PHOTOSYNTHESIS UNDER FLUCTUATING LIGHT, 2nd Edition

EDITED BY: Michele Grieco, Fiamma Longoni, Stefano Santabarbara and Jeremy Harbinson

PUBLISHED IN: Frontiers in Plant Science

frontiers Research Topics

frontiers

ISSN 1664-8714
ISBN 978-2-8325-2790-0
DOI 10.3389/978-2-8325-2790-0

About Frontiers

Frontiers is more than just an open-access publisher of scholarly articles: it is a pioneering approach to the world of academia, radically improving the way scholarly research is managed. The grand vision of Frontiers is a world where all people have an equal opportunity to seek, share and generate knowledge. Frontiers provides immediate and permanent online open access to all its publications, but this alone is not enough to realize our grand goals.

Frontiers Journal Series

The Frontiers Journal Series is a multi-tier and interdisciplinary set of open-access, online journals, promising a paradigm shift from the current review, selection and dissemination processes in academic publishing. All Frontiers journals are driven by researchers for researchers; therefore, they constitute a service to the scholarly community. At the same time, the Frontiers Journal Series operates on a revolutionary invention, the tiered publishing system, initially addressing specific communities of scholars, and gradually climbing up to broader public understanding, thus serving the interests of the lay society, too.

Dedication to Quality

Each Frontiers article is a landmark of the highest quality, thanks to genuinely collaborative interactions between authors and review editors, who include some of the world's best academicians. Research must be certified by peers before entering a stream of knowledge that may eventually reach the public - and shape society; therefore, Frontiers only applies the most rigorous and unbiased reviews.
Frontiers revolutionizes research publishing by freely delivering the most outstanding research, evaluated with no bias from both the academic and social point of view. By applying the most advanced information technologies, Frontiers is catapulting scholarly publishing into a new generation.

What are Frontiers Research Topics?

Frontiers Research Topics are very popular trademarks of the Frontiers Journals Series: they are collections of at least ten articles, all centered on a particular subject. With their unique mix of varied contributions from Original Research to Review Articles, Frontiers Research Topics unify the most influential researchers, the latest key findings and historical advances in a hot research area! Find out more on how to host your own Frontiers Research Topic or contribute to one as an author by contacting the Frontiers Editorial Office: frontiersin.org/about/contact

PHOTOSYNTHESIS UNDER FLUCTUATING LIGHT, 2nd Edition

Topic Editors:
Michele Grieco, Martin Luther University of Halle-Wittenberg, Germany
Fiamma Longoni, Université de Neuchâtel, Switzerland
Stefano Santabarbara, National Research Council (CNR), Italy
Jeremy Harbinson, Wageningen University and Research, Netherlands

Publisher's note: In this 2nd edition, the following articles have been updated: Longoni F, Grieco M, Santabarbara S and Harbinson J (2023) Editorial: Photosynthesis under fluctuating light. Front. Plant Sci. 14:1220360. doi: 10.3389/fpls.2023.1220360; and Schiphorst C, Koeman C, Caracciolo L, Staring K, Theeuwen TPJM, Driever SM, Harbinson J and Wientjes E (2023) The effects of different daily irradiance profiles on Arabidopsis growth, with special attention to the role of PsbS. Front. Plant Sci. 14:1070218. doi: 10.3389/fpls.2023.1070218

Citation: Grieco, M., Longoni, F., Santabarbara, S., Harbinson, J., eds. (2023). Photosynthesis Under Fluctuating Light, 2nd Edition. Lausanne: Frontiers Media SA. doi: 10.3389/978-2-8325-2790-0

Table of Contents

frontiers | Frontiers in Plant Science

TYPE Editorial
PUBLISHED 09 June 2023
DOI 10.3389/fpls.2023.1220360

OPEN ACCESS

EDITED AND REVIEWED BY
Lorenzo Ferroni,
University of Ferrara, Italy

*CORRESPONDENCE
Stefano Santabarbara
stefano.santabarbara@cnr.it

RECEIVED 10 May 2023
ACCEPTED 01 June 2023
PUBLISHED 09 June 2023

CITATION
Longoni F, Grieco M, Santabarbara S and Harbinson J (2023) Editorial: Photosynthesis under fluctuating light. *Front. Plant Sci.* 14:1220360. doi: 10.3389/fpls.2023.1220360

Editorial: Photosynthesis under fluctuating light

Fiamma Longoni[1], Michele Grieco[2], Stefano Santabarbara[3]* and Jeremy Harbinson[4]

[1]Laboratory of Plant Physiology, Institute of Biology, University of Neuchâtel, Neuchâtel, Switzerland, [2]infarm - Indoor Urban Farming B.V., Berlin, Germany, [3]Photosynthesis Research Unit, Institute of Agricultural Biology and Biotechnology, National Research Council (CNR), Milan, Italy, [4]Wageningen University and Research, Wageningen, Netherlands

KEYWORDS

light fluctuation, photosynthesis, combined abiotic stress, light harvesting, plant metabolic regulation

Editorial on the Research Topic
Photosynthesis under fluctuating light

Photosynthetic organisms have colonized a wide variety of habitats in the terrestrial, freshwater and marine biomes. These habitats are characterized by significant differences in key physiological factors, including light intensity and spectral distribution, nutrients and water availability, temperature. The result is a conspicuously complex process that depends on the coordinated activity of several sub-processes whose adaptation underpins the optimisation of the photosynthetic apparatus to the specific habitat. The limited range of techniques available to measure photosynthesis in the field provides only partial insights into the operation and regulation of photosynthesis. The investigation of the diversity of adaptive strategies that have evolved as part of the adaptation of photosynthesis has largely been restricted to laboratory studies made on organisms grown and measured under stable, controlled conditions. This was, and still is, necessary in order to design reproducible, straightforward experiments addressing the fundamental mechanisms underlying the function and regulation of photosynthesis that, however, still eludes complete understanding even under the relatively controlled growth conditions.

Nonetheless, in recent years, there has been a growing interest in improving the understanding of the mechanisms that allow photosynthetic organisms to respond to the fluctuating conditions of the natural environments These fluctuations can be substantial, occurring on different timescales, ranging from the short term (in the sub-second range) to the long term (e.g. seasonal or even slower). Given the variety of adaptive strategies utilised by photosynthetic organism to thrive in specific habitats, the response mechanisms that have evolved to deal with environmental fluctuations are expected to be as diverse and complex.

The papers collected in this Research Topic reflect the variety of approaches employed to address the mechanism of response of photosynthetic organisms to fluctuating light conditions.

Gjindali et al. review both experimental and modelling approaches to address and describe short- and long-term responses to light fluctuations in land plants. A second review by Wang et al. discusses the limitations occurring under very dim light, in some species of vascular plants which generally are considered to have adapted to higher photon fluxes.

Moreover, Ye et al. demonstrate the benefits of mathematical descriptions that do not rely on asymptotic extrapolations to describe the light-saturation curves of net

photosynthesis, carbon and oxygen fixation in land plants. Hommel et al. present a comparative study of short-term fluctuation and rapid responses of the photosynthetic apparatus to light-dark and spectral transitions, highlighting both similarities, as well as differences, in these responses in the model vascular plant *Arabidopsis thaliana*.

Other papers describe experimental investigations of different aspects responses to fluctuating light in plants, including species with agricultural potential. Tula et al. used the recombinant expression of flavodiiron (flv) proteins from *Synechocystis* sp.PCC6803, a recently discovered alternative electron sinks in cyanobacteria, algae and mosses (Ilík et al., 2017), to reduce the photoinhibition of Photosystem II under light fluctuation in Arabidopsis. The paper shows that Flv protein can be introduced in angiosperms and contribute in improving the photosynthetic electron transport efficiency. The study by Kaiser et al., performed in tomato, addresses the importance of stomatal conductance in ensuring a rapid establishment of photosynthetic fluxes upon dark-light transitions. Although Kaiser et al. present evidence that gas exchange can represent a limiting factor for the establishment of photosynthetic fluxes, and its increase appears therefore beneficial, it occurs at the expenses of water use efficiency. Therefore, there is a need to balance these two important factors which are often changing antagonistically. The importance of water use efficiency is also addressed in the paper by Dellero et al., showing that this factor is the most affected by the phenological variation in rapeseed leaves, despite a general trend of decreasing photosynthetic efficiency and carbon assimilation with age.

The study of Zhao et al. address the genetic factors controlling the production of anthocyanin in peach, particularly the promotion of their biosynthesis by UVA and UVB irradiance. Beside their role in fruit coloration, these pigments may also have an important screening effect to protect the organism from ultraviolet radiation. The generality of the photomorphogenic control is further demonstrated by Arabidopsis carrying the peach-derived regulatory elements.

The study by Ohkubo et al. compares different rice cultivars under fluctuating light and elevated CO_2, showing a correlation between the best performing variety and the efficiency of nitrogen utilisation. Responses to fluctuating light are also a relevant factor in understanding the adaptation of plants to specific ecological niches, as shown by Kang et al. Their paper addresses the importance not only of light fluctuation, but also of the leaf temperature changes in response to fluctuating light; these act as synergistic factors, particularly in shade-tolerant plants. The acclimatory responses to light fluctuation can help us understand the ecological success of invasive species. The study of Mlinaric et al. showed that fast growth rate and invasive nature of the Japanese knotweed could be correlated with the increase ability to respond to light fluctuation, possibly linked to the ability of redirecting the photosynthetic electron transfer fluxes toward the cyclic electron transport pathway.

Further contributions to the Research Topic use unicellular cyanobacteria to investigate the acclimation to light changes at subcellular and molecular level. The study of Canonico et al. shows that controlled light oscillations have a significant effect on the average distribution of photosynthetic supercomplexes in defined membrane compartments. At the same time, the photosynthetic supercomplex distribution shows a broad variation on a cell-to-cell basis, which is suggested to represent a possible marker for phenotypic heterogeneity. The study of Bernat et al. addresses the effect of specific wavelengths on the composition of the photosynthetic apparatus of a picocyanobacterium, which displays a great plasticity. They report that cells illuminated with spectral ranges, particularly at the red edge of visible light (wavelengths longer than 680 nm), employ strategies previously considered exclusive to high light conditions.

On the whole, this Research Topic highlights the broad range of strategies that photosynthetic organisms may employ to adapt to ambient fluctuations, and how these strategies may not only depend on given taxa, but being highly heterogeneous down to leaf or cellular level.

Author contributions

All authors listed have made a substantial, direct, and intellectual contribution to the work and approved it for publication.

Funding

FL was supported by the University of Neuchâtel and the Swiss National Science Foundation (31003A_179417). SS acknowledges support from Regione Lombardia through the project "Enhancing Photosynthesis" (DSS 16652 30/11/2021) on behalf of the winners of the "Lombardia è Ricerca – 2020" award.

Conflict of interest

Author MG was employed by infarm - Indoor Urban Farming B.V.

The remaining authors declare that the research was conducted in the absence of any commercial or financial relationships that could be construed as a potential conflict of interest.

Publisher's note

Reference

Ilík, P., Pavlovič, A., Kouřil, R., Alboresi, A., Morosinotto, T., Allahverdiyeva, Y., et al. (2017). Alternative electron transport mediated by flavodiiron proteins is operational in organisms from cyanobacteria up to gymnosperms. *N. Phytol.* 214, 967–972. doi: 10.1111/nph.14536

frontiers in Plant Science

ORIGINAL RESEARCH
published: 25 June 2020
doi: 10.3389/fpls.2020.00902

Providing an Additional Electron Sink by the Introduction of Cyanobacterial Flavodiirons Enhances Growth of *A. thaliana* Under Various Light Intensities

Suresh Tula[1], Fahimeh Shahinnia[1], Michael Melzer[1], Twan Rutten[1], Rodrigo Gómez[2], Anabella F. Lodeyro[2], Nicolaus von Wirén[1], Néstor Carrillo[2] and Mohammad R. Hajirezaei[1]**

[1] Molecular Plant Nutrition, Department of Physiology and Cell Biology, Leibniz Institute of Plant Genetics and Crop Plant Research, Seeland, Germany, [2] Instituto de Biología Molecular y Celular de Rosario (IBR-UNR/CONICET), Facultad de Ciencias Bioquímicas y Farmacéuticas, Universidad Nacional de Rosario, Rosario, Argentina

OPEN ACCESS

Edited by:
Jeremy Harbinson, Wageningen University & Research, Netherlands

Reviewed by:
Peter J. Gollan, University of Turku, Finland
Xenie Johnson, Commissariat à l'Energie Atomique et aux Energies Alternatives (CEA), France

***Correspondence:**
Néstor Carrillo
carrillo@ibr-conicet.gov.ar
Mohammad R. Hajirezaei
mohammad@ipk-gatersleben.de

Specialty section:
This article was submitted to Plant Abiotic Stress, a section of the journal Frontiers in Plant Science

Received: 13 February 2020
Accepted: 02 June 2020
Published: 25 June 2020

Citation:
Tula S, Shahinnia F, Melzer M, Rutten T, Gómez R, Lodeyro AF, von Wirén N, Carrillo N and Hajirezaei MR (2020) Providing an Additional Electron Sink by the Introduction of Cyanobacterial Flavodiirons Enhances Growth of A. thaliana Under Various Light Intensities. Front. Plant Sci. 11:902. doi: 10.3389/fpls.2020.00902

The ability of plants to maintain photosynthesis in a dynamically changing environment is of central importance for their growth. As the photosynthetic machinery is a sensitive and early target of adverse environmental conditions as those typically found in the field, photosynthetic efficiency is not always optimal. Cyanobacteria, algae, mosses, liverworts and gymnosperms produce flavodiiron proteins (Flvs), a class of electron sinks not represented in angiosperms; these proteins act to mitigate the photoinhibition of photosystem I under high or fluctuating light. Here, genes specifying two cyanobacterial Flvs have been expressed in the chloroplasts of *Arabidopsis thaliana* in an attempt to improve plant growth. Co-expression of *Flv1* and *Flv3* enhanced the efficiency of light utilization, boosting the plant's capacity to accumulate biomass as the growth light intensity was raised. The *Flv1*/*Flv3* transgenics displayed an increased production of ATP, an acceleration of carbohydrate metabolism and a more pronounced partitioning of sucrose into starch. The results suggest that Flvs are able to establish an efficient electron sink downstream of PSI, thereby ensuring efficient photosynthetic electron transport at moderate to high light intensities. The expression of Flvs thus acts to both protect photosynthesis and to control the ATP/NADPH ratio; together, their presence is beneficial for the plant's growth potential.

Keywords: *A. thaliana*, cyanobacteria, flavodiiron proteins, photosynthesis, electron sink, primary metabolism, biomass

INTRODUCTION

Plant growth and development, fueled by photosynthesis, depend on the capture of light energy, a process carried out by the chloroplast (Stitt et al., 2010). Photosynthesis can be down-regulated by many factors, including an inadequate pool of ATP or an imbalance between the quantity of ATP and NADPH present (Avenson et al., 2005; Cruz et al., 2005; Amthor, 2010). Additional ATP is provided by the cyclic electron transport (CET) pathway, without production of extra NADPH.

Photosynthesis is also affected by environmental conditions that might limit CO_2 availability (e.g., stomatal closure) or CO_2 assimilation by inhibition of the Calvin-Benson cycle (Czarnocka and Karpiński, 2018). One of the consequences of decreased photosynthetic efficiency is the over-reduction of the photosynthetic electron transport chain (PETC) and the stroma due to limitations in oxidized acceptors ($NADP^+$), which may in turn promote the production of reactive oxygen species (ROS) by adventitious electron and/or energy transfer to O_2 (Gómez et al., 2019). Since the functioning of both PSI and PSII are compromised by the presence of ROS (Miyake, 2010), the result is a further decrease in the plant's capacity to assimilate CO_2 (Zivcak et al., 2015a,b; Takagi et al., 2016). Alterations in plastid redox poise and ROS build-up affect chloroplast signaling and nuclear gene expression (Gollan et al., 2017). Thus, avoiding PSI electron acceptor limitation or introducing additional electron dissipating pathways into the chloroplast have the potential to improve photosynthetic efficiency and hence increase plant's productivity.

Algae, cyanobacteria, non-vascular plants (mosses and liverworts) and gymnosperms have evolved an alternative electron flow (AEF) pathway, driven by the so-called flavodiiron proteins (Flvs). Analysis of the genome of the cyanobacterium *Synechocystis* sp. PCC6803 has identified the presence of four *Flv* genes. Their products, in the form of the heterodimers Flv1/Flv3 and Flv2/Flv4, drive oxygen-dependent electron flow under low (ambient) levels of CO_2 availability and fluctuating and/or high light conditions (Zhang et al., 2012; Allahverdiyeva et al., 2013; Hayashi et al., 2014; Shimakawa et al., 2015). The Flv1/Flv3 heterodimer generates an electron sink downstream of PSI and directs the electron flow to reduce O_2 to H_2O without ROS formation, thereby protecting PSI (Allahverdiyeva et al., 2013). According to Yamamoto et al. (2016), expression of the *Physcomitrella patens* Flv1/Flv3 orthologs in the *Arabidopsis thaliana pgr5* mutant (deficient in the main CET pathway) provides partial compensation for the impairment of CET, demonstrating that Flvs could be functionally beneficial in an angiosperm. Shimakawa et al. (2017) have shown that in the liverwort *Marchantia polymorpha,* Flv1/Flv3 contributes to P700 oxidation and hence protects PSI against photoinhibition. When Gómez et al. (2018) co-expressed *Synechocystis Flv1* and *Flv3* in tobacco chloroplasts, the photosynthetic performance of the resulting transgenic plants under steady-state illumination proved to be comparable to that of wild-type (WT) leaves, while the induction of electron transport and non-photochemical quenching during a dark-to-light transition was significantly faster. Also, expression of *P. patens Flv1* and *Flv3* in the rice *pgr5* or *NDH* mutants has been shown to rescue biomass accumulation (Wada et al., 2018). Moreover, the enhancement of ATP synthesis resulting from over-expression of *Flv3* in *Synechocystis* led to accumulation of glycogen and a consequent increase in cell dry weight (Hasunuma et al., 2014).

The purpose of the present investigation was to determine the phenotypic effect of expressing *Synechocystis Flv1/Flv3* genes in *A. thaliana* plants grown under various light intensities. The focus was to establish whether heterologously expressed Flvs could act as electron sink within the PETC, and if so, whether this capacity had the potential to boost the plant's productivity.

MATERIALS AND METHODS

Expression of Cyanobacterial Flv1/Flv3 in *A. thaliana* and Localization of the Transgenic Products

Arabidopsis thaliana Col-0 lines constitutively expressing *Flv1* and *Flv3* were generated by floral dip (Clough and Bent, 1998), using the pCHF3-derived plasmid described by Gómez et al. (2018), in which the two *Flv* genes were cloned in the same vector backbone between the left and right borders of T-DNA (**Figure 1A**). Transgene expression was driven by separate cauliflower mosaic virus (CaMV) 35S promoters, and a sequence encoding a pea ferredoxin-$NADP^+$ reductase (FNR) transit peptide was fused in-frame to the 5′-end of each *Flv* gene to direct expression of the corresponding products to the chloroplast (**Figure 1B**). Homozygotes were selected by segregation analysis and confirmed by proportional increases in gene contents as determined by PCR amplification with the primers given in **Supplementary Table S1** (*Flv1* F/R and *Flv3* F/R). Three independent transformants were developed into stable transgenic lines (L1-L3). *Flv* transcript levels were monitored using a quantitative real-time PCR (qRT-PCR) assay (**Supplementary Figure S1**).

Chloroplast targeting of the transgenes was validated by fusing the *GFP* sequence (encoding green fluorescent protein) to the 3′-end of the *Flv* coding regions, taking advantage of PGBW5 Gateway binary vectors driven by the CaMV 35S promoter (**Supplementary Figure S2a**). Vectors containing the *Flv* transgenes were transferred into *Agrobacterium tumefaciens* strain EHA105 by the Dower et al. (1988) electroporation method and thence into leaves of *Nicotiana benthamiana* using agroinfiltration as described by Sainsbury and Lomonossoff (2008). Leaves sampled 48 h after infiltration were subjected to confocal laser scanning microscopy (CLSM) to monitor GFP fluorescence (**Supplementary Figure S2b**).

Growth Conditions

Seeds of WT and *Flv*-expressing lines were surface-sterilized by immersion in 70% (v/v) ethanol and 0.05% (v/v) Tween-20 for 15 min, and then rinsed in 96% (v/v) ethanol for 30 s. After air drying, seeds were held at 4°C for 48 h, plated on vertically oriented agar containing half strength Murashige and Skoog (1962) medium and grown under an 8-h photoperiod (160 μmol photons m^{-2} s^{-1}) at 22°C. After 2 weeks, seedlings were potted into a mixture of 70 L substrate 1 (Düsseldorf, Germany), 23 L vermiculite and 372 g plantacote depot 4 m, and held at 22°C, 80% relative humidity under an 8-h photoperiod provided by Master HPI-T Plus 250 W fluorescent lights (Philips, Netherlands) at four different light intensities: low (50 μmol photons m^{-2} s^{-1}), moderate (160 μmol photons m^{-2} s^{-1}), moderately high (300 μmol photons m^{-2} s^{-1}) and high (600 μmol photons m^{-2} s^{-1}). The CO_2 level was maintained at

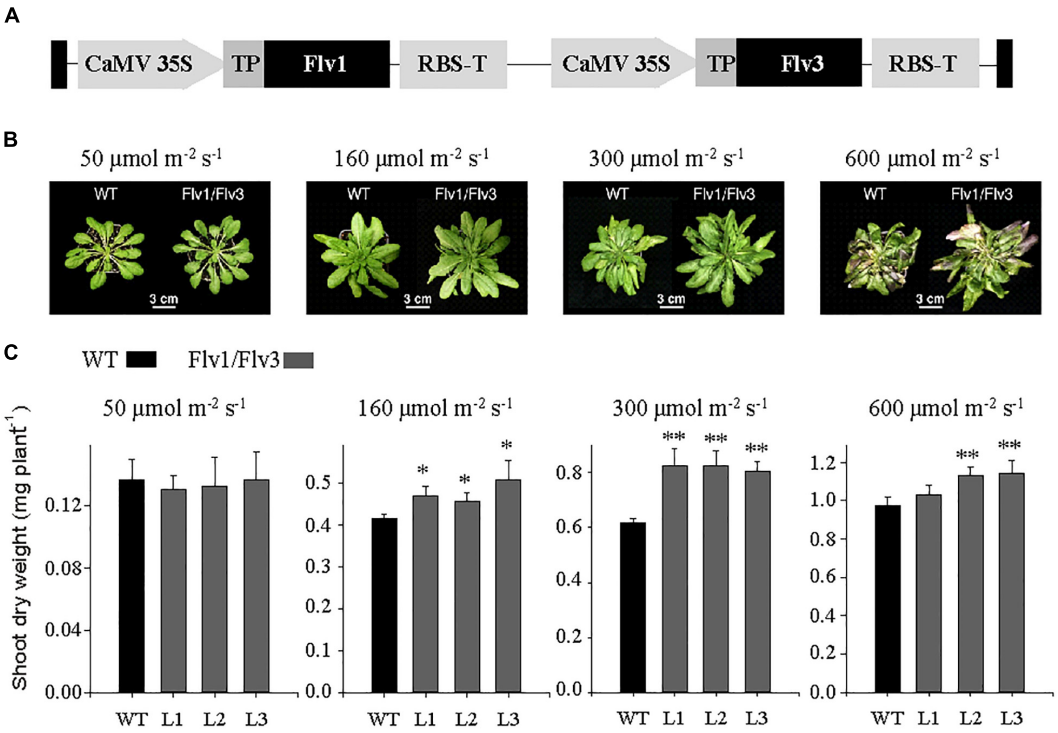

FIGURE 1 | Growth of *A. thaliana* plants heterologously expressing cyanobacterial *Flv* genes. **(A)** Design of the transgene construct pCHF3-*Flv1/Flv3*. The sequence encoding the transit peptide of pea FNR (TP, gray box) was fused to the 5′-end of each *Flv* coding region to target the corresponding fusion products to chloroplasts. Each construct was placed between individual CaMV 35 promoters and RBS (RubiscoS-E9) terminators. **(B)** Phenotypes of 6 weeks old plants exposed to an 8-h photoperiod at a variety of light intensities. **(C)** Shoot dry weight: data are shown as means ± SE (n = 5–8). *, **: means differ from the performance of WT at $P \leq 0.05$ and $P \leq 0.01$, respectively. L1–L3 represent three independent stable lines expressing Flv1/Flv3 in chloroplasts.

400 ppm and plants were kept fully hydrated. For determination of shoot dry weight, whole rosettes of individual plants were harvested at the end of 6 weeks from date of germination. The plant material was dried for 16 h at 80°C and individual rosette dry weights were measured. For leaf biochemical analyses, rosettes of 6 weeks old plants exposed to 160 µmol photons m^{-2} s^{-1} and harvested at various time points during the diurnal cycle (0, 4, 8, 16, 20, and 24 h) were snap-frozen in liquid nitrogen and ground to powder. Plants were also grown under long-day conditions (16-h photoperiod, 160 µmol photons m^{-2} s^{-1}) for 6 weeks, with all other environmental parameters identical to those used for the short-day grown plants. For determination of total shoot dry weight and seed yield, plants were transferred to the growth conditions with 12 h photoperiod and 160 µmol photons m^{-2} s^{-1} for another 3 weeks (**Figure 2**).

Determination of the Leaf Contents of Carbohydrates, Amino Acids and Metabolites

For the determination of soluble sugars (glucose, fructose, and sucrose) and amino acids, a 50-mg aliquot of powdered frozen leaf tissue was extracted in 0.7 mL of 80% (v/v) ethanol at 80°C for 1 h. Following centrifugation (18,700 *g*, 10 min), the supernatant was evaporated under vacuum at 40°C, and the residue dissolved in 0.2 mL deionized water. Sugar contents were quantified using the enzymatic method of Ahkami et al. (2013), while those of the individual amino acids were determined according to Mayta et al. (2018). The pelleted material was used to assess the leaf's starch content: pellets were rinsed twice in 80% (v/v) ethanol, air-dried at 80°C for 1 h and resuspended in 0.2 M KOH. The resulting suspension was held at 80°C for 1 h, the pH adjusted to neutrality using 1 M acetic acid, then incubated overnight at 37°C in 50 mM NaAc (pH 5.2) containing 7 units mg^{-1} amyloglucosidase. The glucose thereby released was measured as above. The methods used for the quantification of primary metabolites followed Ghaffari et al. (2016).

Determination of the Leaf Contents of Adenine Phosphates

Adenine phosphates were quantified employing an UPLC-based method developed from that described by Haink and Deussen (2003). Prior to the UPLC separation step, 20-µL aliquots of the samples used for the quantification of metabolites (as well as a mixture of ATP, ADP, AMP, and ADPGlc) were derivatized by the addition of 45 µL of 10% (v/v) chloracetaldehyde and 435 µL of 62 mM sodium citrate/76 mM KH_2PO_4 (pH 5.2), followed by a 40-min incubation at 80°C, cooling on ice, and centrifugation (20,000 *g*, 1 min). Reverse-phase UPLC separations were achieved using an Infinity 1200 device (Agilent, Waldbronn, Germany). The gradient

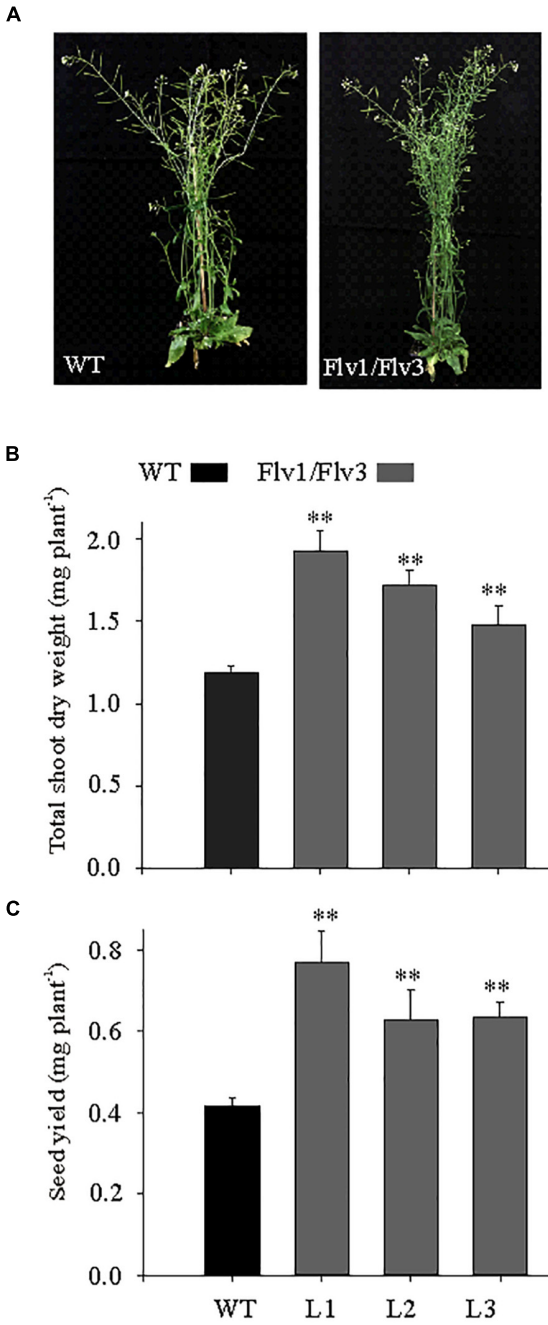

FIGURE 2 | The effect of heterologously expressing *Flv1/Flv3* genes on the development of *A. thaliana* plants grown under long-day photoperiod. **(A)** Phenotypes of WT and *Flv* transgenics. Plants were grown for 6 weeks under a 16-h photoperiod (160 μmol photons m^{-2} s^{-1} of actinic light) and then transferred to ambient conditions for another 3 weeks for determination of **(B)** total shoot dry weight and **(C)** seed yield per plant. Data shown as means ± SE (n = 8). **: means differ from the performance of WT plants at $P \leq 0.01$.

was established employing eluents A (TBAS/KH_2PO_4: 5.7 mM tetrabutylammonium bisulfate/30.5 mM KH_2PO_4, pH 5.8) and B (a 2:1 mixture of acetonitrile and TBAS/KH_2PO_4); the Roti C Solv HPLC reagents were from Roth (Karlsruhe, Germany). The 1.8 μm, 2.1 × 50 mm separation column was an Eclipse plus C18. The column was pre-equilibrated for at least 30 min in a 9:1 mixture of eluents A and B. During the first 2 min of the run, the column contained 9:1 A:B, changed thereafter to 2:3 A:B for 2.3 min followed by a change to 1:9 A:B for 3.1 min and set to initial values of 1:9 for 2.6 min. The flow rate was 0.6 mL min^{-1} and the column temperature was maintained at 37°C. Excitation and emission wavelengths were 280 nm and 410 nm, respectively. Chromatograms were integrated using the MassHunter (release B.04.00) software (Agilent).

Determination of the Leaf Content of Glutathione

Glutathione was extracted from leaves according to Davey et al. (2003). Approximately 100 mg of fresh leaf material were ground to fine powder using tissue homogenizer with 1 mM EDTA and 0.1% (v/v) formic acid at 4°C under green safe light and centrifuged at maximum speed (35,280 *g*) for 10 min. Measurements of oxidized and reduced glutathione were carried out immediately in freshly prepared extracts. Separation and analysis of the desired compounds were performed on a C18 column (HSS T3, 1.8 μm, 2.1 × 150 mm, Waters, Germany) and an UPLC/MS-MS (Infinity ll, 6490 Triple Quadrupole LC/MS, Agilent), respectively. Two μL of extracts and the corresponding standards were injected in the mobile phase consisting of purest water plus 0.1% (v/v) formic acid and pure methanol plus 0.1% (v/v) formic acid. The temperatures of the auto sampler and column were maintained at 8 and 37°C, respectively. Separated compounds were eluted at a flow rate of 0.5 mL min^{-1}, and their quantification was performed using the MassHunter (release B.04.00) software.

Transmission Electron and Confocal Laser Scanning Microscopy

Transmission electron microscopy was performed following Mayta et al. (2018). For ultrastructure analysis, 2-mm^2 cuttings from the central part of three leaves from five different plants of WT and *Flv1/Flv3*-harboring lines were used for conventional and microwave-assisted fixation substitution and resin embedding as detailed in **Supplementary Table S2**. Sectioning and electron microscopy analysis were performed as described previously (Kraner et al., 2017).

To estimate starch accumulation, 100 randomly selected chloroplasts of each WT and *Flv1/Flv3*-harboring plants have been used. Measurements of length, width, area and size of chloroplasts and starch granules were carried out with Image J software[1]. Furthermore, starch bodies per chloroplast have been counted.

Localization analysis of Flv1 and Flv3 fused to GFP at their C-termini and expressed in *N. benthamiana* cells was carried out by CSLM using a Zeiss LSM 780 microscope (Carl Zeiss GmbH, Jena, Germany). GFP was excited with a 488 nm laser line and fluorescence emission detected with a 491–535 nm band-pass filter.

[1]https://imagej.nih.gov/ij

RNA Isolation, cDNA Synthesis and Transcription Analysis

Total RNA was extracted from young leaves following the protocol of Logemann et al. (1987), subjected to DNase treatment (Life Technologies, Darmstadt, Germany) and converted to ss cDNA using a RevertAid first strand cDNA synthesis kit (Life Technologies, Darmstadt, Germany) supplemented with a template of 1 μg total RNA and oligo dT primers. The reaction was carried out at 42°C for 60 min. The primers used for qRT-PCR analysis of *Flv* transgenes are listed in **Supplementary Table S1** (*Flv1*-RT F/R and *Flv3*-RT F/R). The assays were performed in a CFX384 touch real-time system using the SYBR Green Master Mix Kit (Bio-Rad, Feldkirchen, Germany). The relative expression for *Flv* genes was calculated based on the expression of the house-keeping gene *Ubi10* (GenBank accession number *At4g05320*), as WT plants did not contain *Flv* genes. Primers employed to amplify *Ubi10* are also given in **Supplementary Table S1**. Relative transcript abundances were determined with the ΔΔCt method according to Schmittgen and Livak (2008).

Statistical Analysis

Means and standard errors (SE) were calculated using SigmaPlot software[2]. The Student's *t*-test was employed to evaluate for the statistical significance of differences between means.

RESULTS

The Growth Response of *Flv*-Expressing *A. thaliana* Plants to Variations in the Light Intensity

To generate *A. thaliana* plants expressing plastid-targeted Flv1 and Flv3, the coding regions of the corresponding *Flv* genes were fused in-frame to the 3′-end of a DNA sequence encoding the chloroplast transit peptide of pea FNR and placed under the control of the constitutive CaMV 35S promoter in plasmid pCHF3-*Flv1/Flv3* (Gómez et al., 2018; **Figure 1A**). Expression of the *Flv1/Flv3* genes was monitored by measuring the corresponding transcripts using qRT-PCR (**Supplementary Figure S1**). Chloroplast localization of the Flv products was confirmed by introducing a C-terminal GFP tag to both proteins (**Supplementary Figure S2a**) and transiently expressing them in *N. benthamiana*. **Supplementary Figure S2b** shows that GFP fluorescence was confined to plastids in both cases. Image analysis suggests that Flv3 was translocated to all chloroplasts, whilst Flv1 was only detected in a fraction of them (**Supplementary Figure S2b**), most likely affecting the effectivity of heterodimer formation in the transgenic plants. The levels of heterodimer accumulated in *Flv1/Flv3* cells were however sufficient to elicit a growth phenotype in the transformants (see below).

Homozygous lines L1–L3, belonging to the T3 generation, were used for phenotypic characterization. The development of biomass in both WT and *Flv* transgenic plants grown at various light intensities is illustrated in **Figure 1B**. When illuminated at 50 μmol photons m^{-2} s^{-1}, the performance of the transgenic plants was not distinguishable from that of their WT counterparts. However, when the light intensity was increased to either 160 or 300 μmol photons m^{-2} s^{-1}, the transgenic plants were clearly larger (**Figure 1B**). Comparisons of shoot dry weight indicated that transgenic plants harboring *Flv1/Flv3* outperformed WT siblings by 10–30% (**Figure 1C**). Plants expressing *Flv1/Flv3* also grew better at 600 μmol photons m^{-2} s^{-1} (**Figure 1C**), even though they looked stressed at this irradiation levels, as suggested by the color of the leaves, presumably due to anthocyanin accumulation as a typical response to high light (**Figure 1B**).

The Effect of Expressing *Flv1/Flv3* Transgenes on Biomass Accumulation in Plants Grown Under Long-Day Photoperiod

Under a long-day regime, the *Flv* transgenics flowered earlier than WT plants (data not shown), and were more bushy, with increased inflorescences (**Figure 2A**). Shoot dry weight was up to 1.8-fold greater in *Flv*-expressing plants than in WT counterparts (**Figure 2B**). Seed size was unaffected by the presence of the transgenes (data not shown), but seed yield was 1.5- to 1.8-fold greater (**Figure 2C**).

The Effect of Expressing *Flv* Transgenes on Leaf Sugar, Starch and Amino Acid Contents

Yamamoto et al. (2016) and Gómez et al. (2018) have reported that under steady-state illumination conditions, the photosynthetic activity of *Flv*-expressing plants did not differ significantly from their WT siblings. To determine if Flv1/Flv3 expression affected other central metabolic routes, the leaf contents of carbohydrates and amino acids were measured in plants grown at 160 μmol photons m^{-2} s^{-1}, a condition that exhibited significant biomass gains in the transformants relative to the wild-type (**Figure 1**).

Under this light regime, leaves of plants harboring *Flv1/Flv3* accumulated significantly higher sucrose concentrations than those of WT counterparts; in each line, sucrose contents increased gradually during the light period and fell during the dark period (**Figure 3A**). Leaf starch contents did not vary between genotypes at the beginning of the light period, but they increased faster (by as much as 1.7-fold) during the day in *Flv*-transgenic plants than in WT siblings (**Figure 3B**). Moreover, ultrastructural data obtained by transmission electron microscopy indicate that while the average size of starch granules was unaffected by *Flv* expression, their number was enhanced in the leaves of plants expressing *Flv1/Flv3* (**Figure 3C**). Counting starch granules of 100 individual chloroplasts from WT and Flv1/Flv3-expressing plants revealed that the total number of starch granules was 1.24-fold higher in Flv1/Flv3-expressing plants (440) compared to the WT (354) (**Figure 3D**). Furthermore, the ratio of the measured total area of starch granules divided by the total area of chloroplasts was higher by a

[2]www.sigmaplot.co.uk/products/sigmaplot/sigmaplot-details.php

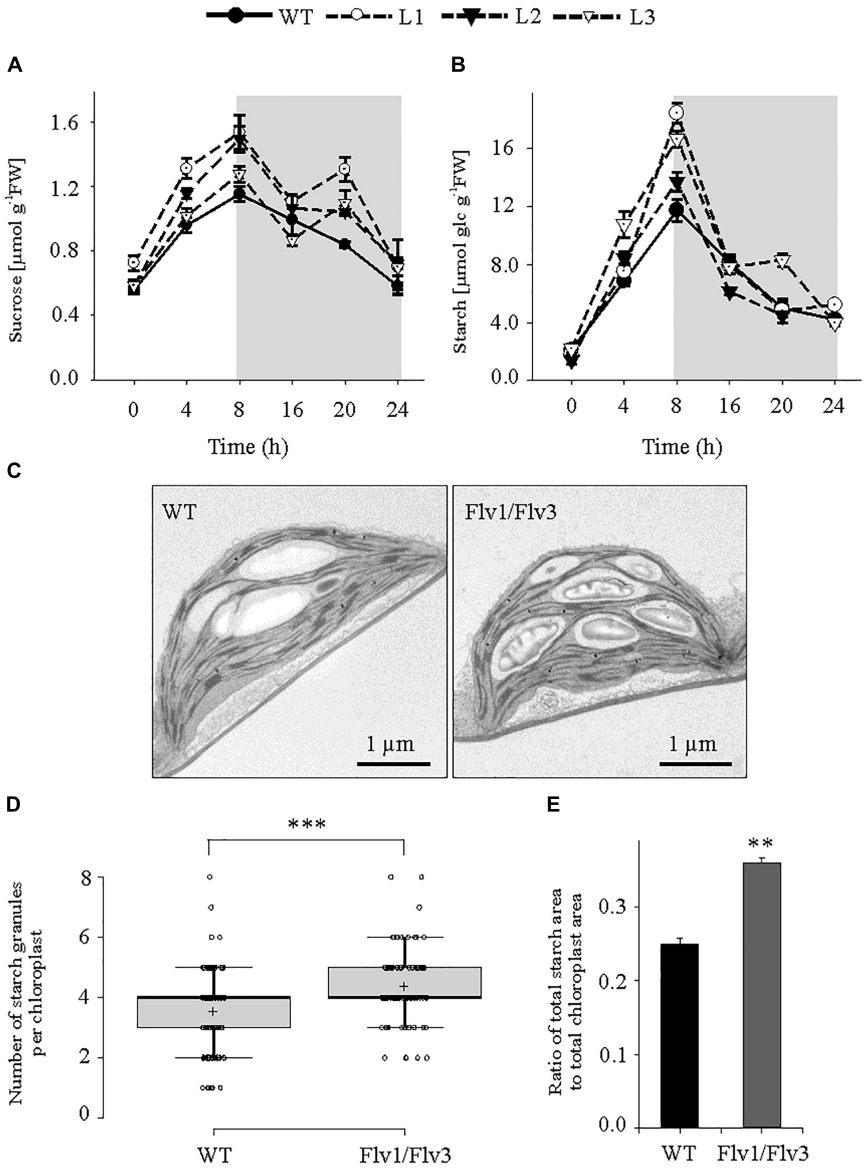

FIGURE 3 | The effect of heterologously expressing *Flv1/Flv3* genes on diurnal variation in carbohydrate metabolism. Temporal variation in the rosette leaves of 6 weeks old plants exposed to 160 µmol photons m^{-2} s^{-1} of actinic light with respect to the contents of **(A)** sucrose and **(B)** starch. Gray boxes indicate the dark period. Data shown as means ± SE (n = 5). FW, fresh weight. **(C)** Representative images of starch granules present in leaves harvested after 5 h of light exposure. **(D)** Number of starch granules per chloroplast [n (chloroplasts) = 100]. **(E)** Ratio of total area of starch granules divided by the total area of chloroplasts. **,***: means differ from the performance of WT plants at $P \leq 0.01$ and $P \leq 0.001$, respectively.

factor of 1.44 in *Flv1/Flv3* expressing plants (680 μm^2/1873 μm^2) than in WT siblings (487 μm^2/1912 μm^2) (**Figure 3E**), indicating that the chloroplasts of *Flv1/Flv3* transgenic plants contained a higher starch volume.

Glucose and fructose contents failed to show consistent differences between lines during the entire photoperiod (**Supplementary Figure S3**). Also, no clear differences were observed with respect to the amounts of any of the amino acids following the plants' exposure to 4 h of light (**Supplementary Table S3**), but by the end of the light period (8 h of light), an increased pool of asparagine, aspartate, glutamine and alanine was observed in *Flv1/Flv3* transgenics with respect to WT plants (**Supplementary Table S4**).

Flv1/Flv3 Expression Increased the ATP Levels of *A. thaliana* Leaves

Leaf contents of ATP, ADP and AMP were measured during both the light (after exposure to 4 and 8 h of illumination) and dark periods (16 h). ATP contents were up to 1.25-fold (after 4 h of illumination), 1.3-fold (after 8 h of illumination only in L1) and 1.3-fold (after 8 h in the dark) higher in *Flv1/Flv3* leaves than in

WT counterparts (**Figure 4a**). The leaf contents of ADP did not differ significantly between lines, whereas the AMP levels were significantly lower up to 1.3-fold in *Flv1/Flv3* transgenic plants compared to WT siblings (**Figures 4b,c**). The ATP/ADP ratio was thus higher at 4 and 16 h by a factor of 1.3- and 1.5-fold, respectively, in all the transgenic lines compared to that of WT siblings (**Figure 4d**). The total adenylate content failed to show differences between lines except for L1, where it was ∼1.2-fold higher than that of WT plants after 8 h of light (**Figure 4e**).

The Effect of Expressing *Flv* Transgenes on the Contents of Glutathione

The contents of both the reduced and oxidized forms of glutathione (GSH and GSSG, respectively) were measured and their ratio was calculated. There was a significant decline of GSH in L3 plants whereas GSSG was statistically higher in line L2 of the transgenic leaves (**Supplementary Figures S4a,b**), resulting in a reduction in the GSH/GSSG ratio of up to 2.5 fold (**Supplementary Figure S4c**).

The Effect of Expressing *Flv* Transgenes on the Leaf Metabolome

The contents of a number of metabolites were affected by the expression of *Flv* transgenes. After a 4-h exposure to light, the concentration of hexose phosphates was raised in all transgenic lines to a level significantly higher than that obtained in WT leaves (**Figure 5A**); however, by the end of the light period, hexose phosphate contents were significantly below those of WT leaves in all transgenic plants (**Figure 5B**). The concentration of the starch precursor ADPGlc was also elevated up to 1.4-fold above the WT level in the *Flv1/Flv3* transformants after 4 h of illumination (**Figure 5C**). When measured again after an 8-h exposure to light, the levels of ADPGlc remained statistically unchanged in the transgenics relative to WT siblings, with the exception of plants from line L2 (**Figure 5D**). With respect to malate, significant increases were only recorded in leaves of line L2 assayed after a 4-h exposure to light, whereas in those of line L3 malate levels were statistically lower after an 8-h exposure to light (**Supplementary Figures S5a,c**). A modest increase in the concentration of citrate was noted with respect to WT levels in the leaves of L3 plants at 4 h and L1 plants at 8 h of illumination (**Supplementary Figures S5b,d**).

DISCUSSION

Photosynthesis is essential for the growth and development of plants, but the process is relatively inefficient since just 8–10% of the overall spectrum of solar radiation is used to convert CO_2 to sugar, while only 2–4% of incident light energy is channeled into growth (Long et al., 2006; Zhu et al., 2010). Most of the solar light intercepted by a leaf is lost by reflection, transmission and absorption by non-photosynthetic pigments, or is simply outside photosynthetically useful wavelengths. In C3 plants, less than 45% of the incident light is harvested, and still a substantial amount is released as heat and fluorescence, or used for photorespiration (Long et al., 2006; Zhu et al.,

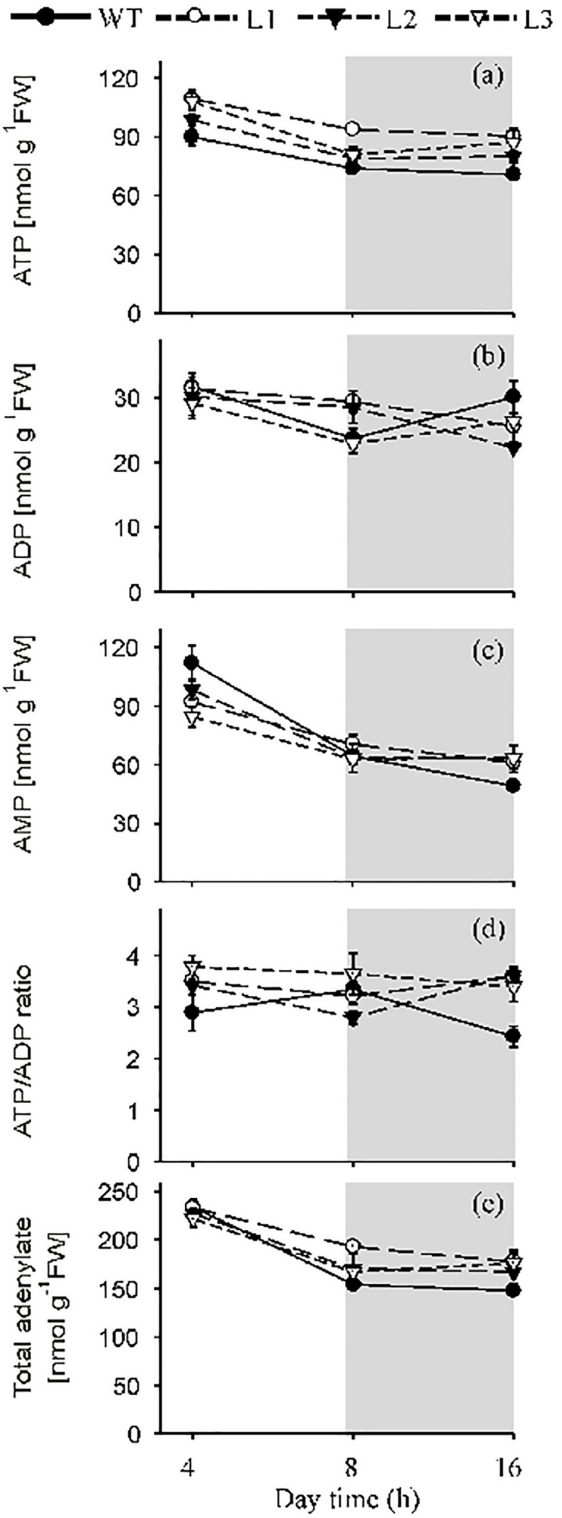

FIGURE 4 | The effect of heterologously expressing *Flv1/Flv3* genes on the contents of ATP, ADP, AMP, the ATP/ADP ratio and total adenylates. Temporal variation in the rosette leaves of 6 weeks old plants exposed to 160 μmol photons m^{-2} s^{-1} of actinic light with respect to **(a)** the contents of ATP, **(b)** ADP and **(c)** AMP, **(d)** the ATP/ADP ratio, **(e)** total adenylates. L1–L3: independent lines harboring *Flv1/Flv3*. Data are shown as means ± SE (n = 5).

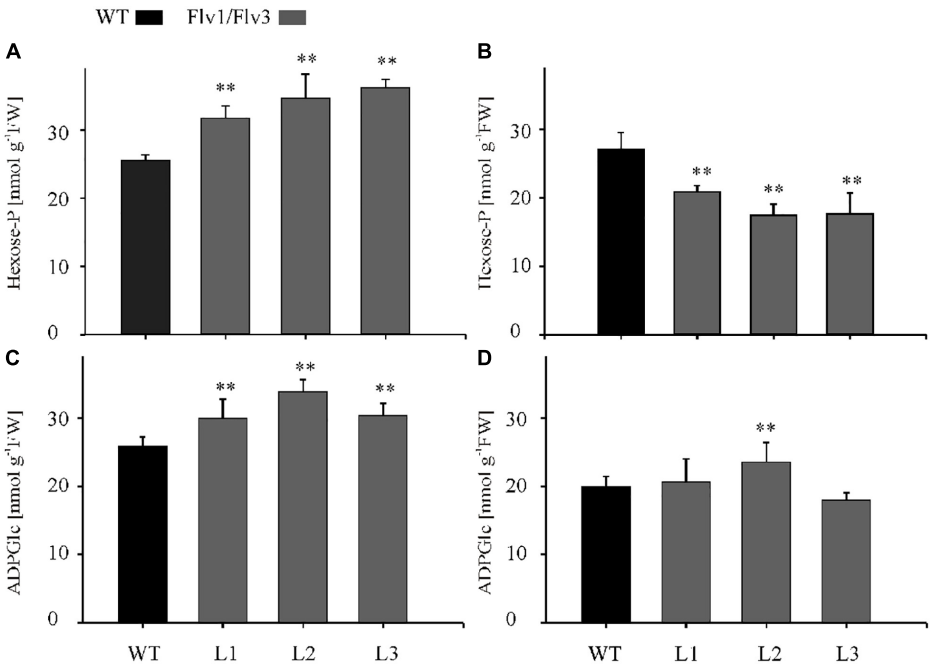

FIGURE 5 | The effect of heterologously expressing *Flv1/Flv3* genes on the contents of primary metabolites. Hexose phosphates **(A,B)** and ADPGlc **(C,D)** were measured in the rosette leaves of 6 weeks old plants after exposure to 4 h **(A,C)** or 8 h **(B,D)** of light. L1–L3: independent lines harboring *Flv1/Flv3*. Data shown as means ± SE (n = 5). **: means differ from the performance of WT plants at $P \leq 0.01$.

2010). In addition, suboptimal conditions such as water and CO_2 limitation, high light, extreme temperatures, etc., might lead to over-reduction of the PETC and uncontrolled ROS production (Gómez et al., 2019). Avoiding these effects by establishing alternative electron sinks in chloroplasts can potentially enhance photosynthesis and overall plant growth.

Flvs have been reported to contribute to photosynthetic redox balance in a number of phototrophs (Jokel et al., 2018; Santana-Sánchez et al., 2019). Moreover, Flv1/Flv3 expressed in angiosperms were shown to act as electron sink for the PETC under certain circumstances (Yamamoto et al., 2016; Wada et al., 2018), especially during dark-light transitions (Gómez et al., 2018). However, the effect of this intervention upon growth and metabolism of the host plants was not reported in those articles. The aim of the present research was to evaluate this by co-expressing *Flv1* and *Flv3* in *A. thaliana* and monitoring growth and metabolic status in the corresponding transformants. The results indicate that plants harboring *Flv1/Flv3* grew significantly better under a range of moderate to high light intensities (**Figure 1**), and displayed increased carbohydrate and ATP levels (**Figures 3**, **4**). The implication of these observations is that Flvs may act as regulators of photosynthesis when expressed in angiosperms, specifically avoiding over-reduction of the PETC as the electron pressure mounted up under increasing light intensities.

In cyanobacteria, the Flv1/Flv3 dimer provides an alternative electron sink at the acceptor side of PSI, preventing over-reduction of the PETC under adverse environmental conditions (Allahverdiyeva et al., 2013; Gerotto et al., 2016; Santana-Sánchez et al., 2019). Likewise, Gómez et al. (2018) have shown that tobacco plants expressing cyanobacterial *Flv1* and *Flv3* showed an improved ability of their dark-adapted leaves to maintain the PETC in a more oxidized state and to enhance proton motive force, again indicating a stronger electron sink in the transformants. The present results suggest a similar interaction of the introduced Flvs with the PETC in the transgenic *A. thaliana*. This hypothesis also agrees with the electron sink activity provided by Flvs in mutants deficient in CET under both high and fluctuating light (Yamamoto et al., 2016; Wada et al., 2018).

In phototrophic organisms, AEF pathways are induced shortly after exposure to light, contributing additional ATP to supply the Calvin–Benson cycle and to support photorespiration during dark-light transitions. As reported by Shikanai and Yamamoto (2017), under steady-state conditions, Flvs have poor access to its putative electron donor Fd, due to activation of the Calvin–Benson cycle, but may regain functionality under highly reduced stromal conditions. Here, *A. thaliana* plants expressing cyanobacterial *Flv1/Flv3* responded differentially to the growth light conditions (**Figure 1**). Under low light intensity, electron transport is typically limited by the availability of photons, so that there is no need of relief with respect to the electron pressure on the PETC. The latter becomes important as the light intensity increases, and the heterologous Flv system was able to dissipate the surplus of reducing equivalents as long as the intensity did not become excessive, as observed for the stressed phenotypes of plants grown at 600 μmol photons m^{-2} s^{-1} and showing anthocyanin accumulation

(**Figure 1B**). When exposed to a long-day regime (16-h photoperiod), the presence of the *Flv* transgenes accelerated flowering (data not shown), and plant biomass accumulation and seed yield were boosted (**Figures 2B,C**), illustrating the benefits of Flv1/Flv3 as additional electron sink under these growth conditions.

In chloroplasts, ATP is generated via the linear and CET pathways (DalCorso et al., 2008), while the mitochondrial respiratory electron transport chain makes an additional contribution during both dark and daylight hours (Liang et al., 2015; Voon et al., 2018). ATP levels were higher in the leaves of *Flv*-expressing transgenics than in those of WT plants after exposure to either 4 or 8 h of light, suggesting that the Flv1/Flv3 dimer was able to dissipate electrons at PSI, enhance linear electron flow and thereby establish the pH gradient required for ATP synthesis (**Figure 4a**). The adenylate pool is also an important regulator of plant metabolism (Geigenberger et al., 2010). In the *Flv* transgenics, an increased ATP level served to boost the activity of the Calvin–Benson cycle, which in turn helped to maintain a high level of hexose phosphates at the middle of the light period (**Figures 5A,B**). Hexose phosphates and ADPGlc accumulated by *Flv*-expressing plants (**Figures 5A–D**) were most likely used to synthesize sucrose and starch during the day, serving to stimulate plant growth (**Figures 3A,B**). The lack of effect of *Flv* expression on the levels of the TCA cycle intermediates citrate and malate implies that these organic acids most likely play at best a minor role in determining biomass production (**Supplementary Figures S5a–d**).

Manipulation of plastid levels of adenylate kinase was shown to increase starch and amino acid contents in potato (Regierer et al., 2002), and to boost the accumulation of amino acids and promote growth in *A. thaliana* (Carrari et al., 2005). In the *Flv* transgenics exposed to 4 h of light, however, there was no evidence for any significant alteration in the leaf's amino acid contents with the exception of alanine (lines L1, L3) and GABA (lines L2, L3), suggesting that by this time

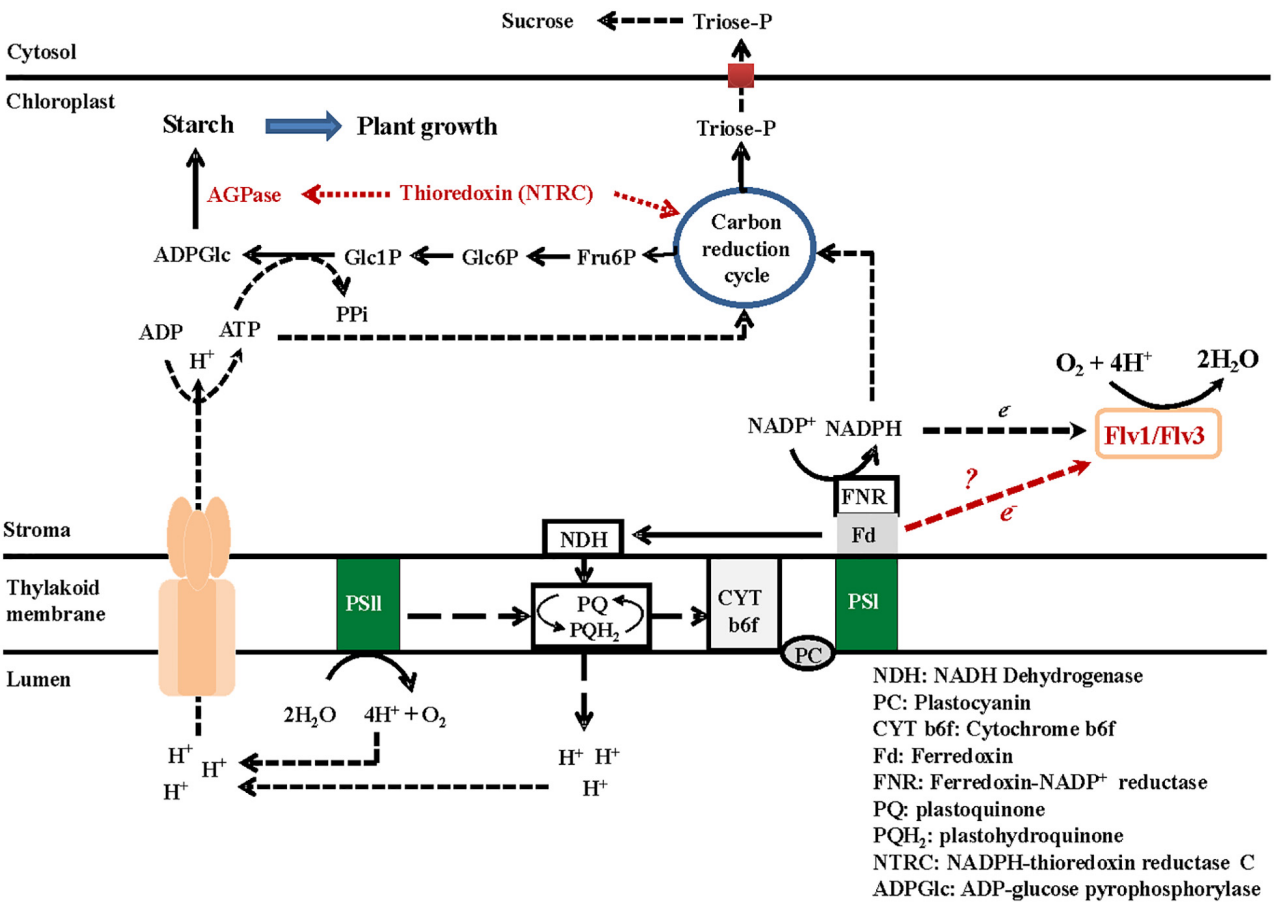

FIGURE 6 | A model describing the metabolic consequences of heterologously expressing *Flv* genes in the chloroplasts of *A. thaliana*. The presence of Flv1/Flv3 creates an electron sink and balances the surplus of the electron flow through PSI and PSII by delivering these electrons to oxygen, which is converted to water. The production of redox equivalents such as NADPH is maintained, resulting in the recycling of carbon through the Calvin–Benson cycle, which in turn generates an increased supply of the phosphorylated metabolites needed for starch synthesis. The energy required for this reaction is provided by ATP, which is synthesized by the H^+-ATP synthase driven by protons pumped by the PETC. The continuous flow of electrons results in acidification of the lumen, which is the driving force for ATP synthesis. ATP is used for the conversion of Glc1P to ADPGlc via ADPGlc pyrophosphorylase. An increased availability of ADPGlc supports a higher level of starch synthesis; starch accumulates when the leaf is exposed to light and is degraded during the dark phase.

illuminated leaves converted most of their photoassimilate into starch (**Supplementary Table S3**). In contrast, the contents of asparagine, arginine, glycine, glutamine, alanine and proline were raised by the plant's exposure to 8 h of light (**Supplementary Table S4**), consistent with the observation that an increase in carbon availability enhances the assimilation of the nitrogen needed for protein synthesis and hence for the continuation of growth in the absence of light (Lawlor, 2002). The glutathione pool was more oxidized in leaves of *Flv*-expressing plants than in their WT siblings (**Supplementary Figure S4**). This was an unexpected result, considering that the presence of Flv1/Flv3 should inhibit the leakage of electrons from the PETC to O_2. It is conceivable that cellular compartments and organelles other than chloroplasts contribute the higher GSSG levels observed in the transgenics (**Supplementary Figure S4b**), but further research will be necessary to properly substantiate this hypothesis.

The levels of both sucrose and ATP were higher in the *Flv* transgenics than in their WT counterparts, not only during illumination, but also during the dark period. According to Sharkey et al. (2004), the levels of sucrose and ATP are highly dependent on carbon metabolism during the night, while Sulpice et al. (2009) and Graf and Smith (2011) have shown that these levels constitute important determinants of biomass accumulation. It seems therefore likely that the growth advantage enjoyed by the *Flv* transgenics reflects their superior capacity to generate photoassimilate and ATP.

Overall, heterologously expressing *Flv1/Flv3* in *A. thaliana* appeared to impact central metabolic routes increasing ATP levels for carbon assimilation and other biosynthetic pathways, and favoring the use of reducing equivalents in productive processes, ultimately boosting growth at moderate to high light intensities (**Figure 6**).

CONCLUSION

The present data have demonstrated that Flv proteins contribute to the efficient functioning of the PETC and that can be introduced in angiosperms with growth and eventually yield benefits. We show that Flvs can act as additional electron sinks when expressed in *A. thaliana*, delivering any excess of reducing equivalents to oxygen, and generating the phosphorylated metabolites required for starch synthesis. The energy needed for this reaction is provided by ATP, which is produced via electron transport and lumen acidification. ATP is also used for the conversion of Glc1P to ADPGlc, mediated by ADPGlc pyrophosphorylase activity. The promotion of ADPGlc finally results in an enhanced level of starch synthesis in leaves exposed to light, and the accumulated starch is metabolized during the dark phase allowing for a continuous growth of the plant (**Figure 6**).

DATA AVAILABILITY STATEMENT

All datasets generated for this study are included in the article/**Supplementary Material**.

AUTHOR CONTRIBUTIONS

MH and NC made substantial contributions to conception and design, interpretation of the results, and preparation of the manuscript. ST made all practical work and did the acquisition and analysis of data, and contributed to preparation of the manuscript. FS and MM were involved in drafting and revising the manuscript, and preparation of the figures. TR, RG, and AL were involved in preparation of microscopy figures (TR), interpretation of the data, and revising the manuscript (RG and AL). NW contributed to the final revision and gave the final approval of the manuscript. All authors contributed to the article and approved the submitted version.

FUNDING

This work was supported by grant FKZ 031A280 from Federal Ministry of Education and Research (BMBF) and by grants PICT 2017-3080 to AL and PICT 2015-3828 to NC from the National Agency for the Promotion of Science and Technology (ANPCyT, Argentina).

ACKNOWLEDGMENTS

We wish to thank Kirsten Hoffie, Marion Benecke, Melanie Ruff, and Nicole Schäfer for excellent technical assistance in molecular and structural analysis at the IPK. This manuscript has been released as a pre-print at bioRxiv 2020.02.05.935346 (Tula et al., 2020).

SUPPLEMENTARY MATERIAL

The Supplementary Material for this article can be found online at: https://www.frontiersin.org/articles/10.3389/fpls.2020.00902/full#supplementary-material

FIGURE S1 | Expression of Flv1/Flv3 in *A. thaliana*. Levels of *Flv* transcripts in the transgenic plants as determined by qRT-PCR. Experimental details are given in section "Materials and Methods." L1–L3: independent lines harboring *Flv1/Flv3*.

FIGURE S2 | Subcellular localization of recombinant Flv1/Flv3. **(a)** Schematic representation of the binary vectors for localization of the *Flv1/GFP* and *Flv3/GFP* fusion transgenes transiently expressed in *N. benthamiana*. The *Flv* genes were fused in-frame to DNA sequences encoding the pea FNR transit peptide (TP) at their 5′-end and *GFP* at their 3′-end, taking advantage of PGBW5 Gateway binary vectors driven by the CaMV 35S promoter. **(b)** GFP fluorescence in the chloroplasts of *N. benthamiana* transformed with *GFP*-tagged *Flv1* and *Flv3* genes. The left panels show GFP fluorescence, the central panels, chlorophyll autofluorescence and the right panels, the merged images.

FIGURE S3 | Diurnal variation in the sugar contents of rosette leaves in 6 weeks old plants heterologously expressing *Flv1/Flv3* genes. Levels of **(a)** glucose and **(b)** fructose were determined in transgenic leaves harboring *Flv1/Flv3*. Data shown as means ± SE (n = 5).

FIGURE S4 | The effect of heterologously expressing *Flv1/Flv3* genes on the contents of GSH **(a)** and GSSG **(b)**, and on the ratio of GSH to GSSG **(c)**. Rosette leaves were sampled at the end of the light period (8-h photoperiod). Data shown as means ± SE (n = 5).

FIGURE S5 | The effect of heterologously expressing *Flv1/Flv3* genes on the leaf contents of organic acids. Malate **(a,c)** and citrate **(b,d)** were measured after plants had been exposed to 4 h **(a,b)** or 8 h **(c,d)** of light. L1–L3: lines harboring *Flv1/Flv3*. Data shown as means ± SE (n = 5). *, **: means differ from the performance of WT plants at $P \leq 0.05$ and $P \leq 0.01$, respectively.

TABLE S1 | List of primers used for PCR and qRT-PCR determinations.

TABLE S2 | Protocol for combined conventional and microwave-driven fixation, dehydration and resin embedding of *A. thaliana* leaf tissue for ultrastructural analysis.

TABLE S3 | Amino acid contents in WT and transgenic lines expressing *Flv1/Flv3* genes. Measurements were carried out after 4 h of illumination. Plants were 6 weeks old. Results are expressed as means ± SE of 5 independent replicates. Significant differences are indicated by asterisks according to Student's t-test ($^*P \leq 0.05$).

TABLE S4 | Amino acid contents in WT and transgenic lines expressing Flv1/Flv3 genes. Measurements were carried out after 8 h of illumination. Plants were 6 weeks old. Results are expressed as means ± SE of 5 independent replicates. Significant differences are indicated by asterisks according to Student's t-test ($^*P \leq 0.05$ and $^{**}P \leq 0.01$).

REFERENCES

Ahkami, A. H., Melzer, M., Ghaffari, M. R., Pollmann, S., Ghorbani Javid, M., Shahinnia, F., et al. (2013). Distribution of indole-3-acetic acid in *Petunia hybrida* shoot tip cuttings and relationship between auxin transport, carbohydrate metabolism and adventitious root formation. *Planta* 238, 499–517. doi: 10.1007/s00425-013-1907-z

Allahverdiyeva, Y., Mustila, H., Ermakova, M., Bersanini, L., Richaud, P., Ajlani, G., et al. (2013). Flavodiiron proteins Flv1 and Flv3 enable cyanobacterial growth and photosynthesis under fluctuating light. *Proc. Natl. Acad. Sci. U.S.A.* 110, 4111–4116. doi: 10.1073/pnas.1221194110

Amthor, J. S. (2010). From sunlight to phytomass: on the potential efficiency of converting solar radiation to phyto-energy. *New Phytol.* 188, 939–959. doi: 10.1111/j.1469-8137.2010.03505.x

Avenson, T. J., Kanazawa, A., Cruz, J. A., Takizawa, K., Ettinger, W. E., and Kramer, D. M. (2005). Integrating the proton circuit into photosynthesis: progress and challenges. *Plant Cell Environ.* 28, 97–109. doi: 10.1111/j.1365-3040.2005.01294.x

Carrari, F., Coll-García, D., Schauer, N., Lytovchenko, A., Palacios-Rojas, N., and Balbo, I. (2005). Deficiency of a plastidial adenylate kinase in *Arabidopsis* results in elevated photosynthetic amino acid biosynthesis and enhanced growth. *Plant Physiol.* 137, 70–82. doi: 10.1104/pp.104.056143

Clough, S. J., and Bent, A. F. (1998). Floral dip: a simplified method for *Agrobacterium* mediated transformation of *Arabidopsis thaliana*. *Plant J.* 16, 735–743. doi: 10.1046/j.1365-313x.1998.00343.x

Cruz, J. A., Avenson, T. J., Kanazawa, A., Takizawa, K., Edwards, G. E., and Kramer, D. M. (2005). Plasticity in light reactions of photosynthesis for energy production and photoprotection. *J. Exp. Bot.* 56, 395–406. doi: 10.1093/jxb/eri022

Czarnocka, W., and Karpiński, S. (2018). Friend or foe? Reactive oxygen species production, scavenging and signaling in plant response to environmental stresses. *Free Radic. Biol. Med.* 122, 4–20. doi: 10.1016/j.freeradbiomed.2018.01.01

DalCorso, G., Pesaresi, P., Masiero, S., Aseeva, E., Schunemann, D., and Finazzi, G. (2008). A complex containing PGRL1 and PGR5 is involved in the switch between linear and cyclic electron flow in *Arabidopsis*. *Cell* 132, 273–285. doi: 10.1016/j.cell.2007.12.028

Davey, M. W., Dekempeneer, E., and Keulemans, J. (2003). Rocket-powered high performance liquid chromatographic analysis of plant ascorbate and glutathione. *Anal. Biochem.* 316, 74–81. doi: 10.1016/s0003-2697(03)00047-2

Dower, W. J., Miller, J. F., and Ragsdale, C. W. (1988). High efficiency transformation of *E. coli* by high voltage electroporation. *Nucleic Acids Res.* 16, 6127–6145. doi: 10.1093/nar/16.13.6127

Geigenberger, P., Riewe, D., and Fernie, A. R. (2010). The central regulation of plant physiology by adenylates. *Trends Plant Sci.* 15, 98–105. doi: 10.1016/j.tplants.2009.11.004

Gerotto, C., Alboresi, A., Meneghesso, A., Jokel, M., Suorsa, M., Aro, E. M., et al. (2016). Flavodiiron proteins act as safety valve for electrons in *Physcomitrella patens*. *Proc. Natl. Acad. Sci. U.S.A.* 113, 12322–12327. doi: 10.1073/pnas.1606685113

Ghaffari, M. R., Shahinnia, F., Usadel, B., Junker, B., Schreiber, F., Sreenivasulu, N., et al. (2016). The metabolic signature of biomass formation in barley. *Plant Cell Physiol.* 57, 1943–1960. doi: 10.1093/pcp/pcw117

Gollan, P. J., Lima-Melo, Y., Tiwari, A., Tikkanen, M., and Aro, E. M. (2017). Interaction between photosynthetic electron transport and chloroplast sinks triggers protection and signalling important for plant productivity. *Philos. Trans. R. Soc. Lond. B Biol. Sci.* 372, 1730. doi: 10.1098/rstb.2016.0390

Gómez, R., Carrillo, N., Morelli, M. P., Tula, S., Shahinnia, F., Hajirezaei, M. R., et al. (2018). Faster photosynthetic induction in tobacco by expressing cyanobacterial flavodiiron proteins in chloroplasts. *Photosynth. Res.* 136, 129–138. doi: 10.1007/s11120-017-0449-9

Gómez, R., Vicino, P., Carrillo, N., and Lodeyro, A. F. (2019). Manipulation of oxidative stress responses as a strategy to generate stress-tolerant crops. From damage to signaling to tolerance. *Crit. Rev. Biotechnol.* 39, 693–708. doi: 10.1080/07388551.2019.1597829

Graf, A., and Smith, A. M. (2011). Starch and the clock: the dark side of plant productivity. *Trends Plant Sci.* 16, 169–175. doi: 10.1016/j.tplants.2010.12.003

Haink, G., and Deussen, A. (2003). Liquid chromatography method for the analysis of adenosine compounds. *J. Chromatogr. B Anal. Technol. Biomed. Life Sci.* 784, 189–193. doi: 10.1016/s1570-0232(02)00752-3

Hasunuma, T., Matsuda, M., Senga, Y., Aikawa, S., Toyoshima, M., Shimakawa, G., et al. (2014). Overexpression of flv3 improves photosynthesis in the cyanobacterium *Synechocystis* sp. PCC6803 by enhancement of alternative electron flow. *Biotechnol. Biofuels* 7:493. doi: 10.1186/s13068-014-0183-x

Hayashi, R., Shimakawa, G., Shaku, K., Shimizu, S., Akimoto, S., Yamamoto, H., et al. (2014). O_2-dependent large electron flow functioned as an electron sink, replacing the steady-state electron flux in photosynthesis in the cyanobacterium *Synechocystis* sp. PCC 6803, but not in the cyanobacterium *Synechococcus* sp. PCC 7942. *Biosci. Biotechnol. Biochem.* 78, 384–393. doi: 10.1080/09168451.2014.882745

Jokel, M., Johnson, X., Peltier, G., Aro, E. M., and Allahverdiyeva, Y. (2018). Hunting the main player enabling *Chlamydomonas reinhardtii* growth under fluctuating light. *Plant J.* 94, 822–835. doi: 10.1111/tpj.13897

Kraner, M., Link, K., Melzer, M., Ekici, A. B., Uebe, S., Tarazona Corrales, P., et al. (2017). Choline transporter-like1 (CHER1) is crucial for plasmodesmata maturation in *Arabidopsis thaliana*. *Plant J.* 89, 394–406. doi: 10.1111/tpj.13393

Lawlor, D. W. (2002). Carbon and nitrogen assimilation in relation to yield: mechanisms are the key to understanding production systems. *J. Exp. Bot.* 53, 773–787. doi: 10.1093/jexbot/53.370.773

Liang, C., Zhang, Y., Cheng, S., Osorio, S., Sun, Y., Fernie, A. R., et al. (2015). Impacts of high ATP supply from chloroplasts and mitochondria on the leaf metabolism of *Arabidopsis thaliana*. *Front. Plant Sci.* 6:922. doi: 10.3389/fpls.2015.00922

Logemann, J., Shell, J., and Willmitzer, L. (1987). Improved method for the isolation of RNA from plant tissue. *Anal. Biochem.* 163, 16–20. doi: 10.1016/0003-2697(87)90086-8

Long, S. P., Zhu, X. G., Naidu, S. L., and Ort, D. R. (2006). Can improvement in photosynthesis increase crop yields? *Plant Cell Physiol.* 29, 315–330. doi: 10.1111/j.1365-3040.2005.01493.x

Mayta, M. L., Lodeyro, A. F., Guiamet, J. J., Tognetti, V. B., Melzer, M., Hajirezaei, M. R., et al. (2018). Expression of a plastid-targeted flavodoxin decreases chloroplast reactive oxygen species accumulation and delays senescence in aging tobacco leaves. *Front. Plant Sci.* 9:1039. doi: 10.3389/fpls.2018.01039

Miyake, C. (2010). Alternative electron flows (water-water cycle and cyclic electron flow around PSI) in photosynthesis: molecular mechanisms and physiological functions. *Plant Cell Physiol.* 51, 1951–1963. doi: 10.1093/pcp/pcq173

Murashige, T., and Skoog, F. (1962). A revised medium for rapid growth and bio assays with tobacco tissue cultures. *Physiol. Plant.* 15, 473–497.

Regierer, B., Fernie, A. R., Springer, F., Pérez-Melis, A., Leisse, A., and Koehl, K. (2002). Starch content and yield increase as a result of altering adenylate pools in transgenic plants. *Nat. Biotechnol.* 20, 1256–1260. doi: 10.1038/nbt760

Sainsbury, F., and Lomonossoff, G. P. (2008). Extremely high-level and rapid transient protein production in plants without the use of viral replication. *Plant Physiol.* 148, 1212–1218. doi: 10.1104/pp.108.126284

Santana-Sánchez, A., Solymosi, D., Mustila, H., Bersanini, L., Aro, E. M., and Allahverdiyeva, Y. (2019). Flv1-4 proteins function in versatile combinations in O_2 photoreduction in cyanobacteria. *eLife* 8:e45766.

Schmittgen, T., and Livak, K. (2008). Analyzing real-time PCR data by the comparative CT method. *Nat. Protoc.* 3, 1101–1108. doi: 10.1038/nprot.2008.73

Sharkey, T. D., Laporte, M. M., Lu, Y., Weise, S. E., and Weber, A. P. M. (2004). Engineering plants for elevated CO_2: a relationship between sugar sensing and starch degradation. *Plant Biol.* 6, 280–288. doi: 10.1055/s-2004-817911

Shikanai, T., and Yamamoto, H. (2017). Contribution of cyclic and pseudo-cyclic electron transport to the formation of proton motive force in chloroplasts. *Mol. Plant* 10, 20–29. doi: 10.1016/j.molp.2016.08.004

Shimakawa, G., Ishizaki, K., Tsukamoto, S., Tanaka, M., Sejima, T., and Miyake, C. (2017). The liverwort, *Marchantia*, drives alternative electron flow using a flavodiiron protein to protect PSI. *Plant Physiol.* 173, 1636–1647. doi: 10.1104/pp.16.01038

Shimakawa, G., Shaku, K., Nishi, A., Hayashi, R., Yamamoto, H., Sakamoto, K., et al. (2015). FLAVODIIRON2 and FLAVODIIRON4 proteins mediate an oxygen-dependent alternative electron flow in *Synechocystis* sp. PCC 6803 under CO_2-limited conditions. *Plant Physiol.* 167, 472–480. doi: 10.1104/pp.114.249987

Stitt, M., Lunn, J., and Usadel, B. (2010). *Arabidopsis* and primary photosynthetic metabolism–more than the icing on the cake. *Plant J.* 61, 1067–1091. doi: 10.1111/j.1365-313X.2010.04142.x

Sulpice, R., Pyl, E. T., Ishihara, H., Trenkamp, S., Steinfath, M., Witucka-Wall, H., et al. (2009). Starch as a major integrator in the regulation of plant growth. *Proc. Natl. Acad. Sci. U.S.A.* 106, 10348–10353. doi: 10.1073/pnas.0903478106

Takagi, D., Takumi, S., Hashiguchi, M., Sejima, T., and Miyake, C. (2016). Superoxide and singlet oxygen produced within the thylakoid membranes both cause photosystem I photoinhibition. *Plant Physiol.* 171, 1626–1634. doi: 10.1104/pp.16.00246

Tula, S., Shahinnia, F., Melzer, M., Rutten, T., Gómez, R., Lodeyro, A. F., et al. (2020). Providing an additional electron sink by the introduction of cyanobacterial flavodiirons enhances the growth of *Arabidopsis thaliana* in varying light. *bioRxiv* [Preprint]. doi: 10.1101/2020.02.05.935346 bioRxiv: 2020.02.05.935346,

Voon, C. P., Guan, X., and Sun, Y. (2018). ATP compartmentation in plastids and cytosol of *Arabidopsis thaliana* revealed by fluorescent protein sensing. *Proc. Natl. Acad. Sci. U.S.A.* 115, 10778–10787. doi: 10.1073/pnas.1711497115

Wada, S., Yamamoto, H., Suzuki, Y., Yamori, W., Shikanai, T., and Makino, A. (2018). Flavodiiron protein substitutes for cyclic electron flow without competing CO_2 assimilation in rice. *Plant Physiol.* 176, 1509–1518. doi: 10.1104/pp.17.01335

Yamamoto, H., Takahashi, S., Badger, M. R., and Shikanai, T. (2016). Artificial remodelling of alternative electron flow by flavodiiron proteins in *Arabidopsis*. *Nat. Plants* 2, 16012. doi: 10.1038/nplants.2016.12

Zhang, P., Eisenhut, M., Brandt, A. M., Carmel, D., Silén, H. M., Vass, I., et al. (2012). Operon *flv4-flv2* provides cyanobacterial photosystem II with flexibility of electron transfer. *Plant Cell* 24, 1952–1971. doi: 10.1105/tpc.111.094417

Zhu, X., Long, S. P., and Ort, D. R. (2010). Improving photosynthetic efficiency for greater yield. *Annu. Rev. Plant Biol.* 61, 235–261. doi: 10.1146/annurev-arplant-042809-112206

Zivcak, M., Brestic, M., Kunderlikova, K., Olsovska, K., and Allakhverdiev, S. I. (2015a). Effect of photosystem I inactivation on chlorophyll *a* fluorescence induction in wheat leaves: does activity of photosystem I play any role in OJIP rise? *J. Photochem. Photobiol. B* 152, 318–324. doi: 10.1016/j.jphotobiol.2015.08.024

Zivcak, M., Brestic, M., Kunderlikova, K., Sytar, O., and Allakhverdiev, S. I. (2015b). Repetitive light pulse-induced photoinhibition of photosystem I severely affects CO_2 assimilation and photoprotection in wheat leaves. *Photosynth. Res.* 126, 449–463. doi: 10.1007/s11120-015-0121-1

Conflict of Interest: The authors declare that the research was conducted in the absence of any commercial or financial relationships that could be construed as a potential conflict of interest.

frontiers in Plant Science

ORIGINAL RESEARCH
published: 07 August 2020
doi: 10.3389/fpls.2020.01216

Concurrent Increases in Leaf Temperature With Light Accelerate Photosynthetic Induction in Tropical Tree Seedlings

Hui-Xing Kang[1], *Xin-Guang Zhu*[2], *Wataru Yamori*[3] *and Yan-Hong Tang*[1]*

[1] Institute of Ecology, College of Urban and Environmental Sciences and Key Laboratory for Earth Surface Processes of Ministry of Education, Peking University, Beijing, China, [2] Center of Excellence for Molecular Plant Sciences and State Key Laboratory of Plant Molecular Genetics, Chinese Academy of Sciences, Shanghai, China, [3] Institute for Sustainable Agro-Ecosystem Services, Graduate School of Agricultural and Life Sciences, The University of Tokyo, Tokyo, Japan

Leaf temperature changes with incident light intensity, but it is unclear how the concurrent changes influence leaf photosynthesis. We examined the time courses of CO_2 gas exchanges and chlorophyll fluorescence of seedling leaves in four tropical tree species in response to lightflecks under three different temperature conditions. The three conditions were two constant temperatures at 30°C (T_{30}) and 40°C (T_{40}), and a simulated gradually changing temperature from 30 to 40°C (T_{dyn}). The time required to reach 50% of the full photosynthetic induction under T_{40} was similar to, or even larger than, that under T_{30}. However, the induction of assimilation rate (A) and electron transport rate of photosystem II (ETR II) and Rubisco activation process were generally accelerated under T_{dyn} compared to those at either T_{30} or T_{40}. The acceleration in photosynthetic induction under T_{dyn} was significantly greater in the shade-tolerant species than in the shade-intolerant species. A modified photosynthetic limitation analysis indicated that the acceleration was likely to be mainly due to ETR II at the early stage of photosynthetic induction. The study suggests that concurrent increases in leaf temperature with light may increase leaf carbon gain under highly fluctuating light in tropical tree seedlings, particularly in shade-tolerant species.

Keywords: dynamic photosynthesis, photosynthetic induction, Rubisco, shade tolerance, sunflecks, temperature

OPEN ACCESS

Edited by:
Jeremy Harbinson, Wageningen University and Research, Netherlands

Reviewed by:
Elias Kaiser, Wageningen University and Research, Netherlands
Tao Li, Institute of Environment and Sustainable Development in Agriculture (CAAS), China

***Correspondence:**
Yan-Hong Tang
tangyh@pku.edu.cn

Specialty section:
This article was submitted to Plant Abiotic Stress, a section of the journal Frontiers in Plant Science

Received: *04 June 2020*
Accepted: *27 July 2020*
Published: *07 August 2020*

Citation:
Kang H-X, Zhu X-G, Yamori W and Tang Y-H (2020) Concurrent Increases in Leaf Temperature With Light Accelerate Photosynthetic Induction in Tropical Tree Seedlings. Front. Plant Sci. 11:1216. doi: 10.3389/fpls.2020.01216

INTRODUCTION

Most of our understanding on plant photosynthesis so far is almost completely based on the measurements made under so-called steady-state or temporally constant environments. However, photosynthesis in nature rarely or even never occurs under constant environments, but under fluctuating light, and changing temperature and other environmental variables. Field observations showed considerable variation in photosynthetically active radiation (PAR) at different temporal scales from seconds to days under tropical forest canopies (Pearcy, 1983; Tang et al., 1999). Efficient utilization of temporally variable light has been considered to be critical for leaf carbon gain (Pearcy, 1990; Kaiser et al., 2015; Tomimatsu and Tang, 2016; Yamori, 2016).

Temporal changes in PAR under forest canopies are often accompanied with changes in leaf temperature (T_{leaf}; Singsaas and Sharkey, 1998; Wise et al., 2004). Changes in T_{leaf} can be closely associated with changes of PAR. For example, leaf temperature increased from 32 to 39°C within several min due to sunflecks (Leakey et al., 2003). Despite of a limited number of observations indicating a close relationship between changes in T_{leaf} and changes in light intensity, there is no detailed quantitative description, within our knowledge, for T_{leaf} changes in response to a step change in light intensity. Nonetheless, such associated changes in temperature with light are expected to influence photosynthesis in nature because leaf photosynthesis is a highly temperature-dependent process (Berry and Björkman, 1980). Recent studies further suggest that photosynthetic induction in response to an increase in PAR varied at different constant temperatures (Leakey et al., 2003; Kaiser et al., 2017; Wachendorf and Küppers, 2017). Moreover, thermal responses of photosynthesis are highly species specific (Slot et al., 2016; Slot and Winter, 2017a; Slot and Winter, 2017b; Fauset et al., 2018). However, very little knowledge has been accumulated regarding concurrent changes in leaf temperature with light on dynamic photosynthesis, despite the fact that the changes may be potentially important for leaf carbon gain under fluctuating light and temperature conditions in nature.

In this study, we characterized induction kinetics in four lowland tropical tree species under two constant temperatures and a simulated dynamic temperature condition, aiming to address (1) how the concurrent changes in leaf temperature with light affect the photosynthetic induction process, (2) if and how major physiological and biochemical processes contribute to the effect(s), and (3) whether there are any differences in the effect(s) between shade-tolerant and shade-intolerant tree species in tropical rain forests.

MATERIALS AND METHODS

Study Site and Plant Species

The study was conducted in a lowland tropical rain forest in Pasoh Forest Reserve (2°59′N, 102°08′E), Malaysia. This is a primary Dipterocarp forest with an averaged leaf area index estimated as 6.52 in the core area of the reserve (Tani et al., 2003b). The annual rainfall of the normal years, i.e., no El Niño years, observed by the meteorological station within the reserve averaged 1809 mm during the period from 1983 to 1990. Most rainfall was observed during the rainy season from March to May and from October to December. Mean annual temperature at 52 m above the forest floor was 25.6°C, ranging from 22.6 to 29.9°C (Tani et al., 2003a).

The study species were two shade-intolerant species, *Croton argyratus* Blume and *Shorea leprosula* Miq., and two shade-tolerant species, *Neobalanocarpus heimii* (King) Ashton and *Lepisanthes senegalensis* (Poir.) Leenh, which are all native to lowland forests (Thomas et al., 2003). Five to six seedlings from different light regimes were selected for each species. Light regime was characterized as averaged daily light integral (DLI) of 60 days prior to the experiment (unit mol m^{-2} d^{-1}), which was estimated from hemispherical photographs using SOLARCALC 7.0 (Mailly et al., 2013). All field measurements were conducted between August and October 2018.

Leaf Gas Exchange and Chlorophyll Fluorescence

Photosynthetic induction responses were measured using a LI-6800 (LI-COR, Lincoln NE, USA) fitted with a LI-6800-01 fluorometer (90% red and 10% blue) on a fully expanded and healthy leaf in each selected seedling. Leaves were first acclimated to the irradiance at 50 μmol m^{-2} s^{-1} for at least 20 min until steady-state assimilation rate (A) and stomatal conductance for H_2O (g_{sw}) were visibly reached, after which light was raised to 1000 μmol m^{-2} s^{-1} for 32 min. A, g_{sw}, and intercellular CO_2 concentration (C_i) were logged every second. To avoid any artefacts from correctional changes in temperature or relative humidity, temperature of the heat exchanger (T_{exchg}) was controlled. Photosynthetic induction was measured under three different temperature conditions, i.e., two constant temperature conditions with 30°C (T_{30}) and 40°C (T_{40}), and a simulated dynamic temperature condition (T_{dyn}). For the two constant temperatures, T_{leaf} reached a constant value around 30.7°C under T_{30} and 36.6°C under T_{40} prior to the increase in light. Under the T_{dyn} condition, T_{exchg} was kept at 30°C before the increase in light and then set to an expected value of 40°C at the same time when light increased. The warming speed of leaf temperature was similar to our observation within the same forest (**Figure S1**). Prior to the induction, leaf-to-air vapor-pressure deficit (VPD) was kept steady around 1 kPa under T_{dyn} and T_{30} and 2.3 kPa under T_{40} to mimic the natural levels at each temperature, according to our records of within-canopy microenvironments (see **Figure S2**). Reference CO_2 concentration was maintained at 400 μmol mol^{-1}. Photosynthetic CO_2 response curves were generated with a LI-6400XT equipped with a LI-6400-02B LED light source on the same leaves at a block temperature of 30 and 40°C. Leaves were first fully induced under 400 μmol mol^{-1} and 1000 μmol m^{-2} s^{-1}. Then, the reference CO_2 concentration was reduced to 50 μmol mol^{-1} in a stepwise manner, after which it returned to the starting level. When steady-state A was again reached, the CO_2 concentration was increased to 1500 μmol mol^{-1} in several steps. Flow rate was maintained at 350 μmol s^{-1}, and relative humidity was controlled at 70%, which yield a VPD similar to that reached at the end of induction.

All measurements were repeated with the same environmental settings as the measurement of photosynthetic induction course to produce the time courses of chlorophyll fluorescence signals using the same LI-6800. Hence, we obtained two sets of induction curves, one with gas exchange only and the other with both gas exchange and chlorophyll fluorescence. Leaf samples were placed in dark for at least 2 h. Then, light was increased to 50 μmol m^{-2} s^{-1} until gas exchange parameters reached steady state, which typically took 20 min, followed by 30 min of induction. However, due to weather and insufficient time, some chlorophyll fluorescence measurements under T_{dyn} started from a light intensity of 50 μmol m^{-2} s^{-1} directly without dark adaptation. For these measurements, less time (~10 min) was required to reach steady state under low light. Gas

exchange parameters were recorded every 5 s, and chlorophyll fluorescence was recorded every minute. Recorded chlorophyll fluorescence signals include F_o and F_M, if leaves were dark adapted, F_s, F_M', and F_o' by turning off the actinic light and then applying far-red light. We used the multi-phase flash (MPF) protocol of the fluorometer for measuring F_M and F_M'. MPF settings were as factory default, including 8000 μmol m^{-2} s^{-1} for flash beam intensity, 40% ramp reduction during the 2nd phase of the MPF, and 0.3 s duration of each flash phase. The quantum yields of photosystem II [Y(II)] were calculated after Yamori et al. (2012). The electron transport rates of photosystem II (ETR II) were calculated using the following equation: ETR II = 0.5 × α × I × Y (II), where 0.5 is the fraction of absorbed light allocated to photosystems II, α is leaf light absorptance (see below), and I is light intensity. The quantum yields of photochemical quenching based on the puddle (qP) and the lake model (qL) and non-photochemical quenching (NPQ) were calculated as described by Kalaji et al. (2017). Data obtained without dark adaptation were excluded from NPQ calculation.

Light Absorptance

Leaf light absorptance was calculated from measured reflectance and transmittance. For each species, four to six branches from seedlings other than those for photosynthesis measurements were sampled around 18:00 h, with the cut end submerged in water immediately. Samples were kept in dark and then measured within 6 h using a Maya-2000-Pro spectrometer (Ocean Optics, Dunedin, FL, USA). Four to six healthy, fully expanded leaves in each sampled branch and three to four discs per leaf were measured. Light absorptance was calculated with respect to the irradiance spectrum of the LI-6800-01 fluorometer, which was also measured with the same spectrometer. This yield leaf light absorptance of 0.88, 0.87, 0.90, and 0.92 for *N. heimii*, *L. senegalensis*, *C. argyratus*, and *S. leprosula*, respectively.

Data Analysis

For those measurements made under T_{dyn}, the time course of H_2O concentration in the sample cell (H_2O_s) exhibited an unusually steep peak within the first minute, since the LI-6800 started to elevate T_{exchg}. As a result, stomatal conductance doubled and C_i increased during the first minute since LED light and T_{exchg} concurrently changed. After excluding the possibility of a contaminated leaf chamber by repeating the same measurement settings with a brand new LI-6800 later, we suspected that such errors were induced by the heat exchanger itself. We matched the LI-6800 only immediately before each measurement, and the differences in match adjustment factor between two consecutive measurements were small compared to the differences in water concentrations result from foliar transpiration. Thus, we proposed an empirical method to sequentially correct H_2O_s, transpiration rate, A, g_{sw}, and C_i (for detailed information, see **Supplementary File S1**).

To determine the maximum rate of increase in A ($\frac{dA}{dt}_{\max}$), the time courses of A during induction (gas exchange only) were fitted to the Boltzmann sigmoidal model proposed by Drake et al. (2013):

$$A(t) = \frac{a_1 - a_2}{1 + e^{(t-t_0)}/\Delta t_A} + a_2 \quad (1)$$

where a_1 and a_2 are the left and right horizontal asymptotes, respectively, t_0 is the point of inflection, and Δt_A describes the steepness of the curve. The maximum rate of increase is the value of the derivative of Equation (1), where $t = t_0$. The maximum rate of increase in g_{sw} ($\frac{dg}{dt}_{\max}$) was calculated in the same way.

To assess if sunfleck utilization was improved or inhibited under T_{dyn} and T_{40}, induction carbon gain (ICG) at time t was calculated after Chazdon and Pearcy (1986a):

$$\mathrm{ICG}(t) = \int_0^t A(t)dt - t * A_{\mathrm{ini}} \quad (2)$$

where A_{ini} is the steady-state A prior to the induction.

To identify the transition point between Rubisco and RuBP regeneration limitation ($C_{i,trans}$) at high temperature, photosynthetic CO_2 response curves were fitted after Bellasio et al. (2016), assuming a constant $R_L : R_d$ ratio of 60% (Way et al., 2019). R_d was calculated by averaging the readings over the last minute in the dark period during chlorophyll fluorescence measurements. $C_{i,trans}$ was determined as:

$$C_{i,\mathrm{trans}} = \frac{8\Gamma^* V_{c,\max} - K_m J_{1000}}{J_{1000} - 4V_{c,\max}} \quad (3)$$

where $V_{c,max}$ is the apparent maximum carboxylation rate of Rubisco, J_{1000} is the potential electron transport rate under 1000 μmol m^{-2} s^{-1}, $\Gamma^\star$ is the CO_2 photocompensation point, and K_m is the effective Michaelis-Menten constant for Rubisco after Bernacchi et al. (2001).

To obtain the apparent time constant of Rubisco activation ($\tau_{Rubisco}$), transient A, recorded during chlorophyll fluorescence measurements, was corrected to steady-state C_i reached at the end of induction ($C_{i,f}$) with respect to transient T_{leaf} after Urban et al. (2007) and then fitted to the exponential function proposed by Woodrow and Mott (1989):

$$A^*(t) = A_f^* - (A_f^* - A_i) * \exp(-t/\tau_{\mathrm{Rubisco}}) \quad (4)$$

where A_f^* is the final corrected A and A_i is the estimated initial A prior to the induction. For modeling convenience, we assumed that Rubisco is a one-phase process and used the data from whole induction curves for fitting. In the prior test, we found that fitting the whole curves yield higher R^2 and smaller confidence intervals than only fitting the data from minute 2 to 10 after the light increase in 25 among 30 cases. We also acknowledge that using the data from whole curve could underestimate $\tau_{Rubisco}$. Using transient C_i recorded during chlorophyll fluorescence measurements, we calculated the potential A supported by transient ETR II (A_j) and that supported by transient carboxylation rate with respect to transient T_{leaf} (A_c):

$$A_j(t) = \mathrm{ETR}(t)\frac{C_i(t) - \Gamma^*(T)}{4C_i(t) + 8\Gamma^*(T)} - R_L(T) \quad (5)$$

$$A_c(t) = V_c(t)\frac{C_i(t) - \Gamma^*(T)}{C_i(t) + K_m(T)} - R_L(T) \quad (6)$$

The temperature response of R_d was described for each leaf studied using an exponential model with Q_{10} (Vanderwel et al., 2015). The temperature dependency of Γ* for each leaf was described by the Arrhenius function using the CO_2 response curves:

$$\Gamma^*(T) = \Gamma^*(25) * \exp\left[\frac{E_a * 10^3 (T - 298.15)}{298.15 * R * T}\right] \quad (7)$$

where Γ*(25) is Γ* at 25°C and E_a is the activation energy term. R is the molar gas constant. For simplicity, we assume that R_L, K_m, and Γ*, which respond to fluctuations in temperature instantaneously, and components of ETR II, i.e., fraction of absorbed light allocated to photosystems II and leaf light absorptance, remain constant during induction. Considerations of these assumptions are described in detail in Discussion. Transient carboxylation rate (V_c) was estimated in analogy to Eqn. (1):

$$V_c(t) = V_{c,f} - (V_{c,f} - V_{c,ini}) * \exp(-t/\tau_{Rubisco}) \quad (8)$$

$V_{c,f}$ and $V_{c,ini}$ were estimated from the so-called one-point method (De Kauwe et al., 2016) using data recorded before and at the end of induction, respectively. Assimilation rate decreased during induction in some measurements made under T_{dyn}.

ETR II obtained under photorespiratory condition was likely to deviate from true linear electron transport rate, leading to incorrect A_j. Considerations on how to model the midway decrease in A during induction and necessary calibration of ETR II are described in detail in **Supplementary File S2**. We compared $A_c(t)$ against $A_j(t)$ to determine whether photosynthetic rate was limited by Rubisco carboxylation or RuBP regeneration at time t.

Statistical Analysis

To determine the effects of measurement temperature condition, data were compared by one-way ANOVA test. Data were log-transformed to meet the assumptions of normality and homogeneity of variances when necessary. Otherwise, a non-parametric Kruskal-Wallis test was used. All tests were conducted using SPSS Statistics Version 20.0 (IBM Corp., New York, USA). To examine whether the variances in the induction responses between T_{30} and T_{dyn} were related to species-specific shade tolerance (S) and DLI, we performed a two-way ANOVA analysis using S and DLI as the main factors and $S \times$ DLI as the interaction factor. The differences in induction responses were represented as the percentage change of a parameter. These tests were carried out in R version 3.5.0 (R Core Team, 2018).

RESULTS

Photosynthetic Induction Response

Time courses of photosynthetic induction under three different temperature conditions are shown in **Figure 1**. After full acclimation under T_{40}, both initial photosynthetic rate (A_{ini})

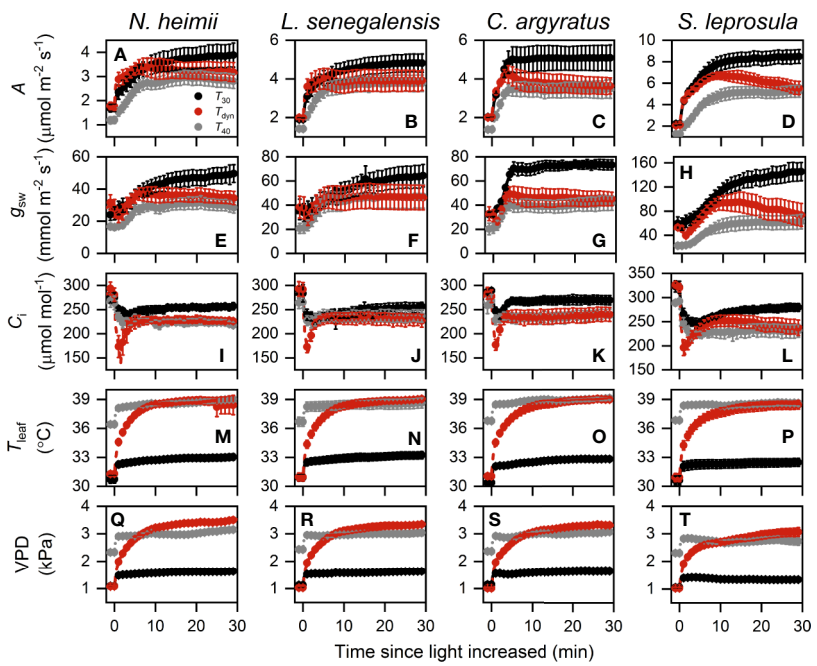

FIGURE 1 | Time courses of A **(A–D)**, g_{sw} **(E–H)**, C_i **(I–L)**, T_{leaf} **(M–P)**, and VPD **(Q–T)** during photosynthetic induction in *N. heimii* **(A, E, I, M, Q)**, *L. senegalensis* **(B, F, J, N, R)**, *C. argyratus* **(C, G, K, O, S)**, and *S. leprosula* **(D, H, L, P, T)**. Shown are the data recorded during gas exchange only measurements under constant 30°C (T_{30}) and 40°C (T_{40}) and simulated dynamic temperature condition (T_{dyn}). Values are the means (± SE) of five to six individual seedlings for each species. A, assimilation rate; g_{sw}, stomatal conductance for H_2O; C_i, intercellular CO_2 concentration; T_{leaf}, leaf temperature; VPD, leaf-to-air vapor pressure deficit.

and final steady-state photosynthetic rate (A_f) were significantly smaller than those under T_{30} (**Table 1**). The maximum rate of increase in $A(\frac{dA}{dt}_{max})$ under T_{40} decreased by 31–64% compared to that under T_{30}.

Photosynthetic rate increased faster under T_{dyn} than either T_{30} or T_{40} and showed an overshoot within 10 min after light intensity increased. A_f under T_{dyn} was similar to that under T_{40}. The time required to reach 50% of full photosynthetic induction ($IT_{f50\%}$) under T_{dyn} was 69–86% lower and 73–89% lower than that under T_{30} and T_{40}, respectively (**Table 1**). The difference in $\frac{dA}{dt}_{max}$ between T_{30} and T_{dyn} was significant in the shade-tolerant species.

Stomatal conductance before and at the end of induction decreased in all species under T_{40} compared to those under T_{30} (**Table 1**). The maximum rate of increase in g_{sw} was larger under T_{30} than T_{dyn}, except for *N. heimii*. A larger depletion in C_i during induction was observed under T_{dyn} than T_{30} and T_{40} in all species (**Figure 1**).

Photosynthetic Sub-Processes Under Different Temperature Conditions

The time required for ETR II to reach 50% of full induction ($ETR_{50\%}$) was 17–44% lower under T_{dyn} than T_{30} (**Table 2**). ETR II reached a maximum within 10 min and decreased afterward under T_{dyn} (**Figure 2**). The dynamics of qP and qL were similar among the three temperature conditions. In comparison with T_{30}, NPQ increased faster under T_{40} in all species and under T_{dyn} in *N. heimii* and *C. argyratus*.

Steady-state V_c reached at the end of induction was higher under T_{dyn} and T_{40} than that under T_{30} (**Table 2**). The time constants of Rubisco activation were larger under T_{40} in all species, except for a small decrease in *N. heimii*. In comparison with T_{30}, $\tau_{Rubisco}$ decreased under T_{dyn} in all species, except for a small increase in *C. argyratus*.

Primary Limiting Factor During Photosynthetic Induction

As shown in **Figure 3**, estimated A_c matched the time course of measured *A*. We noted that *A* was limited by A_j only for the first several min (**Figure S3**), after which *A* was limited by A_c instead. The averaged time length of A_j limitation ranged from 1.4 to 2.7 min under T_{30}, while the rest of photosynthetic induction was occupied by A_c limitation. Limitation from A_c almost dominated the entire induction process under T_{40} (**Figure S3**). This was consistent with CO_2 response curves obtained at T_{40}, as the transition point between Rubisco and RuBP regeneration

TABLE 1 | Parameters of photosynthetic induction since the increase in irradiance from 50 to 1000 μmol m^{-2} s^{-1} in four tropical woody species under constant 30°C (T_{30}), 40°C (T_{40}), and simulated dynamic temperature condition (T_{dyn}). A_{ini}, A_f, $g_{sw,ini}$, $g_{sw,f}$, $C_{i,ini}$, and $C_{i,f}$ were *A*, g_{sw}, and C_i reached before and at the end of photosynthetic induction, respectively, calculated by averaging single values over the last minute of each period; $IT_{f50\%}$, the time required to reach 50% of the difference between A_{ini} and A_f; $\frac{dA}{dt}_{max}$ and $\frac{dg}{dt}_{max}$ were the maximum increasing rate of *A* and g_{sw}, respectively.

Species	Temperature	A_{ini}	A_f	$g_{sw,ini}$	$g_{sw,f}$	$C_{i,ini}$	$C_{i,f}$	$IT_{f50\%}$	$\frac{dA}{dt}_{max}$	$\frac{dg}{dt}_{max}$
Abbreviation	Condition	(μmol m^{-2} s^{-1})		(mmol m^{-2} s^{-1})		(μmol mol^{-1})		(s)	(μmol m^{-2} s^{-2})	(mmol m^{-2} s^{-2})
C. argyratus	T_{30}	1.99 ± 0.03a	5.09 ± 0.60a	32.0 ± 1.9a	73.1 ± 4.0a	288 ± 4	267 ± 9	80.0 ± 13.9a	0.035 ± 0.002a	0.560 ± 0.259a
	T_{dyn}	2.18 ± 0.08a	3.63 ± 0.38b	28.7 ± 3.7ab	45.5 ± 4.9b	271 ± 13	241 ± 13	24.9 ± 14.4b	0.046 ± 0.005a	0.281 ± 0.026ab
	T_{40}	1.40 ± 0.12b	3.50 ± 0.44b	21.0 ± 4.1b	42.7 ± 5.5b	268 ± 12	241 ± 11	91.9 ± 17.6a	0.017 ± 0.005b	0.195 ± 0.034b
S. leprosula	T_{30}	2.20 ± 0.07a	8.51 ± 0.57a	58.6 ± 8.9a	146.0 ± 14.0a	323 ± 10a	279 ± 8a	130.5 ± 22.3a	0.065 ± 0.004a	0.270 ± 0.036
	T_{dyn}	2.16 ± 0.17a	5.45 ± 0.56b	55.4 ± 8.6a	72.2 ± 16.8b	323 ± 12a	237 ± 14b	29.7 ± 5.3b	0.074 ± 0.008a	0.189 ± 0.037
	T_{40}	1.27 ± 0.20b	5.35 ± 0.53b	23.2 ± 4.5b	65.1 ± 11.3b	288 ± 6b	234 ± 13b	233.1 ± 15.7c	0.023 ± 0.004b	0.275 ± 0.135
N. heimii	T_{30}	1.70 ± 0.14a	3.90 ± 0.45a	23.7 ± 3.0	49.9 ± 5.0a	274 ± 10	257 ± 5a	203.3 ± 65.2ab†	0.032 ± 0.007a	0.158 ± 0.053
	T_{dyn}	1.96 ± 0.10a	2.91 ± 0.30ab	23.5 ± 4.6	31.0 ± 2.7b	257 ± 18	226 ± 7b	33.8 ± 27.2a†	0.060 ± 0.007b	0.516 ± 0.401
	T_{40}	1.18 ± 0.13b	2.74 ± 0.27b	16.7 ± 2.0	28.0 ± 3.0b	264 ± 16	219 ± 5b	174.1 ± 20.3b†	0.022 ± 0.009a	0.078 ± 0.024
L. senegalensis	T_{30}	1.90 ± 0.06a	4.83 ± 0.43	34.7 ± 7.9	63.9 ± 8.8	284 ± 17	255 ± 9	106.3 ± 20.3a†	0.046 ± 0.005a	0.120 ± 0.029
	T_{dyn}	2.07 ± 0.08a	3.91 ± 0.48	38.2 ± 9.3	45.8 ± 9.1	290 ± 16	227 ± 11	15.0 ± 2.7b†	0.069 ± 0.008b	0.096 ± 0.021
	T_{40}	1.42 ± 0.10b	3.78 ± 0.40	20.5 ± 3.7	46.6 ± 8.9	264 ± 10	235 ± 11	137.7 ± 3.0a†	0.022 ± 0.004c	0.114 ± 0.017

Shown are data recorded during gas exchange only measurements. Values are the means of five to six individual seedlings for each species (± standard error). Different letters following means indicate significant difference across different temperature conditions within each species, according to a LSD test conducted at P = 0.05 level. Absence of letters denotes absence of significant difference.

†*Statistical analysis using one-way ANOVA and Dunnett's T3 test.*

TABLE 2 | Parameters of the time courses of ETR II and V_c during photosynthetic induction since the increase in irradiance from 50 to 1000 μmol m^{-2} s^{-1} in four tropical woody species under constant 30°C (T_{30}), 40°C (T_{40}), and dynamic temperature condition (T_{dyn}).

Species abbreviation	Temperature condition	ETR_f (μmol m^{-2} s^{-1})	ETR_m (μmol m^{-2} s^{-1})	$V_{c,f}$ (μmol m^{-2} s^{-1})	$ETR_{50\%}$(s)	$\tau_{Rubisco}$(s)
C. argyratus	T_{30}	38.5 ± 3.1	39.8 ± 3.3	34.3 ± 3.0a	78.2 ± 9.4	73.2 ± 7.2
	T_{dyn}	36.9 ± 3.6	40.7 ± 3.8	45.0 ± 3.3b	64.7 ± 2.4	87.8 ± 9.7
	T_{40}	32.1 ± 2.3	36.6 ± 2.7	43.5 ± 2.1b	75.5 ± 10.5	114.4 ± 21.1
S. leprosula	T_{30}	72.4 ± 7.1	72.7 ± 7.1	51.8 ± 4.4	92.6 ± 16.9 †	139.6 ± 20.6ab
	T_{dyn}	61.9 ± 8.4	69.7 ± 7.9	57.2 ± 9.0	72.9 ± 5.2 †	117.9 ± 13.5a
	T_{40}	53.1 ± 8.9	54.5 ± 8.7	57.2 ± 9.3	78.8 ± 32.4 †	253.1 ± 68.2b
N. heimii	T_{30}	46.6 ± 6.5	47.4 ± 6.4	37.2 ± 4.5	107.5 ± 17.9a	248.9 ± 48.9
	T_{dyn}	39.4 ± 3.9	43.5 ± 4.0	44.2 ± 5.5	60.1 ± 4.1b	170.6 ± 10.3
	T_{40}	34.2 ± 4.4	35.9 ± 4.5	37.6 ± 4.8	43.3 ± 9.0b	232.1 ± 30.4
L. senegalensis	T_{30}	48.6 ± 6.9	49.6 ± 7.0	45.8 ± 5.2	120.9 ± 11.0a	150.2 ± 25.7ab †
	T_{dyn}	48.4 ± 7.5	49.0 ± 7.5	63.7 ± 8.4	80.6 ± 2.0b	111.6 ± 3.2a †
	T_{40}	47.0 ± 4.3	47.7 ± 4.5	61.3 ± 4.5	123.7 ± 8.9a	214.0 ± 18.3b †

ETR_f and $V_{c,f}$, ETR II and V_c reached at the end of photosynthetic induction, respectively; ETR_m, maximum ETR II reached during photosynthetic induction; $ETR_{50\%}$, the time required for ETR II to reach 50% of full induction; $\tau_{Rubisco}$, the apparent time constant of Rubisco activation. Estimation was based on data recorded during chlorophyll flouresence measurements. Values are means of four to six individual seedlings for each species (± standard error). Different letters following means indicate significant difference across different temperature conditions within each species, according to a LSD test conducted at P = 0.05 level. Absence of letters denotes absence of significant difference.
†Statistical analysis using one-way ANOVA and Dunnett's T3 test.

limitation was much higher than transient C_i during induction in all species (**Figure 4**).

Carbon Gain

ICG within the first 5 min under T_{40} was 45–83% of that under T_{30} (**Figure 5**). However, ICG within the first minute increased by 38–153% under T_{dyn} compared to that under T_{30}. The differences in ICG between T_{dyn} and T_{30} decreased as the integration interval increased. ICG over 30 min (ICG_{30min}) was 20–38% lower under T_{dyn} than that under T_{30}. The shade-tolerant species showed larger increments in ICG under T_{dyn} and smaller decreases under both T_{dyn} and T_{40} than the shade-intolerant species.

The Effects of Species-Specific Shade Tolerance and Growth Light Environment

In comparison with T_{30}, increments in $\frac{dA}{dt}_{max}$ and ICG_{1min} under T_{dyn} were significantly related to species-specific shade tolerance (**Table 3**). The decrease in $IT_{f50\%}$ was related to individual averaged DLI, as seedlings with low DLI showed greater reduction in ETR_f than those with high DLI (**Figure S4**).

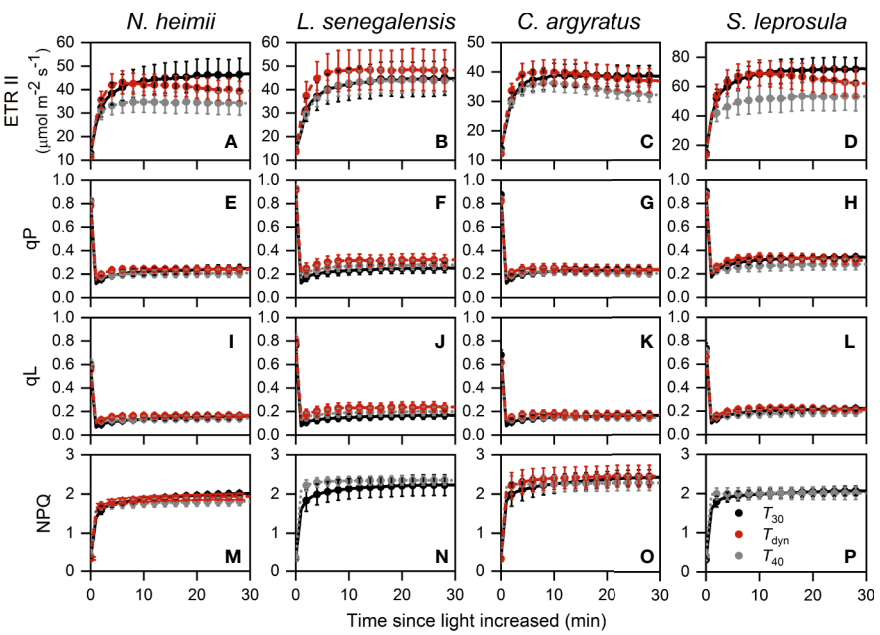

FIGURE 2 | Time courses of ETR II **(A–D)**, qP **(E–H)**, qL **(I–L)**, and NPQ **(M–P)** during photosynthetic induction in *N. heimii* **(A, E, I, M)**, *L. senegalensis* **(B, F, J, N)**, *C. argyratus* **(C, G, K, O)**, and *S. leprosula* **(D, H, L, P)**. Values are the means (± SE) of three to six individual seedlings for each species under constant 30°C (T_{30}) and 40°C (T_{40}) and dynamic temperature condition (T_{dyn}). NPQ in *L. senegalensis* and *S. leprosula* was not shown due to insufficient replicates (n < 3, see *Materials and Methods*). ETR II, electron transport rate of photosystem II; qP and qL are photochemical quenching based on the puddle and the lake model, respectively; NPQ, non-photochemical quenching.

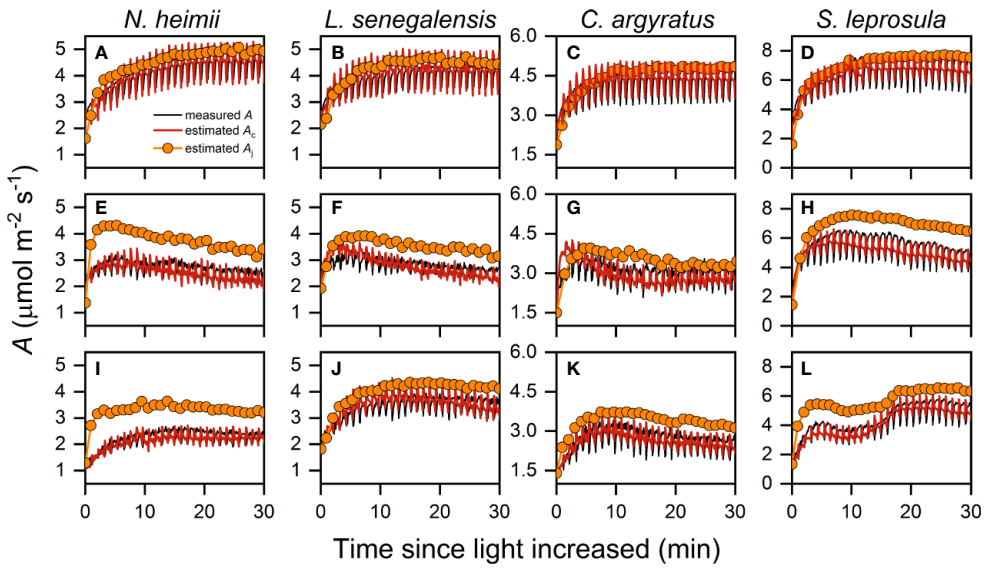

FIGURE 3 | Representative time courses of measured A (open symbols), estimated A_c (red solid line), and estimated A_j (orange symbols with solid line) during photosynthetic induction in *N. heimii* **(A, E, I)**, *L. senegalensis* **(B, F, J)**, *C. argyratus* **(C, G, K)**, and *S. leprosula* **(D, H, L)** under constant 30°C [T_{30} **(A–D)**] simulated dynamic temperature [T_{dyn} **(E–H)**] and constant 40°C condition [T_{40} **(I–L)**], respectively. Measured A were those simultaneously recorded during chlorophyll fluorescence measurements. Estimated A_c and A_j were the potential A supported by V_c and ETR II, respectively. Periodic oscillations of A were inevitable due to the periodic dark pulses necessary for determining fluorescence yield.

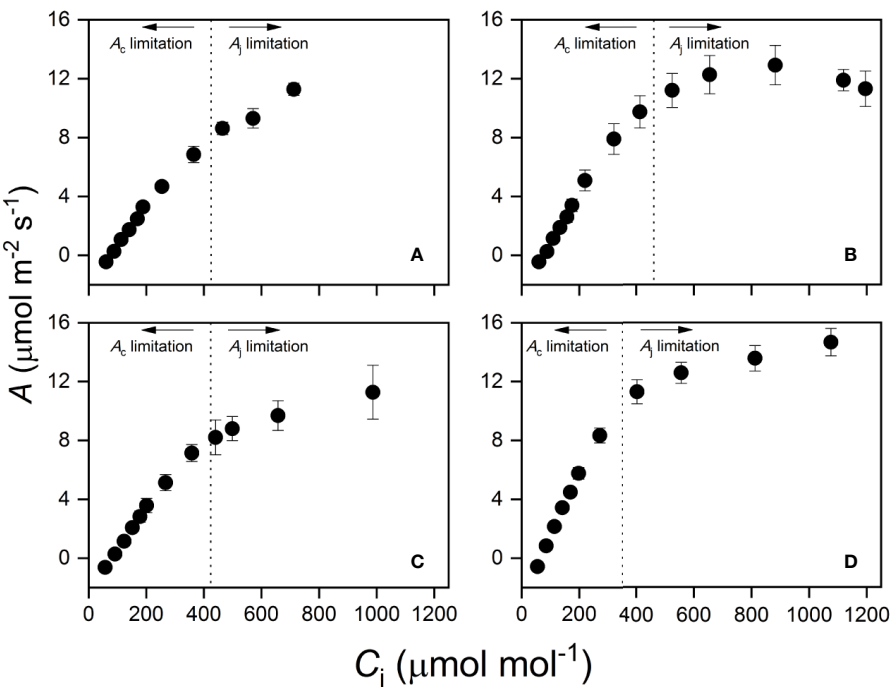

FIGURE 4 | Photosynthetic CO_2 response curve at high temperature (T_{40}) in *N. heimii* **(A)**, *L. senegalensis* **(B)**, *C. argyratus* **(C)**, and *S. leprosula* **(D)**. Assimilation rate (A) was recorded under 1000 μmol m^{-2} s^{-1} at an average leaf temperature of 36.7°C.The x-intercept of vertical dotted lines represents the averaged transition CO_2 concentration in each species, above which the primary limitation imposed on photosynthesis switched from A_c to A_j. Values are the means (± SE) of five to six individual seedlings for each species. A, assimilation rate; C_i, intercellular CO_2 concentration.

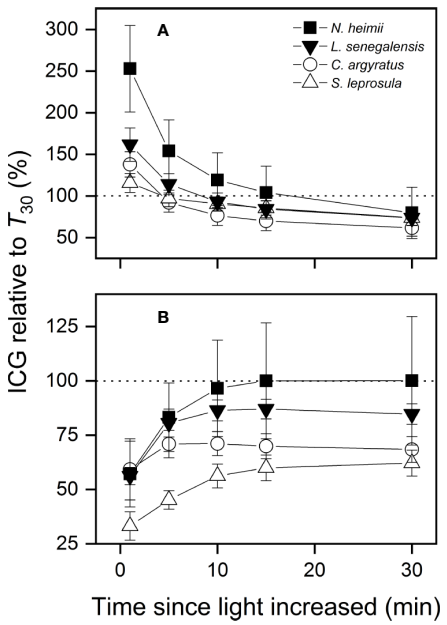

FIGURE 5 | ICG under simulated dynamic temperature condition [T_{dyn} **(A)**] and under constant 40°C [T_{40} **(B)**] relative to that under constant 30°C (T_{30}) as a function of the time since light increased in tree seedlings of four tropical woody species. Shown are data recorded during gas exchange only measurements. The dotted lines indicate equal amount of ICG between two temperature conditions. Open and closed symbols represent data from shade-intolerant and shade-tolerant species, respectively. Values are the means (± SE) of five to six individual seedlings for each species. No significant differences were found across species at $P = 0.05$ level.

TABLE 3 | The influences of species-specific shade tolerance (*S*) and average DLI on the differences in induction responses between T_{30} and T_{dyn}.

	Factors		
	Species-specific shade tolerance (*S*)	**Average daily light integral (DLI)**	***S* × DLI**
$IT_{f50\%}$	1.399	1.600	2.664
$\overline{\frac{dA}{dt}}_{max}$	5.731*	0.073	0.334
$ETR_{50\%}$	4.032	3.698	4.812*
$\tau_{Rubisco}$	0.054	0.012	0.533
ICG_{1min}	5.455*	0.444	0.006
A_f	1.799	0.484	1.311
$g_{sw,f}$	1.217	0.804	1.044
ETR_f	0.141	14.052**	0.329
ICG_{30min}	0.922	0.041	0.241

*The differences in induction responses were represented as the percentage change of a parameter. Shown are F statistics followed by significance symbols, which are *P < 0.05 and **P < 0.01 respectively.*

DISCUSSION

A Gradual Increase in Leaf Temperature Affects Photosynthetic Induction Process

Photosynthesis consists of a number of temperature-dependent biochemical processes (Berry and Björkman, 1980), and the induction process of photosynthesis thus depends on temperature. Recent studies showed that photosynthetic induction can be greatly altered by steady-state environmental temperature (Kaiser et al., 2017; Wachendorf and Küppers, 2017). It is however important to know how changing leaf temperature, accompanied with light changes, would affect photosynthetic induction rate. By comparing gradually increasing leaf temperature with two constant leaf temperatures after an increase in light, it is evident that an elevating leaf temperature from 30 to 40°C accelerates photosynthetic rate at the early-stage induction more than the two extreme constant temperatures of 30 and 40°C (**Figure 1**). This conclusion can be confirmed by the smaller $IT_{f50\%}$ and larger $\overline{\frac{dA}{dt}}_{max}$ (**Table 1**). The increase in simulated ETR at the early stage of the induction response also supports the conclusion (**Figure 2**). It should be also noticed that photosynthetic rate reached the steady-state much faster under the gradual increasing leaf temperature than either constant leaf temperatures, particularly in the shade-tolerant species (**Figure 1**). A full induction state of photosynthetic rate was achieved (within 2–3 min often) even before the leaf temperature reached its steady-state (about 10 min). This fact may indicate that a combined effect of changing leaf temperature, associated with an increase in light, on photosynthetic induction could include some different thermal processes rather than only under constant temperature conditions, which, to our knowledge, is being observed for the first time and deserves further clarification.

Factors Involved in the Induction Process Under Different Temperature Conditions

During the first several min after an increase in light intensity, the increase in photosynthetic rate is often constrained by RuBP regeneration, which is further limited by ETR, light activation of Rubisco, and stomatal opening (Way and Pearcy, 2012; Kaiser et al., 2015; Yamori et al., 2020). All these factors are thermal sensitive, but the time constants of temperature and light stimulations could be considerably different (Leakey et al., 2003; Kaiser et al., 2017; Wachendorf and Küppers, 2017). It is difficult to elucidate individual effects of these factors only based on the gas change and chlorophyll fluorescence observations in this study. We tried to address how these factors contribute to photosynthetic induction under T_{dyn} using photosynthetic limitation analysis.

The acceleration of linear electron transport between photosystem II and I plays an evident role in the acceleration of early-stage induction of photosynthetic rate after increase of light, particularly in the shade-intolerant species (**Table 2**). In this study, the limitation of A_j dominates over the first 4–5 min under T_{30} (**Figure 3** and **Figure S3**), which was longer than those reported for soybean before (Sassenrath-Cole and Pearcy, 1992; Way and Pearcy, 2012). Crop plants grown under controlled environments may have higher RuBP concentration and/or higher activation rate of RuBP regeneration in comparison with plants growing within tropical forests. Decreased $ETR_{50\%}$ under T_{dyn} also indicated that accelerated induction of ETR was related to faster photosynthetic induction at the early stage under T_{dyn}. Constant temperatures strongly affect RuBP regeneration

during photosynthetic induction process (Kaiser et al., 2017). Thus, accelerated induction of ETR II is expected to benefit faster relaxation of limitation through RuBP regeneration process.

An increase in leaf temperature will result in increases in VPD in natural environment. Changes in VPD will affect photosynthetic induction by itself. For example, an increase in VPD reduced g_{sw} and thus increased diffusional limitation (Kaiser et al., 2017). On the other hand, when VPD was held constant, g_{sw} and C_i would increase with increasing T_{leaf} (Urban et al., 2017). In our study, if we assume that g_{sw} and C_i should remain the same as those reached under T_{30}, then A_f under T_{dyn} would increase by 16% on average. If we focus on the early-stage of induction, then effects of changes in VPD can be neglected since stomatal opening and photosynthetic induction didn't change much by VPD at this stage (Tinoco-Ojanguren and Pearcy, 1993; Kaiser et al., 2017). Therefore, concurrent increases in VPD with rising T_{leaf} will not significantly change our current conclusion in this study.

The overshoots during photosynthetic induction under T_{dyn} may be due to inhibition of some physiological processes by high VPD and T_{leaf}. At the early-stage of induction when VPD and T_{leaf} were not so high, Rubisco was activated and stomata gradually opened. As VPD and T_{leaf} rose over a critical point, g_{sw} (**Figures 1E–H**), ETR II (**Figures 2A–D**), and possibly activation state of Rubisco (Yamori et al., 2006; Scafaro et al., 2016; Busch and Sage, 2017) decreased and thus A decreased. Nonetheless, the overshoots need to be clarified in the future.

Photosynthetic Limitation Analysis

As discussed above, we determined the limiting process imposed on photosynthetic induction by comparing A_c and A_j after Farquhar et al. (1980). The classic photosynthetic limitation analysis defines photosynthetic limitation as a reduction in actual transient A compared with that estimated if biochemical or diffusional limitation was removed in one step. On the contrary, a stepwise method, which compares previous and subsequent photosynthesis state, produces smaller error than the one-step method, especially when time intervals between two states are small enough (Deans et al., 2019). The limitation analysis developed in this study is a stepwise method. Dynamic A-C_i analyses use high time-resolution dynamics of V_c and J by constructing induction curves at a wide range of different CO_2 concentrations (Soleh et al., 2016; Taylor and Long, 2017; Salter et al., 2019). This method is time-consuming and risky due to the dependency of Rubisco activation state on CO_2 concentration (Mott and Woodrow, 1993; Woodrow et al., 1996; Tomimatsu et al., 2019). Our method provides a compromise between convenience and accuracy and can be promoted with higher time-resolution fluorescence signals for both PSI and PSII.

Our observations showed that T_{leaf} changed by <0.2°C/s for the first min and <0.05°C/s for the rest of induction (**Figure 1**). Such changes in T_{leaf} should result in small changes in the steady-state R_L and Γ*. Thus, assuming instantaneous response of both parameters imposed little influence (<0.1%) on estimated A_c or A_j. The effect of a time lag in K_m response is also limited. If K_m changes by 50% of difference between two consecutive steady-states, A_c under T_{dyn} changes by less than 5%, in comparison with that assuming instantaneous response of K_m. A decrease in leaf absorptance and/or fraction of absorbed light allocation to PSII is likely to occur when a shaded leaf is exposed to high light for long (Davis et al., 2011; Dutta et al., 2015; Mekala et al., 2015). A survey from 24 species indicates that leaf absorptance of PAR decreased by ~5% after 2 h exposure to high light (Davis et al., 2011), which alone may lead to an overestimation of A_j by ~5% and hence underestimation of A_j limitation. Simulation from Morales et al. (2018) also indicate small influences on A from changes in leaf absorptance. If allocation fraction should be 0.45 from the very beginning of induction, then A_j decreased by ~10%. This would increase the duration of A_j limitation, thus the dominant role of A_j over the early-stage of induction still holds.

Ecological Consequences of Changing Leaf Temperature With PAR

Concurrent change of leaf temperature with PAR may play an important role in leaf carbon uptake and energy balance under temporally variable light environments. Leakey et al. (2003) reported a decrease in ICG in *S. leprosula* seedlings at elevated constant temperature. In this study, we demonstrate that leaf carbon gain is enhanced within the first several min under T_{dyn}, although photosynthetic rate was depressed at the steady-state under 40°C (**Table 1**). Since most sunflecks occurring under dense forest canopies last only a few min (Pearcy, 1983; Chazdon and Pearcy, 1986b), the acceleration of photosynthetic rate accompanied with the increase in leaf temperature at the early stage of the induction suggests that short sunflecks may contribute more leaf carbon gain than previously estimated under constant temperature.

Moreover, it is still debated whether shade-tolerant species can use sunflecks more efficiently than shade-intolerant species (Naumburg and Ellsworth, 2000; Rijkers et al., 2000; Way and Pearcy, 2012). However, the argument is based on the knowledge obtained only under single constant temperature. When taking variation of leaf temperature into account, more leaf carbon gain may be achieved for shade-tolerant species because these species showed higher acceleration of photosynthetic rate than the shade-intolerant species under the changing leaf temperature in this study.

ecent studies suggest that shade-intolerant species from tropical regions have higher photosynthetic temperature optimum, lower T_{leaf}, and a wider temperature range for photosynthesis (Cheesman and Winter, 2013; Slot and Winter, 2017a; Slot and Winter, 2017b) and thus seem more competitive than shade-tolerant species in a warming world. A less strong reduction in ICG found in the shade-tolerant species under T_{dyn} and T_{40} (**Figure 5**), however, provides some contrasting evidence. Detailed assessments on photosynthetic response and energy balance under dynamic environments, particularly under changing light and temperature conditions, are urgently needed to understand the effect of climate change on plants in tropical forests.

CONCLUSION

We provide the first evidence that increase in leaf temperature, associated with increase in light, accelerates photosynthetic rate at the early stage of induction process. We further

demonstrated that the acceleration is likely to be mainly due to accelerated induction of ETR II. These results extend our understanding of dynamic photosynthesis to cover the effects of concurrent changes in leaf temperature and light. However, there are a number of limitations in this preliminary study, and further studies are needed to understand physiological controls of the concurrent changes, particularly in relation to leaf energy budget.

DATA AVAILABILITY STATEMENT

The raw data supporting the conclusions of this article will be made available by the authors, without undue reservation.

AUTHOR CONTRIBUTIONS

H-XK and Y-HT contributed to conception and design of the study. H-XK performed the experiments and the statistical analysis. H-XK wrote the manuscript. X-GZ, WY, and Y-HT provided editorial and scientific advice. All authors contributed to the article and approved the submitted version.

FUNDING

This study was funded by the Key Research of Plant Functional Ecology Program of Peking University (no. 7101302307). This work was supported in part by JSPS KAKENHI (grant numbers JP16H06552, JP18H02185 and JP18KK0170 to W.Y).

ACKNOWLEDGMENTS

We thank Kouki Hikosaka for his constructive comments and stimulating discussion. We thank Azizi Ripin for identifying plant species. Our thanks are also due to Yao Tze-Leong and other staff at the Pasoh Forest Reserve for their generous help.

SUPPLEMENTARY MATERIAL

The Supplementary Material for this article can be found online at: https://www.frontiersin.org/articles/10.3389/fpls.2020.01216/full#supplementary-material

REFERENCES

Bellasio, C., Beerling, D. J., and Griffiths, H. (2016). An Excel tool for deriving key photosynthetic parameters from combined gas exchange and chlorophyll fluorescence: theory and practice. *Plant Cell Environ.* 39 (6), 1180–1197. doi: 10.1111/pce.12560

Bernacchi, C. J., Singsaas, E. L., Pimentel, C., Portis, A. R., and Long, S. P. (2001). Improved temperature response functions for models of Rubisco-limited photosynthesis. *Plant Cell Environ.* 24, 253–259. doi: 10.1111/j.1365-3040.2001.00668.x

Berry, J., and Björkman, O. (1980). Photosynthetic response and adaptation to temperature in higher plants. *Annu. Rev. Plant Biol.* 31, 491–543. doi: 10.1146/annurev.pp.31.060180.002423

Busch, F. A., and Sage, R. F. (2017). The sensitivity of photosynthesis to O_2 and CO_2 concentration identifies strong Rubisco control above the thermal optimum. *New Phytol.* 213 (3), 1036–1051. doi: 10.1111/nph.14258

Chazdon, R. L., and Pearcy, R. W. (1986a). Photosynthetic responses to light variation in rainforest species II. Carbon gain and photosynthetic efficiency during lightflecks. *Oecologia* 69, 524–531. doi: 10.1007/BF00410358

Chazdon, R. L., and Pearcy, R. W. (1986b). Photosynthetic responses to light variation in rainforest species: I. Induction under constant and fluctuating light conditions. *Oecologia* 69, 517–523. doi: 10.1007/BF00410357

Cheesman, A. W., and Winter, K. (2013). Growth response and acclimation of CO_2 exchange characteristics to elevated temperatures in tropical tree seedlings. *J. Exp. Bot.* 64 (12), 3817–3828. doi: 10.1093/jxb/ert211

Davis, P. A., Caylor, S., Whippo, C. W., and Hangarter, R. P. (2011). Changes in leaf optical properties associated with light-dependent chloroplast movements. *Plant Cell Environ.* 34 (12), 2047–2059. doi: 10.1111/j.1365-3040.2011.02402.x

De Kauwe, M. G., Lin, Y. S., Wright, I. J., Medlyn, B. E., Crous, K. Y., Ellsworth, D. S., et al. (2016). A test of the 'one-point method' for estimating maximum carboxylation capacity from field-measured, light-saturated photosynthesis. *New Phytol.* 210 (3), 1130–1144. doi: 10.1111/nph.13815

Deans, R. M., Farquhar, G. D., and Busch, F. A. (2019). Estimating stomatal and biochemical limitations during photosynthetic induction. *Plant Cell Environ.* 42 (12), 3227–3240. doi: 10.1111/pce.13622

Drake, P. L., Froend, R. H., and Franks, P. J. (2013). Smaller, faster stomata: scaling of stomatal size, rate of response, and stomatal conductance. *J. Exp. Bot.* 64 (2), 495–505. doi: 10.1093/jxb/ers347

Dutta, S., Cruz, J. A., Jiao, Y., Chen, J., Kramer, D. M., and Osteryoung, K. W. (2015). Non-invasive, whole-plant imaging of chloroplast movement and chlorophyll fluorescence reveals photosynthetic phenotypes independent of chloroplast photorelocation defects in chloroplast division mutants. *Plant J.* 84 (2), 428–442. doi: 10.1111/tpj.13009

Farquhar, G. D., von Caemmerer, S., and Berry, J. A. (1980). A biochemical model of photosynthetic CO_2 assimilation in leaves of C_3 species. *Planta* 149, 78–90. doi: 10.1007/BF00386231

Fauset, S., Freitas, H. C., Galbraith, D. R., Sullivan, M. J. P., Aidar, M. P. M., Joly, C. A., et al. (2018). Differences in leaf thermoregulation and water use strategies between three co-occurring Atlantic forest tree species. *Plant Cell Environ.* 41 (7), 1618–1631. doi: 10.1111/pce.13208

Kaiser, E., Morales, A., Harbinson, J., Kromdijk, J., Heuvelink, E., and Marcelis, L. F. (2015). Dynamic photosynthesis in different environmental conditions. *J. Exp. Bot.* 66 (9), 2415–2426. doi: 10.1093/jxb/eru406

Kaiser, E., Kromdijk, J., Harbinson, J., Heuvelink, E., and Marcelis, L. F. (2017). Photosynthetic induction and its diffusional, carboxylation and electron transport processes as affected by CO_2 partial pressure, temperature, air humidity and blue irradiance. *Ann. Bot.* 119 (1), 191–205. doi: 10.1093/aob/mcw226

Kalaji, H. M., Schansker, G., Brestic, M., Bussotti, F., Calatayud, A., Ferroni, L., et al. (2017). Frequently asked questions about chlorophyll fluorescence, the sequel. *Photosynth. Res.* 132 (1), 13–66. doi: 10.1007/s11120-016-0318-y

Leakey, A. D., Press, M. C., and Scholes, J. D. (2003). High-temperature inhibition of photosynthesis is greater under sunflecks than uniform irradiance in a tropical rain forest tree seedling. *Plant Cell Environ.* 26, 1681–1690. doi: 10.1046/j.1365-3040.2003.01086.x

Mailly, D., Turbis, S., and Chazdon, R. L. (2013). solarcalc 7.0: An enhanced version of a program for the analysis of hemispherical canopy photographs. *Comput. Electron. Agric.* 97, 15–20. doi: 10.1016/j.compag.2013.06.004

Mekala, N. R., Suorsa, M., Rantala, M., Aro, E. M., and Tikkanen, M. (2015). Plants Actively Avoid State Transitions upon Changes in Light Intensity: Role of Light-Harvesting Complex II Protein Dephosphorylation in High Light. *Plant Physiol.* 168 (2), 721–734. doi: 10.1104/pp.15.00488

Morales, A., Kaiser, E., Yin, X., Harbinson, J., Molenaar, J., Driever, S. M., et al. (2018). Dynamic modelling of limitations on improving leaf CO_2 assimilation under fluctuating irradiance. *Plant Cell Environ.* 41 (3), 589–604. doi: 10.1111/pce.13119

Mott, K. A., and Woodrow, I. E. (1993). Effects of O_2 and CO_2 on nonsteady-state photosynthesis. Further evidence for ribulose-l,5-bisphosphate carboxylase/oxygenase limitation. *Plant Physiol.* 102, 859–866. doi: 10.1104/pp.102.3.859

Naumburg, E., and Ellsworth, D. S. (2000). Photosynthetic sunfleck utilization potential of understory saplings growing under elevated CO_2 in FACE. *Oecologia* 122, 163–174. doi: 10.1007/PL00008844

Pearcy, R. W. (1983). The light environment and growth of C_3 and C_4 tree species in the understory of a Hawaiian forest. *Oecologia* 58, 19–25. doi: 10.1007/BF00384537

Pearcy, R. W. (1990). Sunflecks and photosynthesis in plant canopies. *Annu. Rev. Plant Physiol. Plant Mol. Biol.* 41, 421–453. doi: 10.1146/annurev.pp.41.060190.002225

R Core Team. (2018). R: A language and environment for statistical computing. (Vienna, Austria: R Foundation). https://www.r-project.org/

Rijkers, T., de Vries, P. J., Pons, T. L., and Bongers, F. (2000). Photosynthetic induction in saplings of three shade-tolerant tree species: comparing understorey and gap habitats in a French Guiana rain forest. *Oecologia* 125 (3), 331–340. doi: 10.1007/s004420000459

Salter, W. T., Merchant, A. M., Richards, R. A., Trethowan, R., and Buckley, T. N. (2019). Rate of photosynthetic induction in fluctuating light varies widely among genotypes of wheat. *J. Exp. Bot.* 70 (10), 2787–2796. doi: 10.1093/jxb/erz100

Sassenrath-Cole, G. F., and Pearcy, R. W. (1992). The role of Ribulose-1,5-Bisphosphate regeneration in the induction requirement of photosynthetic CO_2 exchange under transient light conditions. *Plant Physiol.* 99, 227–234. doi: 10.1104/pp.99.1.227

Scafaro, A. P., Galle, A., Van Rie, J., Carmo-Silva, E., Salvucci, M. E., and Atwell, B. J. (2016). Heat tolerance in a wild *Oryza* species is attributed to maintenance of Rubisco activation by a thermally stable Rubisco activase ortholog. *New Phytol.* 211 (3), 899–911. doi: 10.1111/nph.13963

Singsaas, E. L., and Sharkey, T. D. (1998). The regulation of isoprene emission responses to rapid leaf temperature fluctuations. *Plant Cell Environ.* 21, 1181–1188. doi: 10.1046/j.1365-3040.1998.00380.x

Slot, M., and Winter, K. (2017a). In situ temperature relationships of biochemical and stomatal controls of photosynthesis in four lowland tropical tree species. *Plant Cell Environ.* 40 (12), 3055–3068. doi: 10.1111/pce.13071

Slot, M., and Winter, K. (2017b). Photosynthetic acclimation to warming in tropical forest tree seedlings. *J. Exp. Bot.* 68 (9), 2275–2284. doi: 10.1093/jxb/erx071

Slot, M., Garcia, M. N., and Winter, K. (2016). Temperature response of CO_2 exchange in three tropical tree species. *Funct. Plant Biol.* 43 (5), 468-478. doi: 10.1071/fp15320

Soleh, M. A., Tanaka, Y., Nomoto, Y., Iwahashi, Y., Nakashima, K., Fukuda, Y., et al. (2016). Factors underlying genotypic differences in the induction of photosynthesis in soybean [*Glycine max* (L.) Merr]. *Plant Cell Environ.* 39 (3), 685–693. doi: 10.1111/pce.12674

Tang, Y. H., Kachi, N., Furukawa, A., and Awang, M. B. (1999). Heterogeneity of light availability and its effects on simulated carbon gain of tree leaves in a small gap and the understory in a tropical rain forest. *Biotropica* 31 (2), 268–278. doi: 10.1111/j.1744-7429.1999.tb00138.x

Tani, M., Nik, A. R., Ohtani, Y., Yasuda, Y., Sahat, M. M., Kasran, B., et al. (2003a). "Characteristics of energy exchanges and surface conductance of a tropical rain forest in Peninsular Malaysia," in *Pasoh: Ecology of a Lowland Rain Forest in Southeast Asia*. Eds. T. Okuda, N. Manokaran, Y. Matsumoto, K. Niiyama, S. C. Thomas and P. S. Ashton (Tokyo, Japan: Springer), 73–89.

Tani, M., Nik, A. R., Yasuda, Y., Noguchi, S., Shamsuddin, S. A., Sahat, M. M., et al. (2003b). "Long-term estimation of evapotranspiration from a tropical rain forest in Peninsular Malaysia," in *Water Resource Systems - Water Availablity and Global Change*. Eds. S. Franks, G. Bloschl, M. Kumagai, K. Musiake and D. Rosbjerg (IAHS Publication), 280, 267–274.

Taylor, S. H., and Long, S. P. (2017). Slow induction of photosynthesis on shade to sun transitions in wheat may cost at least 21% of productivity. *Philos. Trans. R. Soc. B: Biol. Sci.* 372 (1730), 1–9. doi: 10.1098/rstb.2016.0543

Thomas, S. C., Noor, N. S. M., Mansor, M., Nadarajan, J., Cheng, K. A., Ishida, A., et al. (2003). *Part III. Plant population and functional biology* (Tokyo: Springer-Verlag).

Tinoco-Ojanguren, C., and Pearcy, R. W. (1993). Stomatal dynamics and its importance to carbon gain in two rainforest *Piper* species I. VPD effects on the transient stomatal response to lightflecks. *Oecologia* 94, 388–394. doi: 10.1007/BF00317115

Tomimatsu, H., and Tang, Y. (2016). Effects of high CO_2 levels on dynamic photosynthesis: carbon gain, mechanisms, and environmental interactions. *J. Plant Res.* 129 (3), 365–377. doi: 10.1007/s10265-016-0817-0

Tomimatsu, H., Sakata, T., Fukayama, H., and Tang, Y. (2019). Short-term effects of high CO_2 accelerate photosynthetic induction in *Populus koreana* x *trichocarpa* with always-open stomata regardless of phenotypic changes in high CO_2 growth conditions. *Tree Physiol.* 39 (3), 474–483. doi: 10.1093/treephys/tpy078

Urban, O., Košvancová, M., Marek, M. V., and Lichtenthaler, H. K. (2007). Induction of photosynthesis and importance of limitations during the induction phase in sun and shade leaves of five ecologically contrasting tree species from the temperate zone. *Tree Physiol.* 27, 1207–1215. doi: 10.1093/treephys/27.8.1207

Urban, J., Ingwers, M. W., McGuire, M. A., and Teskey, R. O. (2017). Increase in leaf temperature opens stomata and decouples net photosynthesis from stomatal conductance in *Pinus taeda* and *Populus deltoides x nigra*. *J. Exp. Bot.* 68 (7), 1757–1767. doi: 10.1093/jxb/erx052

Vanderwel, M. C., Slot, M., Lichstein, J. W., Reich, P. B., Kattge, J., Atkin, O. K., et al. (2015). Global convergence in leaf respiration from estimates of thermal acclimation across time and space. *New Phytol.* 207 (4), 1026–1037. doi: 10.1111/nph.13417

Wachendorf, M., and Küppers, M. (2017). Effects of leaf temperature on initial stomatal opening and their roles in overall and biochemical photosynthetic induction. *Trees* 31 (5), 1667–1681. doi: 10.1007/s00468-017-1577-8

Way, D. A., and Pearcy, R. W. (2012). Sunflecks in trees and forests: from photosynthetic physiology to global change biology. *Tree Physiol.* 32 (9), 1066–1081. doi: 10.1093/treephys/tps064

Way, D. A., Aspinwall, M. J., Drake, J. E., Crous, K. Y., Campany, C. E., Ghannoum, O., et al. (2019). Responses of respiration in the light to warming in field-grown trees: a comparison of the thermal sensitivity of the Kok and Laisk methods. *New Phytol.* 222 (1), 132–143. doi: 10.1111/nph.15566

Wise, R. R., Olson, A. J., Schrader, S. M., and Sharkey, T. D. (2004). Electron transport is the functional limitation of photosynthesis in field-grown Pima cotton plants at high temperature. *Plant Cell Environ.* 27, 717–724. doi: 10.1111/j.1365-3040.2004.01171.x

Woodrow, I. E., and Mott, K. A. (1989). Rate limitation of non-steady-state photosynthesis by ribulose-1,5-bisphosphate carboxylase in spinach. *Aust. J. Plant Physiol.* 16, 487–500. doi: 10.1071/PP9890487

Woodrow, I. E., Kelly, C. K., and Mott, K. A. (1996). Limitation of the rate of ribulosebisphosphate carboxylase activation by carbamylation and ribulosebisphosphate carboxylase activase activity: development and tests of a mechanistic model. *Aust. J. Plant Physiol.* 23, 141–149. doi: 10.1071/PP9960141

Yamori, W., Suzuki, K., Noguchi, K. O., Nakai, M., and Terashima, I. (2006). Effects of Rubisco kinetics and Rubisco activation state on the temperature dependence of the photosynthetic rate in spinach leaves from contrasting growth temperatures. *Plant Cell Environ.* 29 (8), 1659–1670. doi: 10.1111/j.1365-3040.2006.01550.x

Yamori, W., Masumoto, C., Fukayama, H., and Makino, A. (2012). Rubisco activase is a key regulator of non-steady-state photosynthesis at any leaf temperature and, to a lesser extent, of steady-state photosynthesis at high temperature. *Plant J.* 71 (6), 871–880. doi: 10.1111/j.1365-313X.2012.05041.x

Yamori, W., Kusumi, K., Iba, K., and Terashima, I. (2020). Increased stomatal conductance induces rapid changes to photosynthetic rate in response to naturally fluctuating light conditions in rice. *Plant Cell Environ.* 43, 1230–1240. doi: 10.1111/pce.13725

Yamori, W. (2016). Photosynthetic response to fluctuating environments and photoprotective strategies under abiotic stress. *J. Plant Res.* 129 (3), 379–395. doi: 10.1007/s10265-016-0816-1

Conflict of Interest: The authors declare that the research was conducted in the absence of any commercial or financial relationships that could be construed as a potential conflict of interest.

frontiers in Plant Science

ORIGINAL RESEARCH
published: 25 August 2020
doi: 10.3389/fpls.2020.01317

High Stomatal Conductance in the Tomato *Flacca* Mutant Allows for Faster Photosynthetic Induction

Elias Kaiser[1]*, *Alejandro Morales*[2,3,4], *Jeremy Harbinson*[1†], *Ep Heuvelink*[1] *and Leo F. M. Marcelis*[1]

[1] Horticulture and Product Physiology, Department of Plant Sciences, Wageningen University, Wageningen, Netherlands, [2] Centre for Crop Systems Analysis, Department of Plant Sciences, Wageningen University, Wageningen, Netherlands, [3] Molecular Plant Physiology, Institute of Environmental Biology, Utrecht University, Utrecht, Netherlands, [4] Plant Ecophysiology, Institute of Environmental Biology, Utrecht University, Utrecht, Netherlands

OPEN ACCESS

Edited by:
Diana Santelia, ETH Zürich, Switzerland

Reviewed by:
Christine Helen Foyer, University of Birmingham, United Kingdom
Thomas D. Sharkey, Michigan State University, United States

***Correspondence:**
Elias Kaiser
elias.kaiser@wur.nl

†Present address:
Jeremy Harbinson, Laboratory of Biophysics, Wageningen University, Wageningen, Netherlands

Specialty section:
This article was submitted to Plant Abiotic Stress, a section of the journal Frontiers in Plant Science

Received: *07 June 2020*
Accepted: *11 August 2020*
Published: *25 August 2020*

Citation:
Kaiser E, Morales A, Harbinson J, Heuvelink E and Marcelis LFM (2020) High Stomatal Conductance in the Tomato Flacca Mutant Allows for Faster Photosynthetic Induction. Front. Plant Sci. 11:1317. doi: 10.3389/fpls.2020.01317

Due to their slow movement and closure upon shade, partially closed stomata can be a substantial limitation to photosynthesis in variable light intensities. The abscisic acid deficient *flacca* mutant in tomato (*Solanum lycopersicum*) displays very high stomatal conductance (g_s). We aimed to determine to what extent this substantially increased g_s affects the rate of photosynthetic induction. Steady-state and dynamic photosynthesis characteristics were measured in *flacca* and wildtype leaves, by the use of simultaneous gas exchange and chlorophyll fluorometry. The steady-state response of photosynthesis to CO_2, maximum quantum efficiency of photosystem II photochemistry (F_v/F_m), as well as mesophyll conductance to CO_2 diffusion were not significantly different between genotypes, suggesting similar photosynthetic biochemistry, photoprotective capacity, and internal CO_2 permeability. When leaves adapted to shade (50 µmol m^{-2} s^{-1}) at 400 µbar CO_2 partial pressure and high humidity (7 mbar leaf-to-air vapour pressure deficit, VPD) were exposed to high irradiance (1500 µmol m^{-2} s^{-1}), photosynthetic induction was faster in *flacca* compared to wildtype leaves, and this was attributable to high initial g_s in *flacca* (~0.6 mol m^{-2} s^{-1}): in *flacca*, the times to reach 50 (t_{50}) and 90% (t_{90}) of full photosynthetic induction were 91 and 46% of wildtype values, respectively. Low humidity (15 mbar VPD) reduced g_s and slowed down photosynthetic induction in the wildtype, while no change was observed in *flacca*; under low humidity, t_{50} was 63% and t_{90} was 36% of wildtype levels in *flacca*. Photosynthetic induction in low CO_2 partial pressure (200 µbar) increased g_s in the wildtype (but not in *flacca*), and revealed no differences in the rate of photosynthetic induction between genotypes. Effects of higher g_s in *flacca* were also visible in transients of photosystem II operating efficiency and non-photochemical quenching. Our results show that at ambient CO_2 partial pressure, wildtype g_s is a substantial limitation to the rate of photosynthetic induction, which *flacca* overcomes by keeping its stomata open at all times, and it does so at the cost of reduced water use efficiency.

Keywords: abscisic acid, air humidity, CO_2 concentration, fluctuating irradiance, dynamic photosynthesis, stomatal conductance

INTRODUCTION

In the leaves of higher plants, stomata balance carbon uptake against water loss. They achieve this balance by dynamically regulating stomatal aperture in response to intrinsic and extrinsic factors. Typically, stomatal aperture decreases in low irradiance or darkness, and increases in high irradiance. Stomatal opening after sudden increases in irradiance is slow compared to changes in Calvin cycle metabolism (McAusland et al., 2016), with time constants in the range of 4 to 29 min (Vico et al., 2011). Due to the slow opening of stomata, the increase of stomatal conductance (g_s, mol m^{-2} s^{-1}) from a low initial value is assumed to be one of the three main limitations of net photosynthesis rate (A, μmol m^{-2} s^{-1}) in response to increases in irradiance (e.g., Urban et al., 2008; Kaiser et al., 2016; Li et al., 2016; Kaiser et al., 2017a; Zhang et al., 2018; Zhang et al., 2020). Given that solar irradiance incident on a leaf often fluctuates, these dynamic limitations of photosynthesis decrease photosynthetic irradiance use efficiency (Morales et al., 2018). Improving g_s, including its dynamics, is an attractive means with which to improve both irradiance and water use efficiency (Lawson and Blatt, 2014; Vialet-chabrand et al., 2017). Increases in the limitation imposed upon A by g_s can be identified via transient decreases of leaf internal CO_2 partial pressure (C_i, μbar). The other two main limitations during photosynthetic induction arise from slow rates of change in the activity of enzymes involved in ribulose-1,5-bisphosphate (RuBP) regeneration, and from slow activation of Rubisco (Pearcy et al., 1996; Way and Pearcy, 2012; Kaiser et al., 2015; Kaiser et al., 2018). These limitations occur additionally to the limitations at steady state due to, e.g., the rate of electron transport, Calvin cycle metabolism, sucrose metabolism, or mesophyll conductance (g_m, mol m^{-2} s^{-1}).

Disentangling stomatal and other limitations during photosynthetic induction is difficult. Many treatments affecting g_s also affect other transient limitations of photosynthetic induction, such as leaf temperature (Kaiser et al., 2017a) and salt stress (Zhang et al., 2018). Similarly, some genetic mutations affecting g_s, such as the abscisic acid (ABA) deficient *aba2-1* mutant in *Arabidopsis thaliana*, showed enhanced A/C_i responses compared to its wildtype, Col-0 (Kaiser et al., 2016), suggesting pleiotropic effects, which may confound effects of altered g_s. Also, models estimating transient stomatal limitation have often been based on linear – not curvilinear – A/C_i relationships (Woodrow and Mott, 1989; Tinoco-Ojanguren and Pearcy, 1993), or are based on steady-state A/C_i responses (Kaiser et al., 2017a). In fact, the maximum rate of carboxylation (V_{cmax}), for example, increases strongly during photosynthetic induction (Soleh et al., 2016; Taylor and Long, 2017). In another approach, the limitation during induction was attributed to g_s alone up to the point where A reached 95% of the steady-state value (McAusland et al., 2016), entirely ignoring limitations by RuBP regeneration and Rubisco activation kinetics. Tools to better separate stomatal from other limitations are thus warranted, and mutants or transformants with substantially altered stomatal characteristics but similar photosynthetic biochemistry (Raissig et al., 2017; Papanatsiou et al., 2019; Tomimatsu et al., 2019; Kimura et al., 2020; Yamori et al., 2020) can be counted among such tools.

The tomato (*Solanum lycopersicum* L.) *flacca* mutant has a 80% to 90% lower ABA content than its wildtype (Tal and Nevo, 1973; Sagi et al., 2002). *Flacca* leaves exhibit a very high g_s, without affecting the A/C_i response, suggesting that photosynthetic capacity is independent of ABA (Bradford et al., 1983). Lack of ABA has not been found to affect g_m in the *aba-1* mutant of *Nicotiana plumbaginifolia* (Mizokami et al., 2015) but to our knowledge has not been determined in *flacca*. The aim of this study is to determine the dynamic limitations of photosynthetic induction due to g_s in tomato leaves. For this, steady-state and dynamic photosynthesis characteristics were measured in the ABA-deficient *flacca* mutant and its wildtype, by the use of simultaneous gas exchange and chlorophyll fluorometry.

Abbreviations: A, net photosynthesis rate; A_g, gross photosynthesis rate; ABA, abscisic acid; ANOVA, analysis of variance; C_a, leaf external CO_2 partial pressure; C_c, chloroplast CO_2 partial pressure; C_i, substomatal CO_2 partial pressure; F, fluorescence emission from leaves under actinic irradiance; F_m, maximal fluorescence in dark-adapted leaves; F_m', maximal fluorescence in light-adapted leaves; F_o, minimal fluorescence in dark-adapted leaves; F_v/F_m, maximum quantum efficiency of PSII photochemistry; F_v'/F_m', efficiency of open PSII traps; g_m, mesophyll conductance; g_s, stomatal conductance; J, rate of linear electron transport; MPF, multi-phase flash protocol; PAR, photosynthetically active radiation; qP, coefficient of photochemical quenching; R_d, mitochondrial respiration; s, lumped parameter used to convert Φ_{PSII} to J; TPU, triose phosphate utilization capacity; WUE_i, intrinsic water use efficiency; V_{cmax}, maximum rate of carboxylation; VPD, leaf-to-air vapour pressure deficit; Γ^*, CO_2 compensation point in the absence of mitochondrial respiration; Φ_{PSII}, photosystem II operating efficiency.

MATERIALS AND METHODS

Plant Material

Seeds of tomato cv. Rheinlands Ruhm wildtype (LA0535) and *flacca* (LA0673) were obtained from the Tomato Genetics Resource Center (University of California, Davis, USA). Seeds were germinated in stonewool plugs (Grodan, Roermond, NL). A week after sowing, they were transferred to stonewool cubes (10 cm × 10 cm × 7 cm; Grodan). Plants were grown in a climate chamber under a day/night cycle of 16/8 h (day/night), 20/18°C temperature, ambient CO_2 partial pressure, 70% relative air humidity, and 154 μmol m^{-2} s^{-1} photosynthetically active radiation (PAR; measured 10 cm above table height), which was provided by fluorescent tubes (Master TL-D 58W/840 Reflex Eco; Philips, Eindhoven, the Netherlands). Stonewool cubes were standing in a layer (height, 1–2 cm) of nutrient solution (Yara Benelux B.V., Vlaardingen, the Netherlands), which was replenished every 1 to 2 days and contained 12.4 mM NO_3^-, 7.2 mM K^+, 4.1 mM Ca^{2+}, 3.3 mM SO_4^{2-}, 1.8 mM Mg^{2+}, 1.2 mM NH_4^+, 1.1 mM PO_4^{3-}, 30 μM BO_3^{3-}, 25 μM Fe^{3+}, 10 μM Mn^{2+}, 5 μM Zn^{2+}, 0.75 μM Cu^+, and 0.5 μM MoO_4^{2-} (EC 2.1 dS m^{-1}, pH 5.5). Between 1 and 4 weeks after sowing, *flacca* plants were sprayed daily with a solution containing 10 μM ABA, 0.01% (w/v) Triton-X, and 0.1% (v/v) ethanol (Bradford et al., 1983), using commercially available horticultural hand sprayers. Wildtype plants were sprayed with a control solution containing

0.01% Triton-X and 0.1% ethanol. Untreated *flacca* plants are smaller and show much higher transpiration rates than the wildtype, together with leaf epinasty and strong root formation along the stem (Tal, 1966). Growing *flacca* with application of ABA causes plants to grow similarly well as the wildtype (Imber and Tal, 1970). When the application of ABA is stopped, *flacca* reverts to its mutant phenotype within days, including always-open stomata (Imber and Tal, 1970). All chemicals were purchased from Sigma (St. Louis, MO, USA).

Measurements

When plants were between 5 and 6 weeks old, the fourth leaf, counting from the bottom, was selected for measurements. ABA spraying was stopped seven days before the start of measurements, to allow the high g_s phenotype of *flacca* to reassert itself. Measurements were performed in a lab, using the LI-6400 XT photosynthesis system (LI-COR Biosciences, Lincoln, Nebraska, USA) equipped with a fluorescence chamber (leaf area: 2 cm^2). Conditions inside the leaf chamber during measurements were: 25°C chamber temperature, 7 mbar leaf-to-air vapour pressure deficit (VPD; except when stated otherwise) and a flow rate of 500 µmol s^{-1}. Irradiance was provided by LEDs in a 90/10 red/blue irradiance mixture, with peak intensities at wavelengths of 635 and 465 nm, respectively. For all measurements, five plants per genotype were used (n = 5).

All measurements were performed on the same spot of a leaf, to reduce measurement noise caused by spatial variation (Lawson and Weyers, 1999; Matthews et al., 2017): (a) dark-adapted F_v/F_m, (b) A/PAR curves at 2% oxygen, (c) A/C_i curves at 2% oxygen, (d) A/C_i curves at 21% oxygen, (e-g) photosynthetic induction under three different environmental conditions (described below). While measurements a-d were performed in the same sequence, the order of photosynthetic induction measurements was randomized for each plant. Values of A were corrected for CO_2 leakage based on the manufacturers' suggestions. Measurements were started at 7:30 in the morning and took 8 to 9 h to complete per leaf.

Dark-Adapted F_v/F_m and Net CO_2 Exchange in Darkness

Leaves were dark-adapted for 20 minutes. Then, net CO_2 exchange in darkness (A_{dark}) was logged, after which a weak measuring beam was turned on to measure F_o. Then, F_m was determined by exposing the leaf to a single-pulse saturating flash of ~9.000 µmol m^{-2} s^{-1} intensity and 1-s duration. Dark-adapted F_v/F_m was calculated as $F_v/F_m = (F_m - F_o)/F_m$.

A/PAR Curves at 2% Oxygen

A gas mixture containing 2% oxygen and 98% nitrogen was fed to the inlet of the LI-6400 XT. Leaf external CO_2 partial pressure (C_a) was set to 2000 µbar, and irradiance was set to 200 µmol m^{-2} s^{-1}. After reaching steady-state A, irradiance was decreased in steps of 150, 100, 70, 50, and 30 µmol m^{-2} s^{-1}, and A was logged for 30 s after reaching steady-state A, at steps of 5 s. Values were later averaged at each step to reduce measurement noise.

A/C_i Curves at 2% Oxygen

A gas mixture containing 2% oxygen and 98% nitrogen was fed to the inlet of the LI-6400 XT. Irradiance was set to 1,500 µmol m^{-2} s^{-1}, and C_a was set to 150 µbar. After reaching steady-state A, C_a was decreased in steps of 130, 100, 70, and 50 µbar. A and C_i were logged as described above. At each C_a, the infrared gas analysers were matched.

A/C_i Curves at 21% Oxygen

Irradiance was set to 1,500 µmol m^{-2} s^{-1}, and C_a was set to 400 µbar. After reaching steady-state A, C_a was decreased in steps of 300, 200, 130, 100, 70 and 50 µbar. Then, C_a was raised to 400 µbar and after reaching steady-state A, C_a was increased in steps of 600, 750, 900, 1,100, 1,400, 1,700, and 2,000 µbar. A and C_i were logged after reaching steady-state (3–5 min per step) as described above. At each C_a, the infrared gas analysers were matched. Parameters describing maximum rate of carboxylation (V_{cmax}), rate of linear electron transport at the measuring irradiance (J_{1500}) and triose phosphate utilization capacity (TPU) were determined using the excel solver tool by Sharkey (2016). Additionally, operating and maximal fluorescence in light-adapted leaves (F and F_m', respectively) were determined at each C_a by using a multi-phase flash protocol (MPF; Loriaux et al., 2013). The maximum intensity of the MPF was ~9.000 µmol m^{-2} s^{-1}, the durations of the three phases were 0.3, 0.7 and 0.4 s respectively, and the percentage decrease of flash intensity during phase two was 60%. These MPF settings were found to yield the most accurate results in pilot experiments (data not shown). Photosystem II operating efficiency (Φ_{PSII}) was calculated as $\Phi_{PSII} = (F_m' - F)/F_m'$. Mesophyll conductance (g_m) was determined following the variable J method proposed by Harley et al. (1992); the variables A, C_i, and Φ_{PSII} to calculate g_m were determined at a C_a of 400 µbar and an irradiance of 1500 µmol m^{-2} s^{-1}. Parameters to calculate g_m, namely R_d, Γ^* and s, were determined from A/C_i and A/PAR measurements at 2 and 21% oxygen following Yin et al. (2009).

Photosynthetic Induction

Leaves were adapted to 50 µmol m^{-2} s^{-1} until g_s was constant (40–60 minutes). Irradiance was then increased to 1500 µmol m^{-2} s^{-1} in a step change, and gas exchange values were logged every 2 s for 60 min. These measurements were performed at C_a and air humidity close to the plant's growth conditions (400 µbar C_a, 7 mbar VPD), termed "control" hereafter. Photosynthetic induction was additionally assessed under two other conditions: "high VPD" (15 mbar) and "low CO_2" (200 µbar), keeping all other conditions the same. During photosynthetic induction, chlorophyll fluorescence was measured using a saturating MPF (described above) once every minute during the first ten minutes, and once every two minutes thereafter. Photosynthetic induction (PI, %) was calculated as a percentage of the total change between initial A (A_i) and final A (A_f) of each transient: $PI = (A-A_i)/(A_f-A_i)*100$. Intrinsic water use efficiency (WUE_i) was calculated as $WUE_i = A/g_s$. Non-photochemical quenching (NPQ) during photosynthetic induction was calculated as $NPQ = (F_m - F_m')/F_m'$. The coefficient of photochemical quenching (qP) and the

efficiency of open photosystem II traps (F_v'/F_m') were calculated after Oxborough and Baker (1997), as $qP = (F_m' - F)/(F_m' - F_o')$ and $F_v'/F_m' = (F_m' - F_o')/F_m'$, where F_o' is minimal fluorescence from irradiance- adapted leaves. F_o' was calculated after Oxborough and Baker (1997).

Statistical Analysis

All statistical tests were performed at P=0.05 as threshold for significance. Where appropriate, a two-sided Student's t-test was used to determine significant differences between genotypes. For photosynthetic induction under different environmental conditions, a two-way analysis of variance (ANOVA) was performed, and interaction means were separated based on Fisher's least significant difference test. Residuals were tested for normal distribution (Shapiro-Wilk test) and equal variances were assumed for treatment groups. If the requirement for normal distribution was not fulfilled, the procedure was repeated on log-transformed data. If after log transformation residuals still did not show normality, Kruskal-Wallis one-way ANOVA, considering six treatments (three environmental conditions times two genotypes), was performed using the original data. In case of significant treatment effects, Dunn's test of multiple comparisons was performed to identify differences between the six treatments. All statistical tests were performed in Genstat (VSN international, Hempstead, UK) except for Dunn's test, which was performed in R (R Core Team, 2020) using the dunn.test package (Dinno, 2017).

RESULTS

Steady-State CO_2 and Irradiance Responses of Photosynthesis

Wildtype and *flacca* leaves showed very similar responses of A and Φ_{PSII} to C_i (**Figure 1**). In the CO_2 range 50 to 300 µbar, A increased near-linearly, then peaked at ~500 µbar and with further increases in C_i, A declined in both genotypes. Compared to A, Φ_{PSII} peaked at lower C_i (~300 µbar) and exhibited a stronger decline with further increases in C_i. Parameters describing photosynthetic capacity, i.e., V_{cmax}, J_{1500} and TPU, were not significantly different between genotypes (**Figure 1**, insert). Mesophyll conductance and its components were not significantly different between genotypes (except C_i, which was significantly greater in *flacca*, **Figure 2C**), although *flacca* tended to show greater values for A, J, R_d, and C_c (**Figure 2**). In dark-adapted leaves, A was −1.2 ± 0.1 µmol m^{-2} s^{-1} in wildtype and −1.9 ± 0.1 µmol m^{-2} s^{-1} in *flacca* leaves (p=0.008). At low irradiance (50 µmol m^{-2} s^{-1}), on the other hand, A was similar between genotypes (**Table 1**).

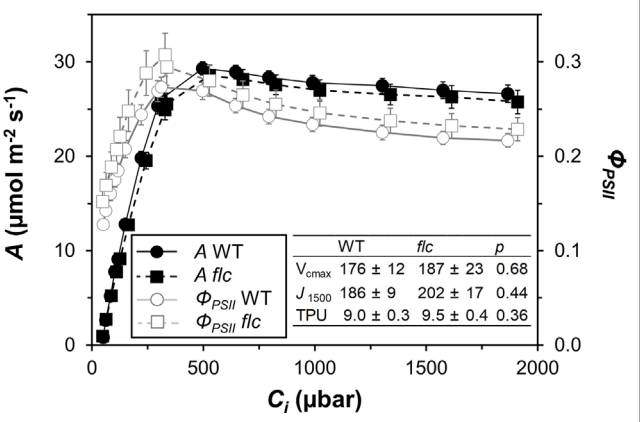

FIGURE 1 | Steady-state responses of net photosynthesis rate (A) and photosystem II operating efficiency (Φ_{PSII}) to leaf internal CO_2 partial pressure (C_i), in wildtype (WT) and *flacca* (*flc*) leaves, measured at 21% oxygen. Insert: parameters derived from curve fitting (after Sharkey, 2016) to A/C_i response (unit for all: µmol m^{-2} s^{-1}), namely maximum rate of carboxylation (V_{cmax}), rate of linear electron transport at 1500 µmol m^{-2} s^{-1} PAR (J_{1500}) and triose phosphate utilisation capacity (TPU); P values for comparisons between WT and *flc* based on two-sided t-test. Symbols and numbers represent averages ± SEM, n = 5.

Response of Photosynthetic Gas Exchange to a Stepwise Irradiance Increase

Next, we tested how gas exchange in wildtype and *flacca* leaves that had been adapted to low irradiance (50 µmol m^{-2} s^{-1}) reacted to a stepwise increase to high irradiance (1500 µmol m^{-2} s^{-1}). In wildtype leaves, the rate of photosynthetic induction was slower at high VPD, compared to the other two treatments (low CO_2 or high VPD; **Figure 3A**), while in *flacca*, there was no difference between control and high VPD treatments (**Figure 3B**). However, while in wildtype leaves the rate of photosynthetic induction was the same in the control and low CO_2 treatments, in *flacca*, induction at low CO_2 was slower than in the control treatment (**Figures 3A, B**). The *flacca* mutation had significant effects on the times to reach 50 (t_{50}) and 90% (t_{90}) of full photosynthetic induction: under control conditions, t_{50} was 91% and t_{90} was 46% of wildtype values in *flacca*, while under high VPD, t_{50} was 63% and t_{90} was 36% of wildtype values in *flacca* (**Figure 4**). Both indices were not significantly different between genotypes under low CO_2 (**Figure 4**). Transient A was higher in *flacca* than in wildtype leaves, and in both genotypes was slightly higher in control than in high VPD, as well as substantially reduced at low CO_2 (insets in **Figures 3A, B**; **Table 1**).

In *flacca*, A showed a small decrease between ~1.5 and 2.0 min after the stepwise increase in irradiance under control and high VPD conditions (**Figure S1B**). These dynamics are very similar to those previously seen in shade-adapted wildtype tomato leaves undergoing photosynthetic induction under high CO_2 partial pressure (Kaiser et al., 2017b), and in the present study were observed neither at low CO_2 (**Figure S1B**), nor in wildtype leaves (**Figure S1A**). The most likely explanation for this phenomenon is a transient mismatch between the rate of CO_2 fixation in the Calvin cycle and downstream sucrose metabolism, which would transiently limit the availability of free phosphate in the chloroplast (Prinsley and Leegood, 1986; Stitt and Grosse, 1988; Stitt and Quick, 1989).

During the complete trajectory of photosynthetic induction, stomatal conductance (g_s) in wildtype leaves was strongly increased by lowering CO_2, and substantially reduced by increasing VPD (**Figure 3C**; **Table 1**). In *flacca*, g_s was lower

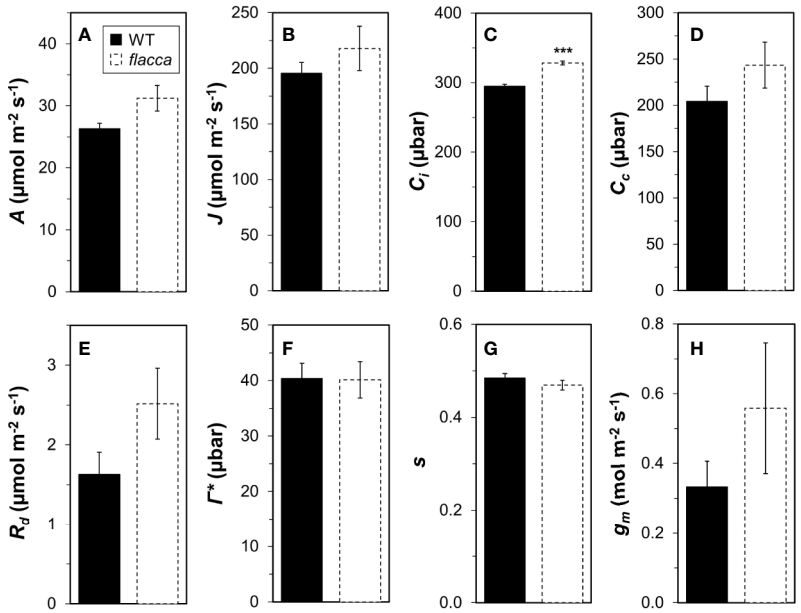

FIGURE 2 | Analysis of mesophyll conductance (g_m) and its components in wildtype (WT) and *flacca* leaves. **(A)** net photosynthesis rate (A); **(B)**, linear electron transport rate (J); **(C)** substomatal CO_2 partial pressure (C_i); **(D)** chloroplast CO_2 partial pressure (C_c); **(E)** mitochondrial respiration (R_d); **(F)** CO_2 compensation point in the absence of mitochondrial respiration (Γ^*); **(G)** lumped parameter to convert Φ_{PSII} to J (s); **(H)**, g_m. A, J and C_i were determined under 1000 µmol m^{-2} s^{-1} PAR, 400 µbar CO_2 atmospheric partial pressure and 25°C chamber temperature. R_d, Γ^*, and s were determined from A/C_i and A/PAR curves under photorespiratory and non-photorespiratory conditions after Yin et al. (2009). Bars and error bars represent averages ± SEM, n = 5. ***P<0.01.

TABLE 1 | Steady-state gas exchange traits at 50 and 1500 µmol m^{-2} s^{-1} PAR.

Treatment	Gen	50 µmol m^{-2} s^{-1}												1500 µmol m^{-2} s^{-1}											
		A				g_s				C_i				A				g_s				C_i			
Control	WT	2.0	±	0.1	b	0.22	±	0.04	b	379	±	4	c	26.0	±	1.0	B	0.60	±	0.04	b	311	±	2	bc
	flc	1.9	±	0.1	b	0.62	±	0.06	d	390	±	1	d	28.4	±	1.4	B	1.03	±	0.05	de	336	±	3	c
Low CO_2	WT	1.7	±	0.1	a	0.34	±	0.04	c	192	±	1	a	14.8	±	0.6	A	0.71	±	0.04	c	159	±	1	a
	flc	1.7	±	0.1	a	0.58	±	0.09	d	194	±	1	ab	16.7	±	1.2	Ab	1.09	±	0.06	e	165	±	1	a
High VPD	WT	1.9	±	0.1	ab	0.14	±	0.01	a	369	±	2	bc	24.4	±	0.8	B	0.41	±	0.01	a	281	±	3	ab
	flc	1.8	±	0.1	ab	0.58	±	0.07	d	385	±	1	cd	26.6	±	1.5	B	0.88	±	0.06	d	329	±	2	bc
Genotype																									
Treatment					*																				
Treatment x Gen									*												*				
Kruskal-Wallis χ^2												***				***									***

*Wildtype and flacca leaves were exposed to 400 µbar CO_2 and 7 mbar VPD (Control), 200 instead of 400 µbar ("low CO_2") and 15 instead of 7 mbar ("high VPD"). Net photosynthesis rate (A, µmol m^{-2} s^{-1}), stomatal conductance (g_s, mol m^{-2} s^{-1}) and leaf internal CO_2 partial pressure (C_i, µbar) are shown as averages ± SEM. Two-way ANOVA was used to indicate significant effects of genotype, treatment or genotype x treatment interactions. When appropriate, a Kruskal-Wallis one-way ANOVA was used. Symbols: *P<0.05, ***P<0.001. Different letters per column indicate statistically significant (P=0.05) differences between treatments as determined by Fisher's least significant difference test or by Dunn's test (in case of Kruskal-Wallis one-way ANOVA).*

in the high VPD treatment compared to both other treatments during photosynthetic induction (**Figure 3D**; **Table 1**). Intriguingly, while the low irradiance adapted (initial) g_s in wildtype leaves reacted to the treatment levels in a predictable way, i.e., decreasing under high VPD and increasing under low CO_2 relative to control (**Figure 3C**), initial g_s in *flacca* did not (**Figure 3D**; **Table 1**). Also, g_s in *flacca* was substantially higher than that in wildtype leaves in all cases, as would be expected of an ABA mutant.

In control conditions, C_i in wildtype leaves showed an initial decrease in the first 10 minutes of photosynthetic induction, after which it gradually increased as stomata opened (**Figure 3E**). This decrease was exacerbated in the high VPD treatment. Even after partial recovery of C_i due to stomatal opening, C_i did not reach control values when approaching steady state (**Figure 3E**; **Table 1**). In *flacca* leaves, C_i decreased less strongly under both control and high VPD conditions, and did not increase much during the remainder of photosynthetic induction (**Figure 3F**).

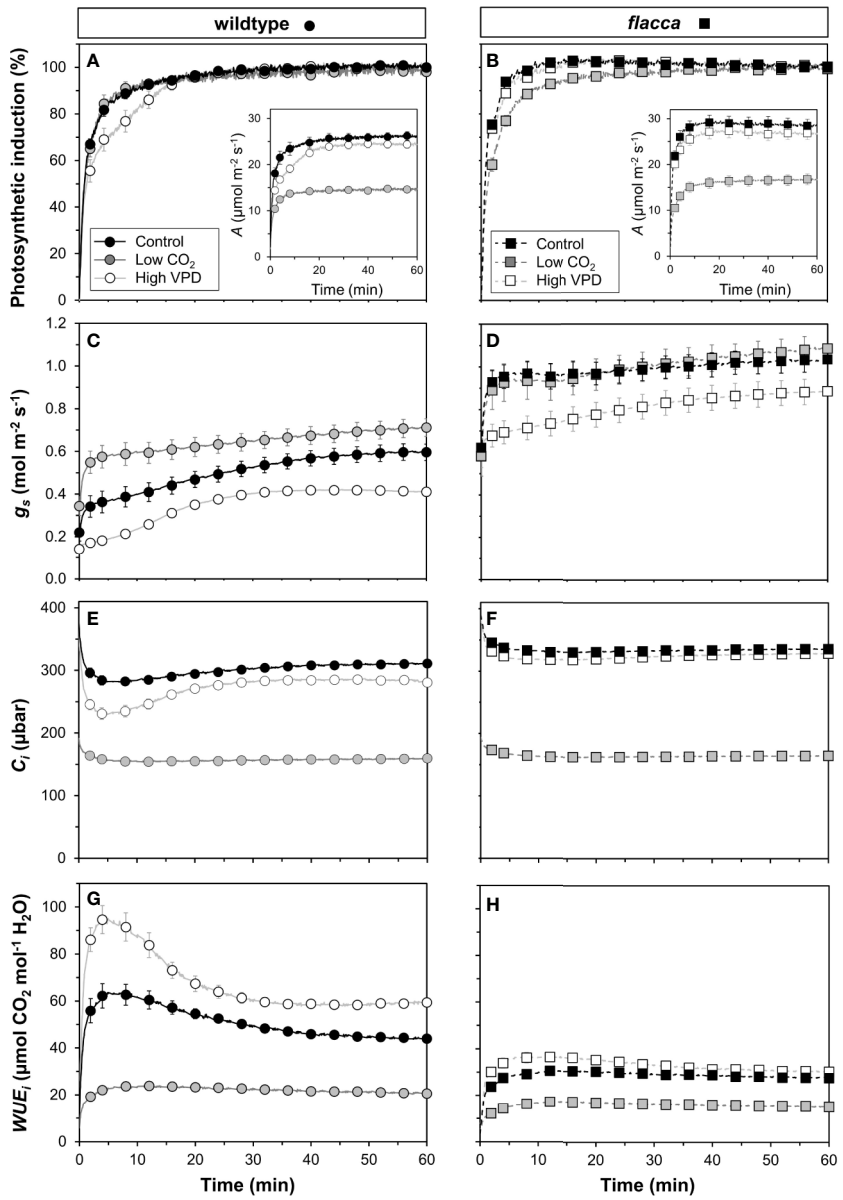

FIGURE 3 | Time courses of gas exchange in wildtype (left panel) and *flacca* leaves (right panel) after a transition from low to high irradiance: **(A, B)** photosynthetic induction; **(C, D)** stomatal conductance (g_s); **(E, F)** leaf internal CO_2 partial pressure (C_i); **(G, H)** intrinsic water use efficiency (WUE_i). Insets in **(A, B)** show net photosynthesis rates (A). Leaves initially adapted to 50 µmol m^{-2} s^{-1} PAR were exposed to 1500 µmol m^{-2} s^{-1} PAR at time = 0 min. Data were logged at 400 µbar CO_2 and 7 mbar leaf-to-air VPD (Control), 200 instead of 400 µbar (Low CO_2) and 15 instead of 7 mbar (High VPD). Lines and symbols represent averages ± SEM, n = 5.

Also, C_i time courses in both of these treatments were virtually indistinguishable in *flacca*, which is explained by the diminished reduction of g_s under high VPD (**Figure 3D**). Under low CO_2, C_i was similar in wildtype and *flacca*, displaying only small decreases in the beginning of photosynthetic induction without subsequent recovery (**Figures 3E, F**).

Intrinsic water use efficiency (WUE_i) was roughly twice as high in wildtype compared to *flacca* leaves (**Figures 3G, H**). In the wildtype, a high VPD resulted in large increases (+31%), and a low CO_2 in large decreases (−56%), of WUE_i relative to control conditions (**Figure 3G**). In *flacca*, WUE_i was markedly reduced (−50%) under low CO_2 relative to the other two conditions (**Figure 3H**). While WUE_i showed strong dynamics in the first 30 minutes after exposure to high irradiance under high VPD and control conditions in the wildtype, it plateaued early after an initial increase (<5 min) in all other cases (**Figures 3G, H**).

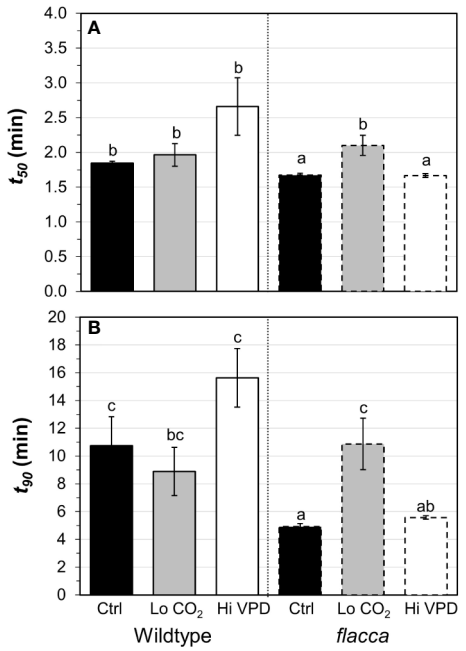

FIGURE 4 | Time to reach 50 (**A**, t_{50}) and 90% (**B**, t_{90}) full photosynthetic induction of wildtype and *flacca* leaves after a step change from low to high irradiance. Experimental conditions identical to those described under **Figure 3**. Different letters depict significant differences ($P<0.05$) between ranks, as determined by Dunn's test. Bars and error bars represent averages ± SEM, n = 5.

Chlorophyll Fluorescence Dynamics During Photosynthetic Induction

In wildtype leaves, an initial rapid increase in Φ_{PSII} within the first ~8 min was followed by a slower, more gradual increase towards a steady state under control and high VPD conditions until ~40 min (**Figure 5A**). In *flacca* leaves in control and high VPD conditions, a gradual decrease was observed after the initial increase in Φ_{PSII} (**Figure 5B**). In both genotypes, Φ_{PSII} under low CO_2 stabilized quickly at lower values and then plateaued. Dark-adapted F_v/F_m was ~0.82 in both genotypes (n.s., **Figure 5B**, inset). A rapid increase in *NPQ* in the first five minutes was followed by a decrease until 10 to 20 min, which was followed by a slower increase until the final measurement after 60 minutes (**Figures 5C, D**). Under control and high VPD conditions, *NPQ* initially rose to much higher values in wildtype (1.6–1.7) compared to *flacca* leaves (1.4–1.5). The subsequent decrease to a local minimum showed a greater amplitude in wildtype (~0.1) compared to *flacca* leaves (~0.05). Under low CO_2, *NPQ* tended to be greater in both genotypes compared to the other treatments. The coefficient of photochemical quenching (*qP*) showed dynamics similar to those of Φ_{PSII} (**Figures 5E, F**). *qP* and Φ_{PSII} were highly correlated in all treatments (R^2 >0.99). The efficiency of open photosystem II traps (F_v'/F_m') showed dynamics that were the inverse of those of *NPQ* (**Figures 5G, H**); *NPQ* and F_v'/F_m' were highly correlated (R^2 >0.99). These correlations suggest that Φ_{PSII} dynamics were largely due to changes in *qP* rather than changes in F_v'/F_m' or *NPQ* (Baker et al., 2007).

Stomatal Effects on Rate of Photosynthetic Induction

Next, we explored several ways to visualize the effects of (partially) closed stomata on photosynthetic induction. First, initial, low-irradiance adapted g_s was plotted against t_{90} (**Figure 6A**). Across both genotypes, there was a consistent threshold-type relationship between initial g_s and t_{90}: at initial g_s <0.4 mol m^{-2} s^{-1}, t_{90} increased strongly with decreases in initial g_s, reaching values of ~15 min at an initial g_s of 0.11 mol m^{-2} s^{-1}. At initial g_s >0.4 mol m^{-2} s^{-1}, the value of t_{90} (~5 min) was unaffected by further increases in initial g_s. Roughly, a similar threshold was visible between t_{50} and initial g_s, as initial g_s <0.2 mol m^{-2} s^{-1} tended to increase t_{50}, while t_{50} was unaffected by differences in initial g_s in the range 0.2 to 0.8 (**Figure 6A**, inset). Initial g_s versus t_{50} or t_{90} did not show a similar relationship at low CO_2 (**Figure S2**) and was therefore omitted from **Figure 6A**.

Photosynthesis integrated over the initial five minutes of photosynthetic induction scaled well with C_i integrated over the same period (**Figure 6C**). This suggests that *A* was affected by C_i, while the change in C_i was due to treatment and/or genotype effects on g_s. Finally, plotting *J* vs. gross photosynthesis rates (A_g, calculated as *A* plus R_d) produced very similar results between control and high VPD conditions in *flacca* leaves (**Figure 6D**), while in wildtype leaves A_g showed higher values for the same *J* in control compared to high VPD conditions (**Figure 6B**). Under low CO_2, both genotypes showed decreased A_g for a given *J*. Also, while in *flacca* leaves the plots of A_g vs. *J* were highly linear (**Figure 6D**), in wildtype leaves they showed an upwards curvature at higher A_g/J values, i.e., A_g increased more strongly than *J* (**Figure 6B**). This upwards curvature is indicative of an increase in the rate of carboxylation relative to the rate of oxygenation, most likely caused by an increase in C_i due to increased stomatal opening (Kaiser et al., 2017a; Zhang et al., 2018).

DISCUSSION

In recent years, the dynamic responses of photosynthesis to fluctuating light, and their limitations, have received more attention. It is now widely recognised that increasing photosynthesis is a pathway to increasing crop productivity (Ort et al., 2015), that crops frequently encounter light intensity fluctuations (Kaiser et al., 2018), and that alleviating some of the limitations acting on photosynthesis transients can strongly increase biomass (Kromdijk et al., 2016). Indeed, research looking into reductions of limitations acting on dynamic photosynthesis currently receives a lot of attention (Tanaka et al., 2019; Acevedo-Siaca et al., 2020; Kimura et al., 2020; Yamori et al., 2020).

Greater Stomatal Conductance Increases the Rate of Photosynthetic Induction

Responses of *A* to C_i, as well as mesophyll conductance, were similar between the *flacca* mutant and the wildtype (**Figures 1** and **2**), while stomatal conductance was strongly enhanced in *flacca* leaves

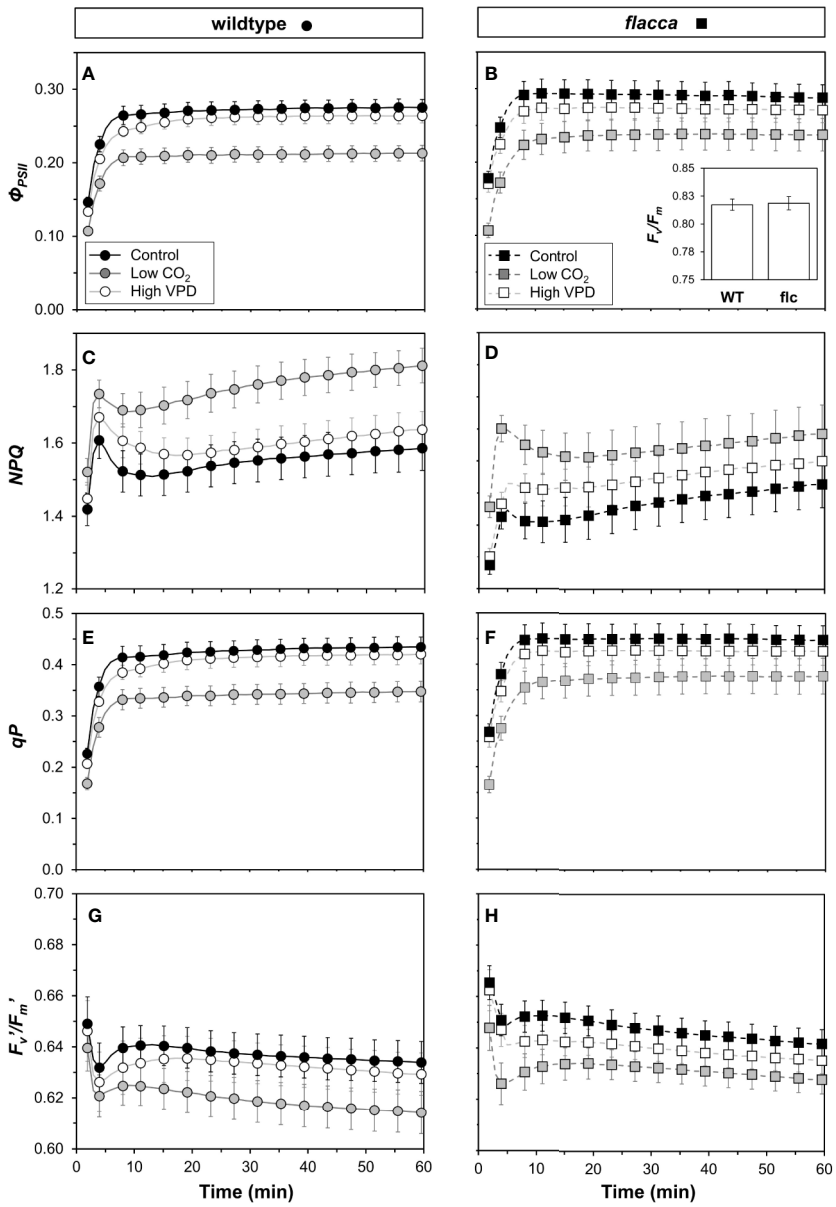

FIGURE 5 | Time courses of chlorophyll fluorescence in wildtype (WT, left panel) and *flacca* leaves (*flc*, right panel) after a transition from low to high irradiance. **(A, B)** photosystem II operating efficiency (Φ_{PSII}); **(C, D)** non-photochemical chlorophyll fluorescence quenching (*NPQ*); **(E, F)** coefficient of photochemical quenching (*qP*); **(G, H)** efficiency of open photosystem II traps (F_v'/F_m'). Experimental conditions identical to those described under **Figure 3**. Lines and symbols represent averages ± SEM, n = 5.

(**Figures 3C, D**). This confirms our hypothesis that the *flacca* mutant is a useful system for strongly reducing stomatal limitations and, via their reduction, better understanding their effects. This is similar to earlier reports using genotypes with "always-open" stomata (Tomimatsu and Tang, 2012; Tomimatsu et al., 2019; Kimura et al., 2020; Yamori et al., 2020). Our results further suggest that the faster photosynthetic induction observed in *flacca* compared to wildtype leaves under control and high VPD conditions (**Figures 3A, B** and **4**) was indeed due to much higher stomatal conductance (difference between genotypes in initial g_s was ~0.4 mol m^{-2} s^{-1}). Initial g_s in leaves adapted to darkness or shade strongly impacts on rates of photosynthetic induction upon illumination with high irradiance. It has been reported previously that parameters such as the time needed to reach 50 or 90% of full photosynthetic induction (t_{50} and t_{90}, respectively) show a strong bimodal relationship with initial g_s (Valladares et al., 1997; Allen and Pearcy, 2000; Kaiser et al., 2016), similar as shown in the present study (**Figure 6A**).

The decrease in initial g_s in the wildtype upon high VPD (**Figure 3C**) translated into a marked decrease in C_i during

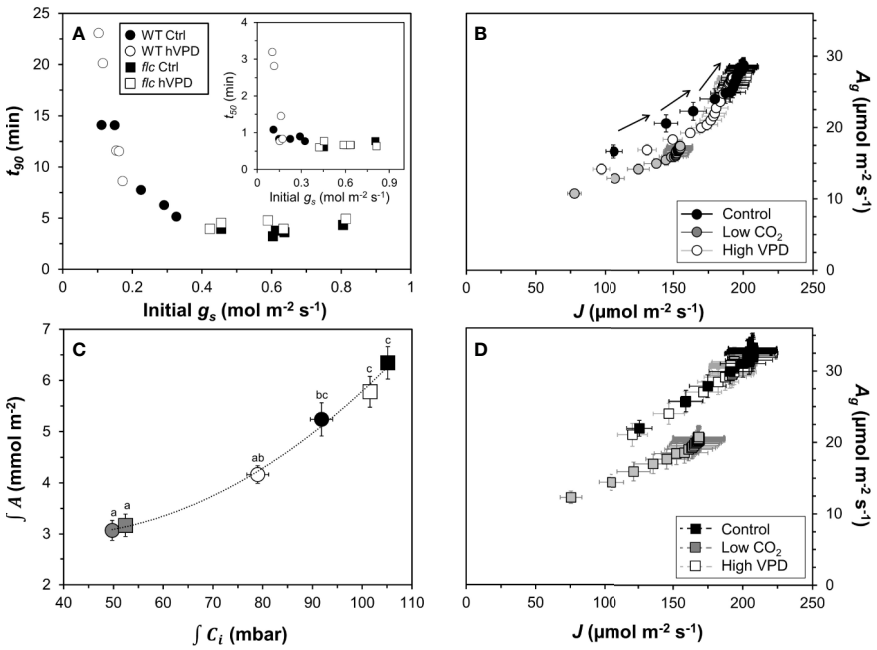

FIGURE 6 | Effects of stomatal conductance on photosynthetic induction. **(A)** relationship between stomatal conductance of leaves adapted to 50 µmol m^{-2} s^{-1} PAR (initial g_s) and time to reach 90% of full photosynthetic induction (t_{90}) after a switch to high irradiance, inset: relationship between initial g_s and t_{50}; **(B)** relationship between electron transport rate (J) and gross photosynthesis rate (A_g) in the wildtype, arrows show sequence in which data were logged; **(C)** relationship between integrated net photosynthesis rate ($\int A$) and integrated leaf internal CO_2 partial pressure ($\int C_i$) during the first five minutes of photosynthetic induction, different letters indicate statistically significant (P<0.05) differences between treatments; **(D)** relationship between J and A_g in *flacca*. Experimental conditions identical to those described under **Figure 3**. Symbols represent averages ± SEM, n = 5.

photosynthetic induction (**Figures 3E** and **6C**). This decrease was less strong in control conditions and was barely visible in *flacca* under control or high VPD (**Figure 3F**), as initial g_s in *flacca* did not react to high VPD (**Figure 3D**). The reduced transient availability of C_i decreased the rate of photosynthetic induction in the wildtype under high VPD (**Figure 3A**). This reduction, in turn, fed back on dynamic Φ_{PSII} (which was slowed down; first 15 minutes in **Figure 5A**), *NPQ* (which initially increased to higher levels and then relaxed less quickly than under control conditions; **Figure 5C**) and the relationship between gross photosynthesis and electron transport (**Figure 6B**). Unlike initial g_s, stomatal opening (difference between initial and final g_s) was not different between wildtype and *flacca* leaves under control (~0.4 mol m^{-2} s^{-1}) and high VPD conditions (~0.3 mol m^{-2} s^{-1}; **Table 1**).

Perhaps surprisingly, photosynthetic induction was not different between genotypes under low CO_2 partial pressure (**Figures 3** and **4**). This may be explained in two ways: firstly, initial g_s in the wildtype increased, from 0.22 mol m^{-2} s^{-1} at 400 µbar to 0.34 mol m^{-2} s^{-1} at 200 µbar, while that in *flacca* did not (**Table 1**). This g_s increase in wildtype leaves almost halved the difference in initial g_s between genotypes (0.4 → 0.24 mol m^{-2} s^{-1}). Secondly, any positive effect that the remaining difference in initial g_s may have had on photosynthetic induction in *flacca* was probably additionally decreased by low CO_2 availability.

Initial g_s in Leaves Lacking ABA Does Not React to Low CO_2 or High VPD

A striking finding of the present study was that while g_s in wildtype leaves (as expected) increased upon reductions in CO_2 partial pressure (**Figure 3C**, **Table 1**), g_s in *flacca* was virtually unchanged (**Figure 3D**). This confirms that ABA is part of the CO_2 signalling pathway in stomatal regulation (reviewed in Engineer et al., 2016). Under high VPD (15 mbar), g_s in *flacca* leaves adapted to low irradiance was similar to that at low VPD (7 mbar; **Figure 3D**). In wildtype leaves, stomata again responded as expected, by reducing their aperture under increased VPD (**Figure 3C**). At high irradiance, however, g_s in *flacca* did respond to the increase in VPD, as its value was reduced by ~0.15 mol m^{-2} s^{-1} compared to that at 7 mbar (**Table 1**). While there is ongoing controversy about the role of ABA in stomatal sensing of humidity, Merilo et al. (2018) showed that a number of genotypes that are either ABA deficient or ABA insensitive closed their stomata when exposed to an increase in VPD (at 150–500 µmol m^{-2} s^{-1} PAR). The authors explained this phenomenon (which is at variance with Mcadam et al., 2015; McAdam et al., 2016) as most likely being a hydropassive response, resulting from much higher initial g_s in ABA mutants, and thus a greater drop in humidity in the substomatal cavity (Merilo et al., 2018).

Limitations of the Study

In this study, we only used one mutant (*flacca*, LA0673) to examine the effects of open stomata on the rate of photosynthetic induction. Ideally, a larger number of mutants, each resulting in differential g_s relative to its wildtype, should be used; this to make sure that the observed effects on photosynthetic induction were truly caused by g_s rather than some other putative effects of the flacca mutation. Secondly, during growth *flacca* plants were regularly sprayed with ABA, following the recommendations of Imber and Tal (1970). It may be that this ABA application triggered unwanted responses in the plants, although based on all results presented here it seems that photosynthesis was fully functional in *flacca*.

CONCLUSIONS AND OUTLOOK

The current study suggests that in wildtype leaves, g_s exerts a substantial limitation on non-steady state photosynthesis. The *flacca* mutant can partially overcome this limitation through stomata that remain open in low light, resulting in substantially reduced t_{90} in ambient CO_2 partial pressure (t_{90} was 36–46% in in *flacca* relative to wildtype values). Nevertheless, while *flacca* is a good system for testing (dynamic) stomatal limitation in the laboratory, breeding for a similar stomatal behaviour will not be useful for most crops (except possibly for production in wetland areas), as this improvement of photosynthesis in fluctuating light will come with a significant reduction in water use efficiency and a major fitness disadvantage. A more promising approach may be to improve stomatal responsiveness to light intensity fluctuations, as this can potentially increase both light and water use efficiency under fluctuating light intensities. Recent, promising examples of increased g_s responsiveness are the BLINK1 transformant (Papanatsiou et al., 2019) and the PATROL1 overexpressor (Kimura et al., 2020).

DATA AVAILABILITY STATEMENT

All datasets presented in this study are included in the article/ **Supplementary Material**.

AUTHOR CONTRIBUTIONS

EK and AM designed the study with input from all other authors. EK performed measurements and data analysis. EK wrote the manuscript with input from all other authors.

ACKNOWLEDGMENTS

We thank the C.M. Rick Tomato Genome Resource Center (TGRC) for kindly supplying us with *flacca* and wildtype seeds.

SUPPLEMENTARY MATERIAL

The Supplementary Material for this article can be found online at: https://www.frontiersin.org/articles/10.3389/fpls.2020.01317/full#supplementary-material

REFERENCES

Acevedo-Siaca, L. G., Coe, R., Wang, Y., Kromdijk, J., Quick, W. P., and Long, S. P. (2020). Variation in photosynthetic induction between rice accessions and its potential for improving productivity. *New Phytol.* 227, 1097–1108. doi: 10.1111/nph.16454. 10.1111/np.

Allen, M. T., and Pearcy, R. W. (2000). Stomatal behavior and photosynthetic performance under dynamic light regimes in a seasonally dry tropical rain forest. *Oecologia* 122, 470–478. doi: 10.1007/s004420050968

Baker, N. R., Harbinson, J., and Kramer, D. M. (2007). Determining the limitations and regulation of photosynthetic energy transduction in leaves. *Plant Cell Environ.* 30, 1107–1125. doi: 10.1111/j.1365-3040.2007.01680.x

Bradford, K. J., Sharkey, T. D., and Farquhar, G. D. (1983). Gas exchange, stomatal behavior, and delta13C values of the flacca tomato mutant in relation to abscisic acid. *Plant Physiol.* 72, 245–250. doi: 10.1104/pp.72.1.245

Dinno, A. (2017).Dunn's Test of Multiple Comparisons Using Rank Sums. Available at: https://cran.r-project.org/web/packages/dunn.test/dunn.test.pdf (Accessed last accessed June 7, 2020).

Engineer, C. B., Hashimoto-Sugimoto, M., Negi, J., Israelsson-Nordström, M., Azoulay-Shemer, T., Rappel, W.-J., et al. (2016). CO2 sensing and CO2 regulation of stomatal conductance: advances and open questions. *Trends Plant Sci.* 21, 16–30. doi: 10.1016/j.tplants.2015.08.014

Harley, P. C., Loreto, F., Di Marco, G., and Sharkey, T. D. (1992). Theoretical considerations when estimating the mesophyll conductance to CO2 flux by analysis of the response of photosynthesis to CO2. *Plant Physiol.* 98, 1429–1436. doi: 10.1104/pp.98.4.1429

Imber, D., and Tal, M. (1970). Phenotypic reversion of flacca, a wilty mutant of tomato, by abscisic acid. *Sci. (80-.).* 169, 592–593. doi: 10.1126/science.169.3945.592

Kaiser, E., Morales, A., Harbinson, J., Kromdijk, J., Heuvelink, E., and Marcelis, L. F. M. (2015). Dynamic photosynthesis in different environmental conditions. *J. Exp. Bot.* 66, 2415–2426. doi: 10.1093/jxb/eru406

Kaiser, E., Morales, A., Harbinson, J., Heuvelink, E., Prinzenberg, A. E., and Marcelis, L. F. M. (2016). Metabolic and diffusional limitations of photosynthesis in fluctuating irradiance in Arabidopsis thaliana. *Sci. Rep.* 6 (31252), 1–13 .doi: 10.1038/srep31252. 10.1038/sr.

Kaiser, E., Kromdijk, J., Harbinson, J., Heuvelink, E., and Marcelis, L. F. M. (2017a). Photosynthetic induction and its diffusional, carboxylation and electron transport processes as affected by CO2 partial pressure, temperature, air humidity and blue irradiance. *Ann. Bot.* 119, 191–205. doi: 10.1002/dvdy

Kaiser, E., Zhou, D., Heuvelink, E., Harbinson, J., Morales, A., and Marcelis, L. F. M. (2017b). Elevated CO2 increases photosynthesis in fluctuating irradiance regardless of photosynthetic induction state. *J. Exp. Bot.* 68, 5629–5640. doi: 10.1093/jxb/erx357

Kaiser, E., Morales, A., and Harbinson, J. (2018). Fluctuating light takes crop photosynthesis on a rollercoaster ride. *Plant Physiol.* 176, 977–989. doi: 10.1104/pp.17.01250

Kimura, H., Hashimoto-Sugimoto, M., Iba, K., Terashima, I., and Yamori, W. (2020). Improved stomatal opening enhances photosynthetic rate and biomass production in fluctuating light. *J. Exp. Bot.* 71, 2339–2350. doi: 10.1093/jxb/eraa090

Kromdijk, J., Glowacka, K., Leonelli, L., Gabilly, S. T., Iwai, M., Niyogi, K. K., et al. (2016). Improving photosynthesis and crop productivity by accelerating recovery from photoprotection. *Sci. (80-.).* 354, 857–861. doi: 10.1126/science.aai8878

Lawson, T., and Blatt, M. R. (2014). Stomatal size, speed, and responsiveness impact on photosynthesis and water use efficiency. *Plant Physiol.* 164, 1556–1570. doi: 10.1104/pp.114.237107

Lawson, T., and Weyers, J. (1999). Spatial and temporal variation in gas exchange over the lower surface of Phaseolus vulgaris L. primary leaves. *J. Exp. Bot.* 50, 1381–1391. doi: 10.1093/jxb/50.337.1381

Li, T., Kromdijk, J., Heuvelink, E., van Noort, F. R., Kaiser, E., and Marcelis, L. F. M. (2016). Effects of diffuse light on radiation use efficiency of two Anthurium cultivars depend on the response of stomatal conductance to dynamic light intensity. *Front. Plant Sci.* 7, 56. doi: 10.3389/fpls.2016.00056

Loriaux, S. D., Avenson, T. J., Welles, J. M., McDermitt, D. K., Eckles, R. D., Riensche, B., et al. (2013). Closing in on maximum yield of chlorophyll fluorescence using a single multiphase flash of sub-saturating intensity. *Plant Cell Environ.* 36, 1755–1570. doi: 10.1111/pce.12115

Matthews, J. S. A., Vialet-Chabrand, S. R. M., and Lawson, T. (2017). Diurnal variation in gas exchange: the balance between carbon fixation and water loss. *Plant Physiol.* 174, 614–623. doi: 10.1104/pp.17.00152

Mcadam, S. A. M., Sussmilch, F. C., Brodribb, T. J., and Ross, J. J. (2015). Molecular characterization of a mutation affecting abscisic acid biosynthesis and consequently stomatal responses to humidity in an agriculturally important species. *AoB Plants* 7, 1–11. doi: 10.1093/aobpla/plv091

McAdam, S. A. M., Sussmilch, F. C., and Brodribb, T. J. (2016). Stomatal responses to vapour pressure deficit are regulated by high speed gene expression in angiosperms. *Plant Cell Environ.* 39, 485–491. doi: 10.1111/pce.12633

McAusland, L., Vialet-Chabrand, S., Davey, P., Baker, N. R., Brendel, O., and Lawson, T. (2016). Effects of kinetics of light-induced stomatal responses on photosynthesis and water-use efficiency. *New Phytol.* 211, 1209–1220. doi: 10.1111/nph.14000

Merilo, E., Yarmolinsky, D., Jalakas, P., Parik, H., Tulva, I., Rasulov, B., et al. (2018). Stomatal VPD response: there is more to the story than ABA. *Plant Physiol.* 176, 851–864. doi: 10.1104/pp.17.00912

Mizokami, Y., Noguchi, K., Kojima, M., Sakakibara, H., and Terashima, I. (2015). Mesophyll conductance decreases in the wild type but not in an ABA-deficient mutant (aba1) of Nicotiana plumbaginifolia under drought conditions. *Plant Cell Environ.* 38, 388–398. doi: 10.1111/pce.12394

Morales, A., Kaiser, E., Yin, X., Harbinson, J., Molenaar, J., Driever, S. M., et al. (2018). Dynamic modelling of limitations on improving leaf CO2 assimilation under fluctuating irradiance. *Plant Cell Environ.* 41, 589–604. doi: 10.1111/pce.13119

Ort, D. R., Merchant, S. S., Alric, J., Barkan, A., Blankenship, R. E., Bock, R., et al. (2015). Redesigning photosynthesis to sustainably meet global food and bioenergy demand. *Proc. Natl. Acad. Sci.* 112, 8529–8536. doi: 10.1073/pnas.1424031112

Oxborough, K., and Baker, N. R. (1997). Resolving chlorophyll a fluorescence images of photosynthetic efficiency into photochemical and non-photochemical components - Calculation of qP and Fv'/Fm' without measuring Fo'. *Photosynth. Res.* 54, 135–142. doi: 10.1023/A:1005936823310

Papanatsiou, M., Petersen, J., Henderson, L., Wang, Y., Christie, J. M., and Blatt, M. R. (2019). Optogenetic manipulation of stomatal kinetics improves carbon assimilation,water use, and growth. *Sci. (80-.).* 363, 1456–1459. doi: 10.1126/science.aaw0046

Pearcy, R. W., Krall, J. P., and Sassenrath-Cole, G. F. (1996). "Photosynthesis in fluctuating light environments," in *Photosynthesis and the Environment*. Ed. N. R. Baker (Dordrecht, the Netherlands: Kluwer Academic), 321–346. doi: 10.1007/0-306-48135-9_13

Prinsley, R. T., and Leegood, R. C. (1986). Factors affecting photosynthetic induction in spinach leaves. *Biochim. Biophys. Acta* 849, 244–253. doi: 10.1016/0005-2728(86)90031-9

R Core Team. (2020). R: A language and environment for statistical computing. (Vienna, Austria: R Foundation for Statistical Computing). Available at: https://www.R-project.org/.

Raissig, M. T., Matos, J. L., Gil, M. X. A., Kornfeld, A., Bettadapur, A., Abrash, E., et al. (2017). Mobile MUTE specifies subsidiary cells to build physiologically improved grass stomata. *Sci. (80-.).* 355, 1215–1218. doi: 10.1126/science.aal3254

Sagi, M., Scazzocchio, C., and Fluhr, R. (2002). The absence of molybdenum cofactor sulfuration is the primary cause of the flacca phenotype in tomato plants. *Plant J.* 31, 305–317. doi: 10.1046/j.1365-313X.2002.01363.x

Sharkey, T. D. (2016). What gas exchange data can tell us about photosynthesis. *Plant Cell Environ.* 39, 1161–1163. doi: 10.1111/pce.12641

Soleh, M. A., Tanaka, Y., Nomoto, Y., Iwahashi, Y., Nakashima, K., Fukuda, Y., et al. (2016). Factors underlying genotypic differences in the induction of photosynthesis in soybean [Glycine max (L.) Merr.]. *Plant Cell Environ.* 131, 305–315 .doi: 10.1111/pce.12674

Stitt, M., and Grosse, H. (1988). Interactions between sucrose synthesis and CO2 fixation I. Secondary kinetics during photosynthetic induction are related to a delayed activation of sucrose synthesis. *J. Plant Physiol.* 133, 129–137. doi: 10.1016/S0176-1617(88)80127-5

Stitt, M., and Quick, W. P. (1989). Photosynthetic carbon partitioning: its regulation and posibilities for manipulation. *Physiol. Plant* 77, 633–641. doi: 10.1111/j.1399-3054.1989.tb05402.x

Tal, M., and Nevo, Y. (1973). Abnormal stomatal behavior and root resistance, and hormonal imbalance in three wilty mutants of tomato. *Biochem. Genet.* 8, 291–300. doi: 10.1007/BF00486182

Tal, M. (1966). Abnormal Stomatal Behavior in Wilty Mutants of Tomato. *Plant Physiol.* 41, 1387–1391. doi: 10.1104/pp.41.8.1387

Tanaka, Y., Adachi, S., and Yamori, W. (2019). Natural genetic variation of the photosynthetic induction response to fluctuating light environment. *Curr. Opin. Plant Biol.* 49, 52–59. doi: 10.1016/j.pbi.2019.04.010

Taylor, S. H., and Long, S. P. (2017). Slow induction of photosynthesis on shade to sun transitions in wheat may cost at least 21% of productivity. *Philos. Trans. R. Soc B* 372, 1–9. doi: 10.1098/rstb.2016.0543

Tinoco-Ojanguren, C., and Pearcy, R. W. (1993). Stomatal dynamics and its importance to carbon gain in two rainforest Piper species. II. Stomatal versus biochemical limitations during photosynthetic induction. *Oecologia* 94, 395–402.

Tomimatsu, H., and Tang, Y. (2012). Elevated CO2 differentially affects photosynthetic induction response in two Populus species with different stomatal behavior. *Oecologia* 169, 869–878. doi: 10.1007/s00442-012-2256-5

Tomimatsu, H., Sakata, T., Fukayama, H., and Tang, Y. (2019). Short-term effects of high CO2 accelerate photosynthetic induction in Populus koreana × trichocarpa with always-open stomata regardless of phenotypic changes in high CO2 growth conditions. *Tree Physiol.* 39, 474–483. doi: 10.1093/treephys/tpy078

Urban, O., Šprtová, M., Košvancová, M., Lichtenthaler, H. K., and Marek, M. V. (2008). Comparison of photosynthetic induction and transient limitations during the induction phase in young and mature leaves from three poplar clones. *Tree Physiol.* 28, 1189–1197. doi: 10.1093/treephys/28.8.1189

Valladares, F., Allen, M. T., and Pearcy, R. W. (1997). Photosynthetic responses to dynamic light under field conditions in six tropical rainforest shrubs occuring along a light gradient. *Oecologia* 111, 505–514. doi: 10.1007/s004420050264

Vialet-chabrand, S. R. M., Matthews, J. S. A., McAusland, L., Blatt, M. R., Griffiths, H., and Lawson, T. (2017). Temporal dynamics of stomatal behavior: Modeling and implications for photosynthesis and water use. *Plant Physiol.* 174, 603–613. doi: 10.1104/pp.17.00125

Vico, G., Manzoni, S., Palmroth, S., and Katul, G. (2011). Effects of stomatal delays on the economics of leaf gas exchange under intermittent light regimes. *New Phytol.* 192, 640–652. doi: 10.1111/j.1469-8137.2011.03847.x

Way, D. A., and Pearcy, R. W. (2012). Sunflecks in trees and forests: from photosynthetic physiology to global change biology. *Tree Physiol.* 32, 1066–1081. doi: 10.1093/treephys/tps064

Woodrow, I. E., and Mott, K. A. (1989). Rate limitation of non-steady-state photosynthesis by Ribulose-1,5-bisphosphate Carboxylase in spinach. *Aust. J. Plant Physiol.* 16, 487–500. doi: 10.1071/PP9890487

Yamori, W., Kusumi, K., Iba, K., and Terashima, I. (2020). Increased stomatal conductance induces rapid changes to photosynthetic rate in response to naturally fluctuating light conditions in rice. *Plant Cell Environ.* 43, 1230–1240. doi: 10.1111/pce.13725

Yin, X., Struik, P. C., Romero, P., Harbinson, J., Evers, J. B., Van Der Putten, P. E. L., et al. (2009). Using combined measurements of gas exchange and

chlorophyll fluorescence to estimate parameters of a biochemical C3 photosynthesis model: a critical appraisal and a new integrated approach applied to leaves in a wheat (Triticum aestivum) canopy. *Plant Cell Environ.* 32, 448–464. doi: 10.1111/j.1365-3040.2009.01934.x

Zhang, Y., Kaiser, E., Zhang, Y., Yang, Q., and Li, T. (2018). Short-term salt stress strongly affects dynamic photosynthesis, but not steady-state photosynthesis, in tomato (Solanum lycopersicum). *Environ. Exp. Bot.* 149, 109–119. doi: 10.1016/j.envexpbot.2018.02.014

Zhang, Y., Kaiser, E., Marcelis, L. F. M., Yang, Q., and Li, T. (2020). Salt stress and fluctuating light have separate effects on photosynthetic acclimation, but interactively affect biomass. *Plant Cell Environ.* 1–15. doi: 10.1111/pce.13810

Conflict of Interest: The authors declare that the research was conducted in the absence of any commercial or financial relationships that could be construed as a potential conflict of interest.

frontiers in Plant Science

ORIGINAL RESEARCH
published: 01 September 2020
doi: 10.3389/fpls.2020.01308

Rice Cultivar Takanari Has Higher Photosynthetic Performance Under Fluctuating Light Than Koshihikari, Especially Under Limited Nitrogen Supply and Elevated CO_2

Satoshi Ohkubo[1], *Yu Tanaka*[2], *Wataru Yamori*[3*] *and Shunsuke Adachi*[1,4*]

[1] Institute of Global Innovation Research, Tokyo University of Agriculture and Technology, Fuchu, Japan, [2] Graduate School of Agriculture, Kyoto University, Kyoto, Japan, [3] Graduate School of Agricultural and Life Sciences, Institute for Sustainable Agro-Ecosystem Services, The University of Tokyo, Nishitokyo, Japan, [4] College of Agriculture, Ibaraki University, Inashiki, Japan

OPEN ACCESS

Edited by:
Paolo Longoni,
Université de Neuchâtel, Switzerland

Reviewed by:
Wei Huang,
Chinese Academy of Sciences, China
Elias Kaiser,
Wageningen University and Research, Netherlands

***Correspondence:**
Wataru Yamori
yamori@g.ecc.u-tokyo.ac.jp
Shunsuke Adachi
shunsuke.adachi.0210@vc.ibaraki.ac.jp

Specialty section:
This article was submitted to Plant Abiotic Stress, a section of the journal Frontiers in Plant Science

Received: 12 June 2020
Accepted: 11 August 2020
Published: 01 September 2020

Citation:
Ohkubo S, Tanaka Y, Yamori W and Adachi S (2020) Rice Cultivar Takanari Has Higher Photosynthetic Performance Under Fluctuating Light Than Koshihikari, Especially Under Limited Nitrogen Supply and Elevated CO_2. Front. Plant Sci. 11:1308. doi: 10.3389/fpls.2020.01308

Plants in the field experience dynamic changes of sunlight rather than steady-state irradiation. Therefore, increasing the photosynthetic rate of an individual leaf under fluctuating light is essential for improving crop productivity. The high-yielding *indica* rice (*Oryza sativa* L.) cultivar Takanari is considered a potential donor of photosynthesis genes because of its higher steady-state photosynthesis at both atmospheric and elevated CO_2 concentrations than those of several Japanese commercial cultivars, including Koshihikari. Photosynthetic induction after a sudden increase in light intensity is faster in Takanari than in Koshihikari, but whether the daily carbon gain of Takanari outperforms that of Koshihikari under fluctuating light in the field is unclear. Here we report that Takanari has higher non-steady-state photosynthesis, especially under low nitrogen (N) supply, than Koshihikari. In a pot experiment, Takanari had greater leaf carbon gain during the initial 10 min after a sudden increase in irradiation and higher daily CO_2 assimilation under simulated natural fluctuating light, at both atmospheric (400 ppm) and elevated (800 ppm) CO_2 concentrations. The electron transport rate during a day under field conditions with low N supply was also higher in Takanari than in Koshihikari. Although the advantages of Takanari were diminished under high N supply, photosynthetic N use efficiency was consistently higher in Takanari than in Koshihikari, under both low and high N supply. This study demonstrates that Takanari is a promising donor parent to use in breeding programs aimed at increasing CO_2 assimilation in a wide range of environments, including future higher CO_2 concentrations.

Keywords: CO_2, electron transport, nitrogen, non-steady-state photosynthesis, rice, stomatal conductance

INTRODUCTION

Most of the research programs conducted to improve photosynthetic performance of leaves through genetic engineering and conventional breeding have examined CO_2 assimilation rate (A) at steady-state conditions in stable light environments (Yamori et al., 2016; Sage et al., 2017; Simkin et al., 2019). However, plants grown in the field often experience fluctuating sunlight during the day due

to clouds, wind, and self-shading, and they rarely display steady-state photosynthesis (Pearcy, 1990; Pearcy et al., 1996; Leakey et al., 2004; Lawson et al., 2012; Slattery et al., 2018). In a soybean (*Glycine max* (L.) Merr.) canopy, for example, sunflecks contribute 40–90% of daily photosynthetic photon flux density (PPFD), with approximately one-third contributed by sunflecks shorter than 10 s (Pearcy, 1990). When the crop canopy is exposed to a sunfleck, leaf *A* gradually increases to reach a new steady-state level, which takes several seconds to minutes (Pearcy, 1990; Yamori, 2016; Tanaka et al., 2019). This process, which is termed photosynthetic induction, may reduce photosynthetic light use efficiency, and the photosystems may be damaged by excess sunlight (Yamori, 2016). The carbon loss due to photosynthetic induction was estimated to be at least 21.0% in wheat and 21.2% in soybean relative to steady-state light (Taylor and Long, 2017; Tanaka et al., 2019). Therefore, improving non-steady-state photosynthesis under fluctuating light is an essential challenge to increase crop productivity.

Natural genetic resources are potential donors for improvement of leaf photosynthesis (Flood et al., 2011; van Bezouw et al., 2019; Adachi et al., 2020). In rice (*Oryza sativa* L.), the steady-state *A* of the uppermost expanded leaves at reproductive stages varies from 11.9 to 32.1 μmol m^{-2} s^{-1} among 65 cultivars and landraces from the 'world core collection' harboring approximately 90% of worldwide allelic variation (Kojima et al., 2005; Kanemura et al., 2007). A wide range of genetic variation in steady-state *A* has also been observed among cultivars and breeding lines in rice (Jahn et al., 2011; Qu et al., 2017), wheat (*Triticum aestivum* L.; Carmo-Silva et al., 2017), soybean (Sakoda et al., 2016), and maize (*Zea mays* L.; Choquette et al., 2019). Quantitative trait locus analysis and genome-wide association studies were conducted to use these variations in crop breeding (Adachi et al., 2011; Adachi et al., 2019b; Wang et al., 2020). Very recently, Acevedo-Siaca et al. (2020) reported a difference of 109% in the total amount of CO_2 fixed during the first 5 min of induction after a sudden increase in irradiance (CCF_5) among 14 rice accessions. Wide differences of carbon gain during photosynthetic induction between cultivars have also been observed in wheat with percentage genetic difference of 80% in the time required for 95% induction (Salter et al., 2019), and soybean with percentage genetic difference of 580% in CCF_5 (Soleh et al., 2016; Soleh et al., 2017). However, our understanding of genetic variation of non-steady-state photosynthesis is still limited relative to that of steady-state photosynthesis, which prohibits to develop breeding strategies for enhancing canopy photosynthetic capacity in the field conditions (Tanaka et al., 2019).

Koshihikari and Takanari have been considered model rice cultivars for the past decade owing to the contrasting properties of their photosynthesis (Taylaran et al., 2011). The *japonica* cultivar Koshihikari is the most widely grown cultivar in Japan owing to its high grain quality, despite its moderate photosynthetic capacity and grain yield (Adachi et al., 2020). The *indica* cultivar Takanari, developed for forage and processing rather than human consumption, has one of the highest grain yields among Japanese rice cultivars (Xu et al., 1997; Imbe et al., 2004). Takanari has one of the highest steady-state *A* values of the flag leaf among the 65 abovementioned cultivars (Kanemura et al., 2007). Its high *A* is largely explained by high leaf nitrogen (N) content due to high N accumulation, and high stomatal conductance (g_s) due to large water uptake capacity (Taylaran et al., 2011; Muryono et al., 2017), and could be also associated with higher mesophyll conductance (g_m) than that of Koshihikari (Chen et al., 2014). The high leaf photosynthetic capacity of Takanari, especially at the reproductive stage, increases crop growth rate and eventually yield (Xu et al., 1997; Takai et al., 2006; Taylaran et al., 2011). Koshihikari, Takanari, and their introgression lines have been widely used for genetic studies of photosynthesis (Takai et al., 2013; Adachi et al., 2019b) and other physiological traits (Takai et al., 2014; Ookawa et al., 2016; San et al., 2018). Takanari also has higher steady-state photosynthesis than Koshihikari at elevated CO_2 in free-air CO_2 enrichment (FACE) experiments (Chen et al., 2014; Ikawa et al., 2019). We have reported that Takanari has a greater photosynthetic induction response to a sudden increase in irradiance than Koshihikari, which could be explained by a combination of a faster response of electron transport rate, larger accumulation of metabolites in the Calvin cycle, and rapid elevation of g_s (Adachi et al., 2019a). Although Takanari has high steady-state *A* and fast photosynthetic induction, its photosynthesis must be evaluated under field conditions with fluctuating light for judgment of its potential value as a donor cultivar in rice breeding programs.

Nitrogen is the primary determinant of leaf photosynthesis because large amounts of leaf N are allocated to ribulose-1,5-bisphosphate carboxylase/oxygenase (Rubisco) and other photosynthetic proteins (Makino et al., 2003). Leaf N content is closely correlated with steady-state *A* in rice (Cook and Evans, 1983; Hirasawa et al., 2010). It was recently reported that elevated leaf N content enhances the photosynthetic induction response in rice (Sun et al., 2016). High N supply also alleviates heat stress under fluctuating light in rice (Huang et al., 2017). Therefore, N may play an important role in the non-steady-state photosynthesis as well as steady-state photosynthesis. Elevated CO_2 concentration facilitates photosynthetic induction under fluctuating light (Leakey et al., 2002; Kaiser et al., 2017), which can be explained by a decreased limitation of CO_2 diffusion from air into chloroplasts, increased post-irradiance CO_2 fixation, and decreased post-irradiance CO_2 burst (Leakey et al., 2004). It is reported that a poplar species with low stomatal conductance showed lower photosynthetic induction than another poplar species with high stomatal conductance under atmospheric CO_2, but the difference was disappeared under elevated CO_2 due to the decreased limitation of stomata (Tomimatsu and Tang, 2012). To develop breeding strategies to enhance photosynthesis under elevated CO_2, the genetic interactions of photosynthetic induction with N supply and CO_2 concentration should be investigated.

Here, we evaluated the photosynthetic responses of Koshihikari and Takanari to a sudden increase in irradiance and the daily photosynthetic carbon gain under fluctuating light conditions mimicking a typical summer day, with different N supplies and at different CO_2 concentrations. We also examined the dynamics of electron transport rate using a pulse-amplitude-modulation (PAM) chlorophyll fluorometer in the field. We

conclude that Takanari is a promising genetic resource for improving non-steady-state photosynthesis, especially under limited N supply at high CO_2 concentrations.

MATERIALS AND METHODS

Plant Materials and Growth Conditions for Pot Experiments

Seeds of rice cultivars Takanari and Koshihikari were sown in nursery boxes filled with artificial soil, and the seedlings were grown until the 4th leaf stage in a greenhouse in 2018. The minimum and maximum temperatures inside the greenhouse were approximately 10 and 35°C, respectively. The seedlings were transplanted into 3-L pots (one per pot) with two different rates of N fertilization. For the low N supply (LN), the pots were filled with a 14:3:3 (v/v/v) mixture of sand, paddy soil (an alluvial clay loam), and upland soil (a diluvial volcanic ash) containing fertilizer (0.3 g of N as ammonium nitrate, and 0.5 g each of P as P_2O_5 and K as K_2O per pot). For the high N supply (HN), the pots were filled with a 1:1 (v/v) mixture of paddy and upland soils containing fertilizer (0.5 g of N as ammonium nitrate and 0.5 g each of P as P_2O_5 and K as K_2O per pot); additional fertilizer (0.5 g of N as ammonium nitrate per pot) was applied at 36 and 50 days after transplanting. The pots were placed in an experimental field of Tokyo University of Agriculture and Technology in Fuchu, Japan (35°41′N, 139°29′E), and the level of standing water was maintained at 2 to 4 cm above the soil. The minimum and maximum temperatures during the growth were approximately 10 and 32°C, and peak PPFD value on clear days was 1,200 μmol photons m^{-2} s^{-1}.

Measurements and Calculations of Photosynthetic Induction

The response of photosynthesis to a sudden increase in irradiance was measured with a LI-6400XT portable photosynthesis system (Li-Cor, Lincoln, NE, USA) using a leaf chamber fluorometer (LI-6400-40). Plants in their pots were transferred to a dark room in the evening before each measurement. Next morning, leaves were enclosed in the leaf chamber of the LI-6400XT and adapted to the background irradiance (50 μmol photons m^{-2} s^{-1}) at either 400 or 800 ppm CO_2 for 20 min at 28°C of leaf chamber temperature. Then irradiance was suddenly increased to 1,500 μmol photons m^{-2} s^{-1}. Gas exchange parameters were automatically recorded every 10 s. The A and g_s values during photosynthetic induction were individually fitted to sigmoidal curves according to Kaiser et al. (2017). Cumulative CO_2 fixation (CCF_{10}) after the step increase in irradiance was calculated as the integrated sum of A over 10 min. After the measurement of photosynthetic induction, the responses to different levels of PPFD and CO_2 were measured according to Yamori et al. (2020). Maximum rates of carboxylation (V_{cmax}) and electron transport (J_{max}) were estimated from A–C_i response curves as in Adachi et al. (2017), except that some parameters were changed to those in Bernacchi et al. (2001) at 30°C which is the average value of leaf temperature during A–C_i response curve measurements (K_c = 690.05 μmol m^{-2} s^{-1}, K_o = 353.02 mmol m^{-2} s^{-1}, Γ^* = 55.22 μmol mol^{-1}, R_d = 1.37 μmol m^{-2} s^{-1}). The biochemical and diffusional limitation during photosynthetic induction were analyzed according to Kaiser et al. (2017).

Photosynthesis Under Simulated Field Light Condition

The diurnal changes in gas exchange rate were measured with the LI-6400XT and the LI-6400-40. To mimic a typical light environment in the canopy, PPFD values were recorded in the paddy field as in Adachi et al. (2019a). Typical daily light conditions over 12 h were replicated in the LI-6400XT chamber under the control of an auto-measuring program. Plants in their pots were transferred to a dark room in the evening before each measurement. The same leaf as was used for the photosynthetic induction measurement was also used for this measurement, but in a different part to avoid damage from the previous measurement. The leaf was enclosed in the leaf chamber at 05:55, kept in the dark for 3 min, and then irradiated at 70 μmol photons m^{-2} s^{-1} for 2 min. The auto-measuring program was initiated at 06:00. Gas exchange parameters were automatically recorded every 10 s and chlorophyll fluorescence parameters every 2 min for 12 h. Leaf chamber temperature was maintained at 28°C and CO_2 concentration at either 400 or 800 ppm. The air flow rate into the chamber was set to 300 μmol s^{-2}. The leaf-to-air vapor pressure difference was 1.1–1.3 kPa. The blue and red ratio of the actinic light by LED-irradiance light source was kept at 10 and 90%, respectively. The intensity of a modulated measuring beam was 0.01 μmol photons m^{-2} s^{-1} during measurements. The steady-state fluorescence (F_s) and maximum fluorescence during a light-saturating pulse of ~8000 μmol photons m^{-2} s^{-1} (F_m') *via* multiple turnover flash were measured. The electron transport rate (ETR) through photosystem II (PSII) was calculated as:

$$ETR = 0.5 \times 0.84 \times \left(F_m' - F_s\right)/F_m' \times PPFD \quad (1)$$

where 0.5 is the fraction of absorbed light reaching PSII and 0.84 is the leaf absorptance (Kumagai et al., 2010; Dallagnol et al., 2015; Yamori et al., 2020). The value of nonphotochemical quenching (NPQ) was also calculated following to Yamori et al. (2011) and Shimadzu et al. (2019). The total daily carbon gain (integrated A) was calculated as the integrated sum of A values over the 12-h experiment.

Quantification of Nitrogen, Rubisco, and Chlorophyll Contents

Immediately after gas exchange measurement for 12 h, two 30-mm-long segments were excised from the center of each leaf used for the gas exchange measurements. One segment was quickly frozen in liquid nitrogen and stored at −80°C, and the other was dried at 80°C for 24 h. The dried sample was used for quantification of nitrogen content with a CN analyzer (MT700 Mark II, Yanako, Kyoto, Japan). The frozen sample was used for quantification of Rubisco and chlorophyll contents according to Yamori et al. (2012) with slight modifications. In brief, the leaf was ground in liquid nitrogen

with a mortar and pestle, and homogenized in 800 µl of extraction buffer (50 mM HEPES, pH 7.8, 10 mM $MgCl_2$, 1 mM EDTA·2Na, 0.1% [v/v] Triton X-100, 1.6% [w/v] polyvinyl pyrrolidone, and 5 mM (±)-dithiothreitol) and 24 µl of 25× cOmplete Protease Inhibitor Cocktail (Roche Diagnostics, Basel, Switzerland). After thorough mixing, a 100-µl aliquot was used for quantification of chlorophyll content, and the rest of the homogenate was used for quantification of Rubisco content. Chlorophylls were extracted with 80% (v/v) acetone and the concentrations of chlorophylls *a* and *b* were determined as in Porra et al. (1989). For Rubisco quantification, the homogenate was centrifuged (19,000× *g*, 4°C, 1 min) and 100-µl of supernatant was mixed with an equal volume of sample buffer (125 mM Tris·HCl, pH 6.8, 4% sodium dodecyl sulfate, 15% glycerol, and 0.02% bromophenol blue). The sample was heated at 95°C for 6 min and centrifuged (25,000× *g*, room temperature, 2 min). Proteins in the supernatant were separated by polyacrylamide gel electrophoresis (4.5% stacking gel and 12.5% resolving gel). The gel was stained with GelCode Blue Stain Reagent (Thermo Scientific, Waltham, MA, USA) and scanned with an optical scanner. The amount of Rubisco large subunit was determined in ImageJ software (National Institutes of Health, https://imagej.nih.gov/ij/) using bovine serum albumin as standard.

Chlorophyll Fluorescence Analysis Under Field Conditions

Seeds of Takanari and Koshihikari were sown in nursery boxes filled with artificial soil, and the seedlings were grown until the 4th leaf stage in a greenhouse in 2019. Plants were transplanted into a paddy field of Tokyo University of Agriculture and Technology (35°39′N, 139°28′E) on 22 May with the chemical fertilizers of 30 kg N, 60 kg P, and 60 kg K ha^{-1} as a basal dressing. The plant density was 22.2 plants m^{-2} (at a spacing of 30 cm × 15 cm). The experimental plots (each 4 m × 4.5 m) was arranged in a complete randomized block design with three replicates. To avoid border effects, a single plant near the center of each plot was selected for the measurements. Diurnal changes in chlorophyll fluorescence parameters were measured with six measuring heads attached to a Monitoring-PAM fluorometer (Waltz, Effeltrich, Germany) as described in Ikeuchi et al. (2014) and Ishida et al. (2014). Three measuring heads were applied for Koshihikari leaves and another three for Takanari leaves. The leaf clips of the fluorometer were fixed on the south-facing upright leaves. The fluorescence parameters and PPFD of sunlight were recorded every 3 min from 04:48 to 18:48 on 14 August. ETR was calculated as described above.

Statistical Analysis

All statistical analyses were performed in the R environment (R Core Team, 2018). The effects of genotype and N application on leaf N, Rubisco and chlorophyll contents, and parameters of steady-state photosynthesis were analyzed using two-way analysis of variance (ANOVA). The significance of the differences among four experimental groups (genotypes × N treatments) was tested with Tukey–Kramer's test using the *multcomp* R package. The differences in CCF_{10} and integrated *A* among eight experimental groups (genotypes × N treatments × CO_2 partial pressures) were also tested with Tukey–Kramer's test.

RESULTS

Steady-State Photosynthesis Under Different N Levels

The contents of leaf N, Rubisco, and chlorophyll, and steady-state photosynthesis values of plants grown in pots at different N levels are shown in **Table 1**. Under LN, leaf N and Rubisco contents were similar in Koshihikari and Takanari, but chlorophyll content was slightly higher in Takanari. Takanari had higher steady-state A_{400} by 29.8% and A_{800} by 32.0% than Koshihikari, and also had higher photosynthetic parameters including g_{s400}, g_{s800}, ETR_{400}, ETR_{800}, V_{cmax}, and J_{max} than Koshihikari. Thus, Takanari had higher photosynthetic capacity than Koshihikari under LN regardless of CO_2 concentrations. Under HN, leaf N content was lower, but Rubisco and chlorophyll contents were slightly higher in Takanari than in Koshihikari. Takanari had significantly lower values of ETR_{400} and J_{max} and tended to have lower A_{400}, A_{800}, ETR_{800}, and V_{cmax} than Koshihikari. These results indicate that an increase in N supply led to a higher N leaf accumulation in Koshihikari than in Takanari, resulting in higher photosynthetic capacity of Koshihikari. Takanari had higher *A* and ETR values at different values of C_i under LN, and lower *A* and ETR values under HN compared with Koshihikari (**Supplementary Figure S1**). Similar results were obtained for A_{400} and A_{800} responses to PPFD (**Supplementary Figure S2**).

At the same leaf N content, A_{400} and A_{800} (**Supplementary Figure S3A**), g_s (**Supplementary Figure S3B**), V_{cmax} (**Supplementary Figure S3C**), and J_{max} (**Supplementary Figure S3D**) were higher in Takanari than in Koshihikari. These results indicate that Takanari had higher photosynthetic N use efficiency owing to the elevated photochemical capacity, enzymatic activity, and gas diffusion conductance per leaf N content.

Initial Photosynthetic Carbon Gain After a Sudden Increase in Irradiation

After a sudden increase in irradiation, the A_{400} and A_{800} values of Takanari rapidly increased and became higher than those of Koshihikari under LN, but were similar to those of Koshihikari under HN (**Supplementary Figures S4A, B**). The g_s value increased faster in Takanari than in Koshihikari under all experimental settings (**Supplementary Figures S4C, D**). At both CO_2 concentrations, CCF_{10} was higher in Takanari under LN but not under HN (**Figure 1**). These results indicate that Takanari gains more carbon during photosynthetic induction under low N supply than does Koshihikari.

The biochemical limitation during photosynthetic induction was almost similar between the cultivars at any settings, except Koshihikari had higher biochemical limitation than Takanari at LN with 800 ppm CO_2 (**Supplementary Figures S5A, B**). The diffusional limitation in Takanari at 400 ppm CO_2 was remarkably lower than Koshihikari, while it was similar at 800 ppm CO_2 (**Supplementary Figures S5C, D**). This result indicates that the elevated g_s in Takanari especially increased photosynthetic induction at the ambient CO_2 condition. iWUE in Takanari during photosynthetic induction was consistently lower across the environments (**Supplementary Figures S4E, F**).

TABLE 1 | Leaf contents of N, Rubisco, and chlorophyll, and parameters of steady-state photosynthesis.

	Koshihikari		Takanari		ANOVA		
	LN	HN	LN	HN	Nitrogen(N)	Cultivar(C)	N × C
N (mmol m^{-2})	71 ± 1^{a}	136 ± 2^{c}	71 ± 2^{a}	110 ± 2^{b}	***	***	***
Rubisco (μmol m^{-2})	2.13 ± 0.10^{a}	4.37 ± 0.13^{b}	2.10 ± 0.22^{a}	4.79 ± 0.13^{b}	***	N.S.	N.S.
Chlorophyll (μmol m^{-2})	85 ± 3^{a}	221 ± 10^{b}	106 ± 5^{a}	244 ± 5^{c}	***	**	N.S.
A_{400} (μmol m^{-2} s^{-1})	14.4 ± 0.5^{a}	26.3 ± 1.9^{c}	18.7 ± 0.7^{ab}	23.2 ± 1.6^{bc}	***	N.S.	*
ETR_{400} (μmol m^{-2} s^{-1})	156 ± 3^{a}	235 ± 7^{c}	177 ± 7^{a}	202 ± 3^{b}	***	N.S.	***
g_{s400} (mol m^{-2} s^{-1})	0.27 ± 0.02^{a}	0.48 ± 0.07^{b}	0.46 ± 0.03^{b}	0.53 ± 0.04^{b}	**	*	N.S.
$C_i/C_{a\ 400}$	0.74 ± 0.01^{ab}	0.71 ± 0.01^{a}	0.79 ± 0.01^{c}	0.76 ± 0.01^{bc}	**	***	N.S.
A_{800} (μmol m^{-2} s^{-1})	23.1 ± 0.6^{a}	37.8 ± 1.4^{c}	30.5 ± 0.9^{b}	34.6 ± 0.7^{c}	***	*	***
ETR_{800} (μmol m^{-2} s^{-1})	162 ± 12^{a}	235 ± 2^{c}	193 ± 3^{b}	207 ± 6^{bc}	***	N.S.	**
g_{s800} (mol m^{-2} s^{-1})	0.22 ± 0.01^{a}	0.36 ± 0.02^{b}	0.40 ± 0.02^{b}	0.41 ± 0.03^{b}	**	***	**
$C_i/C_{a\ 800}$	0.75 ± 0.01^{a}	0.73 ± 0.02^{a}	0.80 ± 0.01^{b}	0.77 ± 0.01^{ab}	*	**	N.S.
V_{cmax} (μmol m^{-2} s^{-1})	85 ± 2^{a}	184 ± 6^{c}	120 ± 4^{b}	169 ± 7^{c}	***	*	***
J_{max} (μmol m^{-2} s^{-1})	125 ± 2^{a}	202 ± 6^{d}	157 ± 4^{b}	177 ± 5^{c}	***	N.S.	***
J_{max}/V_{cmax}	1.47 ± 0.05^{c}	1.10 ± 0.02^{a}	1.31 ± 0.04^{b}	1.05 ± 0.02^{a}	***	*	N.S.

*CO_2 concentrations (400 or 800 ppm) used to measure steady-state photosynthetic parameters are indicated by subscript numbers. ***P < 0.001; **P < 0.01; *P < 0.05; N.S., not significant at 0.05 probability level. Values are means ± SE (n = 8). Values followed by the same letter do not differ significantly among groups at P < 0.05 by Tukey–Kramer multiple comparison test.*

This indicates that Takanari is inferior in terms of water use efficiency due to its excess transpiration.

Photosynthetic Dynamics Under Simulated Fluctuating Light

The auto-measuring program allowed gas exchange measurements under fluctuating light mimicking that in the field (**Figure 2**, **Supplementary Figure S6**). Under LN, Takanari had higher A, g_s, and ETR than Koshihikari throughout the day at both CO_2 concentrations (**Figures 2A, B, E, F, Q, R**, **Supplementary Table S1**). The NPQ values tended to be lower in Takanari, especially at the high light phase, however no significant difference in daily mean NPQ was found between Takanari and Koshihikari (**Figures 2U, V**, **Supplementary Table S1**). The superior photosynthesis under LN in Takanari was also evident from the plots of A and g_s *versus* PPFD (**Supplementary Figure S7**).

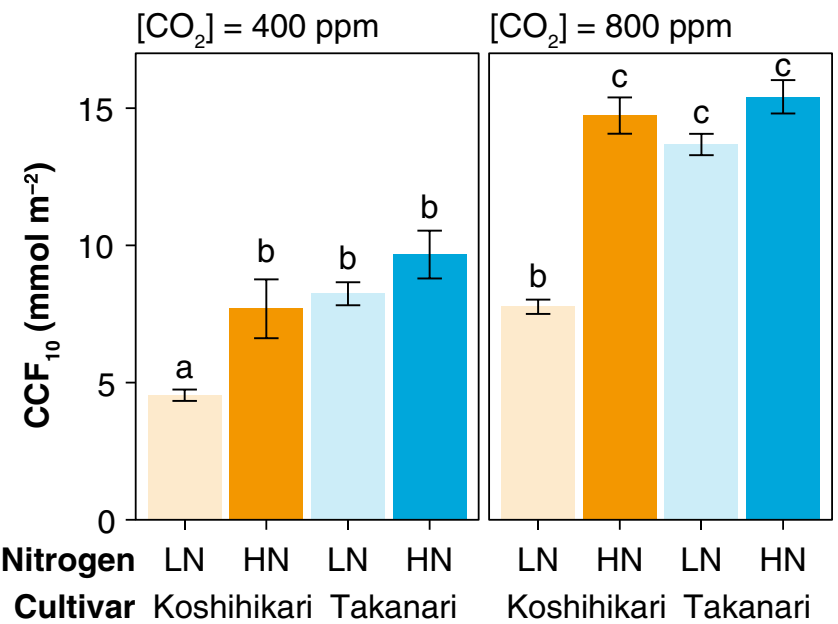

FIGURE 1 | Cumulative CO_2 fixation (CCF_{10}) during the first 10 min of photosynthetic induction after transition from low to high irradiation at different CO_2 concentrations. LN, low N supply; HN, high N supply. Values are means ± SE (n = 4). The same letter indicates no significant differences between groups at P < 0.05 by Tukey–Kramer multiple comparison test.

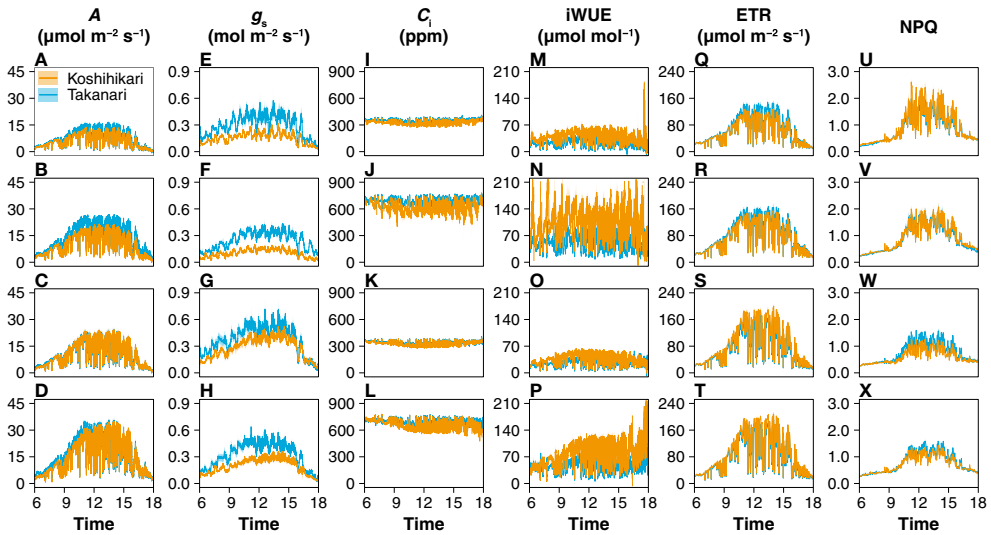

FIGURE 2 | Diurnal patterns of photosynthesis under simulated light conditions mimicking a typical summer day. **(A–D)** CO_2 assimilation rate (*A*), **(E–H)** stomatal conductance (g_s), **(I–L)** internal CO_2 concentration (C_i), **(M–P)** intrinsic water use efficiency (iWUE), **(Q–T)** electron transport rate (ETR), and **(U–X)** nonphotochemical quenching (NPQ). The combinations of the levels of N fertilization (LN, low N supply; HN, high N supply) and CO_2 concentrations (400 or 800 ppm) are shown on the left of the panels. Values are means ± SE (n = 4).

Under HN, the *A* values were similar between the cultivars at both CO_2 concentrations, whereas Takanari had higher g_s and lower ETR than Koshihikari (**Figures 2C, D, G, H, S, T**, **Supplementary Table S1**). NPQ values of Takanari tended to be higher than Koshihikari under HN, however no significant difference in daily mean NPQ was found (**Figures 2W, X**, **Supplementary Table S1**). The C_i value was significantly higher in Takanari than in Koshihikari under LN at 800 ppm CO_2, and tended to be higher in the other treatments, indicating that CO_2 diffusion from air (*i.e.*, CO_2 supply) *versus* biochemical demand in Takanari was always higher than Koshihikari (**Figures 2I–L**, **Supplementary Table S1**). The value of iWUE of Takanari was lower than Koshihikari throughout a day at the most of settings, indicating that Takanari has lower water use efficiency at any environmental conditions (**Figures 2M–P**, **Supplementary Table S1**). The cumulative values of *A* (integrated over a day) tended to be higher under LN at both CO_2 concentrations in Takanari than in Koshihikari, but were similar between the cultivars under HN (**Figure 3**). These values correlated with CCF_{10} irrespective of cultivar and treatment (**Figure 4A**), suggesting that a higher carbon gain during photosynthetic induction leads to a higher daily carbon gain under fluctuating light. Integrated *A* also correlated with steady-state *A* (**Figure 4B**), indicating that photosynthetic capacity is the primary determinant of the daily carbon gain. We also represented the correlation matrix of the observed parameters in **Supplementary Figure S8**.

At the same leaf N content and CO_2 concentration, integrated *A* was higher in Takanari than in Koshihikari (**Figure 4C**). Hence, the photosynthetic N use efficiency is higher in Takanari than in Koshihikari not only under steady-state (**Supplementary Figure S3A**) but also non-steady-state conditions, regardless of CO_2 concentration.

Photosynthetic Dynamics Under Field Conditions

In the field experiment, Takanari had higher ETR than Koshihikari, especially in the afternoon (**Figure 5B**), and a higher ETR in response to PPFD (**Figures 5A, C**). The integrated value of ETR in Takanari (3.44 ± 0.06 mol m^{-2} day^{-1}) was significantly higher in Koshihikari (2.86 ± 0.11 mol m^{-2} day^{-1}) (*t*-test, P = 0.017). These results indicate that Takanari has high photosynthetic performance under natural field conditions.

DISCUSSION

Enhancing photosynthesis of field crops is essential for further increase of food production. Selection and characterization of potential donor cultivars with efficient photosynthesis would contribute to establishing breeding strategies for increasing yield (Flood et al., 2011; van Bezouw et al., 2019; Furbank et al., 2020). Here, we found that the high-yielding *indica* cultivar Takanari has higher *A* under fluctuating light than the Japanese commercial cultivar Koshihikari, especially under LN and elevated CO_2 concentration.

Under LN and saturating irradiation, the steady-state A_{400} and A_{800} were higher in Takanari than in Koshihikari by approximately 30% (**Table 1**). This difference could be explained by the higher g_s, V_{cmax}, and J_{max} in Takanari, but not by the leaf N content (**Table 1**). Takanari had higher CCF_{10}

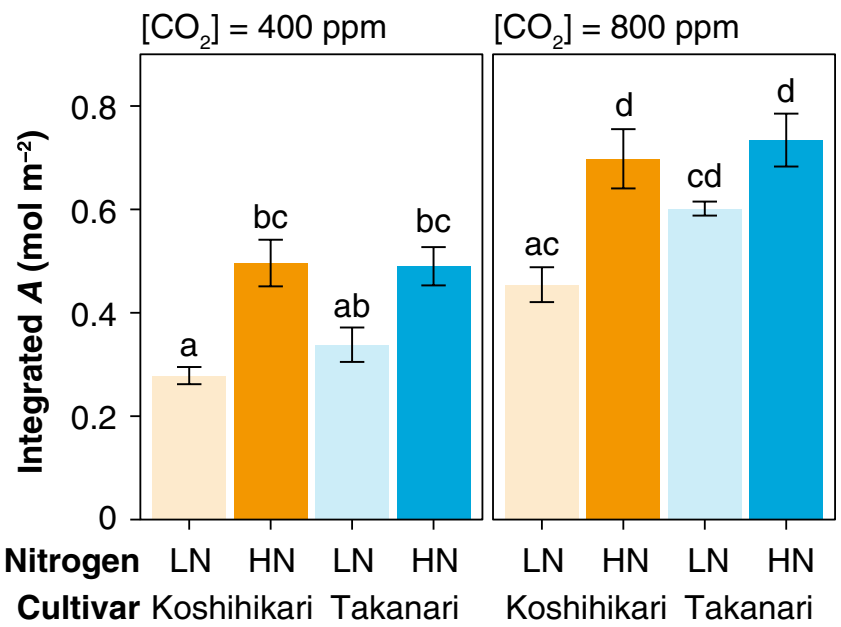

FIGURE 3 | Total daily carbon gain (integrated *A*) under simulated light conditions at different CO_2 concentrations. LN, low N supply; HN, high N supply. Data are integrated *A* values from **Figures 2A–D**. Values are means ± SE (n = 4). The same letter indicates no significant differences between groups at $P < 0.05$ by Tukey–Kramer multiple comparison test.

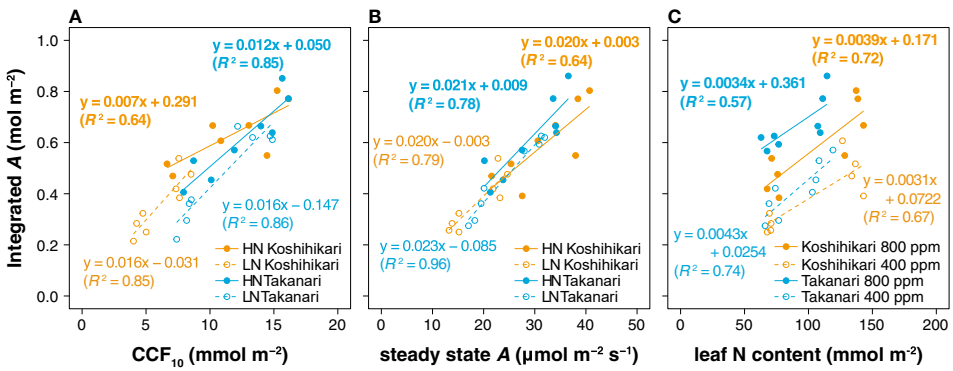

FIGURE 4 | Relationships between total daily carbon gain (integrated *A*) and **(A)** cumulative CO_2 fixation during the first 10 min of photosynthetic induction (CCF_{10}), **(B)** steady-state CO_2 assimilation rate (*A*), and **(C)** leaf nitrogen (N) content. Regression lines and equations are shown for individual cultivars and **(A, B)** N fertilization levels (LN, low N supply; HN, high N supply) or **(C)** CO_2 concentrations. R^2 values are determination coefficients.

at both CO_2 concentrations (**Figure 1**), indicating a larger carbon gain during photosynthetic induction after a sudden increase in irradiance. At both CO_2 concentrations, Takanari tended to have higher integrated *A* over a day under simulated fluctuating light conditions than Koshihikari (**Figure 3**). Takanari also showed higher ETR, a proxy for CO_2 assimilation, in a field with relatively low N input (**Figure 5**). Thus, Takanari had higher photosynthesis under both steady-state and non-steady-state conditions at both CO_2 concentrations tested. Higher steady-state photosynthesis in Takanari than in Koshihikari at a wide range of CO_2 concentrations has been reported (Taylaran et al., 2011; Chen et al., 2014; Ikawa et al., 2018; Adachi et al., 2019b; Ikawa et al., 2019). The published data and our current study strongly suggest that Takanari is a promising donor cultivar for genes useful for enhancing photosynthesis under field conditions at current and future CO_2 concentrations.

Excess light energy can induce photoinhibition, a photodamage of photosystems II and I, which is amplified by fluctuating light in natural field condition (Yamori, 2016). A leaf with lower photosynthetic capacity is subject to photoinhibition because the

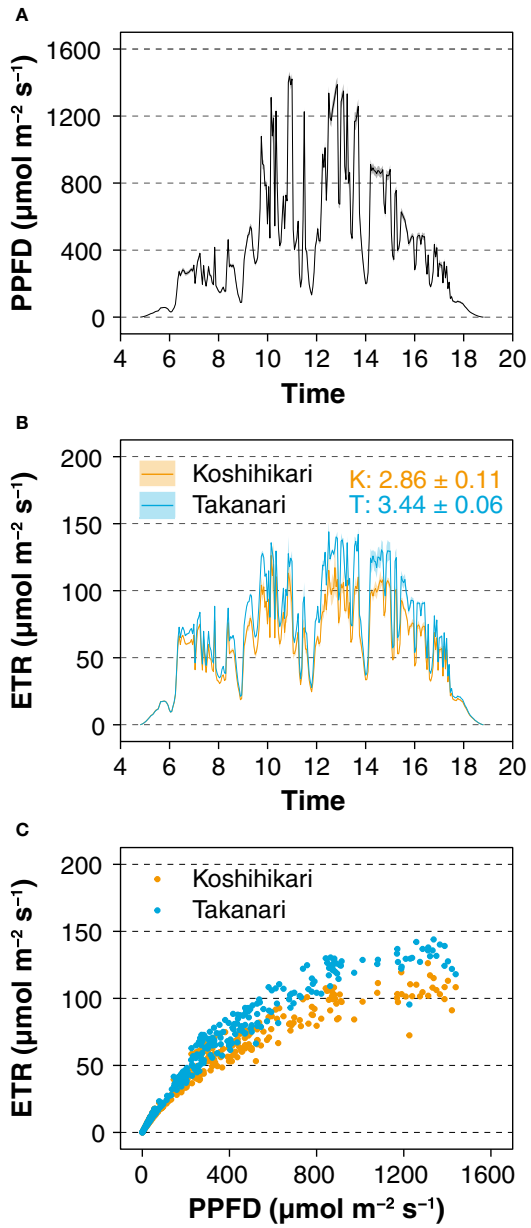

FIGURE 5 | Electron transport rate (ETR) measured by a pulse-amplitude-modulation (PAM) chlorophyll fluorometer in the field. **(A)** Diurnal pattern of photosynthetic photon flux density (PPFD). Values are means ± SE (n = 6). **(B)** Diurnal patterns of ETR. Values are means ± SE (n = 3). Numbers within the panel are integrated ETR values (means ± SE, n = 3) of Koshihikari (K) and Takanari (T). **(C)** Relationship between ETR and PPFD. The data were recorded every 3 min from 04:48 to 18:48 on 14 August 2019.

excess electrons accumulate in the photosystems and produce ROS within the thylakoid membranes, leading to degradation of photosynthetic proteins (Demmig-Adams et al., 1996). Therefore, photoinhibition in Koshihikari leaves under LN might be severer than Takanari, which could be anticipated by the lower A and the elevated thermal dissipation (*i.e.* NPQ) especially at the high light intensity during a day (**Figure 2**). Photoinhibition induced for several hours and days could decrease electron transport rate on the thylakoid membrane and eventually CO_2 assimilation rate (Aro et al., 1993; Long et al., 1994). The difference in CO_2 assimilation rate between Koshihikari and Takanari could be increased after several days of fluctuating light, which may enhance yield gap between the cultivars. The changes of photoinhibition for even longer period should be evaluated in future research.

Under HN, however, leaf photosynthesis differed less between the two cultivars than under LN, likely because of the higher leaf N accumulation in Koshihikari than in Takanari, resulting in similar g_s values and slightly higher V_{cmax} and J_{max} values in Koshihikari at both CO_2 concentrations (**Table 1**). These properties decreased the difference in CCF_{10} and integrated A under HN at both CO_2 concentrations (**Figures 1–3**). Although Takanari can take up larger amounts of N owing to its larger root system and greater hydraulic stream than those in Koshihikari, the difference in plant N uptake becomes smaller with increasing N supply (Adachi et al., 2011; Taylaran et al., 2011; Muryono et al., 2017; Hasegawa et al., 2019). Furthermore, the N allocation rate to the leaves is inherently lower in Takanari than in Koshihikari (Adachi et al., 2011; Muryono et al., 2017). These data suggest that Takanari accumulates a larger proportion of N in stems and roots than does Koshihikari under HN, resulting in similar leaf photosynthesis under both steady-state and non-steady-state conditions.

Steady-state A (**Supplementary Figure S3A**) and integrated A (**Figure 4C**) plotted as a function of leaf N were consistently higher in Takanari than in Koshihikari, regardless of N supply and CO_2 concentration. This higher photosynthetic N use efficiency of Takanari was likely attributable to the higher V_{cmax}, J_{max}, and g_s per leaf N content (**Supplementary Figures S3B–D**). The higher V_{cmax} and J_{max} per leaf N content in Takanari probably indicate preferential allocation of leaf N to thylakoid membrane proteins and Calvin-cycle enzymes than to leaf structural components (Evans and Clarke, 2019). The higher g_s per leaf N content would be attributable to superior stomatal traits such as density and size of each stomatal pore (Ohsumi et al., 2007). The higher hydraulic conductance from roots to leaves, which increases leaf water potential, and higher cytokinin activity in the leaves also potentially associate with the higher g_s in Takanari (Taylaran et al., 2011; Adachi et al., 2019a). The above data show that photosynthetic N use efficiency is greater in Takanari than in Koshihikari, which would retain photosynthesis better with decreased N input (Hasegawa et al., 2019).

Doubling ambient CO_2 concentration increased steady-state A by 44–60% in Koshihikari and by 49–63% in Takanari, regardless of N supply (**Table 1**). These values were similar to those for integrated A (40–61% and 49–76%, respectively; **Figure 3**). These results indicate that elevated CO_2 affects the photosynthesis of Koshihikari and Takanari similarly regardless of light conditions. Elevated CO_2 has additional effects on non-steady-state photosynthesis to those on steady-state photosynthesis by a decreased limitation of CO_2 diffusion from air into chloroplasts, increased post-irradiance CO_2 fixation, and decreased post-

irradiance CO_2 burst (Leakey et al., 2004; Tomimatsu and Tang, 2016). However, our results of integrated *A* at elevated CO_2 did not show these effects. This might be caused by a lot of sunfleck events with high light leading to high CO_2 fixation, masking the benefit during light fluctuation. The effects of elevated CO_2 on total carbon gain are probably more important under light-limited environments such as the bottom of a crop canopy and the closed-forest understory, where the contribution of sunflecks to the daily carbon gain is greater than that in the top canopy (Leakey et al., 2002).

In general, elevated growth CO_2 may decrease the contents of Rubisco and other soluble proteins due to the acclimation to high CO_2 condition, reducing V_{cmax} and J_{max} (Ainsworth and Long, 2005). Here, we grew rice plants outdoors at the atmospheric CO_2 concentration and hence we cannot identify the genetic difference in acclimatization to elevated CO_2. In a FACE experiment (590 ppm CO_2 on average), Takanari maintained higher g_s, V_{cmax}, and J_{max} than did Koshihikari, even though these values were slightly lower in both cultivars at the atmospheric CO_2 concentration (390 ppm on average) (Chen et al., 2014). Therefore, we hypothesize that Takanari would have higher photosynthesis under fluctuating light and elevated growth CO_2 than Koshihikari; this hypothesis must be examined in the future.

A close correlation between steady-state *A* and non-steady-state *A* was found regardless of cultivar and N fertilization level (**Figure 4B**), suggesting that genetic improvement of steady-state *A* may boost daily carbon gain under fluctuating light conditions. We identified several quantitative trait loci for steady-state *A* using several sets of introgression lines derived from Koshihikari and Takanari (Adachi et al., 2019b). Map-based cloning using the same lines identified a gene, *GREEN FOR PHOTOSYNTHESIS*, associated with the difference in steady-state *A* between Koshihikari and Takanari (Takai et al., 2013). We expect that these genetic factors will allow breeders to improve non-steady-state and steady-state *A*. Transgenic approaches are also expected to improve non-steady-state photosynthesis (Slattery et al., 2018). Kromdijk et al. (2016) showed that accelerating recovery from photoprotection by overproduction of three proteins in tobacco (*Nicotiana tabacum* L.) increased plant biomass under field conditions. Yamori et al. (2012) reported that the overexpression of Rubisco activase in rice accelerated photosynthetic induction, especially under heat stress. A mutant of *SLAC1*, encoding an anion channel of guard cells, has increased stomatal aperture and carbon gain during photosynthetic induction and under fluctuating light mimicking field conditions in rice (Yamori et al., 2020) and *Arabidopsis* (Kimura et al., 2020). Genetic modifications of thylakoid membrane proteins, Calvin-cycle enzymes, and proteins that control CO_2 diffusion could independently promote non-steady-state photosynthesis. Combining natural alleles and transgenes could boost photosynthesis and plant growth under field conditions.

In conclusion, we found that Takanari has higher photosynthesis under fluctuating light, especially under limited N supply and elevated CO_2, than Koshihikari. Photosynthetic N use efficiency was also higher in Takanari regardless of N supply and CO_2 conditions. We propose that Takanari is a promising donor cultivar for genes useful in rice breeding aimed at increasing photosynthesis under current and future climates.

DATA AVAILABILITY STATEMENT

The original contributions presented in the study are included in the article/**Supplementary Material**; further inquiries can be directed to the corresponding authors.

AUTHOR CONTRIBUTIONS

YT, WY, and SA designed the experiments. SO and SA performed the experiments. SO, WY, and SA wrote the manuscript.

FUNDING

This work was supported in part by the Japan Science and Technology Agency, CREST grant number JPMJCR15O2 (to SA), and by JSPS KAKENHI (grant numbers JP16H06552, JP18H02185 and JP18KK0170 to WY, and JP18K05585, JP19H02940, JP19H02939 and 19K05987 to SA).

ACKNOWLEDGMENTS

We are grateful to Mr. H. Kimura for assistance with Rubisco quantification, and to Ms. T. Yamanouchi and Ms. Y. Yamashita for assistance with rice cultivation.

SUPPLEMENTARY MATERIAL

The Supplementary Material for this article can be found online at: https://www.frontiersin.org/articles/10.3389/fpls.2020.01308/full#supplementary-material

REFERENCES

Acevedo-Siaca, L. G., Coe, R., Wang, Y., Kromdijk, J., Quick, W. P., and Long, S. P. (2020). Variation in photosynthetic induction between rice accessions and its potential for improving productivity. *New Phytol.* 227, 1097–1108. doi: 10.1111/nph.16454

Adachi, S., Tsuru, Y., Nito, N., Murata, K., Yamamoto, T., Ebitani, T., et al. (2011). Identification and characterization of genomic regions on chromosomes 4 and 8 that control the rate of photosynthesis in rice leaves. *J. Exp. Bot.* 62, 1927–1938. doi: 10.1093/jxb/erq387

Adachi, S., Yoshikawa, K., Yamanouchi, U., Tanabata, T., Sun, J., Ookawa, T., et al. (2017). Fine mapping of carbon assimilation rate 8, a quantitative trait locus for flag leaf nitrogen content, stomatal conductance and photosynthesis in rice. *Front. Plant Sci.* 8, 60. doi: 10.3389/fpls.2017.00060

Adachi, S., Tanaka, Y., Miyagi, A., Kashima, M., Tezuka, A., Toya, Y., et al. (2019a). High-yielding rice Takanari has superior photosynthetic response

under fluctuating light to a commercial rice Koshihikari. *J. Exp. Bot.* 70, 5287–5297. doi: 10.1093/jxb/erz304

Adachi, S., Yamamoto, T., Nakae, T., Yamashita, M., Uchida, M., Karimata, R., et al. (2019b). Genetic architecture of leaf photosynthesis in rice revealed by different types of reciprocal mapping populations. *J. Exp. Bot.* 70, 5131–5144. doi: 10.1093/jxb/erz303

Adachi, S., Ohkubo, S., San, N. S., and Yamamoto, T. (2020). Genetic determination for source capacity to support breeding of high-yielding rice (*Oryza sativa*). *Mol. Breed.* 40, 20. doi: 10.1007/s11032-020-1101-5

Ainsworth, E. A., and Long, S. P. (2005). What have we learned from 15 years of free-air CO_2 enrichment (FACE)? A meta-analytic review of the responses of photosynthesis, canopy properties and plant production to rising CO_2. *New Phytol.* 165, 351–372. doi: 10.1111/j.1469-8137.2004.01224.x

Aro, E. M., Virgin, I., and Andersson, B. (1993). Photoinhibition of photosystem II. Inactivation, protein damage and turnover. *BBA Bioenerg.* 1143, 113–134. doi: 10.1016/0005-2728(93)90134-2

Bernacchi, C. J., Singaas, E. L., Pimentel, C., Portis, A. R.Jr., and Long, S. P. (2001). Improved temperature response functions for models of Rubisco-limited photosynthesis. *Plant Cell Environ.* 24, 253–259. doi: 10.1111/j.1365-3040.2001.00668.x

Carmo-Silva, E., Andralojc, P. J., Scales, J. C., Driever, S. M., Mead, A., Lawson, T., et al. (2017). Phenotyping of field-grown wheat in the UK highlights contribution of light response of photosynthesis and flag leaf longevity to grain yield. *J. Exp. Bot.* 68, 3473–3486. doi: 10.1093/jxb/erx169

Chen, C. P., Sakai, H., Tokida, T., Usui, Y., Nakamura, H., and Hasegawa, T. (2014). Do the rich always become richer? Characterizing the leaf physiological response of the high-yielding rice cultivar Takanari to free-air CO_2 enrichment. *Plant Cell Physiol.* 55, 381–391. doi: 10.1093/pcp/pcu009

Choquette, N. E., Ogut, F., Wertin, T. M., Montes, C. M., Sorgini, C. A., Morse, A. M., et al. (2019). Uncovering hidden genetic variation in photosynthesis of field-grown maize under ozone pollution. *Global Change Biol.* 25, 4327–4338. doi: 10.1111/gcb.14794

Cook, M., and Evans, L. (1983). Some physiological aspects of the domestication and improvement of rice (*Oryza* spp.). *Field Crops Res.* 6, 219–238. doi: 10.1016/0378-4290(83)90062-X

Dallagnol, L. J., Martins, S. C. V., DaMatta, F. M., and Rodrigues, F.Á. (2015). Brown spot negatively affects gas exchange and chlorophyll a fluorescence in rice leaves. *Trop. Plant Pathol.* 40, 275–278. doi: 10.1007/s40858-015-0026-8

Demmig-Adams, B., Adams, W. W. III, Barker, D. H., Logan, B. A., Bowling, D. R., and Verhoeven, A. S. (1996). Using chlorophyll fluorescence to assess the fraction of absorbed light allocated to thermal dissipation of excess excitation. *Physiol. Plant* 98, 253–264. doi: 10.1034/j.1399-3054.1996.980206.x

Evans, J. R., and Clarke, V. C. (2019). The nitrogen cost of photosynthesis. *J. Exp. Bot.* 70, 7–15. doi: 10.1093/jxb/ery366

Flood, P. J., Harbinson, J., and Aarts, M. G. (2011). Natural genetic variation in plant photosynthesis. *Trends Plant Sci.* 16, 327–335. doi: 10.1016/j.tplants.2011.02.005

Furbank, R. T., Sharwood, R., Estavillo, G. M., Silva-Perez, V., and Condon, A. G. (2020). Photons to food: Genetic improvement of cereal crop photosynthesis. *J. Exp. Bot.* 71, 2226–2238. doi: 10.1093/jxb/eraa077

Hasegawa, T., Sakai, H., Tokida, T., Usui, Y., Nakamura, H., Wakatsuki, H., et al. (2019). A high-yielding rice cultivar "Takanari" shows no N constraints on CO_2 fertilization. *Front. Plant Sci.* 10, 361. doi: 10.3389/fpls.2019.00361

Hirasawa, T., Ozawa, S., Taylaran, R. D., and Ookawa, T. (2010). Varietal differences in photosynthetic rates in rice plants, with special reference to the nitrogen content of leaves. *Plant Prod. Sci.* 13, 53–57. doi: 10.1626/pps.13.53

Huang, G., Zhang, Q., Wei, X., Peng, S., and Li, Y. (2017). Nitrogen can alleviate the inhibition of photosynthesis caused by high temperature stress under both steady-state and flecked irradiance. *Front. Plant Sci.* 8, 945. doi: 10.3389/fpls.2017.00945

Ikawa, H., Chen, C. P., Sikma, M., Yoshimoto, M., Sakai, H., Tokida, T., et al. (2018). Increasing canopy photosynthesis in rice can be achieved without a large increase in water use—A model based on free-air CO_2 enrichment. *Global Change Biol.* 24, 1321–1341. doi: 10.1111/gcb.13981

Ikawa, H., Sakai, H., Chen, C. P., Soong, T. H., Yonemura, S., Taniguchi, Y., et al. (2019). High mesophyll conductance in the high-yielding rice cultivar Takanari quantified with the combined gas exchange and chlorophyll fluorescence measurements under free-air CO_2 enrichment. *Plant Prod. Sci.* 22, 395–406. doi: 10.1080/1343943X.2019.1626253

Ikeuchi, M., Uebayashi, N., Sato, F., and Endo, T. (2014). Physiological functions of PsbS-dependent and PsbS-independent NPQ under naturally fluctuating light conditions. *Plant Cell Physiol.* 55, 1286–1295. doi: 10.1093/pcp/pcu069

Imbe, T., Akama, Y., Nakane, A., Hata, T., Ise, K., Ando, I., et al. (2004). Development of a multipurpose high-yielding rice variety "Takanari". *Bull. Natl. Inst. Crop Sci.* 5, 35–51.

Ishida, S., Uebayashi, N., Tazoe, Y., Ikeuchi, M., Homma, K., Sato, F., et al. (2014). Diurnal and developmental changes in energy allocation of absorbed light at PSII in field-grown rice. *Plant Cell Physiol.* 55, 171–182. doi: 10.1093/pcp/pct169

Jahn, C. E., Mckay, J. K., Mauleon, R., Stephens, J., Mcnally, K. L., Bush, D. R., et al. (2011). Genetic variation in biomass traits among 20 diverse rice varieties. *Plant Physiol.* 155, 157–168. doi: 10.1104/pp.110.165654

Kaiser, E., Zhou, D., Heuvelink, E., Harbinson, J., Morales, A., and Marcelis, L. F. M. (2017). Elevated CO_2 increases photosynthesis in fluctuating irradiance regardless of photosynthetic induction state. *J. Exp. Bot.* 68, 5629–5640. doi: 10.1093/jxb/erx357

Kanemura, T., Homma, K., Ohsumi, A., Shiraiwa, T., and Horie, T. (2007). Evaluation of genotypic variation in leaf photosynthetic rate and its associated factors by using rice diversity research set of germplasm. *Photosynth. Res.* 94, 23–30. doi: 10.1007/s11120-007-9208-7

Kimura, H., Hashimoto-Sugimoto, M., Iba, K., Terashima, I., and Yamori, W. (2020). Improved stomatal opening enhances photosynthetic rate and biomass production in fluctuating light. *J. Exp. Bot.* 71, 2339–2350. doi: 10.1093/jxb/eraa090

Kojima, Y., Ebana, K., Fukuoka, S., Nagamine, T., and Kawase, M. (2005). Development of an RFLP-based rice diversity research set of germplasm. *Breed. Sci.* 55, 431–440. doi: 10.1270/jsbbs.55.431

Kromdijk, J., Głowacka, K., Leonelli, L., Gabilly, S. T., Iwai, M., Niyogi, K. K., et al. (2016). Improving photosynthesis and crop productivity by accelerating recovery from photoprotection. *Science* 354, 857–861. doi: 10.1126/science.aai8878

Kumagai, E., Araki, T., and Ueno, O. (2010). Comparison of susceptibility to photoinhibition and energy partitioning of absorbed light in photosystem II in flag leaves of two rice (*Oryza sativa* L.) cultivars that differ in their responses to nitrogen-deficiency. *Plant Prod. Sci.* 13, 11–20. doi: 10.1626/pps.13.11

Lawson, T., Kramer, D. M., and Raines, C. A. (2012). Improving yield by exploiting mechanisms underlying natural variation of photosynthesis. *Curr. Opin. Biotech.* 23, 215–220. doi: 10.1016/j.copbio.2011.12.012

Leakey, A., Press, M., Scholes, J., and Watling, J. (2002). Relative enhancement of photosynthesis and growth at elevated CO_2 is greater under sunflecks than uniform irradiance in a tropical rain forest tree seedling. *Plant Cell Environ.* 25, 1701–1714. doi: 10.1046/j.1365-3040.2002.00944.x

Leakey, A., Scholes, J., and Press, M. (2004). Physiological and ecological significance of sunflecks for dipterocarp seedlings. *J. Exp. Bot.* 56, 469–482. doi: 10.1093/jxb/eri055

Long, S. P., Humphries, S., and Falkowski, P. G. (1994). Photoinhibition of photosynthesis in nature. *Ann. Rev. Plant Biol.* 45, 633–662. doi: 10.1146/annurev.pp.45.060194.003221

Makino, A., Sakuma, H., Sudo, E., and Mae, T. (2003). Differences between maize and rice in N-use efficiency for photosynthesis and protein allocation. *Plant Cell Physiol.* 44, 952–956. doi: 10.1093/pcp/pcg113

Muryono, M., Chen, C. P., Sakai, H., Tokida, T., Hasegawa, T., Usui, Y., et al. (2017). Nitrogen distribution in leaf canopies of high-yielding rice cultivar Takanari. *Crop Sci.* 57, 2080–2088. doi: 10.2135/cropsci2016.07.0589

Ohsumi, A., Kanemura, T., Homma, K., Horie, T., and Shiraiwa, T. (2007). Genotypic variation of stomatal conductance in relation to stomatal density and length in rice (*Oryza sativa* L.). *Plant Prod. Sci.* 10, 322–328. doi: 10.1626/pps.10.322

Ookawa, T., Aoba, R., Yamamoto, T., Ueda, T., Takai, T., Fukuoka, S., et al. (2016). Precise estimation of genomic regions controlling lodging resistance using a set of reciprocal chromosome segment substitution lines in rice. *Sci. Rep.* 6, 30572. doi: 10.1038/srep30572

Pearcy, R. W., Krall, J. P., and Sassenrath-Cole, G. F. (1996). "Photosynthesis in fluctuating light environments," in *Photosynthesis and the Environment*, ed. N. R. Baker (Dordrecht: Springer), 321–346.

Pearcy, R. W. (1990). Sunflecks and photosynthesis in plant canopies. *Ann. Rev. Plant Biol.* 41, 421–453. doi: 10.1146/annurev.pp.41.060190.002225

Porra, R., Thompson, W., and Kriedemann, P. (1989). Determination of accurate extinction coefficients and simultaneous equations for assaying chlorophylls a and b extracted with four different solvents: verification of the concentration of chlorophyll standards by atomic absorption spectroscopy. *BBA Bioenerg.* 975, 384–394. doi: 10.1016/S0005-2728(89)80347-0

Qu, M., Zheng, G., Hamdani, S., Essemine, J., Song, Q., Wang, H., et al. (2017). Leaf photosynthetic parameters related to biomass accumulation in a global rice diversity survey. *Plant Physiol.* 175, 248–258. doi: 10.1104/pp.17.00332

R Core Team (2018). *R: A language and environment for statistical computing* (Vienna, Austria: R Foundation for Statistical Computing).

Sage, R. F., Adachi, S., and Hirasawa, T. (2017). "Improving photosynthesis in rice: from small steps to giant leaps," in *Achieving sustainable cultivation of rice Volume 1*. ed. T. Sasaki (London: Burleigh Dodds Science Publishing), 99–130.

Sakoda, K., Tanaka, Y., Long, S. P., and Shiraiwa, T. (2016). Genetic and physiological diversity in the leaf photosynthetic capacity of soybean. *Crop Sci.* 56, 2731–2741. doi: 10.2135/cropsci2016.02.0122

Salter, W. T., Merchant, A. M., Richards, R. A., Trethowan, R., and Buckley, T. N. (2019). Rate of photosynthetic induction in fluctuating light varies widely among genotypes of wheat. *J. Exp. Bot.* 70, 2787–2796. doi: 10.1093/jxb/erz100

San, N. S., Ootsuki, Y., Adachi, S., Yamamoto, T., Ueda, T., Tanabata, T., et al. (2018). A near-isogenic rice line carrying a QTL for larger leaf inclination angle yields heavier biomass and grain. *Field Crops Res.* 219, 131–138. doi: 10.1016/j.fcr.2018.01.025

Shimadzu, S., Seo, M., Terashima, I., and Yamori, W. (2019). Whole irradiated plant leaves showed faster photosynthetic induction than individually irradiated leaves via improved stomatal opening. *Front. Plant Sci.* 10, 1512. doi: 10.3389/fpls.2019.01512

Simkin, A. J., López-Calcagno, P. E., and Raines, C. A. (2019). Feeding the world: improving photosynthetic efficiency for sustainable crop production. *J. Exp. Bot.* 70, 1119–1140. doi: 10.1093/jxb/ery445

Slattery, R. A., Walker, B. J., Weber, A. P. M., and Ort, D. R. (2018). The impacts of fluctuating light on crop performance. *Plant Physiol.* 176, 990–1003. doi: 10.1104/pp.17.01234

Soleh, M. A., Tanaka, Y., Nomoto, Y., Iwahashi, Y., Nakashima, K., Fukuda, Y., et al. (2016). Factors underlying genotypic differences in the induction of photosynthesis in soybean [*Glycine max* (L.) Merr.]. *Plant Cell Environ.* 49, 685–693. doi: 10.1111/pce.12674

Soleh, M. A., Tanaka, Y., Kim, S. Y., Huber, S. C., Sakoda, K., and Shiraiwa, T. (2017). Identification of large variation in the photosynthetic induction response among 37 soybean [*Glycine max* (L.) Merr.] genotypes that is not correlated with steady-state photosynthetic capacity. *Photosynth. Res.* 131, 305–315. doi: 10.1007/s11120-016-0323-1

Sun, J., Ye, M., Peng, S., and Li, Y. (2016). Nitrogen can improve the rapid response of photosynthesis to changing irradiance in rice (*Oryza sativa* L.) plants. *Sci. Rep.* 6, 31305. doi: 10.1038/srep31305

Takai, T., Matsuura, S., Nishio, T., Ohsumi, A., Shiraiwa, T., and Horie, T. (2006). Rice yield potential is closely related to crop growth rate during late reproductive period. *Field Crops Res.* 96, 328–335. doi: 10.1016/j.fcr.2005.08.001

Takai, T., Adachi, S., Taguchi-Shiobara, F., Sanoh-Arai, Y., Iwasawa, N., Yoshinaga, S., et al. (2013). A natural variant of *NAL1*, selected in high-yield rice breeding programs, pleiotropically increases photosynthesis rate. *Sci. Rep.* 3, 2149. doi: 10.1038/srep02149

Takai, T., Ikka, T., Kondo, K., Nonoue, Y., Ono, N., Arai-Sanoh, Y., et al. (2014). Genetic mechanisms underlying yield potential in the rice high-yielding cultivar Takanari, based on reciprocal chromosome segment substitution lines. *BMC Plant Biol.* 14, 295. doi: 10.1186/s12870-014-0295-2

Tanaka, Y., Adachi, S., and Yamori, W. (2019). Natural genetic variation of the photosynthetic induction response to fluctuating light environment. *Curr. Opin. Plant Biol.* 49, 52–59. doi: 10.1016/j.pbi.2019.04.010

Taylaran, R. D., Adachi, S., Ookawa, T., Usuda, H., and Hirasawa, T. (2011). Hydraulic conductance as well as nitrogen accumulation plays a role in the higher rate of leaf photosynthesis of the most productive variety of rice in Japan. *J. Exp. Bot.* 62, 4067–4077. doi: 10.1093/jxb/err126

Taylor, S. H., and Long, S. P. (2017). Slow induction of photosynthesis on shade to sun transitions in wheat may cost at least 21% of productivity. *Philos. Trans. R. Soc Lond. B Biol. Sci.* 372, 20160543. doi: 10.1098/rstb.2016.0543

Tomimatsu, H., and Tang, Y. (2012). Elevated CO_2 differentially affects photosynthetic induction response in two Populus species with different stomatal behavior. *Oecologia* 169, 869–878. doi: 10.1007/s00442-012-2256-5

Tomimatsu, H., and Tang, Y. (2016). Effects of high CO_2 levels on dynamic photosynthesis: carbon gain, mechanisms, and environmental interactions. *J. Plant Res.* 129, 365–377. doi: 10.1007/s10265-016-0817-0

van Bezouw, R. F., Keurentjes, J. J., Harbinson, J., and Aarts, M. G. (2019). Converging phenomics and genomics to study natural variation in plant photosynthesis efficiency. *Plant J.* 97, 112–133. doi: 10.1111/tpj.14190

Wang, L., Yang, Y., Zhang, S., Che, Z., Yuan, W., and Yu, D. (2020). GWAS reveals two novel loci for photosynthesis-related traits in soybean. *Mol. Genet. Genom.* 295, 705–716. doi: 10.1007/s00438-020-01661-1

Xu, Y.-F., Ookawa, T., and Ishihara, K. (1997). Analysis of the dry matter production process and yield formation of the high-yielding rice cultivar Takanari, from 1991 to 1994. *Jpn. J. Crop Sci.* 66, 42–50. doi: 10.1626/jcs.66.42

Yamori, W., Sakata, N., Suzuki, Y., Shikanai, T., and Makino, A. (2011). Cyclic electron flow around photosystem I via chloroplast NAD(P)H dehydrogenase (NDH) complex performs a significant physiological role during photosynthesis and plant growth at low temperature in rice. *Plant J.* 68, 966–976. doi: 10.1111/j.1365-313X.2011.04747.x

Yamori, W., Masumoto, C., Fukayama, H., and Makino, A. (2012). Rubisco activase is a key regulator of non-steady-state photosynthesis at any leaf temperature and, to a lesser extent, of steady-state photosynthesis at high temperature. *Plant J.* 71, 871–880. doi: 10.1111/j.1365-313X.2012.05041.x

Yamori, W., Irving, L. J., Adachi, S., and Busch, F. A. (2016). "Strategies for Optimizing Photosynthesis with Biotechnology to Improve Crop Yield," in *Handbook of Photosynthesis, 3rd ed.* ed. M. Pessarakli (Florida, Francis Publishing Company), 741–759.

Yamori, W., Kusumi, K., Iba, K., and Terashima, I. (2020). Increased stomatal conductance induces rapid changes to photosynthetic rate in response to naturally fluctuating light conditions in rice. *Plant Cell Environ.* 43, 1230–1240. doi: 10.1111/pce.13725

Yamori, W. (2016). Photosynthetic response to fluctuating environments and photoprotective strategies under abiotic stress. *J. Plant Res.* 129, 379–395. doi: 10.1007/s10265-016-0816-1

Conflict of Interest: The authors declare that the research was conducted in the absence of any commercial or financial relationships that could be construed as a potential conflict of interest.

frontiers in Plant Science

PERSPECTIVE
published: 15 September 2020
doi: 10.3389/fpls.2020.581851

Modeling Light Response of Electron Transport Rate and Its Allocation for Ribulose Biphosphate Carboxylation and Oxygenation

Zi-Piao Ye[1†], *Hua-Jing Kang*[2†], *Ting An*[1], *Hong-Lang Duan*[3], *Fu-Biao Wang*[1], *Xiao-Long Yang*[1*] *and Shuang-Xi Zhou*[4*]

[1] Maths and Physics College, Jinggangshan University, Ji'an, China, [2] Department of Landscape and Water Conservancy Engineering, Wenzhou Vocational College of Science and Technology, Wenzhou, China, [3] Jiangxi Provincial Key Laboratory for Restoration of Degraded Ecosystems & Watershed Ecohydrology, Nanchang Institute of Technology, Nanchang, China, [4] The New Zealand Institute for Plant and Food Research Limited, Hawke's Bay, New Zealand

OPEN ACCESS

Edited by:
Stefano Santabarbara, National Research Council (CNR), Italy

Reviewed by:
Yanbo Hu, Northeast Forestry University, China
John A. Morgan, Purdue University, United States

***Correspondence:**
Shuang-Xi Zhou
shuangxi.zhou@plantandfood.co.nz
Xiao-Long Yang
yxl327813040@163.com

[†]These authors have contributed equally to this work

Specialty section:
This article was submitted to Plant Abiotic Stress, a section of the journal Frontiers in Plant Science

Received: 10 July 2020
Accepted: 25 August 2020
Published: 15 September 2020

Citation:
Ye Z-P, Kang H-J, An T, Duan H-L, Wang F-B, Yang X-L and Zhou S-X (2020) Modeling Light Response of Electron Transport Rate and Its Allocation for Ribulose Biphosphate Carboxylation and Oxygenation. Front. Plant Sci. 11:581851. doi: 10.3389/fpls.2020.581851

Accurately describing the light response curve of electron transport rate (J–I curve) and allocation of electron flow for ribulose biphosphate (RuBP) carboxylation (J_C–I curve) and that for oxygenation (J_O–I curve) is fundamental for modeling of light relations of electron flow at the whole-plant and ecosystem scales. The non-rectangular hyperbolic model (hereafter, NH model) has been widely used to characterize light response of net photosynthesis rate (A_n; A_n–I curve) and J–I curve. However, NH model has been reported to overestimate the maximum A_n (A_{nmax}) and the maximum J (J_{max}), largely due to its asymptotic function. Meanwhile, few efforts have been delivered for describing J_C–I and J_O–I curves. The long-standing challenge on describing A_n–I and J–I curves have been resolved by a recently developed A_n–I and J–I models (hereafter, Ye model), which adopt a nonasymptotic function. To test whether Ye model can resolve the challenge of NH model in reproducing J–I, J_C–I and J_O–I curves over light-limited, light-saturated, and photoinhibitory I levels, we compared the performances of Ye model and NH model against measurements on two C_3 crops (*Triticum aestivum* L. and *Glycine max* L.) grown in field. The results showed that NH model significantly overestimated the A_{nmax} and J_{max} for both species, which can be accurately obtained by Ye model. Furthermore, NH model significantly overestimated the maximum electron flow for carboxylation ($J_{C\text{-}max}$) but not the maximum electron flow for oxygenation ($J_{O\text{-}max}$) for both species, disclosing the reason underlying the long-standing problem of NH model—overestimation of J_{max} and A_{nmax}.

Keywords: photosynthesis, light response curve, electron flow partitioning, maximum *J*, saturation light intensity, ribulose biphosphate carboxylation, ribulose biphosphate oxygenation, model

INTRODUCTION

Light intensity (I) is one of the most important environmental drivers affecting electron flow and its allocation for carboxylation versus oxygenation of ribulose biphosphate (RuBP). At I levels before reaching saturation intensity, the non-rectangular hyperbolic model (hereafter, NH model) is a sub-model which is widely used to characterize the light-response curve of electron transport rate (J–I curve) and to estimate the maximum J (J_{max}) in C_3 photosynthesis model (e.g., Farquhar et al., 1980; Farquhar and Wong, 1984; von Caemmerer, 2000; Farquhar et al., 2001; Long and Bernacchi, 2003; von Caemmerer et al., 2009; Bernacchi et al., 2013; Bellasio et al., 2015; Busch and Sage, 2017; Walker et al., 2017; Cai et al., 2018) and in C_4 photosynthesis model (Berry and Farquhar, 1978; von Caemmerer and Furbank, 1999; von Caemmerer, 2013). At light saturation, J_{max} is estimated by the C_3 photosynthesis model (Farquhar et al., 1980; von Caemmerer, 2013; Farquhar and Busch, 2017). Accurate estimation of J_{max} is important for understanding photosynthesis of C_3 and C_4 species. J_{max} is a key quantity to represent plant photosynthetic status under different environmental conditions when the net photosynthesis rate (A_n) is limited by the regeneration of RuBP, associated with the partitioning of electron flow through photosystem II (PSII) for RuBP carboxylation (J_C) versus that for RuBP oxygenation (J_O) (Farquhar et al., 1980; Long and Bernacchi, 2003).

By simulating light-response curves of photosynthesis (A_n–I curve), NH model has been widely used to obtain key photosynthetic characteristics (e.g., the maximum net photosynthetic rate, A_{nmax}; light compensation point when $A_n = 0$, I_c; dark respiration rate, R_d) for various species under different environmental conditions (e.g., Ögren & Evans, 1993; Thornley, 1998; Ye, 2007; Aspinwall et al., 2011; dos Santos et al., 2013; Mayoral et al., 2015; Sun et al., 2015; Park et al., 2016; Quiroz et al., 2017; Yao et al., 2017; Xu et al., 2019; Yang et al., 2020; Ye et al., 2020). Significant difference between observed A_{nmax} values and that estimated by NH model for various species has been widely reported (e.g., Chen et al., 2011; dos Santos et al., 2013; Lobo et al., 2014; Ogawa, 2015; Sun et al., 2015; Quiroz et al., 2017; Poirier-Pocovi et al., 2018; Ye et al., 2020). This long-standing challenge has been resolved by an A_n–I model, which adopts a nonasymptotic function and can accurately reproduce A_n–I curve over light-limited, light-saturated and photoinhibitory I levels (Ye et al., 2013) (hereafter, Ye model).

Recently, Buckley and Diaz-Espejo (2015) proposed that NH model would overestimate J_{max} due to its asymptotic function. A robust model which can accurately reproduce the observed J–I curve, and obtain J_{max}, is urgently needed (Buckley and Diaz-Espejo, 2015). Furthermore, the light response of J partitioning for RuBP carboxylation and oxygenation (J_C–I and J_O–I curves), and the key quantities to describe the curves (e.g., the maximum J_C, $J_{C\text{-}max}$, and the maximum J_O, $J_{O\text{-}max}$, as well as their corresponding saturation light intensities) are rarely studied. Meanwhile, for the first time, we compared the performances of the two models in reproducing J_C–I and J_O–I curves.

This study aimed to fill these important gaps using an observation-modeling intercomparison approach. We firstly measured leaf gas exchange and chlorophyll fluorescence over a wide range of I levels for two C_3 species [winter wheat (*Triticum aestivum* L.) and soybean (*Glycine max* L.)]. We then incorporated Ye model to reproduce A_n–I, J–I, J_C–I, and J_O–I curves and return key quantities defining the curves, and evaluated its performance against NH model and observations.

MATERIALS AND METHODS

Plant Material and Measurements of Leaf Gas Exchange and Chlorophyll Fluorescence

The experiment was conducted in the Yucheng Comprehensive Experiment Station of the Chinese Academy of Science. The detailed descriptions about soil and meteorological conditions in this experiment station were referred to Ye et al. (2019; 2020). Winter wheat was planted on October 4th, 2011 and the measurements were conducted on April 23th, 2012. Soybean was sown in on May 6th, 2013, and the measurements were performed on 27th July, 2013. Using the Li-6400-40 portable photosynthesis system (Li-Cor, Lincoln, NE, USA), measurements on leaf gas exchange and chlorophyll fluorescence were simultaneously performed on mature fully-expanded sun-exposed leaves in sunny days. J was calculated as $J = \Phi_{PSII} \times I \times 0.5 \times 0.84$, where Φ_{PSII} is the effective quantum yield of PSII (Genty et al., 1989; Krall and Edward, 1992).

For soybean, A_n–I curves and J–I curves were generated from applying different light intensities in a descending order of 2000, 1800, 1600, 1400, 1200, 1000, 800, 600, 400, 200, 150, 100, 80, 50, and 0 μmol m^{-2} s^{-1}. For winter wheat, the light intensity gradient started from 1800 μmol m^{-2} s^{-1} as the maximum, in alignment with environmental light availability from October to April. At each I step, CO_2 assimilation was monitored until a steady state was reached before logging a reading. Ambient CO_2 concentration in the cuvette (C_a) was kept constant at 380 μmol mol^{-1}. Leaf temperature in the cuvette was kept at about 30°C for winter wheat and 36°C for soybean, respectively. The observation-modeling intercomparison was conducted within each species.

A_n–I and J–I Analytical Models

NH model describes J–I curve as follows (Farquhar and Wong, 1984; von Caemmerer, 2000; von Caemmerer, 2013):

$$J = \frac{\alpha_e I + J_{max} - \sqrt{(\alpha_e I + J_{max})^2 - 4\alpha_e \theta J_{max} I}}{2\theta} \quad (1)$$

where α_e is the initial slope of J–I curve, θ is the curve convexity, I is the light intensity, and J_{max} is the maximum electron transport rate.

NH model describes A_n–I curve as follows (Ögren and Evans, 1993; Thornley, 1998; von Caemmerer, 2000):

$$A_n = \frac{\alpha I + A_{nmax} - \sqrt{(\alpha I + A_{nmax})^2 - 4\alpha\theta A_{nmax} I}}{2\theta} - R_d \quad (2)$$

where α is the initial slope of A_n–I curve, A_{nmax} is the maximum net photosynthetic rate, and R_d is the dark respiration rate when

I = 0 μmol m^{-2} s^{-1}. NH model cannot return the corresponding saturation light intensities for J_{max} or A_{nmax} due to its asymptotic function.

The model developed by Ye et al. (2013, 2019; hereafter, Ye model) describes *J*–*I* curve as follows:

$$J = \alpha_e \frac{1 - \beta_e I}{1 + \gamma_e I} I \tag{3}$$

where α_e is the initial slope of *J*–*I* curve, and β_e and γ_e are the photoinhibition coefficient and light-saturation coefficient of *J*–*I* curve, respectively.

The saturation irradiance corresponding to the J_{max} ($I_{e\text{-}sat}$) can be calculated as follows:

$$I_{e-sat} = \frac{\sqrt{(\beta_e + \gamma_e)/\beta_e} - 1}{\gamma_e} \tag{4}$$

Using Ye model, J_{max} can be calculated as follows:

$$J_{max} = \alpha_e \left(\frac{\sqrt{\beta_e + \gamma_e} - \sqrt{\beta_e}}{\gamma_e} \right)^2 \tag{5}$$

Ye model describes A_n–*I* curve as follows (Ye, 2007; Ye et al., 2013):

$$A_n = \alpha \frac{1 - \beta I}{1 + \gamma I} I - R_d \tag{6}$$

where α is the initial slope of A_n–*I* curve, β and γ are the photoinhibition coefficient and light-saturation coefficient of A_n–*I* curve, respectively.

The saturation irradiance corresponding to A_{nmax} (I_{sat}) can be calculated as follows:

$$I_{sat} = \frac{\sqrt{(\beta + \gamma)/\beta} - 1}{\gamma} \tag{7}$$

Using Ye model, A_{nmax} can be calculated as follows:

$$A_{nmax} = \alpha \left(\frac{\sqrt{\beta + \gamma} - \sqrt{\beta}}{\gamma} \right) - R_d \tag{8}$$

J_C and J_O Estimation and J_C –*I* and J_O –*I* Analytical Models

Combining measurements of gas exchange and chlorophyll fluorescence was a reliable and easy-to-use technique widely used to determine J_O and J_C (e.g., Peterson, 1990; Comic and Briantais, 1991). In C_3 plants, carbon assimilation and photorespiration are two closely linked processes catalyzed by the key photosynthetic enzyme—RuBP carboxylase/oxygenase. Photorespiration is considered as an alternative sink for light-induced photosynthetic electron, and as a process helping consume extra photosynthetic electrons under high irradiance or other stressors limiting CO_2 availability at Rubisco (Stuhlfauth et al., 1990; Valentini et al., 1995; Long and Bernacchi, 2003). When the other alternative electron sinks are ignored or kept constant, the electron flow is mainly allocated for RuBP carboxylation and RuBP oxygenation (e.g. Farquhar et al., 1980; von Caemmerer, 2000; Farquhar et al., 2001; Long and Bernacchi, 2003; von Caemmerer et al., 2009; Bernacchi et al., 2013; von Caemmerer, 2013), and J_C and J_O can be respectively calculated as follows (Valentini et al., 1995):

$$J_C = \frac{1}{3}\left[J + 8\left(A_n + R_{day}\right)\right] \tag{9}$$

$$J_O = \frac{2}{3}\left[J - 4\left(A_n + R_{day}\right)\right] \tag{10}$$

where R_{day} is the day respiration rate, and following Fila et al. (2006), R_{day} = 0.5 R_d. In this study, J_C and J_O values calculated from Eqs. 9 and 10 were viewed as experimental observations—to be compared with modelled values derived from NH model and Ye model, respectively.

Using the same *J*–*I* modeling framework by Ye model, the light response of J_C (J_C–*I*) can be described as follows:

$$J_C = \alpha_C \frac{1 - \beta_C I}{1 + \gamma_C I} I \tag{11}$$

where α_C is the initial slope of J_C–*I* curve, and β_C and γ_C are two coefficient of J_C–*I* curve. The maximum J_C ($J_{C\text{-}max}$) and the saturation irradiance corresponding to the $J_{C\text{-}max}$ ($I_{C\text{-}sat}$) can be calculated as follows:

$$J_{C-max} = \alpha_C \left(\frac{\sqrt{\beta_C + \gamma_C} - \sqrt{\beta_C}}{\gamma_C} \right)^2 \tag{12}$$

$$I_{C-sat} = \frac{\sqrt{(\beta_C + \gamma_C)/\beta_C} - 1}{\gamma_C} \tag{13}$$

Using the same *J*–*I* modeling framework by Ye model, the light response of J_O (J_O–*I*) can be described as follows:

$$J_O = \alpha_O \frac{1 - \beta_O I}{1 + \gamma_O I} I \tag{14}$$

where α_O is the initial slope of J_O–*I* curve, and β_O and γ_O are two coefficient of J_O–*I* curve. The maximum J_O ($J_{O\text{-}max}$) and the saturation irradiance corresponding to the $J_{O\text{-}max}$ ($I_{O\text{-}sat}$) can be calculated as follows:

$$J_{O-max} = \alpha_O \left(\frac{\sqrt{\beta_O + \gamma_O} - \sqrt{\beta_O}}{\gamma_O} \right)^2 \tag{15}$$

$$I_{O-sat} = \alpha_O \frac{\sqrt{\beta_O + \gamma_O/\beta_O} - 1}{\gamma_O} \tag{16}$$

Meanwhile, NH model can describe the J_C–*I* and J_O–*I* curves as follows:

$$J_C = \frac{\alpha_C I + J_{C-max} - \sqrt{(\alpha_C I + J_{C-max})^2 - 4\alpha_C \theta J_{C-max} I}}{2\theta} \tag{17}$$

where α_C is the initial slope of J_C–*I* curve, θ is the curve convexity, and $J_{C\text{-}max}$ is the maximum J_C, and

$$J_O = \frac{\alpha_O I + J_{O-max} - \sqrt{(\alpha_O I + J_{O-max})^2 - 4\alpha_O \theta J_{O-max} I}}{2\theta} \quad (18)$$

where α_O is the initial slope of J_O–I curve, θ is the curve convexity, and $J_{O\text{-}max}$ is the maximum J_O. NH model—Eqs. 17 and 18—cannot return the corresponding saturation light intensities for $J_{C\text{-}max}$ or $J_{O\text{-}max}$ due to its asymptotic function.

Statistical Analysis

Statistical tests were performed using the statistical package SPSS 18.5 statistical software (SPSS, Chicago, IL). One-Way ANOVA was used to examine differences between parameter values estimated by NH model, Ye model and observed values of each parameter (A_{nmax}, I_{sat}, J_{max}, $I_{e\text{-}sat}$, $J_{C\text{-}max}$, $I_{C\text{-}sat}$, $J_{O\text{-}max}$, $I_{O\text{-}sat}$, etc.). Goodness of fit of the mathematical model to experimental observations was assessed using the coefficient of determination (R^2 = 1 – SSE/SST, where SSE is the error sum of squares, and SST is the total sum of squares).

RESULTS

Light Response of A_n and J

Soybean and winter wheat exhibited an immediate and rapid initial increase of A_n (α) and J (α_e) with the increasing I (**Figure 1**

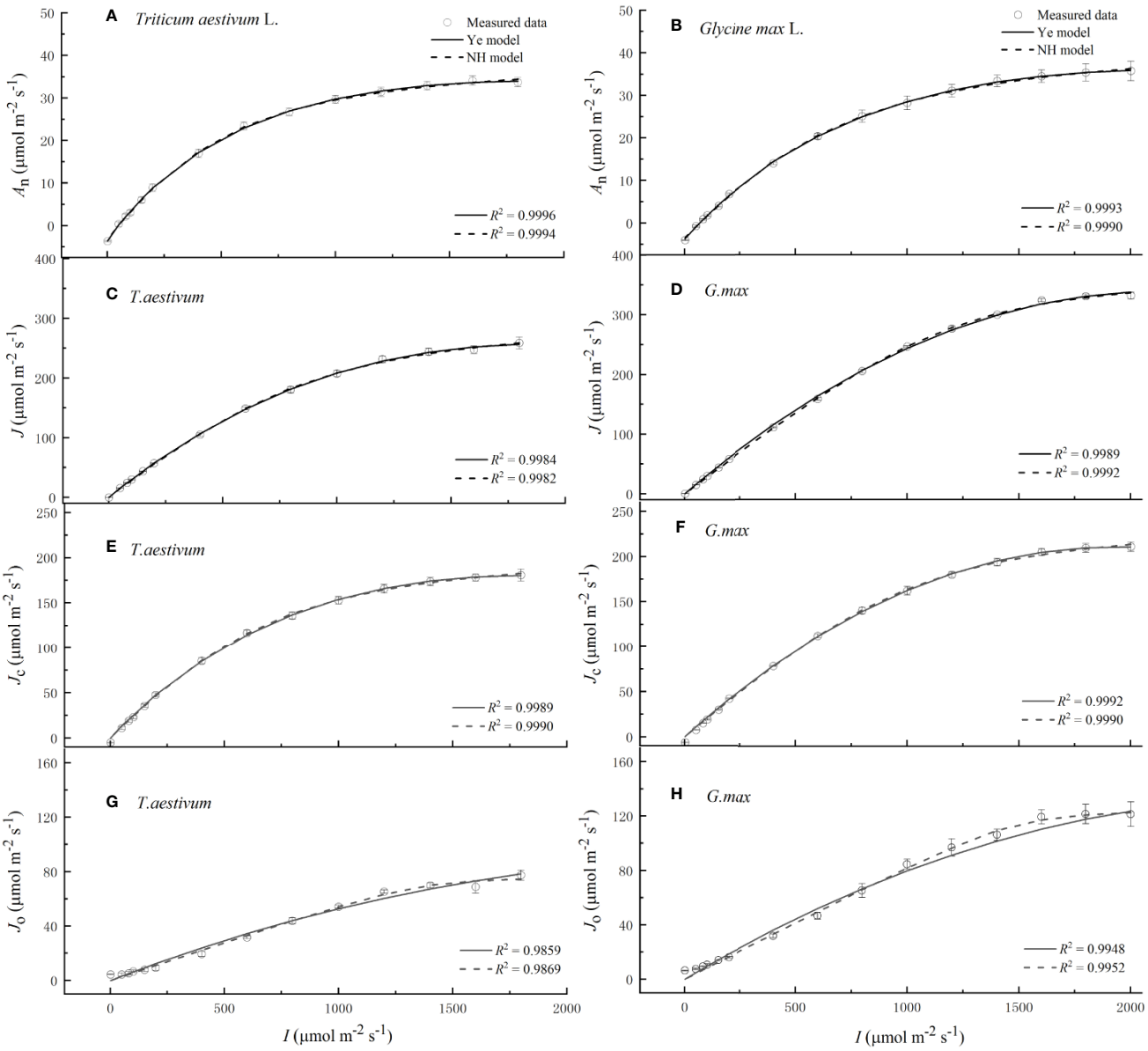

FIGURE 1 | Light response curves of net photosynthetic rate **(A, B),** electron transport rate **(C, D),** electron flow for RuBP carboxylation **(E, F)** and the electron flow for RuBP oxygenation **(G, H)** for winter wheat (*Triticum aestivum* L.) and soybean (*Glycine max* L.), respectively, over the irradiance range from 0 to 2000 μmol m^{-2} s^{-1}. Solid curves were fitted using Ye model, and dash curves were fitted using NH model. Values are means ± standard errors (n = 3).

and **Table 1**). The increase of A_n and J continued until I reached the cultivar-specific maximum values (A_{nmax} and J_{max}) at their corresponding saturation light intensities (I_{sat} and $I_{e\text{-}sat}$) (**Figure 1** and **Table 1**). Both NH model (Eqs. 1 and 2) and Ye model (Eqs. 3 and 6) showed high level of goodness of fit (R^2) to experimental observations of two species (**Figure 1** and **Table 1**). However, compared with observations, NH model significantly overestimated A_{nmax} and J_{max} ($P < 0.05$) for both soybean and winter wheat (**Table 1**). In contrast, A_{nmax} and J_{max} values returned by Ye model were in very close agreement with the observations for both species (**Table 1**).

Light Response of J_C and J_O

Both species exhibited an immediate and rapid initial increase of J_C (α_C) with the increasing I (**Figure 1** and **Table 1**). The increase of J_C continued until I reached the cultivar-specific maximum values ($J_{C\text{-}max}$) at the corresponding saturation light intensity ($I_{C\text{-}sat}$) (**Figure 1** and **Table 1**). Both Ye model (Eq. 11) and NH model (Eq. 17) showed high level of goodness of fit (R^2) to experimental observations of both species (**Figure 1** and **Table 1**). However, compared with observations, NH model significantly overestimated $J_{C\text{-}max}$ ($P < 0.05$) for both soybean and winter wheat (**Table 1**). In contrast, $J_{C\text{-}max}$ values returned by Ye model were in very close agreement with the observations for both species (**Table 1**).

Compared to the light-response rapidness of J_C, J_O exhibited a much slower initial increase (α_O) with the increasing I (**Figure 1** and **Table 1**). No species showed significant difference between the observed value of $J_{O\text{-}max}$ and that estimated by Ye model (Eq. 14) or NH model (Eq. 18) (**Table 1**). Both models showed high level of goodness of fit (R^2) to experimental observations of both species (**Figure 1** and **Table 1**).

TABLE 1 | Fitted (Ye model and NH model) and measured values (Obs.) of parameters defining the light-response curve of photosynthesis (A_n–I curve), electron transport rate (J–I curve), electron transport rate for RuBP carboxylation (J_C–I curve), and electron transport rate for RuBP oxygenation (J_O–I curve) for wheat and soybean species, respectively.

Parameters	*T. aestivum*			*G. max*		
	Ye model	NH model	Obs.	Ye model	NH model	Obs.
A_n–I curve						
θ (dimensionless)	–	0.659 ± 0.046	–	–	0.644 ± 0.073	–
α (μmol μmol $^{-1}$)	0.077 ± 0.005^a	0.069 ± 0.005^a	–	0.059 ± 0.002^a	0.055 ± 0.002^a	–
β (m^2 s μmol $^{-1}$)	(1.31 ± 0.07) × 10 $^{-4}$	–	–	(1.40 ± 0.08) × 10 $^{-4}$	–	–
γ (m^2 s μmol $^{-1}$)	(1.02 ± 0.16) × 10 $^{-3}$	–	–	(5.76 ± 0.43) × 10 $^{-4}$	–	–
A_{nmax} (μmol m^{-2} s^{-1})	33.91 ± 1.14^b	43.30 ± 1.28^a	33.71 ± 1.12^b	36.04 ± 2.11^b	47.74 ± 2.08^a	35.74 ± 2.29^b
I_{sat} (μmol m^{-2} s^{-1})	1870.58 ± 26.45^a	–	1799.59 ± 0.78^a	2199.05 ± 78.46^a	–	1999.73 ± 0.79^a
I_c (μmol m^{-2} s^{-1})	50.08 ± 6.61^a	50.42 ± 6.71 ^{a}	50.20 ± 6.67^a	66.72 ± 2.93^a	67.38 ± 2.81^a	66.82 ± 2.95^a
R_d (μmol m^{-2} s^{-1})	3.60 ± 0.21^a	3.29 ± 0.15^a	3.73 ± 0.14^a	3.76 ± 0.26^a	3.58 ± 0.13^a	4.03 ± 0.08^a
Residuals	1.12 ± 0.15^a	1.52 ± 0.34^a	–	2.26 ± 0.14^a	2.94 ± 0.84^a	–
J–I curve						
θ (dimensionless)	–	0.816 ± 0.009	–	–	0.924 ± 0.005	–
α_e (μmol μmol $^{-1}$)	0.295 ± 0.012^a	0.282 ± 0.012^a	–	0.299 ± 0.006^a	0.282 ± 0.005^a	–
β_e (m^2 s μmol $^{-1}$)	(2.42 ± 0.28) × 10 $^{-3}$	–	–	(3.07 ± 0.08) × 10 $^{-4}$	–	–
γ_e (m^2 s μmol $^{-1}$)	(1.26 ± 0.66) × 10 $^{-4}$	–	–	(-1.50 ± 0.24) × 10 $^{-4}$	–	–
J_{max} (μmol m^{-2} s^{-1})	257.23 ± 7.36^b	304.91 ± 7.11^a	261.56 ± 7.32^b	332.79 ± 5.16^b	373.87 ± 5.47^a	332.86 ± 5.01^b
$I_{e\text{-}sat}$ (μmol m^{-2} s^{-1})	1873.37 ± 109.46^a	–	1734.16 ± 66.15^a	1906.01 ± 19.97^a	–	1933.23 ± 66.27^a
Residuals	197.76 ± 119.18^a	224.69 ± 81.52^a	–	69.69 ± 6.00^a	139.25 ± 19.30^a	–
J_C–I curve						
θ (dimensionless)	–	0.770 ± 0.040	–	–	0.871 ± 0.011	–
α_C (μmol μmol $^{-1}$)	0.266 ± 0.012 a	0.248 ± 0.014^a	–	0.221 ± 0.003^a	0.207 ± 0.002^b	–
β_C (m^2 s μmol $^{-1}$)	(2.07 ± 0.10) × 10 $^{-4}$	–	–	(2.54 ± 0.03) × 10 $^{-4}$	–	–
γ_C (m^2 s μmol $^{-1}$)	(3.75 ± 0.75) × 10 $^{-4}$	–	–	(1.67 ± 1.37) × 10 $^{-5}$	–	–
$J_{C\text{-}max}$ (μmol m^{-2} s^{-1})	180.49 ± 5.16^b	210.90 ± 4.85^a	182.48 ± 5.10^b	210.66 ± 4.79^b	242.42 ± 3.43^a	210.76 ± 5.15^b
$I_{C\text{-}sat}$ (μmol m^{-2} s^{-1})	1813.42 ± 12.16^a	–	1734.16 ± 66.15^a	1938.65 ± 0.66^b	–	1999.73 ± 0.79^a
Residuals	72.25 ± 21.53^a	62.74 ± 8.96^a	–	78.54 ± 18.52^a	83.50 ± 5.26^a	–
J_O–I curve						
θ (dimensionless)	–	0.839 ± 0.159	–	–	0.987 ± 0.008	–
α_O (μmol μmol $^{-1}$)	0.062 ± 0.007^a	0.060 ± 0.007^a	–	0.087 ± 0.005^a	0.084 ± 0.005^a	–
β_O (m^2 s μmol $^{-1}$)	(3.45 ± 1.47) × 10 $^{-4}$	–	–	(4.12 ± 0.18) × 10 $^{-4}$	–	–
γ_O (m^2 s μmol $^{-1}$)	(-1.98 ± 2.75) × 10 $^{-4}$	–	–	(-3.71 ± 0.31) × 10 $^{-4}$	–	–
$J_{O\text{-}max}$ (μmol m^{-2} s^{-1})	85.67 ± 7.75^a	91.67 ± 16.52^a	79.08 ± 2.29^a	124.34 ± 7.51^a	127.13 ± 9.43^a	121.61 ± 9.14^a
$I_{O\text{-}sat}$ (μmol m^{-2} s^{-1})	2790.82 ± 1085.62^a	–	1734.16 ± 66.15^a	1860.92 ± 34.19^a	–	1866.73 ± 132.78^a
Residuals	145.10 ± 57.72^a	136.82 ± 60.25^a	–	147.28 ± 14.61^a	150.40 ± 13.62^a	–

For A_n–I curve, the parameters are: the initial slope of the A_n–I curve (α_p), the maximum A_n (A_{nmax}) and the corresponding saturation irradiance (I_{sat}), light compensation point (I_c) and dark respiration rate (R_d). For J–I curve, the parameters are: the initial slope of J–I curve (α_e), the maximum J (J_{max}) and the corresponding saturation irradiance corresponding to J_{max} ($I_{e\text{-}sat}$). For J_C–I curve, the parameters are: the initial slope of J_C–I curve (α_C), the maximum J_C ($J_{C\text{-}max}$) and the corresponding saturation irradiance corresponding to $J_{C\text{-}max}$ ($I_{C\text{-}sat}$). For J_O–I curve, the parameters are: the initial slope of J_O–I curve (α_O), the maximum J_O ($J_{O\text{-}max}$) and the corresponding saturation irradiance corresponding to $J_{O\text{-}max}$ ($I_{O\text{-}sat}$). The observation-modeling intercomparison was only conducted within each species. Within each species the different the letters denote statistically significant differences between the values fitted by Ye model, NH model and measured values (Obs.) for each parameter ($P \leq 0.05$). Values are the mean ± standard errors ($n = 3$).

DISCUSSION

Assessed with an observation-modeling intercomparison approach, the results in this study highlight the robustness of Ye model in accurately reproducing A_n–I, J–I, J_C–I, and J_O–I curves and returning key quantities defining the curves, in particular: A_{nmax}, J_{max}, $J_{C\text{-}max}$, and $J_{O\text{-}max}$. On the contrary, the NH model significantly overestimates A_{nmax}, J_{max}, and $J_{C\text{-}max}$ (**Table 1**). For the first time, our study discloses the previously widely reported overestimation of J_{max} (and A_{nmax}) by the NH model is linked to its overestimation of $J_{C\text{-}max}$ but not $J_{O\text{-}max}$.

The overestimation of A_{nmax} by NH model found in this study is consistent with the previous reports (e.g., Calama et al., 2013; dos Santos et al., 2013; Lobo et al., 2014; Ježilová et al., 2015; Mayoral et al., 2015; Ogawa, 2015; Park et al., 2016; Quiroz et al., 2017; Poirier-Pocovi et al., 2018; Ye et al., 2020). The accurate returning of A_{nmax} by Ye model found in this study is consistent with previous studies using Ye model for various species under different environmental conditions (e.g., Wargent et al., 2011; Zu et al., 2011; Xu et al., 2012a; Xu et al., 2012b; Lobo et al., 2014; Xu et al., 2014; Song et al., 2015; Chen et al., 2016; Ye et al., 2019; Yang et al., 2020; Ye et al., 2020). The robustness of Ye model has also been validated for microalgae observations, including four freshwater and three marine microalgae species (Yang et al., 2020). The Ye model reproduced the A_n–I response well for all microalgae species, and produced I_{sat} closer to the measured values than those by three widely used models for microalgae (Yang et al., 2020). Meanwhile, the overestimation of J_{max} by NH model found in this study supports Buckley and Diaz-Espejo (2015) in highlighting the demerit of the asymptotic function (i.e. NH model).

One key novelty of the present study is its evaluation of both asymptotic and nonasymptotic functions in describing the light response of electron flow allocation for carboxylation and oxygenation respectively (i.e. J_C–I and J_O–I curves). To the best of our knowledge, this is the first study which has experimentally evidenced the robustness of a nonasymptotic function (Eqs. 3, 11, 14) in accurately (1) reproducing J–I, J_C–I, and J_O–I curves and (2) returning J_{max}, $J_{C\text{-}max}$, and $J_{O\text{-}max}$ values, as well as their corresponding the saturation light intensities. These novel findings are of significance for our understanding of light responses of plant carbon assimilation and photorespiration—both are catalyzed by RuBP carboxylase/oxygenase.

The findings, and the approach of bridging experiment and modeling, in the present study remain to be tested for (1) species of different plant function types and/or climatic origin, which could exhibit different response patterns (Ye et al., 2020) and (2) plant response to interaction of multiple environmental factors (e.g., temperature, rainfall pattern, soil type) involving fluctuating light. The explicit and consistent modeling framework and parameter definitions on light responses (i.e. A_n–I, J–I, J_C–I, and J_O–I)—combined with the simplicity and robustness—allows for future transparent scaling-up of leaf-level findings to whole-plant and ecosystem scales.

CONCLUSIONS

Ye model can accurately estimate A_{nmax}, J_{max}, and $J_{C\text{-}max}$ which the NH model would overestimate. Adopting an explicit and transparent analytical framework and consistent definitions on A_n–I, J–I, J_C–I, and J_O–I curves, this study highlights the advantage of Ye model over NH model in terms of (1) its extremely well reproduction of J–I, J_C–I, and J_O–I trends over a wide I range from light-limited to light-inhibitory light intensities, (2) accurately returning the wealth of key quantities defining J–I, J_C–I, and J_O–I curves, particularly J_{max}, $J_{C\text{-}max}$, $J_{O\text{-}max}$, and their corresponding the saturation light intensities (besides A_{nmax} and I_{sat} of A_n–I curve), and (3) being transparent in disclosing that the previously widely reported but poorly explained problem of NH model—overestimation of J_{max} (and the maximum plant carboxylation capacity)—is linked to its overestimation of $J_{C\text{-}max}$ but not $J_{O\text{-}max}$. Besides, NH model cannot obtain their saturation light intensities corresponding to J_{max}, A_{nmax}, $J_{C\text{-}max}$, and $J_{O\text{-}max}$ due to its asymptotic function. This study is of significance for both experimentalists and modelers working on better representation of photosynthetic processes under dynamic irradiance conditions.

DATA AVAILABILITY STATEMENT

The raw data supporting the conclusions of this article will be made available by the authors, without undue reservation.

AUTHOR CONTRIBUTIONS

All authors contributed to the conception of the work. H-JK mainly performed the experiment. Z-PY and S-XZ drafted the original manuscript. All authors critically reviewed and revised the manuscript with new data sets and contributed substantially to the completion of the present study. All authors contributed to the article and approved the submitted version.

FUNDING

This research was supported by the Natural Science Foundation of China (Grant No. 31960054 and 31560069) and the Key Science and Technology Innovation Team Project of Wenzhou City (Grant No. C20150008).

REFERENCES

Aspinwall, M. J., King, J. S., McKeand, S. E., and Domec, J. C. (2011). Leaf-level gas-exchange uniformity and photosynthetic capacity among loblolly pine (*Pinus taeda* L.) genotypes of contrasting inherent genetic variation. *Tree Physiol.* 31, 78–91. doi: 10.1093/treephys/tpq107

Bellasio, C., Beerling, D. J., and Griffiths, H. (2015). An Excel tool for deriving key photosynthetic parameters from combined gas exchange and chlorophyll fluorescence: Theory and practice. *Plant Cell Environ.* 39, 1180–1197. doi: 10.1111/pce.12560

Bernacchi, C. J., Bagley, J. E., Serbin, S. P., Ruiz-Vera, U. M., Rosenthal, D. M., and Vanloocke, A. (2013). Modelling C_3 photosynthesis from the chloroplast to the ecosystem. *Plant Cell Environ.* 36, 1641–1657. doi: 10.1111/pce.12118

Berry, J. A., and Farquhar, G. D. (1978). "The CO2 concentrating function of C4 photosynthesis: a biochemical model," in *The Proceedings of the Fourth International Congress on Photosynthesis*. Eds. D. Hall, J. Coombs and T. Goodwin (London: Biochemical Society of London), 119–131.

Buckley, T. N., and Diaz-Espejo, A. (2015). Reporting estimates of maximum potential electron transport rate. *New Phytol.* 205, 14–17. doi: 10.1111/nph.13018

Busch, F. A., and Sage, R. F. (2017). The sensitivity of photosynthesis to O_2 and CO_2 concentration identifies strong Rubisco control above the thermal optimum. *New Phytol.* 213, 1036–1051. doi: 10.1111/nph.14258

Cai, C., Li, G., Yang, H. L., Yang, J. H., Liu, H., Struik, P. C., et al. (2018). Do all leaf photosynthesis parameters of rice acclimate to elevated CO_2, elevated temperature, and their combination, in FACE environments? *Global Change Biol.* 24, 1685–1707. doi: 10.1111/gcb.13961

Calama, R., Puértolas, J., Madrigal, G., and Pardos, M. (2013). Modeling the environmental response of leaf net photosynthesis in *Pinus pinea* L. natural regeneration. *Ecol. Model.* 51, 9–21. doi: 10.1016/j.ecolmodel.2012.11.029

Chen, Z. Y., Peng, Z. S., Yang, J., Chen, W. Y., and Ou-Yang, Z. M. (2011). A mathematical model for describing light-response curves in nicotiana tabacum l. *Photosynthetica* 49, 467–471. doi: 10.1007/s11099-011-0056-5

Chen, X., Liu, W. Y., Song, L., Li, S., Wu, C. S., and Lu, H. Z. (2016). Adaptation of epiphytic bryophytes in the understorey attributing to the correlations and trade-offs between functional traits. *J. Bryol.* 38, 110–117. doi: 10.1080/03736687.2015.1120370

Comic, G., and Briantais, J. M. (1991). Partitioning of photosynthetic electron flow between CO_2 and O_2 reduction in a C_3 leaf (*Phaseolus vulgaris* L.) at different CO_2 concentrations and during drought stress. *Planta* 183, 178–184. doi: 10.1007/bf00197786

dos Santos, J. U. M., de Carvalho, G. J. F., and Fearnside, P. M. (2013). Measuring the impact of flooding on Amazonian trees: photosynthetic response models for ten species flooded by hydroelectric dams. *Trees* 27, 193–210. doi: 10.1007/s00468-012-0788-2

Farquahr, G. D., and Busch, F. A. (2017). Changes in the chloroplastic CO_2 concentration explain much of the observed Kok effect: a model. *New Phytol.* 214, 570–584. doi: 10.1111/nph.14512

Farquhar, G. D., and Wong, S. C. (1984). An empirical model of stomatal conductance. *Aus. J. Plant Physiol.* 11, 191–210. doi: 10.1071/pp9840191

Farquhar, G. D., von Caemmerer, S., and Berry, J. A. (1980). A biochemical model of photosynthetic CO_2 assimilation in leaves of C_3 species. *Planta* 149, 78–90. doi: 10.1007/BF00386231

Farquhar, G. D., von Caemmerer, S., and Berry, J. A. (2001). Models of photosynthesis. *Plant Physiol.* 125, 42–45. doi: 10.1104/pp.125.1.42

Fila, G., Badeck, F., Meyer, S., Cerovic, Z., and Ghashghaie, J. (2006). Relationships between leaf conductance to CO_2 diffusion and photosynthesis in micropropagated grapevine plants, before and after *ex vitro* acclimatization. *J. Exp. Bot.* 57, 2687–2695. doi: 10.1093/jxb/erl040

Genty, B., Briantais, J. M., and Baker, N. R. (1989). The relationship between the quantum yield of photosynthetic electron transport and quenching of chlorophyll fluorescence. *Biochim. Biophys. Acta* 990, 87–92. doi: 10.1016/s0304-4165(89)80016-9

Ježilová, E., Nožková-Hlaváčková, V., and Duchoslav, M. (2015). Photosynthetic characteristics of three ploidy levels of *Allium oleraceum* L. (Amaryllidaceae) differing in ecological amplitude. *Plant Spec. Biol.* 30, 212–224. doi: 10.1111/1442-1984.12053

Krall, J. P., and Edward, G. E. (1992). Relationship between photosystem II activity and CO_2 fixation in leaves. *Physiol. Plant* 86, 180–187. doi: 10.1111/j.1399-3054.1992.tb01328.x

Lobo, F. D. A., Barros, M. P. D., Dalmagro, H. J., Dalmolin, Â.C., Pereira, W. E., de Souza, É.C., et al. (2014). Fitting net photosynthetic light-response curves with microsoft excel – a critical look at the models. *Photosynthetica* 52, 445–456. doi: 10.1007/s11099-014-0045-6

Long, S. P., and Bernacchi, C. J. (2003). Gas exchange measurements, what can they tell us about the underlying limitations to photosynthesis? Procedures and sources of error. *J. Exp. Bot.* 54, 2393–2401. doi: 10.1093/jxb/erg262

Mayoral, C., Calama, R., Sánchez-González, M., and Pardos, M. (2015). Modelling the influence of light, water and temperature on photosynthesis in young trees of mixed Mediterranean forests. *New For.* 46, 485–506. doi: 10.1007/s11056-015-9471-y

Ogawa, K. (2015). Mathematical consideration of the pipe model theory in woody plant species. *Trees* 29, 695–704. doi: 10.1007/s00468-014-1147-2

Ögren, E., and Evans, J. R. (1993). Photosynthetic light-response curves. *Planta* 189, 182–190. doi: 10.1007/BF00195075

Park, K. S., Bekhzod, K., Kwon, J. K., and Son, J. E. (2016). Development of a coupled photosynthetic model of sweet basil hydroponically grown in plant factories. *Hortic. Environ. Biotechnol.* 57, 20–26. doi: 10.1007/s13580-016-0019-7

Peterson, R. B. (1990). Effects of irradiance on the *in vivo* CO_2:O_2 specificity factor in tobacco using simultaneous gas exchange and fluorescence techniques. *Plant Physiol.* 94, 892–898. doi: 10.1104/pp.94.3.892

Poirier-Pocovi, M., Lothier, J., and Buck-Sorlin, G. (2018). Modelling temporal variation of parameters used in two photosynthesis models: influence of fruit load and girdling on leaf photosynthesis in fruit-bearing branches of apple. *Ann. Bot.* 121, 821–832. doi: 10.1093/aob/mcx139

Quiroz, R., Loayza, H., Barreda, C., Gavilán, C., Posadas, A., and Ramírez, D. A. (2017). Linking process- based potato models with light reflectance data: Does model complexity enhance yield prediction accuracy? *Europ. J. Agron.* 82, 104–112. doi: 10.1016/j.eja.2016.10.008

Song, L., Zhang, Y. J., Chen, X., Li, S., Lu, H. Z., Wu, C. S., et al. (2015). Water relations and gas exchange of fan bryophytes and their adaptations to microhabitats in an Asian subtropical montane cloud forest. *J. Plant Res.* 128, 573–584. doi: 10.1007/s10265-015-0721-z

Stuhlfauth, T. R., Scheuermann, R., and Foek, H. P. (1990). Light energy dissipation under water stress conditions. Contribution of reassimilation and evidence for additional processes. *Plant Physiol.* 92, 1053–1061. doi: 10.1104/pp.92.4.1053

Sun, J. S., Sun, J. D., and Feng, Z. Z. (2015). Modelling photosynthesis in flag leaves of winter wheat (*Triticum aestivum*) considering the variation in photosynthesis parameters during development. *Funct. Plant Biol.* 42, 1036–1044. doi: 10.1071/FP15140

Thornley, J. H. M. (1998). Dynamic model of leaf photosynthesis with acclimation to light and nitrogen. *Ann. Bot.* 81, 431–430. doi: 10.1006/anbo.1997.0575

Valentini, R., Epron, D., Angelis, P. D., Matteucci, G., and Dreyer, E. (1995). *In situ* estimation of net CO_2 assimilation, photosynthetic electron flow and photorespiration of Turkey oak (*Q. cerris* L.) leaves: diurnal cycles under different water supply. *Plant Cell Environ.* 18, 631–640. doi: 10.1111/j.1365-3040.1995.tb00564.x

von Caemmerer, S., and Furbank, R. T. (1999). "Modeling of C4 photosynthesis," in *C4 Plant Biology*. Eds. R. F. Sage and R. Monson (San Diego, CA: Academic Press), 169–207.

von Caemmerer, S., Farquhar, G. D., and Berry, J. A. (2009). "Biochemical model of C3 photosynthesis," in *Photosynthesis in Silico. Understanding Complexity from Molecules to Ecosystemns*. Eds. A. Laisk, L. Nedbal and Govindjee, (Dordrecht, Netherlands: Springer), 209–230.

von Caemmerer, S. (2000). *Biochemical Models of Leaf Photosynthesis* (Victoria, Australia: Csiro Publishing).

von Caemmerer, S. (2013). Steady-state models of photosynthesis. *Plant Cell Environ.* 36, 1617–1630. doi: 10.1111/pce.12098

Walker, B. J., Orr, D. J., Carmo-Silva, E., Parry, M. A., Bernacchi, C. J., and Ort, D. R. (2017). Uncertainty in measurements of the photorespiratory CO_2 compensation point and its impact on models of leaf photosynthesis. *Photosyn. Res.* 132, 245–255. doi: 10.1007/s11120-017-0369-8

Wargent, J. J., Elfadly, E. M., Moore, J. P., and Paul, N. D. (2011). Increased exposure to uv-b radiation during early development leads to enhanced photoprotection and improved long-term performance in lactuca sativa. *Plant Cell Environ.* 34, 1401–1413. doi: 10.1111/j.1365-3040.2011.02342.x

Xu, Z. F., Yin, H. J., Xiong, P., Wan, C., and Liu, Q. (2012a). Short-term responses of *Picea asperata* seedlings of different ages grown in two contrasting forest ecosystems to experimental warming. *Environ. Exp. Bot.* 77, 1–11. doi: 10.1016/j.envexpbot.2011.10.011

Xu, Z. F., Hu, T. X., and Zhang, Y. B. (2012b). Effects of experimental warming on phenology, growth and gas exchange of treeline birch (*Betula utilis*) saplings, Eastern Tibetan Plateau, China. *Eur. J. For. Res.* 131, 811–819. doi: 10.1007/s10342-011-0554-9

Xu, J. Z., Yu, Y. M., Peng, S. Z., Yang, S. H., and Liao, L. X. (2014). A modified nonrectangular hyperbola equation for photosynthetic light-response curves of

leaves with different nitrogen status. *Photosynthetica* 52, 117–123. doi: 10.1007/s11099-014-0011-3

Xu, J., Lv, Y., Liu, X., Wei, Q., and Liao, L. (2019). A general non-rectangular hyperbola equation for photosynthetic light response curve of rice at various leaf ages. *Sci. Rep.* 9, 9909. doi: 10.1038/s41598-019-46248-y

Yang, X. L., Liu, L. H., Yin, Z. K., Wang, X. Y., Wang, S. B., and Ye, Z. P. (2020). Quantifying photosynthetic performance of phytoplankton based on photosynthesis–irradiance response models. *Environ. Sci. Eur.* 32, 24. doi: 10.1186/s12302-020-00306-9

Yao, X., Zhou, H., Zhu, Q., Li, C. H., Zhang, H. J., Hu, J. J., et al. (2017). Photosynthetic response of soybean leaf to wide light-fluctuation in maize-soybean intercropping system. *Front. Plant Sci.* 8, 1695. doi: 10.3389/fpls.2017.01695

Ye, Z. P., Suggett, J. D., Robakowski, P., and Kang, H. J. (2013). A mechanistic model for the photosynthesis-light response based on the photosynthetic electron transport of PS II in C_3 and C_4 species. *New Phytol.* 152, 1251–1262. doi: 10.1111/nph.12242

Ye, Z. P., Liu, Y. G., Kang, H. J., Duan, H. L., Chen, X. M., and Zhou, S. X. (2019). Comparing two measures of leaf photorespiration rate across a wide range of light intensities. *J. Plant Physiol.* 240, 153002. doi: 10.1016/j.jplph.2019.153002

Ye, Z.-P., Ling, Y., Yu, Q., Duan, H.-L., Kang, H.-J., Huang, G.-M., et al. (2020). Quantifying light response of leaf-scale water-use efficiency and its interrelationships with photosynthesis and stomatal conductance in C_3 and C_4 Species. *Front. Plant Sci.* 11, 374. doi: 10.3389/fpls.2020.00374

Ye, Z. P. (2007). A new model for relationship between irradiance and the rate of photosynthesis in *Oryza sativa*. *Photosynthetica* 45, 637–640. doi: 10.1007/s11099-007-0110-5

Zu, Y. G., Wei, X. X., Yu, J. H., Li, D. W., Pang, H. H., and Tong, L. (2011). Responses in the physiology and biochemistry of Korean pine (*Pinus koraiensis*) under supplementary UV-B radiation. *Photosynthetica* 49, 448–458. doi: 10.1007/s11099-011-0057-4

Conflict of Interest: S-XZ was employed by the company The New Zealand Institute for Plant and Food Research Limited.

The remaining authors declare that the research was conducted in the absence of any commercial or financial relationships that could be construed as a potential conflict of interest.

frontiers in Plant Science

ORIGINAL RESEARCH
published: 12 November 2020
doi: 10.3389/fpls.2020.586543

Plasticity of Cyanobacterial Thylakoid Microdomains Under Variable Light Conditions

Myriam Canonico[1,2†], *Grzegorz Konert*[1†] *and Radek Kaňa*[1,2*]

[1] *Institute of Microbiology, CAS, Centrum Algatech, Třeboň, Czechia,* [2] *Faculty of Science, University of South Bohemia, České Budějovice, Czechia*

Photosynthetic light reactions proceed in thylakoid membranes (TMs) due to the activity of pigment–protein complexes. These complexes are heterogeneously organized into granal/stromal thylakoids (in plants) or into recently identified cyanobacterial microdomains (MDs). MDs are characterized by specific ratios of photosystem I (PSI), photosystem II (PSII), and phycobilisomes (PBS) and they are visible as sub-micrometer sized areas with different fluorescence ratios. In this report, the process of long-term plasticity in cyanobacterial thylakoid MDs has been explored under variable growth light conditions using *Synechocystis* sp. *PCC6803* expressing YFP tagged PSI. TM organization into MDs has been observed for all categorized shapes of cells independently of their stage in cell cycle. The heterogeneous PSI, PSII, and PBS thylakoid areas were also identified under two types of growth conditions: at continuous light (CL) and at light-dark (L-D) cycle. The acclimation from CL to L-D cycle changed spatial distribution of photosystems, in particular PSI became more evenly distributed in thylakoids under L-D cycle. The process of the spatial PSI (and partially also PSII) redistribution required 1 week and was accompanied by temporal appearance of PBS decoupling probably caused by the re-organization of photosystems. The overall acclimation we observed was defined as TM plasticity as it resembles higher plants grana/stroma reorganization at variable growth light conditions. In addition, we observed large cell to cell variability in the actual MDs organization. It leads us to suggest that the plasticity, and cell to cell variability in MDs could be a manifestation of phenotypic heterogeneity, a recently broadly discussed phenomenon for prokaryotes.

Keywords: photosynthesis, thylakoid membrane, microdomains and rafts, membrane organization, cyanobacteria, phenotypic heterogeneity, photosystems, phycobilisomes decoupling

OPEN ACCESS

Edited by:
Paolo Longoni,
Université de Neuchâtel, Switzerland

Reviewed by:
Vivek Dogra,
Institute of Himalayan Bioresource Technology (CSIR), India
Yanbo Hu,
Northeast Forestry University, China

***Correspondence:**
Radek Kaňa
kana@alga.cz
orcid.org/0000-0001-5768-6902

† These authors have contributed equally to this work

Specialty section:
This article was submitted to Plant Abiotic Stress, a section of the journal Frontiers in Plant Science

Received: *23 July 2020*
Accepted: *09 October 2020*
Published: *12 November 2020*

Citation:
Canonico M, Konert G and Kaňa R (2020) Plasticity of Cyanobacterial Thylakoid Microdomains Under Variable Light Conditions. Front. Plant Sci. 11:586543. doi: 10.3389/fpls.2020.586543

INTRODUCTION

Photosynthetic light reactions are catalyzed by several protein complexes, namely Photosystem I (PSI), Photosystem II (PSII), cytochrome b_6f complex, and ATPase synthase. The light energy needed to drive electron transfer is funneled to the photosystems by light-harvesting antenna complexes in cyanobacteria represented by Phycobilisomes (PBS). They are localized on the TM peripherally attached to the stromal side of PSI and PSII. It is well known that in higher plants photosystems are heterogeneously distributed with higher PSII content

typically found in granal (stacked) thylakoids (Andersson and Anderson, 1980; Albertsson, 2001). Recently (Strašková et al., 2019), a heterogeneous distribution of the photosystems has also been identified in cyanobacteria *in vivo* without changes in membrane stacking. These heterogeneous TM areas were described as MDs (Konert et al., 2019; Strašková et al., 2019) and defined as membrane regions with different composition of pigment-proteins complexes (PPCs), it means photosystems and PBS. These special membrane zones, sub-micrometer in size, define the mosaic-like structure of TM. The MD structure is very stable in a span of minutes and it seems to restrict the overall mobility of all PPCs in cyanobacteria thylakoids (Strašková et al., 2019).

The importance of TM heterogeneity is still not fully clear (Mullineaux, 2005; Pribil et al., 2014). Several theories were proposed to explain its benefits for photosynthesis, such as: (1) reduction in PSI–PSII energy spillover; (2) solution of long-distance plastoquinone diffusion; (3) acting in fine-tuning of light-harvesting during photoprotection (Herbstova et al., 2012). The last point is in line with the fact that light intensity and/or its fluctuation is a key factor affecting overall photosynthetic efficiency. The periods with excessive light are potentially harmful to photosynthetic proteins, pigments, and lipids due to the formation of ROS (Li et al., 2009). Therefore, there are several photoprotective and light-optimizing processes (see, e.g., reviews for cyanobacteria; Kirilovsky et al., 2014; Calzadilla and Kirilovsky, 2020) that either dissipate excessive irradiation (non-photochemical quenching), regulate excitation energy distribution into/between photosystems (e.g., state transitions; McConnell et al., 2002; Kaňa et al., 2012; antenna decoupling; Kaňa et al., 2009; Tamary et al., 2012) or they cope with accelerated degradation of proteins in light (e.g., photoinhibition; Li et al., 2018). However, a functional link between the response of TM organization and fluctuations in light is still rather fragmented.

The granal/stromal organization of TMs in higher plants is affected by changes in growth light (Kirchhoff, 2013) or by light stress (Herbstova et al., 2012). In the case of cyanobacterial MDs, the effect of high or fluctuating light conditions on membrane organization is less clear. Here we decided to study the plasticity of TM microdomains during a shift from CL to L-D cycle. We also wanted to test whether there is a link between cell shape (regular, elongated, dividing, and string cells) and MD organization of TM. We proved that heterogeneity of thylakoids is not a simple consequence of cell's phase in cell cycle; MDs are present in all types (shapes) of cells. Further, the MD structure is able to respond to a shift from CL to L-D conditions by more even redistribution of PSI in cells. Last but not least, cells kept their heterogeneity in sizes and shapes during the diel cycle that brought the discussion on importance of phenotypic heterogeneity in cyanobacteria.

Abbreviations: Chl, chlorophyll; CL, continuous light; d, cell diameter in μm; L-D, light-dark cycle; MD(s), microdomain(s); OD_{735}, optical density measured at 735 nm; PBS, phycobilisomes; PPCs, pigment–proteins complexes (namely, PSI, PSII, and PBS); PSI, photosystem I; Φ_{PSII}, maximal quantum yield of photosystem II in light or actual PSII efficiency in light; PSI, Photosystem I; PSII, photosystem II; ROS, reactive oxygen species; TM(s), thylakoid membrane(s).

MATERIALS AND METHODS

Strain, Cultivation, Experimental Conditions

We used the PSI-YFP tagged strain (Strašková et al., 2018, 2019) of the glucose-tolerant *Synechocystis* sp. *PCC 6803* (hereafter *Synechocystis PSI-YFP*). Before cultivation in a bioreactor (FMT150, PSI, Brno, Czech Republic, see, e.g., Nedbal et al., 2008), cells were grown in an Erlenmeyer flask for 12 days under CL (fluorescence tubes 35 μmol m^{-2} s^{-1}, 28°C, BG11 medium, continuous shaking) and regularly diluted to keep them in exponential growth phase. 400 mL of culture (OD_{735} = 0.4) was then diluted with 500 mL of BG11 and transferred into a bioreactor. Cells in the bioreactor were acclimated for 2 days to sinusoidal light without dark period and then to the sinusoidal L-D period (12/12 h, white light provided by diodes, maximal intensity of 100 μmol photons m^{-2} s^{-1}, 28°C) for 2 weeks. The culture was regularly diluted to keep cells in the exponential growth phase.

For experiments in Erlenmeyer flasks, stock culture was initially cultivated under CL (for 3 days, fluorescence tubes) and then split into two cultures cultivated differently, either under continuous or sinusoidal L-D cycle for the following 10 days. Subsequently, the light conditions were switched (continuous to sinusoidal and vice versa) and kept for 7 days to follow the reversibility of thylakoid acclimation to each light condition.

Cell Counter and Absorbance Measurements

Cell growth in the Erlenmeyer flasks was monitored by OD_{735} by WPA S800 spectrophotometer (Biochrom Ltd., England). The absorbance spectra of intact cells were measured by Unicam UV-500 (Thermo Spectronic, United States) by the integration sphere (Kaňa et al., 2009) and each data point represents an average of three daily samples (n = 3). Cell counts/sizes were estimated by Coulter Counter (Beckman, Multisizer 4, United States) at constant parameters (50 μL sample dilution in 10 mL of electrolyte made of 0.9% NaCl in deionized water; 50 μm aperture; size threshold level 1–4 μm) and averaged values were acquired by measuring three times per data point (n = 18). The curves of distribution in cell sizes were divided to get a percentage of small (range 1.2–1.6 μm) and large (range 1.601–2.5 μm) cells.

77 K Fluorescence Measurements

Low-temperature fluorescence (at 77 K) was recorded by SM-9000 (Photon Systems Instruments, Brno, Czechia) by averaging three emission spectra and repeated three times per day at different days in the bioreactor (n = 9). Parameters of measurements were as follows: excitation at 461 and 526 nm by LED; spectra detection from cells on GF-F filters (Whatman, United Kingdom); dark-adapted cells (20 min); baseline-correction with blank filter immersed with BG 11 medium.

Confocal Microscopy and Image Processing

Images were acquired using Laser Scanning Microscope LSM 880 (Zeiss, Germany) using the Plan-Apochromat 63 × /1.4 Oil DIC M27 objective. Live *Synechocystis PSI-YFP* cells were imaged in three channels: (1) YFP from PSI-YFP (excitation 514 nm; detected 526–588 nm); (2) PBS (excited at 633 nm; detected at 642–677 nm); (3) Chl from PSII (excited at 488 nm; detected at 696–758 nm). The collected images (8 bit; 512 × 512; 8.24 μs dwell time; 1 Airy unit pinhole) were processed in ImageJ (FIJI distribution). First, the individual cells were cut from the whole pictures, and single-cell parameters were analyzed cell-by-cell. Each cell was characterized by its cell area and total fluorescence of each channel. Further, cells were categorized into one of the four types based on their shape (regular, elongated, dividing, string) in a similar way as described before (Schneider et al., 2007). The categories were selected automatically based on cell circularity (4π*area/perimeter^2), roundness [4*area/(π*major_axis^2)], and feret diameter (the longest distance between any two points along the selection boundary). Category "regular" represented cells approaching circle (circularity > 0.8), "elongated" were ellipse-shaped (circularity < 0.8, roundness < 0.9, feret > 2.2), "dividing" were ellipse-shaped with constriction mark (circularity < 0.85, feret > 2.8). The string cells were constituted by two daughter cells after division (i.e., they were separated based on fluorescence pictures from thylakoids but connected based on transmission pictures) with circularity < 0.7. In required cases, some cells were manually re-assigned to a more fitting category. Total number of cells analyzed per day was between n = 709–1565 for bioreactor and n = 947 for Erlenmeyer flask experiments. In summary, about 10,000 pictures of *Synechocystis PSI-YFP* thylakoids were analyzed and interpreted.

Statistical Analysis

The statistical analysis was carried out with R 3.6.2 (RCoreTeam, 2019) in Rstudio 1.2.5033 (RStudioTeam, 2019). Packages used: dplyr (Wickham et al., 2020), agricolae (de Mendiburu, 2020), and DescTools (Signorell et mult. al, 2020). Data were analyzed with Student's t-test (Student., 1908) or one-way ANOVA (Fisher, 1921) when more than two data points were compared. Subsequent analysis with *post hoc* Duncan test (Duncan, 1955) was used when applicable. All significant points ($p < 0.05$) as compared with initial testing day were marked with asterisk on corresponding figures with colors matching the data being addressed.

RESULTS

Synechocystis sp. PCC 6803 strains with YFP tagged PSI (hereafter *Synechocystis PSI-YFP)* (Strašková et al., 2018, 2019) were first cultivated in CL condition and then shifted into sinusoidal L-D regime in the bioreactor to study the progressive acclimation of *Synechocystis PSI-YFP* to the more natural condition mimicing day-night cycle. The process was monitored *in situ* inside the bioreactor (**Figure 1A**). Cell growth was characterized by an increase in OD_{735} (**Figure 1A**); it indicted that cells grew only in light period and they stopped growth in the dark. This is in line with previous *in situ* observation with single cyanobacteria cell (Yu et al., 2017); it is obvious as *Synechocystis PSI-YFP* rely on light energy from photosynthesis. At maximal light irradiation, cell culture showed a depression in PSII maximal quantum yield (Φ_{PSII}) typical for photoinhibition. Despite the high light induced effect in PSII fluorescence, the overall photosynthetic production of oxygen by PSII was not affected, as O_2 concentration increased during daytime (**Figure 1A**). Photosynthetic activity was also followed by measuring pH of the growths medium in the bioreactor (**Figure 1A**). The culture pH can be used as an indirect measure of photosynthetic CO_2 assimilation, because pH increases when the dissolved CO_2 is removed from the water through photosynthesis. The pH (i.e., CO_2 consumption) of the culture followed a similar pattern as the oxygen evolution (**Figure 1A**).

Synechocystis PSI-YFP cells were collected from bioreactor on regular intervals and the TM structure of *Synechocystis PSI-YFP* cells was monitored by confocal microscope (**Figure 1B**). At the start of the experiment (when cells were still acclimated to CL), thylakoids had characteristic structure, color organization, and intensity as usual photosynthetic MDs in the culture grown under CL conditions (Konert et al., 2019; Strašková et al., 2019), the most typical set-up for laboratory experiments with cyanobacteria. MDs, as they were defined (Strašková et al., 2019), are characterized by typical PSI/PSII/PBS ratios that are reflected in their colors (in RGB color coding) and visible in single-cell images of TMs. Our RGB images thus showed the extent of PSI (green channel), PSII (red channel), and PBS (blue channel) co-localization (**Figure 1B—START**). These three channels images can be used also to identify different types of MDs (see color coding scheme of the seven possible MDs types in **Figure 1B**—green, red, blue, cyan, yellow, magenta, white as defined in Strašková et al., 2019) that are characterized by different ratio of PSI/PSII/PBS fluorescence. MDs were clearly visible in the RGB pictures at the start of the experiment (cells acclimated to CL) with most pronounced colors (MDs) being: (1) green with high PSI content (low PSII and PBS); (2) magenta with high PBS and PSII (low PSI); and (3) white with similarly high PSI, PSII, and PBS content (**Figure 1B**). On the contrary, MDs at the end of the experiment (cells acclimated to L-D cycle) became more "bluish" (**Figure 2C—END**), indicating a relative increase in PBS fluorescence in comparison to PSI-YFP or PSII emission.

This process of MD acclimation during the shift from CL to L-D growth was further explored. First, we characterized changes in cell sizes (**Figures 1C,D** and **Supplementary Figure 1**), and shapes (**Figures 2A,B**). Cell sizes were estimated on the level of single cells (**Figures 1C,D**) or cell suspension (cell counter, **Supplementary Figures 1A,B**) during the diel cycle consisting of 12 h dark and 12 h sinusoidal light (**Figures 2A,B**). Both methods brought the same conclusions: we observed an outline of the diel pattern in *Synechocystis PSI-YFP* cell sizes (**Figures 1C,D** and **Supplementary Figures 1A,B**). Smaller cell (with diameter $d < 1.6$ μm) counts were continuously decreasing until hours 14–16 of diel cycle. On the contrary, the larger cells

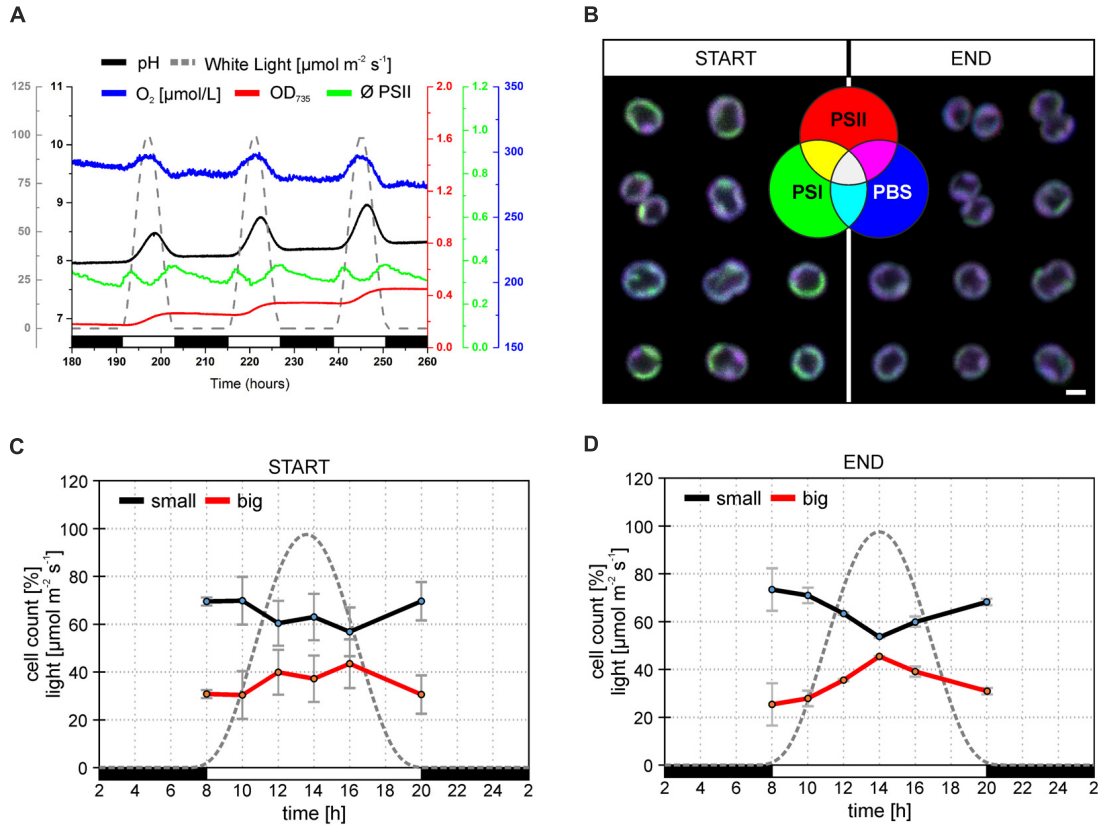

FIGURE 1 | Behavior of *Synechocystis PSI-YFP* cells during cultivation in the bioreactor. The original starting culture ("START"; cells acclimated to continuous light; days 2 and 3 in the bioreactor) was slowly acclimated to the sinusoidal light-dark cycle (12/12 h marked by white/black bars, maximal intensity 100 µmol m^{-2} s^{-1}). The light intensity profile is depicted as a gray dotted line. Cells grew in the bioreactor for 2 weeks to be considered as acclimated to the light-dark cycle ("END"; days 13 and 14 in the bioreactor). **(A)** Dynamic behavior of *Synechocystis PSI-YFP* cells during cultivation in the bioreactor *in situ*. Parameters represent: (1) OD_{735} optical density (red line) measured at 735 nm representing growth of biomass; (2) pH of culture (black line); (3) O_2 dissolved in water (blue line); (4) ϕ_{PSII} (green line) representing actual PSII efficiency under red light; (5) light intensity (µmol m^{-2} s^{-1}; gray dashed line). Data represent typical behavior of the parameters for days 6, 7, and 8 of bioreactor experiment. **(B)** Confocal microscope images of *Synechocystis PSI-YFP* cells at the start (days 2 and 3) and at the end (days 13 and 14) of bioreactor experiment. Three channel RGB pictures represent three acquired fluorescence signals showing localization of three complexes: (1) red—PSII autofluorescence; (2) blue—PBS autofluorescence; (3) green—PSI-YFP fluorescence. A combination of these three signals provides four additional membrane areas reflecting the co-localization of PSI/PSII/PBS. Overlapping signals create: (4) magenta—dominant PSI and PSII (low PBS); (5) cyan—dominant PSI and PBS (low PSII); (6) yellow—dominant PSI and PSII (low PBS); (7) white—PSI, PSII, and PBS are in similar, high content. Pictures represent typical thylakoid membrane organization of *Synechocystis PSI-YFP* during bioreactor experiment. Total number of analyzed cells per day was between n = 709 and 1565. **(C,D)** Confocal microscope measurements of cell sizes during the diel cycle, based on acquired images, two cell categories were counted: small (black line, cell area 2.0–2.8 µm^2); big (red line, cell area 2.8–4.0 µm^2). Data represent averages and SD at the start (**C**; days 2 and 3) and at the end (**D**; days 13 and 14) of the bioreactor experiment. Data represent averages of two different days of the bioreactor experiment.

(d > 1.6 µm) showed the opposite pattern (**Figures 1C,D**). There were no qualitative differences in the diel pattern between the start and the end (**Figures 1C,D** and **Supplementary Figures 1A,B**); changes were just more pronounced at the end of the experiment. Therefore, even though based on macroscopic parameters from bioreactor (**Figure 1A**), the *Synechocystis PSI-YFP* culture seems to be synchronized (which is in line with previous results; van Alphen and Hellingwerf, 2015), it remained heterogeneous on single-cell level (see cell sizes/cell shapes in **Figures 1D**, **2B**). In fact, there was no particular point at which all cells would divide at one moment. *Synechocystis PSI-YFP* cells remained heterogeneous in their sizes during the diel cycle (**Figures 1C,D**). This is visible in the accumulation of elongating and dividing cells around hours 12–14 of the diel cycle (**Figure 2B**). Interestingly, the heterogeneity of cyanobacteria culture is also visible in the TM organization in our *Synechocystis PSI-YFP* (**Figure 1C**). Despite cells and TM heterogeneity, cells tend to keep some averaged parameters (bulk parameters) constant (e.g., equilibration of average sizes between the start and the end; **Supplementary Figure 2**). On the other hand, the huge cell-to-cell heterogeneity in *Synechocystis PSI-YFP* culture (**Figure 2B**) did not allow us to depict a clear diel pattern in the intensity of the 3 fluorescence channels per cell (**Supplementary Figure 3**) that reflected relative changes in PSI-YFP, PSII, and PBS fluorescence/concentration per single cell. We cannot exclude existence of such a dial pattern in single cell PSI-YFP, PSII, and PBS fluorescence as more experimental data are necessary to prove this hypothesis.

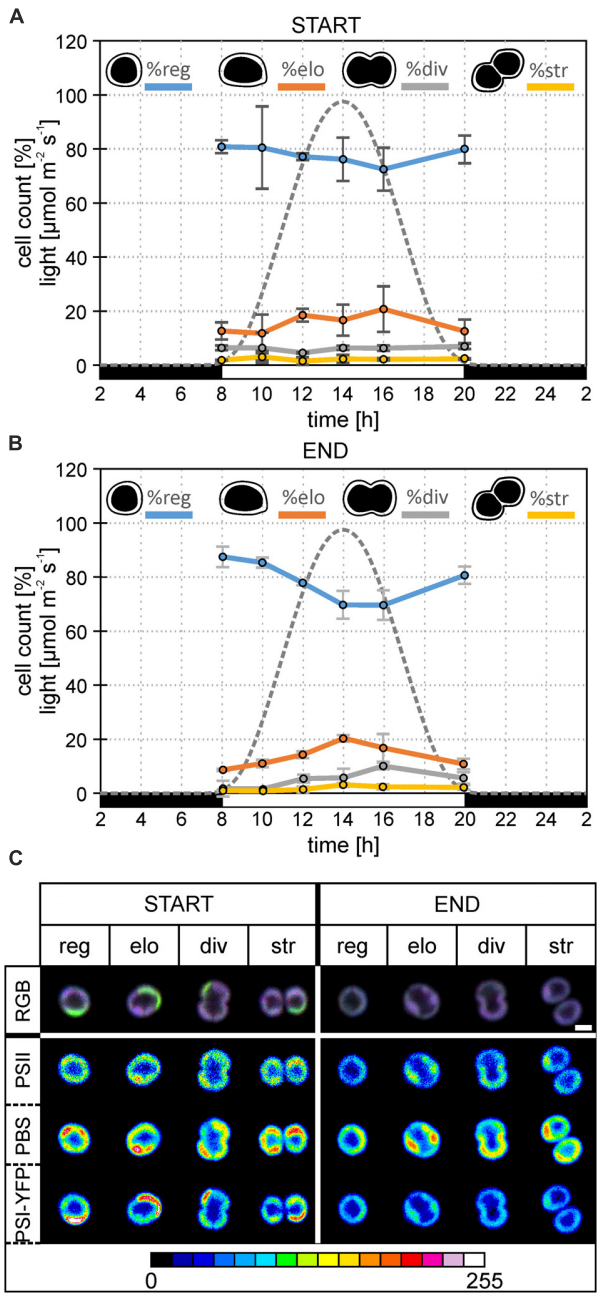

FIGURE 2 | Changes in the diel distribution of cell types and microdomain localization in the particular type of *Synechocystis PSI-YFP* cells. The original starting culture ("START"; cells acclimated to continuous light; days 2 and 3 in the bioreactor) was slowly acclimated in the bioreactor to the sinusoidal light-night cycle ("END", days 13 and 14 in bioreactor). The light intensity profile is shown as a gray dotted line. The figure describes diel changes in the cell counts and microdomains organization in the four cell types based on their shapes, namely: "*reg*"—regular cells; "*elo*"—elongated cells; "*div*"—dividing cells; "*str*"—string cells after division. Total number of cells analyzed per day was between n = 709 and 1565. **(A)** Diel cycle of relative cell counts of four typical cells—regular, elongated, dividing, string—the start of bioreactor experiment (i.e., *Synechocystis PSI–YFP* acclimated acclimated to continuous light). Intensity of sinusoidal light during the day is marked by a gray dotted line. Data represent averages and SD from 2 days of experiment (days 2 and 3). *(Continued)*

FIGURE 2 | Continued
(B) Diel cycle of relative cell counts of four typical cells—regular, elongated, dividing, string—end of bioreactor experiment (i.e., *Synechocystis PSI–YFP* acclimated to light-dark cycle). Intensity of sinusoidal light during the day is marked by a gray dotted line. Data represent averages and SD from 2 days of the experiment (days 13 and 14). **(C)** A typical microdomain organization of four typical cells—regular, elongated, dividing, string. The figure compares the start (days 2 and 3) and at the end (days 13 and 14) of the bioreactor experiment. Total number of cells analyzed per day was between n = 709 and 1565. The first row shows three channels pictures (RGB, 24-bit) with co-localization of PSII, PBS, and PSI-YFP. Colors reflect PSI/PSII/PBS co-localization, the most dominant colors were magenta (dominant PBS and PSII), green (dominant PSI), white (balanced PSI, PSII, and PBS), and blue (dominant PBS). Second, third, and fourth rows depict intensity of single-channel fluorescence of PSII, PBS, and PSI-YFP, respectively. Colors reflect intensity of fluorescence signal per channel (heatmap images) in the 8-bit scale 0–255 (see the color scale bar).

To cope with the inevitable heterogeneity of cyanobacteria cell sizes and its putative effect on thylakoid organization (**Figures 1C,D**), we tried to categorize cells based on their shapes (**Figures 2A,B**) and study their TM heterogeneity separately (**Figure 2A**). For this purpose, acquired images of *Synechocystis PSI-YFP* cells were grouped into four cell types based on their shapes reflecting their stage in the cell cycle, namely: regular, elongated, dividing, and string cells (see description in the legend of **Figure 2**). The diel profiles in the cell types (**Figure 2A**) were very similar with the diel profile of cells sizes (**Figures 1C,D**); we observed a continual decrease in the regular and increase in the number of elongated and dividing cells until midday (14 h in **Figure 2B**) when cells were more prone to cell division.

These four cell categories were then characterized by their MD organization (**Figure 2C**). At first, the heterogeneous structure of *Synechocystis PSI-YFP* thylakoids (defined by co-localization of PSI, PSII, and PBS; **Figure 2A**) was clearly visible for all four types of cells (**Figure 2C**). During the transition from CL to L-D cycle, all cell types become more "bluish" (RGB pictures in **Figure 2C**). This conclusion was confirmed by two additional independent bioreactor experiment (**Supplementary Figure 4**). In all cases, during the transition from CL to L-D cycle, cells have partially lost their green fluorescence signal due to the PSI-YFP decrease. On the other hand, the blue signal (reflecting PBS) was kept almost at the same levels between CL and L-D conditions (**Supplementary Figure 4**). It led to the more "bluish" cells thylakoids in all studied biological replicates (**Figure 2C** and **Supplementary Figure 4A**). When we analyzed the three measured channels independently in more details in the selected bioreactor experiment (see the heatmap in the **Figure 2C**), we clearly observed that the most pronounced spatial variability inside thylakoid was detected for PBS (high fluorescence red-spots in the heatmaps of PBS in **Figure 2B**). Moreover, its heterogeneity remained stable during CL to L-D transition in the bioreactor. On the contrary, the fluorescence signal of PSII (based on Chl autofluorescence) and even more PSI (based on YFP fluorescence) partially lost their heterogeneity during the CL to L-D switch (**Figure 2B**). This led us to conclude that the localization of PSII and especially PSI (in contrast to PBS) became more homogenous in thylakoids (**Figure 2B**) when cells are acclimated to the natural L-D cycle.

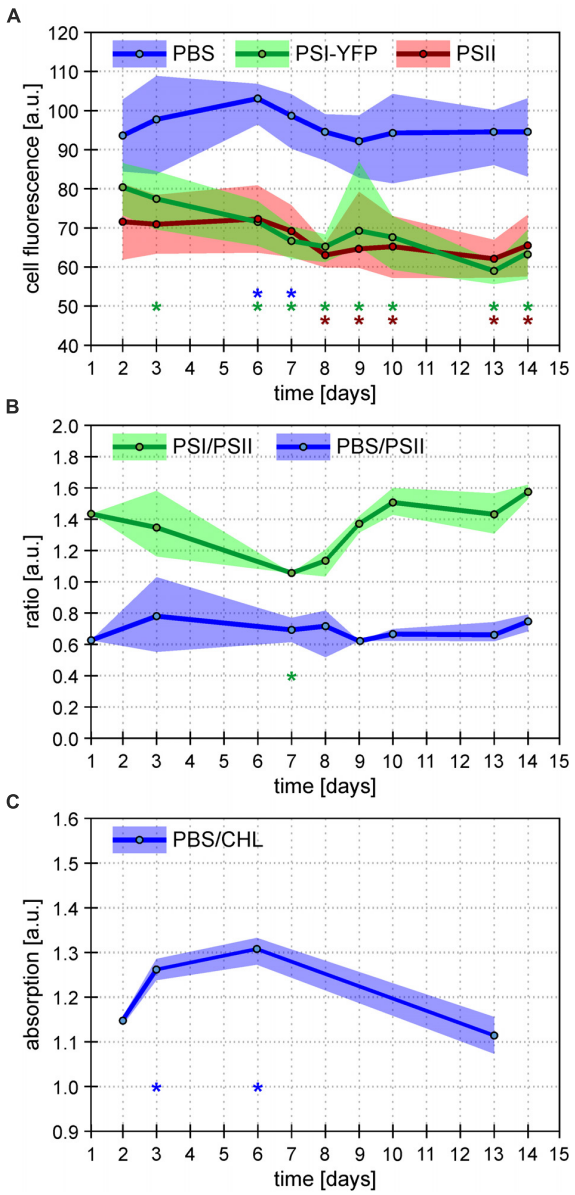

FIGURE 3 | Overall behavior of *Synechocystis PSI-YFP* cells during cultivation in bioreactor. Figures depict continual acclimation of *Synechocystis PSI-YFP* cells after their shift from continuous light (day 0) to day–night cycle in bioreactor (days 1–14). **(A)** Intensity of single-cell fluorescence of pigment–protein complexes calculated from confocal images. Three channels were detected: PSI-YFP (green), PSII (red), and PBS (blue). The day values represent averages from six different time spots per day (see **Supplementary Figure 3** for the whole diel cycle), ranges shows variability during the same day (i.e. maximal/minimal values in the day, not SD). Total number of cells analyzed per day was between $n = 709$ and 1565. Asterisks indicate data points significantly different from corresponding fluorescence value at day 2 ($p < 0.05$; blue = PBS; green = PSI-YFP; red = PSII). **(B)** Bulk measurements of PSI/PSII and PBS/PSII fluorescence ratios measured at 77 K. PSI/PSII fluorescence ratio (green line) reflects ratio of photosystems (excitation at 461 nm, detection at F730/F695 nm). The PBS/PSII fluorescence ratio (blue line) is a measure of PBS decoupling (excitation at 531 nm, detection at F660/F695 nm). Points represent averaged values per day ($n = 9$); ranges show variability during the same day (i.e. maximal/minimal values in the day, not SD). *(Continued)*

FIGURE 3 | Continued
For whole spectra, see **Supplementary Figure 5**. Asterisks indicate data points significantly different from corresponding ratio value at day 2 ($p < 0.05$; green = PSI/PSII; blue = PBS/PSI). **(C)** Bulk measurements of absorbance ratio (623/630 nm) reflecting ratio of phycobilisomes to chlorophylls from photosystems (PBS/CHL). Points represent averaged values of the selected days ($n = 3$); ranges show variability (i.e. maximal/minimal values in the day, not SD) during the same day. Asterisks indicate data points significantly different from corresponding absorption value at day 2 ($p < 0.05$).

The process of this acclimation was quantified by calculating single-cell fluorescence intensity of PSI-YFP, PSII, and PBS (**Figure 3A**). The analysis showed a cell diel pattern in the three channels' fluorescence; an initial decrease in all three channels' fluorescence, and its recovery in the second half of the light phase of the day (**Supplementary Figure 3**). Further, the averaged values per every measured day (**Figure 3A**) clearly proved that PBS fluorescence emitted by single cell was the most stable during the 2 weeks acclimation under L-D cycle; through a slight increase in the first week was leveled down at the end to recover to the original value. On the contrary, PSI-YFP and PSII fluorescence continuously went down by about 20 and 10%, respectively (**Figure 3A**) indicating a decrease in PSI and PSII content or some change in fluorescence yield during acclimation from CL (start) to L-D cycle (end).

To further explore if the effect is either due to some changes in concentration of PPCs or due to a decrease in their fluorescence quantum yield, we estimated independently PSI/PSII ratio by 77 K fluorescence emission (**Figure 3B**). The bulk measurement of PSI/PSII ratio showed an initial decrease during the first 7 days (**Figure 3B**), which correlated with a much faster decrease of PSI fluorescence visible on single cells level (**Figure 3A**). Later, the confocal data from single cells (**Figure 3A**) and PSI/PSII ratio from bulk measurements (**Figure 3B**) behaved slightly differently. We do not know the precise mechanism behind this. It could be caused by a different change in quantum yield of PSI and PSII fluorescence in re-organized MDs due to some activation state transitions or/and some other de-quenching mechanism.

In comparison to photosystems, behavior of PBS fluorescence per cells was totally different during transition from CL to L-D cycle; we have noticed surprising stability of PBS fluorescence between initial and final values (**Figure 3A**). This result was compared with several bulk 77 K fluorescence and RT absorbance measurements. At first, fluorescence ratios of F650/F695 reflecting PBS decoupling (PBS/PSII in **Figure 3B**) has been detected (**Figure 3B** and **Supplementary Figure 5**). Further, the ratio of PBS to total Chls was deduced from the absorbance spectra (A_{630}/A_{682}) (PBS/CHL; **Figure 3C**). In the first 7 days, we found a temporal stimulation of PBS decoupling (day 3 in **Figure 3B** and **Supplementary Figure 5**) together with temporal increase in the PBS content reflected by PBS/CHL (day 3 in **Figure 3C**). The increase correlated with temporal stimulation in PBS fluorescence per single cell (days 3 and 6 in **Figure 3A**). However, all these three temporal effects disappeared after full CL to L-D acclimation (day 14 in **Figures 3A–C**) that shows the final stability of PBS fluorescence per cell (**Figure 3A**). The stability

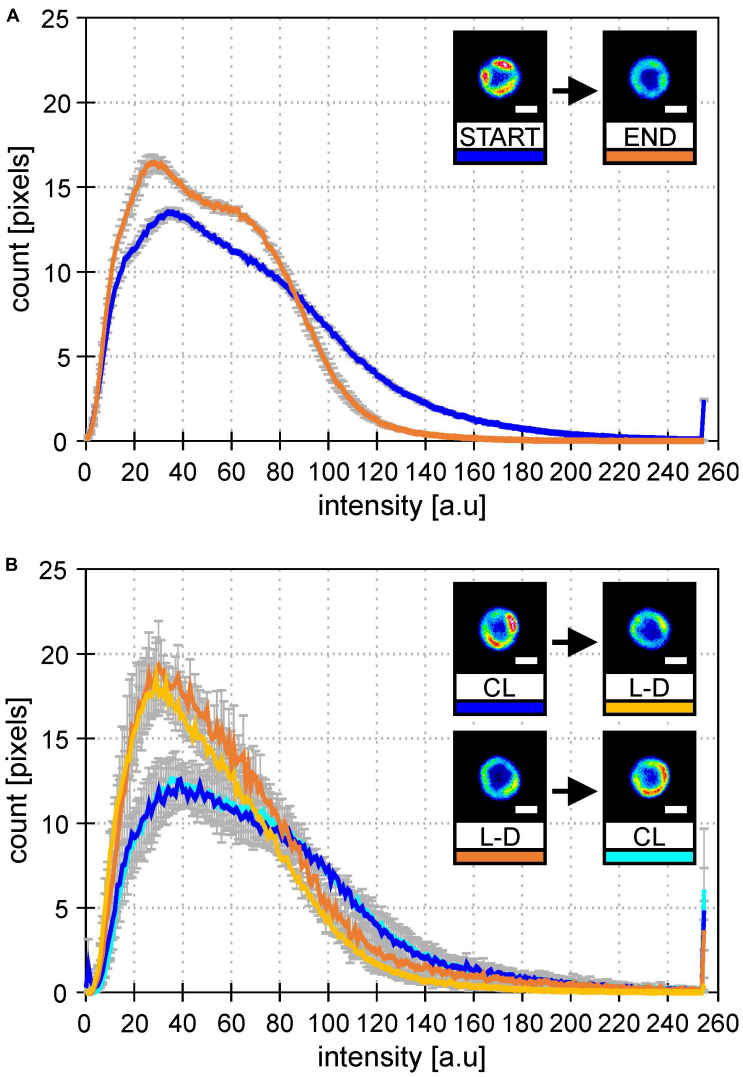

FIGURE 4 | Histograms of PSI-YFP fluorescence intensities from thylakoids of *Synechocystis PSI-YFP* cells. Figures describe distribution of the PSI-YFP fluorescence intensity in cells grown either on continuous light ("CL") or at light-dark cycle ("L-D") in bioreactor and in flask. Histograms represent intensity profiles obtained from 615 **(A)** and 4276 **(B)** cells. Scale bars in the pictures show 1 μm. Total number of cells analyzed per day was $n = 947$. **(A)** Bioreactor data: Figures depicts distribution of PSI-YFP fluorescence intensities at the start (blue; days 2 and 3) and the end (orange; days 13 and 14) of bioreactor experiment. The pictures show typical PSI-YFP thylakoid distribution in cells from the START (cells acclimated to continuous light) and the END (cells acclimated to day–night cycle for 2 weeks) of bioreactor experiment. **(B)** Erlanmeyer flask experiment: Plots of PSI-YFP fluorescence intensity distribution for cells grown in the flask at continuous of light-dark cycle. Histograms and figures describes two experiments: (1) cells grown for 10 days on the continous light ("CL"; blue) were moved into the light-dark condition for 10 days ("L-D"; yellow); (2) cells grown in the light-dark condition ("L-D"; orange) for 10 days were moved into continous light ("CL"; cyan).

in PBS highly contrasted with the behavior of photosystems since their fluorescence decreased during CL to L-D transition (**Figure 3A**). Taking all this together, single *Synechocystis PSI-YFP* cell was more stable considering PBS fluorescence as it showed the same value during CL (days 1 and 2 in bioreactor) and L-D cell (days 13 and 14 in **Figure 3**). On the other hand, photosystems in the membrane were highly re-structured during CL to L-D transition; this is visible on single cell level as a more homogenous PSI distribution inside the cell (**Figure 2C** and **Supplementary Figure 4**). All these data shows that MDs are naturally occurring structures of TM (Strašková et al., 2019) and that they show plasticity in response to light conditions.

To check whether it was L-D cycle and not bioreactor itself causing this MD behavior, we established similar growth conditions in Erlenmeyer flasks. Cultures were switched between CL and L-D and then back to original condition to see the reversibility of the process (**Figure 4**). In both types of cultivation (bioreactor data in **Figure 4A** and flask data in **Figure 4B**), the addition of dark period caused spatial homogenization of PSI-YFP distribution visible in the cell pictures. Further, there was also clear narrowing of the PSI-YFP fluorescence in histograms pointing to the same effect (**Figures 4A,B**). The acclimation from growth without (CL) and with (L-D) dark period was clearly reversible as seen in the switch between CL and L-D for flask

experiment (**Figure 4B**). It seems that *Synechocystis PSI-YFP* cells responded to the addition of a dark period into continuous irradiation by reorganizing PSI into more homogeneous pattern visible at natural L-D cycle (**Figure 3**).

DISCUSSION

We have identified the ability of cyanobacterial TM to acclimate to the switch in light condition by long-term reorganization of photosystems, especially PSI. Except the TM plasticity, we also observed MDs diversity in population of cells in line with previous results (Konert et al., 2019; Strašková et al., 2019). We have raised a hypothesis that the qualitative switch in PSI organization (more homogeneous PSI distribution during L-D than during CL irradiation; **Figure 2C** and **Supplementary Figure 4**) is triggered by the addition of a dark period for L-D cycle. The hypothesis has been proved in the flask experiments when light conditions were switched between CL and L-D and back to the original conditions. The variability in PSI distribution (more homogeneous in L-D, more heterogeneous in CL) and reversibility of the process (**Figure 4B**) shows the plasticity of cyanobacterial MDs. Even though MDs are very stable during short term changes in irradiation (e.g., in minutes; Strašková et al., 2019), some previous data have already indicated process of long-term acclimation in scale of hour(s) on single cell level (Steinbach and Kaňa, 2016) or on cell population level (Konert et al., 2019). Here we show clear response in PSI re-distribution after a long-term change in growth irradiation from CL to L-D conditions.

Our data indicate that the key factor in the acclamation to L-D cycle seems to be the redistribution of photosystems, especially PSI (**Figure 2C**). The special PSI redistribution could be helpful to better cope with diurnal changes in metabolism of cyanobacteria at diel cycles (Welkie et al., 2019). In fact, during the L-D cycles, there is an everyday shift from daytime photosynthesis to night-time oxidative pentose phosphate pathway (Diamond et al., 2015). The night-time is also used for cell detoxification from ROS. It is a question, whether the special redistribution of PSI at L-D cycle is favorable for larger NADPH production (formed in photosynthesis) that is preferentially used (more than NADH) as a reductant source for ROS detoxification (Flores and Herrero, 2005). The similar light-induced response on PSI level is visible also for cyanobacterial cells acclimated to high-light (Kopečná et al., 2012) or to a light of different quality (El Bissati and Kirilovsky, 2001; Luimstra et al., 2020). It is well know that a shift from low-light to high-light growth conditions stimulates decrease in the PSI to PSII ratio due to selective suppression of the amount of functional PSI (Murakami and Fujita, 1993; Murakami et al., 1997). Another important light-induced regulatory mechanism connected with PSI is light induced state transitions (see, e.g., Kirilovsky et al., 2014 for review). Interestingly, one from the older model of state transition proposed also PSI monomerization (Bald et al., 1996) and changes in spatial organization photosystems in TM during state transitions. In that model, PSII particles are aligned in rows in state 1 compared to state 2 with more randomly distributed particles (Olive et al., 1986, 1997). In light with the above-mentioned results, we tend to suggest that also TM plasticity, as we saw it based on PSI/PSII and PBS co-localization (**Figure 2**), is controlled by PSI to PSII ratio. The change in the ratio is induced by light and includes regulation of several genes (Luimstra et al., 2020). However, it is still not clear whether PSI to PSII ratio is a redox-control (El Bissati and Kirilovsky, 2001) or a photoreceptor control process. It needs to be still clarified whether TM plasticity connected with PSI redistribution (see **Figure 2**) is a redox or a photoreceptor control mechanism.

Redox/photoreceptor control is the only well-known control mechanisms of TM plasticity (Baulina, 2012). It needs to include various membrane-connected phenomena from the ion-induced effect on TM electrical double layer (Kaňa and Govindjee., 2016) to some changes in membrane energization (effect of DCMU in Stingaciu et al., 2019). In addition to photosystems, also PBS could be another factor in play, as TM morphology is changed if PBS structure is affected by mutation (Olive et al., 1997; Collins et al., 2012). Indeed, we have found a temporal appearance of the PBS decoupling in the middle of our 2 weeks experiment (**Figures 3B,C** and **Supplementary Figure 5**). The actual importance of PBS decoupling for cyanobacteria physiology and photoprotection is still matter of discussion (see, e.g., Kirilovsky et al., 2014; Calzadilla and Kirilovsky, 2020 for reviews). Several works have been published proposing physiological importance of PBS decoupling at various circumstances including high light stress (Tamary et al., 2012; Steinbach and Kaňa, 2016) or state transitions (Kaňa et al., 2009; Kupper et al., 2009; Chukhutsina et al., 2015; Ranjbar Choubeh et al., 2018). Our data indicate that PBS decoupling could play another role during reorganization of TM proteins. In a situation when photosystems need to be slowly redistributed in thylakoid during few days, PBS are more prone to be decoupled (**Figures 3B,C**) and it can be detected by a typical increase in the PBS emission on single cell level (**Figure 3A**) or in the whole suspension (**Supplementary Figure 5**). As soon as photosystems are reorganized in a new type of a steady distribution (i.e., thylakoids are acclimated to L-D cycle), the PBS fluorescence disappears as the proper PSI–PBS and PSII–PBS interactions are re-established. Indeed, the increase in the PBS fluorescence disappeared on the end of bioreactor experiment, when cells were acclimated to the L-D cycle (**Supplementary Figure 5**). Surprisingly, when comparing the first and the last day during transition from CL to L-D, the PBS composition (deduced from a single cell fluorescence) seems to be unaffected; PBS were then more stable then photosystems (**Figures 3B,C**). Therefore, the increase in the PBS decoupling was only a temporal process that seems to be conditional for successful reorganization of photosystems in TM during changing light conditions.

Our bioreactor experiment showed structural changes in organization of TM proteins within hours/days. Similar short-term structural plasticity of TM (in minutes) is also known as light/dark-induced TM swelling/shrinking visible in electron micrograph (Murakami and Packer, 1970). This process has been recently confirmed by neutron scattering method (Nagy et al., 2011; Stingaciu et al., 2019). However, this effect is probably undetectable by our method as MDs seem to be very stable in short term (Strašková et al., 2019). Recently, there were other

studies proposing the fast reorganization of TM proteins during few minutes of very high light (Sarcina et al., 2006; Tamary et al., 2012; Casella et al., 2017). These data, though, do not correspond with the observed stability of MDs (Strašková et al., 2019). The observed discrepancy could be a result of rather non-physiological high irradiances used in these studies (from tens to hundred thousand μmol m^{-2} s^{-1}). Other explanation could be that such dynamic behavior can be present only in few specific cells (see discussion of phenotypic heterogeneity below). In fact, we agree with these authors that cyanobacterial TM proteins have the ability to be reorganized in thylakoids based on current light conditions. However, our data show rather slower kinetics behind (hours-days). The organization of pigment-proteins in MDs is rather stable in minutes of physiological high-light (Strašková et al., 2019), that is also supported by their very low mobility (see recent reviews, Kirchhoff, 2008; Mullineaux, 2008; Kaňa, 2013). Based on our data, reorganization of TM requires hours (Steinbach and Kaňa, 2016; Konert et al., 2019) or days (**Figures 2C**, **4A,B**) to be clearly visible and detectable on single cell level as different types of MDs. Therefore, instead of the term "dynamics of TM," we prefer to talk about "TM plasticity" in a similar meaning as it is known for higher plants thylakoids (Pribil et al., 2014). Indeed, our cyanobacterial MDs are able to be reorganized in a similar way as it can be seen for granal/stromal thylakoids (Kirchhoff, 2013).

Our data pointed out that TM plasticity needs to be considered in light of cell to cell heterogeneity of cyanobacteria. We provide evidence of *Synechocystis PSI-YFP* population heterogeneity considering their sizes (**Figure 1**) and shapes (**Figure 2**) during the diel cycle. The phenomenon has been already noted by the previous work (Strašková et al., 2019) where count of MDs per single cell was shown to be variable (from one to four). It indicates that research on cyanobacterial response to variable light conditions requires single cell methods because cyanobacterial cells are not uniformed. It seems that such population heterogeneity in cyanobacteria cultures seems to be inevitable as cyanobacteria cells often forms two subpopulations (Martins et al., 2018). It is caused by multiple factors that coordinate cyanobacterial cell growth and division (Yang et al., 2010). The main factors for most of bacteria could be listed as environmental (e.g., light conditions for photothrophs), the internal circadian clock, and the cell-volume control (Nordholt et al., 2020). Those three interacts also in cyanobacteria in a complex manner and form heterogeneous population of cells. For instance, considering volume control, cyanobacteria behave as "adders"—they are prone to divide when a certain volume has been added after division (Yu et al., 2017). Interestingly, it is in contrast to current view on other phototrophs (algae), where the cell cycle progression is considered to be regulated by critical size and algae can be fully synchronized naturally by alternating light/dark period (Nishihama and Kohchi, 2013). Various groups have shown that the cell division and growth in algae are tightly linked to light levels (Bišová and Zachleder, 2014) in contrast to cyanobacteria (Yang et al., 2010). In this prokaryotic photothrophs, cell division is freely "allowed" at certain times of the day and the division window can only be narrowed by light/day cycles (Martins et al., 2018).

Stepping from the single cell level to the cell population level, the phenomenon we observed in single cells, structural plasticity of thylakoid MDs, could also manifest a more general trend typical for bacteria cells: phenotypic heterogeneity (Grote et al., 2015). It describes the inevitable occurrence of "non-conformist" cells (cells with distinct phenotype) within isogenic (cyano)-bacterial populations. The phenotypic heterogeneity allows genotypes to persist in a fluctuating environment (Ackermann, 2015) like our variable L-D cycle. However, we still do not know in details why cyanobacteria keep their MD organization heterogeneous in the population (Konert et al., 2019; Strašková et al., 2019). The plasticity of MDs could be a manifestation of phenotypic heterogeneity, a recently broadly discussed phenomenon of non-genetic cell-to-cell differences in microbial population (Van Boxtel et al., 2017). More experimental work needs to be done to address the connection between the behavior of MDs structure on the single-cell and on the population level.

DATA AVAILABILITY STATEMENT

The original contributions presented in the study are included in the article/**Supplementary Material**. Further inquiries can be directed to the corresponding author/s.

AUTHOR CONTRIBUTIONS

RK designed and supervised the project and wrote the manuscript. MC and GK were involved in the project discussion, carried out all the experimental work, and analyzed the data. GK contributed to confocal microscopy. MC contributed to all other methods. All authors interpreted the data, discussed the results, and commented on the manuscript.

FUNDING

The study was supported by the Czech Science Foundation (Project 19-11494S). The instrumentation at center ALGATECH was supported by the institutional project Algamic (CZ.1.05/2.1.00/19.0392).

ACKNOWLEDGMENTS

We also thank Jiří Šetlík for his help with bioreactor and Barbora Šedivá for the fluorescence measurements and data processing. We would also like to thank Eliška Kuthanová and Minna Koskela for reading the manuscript.

SUPPLEMENTARY MATERIAL

The Supplementary Material for this article can be found online at: https://www.frontiersin.org/articles/10.3389/fpls.2020.586543/full#supplementary-material

REFERENCES

Ackermann, M. (2015). A functional perspective on phenotypic heterogeneity in microorganisms. *Nat. Rev. Microbiol.* 13, 497–508. doi: 10.1038/nrmicro3491

Albertsson, P. -Å (2001). A quantitative model of the domain structure of the photosynthetic membrane. *Trends Plant Sci.* 6, 349–354. doi: 10.1016/s1360-1385(01)02021-0

Andersson, B., and Anderson, J. M. (1980). Lateral heterogeneity in the distribution of chlorophyll-protein complexes of the thylakoid membranes of spinach-chloroplasts. *Biochim. Biophys. Acta* 593, 427–440. doi: 10.1016/0005-2728(80)90078-x

Bald, D., Kruip, J., and Rogner, M. (1996). Supramolecular architecture of cyanobacterial thylakoid membranes: how is the phycobilisome connected with the photosystems? *Photosynth. Res.* 49, 103–118. doi: 10.1007/bf00117661

Baulina, O. I. (2012). "Ultrastructural plasticity of cyanobacteria under dark and high light intensity conditions," in *Ultrastructural Plasticity of Cyanobacteria*, (Berlin: Springer-Verlag), 11–63. doi: 10.1007/978-3-642-32781-0_2

Bišová, K., and Zachleder, V. (2014). Cell-cycle regulation in green algae dividing by multiple fission. *J. Exp. Bot.* 65, 2585–2602. doi: 10.1093/jxb/ert466

Calzadilla, P. I., and Kirilovsky, D. (2020). Revisiting cyanobacterial state transitions. *Photochem. Photobiol. Sci.* 19, 585–603. doi: 10.1039/c9pp00451c

Casella, S., Huang, F., Mason, D., Zhao, G. Y., Johnson, G. N., Mullineaux, C. W., et al. (2017). Dissecting the native architecture and dynamics of cyanobacterial photosynthetic machinery. *Mol. Plant* 10, 1434–1448. doi: 10.1016/j.molp.2017.09.019

Chukhutsina, V., Bersanini, L., Aro, E.-M., and van Amerongen, H. (2015). Cyanobacterial light-harvesting phycobilisomes uncouple from photosystem i during dark-to-light transitions. *Sci. Rep.* 5:14193.

Collins, A. M., Liberton, M., Jones, H. D. T., Garcia, O. F., Pakrasi, H. B., and Timlin, J. A. (2012). Photosynthetic pigment localization and thylakoid membrane morphology are altered in synechocystis 6803 phycobilisome mutants. *Plant Physiol.* 158, 1600–1609. doi: 10.1104/pp.111.192849

de Mendiburu, F. (2020). *agricolae: Statistical Procedures for Agricultural Research*. doi: 10.1104/pp.111.192849. Available online at: https://cran.r-project.org/web/packages/agricolae/index.html

Diamond, S., Jun, D. R., Rubin, B. E., and Golden, S. S. (2015). The circadian oscillator in Synechococcus elongatus controls metabolite partitioning during diurnal growth. *Proc. Natl. Acad. Sci. U.S.A.* 112, E1916–E1925.

Duncan, D. B. (1955). Multiple range and multiple F tests. *Biometrics* 11, 1–42. doi: 10.2307/3001478

El Bissati, K., and Kirilovsky, D. (2001). Regulation of psbA and psaE expression by light quality in *Synechocystis* species PCC 6803. A redox control mechanism. *Plant Physiol.* 125, 1988–2000. doi: 10.1104/pp.125.4.1988

Fisher, R. A. (1921). On the "Probable Error" of a coefficient of correlation deduced from a small sample. *Metron* 1, 3–32.

Flores, E., and Herrero, A. (2005). Nitrogen assimilation and nitrogen control in cyanobacteria. *Biochem. Soc. Trans.* 33, 164–167. doi: 10.1042/bst0330164

Grote, J., Krysciak, D., and Streit, W. R. (2015). Phenotypic heterogeneity, a phenomenon that may explain why quorum sensing does not always result in truly homogenous cell behavior. *Appl. Environ. Microbiol.* 81, 5280–5289. doi: 10.1128/aem.00900-15

Herbstova, M., Tietz, S., Kinzel, C., Turkina, M. V., and Kirchhoff, H. (2012). Architectural switch in plant photosynthetic membranes induced by light stress. *Proc. Natl. Acad. Sci. U.S.A.* 109, 20130–20135. doi: 10.1073/pnas.1214265109

Kaňa, R. (2013). Mobility of photosynthetic proteins. *Photosynth. Res.* 116, 465–479. doi: 10.1007/s11120-013-9898-y

Kaňa, R., and Govindjee. (2016). Role of ions in the regulation of light-harvesting. *Front. Plant Sci.* 7:1849. doi: 10.3389/fpls.2016.01849

Kaňa, R., Kotabová, E., Komárek, O., Šedivá, B., Papageorgiou, G. C., Govindjee, et al. (2012). The slow S to M fluorescence rise in cyanobacteria is due to a state 2 to state 1 transition. *Biochim. Biophys. Acta Bioenerg.* 1817, 1237–1247. doi: 10.1016/j.bbabio.2012.02.024

Kaňa, R., Prášil, O., Komárek, O., Papageorgiou, G. C., and Govindjee. (2009). Spectral characteristic of fluorescence induction in a model cyanobacterium, *Synechococcus* sp (PCC 7942). *Biochim. Biophys. Acta* 1787, 1170–1178. doi: 10.1016/j.bbabio.2009.04.013

Kirchhoff, H. (2008). Significance of protein crowding, order and mobility for photosynthetic membrane functions. *Biochem. Soc. Trans.* 36, 967–970. doi: 10.1042/bst0360967

Kirchhoff, H. (2013). Architectural switches in plant thylakoid membranes. *Photosynth. Res.* 116, 481–487. doi: 10.1007/s11120-013-9843-0

Kirilovsky, D., Kaňa, R., and Prášil, O. (2014). "Mechanisms modulating energy arriving at reaction centers in cyanobacteria," in *Non-Photochemical Quenching and Energy Dissipation in Plants, Algae and Cyanobacteria*, Vol. 40, eds B. Demmig-Adams, G. Garab, W. A. Iii, and Govindjee (Dordrecht: Springer Netherlands), 471–501. doi: 10.1007/978-94-017-9032-1_22

Konert, G., Steinbach, G., Canonico, M., and Kaňa, R. (2019). Protein arrangement factor: a new photosynthetic parameter characterizing the organization of thylakoid membrane proteins. *Physiol. Plant.* 166, 264–277. doi: 10.1111/ppl.12952

Kopečná, J., Komenda, J., Bučinská, L., and Sobotka, R. (2012). Long-term acclimation of the cyanobacterium Synechocystis PCC 6803 to high light is accompanied by an enhanced production of chlorophyll that is preferentially channeled to trimeric PSI. *Plant Physiol.* 160, 2239–2250. doi: 10.1104/pp.112.207274

Kupper, H., Andresen, E., Wiegert, S., Simek, M., Leitenmaier, B., and Šetlik, I. (2009). Reversible coupling of individual phycobiliprotein isoforms during state transitions in the cyanobacterium Trichodesmium analysed by single-cell fluorescence kinetic measurements. *Biochim. Biophys. Acta* 1787, 155–167. doi: 10.1016/j.bbabio.2009.01.001

Li, L., Aro, E. M., and Millar, A. H. (2018). Mechanisms of photodamage and protein turnover in photoinhibition. *Trends Plant Sci.* 23, 667–676. doi: 10.1016/j.tplants.2018.05.004

Li, Z. R., Wakao, S., Fischer, B. B., and Niyogi, K. K. (2009). Sensing and responding to excess light. *Annu. Rev. Plant Biol.* 60, 239–260. doi: 10.1146/annurev.arplant.58.032806.103844

Luimstra, V. M., Schuurmans, J. M., Hellingwerf, K. J., Matthijs, H. C. P., and Huisman, J. (2020). Blue light induces major changes in the gene expression profile of the cyanobacterium *Synechocystis* sp. PCC 6803. *Physiol. Plant.* 170, 10–26. doi: 10.1111/ppl.13086

Martins, B. M. C., Tooke, A. K., Thomas, P., and Locke, J. C. W. (2018). Cell size control driven by the circadian clock and environment in cyanobacteria. *Proc. Natl. Acad. Sci. U.S.A.* 115, E11406–E11424. doi: 10.1002/(sici)1521-1878(200001)22:1<10::aid-bies4>3.0.co;2-a

McConnell, M. D., Koop, R., Vasil'ev, S., and Bruce, D. (2002). Regulation of the distribution of chlorophyll and phycobilin-absorbed excitation energy in cyanobacteria. A structure-based model for the light state transition. *Plant Physiol.* 130, 1201–1212. doi: 10.1104/pp.009845

Mullineaux, C. W. (2005). Function and evolution of grana. *Trends Plant Sci.* 10, 521–525. doi: 10.1016/j.tplants.2005.09.001

Mullineaux, C. W. (2008). Factors controlling the mobility of photosynthetic proteins. *Photochem. Photobiol.* 84, 1310–1316. doi: 10.1111/j.1751-1097.2008.00420.x

Murakami, A., and Fujita, Y. (1993). regulation of stoichiometry between PSI and PSII in response to light regime for photosynthesis observed with synechocystis PCC-6714 – relationship between redox state of CYT B6-F complex and regulation of PSI formation. *Plant Cell Physiol.* 34, 1175–1180.

Murakami, A., Kim, S. J., and Fujita, Y. (1997). Changes in photosystem stoichiometry in response to environmental conditions for cell growth observed with the cyanophyte *Synechocystis* PCC 6714. *Plant Cell Physiol.* 38, 392–397. doi: 10.1093/oxfordjournals.pcp.a029181

Murakami, S., and Packer, L. (1970). Light-induced changes in conformation and configuration of thylakoid membrane of ulva and porphyra chloroplasts in-vivo. *Plant Physiol.* 45, 289–299. doi: 10.1104/pp.45.3.289

Nagy, G., Posselt, D., Kovács, L., Holm, J. K., Szabó, M., Ughy, B., et al. (2011). Reversible membrane reorganizations during photosynthesis in vivo: revealed by small-angle neutron scattering. *Biochem. J.* 436, 225–230. doi: 10.1042/bj20110180

Nedbal, L., Trtílek, M., Cervený, J., Komárek, O., and Pakrasi, H. B. (2008). A photobioreactor system for precision cultivation of photoautotrophic microorganisms and for high-content analysis of suspension dynamics. *Biotechnol. Bioeng.* 100, 902–910. doi: 10.1002/bit.21833

Nishihama, R., and Kohchi, T. (2013). Evolutionary insights into photoregulation of the cell cycle in the green lineage. *Curr. Opin. Plant Biol.* 16, 630–637. doi: 10.1016/j.pbi.2013.07.006

Nordholt, N., van Heerden, J. H., and Bruggeman, F. J. (2020). Biphasic cell-size and growth-rate homeostasis by single *Bacillus* subtilis cells. *Curr. Biol.* 30, 2238–2247.e5.

Olive, J., Ajlani, G., Astier, C., and Recouvreur, M. (1997). Ultrastructure and light adaptation of phycobilisome mutants of Synechocystis PCC 6803. *Biochim. Biophys. Acta* 1319, 275–282. doi: 10.1016/s0005-2728(96)00168-5

Olive, J., Mbina, I., Vernotte, C., Astier, C., and Wollman, F. A. (1986). Randomization of the ef particles in thylakoid membranes of synechocystis-6714 upon transition from state-i to state-ii. *FEBS Lett.* 208, 308–312. doi: 10.1016/0014-5793(86)81039-0

Pribil, M., Labs, M., and Leister, D. (2014). Structure and dynamics of thylakoids in land plants. *J. Exp. Bot.* 65, 1955–1972. doi: 10.1093/jxb/eru090

Ranjbar Choubeh, R., Wientjes, E., Struik, P. C., Kirilovsky, D., and van Amerongen, H. (2018). State transitions in the cyanobacterium *Synechococcus elongatus* 7942 involve reversible quenching of the photosystem II core. *Biochim. Biophys. Acta Bioenerg.* 1859, 1059–1066. doi: 10.1016/j.bbabio.2018.06.008

RCoreTeam (2019). *R: A Language and Environment for Statistical Computing*. Available online at: http://www.r-project.org/index.html

RStudioTeam (2019). *RStudio: Integrated Development Environment for R*. Available online at: http://www.rstudio.com/

Sarcina, M., Bouzovitis, N., and Mullineaux, C. W. (2006). Mobilization of photosystem II induced by intense red light in the cyanobacterium Synechococcus sp PCC7942. *Plant Cell* 18, 457–464. doi: 10.1105/tpc.105.035808

Schneider, D., Fuhrmann, E., Scholz, I., Hess, W. R., and Graumann, P. L. (2007). Fluorescence staining of live cyanobacterial cells suggest non-stringent chromosome segregation and absence of a connection between cytoplasmic and thylakoid membranes. *BMC Cell Biol.* 8:10. doi: 10.1186/1471-2121-8-39

Signorell et mult. al, A. (2020). *DescTools: Tools for Descriptive Statistics*. Available online at: https://cran.r-project.org/package=DescTools

Steinbach, G., and Kaňa, R. (2016). Automated microscopy: macro language controlling a confocal microscope and its external illumination: adaptation for photosynthetic organisms. *Microsc. Microanal.* 22, 258–263. doi: 10.1017/s1431927616000556

Stingaciu, L.-R., O'Neill, H. M., Liberton, M., Pakrasi, H. B., and Urban, V. S. (2019). Influence of chemically disrupted photosynthesis on cyanobacterial thylakoid dynamics in *Synechocystis* sp. PCC 6803. *Sci. Rep.* 9: 5711.

Strašková, A., Knoppová, J., and Komenda, J. (2018). Isolation of the cyanobacterial YFP-tagged photosystem I using GFP-Trap (R). *Photosynthetica* 56, 300–305. doi: 10.1007/s11099-018-0771-2

Strašková, A., Steinbach, G., Konert, G., Kotabová, E., Komenda, J., Tichý, M., et al. (2019). Pigment-protein complexes are organized into stable microdomains in cyanobacterial thylakoids. *Biochim. Biophys. Acta Bioenerg.* 1860:148053. doi: 10.1016/j.bbabio.2019.07.008

Student. (1908). The probable error of a mean. *Biometrika* 6, 1–25. doi: 10.2307/2331554

Tamary, E., Kiss, V., Nevo, R., Adam, Z., Bernat, G., Rexroth, S., et al. (2012). Structural and functional alterations of cyanobacterial phycobilisomes induced by high-light stress. *Biochim. Biophys. Acta Bioenerg.* 1817, 319–327. doi: 10.1016/j.bbabio.2011.11.008

van Alphen, P., and Hellingwerf, K. J. (2015). Sustained circadian rhythms in continuous light in *Synechocystis* sp. PCC6803 growing in a well-controlled photobioreactor. *PLoS One* 10:e0127715. doi: 10.1371/journal.pone.0127715

Van Boxtel, C., Van Heerden, J. H., Nordholt, N., Schmidt, P., and Bruggeman, F. J. (2017). Taking chances and making mistakes: non-genetic phenotypic heterogeneity and its consequences for surviving in dynamic environments. *J. R. Soc. Interface* 14:20170141. doi: 10.1098/rsif.2017.0141

Welkie, D. G., Rubin, B. E., Diamond, S., Hood, R. D., Savage, D. F., and Golden, S. S. (2019). A hard day's night: cyanobacteria in diel cycles. *Trends Microbiol.* 27, 231–242. doi: 10.1016/j.tim.2018.11.002

Wickham, H., François, R., Lionel, H., and Müller, K. (2020). *dplyr: A Grammar of Data Manipulation*. Available online at: https://dplyr.tidyverse.org/

Yang, Q., Pando, B. F., Dong, G., Golden, S. S., and van Oudenaarden, A. (2010). Circadian gating of the cell cycle revealed in single cyanobacterial cells. *Science* 327, 1522–1526. doi: 10.1126/science.1181759

Yu, F. B., Willis, L., Chau, R. M. W., Zambon, A., Horowitz, M., Bhaya, D., et al. (2017). Long-term microfluidic tracking of coccoid cyanobacterial cells reveals robust control of division timing. *BMC Biol.* 15:11. doi: 10.1186/s12915-016-0344-4

Conflict of Interest: The authors declare that the research was conducted in the absence of any commercial or financial relationships that could be construed as a potential conflict of interest.

frontiers in Plant Science

MINI REVIEW
published: 23 November 2020
doi: 10.3389/fpls.2020.573881

Rationale: Photosynthesis of Vascular Plants in Dim Light

Xiaolin Wang[1], Yong Wang[2], Aifeng Ling[2], Zhen Guo[3], Muhammad Asim[1], Fupeng Song[4], Qing Wang[5], Yanguo Sun[1], Rayyan Khan[1], Huifeng Yan[1] and Yi Shi[1]**

[1] Tobacco Research Institute, of Chinese Academy of Agricultural Sciences, Qingdao, China, [2] Liangshan Branch of Sichuan Tobacco Company, Xichang, Qingdao, China, [3] First Institute of Oceanography, Ministry of Natural Resources, Qingdao, China, [4] College of Resources and Environment, Shandong Agricultural University, Tai'an, China, [5] College of Tropical Crops, Hainan University, Haikou, China

Light dominates the earth's climate and ecosystems via photosynthesis, and fine changes of that might cause extensive material and energy alternation. Dim light (typically less than 5 μmol photons m^{-2} s^{-1}) occurs widely in terrestrial ecosystems, while the frequency, duration, and extent of that are increasing because of climate change and urbanization. Dim light is important for the microorganism in the photosynthetic process, but omitted or unconsidered in the vascular plant, because the photosynthesis in the high-light adapted vascular leaves was almost impossible. In this review, we propose limitations of photosynthesis in vascular plant leaves, then elucidate the possibility and evidence of photosynthesis in terms of energy demand, stomatal opening, photosynthetic induction, and photosynthesis-related physiological processes in dim light. This article highlights the potential and noteworthy influence of dim light on photosynthesis in vascular plant leaves, and the research gap of dim light in model application and carbon accounting.

Keywords: dim light, light harvest, stomatal behavior, light induction, carbon consequence, photosynthesis

OPEN ACCESS

Edited by:
Jeremy Harbinson, Wageningen University and Research, Netherlands

Reviewed by:
Lea Hallik, University of Tartu, Estonia
Ryutaro Tokutsu, Graduate University for Advanced Studies, Sokendai, Japan

****Correspondence:***
Huifeng Yan
yanhuifeng@caas.cn
Yi Shi
shiyi@caas.cn

Specialty section:
This article was submitted to Plant Abiotic Stress, a section of the journal Frontiers in Plant Science

Received: *20 June 2020*
Accepted: *15 September 2020*
Published: *23 November 2020*

Citation:
Wang X, Wang Y, Ling A, Guo Z, Asim M, Song F, Wang Q, Sun Y, Khan R, Yan H and Shi Y (2020) Rationale: Photosynthesis of Vascular Plants in Dim Light. Front. Plant Sci. 11:573881. doi: 10.3389/fpls.2020.573881

INTRODUCTION

Plants use light both as a source of energy via photosynthesis and as a source of information (Gaston et al., 2013; Bennie et al., 2016). Leaves are always exposed to the environment with fluctuating light, which rapidly shift from being limiting for photosynthesis to high levels (Retkute et al., 2015). Dim light (typically less than 5 μmol photons m^{-2} s^{-1}) is universal in natural and artificial ecosystems, such as twilight, dawn, and moonlight (Salisbury, 1981; Raven and Cockell, 2006; Bennie et al., 2016), deep ocean (Dubinsky and Schofield, 2010; Ezequiel et al., 2015), understory (Pearcy, 1983; Valladares et al., 2011), and artificial night illumination (Gaston et al., 2013; Bennie et al., 2016; Davies and Smyth, 2018; **Table 1**). Some plants switch light conditions among different intensities. In most cases, dim light is considered as useless light for net carbon fixation, because the levels of photosynthetically active radiation (PAR) are far below the sunlit conditions (between 100 and 2000 μmol photons m^{-2} s^{-1}).

However, dim light is an exclusive energy source for photosynthesis in some species associated with dim light over a long period of time, for instance, algae and photolithotrophs in the oceans must harvest the very low light to drive photosynthesis because the PAR below the sea surface is greatly decreased, especially in the deep ocean (Dubinsky and Schofield, 2010; Ezequiel et al., 2015). Dim light possibly fulfills the energy demand for the metabolism of a unicellular organism, hence,

TABLE 1 | Light intensity of some types of dim light environment.

Light conditions	PPFD (μ mol photons m^{-2} s^{-1})	Data sources
Earth surface at the full moon	0.004	Breitler et al., 2020
300 m below the sea surface	0.02	Raven et al., 2000
Understory of rainforest	0.1	Pearcy et al., 1985
The average intensity of urban light pollution	0.5–1	Gaston et al., 2013
100 W-incandescent lamp	3	Measured in 5-m distance
150 W-fluorescent lamp	5	Measured in 5-m distance

The average light intensity of the incandescent lamp and the fluorescent lamp was measured with an optic spectrometer (AvaSpec-ULS2048XL, Avantes, Netherlands) in Beijing (39°28′N- 41°05′N–115°25′E-117°35′E), China, N = 100.

playing important roles in marine life and marine carbon sequestration. For the multicellular green plants, the use of dim light is also crucial when they are exposed in a dim environment. For example, understory plants have to acclimate as low as 0.1 μmol photons m^{-2} s^{-1} PPFD and complete their lifecycles (Salisbury, 1981; Pearcy, 1983; Valladares et al., 2011; Ezequiel et al., 2015). In actuality, dim light has been more common in recent decades due to the decrease in radiation reaching the earth surface with rising atmospheric aerosol, caused by anthropogenic emissions (Mercado et al., 2009), thus the areas of low light expanded. For another case, increasing urbanization has changed a large area of natural lands to urban lands, which would suffer great shade by urban structures in the daytime and multitudinous light pollution in nighttime (Gerrish et al., 2009; Gaston et al., 2013). To the best of our knowledge, the estimation of carbon sequestration in terrestrial ecosystems failed to take CO_2 assimilation of green plants in dim light into consideration, particularly in urban areas. This might be caused by inconclusive effects of dim light on the CO_2 assimilation sequestration, and the global carbon sequestration needs to be given wide attention.

The photosynthesis in vascular plant leaves is determined not only by energy demand but also stomatal opening and activity of a biochemical enzyme (Rubisco), which is greatly affected by PPFD. The energetic demands for photosynthesis in the vascular green plant were quite different from unicellular organisms. The photosynthesis in dim light in the unicellular organisms was widely investigated, but there were no findings about the response of photosynthetic light reaction and dark reaction to dim light in higher green plants. One of the noticeable problems is whether the high-light adapted vascular plant leaves could take full advantage of dim light for photosynthesis, because the vascular plant leaves need to capture the light and CO_2 passing through the epidermis, cytoderm, cytomembrane, and activate the necessary light-dependent photosynthetic enzymes.

In this review, we presented the limitation of photosynthesis in leaves of the vascular plants and explained the possibility of photosynthesis in terms of the driving force of reaction, stomatal opening, and activation of biochemical reaction in dim light. We critically appraised the evidence of great importance of the dim light in photosynthesis in a vascular plant and emphasized the importance of comprehensive re-consideration to those processes in photosynthetic ecophysiology and carbon sequestration of terrestrial ecosystems.

PHOTOSYNTHESIS IN DIM LIGHT

Limitation of Photosynthesis of Vascular Plants in Dim Light

The lowest photon flux density of PAR at which O_2-evolving photolithotrophs on earth appears to be able to generate photosynthesis is 10 nmol photons m^{-2} s^{-1} (Raven et al., 2000). In addition, Quigg et al. (2003) had also proved that the protein turnover, charge recombination in PSII, and proton leakage and slippage of *Dunaliella tertiolecta* and *Phaeodactylum tricornutum* could generate in dim light, respectively in the value of 30 and 3 μmol photons m^{-2} s^{-1} (Quigg et al., 2003). Photosynthesis in plant cells occurs in the chlorophyll-containing chloroplast and assimilates CO_2 in photosynthetic apparatus (Singhal et al., 2019), whether the initiation of the photosynthesis will mainly depend on the driving force of photoreaction, the capacity of CO_2 supply, and the activity of photosynthetic apparatus. Thus, energy demand, stomatal behavior, and induction of photosynthetic apparatus are the key limitations of photosynthesis under dim light conditions.

The High Energy Transfer Efficiency in Photochemical Systems of Plant Leaves

Plants have a large variety of light-harvesting strategies to adapt nearly everywhere sunlight can penetrate. The interaction of two photosynthetic pigments was synergistic on light harvesting and the absorbed light energy from plenty of antenna pigments focuses on one reaction center (RC) pigment. One typical RC and the surrounded about 250–300 pigment molecules comprise a functional photosynthetic unit (PSU) (Croce and Van Amerongen, 2014). The number of chloroplasts is kept in steady state among most of the plant species (Kura-Hotta et al., 1990; Ono et al., 1995), ranging from tens to hundreds, and thus the total surface areas of chloroplasts are greatly higher than a leaf area. The chloroplast is a typical spheroid with 5–10 μm long axis containing 10^9 chlorophyll molecules per chloroplast (Melis et al., 1998). Therefore, an enormous amount of pigment molecules produces effective energy conversion and transformation in plant leaves, resulting an efficient light harvesting.

The RC would be inactive without an antenna, the capacity of light-harvesting is crucial, especially in light-limited conditions (Croce and Van Amerongen, 2014). Thus in such conditions the antenna pigments transfer their excitation energy typically

within 1 ps to Chl a, and the excitation energy transfer proceeds via Chl a. The arrival of excitation in the RC, typically within 10^{-10} s after initial photon capture by the antenna, leads to efficient electron transfer from a primary donor (P680 of PSII) to the primary acceptor. Upon excitation by light P680 in PSII causes charge separation and releases an electron, which initiates the linear electron transfer pathway, and P680 turns to an excited state (P680*). The electron eventually leads to the reduction of the primary donor P700 of PSI, which is oxidized after it has donated an electron to Fd after light excitation through pheophytin (pheo, 3 ps), plastoquinone (Q_A and Q_B, 200 ps), cytochrome b_6f complex ($Cytb_6f$), quinine sink (PQ), and plastocyanin (PC, 100 to 1000 μs). The period of electron transfer from P680 to P700 takes less than 2 ms calculated from the most time-consuming process (Q_A to PC). The electron in P700* transfers via two electron acceptors (A_0 and A_1) and iron-sulfur cluster (F_x, F_A, and F_B) to ferredoxin (F_d), and finally delivers to oxidized nicotinamide adenine dinucleotide phosphate ($NADP^+$). This process approximately takes 100 μs. $P680^+$ is one of the products of charge separation, which can be reduced by a tyrosine residue (Y_z) in 20–260 ns, and finally be reduced by manganese cluster in 30–1000 μs via state S_1 to state S_4 (Kok et al., 1970; Dismukes and Siderer, 1981). Haumann and Junge (1994) reported that the water oxidation was a millisecond reaction step on transition S_4 to S_0, which finally liberated dioxygen (Haumann and Junge, 1994). The half-rise times of four flashes induced the fast release proton were less than 100 μs at pH 7.4 and 6.3 (Haumann and Junge, 1994). The water oxidation takes less than 2 ms to evolve O_2 on the thylakoid membranes (Mcevoy and Brudvig, 2006). **Figure 1** showed that the whole process of light reaction would take 2–3 ms via the two reaction centers (Haumann and Junge, 1994; Mcevoy and Brudvig, 2006).

There is also a risk for efficient light harvesting in restricted time. The pigments cannot remain excited for a long period, and consequently the energy will be lost as heat, radiation, or in other ways. A delay time recently reported for the PSII antenna in plants is 2 ns (Belgio et al., 2012). Thus, to guarantee a fast enough rate and a high quantum yield, the PSII in plants is mainly organized in a supercomplex (Van Bezouwen et al., 2017; Kouřil et al., 2018). The quantum efficiency of the supercomplex is near 100%, and the delay time is around 0.15 ns (Caffarri et al., 2011). Fast and effective electron transfer prevents quenching and returning of the electron. It has been accepted that the Z scheme for photosynthesis proposed by Hill and Bendall (1960) revealed two photoreaction centers, and each required 4 photons to evolve one molecule of O_2, and require 8 photons assuming the same energy distribution of two photosystems (Putnam-Evans and Barry, 2007). The energy of a single excited chlorophyll molecule cannot exceed 180 kJ mol^{-1}, but the reduction of $NADP^+$ (electron transfer from water to $NADP^+$) needs the energy of 230 kJ·mol^{-1}. Thus, there should be plenty of excited chlorophyll molecules to accomplish a certain "climbing step." The energy needed in reducing CO_2 into carbohydrate is 470 kJ mol^{-1} (Belgio et al., 2012), approximately equivalent to the energy of 8 photons assuming that the efficiency of multiphoton processes is up to 33%.

Experiments of isolated chloroplasts flashing by Joliot et al. (1969) showed that the dark-adapted chloroplasts fail to evolve O_2 after two-millisecond flashings, but the most O_2 could be detected in the third flashing and fourth flashing followed, and after that there was an O_2-evoluting peak every four flashings (Joliot et al., 1969; Joliot, 2003). The O_2-evoluting model presented by Kok reveals that the oxygen-evolving complex (OEC) can store one charge after flashing, and four stored charges can be used for water-splitting (Kok et al., 1970). Therefore, the electrons from charge separation can be stored, rather than quenching or shifting immediately.

Thus, a consequence of the dim light leads to the effective charge separation and recombination in plant leaves. This fast and effective electron transfer prevents quenching and returning of the electron, and the electrons for water splitting can be stored temporarily in the manganese clusters. These features provide feasible ATP and NADPH for photosynthesis. And the huge number of RC and antenna increases the probability of the above processes. Theoretically, the photosynthetic photoreaction in plant leaves can be driven by the energy of dim light.

Stomatal Behavior in the Dark or in Dim Light

Plants require sufficient CO_2 to enter the leaf for photosynthesis. The stomata are formed from two specialized cells (guard cells) in the epidermis, which are morphologically distinct from general epidermal cells and are responsible for regulating stomatal aperture and gas exchange between plants and atmosphere (Blatt, 2000; Julian et al., 2001). Responses of stomata to light are one of the key factors influencing photosynthesis. Stomatal closure at a low light intensity or in darkness results in reduced water loss when the potential photosynthetic rate is low. The stomata of CAM (Crassulacean acid metabolism) species, such as *Ananas comosus, Agave americana L, Opuntia Tourn. ex Mill, Cymbidium* are closed in daytime but open in the nighttime to adapt to an arid environment (Lee, 2010), and in some C_3 and C_4 species, the night-open of stomata were also observed in dark or dim light (Meidner and Mansfield, 1965; Kaufmann, 1976; Grulke et al., 2004; Ogle et al., 2012). The length of the preceding dark period might be more important than light intensity in determining the stomatal opening, which is mainly a behavior of circadian rhythms (Meidner and Mansfield, 1965).

The change in the turgor pressure of the cell causes movement in guard cells, which has been regarded as the major mechanism of blue-light mediated response, whereas the change of the intercellular CO_2 mediated movements of guard and mesophyll cells has been regarded as a major mechanism for regulation of stomatal aperture by photosynthesis (Kaufmann, 1976; Shimazaki et al., 2007; Wang et al., 2008; Lawson, 2009). It has been reported that the dim intensities of white light, down to 10 lux (the equivalent of about 0.81 μmol photons m^{-2} s^{-1}), were found sufficient to induce the response of stomatal nighttime opening (Meidner and Mansfield, 1965; Yamori et al., 2020). The blue light mediated reaction to the stomatal opening can be driven by bioenergy transferred from as low as 3 μmol photons m^{-2} s^{-1} light intensity (Meidner and Mansfield, 1965;

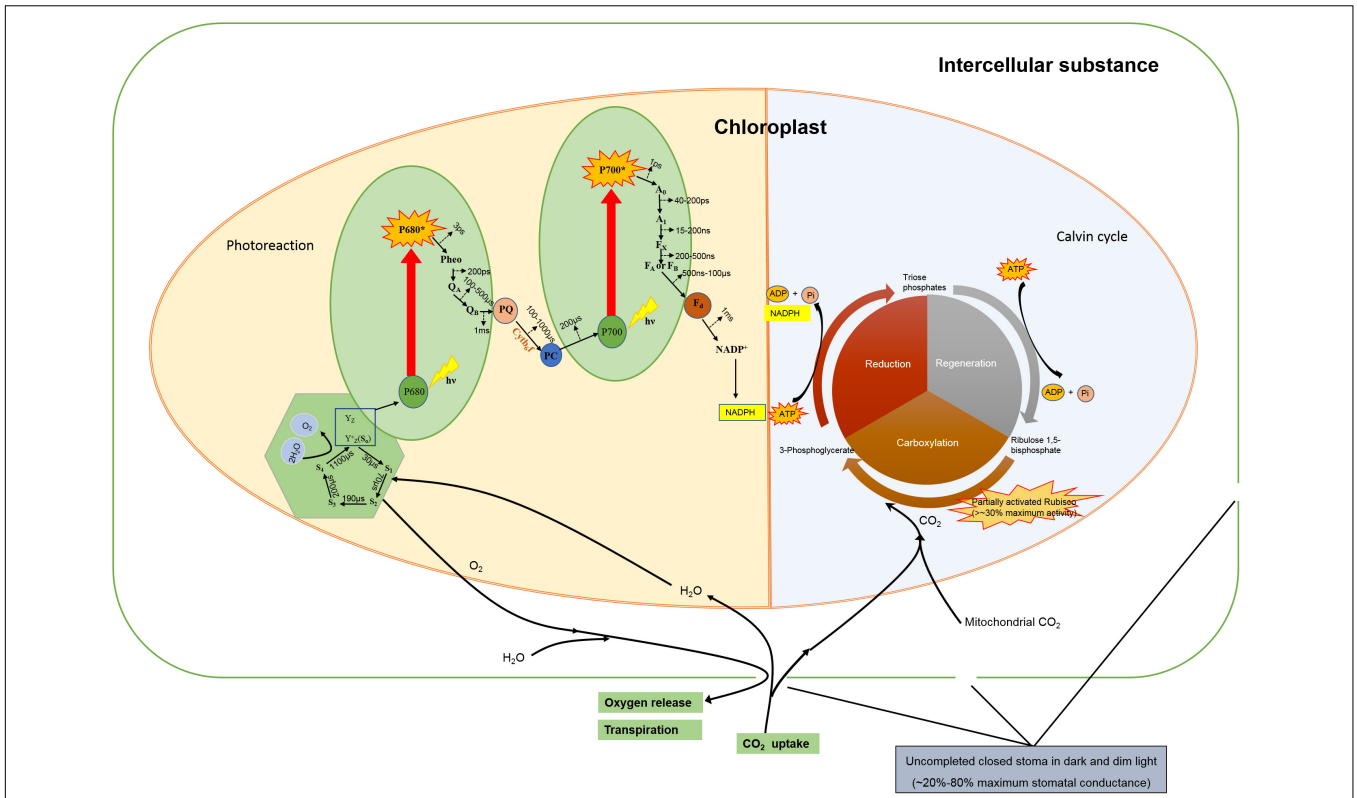

FIGURE 1 | A diagram for linear electron transfer pathway, Rubisco activities and stomatal behavior of a vascular plant leaf in the dim light. The references were showed in the "**Supplementary Material**". P680: reaction center pigment molecules of PSII, $P680^{+}$: oxidation state of P680, P680*: excited state of P680, pheo: pheophytin, Q_A and Q_B: plastoquinone, $Cytb_6f$: cytocrom b6f complex, PQ: quinine sink, PC: plastocyanin, P700: reaction center pigment molecules of PSI, $P700^{+}$: oxidation state of P700, P700*: excited state of P700, A_0: the primary electron acceptor of PSI, A_1: the secondary electron acceptor of PSI, F_x(FA,FB): iron-sulfur cluster, F_d: ferredoxin, Y_z: tyrosine residues of D_1 protein, S_0(S_1, S_2, S_3, S_4): redox state.

Shimazaki et al., 2007). A powerful proof by contradiction is if stomata close in the nighttime, how do they provide oxygen for mitochondrial respiration. Photosynthesis in dim light might be very low, and partial stomatal opening could make standard the CO_2 demand for photosynthesis. The nocturnal stomatal conductance in C_3 and C_4 plants was reported in recent years, which contributes to water loss at night (Hoshika et al., 2018; Resco De Dios et al., 2019). The benefit of the stomatal opening thus remains a confusion for botanists. But from those reports it might suggest that the stoma remain open in dark, let alone generate photosynthesis in dim light (such as moonlight) (Mayoral et al., 2020). The simplest explanation is that plants lack stomatal control during the night, and the stomata remain leaky overnight (Resco De Dios et al., 2019). Thus, the stomata behavior in the dim light fails to present a significant obstacle to carbon assimilation.

Photosynthetic Induction in the Dark or in Dim Light

The photosynthetic apparatus require an induction after a long period in darkness, ranging from minutes to several hours (Osterhout and Haas, 1918). The induction involves the buildup of ribulose-1,5-bisphosphate (RuBP) in the Calvin cycle, the activation of Rubisco (Pearcy et al., 1985; Pearcy, 1988), and stomatal opening (Han et al., 1999; Schulte et al., 2003). Loss of quantum yield in the dark and dim light is one of the important reasons for induction. The period of low light (includes darkness) and intensity of actinic light has great effects on the period of photosynthetic induction (Kirschbaum et al., 2004). The activation level of Rubisco is determined by pH, intercellular CO_2 concentration, and Mg^{2+} concentration, but the mechanisms of the activating reaction of Rubisco have not yet been completely understood (Carmo-Silva and Salvucci, 2013).

Despite this, there is still evidence that the Rubisco in leaves is still activated after a long period of darkness. A significant difference in photosynthetic efficiency was observed in street light pollution with the PAR less than 0.5 μmol photons m^{-2} s^{-1} (Meravi and Kumar Prajapati, 2020). The activity of *in vitro* Rubisco in *Raphanus sativus L* leaves in the dark was 30% before light induction (Caemmerer and Edmondson, 1986; Von Caemmerer, 2000). Salvucci et al. (1986) showed that Rubisco in *Arabidopsis thaliana L. Heynh* could remain active after a 60-min darkness, and the activity of Rubisco could quickly rise when exposed to low light (Salvucci et al., 1986). In addition, Carmo-Silva and Salvucci (2013) reported that the activity of Rubisco in *Arabidopsis thaliana* could remain a maximum of 30–50% in very low light intensity (<30 μmol photons m^{-2} s^{-1})

(Carmo-Silva and Salvucci, 2013). Consequently, after the dark adaption, the Rubisco of leaves remain active, and dim light could partially activate the Rubisco in some species, hence, results in the partial induction of photosynthesis in the leaves of these species without light induction or with somewhat induction by dim light.

CONCLUSION AND FUTURE PERSPECTIVE

The PPFD of O_2-evolving photolithotrophs on earth appears to be able to generate photosynthesis at 10 nmol photons m^{-2} s^{-1}. Vascular plants have a similar photosynthetic process and equivalent energy demand. The numerous antenna pigments harvest photons and focus on one RC, and consequently generate the electronic potential for charge separation in vascular plant leaves. The fast and effective electron transfer prevents quenching and returning of the electron, which remains steady electron flux in the photosynthetic membrane. The electron can be accumulated for water-splitting through state S_0 to S_4, resulting in O_2 evolving. Stomata, which may be different from photolithotrophs, cannot restraint gas exchange in the dim light, even if in darkness. The biochemical reaction Calvin cycle is also proved to be partially active in dim light. From the above, both reactions (dark reaction and light reaction) of photosynthesis can be conducted in dim light. Dim light occurs widely and lasts for a long time in natural and artificial environments, and this article showed that the photosynthesis of plant leaves could occur in this light condition. Thus, the increasing scenes of dim light might cause more contributions from the vascular plant to atmospheric carbon dioxide concentration on local or regional scales, which was closely related to plant development, crop yield, and climate change. In the future, the impact of dim light on plant photosynthesis should be investigated like normal light, and the models for estimation of crop yield and carbon budget should take dim light into consideration. The successful investigation to comprehend the utilization of dim light will require technological advancements to measure light characteristics and detecting methods to measure gas exchange at ecologically relevant levels in various field conditions, with theoretical foundations from this review. We hope that this article could provide some shreds of evidence for the research of carbon budget model, carbon sequestration, urban ecology, and understory ecology, etc.

AUTHOR CONTRIBUTIONS

XW did most of the data collection, XW, YS, HY, YW, AL wrote the first draft and ZG, FS, MA, QW, YS, RK edited and revised it. All authors contributed to the article and approved the submitted version.

FUNDING

This study was funded through National Key R&D Program of China (2018YFD0201100), Agricultural Science and Technology Innovation Program of Chinese Academy of Agricultural Sciences (ASTIP-TRIC03), and Key S&T Program of Sichuan Branch of China Tobacco Company (SCYC201909).

SUPPLEMENTARY MATERIAL

The Supplementary Material for this article can be found online at: https://www.frontiersin.org/articles/10.3389/fpls.2020.573881/full#supplementary-material

REFERENCES

Belgio, E., Johnson, M. P., Jurić, S., and Ruban, A. V. (2012). Higher plant photosystem Ii light-harvesting antenna, not the reaction center, determines the excited-state lifetime-both the maximum and the nonphotochemically quenched *Biophys. J.* 102 2761–2771. doi: 10.1016/j.bpj.2012.05.004

Bennie, J., Davies, T. W., Cruse, D., and Gaston, K. J. (2016). Ecological effects of artificial light at night on wild plants. *J. Ecol.* 104, 611–620. doi: 10.1111/1365-2745.12551

Blatt, M. R. (2000). Cellular signaling and volume control in stomatal movements in plants. *Annu Rev. Cell Dev. Biol.* 16, 221–241. doi: 10.1146/annurev.cellbio.16.1.221

Breitler, J. C., Djerrab, D., Leran, S., Toniutti, L., Guittin, C., Severac, D., et al. (2020). Full moonlight-induced circadian clock entrainment in coffea arabica. *BMC Plant Biol.* 20:24. doi: 10.1186/s12870-020-2238-4

Caemmerer, S., and Edmondson, D. (1986). Relationship between steady-state gas exchange, in vivo ribulose bisphosphate carboxylase activity and some carbon reduction cycle intermediates in raphanus sativus. *Funct. Plant Biol.* 13, 669–688. doi: 10.1071/pp9860669

Caffarri, S., Broess, K., Croce, R., and Amerongen, H. V. (2011). Excitation energy transfer and trapping in higher plant photosystem II complexes with different antenna sizes. *Biophys. J.* 100, 2094–2103. doi: 10.1016/j.bpj.2011.03.049

Carmo-Silva, A. E., and Salvucci, M. E. (2013). The regulatory properties of rubisco activase differ among species and affect photosynthetic induction during light transitions. *Plant Physiol.* 161, 1645–1655. doi: 10.1104/pp.112.213348

Croce, R., and Van Amerongen, H. (2014). Natural strategies for photosynthetic light harvesting. *Nat. Chem. Biol.* 10, 492. doi: 10.1038/nchembio.1555

Davies, T. W., and Smyth, T. (2018). Why artificial light at night should be a focus for global change research in the 21st century. *Glob. Change Biol.* 24, 872–882. doi: 10.1111/gcb.13927

Dismukes, G. C., and Siderer, Y. (1981). Intermediates of a polynuclear manganese center involved in photosynthetic oxidation of water. *Proc. Natl. Acad. Sci. U S A.* 78, 274–278. doi: 10.1073/pnas.78.1.274

Dubinsky, Z., and Schofield, O. (2010). From the light to the darkness: thriving at the light extremes in the oceans. *Hydrobiologia* 639, 153–171. doi: 10.1007/s10750-009-0026-0

Ezequiel, J., Laviale, M., Frankenbach, S., Cartaxana, P., and Serôdio, J. (2015). Photoacclimation state determines the photobehaviour of motile microalgae: the case of a benthic diatom. *J. Exp. Mar. Biol. Ecol.* 468, 11–20. doi: 10.1016/j.jembe.2015.03.004

Gaston, K. J., Bennie, J., Davies, T. W., and Hopkins, J. (2013). The ecological impacts of nighttime light pollution: a mechanistic appraisal. *Biol. Rev.* 88, 912–927. doi: 10.1111/brv.12036

Gerrish, G. A., Morin, J. G., Rivers, T. J., and Patrawala, Z. (2009). Darkness as an ecological resource: the role of light in partitioning the nocturnal niche. *Oecologia* 160, 525–536. doi: 10.1007/s00442-009-1327-8

Grulke, N. E., Alonso, R., Nguyen, T., Cascio, C., and Dobrowolski, W. (2004). Stomata open at night in pole-sized and mature ponderosa pine: implications for O_3 exposure metrics. *Tree Physiol.* 24, 1001–1010. doi: 10.1093/treephys/24.9.1001

Han, Q., Yamaguchi, E., Odaka, N., and Kakubari, Y. (1999). Photosynthetic induction responses to variable light under field conditions in three species grown in the gap and understory of a fagus crenata forest. *Tree Physiol.* 19, 625–634. doi: 10.1093/treephys/19.10.625

Haumann, M., and Junge, W. (1994). Extent and rate of proton release by photosynthetic water oxidation in thylakoids: electrostatic relaxation versus chemical production. *Biochemistry* 33, 864–872. doi: 10.1021/bi00170a003

Hoshika, Y., Osada, Y., De Marco, A., Peñuelas, J., and Paoletti, E. (2018). Global diurnal and nocturnal parameters of stomatal conductance in woody plants and major crops. *Glob. Ecol. Biogeogr.* 27, 257–275. doi: 10.1111/geb.12681

Joliot, P. (2003). Period-four oscillations of the flash-induced oxygen formation in photosynthesis. *Photosyn. Res.* 76, 65–72.

Joliot, P., Barbieri, G., and Chabaud, R. (1969). A new model of photochemical centers in system-2. *Photochem. Photobiol.* 10, 309–329.

Julian, I., Schroeder, Gethyn, J., Allen, Veronique Hugouvieux, June, M., et al. (2001). Guard cell signal transduction. *Annu. Rev. Plant Physiol. Plant Mol. Biol.* 52, 627–658.

Kaufmann, M. R. (1976). Stomatal response of engelmann spruce to humidity, light, and water stress. *Plant Physiol.* 57, 898–901. doi: 10.1104/pp.57.6.898

Kirschbaum, M. U., Ohlemacher, C., and Küppers, M. (2004). Loss of quantum yield in extremely low light. *Planta* 218, 1046–1053. doi: 10.1007/s00425-003-1186-1

Kok, B., Forbush, B., and Mcgloin, M. (1970). Cooperation of charges in photosynthetic O_2 evolution-I. A linear four step mechanism. *Photochem. Photobiol.* 11, 457–475. doi: 10.1111/j.1751-1097.1970.tb06017.x

Kouřil, R., Nosek, L., Semchonok, D., Boekema, E. J., and Ilík, P. (2018). "Organization of Plant Photosystem II and Photosystem I Supercomplexes," in *Membrane Protein Complexes: Structure and Function*, eds J. R. Harris and E. J. Boekema (Singapore: Springer), 259–286. doi: 10.1007/978-981-10-7757-9_9

Kura-Hotta, M., Hashimoto, H., Satoh, K., and Katoh, S. (1990). Quantitative determination of changes in the number and size of chloroplasts in naturally senescing leaves of rice seedlings. *Plant Cell Physiol.* 31, 33–38.

Lawson, T. (2009). Guard cell photosynthesis and stomatal function. *New Phytol.* 181, 13–34. doi: 10.1111/j.1469-8137.2008.02685.x

Lee, J. S. (2010). Stomatal opening mechanism of CAM plants. *J. Plant Biol.* 53, 19–23. doi: 10.1007/s12374-010-9097-8

Mayoral, O., Solbes, J., Canto, J., and Pina, T. (2020). What has been thought and taught on the lunar influence on plants in agriculture? perspective from physics and biology. *Agronomy* 10:955. doi: 10.3390/agronomy10070955

Mcevoy, J. P., and Brudvig, G. W. (2006). Water-splitting chemistry of photosystem II. *Chem. Rev.* 106, 4455–4483. doi: 10.1021/cr0204294

Meidner, H., and Mansfield, T. (1965). Stomatal responses to illumination. *Biol. Rev.* 40, 483–508. doi: 10.1111/j.1469-185x.1965.tb00813.x

Melis, A., Neidhardt, J., and Benemann, J. R. (1998). Dunaliella salina (Chlorophyta) with small chlorophyll antenna sizes exhibit higher photosynthetic productivities and photon use efficiencies than normally pigmented cells. *J. Appl. Phycol.* 10, 515–525.

Meravi, N., and Kumar Prajapati, S. (2020). Effect street light pollution on the photosynthetic efficiency of different plants. *Biol. Rhythm Res.* 51, 67–75. doi: 10.1080/09291016.2018.1518206

Mercado, L. M., Bellouin, N., Sitch, S., Boucher, O., Huntingford, C., Wild, M., et al. (2009). Impact of changes in diffuse radiation on the global land carbon sink. *Nature* 458, 1014. doi: 10.1038/nature07949

Ogle, K., Lucas, R. W., Bentley, L. P., Cable, J. M., Barron-Gafford, G. A., Griffith, A., et al. (2012). Differential daytime and night-time stomatal behavior in plants from north american deserts. *New Phytol.* 194, 464–476. doi: 10.1111/j.1469-8137.2012.04068.x

Ono, K., Hashimoto, H., and Katoh, S. (1995). Changes in the number and size of chloroplasts during senescence of primary leaves of wheat grown under different conditions. *Plant Cell Physiol.* 36, 9–17.

Osterhout, W. J. V., and Haas, A. (1918). On the dynamics of photosynthesis. *J. Gen. Physiol.* 1, 1–16. doi: 10.1007/0-306-48148-0_1

Pearcy, R. W. (1983). The light environment and growth of C_3 and C_4 tree species in the understory of a hawaiian forest. *Oecologia* 58, 19–25. doi: 10.1007/bf00384537

Pearcy, R. W. (1988). Photosynthetic utilisation of lightflecks by understory plants. *Funct. Plant Biol.* 15, 223–238. doi: 10.1071/pp9880223

Pearcy, R. W., Osteryoung, K., and Calkin, H. W. (1985). Photosynthetic responses to dynamic light environments by hawaiian trees time course of CO_2 uptake and carbon gain during sunflecks. *Plant Physiol.* 79, 896–902. doi: 10.1104/pp.79.3.896

Putnam-Evans, C., and Barry, B. A. (2007). Preface for special issue of photosynthesis research "photosynthetic water oxidation". *Photosyn. Res.* 92, 273–274. doi: 10.1007/s11120-007-9226-5

Quigg, A., Beardall, J., and Wydrzynski, T. (2003). Photoacclimation involves modulation of the photosynthetic oxygen-evolving reactions in dunaliella tertiolecta and phaeodactylum tricornutum. *Funct. Plant Biol.* 30, 301–308. doi: 10.1071/fp02140

Raven, J., and Cockell, C. (2006). Influence on photosynthesis of starlight, moonlight, planetlight, and light pollution (reflections on photosynthetically active radiation in the universe). *Astrobiology* 6, 668–675. doi: 10.1089/ast.2006.6.668

Raven, J., Kübler, J., and Beardall, J. (2000). Put out the light, and then put out the light. *J. Mar. Biol. Assoc. U K.* 80, 1–25. doi: 10.1017/s0025315499001526

Resco De Dios, V., Chowdhury, F. I., Granda, E., Yao, Y., and Tissue, D. T. (2019). Assessing the potential functions of nocturnal stomatal conductance in C_3 and C_4 plants. *N. Phytol.* 223, 1696–1706. doi: 10.1111/nph.15881

Retkute, R., Smith-Unna, S. E., Smith, R. W., Burgess, A. J., Jensen, O. E., Johnson, G. N., et al. (2015). Exploiting heterogeneous environments: does photosynthetic acclimation optimize carbon gain in fluctuating light? *J. Exp. Bot.* 66, 2437–2447. doi: 10.1093/jxb/erv055

Salisbury, F. B. (1981). Twilight effect: initiating dark measurement in photoperiodism of *xanthium*. *Plant Physiol.* 67, 1230–1238. doi: 10.1104/pp.67.6.1230

Salvucci, M. E., Portis, A. R., and Ogren, W. L. (1986). Light and CO_2 response of ribulose-1, 5-bisphosphate carboxylase/oxygenase activation in arabidopsis leaves. *Plant Physiol.* 80, 655–659. doi: 10.1104/pp.80.3.655

Schulte, M., Offer, C., and Hansen, U. (2003). Induction of CO_2-gas exchange and electron transport: comparison of dynamic and steady-state responses in fagus sylvatica leaves. *Trees* 17, 153–163. doi: 10.1007/s00468-002-0219-x

Shimazaki, K.-I., Doi, M., Assmann, S. M., and Kinoshita, T. (2007). Light regulation of stomatal movement. *Annu. Rev. Plant Biol.* 58, 219–247.

Singhal, R. K., Kumar, M., and Bose, B. (2019). Eco-physiological responses of artificial night light pollution in plants. *Russ. J. Plant Physiol.* 66, 190–202. doi: 10.1134/s1021443719020134

Valladares, F., Gianoli, E., and Saldaña, A. (2011). Climbing plants in a temperate rainforest understorey: searching for high light or coping with deep shade? *Ann. Bot.* 108, 231–239. doi: 10.1093/aob/mcr132

Van Bezouwen, L. S., Caffarri, S., Kale, R. S., Kouřil, R., Thunnissen, A.-M. W. H., Oostergetel, G. T., et al. (2017). Subunit and chlorophyll organization of the plant photosystem II supercomplex. *Nature Plants* 3:17080.

Von Caemmerer, S. (2000). *Biochemical models of leaf photosynthesis*. Clayton: Csiro publishing.

Wang, Y., Noguchi, K., and Terashima, I. (2008). Distinct light responses of the adaxial and abaxial stomata in intact leaves of helianthus annuus L. *Plant Cell Environ.* 31, 1307–1316. doi: 10.1111/j.1365-3040.2008.01843.x

Yamori, W., Kusumi, K., Iba, K., and Terashima, I. (2020). Increased stomatal conductance induces rapid changes to photosynthetic rate in response to naturally fluctuating light conditions in rice. *Plant Cell Environ.* 43, 1230–1240. doi: 10.1111/pce.13725

Conflict of Interest: YW and AL were both employed by Liangshan Branch of Sichuan Tobacco Company.

The remaining authors declare that the research was conducted in the absence of any commercial or financial relationships that could be construed as a potential conflict of interest.

frontiers in Plant Science

ORIGINAL RESEARCH
published: 18 January 2021
doi: 10.3389/fpls.2020.603178

The Photomorphogenic Transcription Factor PpHY5 Regulates Anthocyanin Accumulation in Response to UVA and UVB Irradiation

*Yun Zhao[1,2], Ting Min[2], Miaojin Chen[3], Hongxun Wang[4], Changqing Zhu[1], Rong Jin[1], Andrew C. Allan[5,6], Kui Lin-Wang[5] and Changjie Xu[1]**

[1] Zhejiang Provincial Key Laboratory of Horticultural Plant Integrative Biology, Zhejiang University, Hangzhou, China, [2] College of Food Science & Engineering, Wuhan Polytechnic University, Wuhan, China, [3] Fenghua Institute of Honey Peach, Fenghua, China, [4] College of Biology and Pharmaceutical Engineering, Wuhan Polytechnic University, Wuhan, China, [5] New Zealand Institute for Plant & Food Research Limited, Auckland, New Zealand, [6] School of Biological Sciences, University of Auckland, Auckland, New Zealand

OPEN ACCESS

Edited by:
Jeremy Harbinson, Wageningen Plant Research, Wageningen University and Research, Netherlands

Reviewed by:
Weiqiang Li, RIKEN, Japan
Yanjun Jing, Institute of Botany, Chinese Academy of Sciences, China

***Correspondence:**
Changjie Xu
chjxu@zju.edu.cn

Specialty section:
This article was submitted to Plant Abiotic Stress, a section of the journal Frontiers in Plant Science

Received: *05 September 2020*
Accepted: *28 December 2020*
Published: *18 January 2021*

Citation:
Zhao Y, Min T, Chen M, Wang H, Zhu C, Jin R, Allan AC, Lin-Wang K and Xu C (2021) The Photomorphogenic Transcription Factor PpHY5 Regulates Anthocyanin Accumulation in Response to UVA and UVB Irradiation. Front. Plant Sci. 11:603178. doi: 10.3389/fpls.2020.603178

Red coloration contributes to fruit quality and is determined by anthocyanin content in peach (*Prunus persica*). Our previous study illustrated that anthocyanin accumulation is strongly regulated by light, and the effect of induction differs according to light quality. Here we showed that both ultraviolet-A (UVA) and ultraviolet-B (UVB) irradiation promoted anthocyanin biosynthesis in "Hujingmilu" peach fruit, and a combination of UVA and UVB had additional effects. The expression of anthocyanin biosynthesis and light signaling related genes, including transcription factor genes and light signaling elements, were induced following UV irradiation as early as 6 h post-treatment, earlier than apparent change in coloration which occurred at 72 h. To investigate the molecular mechanisms for UVA- and UVB-induced anthocyanin accumulation, the genes encoding ELONGATED HYPOCOTYL 5 (HY5), CONSTITUTIVE PHOTOMORPHOGENIC1 (COP1), Cryptochrome (CRY), and UV RESISTANCE LOCUS 8 (UVR8) in peach were isolated and characterized through functional complementation in corresponding Arabidopsis (*Arabidopsis thaliana*) mutants. *PpHY5* and *PpCOP1.1* restored hypocotyl length and anthocyanin content in Arabidopsis mutants under white light; while *PpCRY1* and *PpUVR8.1* restored *AtHY5* expression in Arabidopsis mutants in response to UV irradiation. Arabidopsis *PpHY5/hy5* transgenic lines accumulated higher amounts of anthocyanin under UV supplementation (compared with weak white light only), especially when UVA and UVB were applied together. These data indicated that PpHY5, acting as AtHY5 counterpart, was a vital regulator in UVA and UVB signaling pathway. In peach, the expression of *PpHY5* was up-regulated by UVA and UVB, and PpHY5 positively regulated both its own transcription by interacting with an E-box in its own promoter, and the transcription of the downstream anthocyanin biosynthetic genes *chalcone synthase 1* (*PpCHS1*), *chalcone synthase 2* (*PpCHS2*), and *dihydroflavonol 4-reductase* (*PpDFR1*) as well as the transcription factor gene *PpMYB10.1*. In summary,

functional evidence supports the role of PpHY5 in UVA and UVB light transduction pathway controlling anthocyanin biosynthesis. In peach this is via up-regulation of expression of genes encoding biosynthetic enzymes, as well as the transcription factor *PpMYB10.1* and *PpHY5* itself.

Keywords: peach, anthocyanin, UVA, UVB, *HY5*, photoreceptor, *PpMYB10.1*

INTRODUCTION

Anthocyanins, a group of secondary metabolites known as flavonoid compounds, are important water-soluble pigments widely distributed in plants where they perform a multitude of biological functions such as protecting against a variety of abiotic stresses [ultraviolet (UV) radiation, nutrient deficiency, low temperature, drought, etc.], attracting pollinators and seed dispersers, and defense against pathogens and herbivores (Schaefer et al., 2004; Gould et al., 2010). In addition, they are also recognized to have potential human health benefits in aspects such as prevention from cancer and heart disease (Tsuda, 2012; Zhang et al., 2015). Hence, anthocyanin is considered as an essential determinant for fruit quality.

The anthocyanin biosynthetic pathway has been extensively studied and found to be relatively conserved among plant species (Winkel-Shirley, 2001). Anthocyanins are biosynthesized via the phenylpropanoid pathway, which is catalyzed stepwise by a series of enzymes including phenylalanine ammonia lyase (PAL), cinnamic acid-4-hydroxylase (C4H), 4-coumarate CoA ligase (4CL), chalcone synthase (CHS), chalcone isomerase (CHI), flavanone 3-hydroxylase (F3H), flavonoid 3'-hydroxylase (F3'H), flavonoid 3',5'-hydroxylase (F3'5'H), dihydroflavonol 4-reductase (DFR), anthocyanidin synthase (ANS), and UDP-glucose: flavonoid 3-*O*-glucosyltransferase (UFGT; Jaakola, 2013; Zhang et al., 2014). The expression of the genes that encode these enzymes are transcriptionally regulated by MYB, basic Helix-Loop-Helix (bHLH), and WD40 repeat proteins, often in a form of trimeric protein complex of MYB-bHLH-WD40 (the MBW complex; Lin-Wang et al., 2010; BenSimhon et al., 2011; An et al., 2012; Chagné et al., 2013; Wang N. et al., 2018). In peach (*Prunus persica*), several relevant transcription factors (PpMYB10s, PpbHLH3, and PpWD40-1) have been functionally confirmed to control anthocyanin biosynthesis (Ravaglia et al., 2013; Rahim et al., 2014; Uematsu et al., 2014; Zhou et al., 2014, 2018; Tuan et al., 2015).

Anthocyanin biosynthesis is not only developmentally regulated but also influenced by various environmental and endogenous stimuli as well (Guo et al., 2008). As the primary energy source and an informational signal for regulating plant growth and development, light is one of the most critical environmental factors (Kami et al., 2010). Light profoundly influences complex signaling pathways such as photomorphogenesis, circadian rhythms and the regulation of secondary metabolism throughout the life of plants (Gelderen et al., 2018).

Previous research has revealed the significance of light on the induction of anthocyanin biosynthesis in fruits such as bilberry (*Vaccinium myrtillus*, Uleberg et al., 2012), Chinese bayberry (*Myrica rubra*, Niu et al., 2010), grapes (*Vitis vinifera*, Azuma et al., 2012), raspberry (*Rubus idaeus*, Wang et al., 2009) and cranberry (*Vaccinium macrocarpon*, Zhou and Singh, 2004), etc. The effects of light on anthocyanin accumulation vary with different light wavelengths, where UV light always presents a more profound effect on anthocyanin biosynthesis compared with white light (Zoratti et al., 2014). For instance, ultraviolet-B (UVB) irradiation significantly increased anthocyanin content in the peel of apple (*Malus domestica*) and pear (*Pyrus pyrifolia*) fruits (Hagen et al., 2007; Qian et al., 2013; Sun et al., 2014; Henry-Kirk et al., 2018). Tomato (*Solanum lycopersicum*) grown under ultraviolet-A (UVA) supplementation visibly accumulated more anthocyanin in a short time (Guo and Wang, 2010; Castagna et al., 2014). In strawberries (*Fragaria ananassa*), blue light and UVC irradiation stimulated anthocyanin accumulation and enhanced the antioxidant activities (Li et al., 2014; Xu et al., 2014). In peach, it has also been demonstrated that UV lights are stronger stimulants for anthocyanin accumulation (Zhao et al., 2017).

Higher plants have evolved extremely advanced systems to sense changes in ambient light conditions (Casal, 2013), by being equipped with specialized sensory photoreceptors for specific wavelengths of light, including red/far-red light receptor phytochromes (PHYA to PHYE) (Oh and Montgomery, 2017), blue/UVA light receptor cryptochromes (CRY1 and CRY2) or phototropins (PHOTs; Lin, 2002; Liu et al., 2011; Wang Q. et al., 2018), and UVB light receptor UV RESISTANCE LOCUS 8 (UVR8; Rizzini et al., 2011; Yin and Ulm, 2017; Liang et al., 2019). Photoreceptors are indispensable for light-induced anthocyanin biosynthesis (Yang et al., 2016), as in Arabidopsis (*Arabidopsis thaliana*), the photoreceptor deficient mutants *uvr8* and *cry1cry2* respectively have a weak response in UVB and blue light/UVA-induced photomorphogenesis like blocking the inhibition of hypocotyl elongation and the induction of anthocyanin biosynthesis (Wade et al., 2001; Morales et al., 2013; Wang Q. et al., 2018).

After perceiving light, this signal is transmitted from photoreceptors to downstream light signal transduction factors to regulate the process of light-induced anthocyanin biosynthesis both transcriptionally and post-translationally (Casal, 2013). ELONGATED HYPOCOTYL 5 (HY5), a basic leucine zipper (bZIP) transcription factor, is a master regulator in light signal transduction pathway that acts downstream of multiple photoreceptors to respond to photomorphogenesis (Holm et al., 2002; Gangappa and Botto, 2016). HY5 is considered as a positive regulator to participate in light-induced anthocyanin biosynthesis in Arabidopsis, apple, grape, and pear (Loyola et al., 2016; An et al., 2017; Nawkar et al., 2017; Tao et al., 2018). AtHY5 targets the anthocyanin biosynthetic genes (*CHS*, *F3H*)

and *MYB* [*PRODUCTION OF FLAVONOL GLYCO-SIDES 1* (*PFG1*)/*MYB12*, *MYB75*/*PRODUCTION OF ANTHOCYANIN PIGMENT* 1 (*PAP1*)] to activate their expression by direct binding to the promoters (Chattopadhyay et al., 1998; Lee et al., 2007; Stracke et al., 2010; Shin et al., 2013). In eggplant (*Solanum melongena*) under blue light, SmHY5 has also been revealed to accelerate anthocyanin accumulation by regulating the expression of downstream genes encoding enzymes of the anthocyanin biosynthetic pathway (Jiang et al., 2016). In apple, MdHY5 promoted the expression of *MdMYB10* to regulate anthocyanin accumulation (An et al., 2017). CONSTITUTIVE PHOTOMORPHOGENIC1 (COP1), an E3 ubiquitin ligase, is a crucial repressor for photomorphogenesis and anthocyanin biosynthesis, targeting HY5 for proteasome-mediated degradation (Osterlund et al., 2000; Lau and Deng, 2012). In pear, PpyCOP1 indirectly interacted with PpyHY5 to mediate regulation of anthocyanin accumulation (Tao et al., 2018). Additionally, apple MdCOP1 was also found to be critical for the ubiquitination and degradation of MdMYB1, a positive regulator for anthocyanin biosynthesis, further leading to the negative regulation for the coloration in apple fruit (Li et al., 2012).

Anthocyanin accumulation is essential for the quality of peach fruit. Our previous study revealed that UV light enhances anthocyanin content in peach peel (Zhao et al., 2017). However, how photoreceptors and light signal transduction elements mediate UV light-induced anthocyanin accumulation has not been elucidated. In this study, the effect of UVA and UVB irradiation on the coloration of peach fruit was examined. We cloned and functionally characterized *PpHY5* and provided molecular evidence that PpHY5 plays a vital role in anthocyanin biosynthesis in response to UVA and UVB. These results contributed to our understanding of the mechanism underlying UV light-induced anthocyanin biosynthesis in peach, as well as providing evidence for improving fruit pigmentation.

MATERIALS AND METHODS

Plant Materials and Growth Conditions

The peach cultivar (cv) "Hujingmilu" was used in this study. All fruit were bagged with commercial yellow paper bags at 42 days after full blossom and collected at just before turning stage. For UV irradiation treatment experiments, all collected fruit were transferred to a growth chamber at a constant 20°C and irradiated with continuous UVA (320–400 nm, 1,000 $\mu w/cm^2$) or UVB (280–320 nm, 58 $\mu w/cm^2$) or both together for 0, 6, 12, 24, 48, 72, and 144 h, respectively. The fruit kept in the dark served as the control. Peel tissue from 30 fruit of each treatment were separated simultaneously into three biological replicates (10 fruit for each replicate) at every sampling time, then immediately frozen in liquid nitrogen and stored at −80°C for subsequent experiments.

The Arabidopsis *hy5* (SALK_056405), *cop1* (SALK_022133), *uvr8* (SALK_033468), and *cry1* (SALK_069292) mutants with the Columbia genetic background were obtained from The Arabidopsis Information Resource (TAIR). For hypocotyl length and anthocyanin accumulation assays, seeds of wild type (WT), above-mentioned mutants as well as transgenic lines obtained in this study were sterilized and germinated on Murashige and Skoog plates supplemented with 0.6% agar and 1% sucrose, and subjected to a chilling treatment at 4°C for 2 days in the dark. Then these seedlings were transferred to a growth chamber at 24°C under the long-day condition (16 h photoperiod/8 h dark cycle) of white light in normal intensity (40 w/m^2) for growth. For UV light treatment experiment, seedlings were grown under continuous weak white light (WWL, 40 $\mu w/cm^2$) supplemented with UVA (40 $\mu w/cm^2$) or UVB (10 $\mu w/cm^2$) or both together at 24°C. And the seedlings kept under only WWL served as the control. After growth under different light conditions as indicated for 5 or 7 days, respectively, the hypocotyl length was measured and seedlings were sampled for subsequent experiments.

Color Measurement

Fruit surface color measurement was carried out using a reflectance spectrophotometer (Hunter Lab Mini Scan XE Plus colorimeter) at four evenly distributed equatorial positions of per fruit. The raw data as L* (lightness, from black to white), a* (the degree of green-red variation), b* (the degree of blue-yellow variation) values were recorded and the color index of red grapes (CIRG) was calculated according to the formula $CIRG = (180 - H)/(L^* + C)$, while $H = \arctan(b^*/a^*)$ and $C = [(a^*)^2+(b^*)^2]^{0.5}$ (Carreño et al., 1995; Zhang et al., 2008).

Anthocyanin Extraction and Measurement

Anthocyanin was extracted from peach fruit peel and Arabidopsis seedlings by using the method as described in our previous study (Zhao et al., 2017). High-performance liquid chromatography (HPLC) analysis for quantification of anthocyanin was performed using an Agilent 1260 liquid chromatograph system (Agilent Technologies, CA, United States) equipped with a ZORBAX SB-C18 column following a previously reported protocol (Cheng et al., 2014). The UV-visible light detector wavelength was set at 520 nm. Cyanidin 3-*O*-glucoside chloride was employed as the authentic standard.

RNA Extraction and Reverse Transcription Quantitative PCR Analysis

Total RNA was isolated from peach tissue samples and Arabidopsis by using a modified cetyltrimethylammonium bromide (CTAB) method (Liu et al., 2015) and the TRIzol Reagent Kit (Ambion, Hopkinton, MA, United States), respectively. First-strand cDNA was synthesized with HiScript® II Q Select RT SuperMix (Vazyme) after removal of genomic DNA contamination by TURBO DNase (Ambion) following the manufacturer's protocol. Reverse transcription quantitative PCR (RT-qPCR) was performed using the SsoFast EvaGreen Supermix kit (Bio-Rad, CA, United States) with the CFX96 instrument (Bio-Rad, CA, United States) according to the following program: 95°C for 3 min, followed by 45 cycles of 95°C for 10 s, 60°C for 30 s and then 95°C for 10 s followed by a continuous increase from 65°C to 95°C at the heating rate of 0.5°C/s for dissociation curve analysis (Zhao et al., 2017).

The *PpTEF2* (GenBank accession: No. JQ732180) and *ATACT2* (GenBank accession: No. AT3G18780) genes were used as the internal reference genes to normalize expression values for peach and Arabidopsis, respectively (Tong et al., 2009; Zhou et al., 2013). The primer sequences for RT-qPCR were designed with Primer Premier 5 and listed in **Supplementary Table 1**.

RNA-Seq Analysis

RNA sequencing (RNA-Seq) of peach fruit samples (irradiated with different UV-light conditions for 0, 6, 12, 24, and 48 h) was conducted using the Xten platform by staff at Biomarker (Beijing, China) with three biological replicates for each sample. Data analysis was conducted as described in our previous work (Zhao et al., 2017). Transcript abundances were normalized by calculating FPKM (expected number of Fragments Per Kilobase of transcript sequence per Million base pairs sequenced).

Plasmid Construction

The full-length coding sequence of *PpHY5* (Prupe.1G478400), *PpHYH* (Prupe.1G208500), *PpCOP1.1* (Prupe.5G031300), *PpUVR8.1* (Prupe.4G277200), *PpCRY1* (Prupe.1G517600) was isolated and recombined into the pGreenII 0029 62-SK vector (*PpHY5*-SK, *PpHYH*-SK, *PpCOP1.1*-SK, *PpUVR8.1*-SK, *PpCRY1*-SK). The promoter sequence (1500 bp upstream of the initiation codon) of structural genes (*PpCHS1*, *PpCHS2*, *PpCHI*, *PpF3H*, *PpF3'H*, *PpDFR*, *PpANS*, and *PpUFGT*) and transcription factors (*PpMYB10.1*/*2*/*3*) were constructed into the pGreen II 0800-LUC vector (*PpCHS1*-LUC, *PpCHS2*-LUC, *PpCHI*-LUC, *PpF3H*-LUC, *PpF3'H*-LUC, *PpDFR*-LUC, *PpANS*-LUC, *PpUFGT*-LUC, and *PpMYB10.1*/*2*/*3*-LUC). In experiments for verifying the function of E-box motifs in *PpHY5* promoter, mutations on the *PpHY5* promoter were conducted using the Fast Mutagenesis System Kit (Transgene) and inserted into the pGreenII 0800-LUC vector, named *PpHY5m1*-LUC, *PpHY5m2*-LUC, *PpHY5m3*-LUC, and *PpHY5m4*-LUC, respectively. For subcellular localization analysis, the coding sequence of each gene without stop codon was fused with green fluorescent protein (GFP) and cloned into the pCAMBIA super 1300-eGFP vector (*PpHY5*-GFP, *PpCOP1.1*-GFP). All constructs were transformed into *Agrobacterium tumefaciens* strain GV3101 (MP90) by electroporation with GenePulser Xcell^{TM} Electroporation Systems (Bio-Rad, Hercules, CA, United States) for subsequent experiments. Primers used for plasmid construction were described as listed in **Supplementary Table 2**.

Dual-Luciferase Assay

The dual-luciferase assay was performed with *Nicotiana benthamiana* leaves by using a previously reported protocol (Zhao et al., 2020). *Agrobacterium* cultures containing recombinant pGreenII 0029 62-SK vectors harboring transcription factor genes and the cultures containing recombinant pGreen II 0800-LUC vector harboring target gene promoters were infiltrated into *N. benthamiana* leaves with a ratio of 10:1 (v/v). At three days following infiltration, the firefly luciferase (LUC) and renilla luciferase (REN) activities were measured using dual-Luciferase Reporter Assay System (Promega, MI, United States) with Modulus Luminometer. When the ratio of LUC/REN was over two and the difference was highly significant ($P < 0.01$) as compared with the control, the transcription factor was considered to be able to activate the promoter. For each transcription factor and promoter interaction, dual-luciferase assays were conducted with at least three independent experiments (six replicate reactions in each experiment).

Arabidopsis Transformation and Hypocotyl Length Measurement

The Arabidopsis transformation was performed by using the floral dip method (Zhang et al., 2006). SilwetL-77 (Real-Times, Beijing, China) was applied as a surfactant in *Agrobacterium*-based transformation of Arabidopsis. Transgenic seeds were sterilized and placed on Murashige and Skoog medium containing 50 mg/mL kanamycin for transgenic plant selection. For each target gene, at least three lines were characterized and three of them with highest expression levels of target gene were selected, and individuals of the T2 were used for further phenotype analysis. After growth for 5 or 7 days, the hypocotyl length measurement of at least 30 Arabidopsis seedlings was conducted for each replicate. All experiments were carried out with three independent biological replicates.

Subcellular Localization Analysis

The *Agrobacterium* strain carrying the 35S::*PpHY5*-GFP or 35S::*PpCOP1.1*-GFP recombinant vector was infiltrated into transgenic *N. benthamiana* plant with a red fluorescent nuclear marker (Nucleus-RFP) according to a previous report (Zhao et al., 2020), while 35S::GFP was used as a negative control. The GFP florescence of the transiently expressed leave was observed under a Zeiss LSM710NLO confocal laser scanning microscope.

Cis-regulatory Element Analysis

The predictions of conserved *cis*-regulatory elements in the promoter were analyzed using the PlantCARE database.[1]

Statistical Analysis

The statistical significance of differences was analyzed using SPSS statistical software (SPSS 19.0, SPSS Inc., Chicago, IL, United States) with Student's *t*-test. Graphs were plotted using Origin 8.0 (Origin Lab Corporation, Northampton, MA, United States).

RESULTS

Time Course of Color Development and the Expression of Anthocyanin Biosynthetic Genes Under Continuous UV Treatments

To investigate the influence of different UV light treatments on anthocyanin biosynthesis in peach, the fruit were given

[1]http://bioinformatics.psb.ugent.be/webtools/plantcare/html/

either a continuous UVA or UVB or UVA + UVB treatment. The control fruit was kept in the dark and did not develop red color over time. Under UV irradiation, the peel color remained green within 24 h and a few red spots began to be slightly visible at 48 h. At 72 and 144 h following irradiation, the fruit turned deep red (**Figure 1A**). These observations matched well with the CIRG values (**Figure 1B**). Under dark condition, the concentration of anthocyanin in peel was very low and showed no significant increase over time (**Figure 1B**). In contrast, anthocyanin accumulated following irradiation with UVA or UVB or UVA + UVB, and the effects varied significantly among different UV lights conditions. The concentration of anthocyanin rose sharply to 3.12 mg/100gFW (15-fold higher than the control) under UVA exposure and 2.11 mg/100gFW (10-fold higher than the control) under UVB exposure at 144 h respectively. During the irradiation period, the highest anthocyanin content was detected in fruit under UVA + UVB treatment, reaching 3.47 mg/100gFW at 72 h (2–3 fold higher than UVA or UVB) and 11.59 mg/100gFW at 144 h (3-6 fold higher than UVA or UVB), respectively (**Figure 1B**), which was consistent with the visual appearance.

In order to further explore the molecular mechanisms for anthocyanin accumulation in response to UV lights, we analyzed the transcript levels of genes encoding anthocyanin biosynthetic enzymes (*PpPAL*, *Pp4CL*, *PpCHS1*, *PpCHS2*, *PpCHI*, *PpF3H*, *PpDFR1*, *PpDFR2*, *PpANS*, and *PpUFGT*), transport genes *PpGST1* and regulatory genes (*PpMYB10.1*, *PpMYB10.2*, and *PpMYB10.3*) in peel during the early irradiation period (0, 6, 12, 24, and 48 h) before the appearance of red coloration. Under dark condition, the assayed genes exhibited low expression levels and for some genes such as *PpCHS1*, *PpDFR1*, and *PpUFGT*, the transcript levels showed little change over time (**Figure 2**). In comparison to the low expression levels at the initial point (0 h), the expression profiles of the biosynthetic genes were up-regulated to various degrees in peel of fruit when exposed to the UV treatments. The transcripts of all assayed biosynthetic genes under different UV light conditions were elevated than control (**Figure 2**). After exposure to UV light for 6 h, the expression levels of all analyzed biosynthetic genes sharply increased (**Figure 2**). For example, the transcript levels of *PpCHS1* and *PpUFGT* in the UV light-exposed fruit were at least 6-fold and 9-fold higher than the control. However, after exposure to UV light for 12 h, the transcript levels of *PpCHI*, *PpF3H*, *PpANS*, and *PpGST1* decreased slightly. *Pp4CL* and *PpCHS1* showed the highest expression after 24 h of UV light irradiation. Although there was a slight decline in the transcript abundance of some genes after irradiation for 48 h, the expression was consistently higher than the control, for instance, the transcript levels of *PpDFR1* were at least 7-fold higher, 14-fold higher and 28-fold higher in the UV light-exposed fruit than that in the dark, respectively. In particular, the expression of *PpGST1* continuously remained very low in the fruit under dark condition, while was strongly stimulated by UV light, showing a 43-fold, 155-fold, and 332-fold elevation at 48 h in UVA, UVB, and UVA + UVB light exposed fruit, respectively.

The expression patterns of the regulatory transcription factor genes (*PpMYB10.1*, *PpMYB10.2*, and *PpMYB10.3*) showed elevation by UV, but with different profiles. The transcript level of *PpMYB10.1* was strongly induced by UV light and then decreased after prolonged exposure. The expression of *PpMYB10.2* and *PpMYB10.3* presented little change under UVA irradiation and transcript abundance was lower compared with *PpMYB10.1* (**Figure 2**). The transcript levels of most genes were generally highest in peel of fruit irradiated with UVA + UVB, followed by UVA and UVB, while the expression were almost undetectable or showed low levels in control. Even though there were slight declines in transcription level at some time points, most genes reached the maximum transcription levels when treated with UVA + UVB for 24 h, which ensured the high transcription abundance detected in fruit at later stages. The results suggested

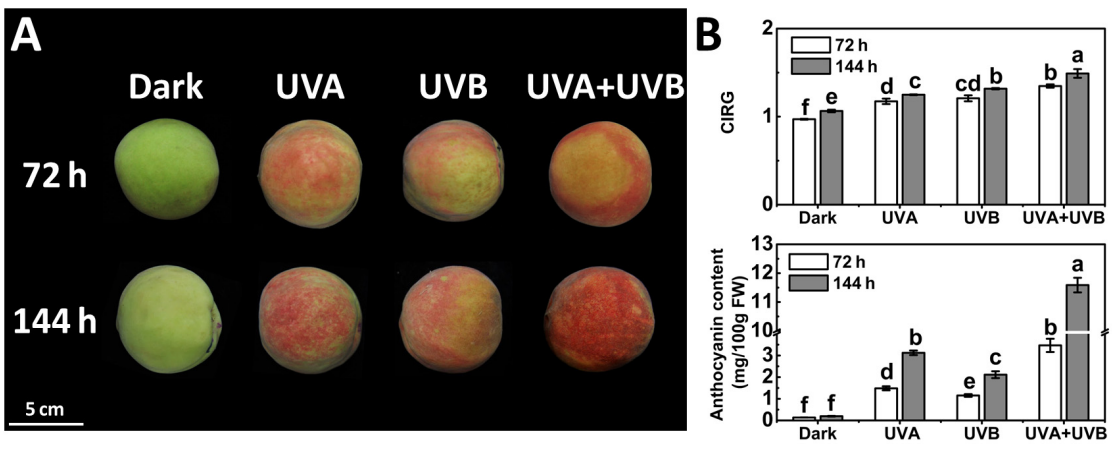

FIGURE 1 | Coloration **(A)** and the color index of red grapes (CIRG) values and anthocyanin content **(B)** in the peach peel after continuous UV irradiation or kept in dark. UVA, 1,000 μw/cm^2; UVB, 58 μw/cm^2. Scale bar indicated 5 cm. Data were presented as means (±SE) from three independent biological replicates. Values labeled with different letters indicated a significant difference at $P < 0.05$.

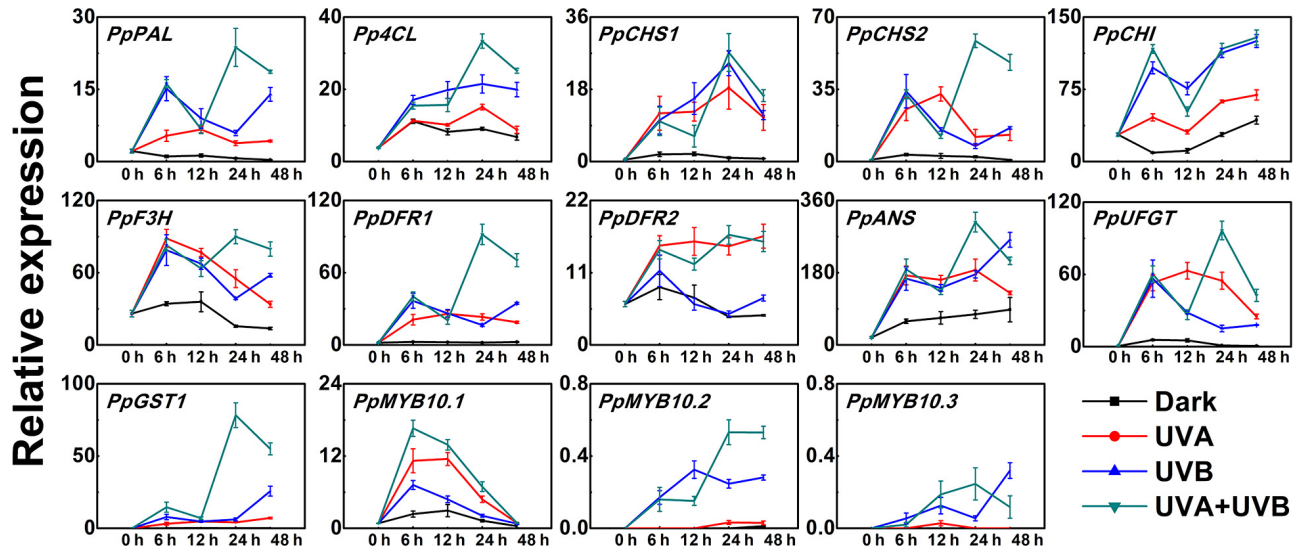

FIGURE 2 | Time course of the transcript levels of anthocyanin biosynthesis related genes in peach peel in response to continuous UV lights. UVA, 1,000 μw/cm^2; UVB, 58 μw/cm^2. Data were presented as means (±SE) from three independent biological replicates.

that the coloration of the peel was able to be induced by the irradiation of UVA or UVB, and there was a synergistic effect of UVA and UVB in stimulating anthocyanin biosynthesis.

Expression Analysis of *PpHY5* and *PpCOP1.1* after UV Light Treatment

In Arabidopsis, it has been demonstrated that *HY5* and *COP1* play vital roles in light signal transduction pathway (Lau and Deng, 2012; Gangappa and Botto, 2016). Previously, we identified potential homologous genes in peach (named *PpHY5*, *PpHYH*, *PpCOP1.1*, and *PpCOP1.2*) (Zhao et al., 2017). To clarify their functions in UV light induced anthocyanin biosynthesis in peach fruit, the expression levels following UV light exposure were monitored.

PpHY5 expression exhibited a strong response to UV light irradiation (**Figure 3**). The transcript level of *PpHY5* was low at the beginning (0 h); with UV there was a sharp increase which peaked within the first 6 h, and showed the highest accumulation level under UVA + UVB (about 4-fold higher than the control); from this peak there was a gradual decrease but expression remained higher than control (**Figure 3**). In Arabidopsis, HY5 HOMOLOG (HYH) has multiple overlapping functions with HY5 (Holm et al., 2002). In our study, the transcript level of *PpHYH* was similar to those of *PpHY5*, which increased at the beginning of irradiation but eventually decreased with continuous UV light (**Figure 3**). By contrast, the expression of *PpCOP1.1* decreased gradually following irradiation with UVA or UVB or UVA + UVB while slightly increased in the control (**Figure 3**). However, *PpCOP1.2* remained at quite low levels of expression with no obvious variation during the entire irradiation period among all different treatments (**Figure 3**). Overall, expression of *PpHY5* and *PpHYH* increased following UV treatment while that of *PpCOP1.1* was reduced. The transcript levels of these genes also responded quickly, within 6 h after the start of the treatment.

PpHY5 and *PpCOP1.1* Restored Hypocotyl Length and Anthocyanin Content in Arabidopsis Mutants under White Light

To confirm the roles of *PpHY5* and *PpCOP1.1* as light signal transduction related genes, we conducted the functional complementation assays with the Arabidopsis *hy5* mutant and *cop1* mutant transformed with *PpHY5* and *PpCOP1.1*, respectively. At least three independent transgenic lines of each background were generated and confirmed by RT-qPCR. The transgenic lines (*PpHY5*/*hy5*, *PpCOP1.1*/*cop1*) with high expression of *PpHY5* or *PpCOP1.1* were chosen to compare with WT and *hy5* or *cop1* mutant by measuring hypocotyl length and anthocyanin content under all conditions in 5-day-old seedlings.

For plants grown under white light for five days, *hy5* exhibited the longest hypocotyl phenotype (11.47 mm), while *cop1* exhibited the shortest hypocotyl phenotype (3.55 mm) (**Figure 4A**). The constitutive overexpression of *PpHY5* or *PpCOP1.1* in corresponding mutant background restored the hypocotyl length under white light (**Figure 4A**). The concentrations of anthocyanin in all lines also showed difference to some degrees (**Figure 4B**). Compared to WT, *cop1* displayed significantly higher accumulation of anthocyanin, and a lower level was observed in *hy5*. The anthocyanin levels were restored and enhanced in *PpHY5*/*hy5* transgenic lines, reaching a level that was about 4.1-fold higher than that in *hy5* mutant background (**Figure 4B**). In comparison, the anthocyanin accumulation was inhibited in the *PpCOP1.1*-complemented lines and decreased by 32% than those in *cop1* mutant background (**Figure 4B**). Likewise, the genes encoding

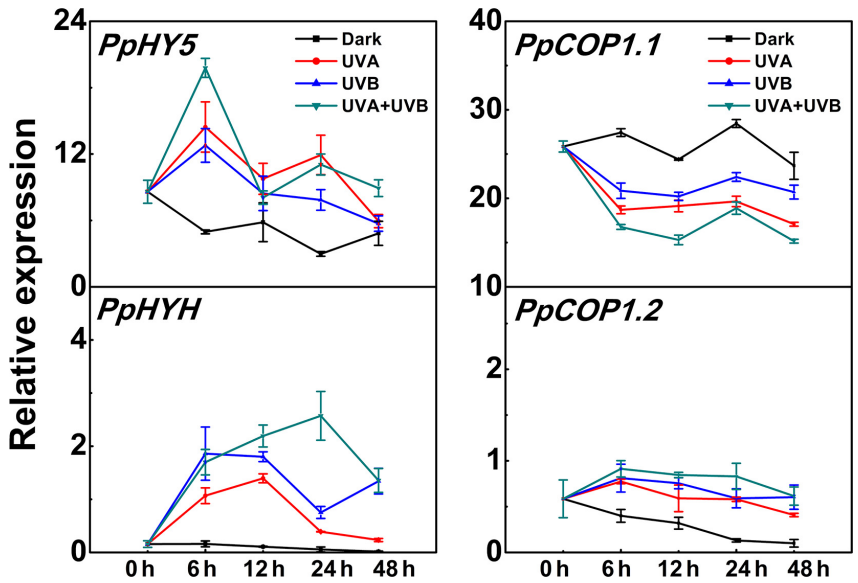

FIGURE 3 | Time course of the transcript levels of *PpHY5*, *PpHYH* and *PpCOP1.1*, *PpCOP1.2* in peach peel in response to continuous UV lights. UVA, 1,000 μw/cm^2; UVB, 58 μw/cm^2. Data were presented as means (±SE) from three independent biological replicates.

enzymes of the anthocyanin biosynthetic pathway (*PAL*, *CHS*, *CHI*, *F3H*, *DFR*, *ANS*, and *UFGT*) exhibited similar transcript accumulation trends consistent with anthocyanin content (**Figure 4C**). All these structural genes were generally lowly expressed in *hy5* and highly expressed in *cop1* relative to WT. For instance, the expression levels of *ANS* and *UFGT* decreased significantly in *hy5* and were about 50 and 75% lower, whereas at least 5-fold and 4-fold higher in *cop1* than that measured in WT. No significant differences in transcript levels of anthocyanin biosynthetic structural genes were found between *PpHY5*/*hy5* or *PpCOP1.1*/*cop1* transgenic lines and WT.

To visualize the subcellular localization of PpHY5 and PpCOP1.1, we performed the confocal microscopy assays of *N. benthamiana* leaves transiently transformed with *PpHY5*-GFP and *PpCOP1.1*-GFP. Our results showed that both PpHY5-GFP and PpCOP1.1-GFP displayed signal in the nucleus under white light (**Supplementary Figure 1**). This was in consistent with the subcellular localization of AtHY5 and AtCOP1 (Hardtke et al., 2000; Osterlund et al., 2000; Lau and Deng, 2012). These data suggested that *PpHY5* and *PpCOP1.1* were the functional orthologous of *AtHY5* and *AtCOP1* and were able to participate in white-light-related photomorphogenesis.

PpHY5 Participated in UVA- and UVB-Induced Anthocyanin Accumulation in a *PpCRY1* and *PpUVR8.1* Dependent Manner

In Arabidopsis, AtHY5 is a key factor in photomorphogenic responses and acts as a downstream signaling intermediate of AtCRY1 and AtUVR8 (Binkert et al., 2014; Marzi et al., 2020). To determine whether the peach counterpart of these genes function in the same signaling cascade in Arabidopsis, we generated the *PpHY5*/*hy5*, *PpCRY1*/*cry1*, and *PpUVR8.1*/*uvr8* transgenic lines. Five-day-old seedlings of WT, *cry1* mutant and *PpCRY1*/*cry1* transgenic lines were exposed to WWL + UVA for periods of 0–24 h and the expression of *AtHY5* was examined. Upon WWL + UVA exposure, the transcript levels of *AtHY5* were up-regulated and reached the maximum at 4 h (the upregulation ratio of *PpCRY1*/*cry1* was 13-fold, for *cry1* mutant it was 3-fold, for WT it was 16-fold), then a decreased occurred with the increment of irradiation time (**Figure 5A**). In comparison, *AtHY5* in *PpCRY1*-overexpression seedling in *cry1* background exhibited a similar transcript accumulation pattern as WT which was consistently higher than *cry1* mutant. With complementation of the *cry1* mutant, it can be concluded that *PpCRY1* was a functional counterpart of *AtCRY1* and could regulate *AtHY5* expression in response to UVA irradiation.

Similarly, after five days growth under white light, WT, *uvr8* mutant and *PpUVR8.1*/*uvr8* transgenic lines were transferred to WWL + UVB condition for periods of 0-24 h. Before WWL + UVB irradiation (0 h), *AtHY5* displayed relatively low transcription levels in all lines (**Figure 5B**). After exposure to WWL + UVB, a UV-induced elevation in *AtHY5* transcription occurred in WT, while no increase was observed in *uvr8*. However, the overexpression of *PpUVR8.1* in *uvr8* restored the ability of UVB to increase *AtHY5* transcription. The transcript levels of *AtHY5* showed a similar pattern in seedlings of *PpUVR8.1*/*uvr8* transgenic lines and WT during the irradiation period, decreasing gradually after a rapid peaking within 4 h. This suggested that the *PpUVR8.1* was a functional counterpart of *AtUVR8* and could regulate the expression of *AtHY5* in response to UVB irradiation.

As described above, *AtHY5* participates in both UVA and UVB signaling pathways in the *PpCRY1* and *PpUVR8.1* dependent

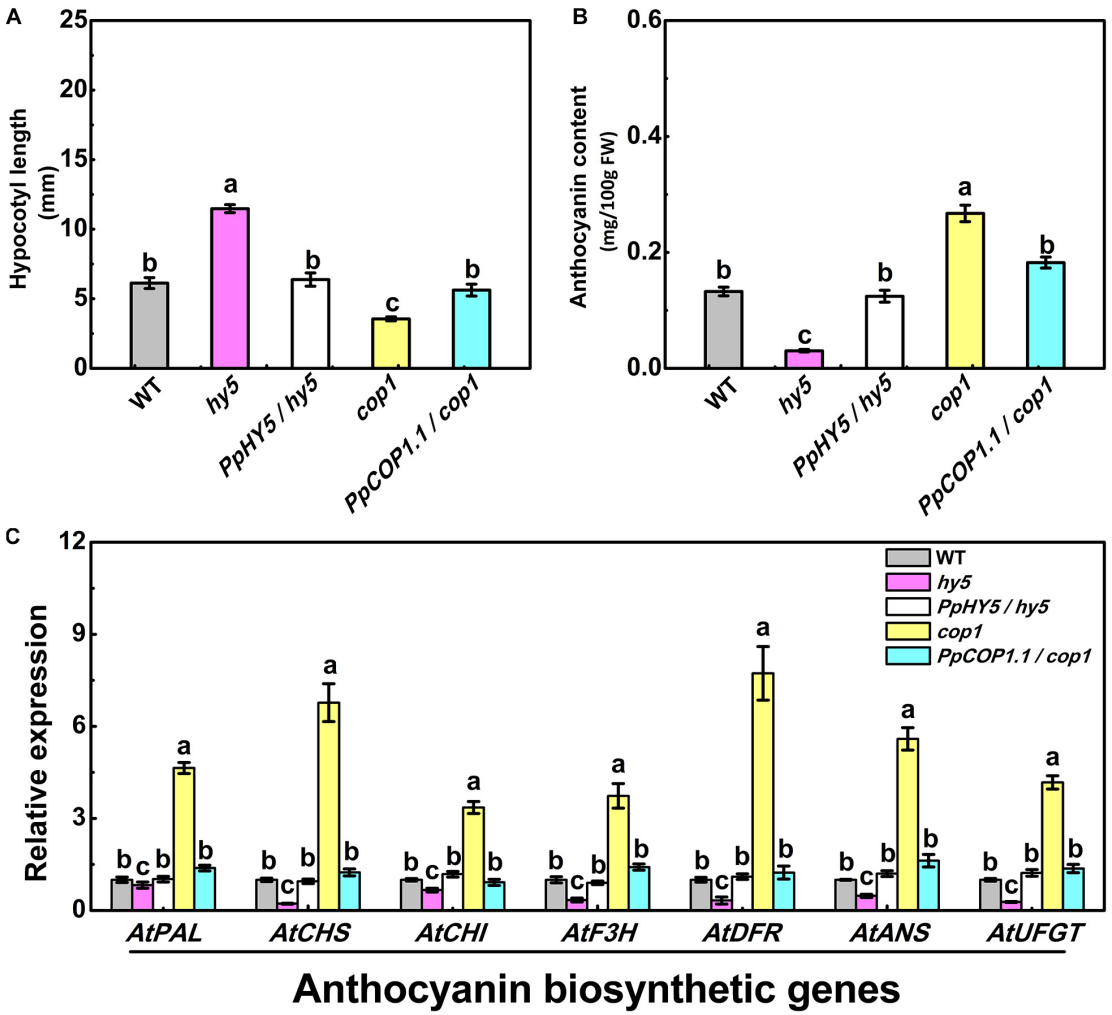

FIGURE 4 | Hypocotyl length **(A)**, anthocyanin content **(B)** and the relative expression levels of anthocyanin biosynthesis related genes **(C)** in 5-day-old seedlings of wild type (WT), mutant (*hy5*, *cop1*) and transgenic plants (*PpHY5*/*hy5*, *PpCOP1.1*/*cop1*) grown under long-day condition (16 h 40 w/m^2 white light/8 h dark cycle). For Arabidopsis transgenic plants, three independent lines for each target gene were used. Data were presented as means (±SE) from three independent biological replicates with 30 or more Arabidopsis seedlings collected for each replicate. Values labeled with different letters indicated a significant difference at $P < 0.05$.

manner respectively, leading to regulation of hypocotyl elongation and anthocyanin biosynthesis. The *PpHY5*/*hy5* transgenic line was used for measuring hypocotyl length and anthocyanin content under WWL, WWL + UVA, WWL + UVB or WWL + UVA + UVB condition. Among *hy5*, WT and *PpHY5*/*hy5* transgenic line under different light conditions, *hy5* consistently showed the longest hypocotyl length and the lowest anthocyanin content relative to other plants (**Figure 6**). When overexpressing *PpHY5* in *hy5*, the phenotypes of inhibition of hypocotyl elongation and anthocyanin accumulation were restored to levels in WT. Upon UV light exposure, the hypocotyl length was suppressed and anthocyanin increased in *PpHY5*/*hy5* transgenic line and WT as compared with those under WWL, but such phenotypes of photomorphogenesis were compromised in *hy5* (**Figure 6**). A more profound effect on photomorphogenesis was observed when irradiated with both UVA and UVB (**Figure 6**). The observation was consistent with the result in peach fruit under UV light treatments, indicating that PpHY5 played a similar role to AtHY5, which directly participated in UVA- and UVB-induced photomorphogenic responses and acted as a central positive regulator downstream of PpCRY1 and PpUVR8.1 photoreceptors.

PpHY5 Activated the Expression of Anthocyanin Biosynthetic Genes, *PpMYB10.1,* and Its Own Expression

Previous studies have demonstrated that Arabidopsis HY5 binds to the G-box (CACGTG) and ACE (ACGT containing element) motifs in the promoters of target genes in response to light (Lee et al., 2007). In Arabidopsis *PpHY5*/*hy5* transgenic lines, it was found that PpHY5 promoted the expression of anthocyanin biosynthetic structural genes (**Figure 4C**). In order to elucidate the function of PpHY5 in the regulation of anthocyanin

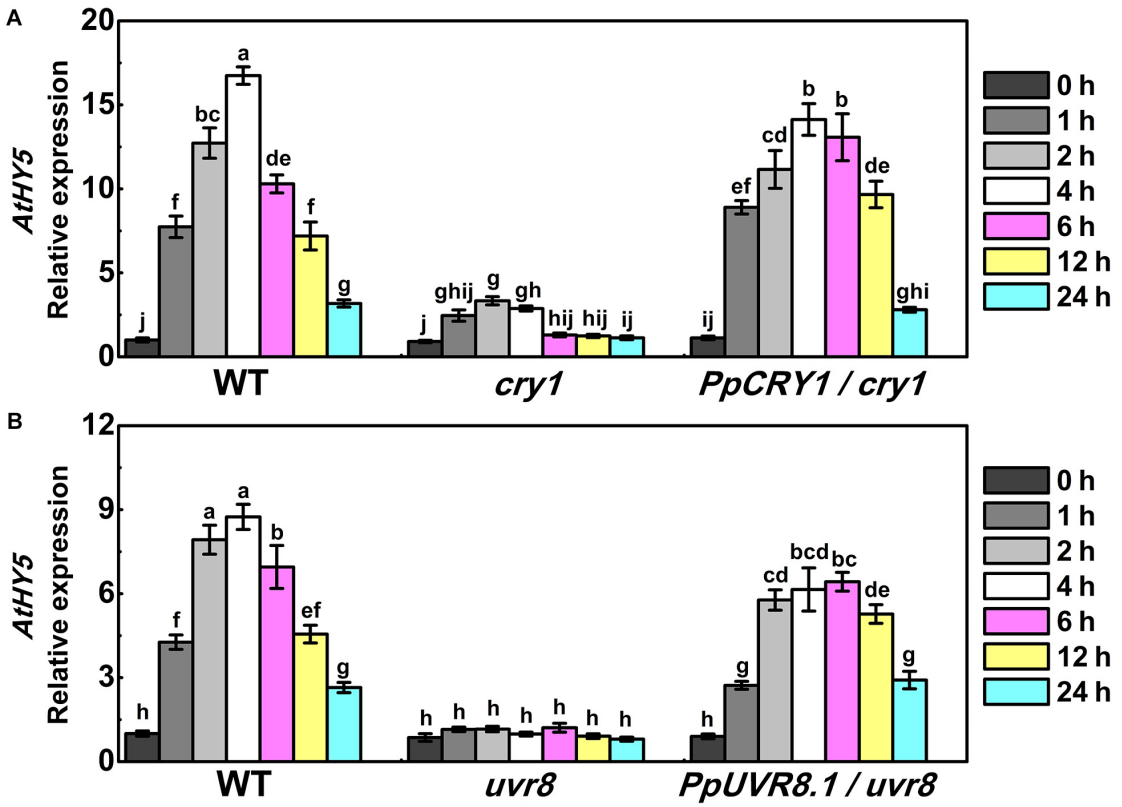

FIGURE 5 | The expression of *AtHY5* in the wild type (WT), *cry1* mutant and *PpCRY1/cry1* transgenic plant with different durations of continuous weak white light (WWL, 40 μw/cm^2) + UVA irradiation (40 μw/cm^2) **(A)** or in the WT, *uvr8* mutant and *PpUVR8.1/uvr8* transgenic plant with different durations of continuous WWL (40 μw/cm^2) + UVB irradiation (10 μw/cm^2) **(B)**. For Arabidopsis transgenic plants, three independent lines for each target gene were used. 5-day-old seedlings grown under constant WWL were subjected to WWL + UVA or WWL + UVB irradiation for the indicated time span. Data were presented as means (±SE) from three independent biological replicates with 30 or more Arabidopsis seedlings collected for each replicate.

accumulation in peach, the promoter regions (1,500 bp length) of anthocyanin biosynthetic genes and *PpMYB10s* were isolated.

Analysis of promoter sequences revealed the presence of putative *cis*-regulatory elements related to light signaling. The HY5-binding motifs (G-box and/or ACE motifs) were distributed in the promoters of 11 genes (*PpCHS1*, *PpCHS2*, *PpCHI*, *PpF3H*, *PpF3'H*, *PpDFR1*, *PpANS*, *PpUFGT*, and *PpMYB10.1/2/3*), with the total number ranging from one to seven for each promoter (**Figure 7A**). For example, five G-box motifs were identified in the *PpCHS1* promoter, four G-box motifs, and one ACE motif were identified in the *PpMYB10.1* promoter, while only one G-box motif and one ACE motif were identified in the *PpANS* promoter (**Figure 7A**). To validate the effect of PpHY5 on the transcription of anthocyanin biosynthetic genes, the promoter sequences of 11 genes were isolated and the dual-luciferase assay was conducted. When co-infiltrated with *PpHY5*, the highest activity was observed in the promoter of *PpCHS1* (5.3-fold) followed by *PpMYB10.1* (4.9-fold), *PpCHS2* (4.1-fold), and *PpDFR1* (3.3-fold) (**Figure 7B**). However, no obvious enhancements in luciferase enzyme activities were detected for other genes. Similarly, infiltration of *PpHYH* was also able to activate the promoters of both *PpCHS1* (2.9-fold) and *PpDFR1* (2.6-fold), while no obvious change in activation was observed on the promoters of either *PpCHS2* or *PpMYB10.1* or other genes (**Figure 7B**). Compared with PpHY5, PpHYH showed a similar but weaker ability to activate the promoters of both *PpCHS1* and *PpDFR1*. Taken together, these findings indicated that PpHY5 functioned as a positive transcriptional regulator for anthocyanin accumulation via activation of anthocyanin biosynthetic genes, possibly via binding directly to their promoters at G−box and ACE motifs.

We also analyzed the effects of PpHY5 and PpHYH on the promoter activity of *PpHY5* itself. PpHY5 and PpHYH significantly stimulated *PpHY5* promoter activity with the ratio of LUC to REN of 6.6 and 4.3 respectively (**Figure 7C**). To investigate the specificity of the interaction between PpHY5 and the *PpHY5* promoter, we performed a combination of *cis*-regulatory element mutations and the dual-luciferase assays to compare the activation levels. Four predicted E-box motifs were found in the promoter of *PpHY5* and designated as E-box-1, E-box-2, E-box-3 and E-box-4 respectively (**Figure 7D**). As shown in **Figure 7E**, when E-box-2 (CAAATG) within the *PpHY5* promoter was mutated to ACAAGT, the trans-activation activity of *PpHY5* on *PpHY5*-m2 promoter was attenuated by 74%. In contrast, PpHY5 still showed similar activation towards other mutated *PpHY5* promoters (*PpHY5*-m1, *PpHY5*-m3 and *PpHY5*-m4) with the induction of 5.6-, 7-, and 6.4-fold, with

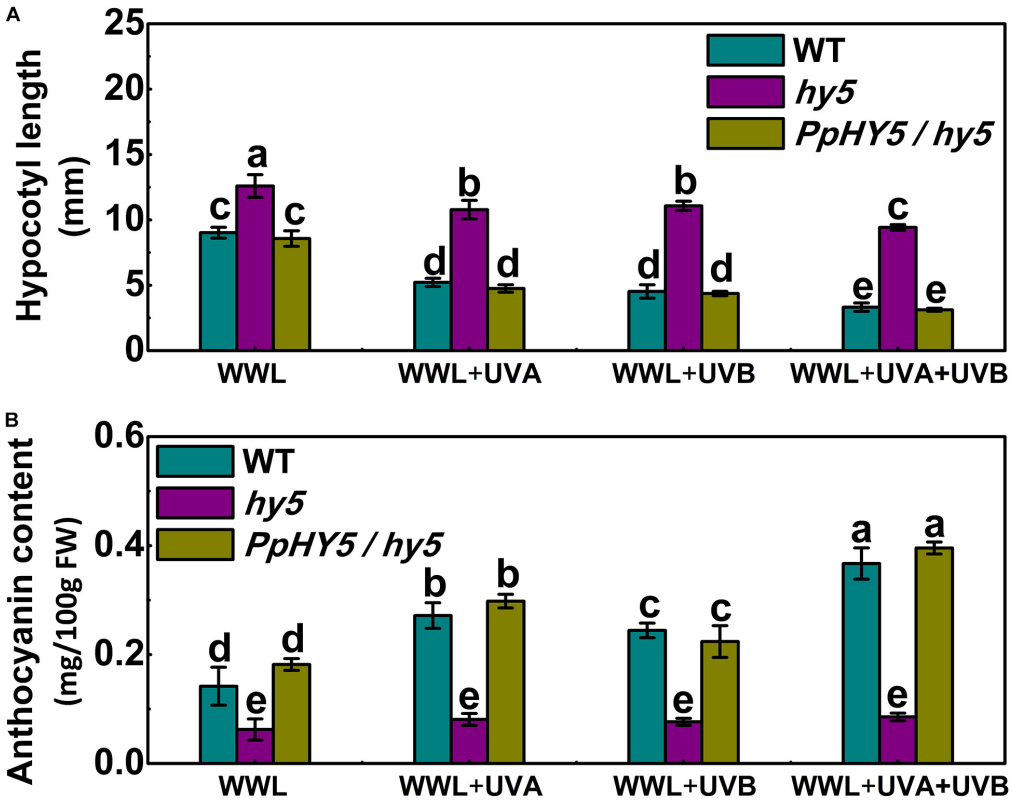

FIGURE 6 | Effect of different light treatments on hypocotyl length **(A)** and anthocyanin content **(B)** of 7-day-old seedlings of wild type (WT), *hy5* mutant and *PpHY5/hy5* transgenic plant. Seedlings were grown under continuous weak white light (WWL, 40 μw/cm^2) supplemented with/without UVA (40 μw/cm^2) or UVB (10 μw/cm^2) or both together for different UV light treatments. For Arabidopsis transgenic plant, three independent lines were used. Data were presented as means (±SE) from three independent biological replicates with 30 or more Arabidopsis seedlings collected for each replicate. Values labeled with different letters indicated a significant difference at $P < 0.05$.

no significant difference relative to the native *PpHY5* promoter (**Figure 7E**). These results suggested that PpHY5 might recognize E-box-2 to specifically activate its own transcription.

DISCUSSION

UVA and UVB Increased Anthocyanin Accumulation in Peach by Up-Regulating the Expression of Anthocyanin-Related Genes

Peach is an economically important fruit crop cultivated worldwide. Fruit coloration is one of the critical traits of exterior quality and commercial value for the consideration in consumer choice. Anthocyanin is the predominant component responsible for red pigmentation in peach fruit (Cheng et al., 2014). Light is an essential environmental factor influencing the production of anthocyanin and fruit coloration in peach, indicating the light signaling pathway is involved in the process (Zoratti et al., 2014). In this study, we conducted the comprehensive analysis of the effects of different UV lights on anthocyanin accumulation in peach. The results showed that peach fruit accumulated anthocyanin under UVA or UVB treatment and the induction was strengthened by the irradiation of UVA and UVB together (**Figure 1**). The induction was due to enhanced expression of genes encoding enzymes of the anthocyanin biosynthetic pathway.

The effects of UV irradiation on anthocyanin accumulation were not apparent until after continuous UV light treatment for 72 and 144 h. However, the transcript levels of multiple genes were induced in a short time (**Figure 2**). The results were similar with the significant elevation in the transcripts of *AtCHS*, *AtF3H*, and *AtDFR* in Arabidopsis under blue light treatment for 1 h (Cominelli et al., 2008). Maximum transcriptional response was observed following irradiation with of UVA + UVB, which correlated with anthocyanin accumulation. The molecular evidence of the synergistic effect of UVA + UVB on the regulation of anthocyanin biosynthesis needs further study.

The Function of PpHY5 Is Conserved in Different Light Signaling Pathways for Anthocyanin Accumulation

HY5, a member of the bZIP family transcription factor, is an essential regulator in multifaceted developmental processes,

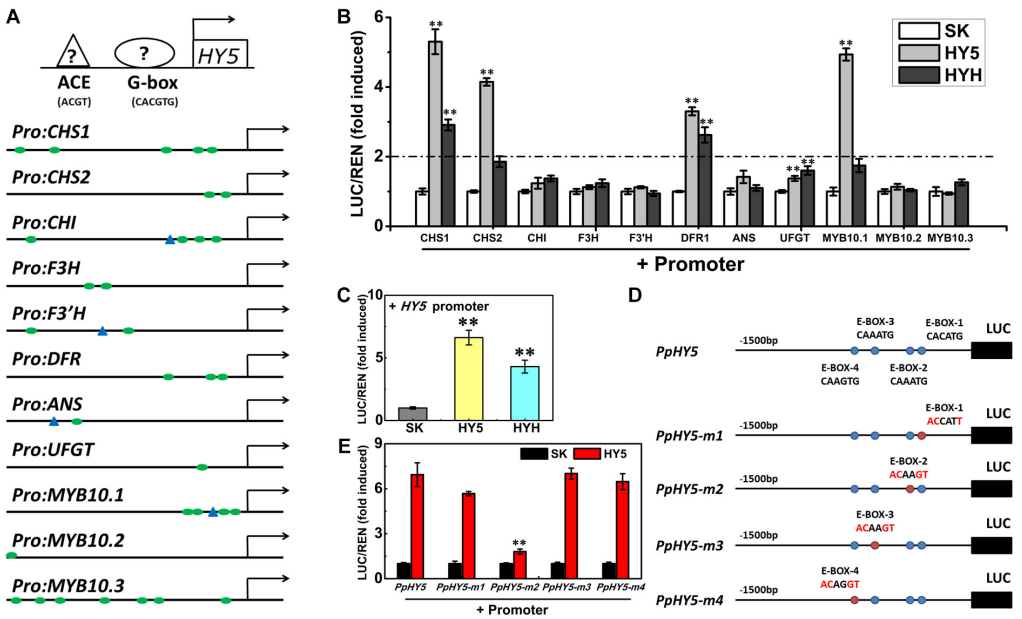

FIGURE 7 | Activation/self-activation of anthocyanin biosynthesis related genes by PpHY5 or PpHYH. **(A)** Upstream sequences (1500 bp) of anthocyanin biosynthesis related genes with G-box and ACGT containing element (ACE) motifs presented as green circles and blue triangles in the promoters, respectively. **(B)** Effects of PpHY5 or PpHYH on the promoter activity of anthocyanin biosynthesis related genes in dual-luciferase assays. **(C)** Effects of PpHY5 or PpHYH on the promoter activity of *PpHY5* in dual-luciferase assays. **(D,E)** Schematic diagrams of motif mutations for the *PpHY5* promoter **(D)** and effects of PpHY5 on the activity of original and mutated promoters in dual-luciferase assays **(E)**. The ratio of LUC/REN of the empty vector (SK) plus promoter was used as the calibrator (set as 1). LUC: firefly luciferase; REN: renilla luciferase; green circles: G-box; blue triangles: ACE motif; blue circles: E-box; red circles: mutated E-box. Data were presented as means (±SE) from six independent biological replicates and Student's *t*-test was used for statistical analyses compared with corresponding control. Asterisks (**) indicated a highly significant difference at $P < 0.01$.

such as photomorphogenesis, pigment accumulation, chloroplast development, nutrient assimilation, and carbon/nitrogen balance (Gangappa and Botto, 2016). HY5 has also been functionally characterized to be involved in the regulation of anthocyanin accumulation in response to light in a variety of plants (Shin et al., 2013; Jiang et al., 2016; An et al., 2017). After exposure to blue light, the transcript level of *SlHY5* in tomato was induced sharply within 3 h, and the SlHY5 protein accumulated steadily and peaked at 48 h (Liu et al., 2018). In peach, *PpHY5* had a strong response to both UVA and UVB at the transcription level, and the expression rapidly increased within 6 h. Expression of *PpHYH*, the closest homolog of *PpHY5*, was also induced by UVA and UVB treatments. Meanwhile, a decrease in the transcription level of *PpCOP1.1* was observed.

In Arabidopsis under white light, the *hy5* mutant exhibited skotomorphogenic phenotype with less anthocyanin content and longer hypocotyl length, conversely the *cop1* mutant presented photomorphogenic phenotype with higher anthocyanin content and short hypocotyl length. Overexpression of *PpHY5* in *hy5* and *PpCOP1.1* in *cop1* restored wild type phenotypes under white light (**Figure 4A**). Moreover, the RT-qPCR analysis showed that anthocyanin biosynthetic structural genes, including *AtPAL*, *AtCHS*, *AtCHI*, *AtF3H*, *AtDFR*, *AtANS*, and *AtUFGT*, were significantly up-regulated in *PpHY5*/*hy5* and down-regulated in *PpCOP1.1*/*cop1* transgenic lines than those in the corresponding mutant (**Figure 4C**). The phenotypes in Arabidopsis transgenic lines and mutants implied that *PpHY5* and *PpCOP1.1* acted as counterparts. Under WWL, *PpHY5* also directly participated in UVA- and UVB-induced anthocyanin accumulation which depended on *PpCRY1* and *PpUVR8.1* photoreceptors, indicating that PpHY5 exhibited a positive regulatory role in anthocyanin biosynthesis in response to various wavelengths of light environment.

We further investigated the role of PpHY5 in the regulation of anthocyanin accumulation using the dual-luciferase assay. PpHY5 positively activated the transcription of *PpCHS1*, *PpDFR1*, *PpCHS2*, and *PpMYB10.1* (**Figure 7B**). This is similar to results seen in tomato, apple, and pear (An et al., 2017; Liu et al., 2018; Tao et al., 2018). We also found that PpHYH had a similar effect to PpHY5 in regulating anthocyanin accumulation (**Figure 7B**). In addition, PpHY5 could bind to the E-box to regulate its own transcription (**Figure 7E**). As hypothesized, UVA and UVB light signals for anthocyanin biosynthesis were via PpHY5 in peach (**Figure 8**). These findings suggested that PpHY5 had a conserved function across different species and various wavelengths of light in regulating anthocyanin accumulation.

PpCRY1 and PpUVR8.1 Contributed to UVA and UVB Signaling Pathways in Peach

Many studies have revealed that the photoreceptors are indispensable for anthocyanin biosynthesis. *VviUVR1* and *MpUVR8*, the UVB receptors in grape and liverwort, played a

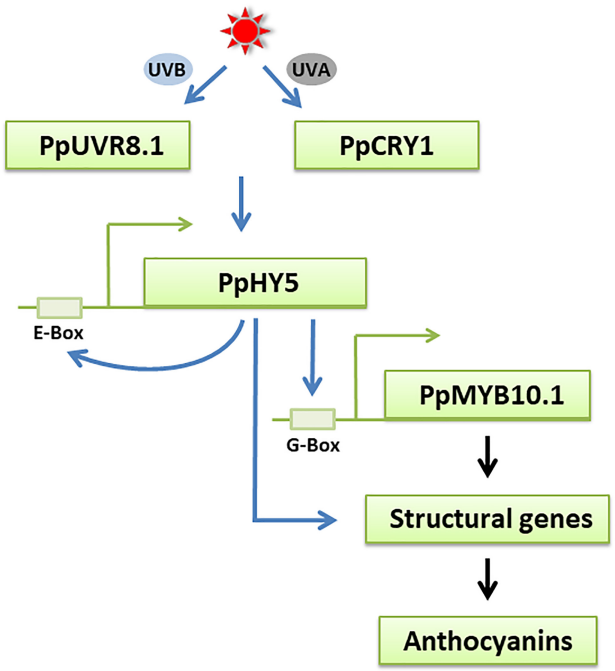

FIGURE 8 | A possible model for UVA- and UVB-induced anthocyanin biosynthesis in peach fruit. The UV light receptors PpCRY1 and PpUVR8.1 respectively perceive UVA and UVB light signals and influences the expression of *PpHY5*, an essential regulator in UVA and UVB signaling pathway. PpHY5 positively induces its own transcription by interacting with an E-box in its own promoter and activates the expression of *PpMYB10.1* to regulate anthocyanin accumulation. The transcription of anthocyanin biosynthetic structural genes is directly regulated by *PpMYB10.1* and some of them were also regulated by *PpHY5*. The blue arrows indicate the pathways verified in the present work. The black arrows indicate the pathways that have been previously reported in peach.

predominant role in the UVB-induced flavonoid accumulation (Loyola et al., 2016; Clayton et al., 2018). The phenotypes of alleviated hypocotyl elongation inhibition and decreased anthocyanin accumulation were observed in the antisense *Brassica napus CRY1* (*BnCRY1*) transgenic plant (Chatterjee et al., 2006). In apple, cryptochrome genes *MdCRY1* and *MdCRY2* have been identified to regulate anthocyanin accumulation and *MdCRY2* also participated in the photoperiodic control of flowering (Li et al., 2013a,b). Overexpression of *SlCRY1a* led to higher anthocyanin accumulation in tomato (Liu et al., 2018) and *SlUVR8* mediated the expression of *SlCHS* in response to the UVB environment (Li et al., 2018). We cloned the *PpCRY1* and *PpUVR8.1* from peach and characterized their functions as UVA and UVB receptors by complementation of Arabidopsis mutants. In our study, overexpressing *PpUVR8.1* or *PpCRY1* in the corresponding transgenic line promoted the expression of *AtHY5* in response to UVA or UVB irradiation, respectively. The results provided evidences that *PpCRY1* and *PpUVR8.1* acted as the photoreceptors of UVA and UVB and were associated with eliciting the transcript accumulation of *HY5*.

In conclusion, our study showed that UVA and UVB accelerated anthocyanin biosynthesis in the peel of "Hujingmilu" peach. The functions of crucial genes and photoreceptors in UV light signaling transduction pathways from peach were clarified. The data suggested that PpHY5 was both involved in UVA- and UVB-induced anthocyanin accumulation via a relatively conserved signaling pathway in PpCRY1-dependent and PpUVR8.1-dependent manner, respectively (**Figure 8**). PpHY5 regulated anthocyanin accumulation by activating the expression of anthocyanin biosynthetic-related genes. However, the results were mainly based on transcriptional control, which still needs to be verified at the post-transcriptional level in future experiments. Additionally, it would be worthy to investigate whether a direct interaction or an indirect interaction containing other unknown factors exists between PpCRY1 or PpUVR8.1 and PpHY5.

DATA AVAILABILITY STATEMENT

The raw data were deposited in NCBI sequence read archive (SRA) under accession number PRJNA665861.

AUTHOR CONTRIBUTIONS

YZ carried out the experiment, analyzed the data, and drafted the manuscript. MC helped to provide the experiment materials. CZ and RJ helped to provide technical assistance. TM, HW, AA, KL-W, and CX were involved in the revision of the manuscript. CX initiated the project, designed the research framework, coordinated the study, and participated in writing the manuscript. All authors read and approved the final manuscript.

FUNDING

This study was supported by the National Natural Science Foundation in China (31572102), Zhejiang Provincial Science and Technology Project for the Belt and Road (2016C04001), and the Open Project Fund of Hubei Key Laboratory for Processing and Transformation of Agricultural Products (2019HBSQGDKFB05).

SUPPLEMENTARY MATERIAL

The Supplementary Material for this article can be found online at: https://www.frontiersin.org/articles/10.3389/fpls.2020.603178/full#supplementary-material

Supplementary Figure 1 | Subcellular localization of PpHY5 and PpCOP1.1 in *Nicotiana benthamiana* leaves under white light. eGFP, GFP channel; Nucleus-RFP, transgenic *N. benthamiana* plants with red florescence in the nucleus; Bright-field, light microscopy image; Merged, merged image of the GFP and Bright channels. Scale bars indicated 20 μm.

Supplementary Table 1 | Primers used for reverse transcription quantitative PCR analysis.

Supplementary Table 2 | Primers used for plasmid construction. The restriction sites are underlined.

REFERENCES

An, J. P., Qu, F. J., Yao, J. F., Wang, X. N., You, C. X., Wang, X. F., et al. (2017). The bZIP transcription factor *MdHY5* regulates anthocyanin accumulation and nitrate assimilation in apple. *Hortic. Res.* 4:17023. doi: 10.1038/hortres.2017.23

An, X. H., Tian, Y., Chen, K. Q., Wang, X. F., and Hao, Y. J. (2012). The apple WD40 protein MdTTG1 interacts with bHLH but not MYB proteins to regulate anthocyanin accumulation. *Plant Physiol.* 169, 710–717. doi: 10.1016/j.jplph.2012.01.015

Azuma, A., Yakushiji, H., Koshita, Y., and Kobayashi, S. (2012). Flavonoid biosynthesis-related genes in grape skin are differentially regulated by temperature and light conditions. *Planta* 236, 1067–1080. doi: 10.1007/s00425-012-1650-x

BenSimhon, Z., Judeinstein, S., NadlerHassar, T., and Trainin, T. (2011). A pomegranate (*Punica granatum* L.) *WD*40-repeat gene is a functional homologue of *Arabidopsis TTG1* and is involved in the regulation of anthocyanin biosynthesis during pomegranate fruit development. *Planta* 234, 865–861. doi: 10.1007/s00425-011-1438-4

Binkert, M., Kozma-Bognár, L., Terecskei, K., De, V. L., Nagy, F., and Ulm, R. (2014). UV-B-responsive association of the Arabidopsis bZIP transcription factor ELONGATED HYPOCOTYL5 with target genes, including its own promoter. *Plant Cell* 26, 4200–4213. doi: 10.1105/tpc.114.130716

Carreño, J., Martínez, A., Almela, L., and Fernández-López, J. A. (1995). Proposal of an index for the objective evaluation of the colour of red table grapes. *Food Res. Int.* 28, 373–377. doi: 10.1016/0963-9969(95)00008-A

Casal, J. J. (2013). Photoreceptor signaling networks in plant responses to shade. *Annu. Rev. Plant Biol.* 64, 403–427. doi: 10.1146/annurev-arplant-050312-120221

Castagna, A., Dall'Asta, C., Chiavaro, E., Galaverna, G., and Ranieri, A. (2014). Effect of post-harvest UV-B irradiation on polyphenol profile and antioxidant activity in flesh and peel tomato fruits. *Food Bioproc. Technol.* 7, 2241–2250. doi: 10.1007/s11947-013-1214-5

Chagné, D., Lin-Wang, K., Espley, R. V., Volz, R. K., How, N. M., Rouse, S., et al. (2013). An ancient duplication of apple MYB transcription factors is responsible for novel red fruit-flesh phenotypes. *Plant Physiol.* 161, 225–239. doi: 10.1104/pp.112.206771

Chatterjee, M., Sharma, P., and Khurana, J. P. (2006). *Cryptochrome 1* from *Brassica napus* is up-regulated by blue light and controls hypocotyl/stem growth and anthocyanin accumulation. *Plant Physiol.* 141, 61–74. doi: 10.1104/pp.105.076323

Chattopadhyay, S., Ang, L. H., Puente, P., Deng, X. W., and Wei, N. (1998). Arabidopsis bZIP protein *HY5* directly interacts with light-responsive promoters in mediating light control of gene expression. *Plant Cell* 10, 673–683. doi: 10.1105/tpc.10.5.673

Cheng, J., Wei, G., Zhou, H., Gu, C., Vimolmangkang, S., Liao, L., et al. (2014). Unraveling the mechanism underlying the glycosylation and methylation of anthocyanins in peach. *Plant Physiol.* 166, 1044–1058. doi: 10.1104/pp.114.246876

Clayton, W. A., Albert, N. W., Thrimawithana, A. H., McGhie, T. K., Deroles, S. C., Schwinn, K. E., et al. (2018). UVR8-mediated induction of flavonoid biosynthesis for UVB tolerance is conserved between the liverwort *Marchantia polymorpha* and flowering plants. *Plant J.* 96, 503–517. doi: 10.1111/tpj.14044

Cominelli, E., Gusmaroli, G., Allegra, D., Galbiati, M., Wade, H. K., and Jenkins, G. I. (2008). Expression analysis of anthocyanin regulatory genes in response to different light qualities in *Arabidopsis thaliana*. *Plant Physiol.* 165, 886–894. doi: 10.1016/j.jplph.2007.06.010

Gangappa, S. N., and Botto, J. F. (2016). The multifaceted roles of HY5 in plant growth and development. *Mol. Plant.* 9, 1353–1365. doi: 10.1016/j.molp.2016.07.002

Gelderen, K. V., Kang, C., and Pierik, R. (2018). Light signaling, root development, and plasticity. *Plant Physiol.* 176, 1049–1060. doi: 10.1104/pp.17.01079

Gould, K. S., Dudle, D. A., and Neufeld, H. S. (2010). Why some stems are red: cauline anthocyanins shield photosystem II against high light stress. *J. Exp. Bot.* 61, 2707–2717. doi: 10.1093/jxb/erq106

Guo, J., and Wang, M. (2010). Ultraviolet A-specific induction of anthocyanin biosynthesis and *PAL* expression in tomato (*Solanum lycopersicum* L.). *Plant Growth Regul.* 62, 1–8. doi: 10.1007/s10725-010-9472-y

Guo, J., Han, W., and Wang, M. H. (2008). Ultraviolet and environmental stresses involved in the induction and regulation of anthocyanin biosynthesis: a review. *Afr. J. Biotechnol.* 7, 4966–4972. doi: 10.5897/AJB08.090

Hagen, S. F., Borge, G., Bengtsson, G. B., Bilger, W., Berge, A., and Haffner, K. (2007). Phenolic contents and other health and sensory related properties of apple fruit (*Malus domestica* Borkh., *cv. Aroma): effect of postharvest UV-B irradiation*. *Postharvest Biol. Technol.* 45, 1–10. doi: 10.1016/j.postharvbio.2007.02.002

Hardtke, C. S., Gohda, K., Osterlund, M. T., Oyama, T., Okada, K., and Deng, X. W. (2000). HY5 stability and activity in arabidopsis is regulated by phosphorylation in its COP1 binding domain. *EMBO J.* 19, 4997–5006. doi: 10.1093/emboj/19.18.4997

Henry-Kirk, R. A., Plunkett, B., Hall, M., McGhie, T., Allan, A. C., Wargent, J. J., et al. (2018). Solar UV light regulates flavonoid metabolism in apple (*Malus domestica*). *Plant Cell Environ.* 41, 675–688. doi: 10.1111/pce.13125

Holm, M., Ma, L. G., Qu, L., and Deng, X. W. (2002). Two interacting bZIP proteins are direct targets of COP1-mediated control of light-dependent gene expression in *Arabidopsis*. *Genes Dev.* 16, 1247–1259. doi: 10.1101/gad.969702

Jaakola, L. (2013). New insights into the regulation of anthocyanin biosynthesis in fruits. *Trends Plant Sci.* 18, 477–483. doi: 10.1016/j.tplants.2013.06.003

Jiang, M., Ren, L., Lian, H., Liu, Y., and Chen, H. (2016). Novel insight into the mechanism underlying light-controlled anthocyanin accumulation in eggplant (*Solanum melongena* L.). *Plant Sci.* 249, 46–58. doi: 10.1016/j.plantsci.2016.04.001

Kami, C., Lorrain, S., Hornitschek, P., and Fankhauser, C. (2010). Light-regulated plant growth and development. *Curr. Top. Dev. Biol.* 91, 29–66. doi: 10.1016/S0070-2153(10)91002-8

Lau, O. S., and Deng, X. W. (2012). The photomorphogenic repressors COP1 and DET1: 20 years later. *Trends Plant Sci.* 17, 584–593. doi: 10.1016/j.tplants.2012.05.004

Lee, J., He, K., Stolc, V., Lee, H., Figueroa, P., Gao, Y., et al. (2007). Analysis of transcription factor HY5 genomic binding sites revealed its hierarchical role in light regulation of development. *Plant Cell* 19, 731–749. doi: 10.1105/tpc.106.047688

Li, D., Luo, Z., Mou, W., Wang, Y., and Ying, T. (2014). ABA and UV-C effects on quality, antioxidant capacity and anthocyanin contents of strawberry fruit (*Fragaria ananassa* Duch.). *Postharvest Biol. Technol.* 90, 56–62. doi: 10.1016/j.postharvbio.2013.12.006

Li, H. R., Li, Y. X., Deng, H., Sun, X. C., Wang, A. Q., Tang, X. F., et al. (2018). Tomato UV-B receptor SlUVR8 mediates plant acclimation to UV-B radiation and enhances fruit chloroplast development via regulating SlGLK2. *Sci Rep.* 8:6097. doi: 10.1038/s41598-018-24309-y

Li, Y. Y., Mao, K., Zhao, C., Zhang, R. F., Zhao, X. Y., Zhang, H. L., et al. (2013a). Molecular cloning of *cryptochromes 1* from apple and its functional characterization in *Arabidopsis*. *Plant Physiol. Biochem.* 67, 169–177. doi: 10.1016/j.plaphy.2013.02.031

Li, Y. Y., Mao, K., Zhao, C., Zhao, X. Y., Zhang, H. L., Shu, H. R., et al. (2012). MdCOP1 ubiquitin E3 ligases interact with MdMYB1 to regulate light-induced anthocyanin biosynthesis and red fruit coloration in apple. *Plant Physiol.* 160, 1011–1022. doi: 10.1104/pp.112.199703

Li, Y. Y., Mao, K., Zhao, C., Zhao, X. Y., Zhang, R. F., Zhang, H. L., et al. (2013b). Molecular cloning and functional analysis of a blue light receptor gene *MdCRY2* from apple (*Malus domestica*). *Plant Cell Rep.* 32, 555–566. doi: 10.1007/s00299-013-1387-4

Liang, T., Yang, Y., and Liu, H. T. (2019). Signal transduction mediated by the plant UV-B photoreceptor UVR8. *New Phytol.* 221, 1247–1252. doi: 10.1111/nph.15469

Lin, C. T. (2002). Blue light receptors and signal transduction. *Plant Cell* 14, 207–225. doi: 10.1105/tpc.000646

Lin-Wang, K., Bolitho, K., Grafton, K., and Karunairetnam, S. (2010). An R2R3 MYB transcription factor associated with regulation of the anthocyanin

biosynthetic pathway in Rosaceae. *BMC Plant Biol.* 10:50. doi: 10.1186/1471-2229-10-50

Liu, C. C., Chi, C., Jin, L. J., Zhu, J. H., Yu, J. Q., and Zhou, Y. H. (2018). The bZip transcription factor *HY5* mediates *CRY1a*-induced anthocyanin biosynthesis in tomato. *Plant Cell Environ.* 41, 1762–1775. doi: 10.1111/pce.13171

Liu, H. T., Liu, B., Zhao, C. X., Pepper, M., and Lin, C. T. (2011). The action mechanisms of plant cryptochromes. *Trends Plant Sci.* 16, 684–691. doi: 10.1016/j.tplants.2011.09.002

Liu, T., Song, S., Yuan, Y. B., Wu, D. J., Chen, M. J., Sun, Q. N., et al. (2015). Improved peach peel color development by fruit bagging. Enhanced expression of anthocyanin biosynthetic and regulatory genes using white non-woven polypropylene as replacement for yellow paper. *Sci. Hortic.* 184, 142–148. doi: 10.1016/j.scienta.2015.01.003

Loyola, R., Herrera, D., Mas, A., Wong, D. C., Holl, J., Cavallini, E., et al. (2016). The photomorphogenic factors UV-B RECEPTOR 1, ELONGATED HYPOCOTYL 5, and HY5 HOMOLOGUE are part of the UV-B signalling pathway in grapevine and mediate flavonol accumulation in response to the environment. *J. Exp. Bot.* 67, 5429–5445. doi: 10.1093/jxb/erw307

Marzi, D., Brunetti, P., Mele, G., Napoli, N., Calò, L., Spaziani, E., et al. (2020). Light controls stamen elongation via cryptochromes, phytochromes and COP1 through HY5 and HYH. *Plant J.* 103, 379–394. doi: 10.1111/tpj.14736

Morales, L. O., Brosche, M., Vainonen, J., Jenkins, G. I., Wargent, J. J., Sipari, N., et al. (2013). Multiple roles for UV RESISTANCE LOCUS8 in regulating gene expression and metabolite accumulation in Arabidopsis under solar ultraviolet radiation. *Plant Physiol.* 161, 744–759. doi: 10.1104/pp.112.211375

Nawkar, G. M., Kang, C. H., Maibam, P., Park, J. H., Jung, Y. J., Chae, H. B., et al. (2017). HY5, a positive regulator of light signaling, negatively controls the unfolded protein response in Arabidopsis. *Proc. Natl. Acad. Sci. U. S. A.* 114, 2084–2089. doi: 10.1073/pnas.1609844114

Niu, S. S., Xu, C. J., Zhang, W. S., Zhang, B., Li, X., Lin-Wang, K., et al. (2010). Coordinated regulation of anthocyanin biosynthesis in Chinese bayberry (*Myrica rubra*) fruit by a R2R3 MYB transcription factor. *Planta* 231, 887–899. doi: 10.1007/s00425-009-1095-z

Oh, S., and Montgomery, B. L. (2017). Phytochromes: Where to start. *Cell* 171, 1254–1256. doi: 10.1016/j.cell.2017.11.020

Osterlund, M. T., Hardtke, C. S., Wei, N., and Deng, X. W. (2000). Targeted destabilization of HY5 during light-regulated development of *Arabidopsis*. *Nature* 405, 462–466. doi: 10.1038/35013076

Qian, M., Zhang, D., Yue, X., Wang, S., and Li, X. (2013). Analysis of different pigmentation patterns in "Mantianhong" (*Pyrus pyrifolia* Nakai) and "Cascade" (*Pyrus communis* L.) *under bagging treatment and postharvest UV-B/visible irradiation conditions*. *Sci. Hortic.* 151, 75–82. doi: 10.1016/j.scienta.2012.12.020

Rahim, M. A., Busatto, N., and Trainotti, L. (2014). Regulation of anthocyanin biosynthesis in peach fruits. *Planta* 240, 913–929. doi: 10.1007/s00425-014-2078-2

Ravaglia, D., Espley, R. V., Henry-Kirk, R. A., Andreotti, C., and Ziosi, V. (2013). Transcriptional regulation of flavonoid biosynthesis in nectarine (*Prunus persica*) by a set of R2R3 MYB transcription factors. *BMC Plant Biol.* 13:68. doi: 10.1186/1471-2229-13-68

Rizzini, L., Favory, J. J., Cloix, C., and Faggionato, D. (2011). Perception of UV-B by the Arabidopsis UVR8 protein. *Science* 332, 103–106. doi: 10.1126/science.1200660

Schaefer, H. M., Schaefer, V., and Levey, D. J. (2004). How plant-animal interactions signal new insights in communication. *Trends Ecol. Evol.* 19, 577–584. doi: 10.1016/j.tree.2004.08.003

Shin, D. H., Choi, M. G., Kim, K., Bang, G., Cho, M., Choi, S. B., et al. (2013). HY5 regulates anthocyanin biosynthesis by inducing the transcriptional activation of the MYB75/PAP1 transcription factor in Arabidopsis. *FEBS Lett.* 587, 1543–1547. doi: 10.1016/j.febslet.2013.03.037

Stracke, R., Favory, J. J., Gruber, H., Bartelniewoehner, L., Bartels, S., Binkert, M., et al. (2010). The Arabidopsis bZIP transcription factor HY5 regulates expression of the PFG1/MYB12 gene in response to light and ultraviolet-B radiation. *Plant Cell Environ.* 33, 88–103. doi: 10.1111/j.1365-3040.2009.02061.x

Sun, Y. W., Qian, M. J., Wu, R. Y., Niu, Q. F., Teng, Y. W., and Zhang, D. (2014). Postharvest pigmentation in red Chinese sand pears (*Pyrus pyrifolia* Nakai) in response to optimum light and temperature. *Postharvest Biol. Technol.* 91, 64–71. doi: 10.1016/j.postharvbio.2013.12.015

Tao, R. Y., Bai, S. L., Ni, J. B., Yang, Q. S., Zhao, Y., and Teng, Y. W. (2018). The blue light signal transduction pathway is involved in anthocyanin accumulation in 'Red Zaosu' pear. *Planta* 248, 37–48. doi: 10.1007/s00425-018-2877-y

Tong, Z., Gao, Z., Wang, F., Zhou, J., and Zhang, Z. (2009). Selection of reliable reference genes for gene expression studies in peach using real-time PCR. *BMC Mol. Biol.* 10:71. doi: 10.1186/1471-2199-10-71

Tsuda, T. (2012). Dietary anthocyanin-rich plants: biochemical basis and recent progress in health benefits studies. *Mol. Nutr. Food Res.* 56, 159–170. doi: 10.1002/mnfr.201100526

Tuan, P. A., Bai, S. L., Yaegaki, H., Tamura, T., Hihara, S., Moriguchi, T., et al. (2015). The crucial role of *PpMYB10.1 in anthocyanin accumulation in peach and relationships between its allelic type and skin color phenotype*. *BMC Plant Biol.* 15:280. doi: 10.1186/s12870-015-0664-5

Uematsu, C., Katayama, H., and Makino, I. (2014). Peace, a MYB-like transcription factor, regulates petal pigmentation in flowering peach 'Genpei' bearing variegated and fully pigmented flowers. *J. Exp. Bot.* 65, 1081–1094. doi: 10.1093/jxb/ert456

Uleberg, E., Rohloff, J., Jaakola, L., Trost, K., Junttila, O., and Haggman, H. (2012). Effects of temperature and photoperiod on yield and chemical composition of northern and southern clones of bilberry (*Vaccinium myrtillus* L.). *J. Agric. Food Chem.* 60, 10406–10414. doi: 10.1021/jf302924m

Wade, H. K., Bibikova, T. N., and Valentine, W. J. (2001). Interactions within a network of phytochrome, cryptochrome and UV-B phototransduction pathways regulate chalcone synthase gene expression in *Arabidopsis* leaf tissue. *Plant J.* 25, 675–685. doi: 10.1046/j.1365-313x.2001.01001.x

Wang, N., Qu, C. Z., Jiang, S. H., Chen, Z. J., Xu, H. F., Fang, H. C., et al. (2018). The proanthocyanidin-specific transcription factor *MdMYBPA1* initiates anthocyanin synthesis under low-temperature conditions in red-fleshed apples. *Plant J.* 96, 39–55. doi: 10.1111/tpj.14013

Wang, Q., Zuo, Z. C., Wang, X., Liu, Q., Gu, L. F., Oka, Y., et al. (2018). Beyond the photocycle-how cryptochromes regulate photoresponses in plants? *Curr. Opin. Plant Biol.* 45, 120–126. doi: 10.1016/j.pbi.2018.05.014

Wang, S. Y., Chen, C. T., and Wang, C. Y. (2009). The influence of light and maturity on fruit quality and flavonoid content of red raspberries. *Food Chem.* 112, 676–684. doi: 10.1016/j.foodchem.2008.06.032

Winkel-Shirley, B. (2001). Flavonoid biosynthesis: a colorful model for genetics, biochemistry, cell biology, and biotechnology. *Plant Physiol.* 126, 485–493. doi: 10.1104/pp.126.2.485

Xu, F., Cao, S., Shi, L., Chen, W., and Su, X. (2014). Blue light irradiation affects anthocyanin content and enzyme activities involved in postharvest strawberry fruit. *J. Agric. Food Chem.* 62, 4778–4783. doi: 10.1021/jf501120u

Yang, D. Y., Seaton, D. D., Krahmer, J., and Halliday, K. J. (2016). Photoreceptor effects on plant biomass, resource allocation, and metabolic state. *Proc. Natl. Acad. Sci. U. S. A.* 113, 7667–7672. doi: 10.1073/pnas.1601309113

Yin, R., and Ulm, R. (2017). How plants cope with UV-B: from perception to response. *Curr. Opin. Plant Biol.* 37, 42–48. doi: 10.1016/j.pbi.2017.03.013

Zhang, W. S., Li, X., Zheng, J. T., Wang, G. Y., Sun, C. D., Ferguson, I. B., et al. (2008). Bioactive components and antioxidant capacity of Chinese bayberry (*Myrica rubra* Sieb. *and Zucc.) fruit in relation to fruit maturity and postharvest storage*. *Eur. Food Res. Technol.* 227, 1091–1097. doi: 10.1007/s00217-008-0824-z

Zhang, X. N., Huang, H. Z., Zhao, X. Y., Lv, Q., Sun, C. D., Li, X., et al. (2015). Effects of flavonoids-rich Chinese bayberry (*Myrica rubra*) pulp extracts on glucose consumption in human HepG2 cells. *J. Funct. Foods.* 14, 144–153. doi: 10.1016/j.jff.2015.01.030

Zhang, X., Henriques, R., Lin, S., Niu, Q., and Chua, N. (2006). *Agrobacterium*-mediated transformation of *Arabidopsis thaliana* using the floral dip method. *Nat. Protoc.* 1, 641–646. doi: 10.1038/nprot.2006.97

Zhang, Y., Butelli, E., and Martin, C. (2014). Engineering anthocyanin biosynthesis in plants. *Curr. Opin. Plant Biol.* 19, 81–90. doi: 10.1016/j.pbi.2014.05.011

Zhao, Y., Dong, W. Q., Wang, K., Zhang, B., Allan, A. C., Lin-Wang, K., et al. (2017). Differential sensitivity of fruit pigmentation to ultraviolet light between two peach cultivars. *Front. Plant Sci.* 8:1552. doi: 10.3389/fpls.2017.01552

Zhao, Y., Dong, W. Q., Zhu, Y. C., Allan, A. C., Lin-Wang, K., and Xu, C. J. (2020). *PpGST1*, an anthocyanin-related glutathione S-transferase gene, is essential for fruit coloration in peach. *Plant Biotechnol. J.* 18, 1284–1295. doi: 10.1111/pbi.13291

Zhou, H., Lin-Wang, K., Wang, F. R., Andrew, A. C., and Han, Y. P. (2018). Activator-type R2R3-MYB genes induce a repressor-type R2R3-MYB gene to balance anthocyanin and proanthocyanidin accumulation. *New Phytol.* 4, 1919–1934. doi: 10.1111/nph.15486

Zhou, Y., and Singh, B. R. (2004). Effect of light on anthocyanin levels in submerged, harvested cranberry fruit. *Biomed. Biotechnol.* 5, 259–263. doi: 10.1155/S1110724304403027

Zhou, Y., Guo, D., Li, J., Cheng, J., Zhou, H., Gu, C., et al. (2013). Coordinated regulation of anthocyanin biosynthesis through photorespiration and temperature in peach (*Prunus persica*). *Tree Genet Genomes.* 9, 265–278. doi: 10.1007/s11295-012-0552-1

Zhou, Y., Zhou, H., Lin-wang, K., Vimolmangkang, S., Espley, R. V., Wang, L., et al. (2014). Transcriptome analysis and transient transformation suggest an ancient duplicated MYB transcription factor as a candidate gene for leaf red coloration in peach. *BMC Plant Biol.* 14:1–13. doi: 10.1186/s12870-014-0388-y

Zoratti, L., Karppinen, K., Escobar, A. L., Haggman, H., and Jaakola, L. (2014). Light-controlled flavonoid biosynthesis in fruits. *Front. Plant Sci.* 5:534. doi: 10.3389/fpls.2014.00534

Conflict of Interest: The authors declare that the research was conducted in the absence of any commercial or financial relationships that could be construed as a potential conflict of interest.

frontiers in Plant Science

ORIGINAL RESEARCH
published: 18 March 2021
doi: 10.3389/fpls.2021.612302

Photomorphogenesis in the Picocyanobacterium *Cyanobium gracile* Includes Increased Phycobilisome Abundance Under Blue Light, Phycobilisome Decoupling Under Near Far-Red Light, and Wavelength-Specific Photoprotective Strategies

Gábor Bernát[1,2], Tomáš Zavřel[3], Eva Kotabová[2], László Kovács[4], Gábor Steinbach[5,6], Lajos Vörös[1], Ondřej Prášil[2], Boglárka Somogyi[1] and Viktor R. Tóth[1]*

[1] Balaton Limnological Institute, Centre for Ecological Research, Tihany, Hungary, [2] Centre Algatech, Institute of Microbiology of the Czech Academy of Sciences, Třeboň, Czechia, [3] Global Change Research Institute, Academy of Sciences of the Czech Republic, Brno, Czechia, [4] Institute of Plant Biology, Biological Research Centre, Eötvös Loránd Research Network, Szeged, Hungary, [5] Institute of Biophysics, Biological Research Centre, Eötvös Loránd Research Network, Szeged, Hungary, [6] Cellular Imaging Laboratory, Biological Research Center, Eötvös Loránd Research Network, Szeged, Hungary

Photomorphogenesis is a process by which photosynthetic organisms perceive external light parameters, including light quality (color), and adjust cellular metabolism, growth rates and other parameters, in order to survive in a changing light environment. In this study we comprehensively explored the light color acclimation of *Cyanobium gracile*, a common cyanobacterium in turbid freshwater shallow lakes, using nine different monochromatic growth lights covering the whole visible spectrum from 435 to 687 nm. According to incident light wavelength, *C. gracile* cells performed great plasticity in terms of pigment composition, antenna size, and photosystem stoichiometry, to optimize their photosynthetic performance and to redox poise their intersystem electron transport chain. In spite of such compensatory strategies, *C. gracile*, like other cyanobacteria, uses blue and near far-red light less efficiently than orange or red light, which involves moderate growth rates, reduced cell volumes and lower electron transport rates. Unfavorable light conditions, where neither chlorophyll nor phycobilisomes absorb light sufficiently, are compensated by an enhanced antenna size. Increasing the wavelength of the growth light is accompanied by increasing photosystem II to photosystem I ratios, which involve better light utilization in the red spectral region. This is surprisingly accompanied by a partial excitonic antenna decoupling, which was the highest in the cells grown under 687 nm light. So far, a similar phenomenon is known to be induced only by strong light; here we demonstrate that under certain physiological conditions such decoupling is also possible to be induced by weak light. This suggests that

OPEN ACCESS

Edited by:
Stefano Santabarbara, National Research Council (CNR), Italy

Reviewed by:
Vivek Dogra, Institute of Himalayan Bioresource Technology (CSIR), India
Tse-Min Lee, National Sun Yat-sen University, Taiwan

***Correspondence:**
Gábor Bernát
bernat.gabor@ecolres.hu

Specialty section:
This article was submitted to Plant Abiotic Stress, a section of the journal Frontiers in Plant Science

Received: *30 September 2020*
Accepted: *15 February 2021*
Published: *18 March 2021*

Citation:
Bernát G, Zavřel T, Kotabová E, Kovács L, Steinbach G, Vörös L, Prášil O, Somogyi B and Tóth VR (2021) Photomorphogenesis in the Picocyanobacterium Cyanobium gracile Includes Increased Phycobilisome Abundance Under Blue Light, Phycobilisome Decoupling Under Near Far-Red Light, and Wavelength-Specific Photoprotective Strategies. Front. Plant Sci. 12:612302. doi: 10.3389/fpls.2021.612302

suboptimal photosynthetic performance of the near far-red light grown *C. gracile* cells is due to a solid redox- and/or signal-imbalance, which leads to the activation of this short-term light acclimation process. Using a variety of photo-biophysical methods, we also demonstrate that under blue wavelengths, excessive light is quenched through orange carotenoid protein mediated non-photochemical quenching, whereas under orange/red wavelengths state transitions are involved in photoprotection.

Keywords: cyanobacteria, photosynthesis, light-quality acclimation, pigment composition, imbalance

INTRODUCTION

To be able to survive in ever-changing environments is a critical biological need, and survival/acclimation strategies rely on complex regulatory processes. Sunlight, which is the most important environmental factor for photoautotrophs, and the energy source for most life on Earth, changes continuously – seasonally, daily and also on more rapid time scales. Temporary and spatial changes in light intensities are often accompanied by spectral changes in the available light both in terrestrial and aquatic habitats. In aquatic environments, photosynthetic microorganisms at the surface of the water column are exposed to intense, red-enriched light, while the spectra of available light at moderate or high depth are dominated by green and blue light (or blue light alone). In optically complex environments, such as in shallow waters, the spectrum of available light is affected by the concentration of organic and/or inorganic particles and by the reflection from the lake/sea floor (Maritorena et al., 1994; Ackleson, 2003). Photosynthetic macro- and microorganisms have developed several molecular mechanisms to respond to changes in light quantity and quality to protect themselves from damage by excess light and to optimize their photochemical efficiency at sub-optimal light conditions.

The central features of oxygenic photosynthesis are two sequentially coupled photosystems, photosystem II (PSII) and photosystem I (PSI), located in the thylakoid membrane and connected by the intersystem electron transport chain. Photoautotrophs must regulate the number of light quanta reaching the reaction centers and also light energy distribution between the two photosystems. In the absence of such regulation, the electron transport chain can become under- or oversaturated; while the former involves sub-optimal photosynthetic performance, the latter promotes formation of triplet chlorophyll (Chl) (primarily triplet P680, primary donor of PSII) and, in turn, reactive oxygen species that cause severe damage to cellular components. Adjusting the light-harvesting antenna size and composition, and tuning PSII/PSI ratios according to incident light is a general phenomenon in long-term light acclimation (Fujita et al., 1994; Fujita, 1997; Dietzel et al., 2008).

Various algae and cyanobacteria are able to sense and respond to spectrally variable ambient light conditions (Fujita et al., 1985; Rockwell et al., 2014; Wiltbank and Kehoe, 2016). In cyanobacteria, specific photosensory proteins, cyanobacteriochromes (CBCRs) are employed to detect the spectral quality of irradiance (Fiedler et al., 2004; Ikeuchi and Ishizuka, 2008; Rockwell and Lagarias, 2010). CBCRs exhibit a broad range of wavelength sensitivities, covering the entire visible and near-UV spectrum. The main CBCR function is the regulation of cyanobacterial chromatic acclimation (CA), the mechanisms responding to changes of the ambient spectral light quality (Gutu and Kehoe, 2012; Montgomery, 2017).

Chromatic acclimation occurs in various freshwater and marine habitats and classified into six different types according to the changes in the pigment composition of the of the cyanobacterial light-harvesting antennae, the phycobilisomes (PBS) (Tandeau de Marsac, 1977; Gutu and Kehoe, 2012). In this classification the two distinct phycobiliproteins (PBPs) of the peripheral PBS rods, phycocyanin (PC) and phycoerythrin (PE) have a central role. Species belonging to Group I fail to exhibit change in either PC or PE content in response to changing light. Group II species can adjust PE levels only: they have high PE content under green and low PE content under red light. Species in Group III perform the most dramatic CA known as "complementary chromatic adaptation" that has been described more than a century ago (Engelmann, 1883). They vary PE levels in a similar way as in group II, but, in addition, adjust PC levels to reverse direction, i.e., increase it under red and decrease it under green light. The fourth type of CA responds to blue and green light (Palenik, 2001), and it is specific to deep marine environments (typical representatives are various *Synechococcus* strains). In CA4, similar to CA1, there are no significant changes in PE or PC levels; however, ratios of the two PE-bound chromophores, phycourobilin (blue light absorbing) and phycoerythrobilin (green light absorbing), do change (Everroad et al., 2006). CA5 and CA6 are involved in acclimation to far-red light and involve specific pigments such as chlorophyll *d* and chlorophyll *f* (Sanfilippo et al., 2019).

Although members of CA Group I, same as CA-incapable strains, do not alter their PC and/or PE levels in response to changing light colors, they do sense light color and perform photomorphogenesis (Fujita et al., 1985, 1987, 1994; Fujita and Murakami, 1987; Fujita, 1997; Fiedler et al., 2004; Bernstein et al., 2014). These studies revealed changes in growth rates, and abundance and stoichiometry of photosystems, cytochrome b_6f, and PBSs in response to the color of growth light. However, most of these investigations are restricted only to a few (most often: two) selected growth lights (e.g., PBP and Chl *a* light), rather than covering the entire visible range. Very recently, Luimstra and her co-workers systematically investigated the paradox, why cyanobacteria utilize blue light much less efficiently than

orange or red light (Luimstra et al., 2018) growing *Synechocystis* sp. PCC 6803 under blue (425 nm), orange (625 nm) or red (660 nm) light. They combined growth rate determinations, O_2-yield measurements and UV-Vis, and fluorescence spectroscopy measurements and found an imbalance between PSII and PSI and a related energy deficiency at PSII in cultures grown under blue light.

In this work, we comprehensively study the photomorphogenesis of the unicellular cyanobacterium *Cyanobium gracile* (a strain without any previous record of CA) over the full visible light range from violet to far red light, using nine monochromatic growth lights. We characterize long-term acclimation strategies in terms of pigment composition, light harvesting and energy distribution, redox homeostasis, and cellular plasticity. *C. gracile* naturally occurs in turbid freshwater shallow lakes with an optically complex environment, like Lake Balaton (Felföldi et al., 2011). However, wavelength-specific acclimation strategies in this strain have not been studied up to date. We observed unusual fluorescence properties of *C. gracile* cells when cultivated under certain wavelengths, similar to those found in strong-light exposed *Synechocystis* with high PBS emission (Tamary et al., 2012). The phenomenon was the most pronounced in cells grown under 687 nm light. We interpreted these properties as a signature of substantial excitonic decoupling induced by continuous weak light under certain physiological conditions. This suggests that suboptimal photosynthetic performance of *C. gracile* cells grown under near far-red light is due to a solid redox- and/or signal-imbalance, which leads to the activation of this light acclimation process. In addition, we found wavelength-specific changes in cell morphology, pigment content, photoprotection, and photosynthetic efficiency, suggesting a high level of light utilization plasticity and previously unrecognized light acclimation strategies in *C. gracile*.

MATERIALS AND METHODS

Strain and Culture Conditions

The *Cyanobium* strain was isolated from Lake Fertő, Austria, and is being deposited as strain ACT 1026 at the Algal Collection Tihany, Hungary. Its 16S rRNA nucleotide sequence shows 100% similarity to that of *Cyanobium gracile* sp. PCC 6307 (Rippka and Cohen-Bazire, 1983; Felföldi et al., 2011). Cells were grown in Erlenmeyer flasks at 24°C in liquid BG11 medium (Stanier et al., 1971) as semi-continuous batch cultures, exposed to 25 μmol photons m^{-2} s^{-1} diffuse light, placed onto a home-built cultivation apparatus with monochromatic light emitting diodes (LEDs), using a 14:10 h light-dark regime. Nine different growth lights, from 435 to 687 nm, were applied, using the following power LEDs: FD-34UV-Y1 (peak wavelength: 435 nm), FD-3B-Y1 (465 nm), FD-32G-Y1 (495 nm), FD-3G-Y1 (520 nm), FD-3Y-Y1 (596 nm), FD-3A-Y1 (615 nm), FD-3R-Y1 (633 nm), FD-333R-Y1 (663 nm), FD-34R-Y1 (687 nm) (Shenzhen Fedy Technology Co., Ltd., Shenzhen, China). LED emission spectra, corrected by the photosynthetically usable radiation, PUR, accessible to the corresponding cultures, are shown in detail in **Figure 1A**. Cultures were shaken manually once a day. By considering the growth rates of the cultures at selected wavelengths (see section "Results"), cultures were diluted to an appropriate cell density in advance (usually 4 days before the measurements), resulting in OD_{750} = 0.2 at the day of the measurements (see the next section for further details). Such setup provided appropriate (long-term) light acclimation and secured keeping the cells in the exponential growth phase.

OD Determination, Cell Counting and Determination of Growth Rates

Optical density of the cultures was determined at 750 nm using a U2900 Hitachi double beam spectrophotometer (Hitachi, Tokyo, Japan). Cells were counted and size-determined using a Cellometer Auto M10 (Nexcelom Bioscience, Lawrence, MA, United States) and an ImageStream MkII imaging flow cytometer (Amnis Corp., Seattle, WA, United States), respectively. Right after harvesting, cells were treated with 2% formaldehyde and incubated for 10 min at room temperature. The fixed cells were stored at –20°C until further use (up to 3 weeks). Prior to further analysis, samples were thawed slowly (during ∼1 h) at room temperature. To discriminate *C. gracile* cells from debris/bacterial contamination, 5 μL of SYBR Green I was added to each sample. During cytometric analysis, gating of the measured populations was applied to discriminate (i) focused objects (*via* combined use of RMS gradient and Threshold Mask features of the IDEAS instrumental software) and (ii) round objects (width/length ratio from 0.9 to 1.0). The imaging flow cytometer was calibrated using non-fluorescent microspheres (1–15 μm, Thermo Fisher Scientific, Waltham, MA, United States), and the results were validated with an Axio Imager 2 light microscope (Carl Zeiss, Oberkochen, Germany). During cytometric analysis, Chl *a* and PBS autofluorescence (excitation: 642 nm, detection: 642–745 nm) were also recorded to validate selection of the cells within all measured objects. Bright field images were used for cell size analysis; and mean cell volumes in the cultures were calculated assuming spherical cell shapes. At OD_{750} = 0.2 cell densities varied between 3.5 and 7.7 × 10^7 cells mL^{-1}. Growth rates were determined by fitting the OD_{750} values by an exponential function.

Photosynthetic Activity Measurements

Photosynthetic performance of *C. gracile* under actinic light (AL) illumination was probed using a Multi-Color-PAM (MC-PAM; Walz, Effeltrich, Germany) by recording fluorescence induction, OJIP and rapid light curves. Photosynthetically relevant parameters [e.g., electron transport rates (ETR)] were determined using saturating pulse (SP) analysis under five different (default) AL and measuring light (ML) wavelengths of the instrument: 440, 480, 540, 590, and 625 nm. In all cases, AL and ML were set to the same color. Importantly, for all but one (**Figure 2A**) figures in the main text 625 nm AL and ML are used and additional data (when relevant) are provided in the **Supplementary Material**. Fluorescence induction curves with 5 min AL period were recorded after 20 min of dark acclimation; AL intensity at each wavelength was set to 100 μmol photons m^{-2} s^{-1}, which (moderate) light intensity was sufficiently high to induce fluorescence transients. AL intensities during rapid light

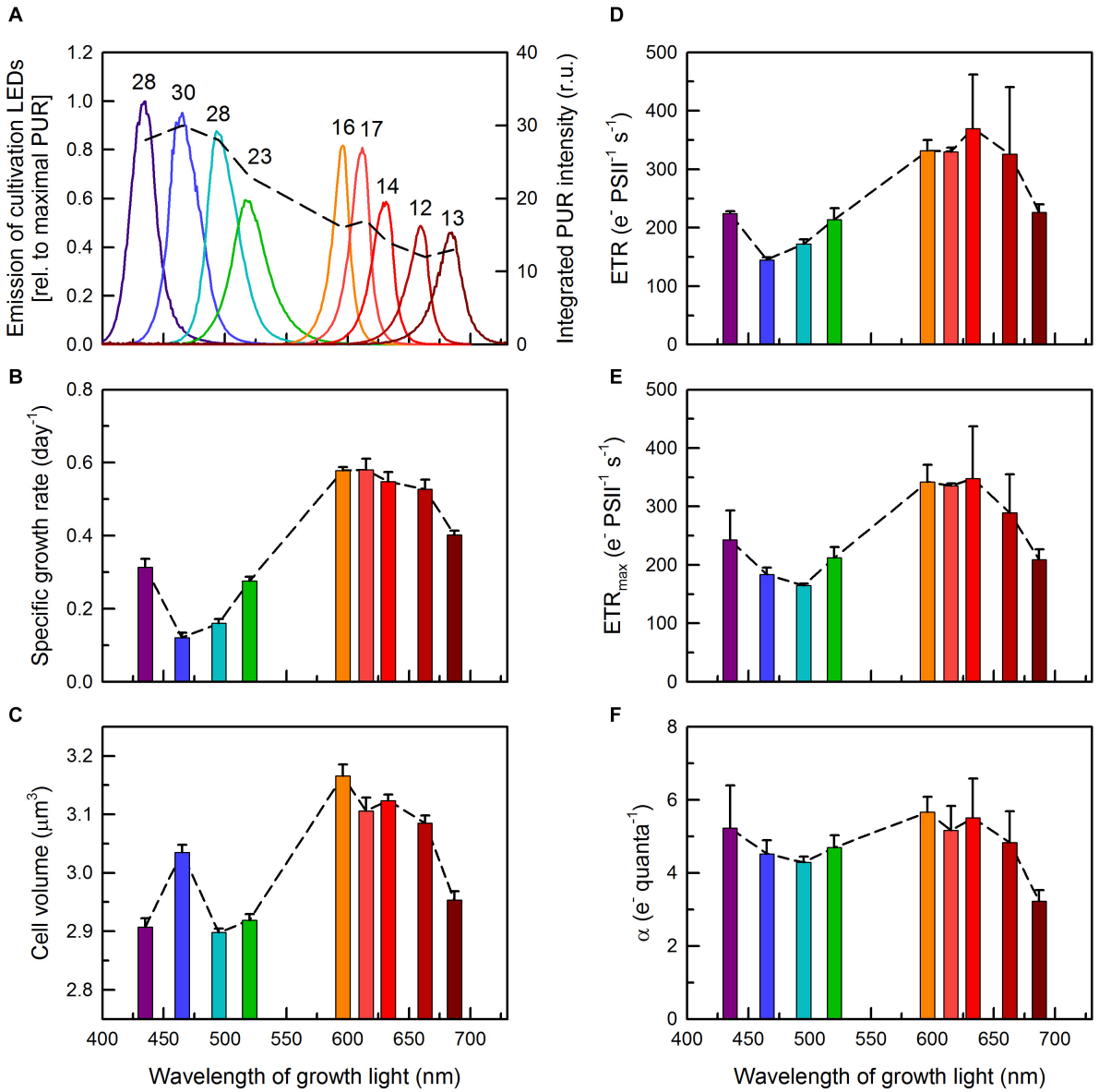

FIGURE 1 | (A) Emission spectra of the LEDs used for cultivation of *C. gracile* ACT 1026 (solid lines, left axis). The areas under the individual spectra correspond with photosynthetically usable radiation (PUR; dashed line and numbers on top, right axis) based on the UV-Vis spectra of the *C. gracile* cells grown under monochromatic lights (as detailed in **Figure 2B**). Growth rates **(B)**, cellular volumes **(C)** and ETR parameters **(D–F)** were determined for *C. gracile* during semi-continuous cultivation under monochromatic lights as shown in panel **(A)**. ETR **(D)**, ETR_{max} (E) and α **(F)** were determined by SP analysis of the corresponding fluorescence induction curves [**(D)**; see also **Supplementary Figure 6**] and rapid light curves **(E,F)** using 625 nm ML and AL. (For other ML's and AL's, see **Supplementary Figure 1**.) Values of three biological replicates were averaged; standard errors are indicated as error bars in panels **(B–F)**. Dashed lines in panels **(A–F)** represent the trend lines.

curve recordings stepwise increased from 0 to 1300–1700 µmol photons m^{-2} s^{-1} (depending on the AL used) through 20 individual steps of 30 s duration each, following default protocol settings defined by the manufacturer. Here, besides the first (dark) step, no extra dark acclimation was applied. Functional absorption cross-section of PSII, σ_{II}, was determined after 20 min of dark acclimation, using the default script "Sigma1000cyano."

Fast fluorescence induction kinetics (OJIP) was recorded by *Fast Kinetics* MC-PAM feature after 360 s of dark acclimation, using *FastKin_Def* trigger settings and saturation pulses of five wavelengths (440, 480, 540, 590, and 625 nm) and of maximal intensity up to 20 000 µmol photons m^{-2} s^{-1}.

Absorption (UV-Vis) Spectroscopy

Whole cell absorption spectra were recorded by Unicam UV 500 scanning spectrophotometer (Thermo Spectronic, Cambridge, United Kingdom) using a pair of 1-mm transparent quartz cuvettes placed into the outer cuvette holder of the instrument

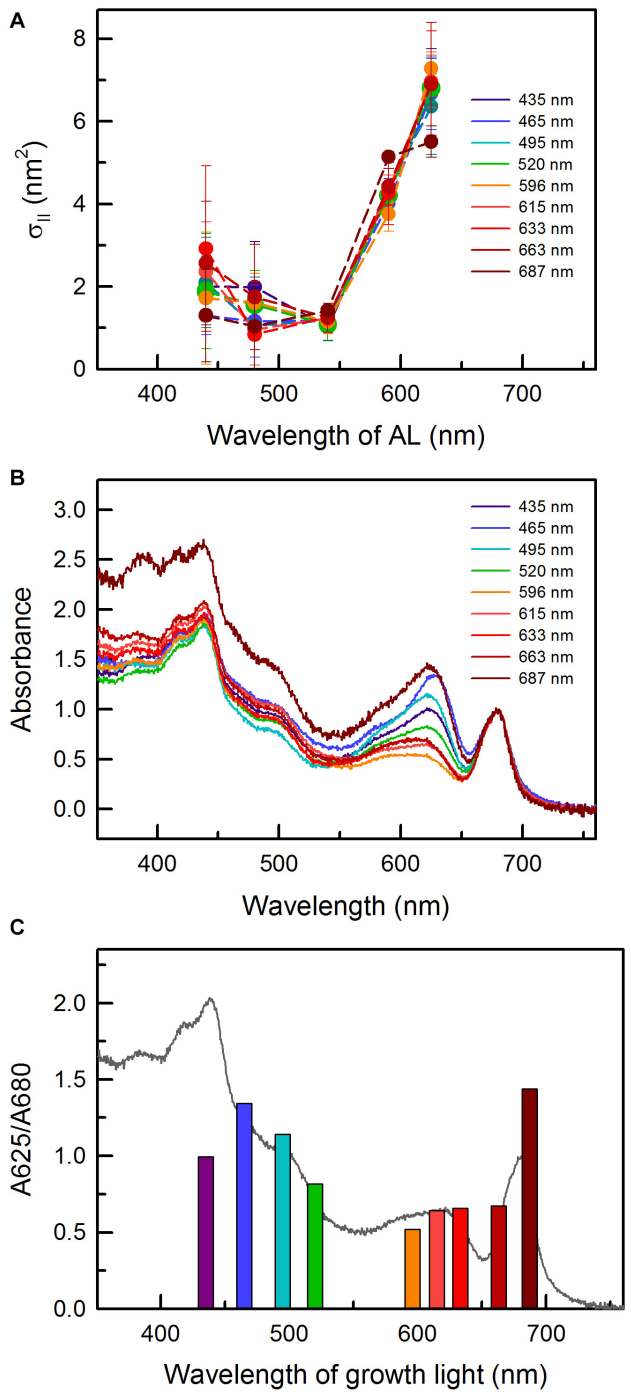

FIGURE 2 | (A) Functional absorption cross-section of PSII, σ_{II}, as a function of actinic light (AL) wavelength in *C. gracile* sp. ACT 1026 cells grown under monochromatic lights (as detailed in **Figure 1A**). Values of three biological replicates were averaged; standard errors are indicated as error bars. **(B)** Absorbance spectra of *C. gracile* grown under particular monochromatic lights. Spectra were baseline corrected and normalized to the 680 nm Chl *a* Q-band. Each spectrum represents the average of three biological replicates; error intervals are not shown for clarity. **(C)** A625/A680 ratios as a function of growth light. Averaged absorbance spectrum of cultures grown under 615 nm light is shown as a reference. The legends in panel **(A,B)** indicate the wavelengths of growth lights.

(with shorter optical path length, which is beneficial for recording absorption spectra of cell suspensions with substantial light scattering). In order to obtain a high signal-to-noise ratio, 120 nm/min scan speed and 2.0 nm bandwidth were applied.

Low Temperature Fluorescence Emission and Excitation Spectroscopy

A total of 10 mL of cell suspension was filtered through a 25 mm GF/B glass microfiber filter (Whatman, Maidstone, United Kingdom) under dim light. Moist, oval-shaped fragments (∼1 cm × 0.3 cm) were cut using a deformed cork drill stored at −80°C prior to use (up to 6 months). For measurements, the fragments were placed into the cavity of a copper finger of a home-made apparatus (Prášil et al., 2009) and were immersed into a transparent Dewar flask filled with liquid nitrogen. A total of 77 K fluorescence emission spectra were recorded using an SM-9000 spectrophotometer (Prášil et al., 2009; Photon System Instruments [PSI], Brno, Czechia) upon excitation with 457 or 534 nm light (20 nm bandwidths) for Chl and phycobilin excitation, respectively. Three individual spectra of three replicates (9 in total) were recorded, baseline-corrected and averaged.

Fluorescence excitation spectra were recorded similarly using an Aminco-Bowman AB2 Luminescence Spectrometer (SLM Spectronic Instruments, Rochester, NY, United States) with fluorescence emission recorded at either 655, 685, 728, 745, or 765 nm. Both the excitation and emission bandwidths were set to 4 nm. Three individual traces of each sample were averaged, and the raw data were divided by the signal from the reference photomultiplier tube to provide a first-order quantum correction.

Pigment Analysis

Phycobiliprotein content was estimated by semi-quantitative analysis of the whole-cell absorption spectra, based on the method of Bennett and Bogorad (1973), and followed by normalizing the phycobilisome content to the respective absorbance at 750 nm. Although the extinction coefficients determined by Bennett and Bogorad (1973) are specific for 1 cm optical path length, due to the linear dependence of the absorbance on path length, they can also be used for semi-quantitative determination e.g., in 1 mm cuvettes.

Chlorophyll and carotenoid contents of the samples were determined by high-performance liquid chromatography (HPLC). Cells from 10 mL cultures aliquots were harvested on a Whatman glass microfiber filter (GF/B; Ø 25 mm) and were kept frozen at –80°C until extraction (for less than 2 weeks). Soluble pigments were extracted by adding 500 μL of pure acetone and concomitant shaking for 30 min at 1,000 rpm in the dark at 25°C. Insoluble constituents were span down at 11 500 × *g* at 4°C for 10 min, and the supernatant was passed through a polytetrafluoroethylene (PTFE) syringe filter with a pore size of 0.2 μm.

Carotenoid composition of the acetonic extracts was analyzed using a Shimadzu Prominence HPLC system (Shimadzu, Kyoto, Japan) consisting of two LC-20AD pumps, a DGU-14A degasser, a SIL-30A automatic sample injector, a column thermostat

and a Nexera X2 1024-element photodiode-array detector. Chromatographic separations were carried out on a Phenomenex Synergi Hydro-RP 250 × 4.6 mm column with a particle size of 4 μm and a pore size of 80 Å. 20 μL aliquots of acetonic extract were injected to the column and the pigments were eluted by a linear gradient from solvent A (acetonitrile, water, trimethylamine; in a ratio of 9:1:0.01) to solvent B (ethyl acetate). The gradient from solvent A to solvent B was run from 0 to 25 min at a flow rate of 1 mL/min. The column temperature was set to 25°C. Eluates were monitored in a wavelength range of 260 to 750 nm. Pigments were identified according to their retention time and absorption spectrum and quantified by integrated chromatographic peak area recorded at the wavelength of maximum absorbance for each pigment using their corresponding absorption coefficient.

Confocal Microscopy

Confocal microscopy were performed using a Leica DMi8 confocal microscope (Leica, Wetzlar, Germany) equipped with a HC PL APO CS2 63×/1.4 oil objective and a TD 488/552/638 main beam splitter. Cells were immobilized on a thin (<1 mm) layer of solid BG11 agar and placed upside down onto a cover slide. Chl *a* and PBS autofluorescence were excited using the 488 and 638 nm lasers, respectively, and were detected over the 690–790 nm and 650–680 nm spectral windows with PMT detectors. The microscope provided a 2048 × 2048 pixel resolution with a 183.65 × 183.65 μm picture size (90 nm/pixel). Images were processed using the ImageJ (1.52c) open source Java image processing program (Schneider et al., 2012). In order to exclude low intensity background images, fluorescence channels were separated and images were converted into a 32 bit floating point format using a macro. The mean fluorescence intensity of the cells was calculated as an average intensity above the threshold. For statistical analysis, intensity profiles for both channels were evaluated along the cellular cross sections and fluorescence intensities of pixels positioned with identical distances from the geometrical center of cells were averaged. Ratios of the fluorescence intensities at centers of cells (first values of the folded datasets) and intensities of membrane regions (corresponding maxima) were calculated.

RESULTS

Growth Rates, Electron Transport Rates, and Overall Fitness of the Cell Cultures

Growth rates of *C. gracile* was found to be wavelength-dependent. Similarly to other cyanobacteria (Wyman and Fay, 1986; Luimstra et al., 2018), *C. gracile* grows slowly under violet, blue and green light, and relatively fast under red light. Plotting the growth rates against wavelength of growth light shows the lowest rates at around 465–495 nm (μ = 0.12–0.16 d^{-1}), and a broad plateau of high growth rates (μ = 0.52–0.58 d^{-1}) from 596 to 663 nm (**Figure 1B**). The observed slow growth at the blue-blue green spectral region was accompanied by low maximal culture densities (data not shown). Reaching the far-red region (687 nm) resulted in considerably slower growth rates again (**Figure 1B**). This pattern does not fit the changes in PUR (in fact, it was more or less the opposite; **Figure 1A**), hence, cannot be explained by changes in light quanta absorbed (see section "Discussion" for further details).

Interestingly, growth rates correlated considerably with cell volumes, i.e., the cells were smaller in most cultures grown under violet to green and under near far-red light, and larger in cultures grown under orange to red light (**Figure 1C**), albeit the relative difference in cell volumes was much smaller (up to 9%) than the corresponding difference in growth rates (up to 4.8-fold). Nevertheless, the insufficient microbial growth under sub-optimal light conditions was accompanied by smaller cell volumes. To elucidate such dramatic wavelength dependence of growth, we further probed how pigment levels, light capture and distribution, and other bio-energetically relevant parameters did also change (or did not change) with varying growth light.

In order to address the latter issue, steady-state and maximal PSII-mediated electron transport rates (ETR(II) and $ETR(II)_{max}$, respectively) were determined by SP analysis of the corresponding fluorescence induction curves and rapid light curves (**Figures 1D,E**, respectively). Irrespective of the applied AL color, the light quality dependences of both parameters were similar to those of the growth rates (**Figure 1B** and **Supplementary Figure 1**), showing, not surprisingly, a tight correlation between photosynthetic performance and growth characteristics. Nevertheless, the relatively large variation in growth rates (4.8-fold, see above) was accompanied by a smaller variation in ETR values (2.1-fold), indicating a non-proportional (linear) relationship between ETR and growth rates. Noteworthy, steady-state ETR(II), apparently, exceeded $ETR(II)_{max}$ in some cases (compare **Figures 1D,E**), which, possibly, was due to the different approach applied at determining these parameters (see section "Materials and Methods") and also state transitions occurred during rapid light curves (see section "Photosynthetic Performance" for details). Slopes of the ETR light curves in the initial, light-limited phase, α (**Figure 1F**) showed similar light quality dependence as the other, above mentioned parameters; however, performed a much smaller overall variability (i.e., photosynthetic performance in the light-limited phase did only weakly depend on growth light). The lowest α value (i.e., theoretical maximal ETR at any light intensity) belonged to the cultures acclimated to 687 nm light, showing an impaired electron transport in these cultures.

Light Absorption and Pigment Composition

The AL-color dependency of the functional absorption cross-section of PSII, σ_{II}, showed a similar pattern to that of *Synechocystis* sp. PCC 6803 (Schreiber et al., 2012): low σ_{II} values up to 540 nm, and a remarkable increase above this wavelength (**Figure 2A**). The AL-color dependency of σ_{II} was irrespective of the growth light with only one exception: the *C. gracile* cells grown under 687 nm showed significantly relatively smaller cross section of PSII as compared to other cultures when 625 nm (i.e., red) AL was applied (one-way ANOVA followed by Tukey's HSD

post hoc test; $p < 0.05$). This smaller functional antenna size may explain the lower α of these cultures (see previous paragraph).

The minimal growth rates of *C. gracile* at 465 and 495 nm (**Figure 1B**) can be explained by the combination of ineffective utilization of the blue-blue green light in cyanobacteria (see also Luimstra et al., 2018, and references therein) and the absorbance profile of the cells showing a remarkable drop in Chl absorption at the red side of the Soret band (**Figure 2B**). In general, the absorbance spectra of *C. gracile* were similar to that of other cyanobacteria (see e.g., Kopečna et al., 2012; Luimstra et al., 2018) with Chl *a* Soret band at 440 nm (together with two shoulders at 387 and 420 nm) and a Q-band at 680 nm, a carotenoid shoulder at 485 nm, and phycocyanobilin absorption peaked at 625 nm. The recorded spectra showed high variability, mainly due to alterations in phycobilin absorption, which displayed strong dependency on the wavelength of the growth light (**Figure 2B**). Plotting the A625/A680 ratios against growth wavelengths revealed high PBS to Chl ratios over the violet to blue-green region with the highest A625/A680 ratio at around 465–495 nm, as well as at 687 nm, and a low, stable PBS abundance between these wavelengths (**Figure 2C**). Semi-quantitative analysis of the cellular PBP content showed a similar trend with the same local maxima, however, with about 60% more PBS in the blue part of the spectra as compared to the near far-red region (**Figure 3A**). These results imply a low Chl content in the 687 nm grown cells, in agreement with direct determination of the Chl *a* levels by HPLC (**Figure 3B**). Unsurprisingly, normalization of the PBP content to the Chl concentration, revealed the same trend as of the A625/A680 ratios (**Figure 2C** and **Supplementary Figure 2**). Besides, the remarkably high absorbance and modified spectral shape of the 687 nm grown cultures in the blue spectral region suggests an elevated carotenoid level in these cells (as compared to Chl *a*), which is also supported by a more intense carotenoid shoulder at 485 nm (**Figure 2B**; Kopečna et al., 2012). This, again, is well supported by HPLC data (**Figures 3C–F**).

High-performance liquid chromatography chromatograms of *C. gracile* cells were dominated by three major bands with retention times of 13.7, 16.6, and 20.4 min, originating from zeaxanthin, Chl *a*, and β-carotene, respectively (**Supplementary Figure 3**; Komárek et al., 1999; note that β-carotene was misidentified as α-carotene that time). In cells grown under blue/blue-green light, Chl *a* allomers, to a certain extent, were also present (**Supplementary Figure 3**), showing an increased level of reactive oxygen substances, which concurs with a reduced plastoquinone (PQ) level in these cells (see section "Photosynthetic Performance" for details). Quantitative analysis of the pigment composition (**Figures 3B–F**) revealed remarkable changes in the Chl and total carotenoid level in the cultures grown under 687 nm light, in particular, lowered Chl *a* and enhanced carotenoid levels, respectively (**Figures 3B,C**). This negative correlation results in a very high ratio of total carotenoids to Chl *a* in these cells (**Figure 3D**). Lower, but still significant (one-way ANOVA followed by Tukey's HSD *post hoc* test; $p < 0.05$) increase in total carotenoids to Chl *a* ratio was also found in *C. gracile* cells grown under violet light (435 nm, **Figure 3D**). In both cases, the enhanced total carotenoid to Chl *a* ratio originated dominantly from the increase of zeaxanthin (**Figure 3E**). As compared to zeaxanthin, the level of β-carotene showed weaker dependence on the growth light (**Figure 3F**). However, we found statistically significant decrease (one-way ANOVA followed by Tukey's HSD *post hoc* test; $p < 0.05$) in β-carotene to Chl *a* ratio in the cells grown at 495 and 520 nm (**Figure 3F**), in correlation with the substantial level of allomeric substances in these cultures (see above).

Excitation of Photosynthetic Pigment-Protein Complexes

Spectral properties of *C. gracile* cells were further examined by low temperature (77 K) fluorescence spectroscopy. Fluorescence emission spectra with 455 nm (Chl *a*) excitation showed three major spectral features: a minor PBP emission at 655 nm; a double emission peak at 685–695 nm, originating from PSII (emitting at both wavelengths) with a variable contribution to the signal by the PBS terminal emitter (emitting at 685 nm only); and a robust PSI emission peaking at 728 nm (**Figure 4A**), indicating small PSII/PSI ratios over the whole visible range, regardless of the growth wavelength. Nevertheless, increasing the growth wavelength from 435 to 663 nm resulted in a remarkable increase in the PSII/PSI ratio (**Figure 4A**, main panel and inset). The proportional increase of the 685 and 695 nm emission suggests only a minor contribution of the PBS terminal emitter. Contrary to this, the cells grown under 687 nm light show an intense fluorescence emission at 685 nm and a distorted shape of the 685–695 nm double band, showing a considerable light emission from the PBS terminal emitter.

This feature is much better seen in **Figure 4B** where fluorescence emission spectra with direct PBS excitation at 590 nm are shown. This series of spectra revealed that PBS decoupling, to a certain extent, took place also at shorter growth wavelengths but it became dominant at 687 nm (**Figure 4B**). Enhancing fluorescence intensities of the 655 nm emission as compared to the PSI emission at 728 nm are in good accordance with the increasing PSII/PSI ratios (**Figure 4A**), and rather than showing increasing PBS levels (c.f. **Figure 2**), they indicate changes in the excitation energy transfer. Besides these, the spectra also show the intensification of two shoulders, at 745 and 765 nm, respectively, with unknown origin. As with increasing growth wavelengths they increase concomitantly with the intensity of the major emission peak of the terminal emitter at 685 nm (**Figure 4B**), they might have a related origin.

The interpretation of the fluorescence emission spectra of the 687 nm grown *C. gracile* cells is well supported by fluorescence excitation measurements. As expected, the 655 nm PBP fluorescence emission peak can exclusively be excited by photons absorbed by phycobilins (**Figure 4C**). The same is true for the 685 nm emission with mixed origin, which confirms our assumption that it originated dominantly from PBS in *C. gracile* grown at 687 nm. In contrast, the 728 nm (PSI) emission band can also effectively be excited by 440 nm blue or 680 nm red light, characteristic for Chl absorption (**Figure 4C**). The shoulders at 745 and 765 nm can also be excited by 440 and 680 nm light, however, to a smaller extent as compared to the 728 nm emission

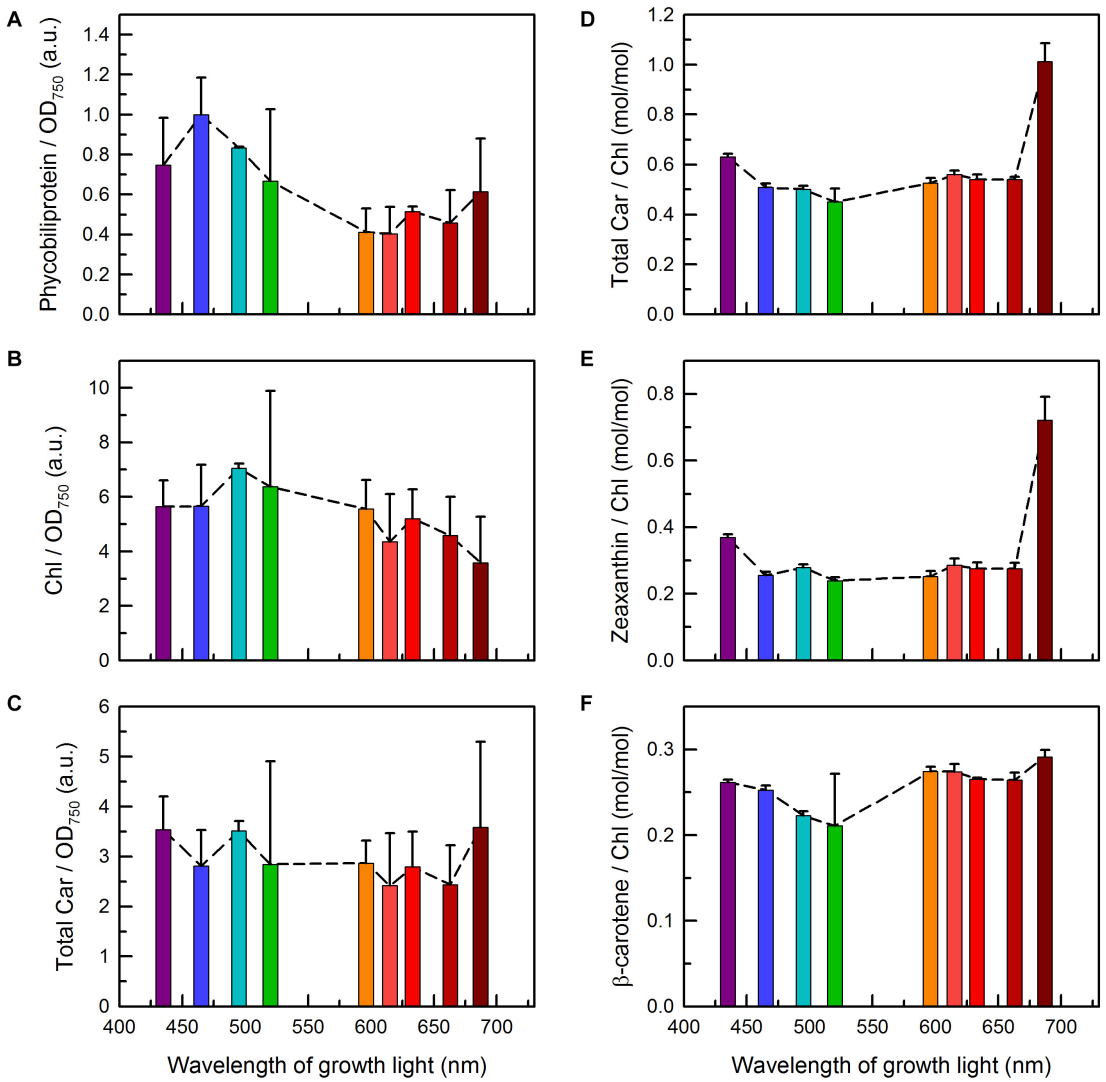

FIGURE 3 | Pigment contents in *C. gracile* sp. ACT 1026 cultures grown under monochromatic lights (as detailed in **Figure 1A**). Total phycobiliprotein content of the cultures **(A)** was determined based on the absorbance spectra shown in **Figure 2B**, while the levels of Chl *a* and carotenoids **(B–F)** were determined by HPLC. Pigment levels were normalized either to OD_{750} [**(A)**, total phycobiliprotein; **(B)**, Chl *a*; **(C)**, total carotenoid] or to the corresponding Chl *a* concentration [**(D)**, total carotenoid; **(E)**, zeaxanthin; **(F)**, β-carotene]. Phycobiliprotein to Chl *a* ratios are shown in **Supplementary Figure 2**. Data are expressed as mean ± standard error (n = 3). Dashed lines in panels **(A–F)** represent trend lines in both panels.

peak. This, again, suggests that both of these shoulders have a PBS-related origin.

We explored the unique fluorescence properties of *C. gracile* cells grown under 687 nm light also by confocal microscopy. **Figure 5** shows multicolor confocal micrographs of the 687 nm grown cells (B) together with control cells grown under 615 nm light (A). Both types of cells are oval shaped with 1.80 ± 0.01 μm (615 nm) and 1.78 ± 0.01 μm (687 nm) mean diameter (see also **Figure 1B**). The control cells grown under 615 nm light showed a typical cellular pattern (Tamary et al., 2012) with intense, ring-shaped autofluorescence from the cell periphery, where thylakoid membranes are located (**Figures 5A,C**). As images were composed of PBS- (green) and Chl *a* (red) autofluorescence, the green-yellow color indicates that the majority of autofluorescence originated from colocalized Chl *a*- and PBS emitters. Quantitative analysis of the images revealed similar, 77.1 ± 14.2% and 80.6 ± 11.0% Chl *a* and PBS fluorescence intensities, respectively, in the central region of the cells grown at 615 nm as compared to the membrane region (**Figure 5C**). Contrary to this, the cells grown under 687 nm light showed fluorescence patterns to be more homogenous pattern across the cells and dominated by green color (**Figure 5B**). This latter indicates increased PBS/Chl *a* fluorescence ratios in these cells, in good agreement with the fluorescence spectroscopy data (**Figure 4**). Image analysis resulted in 1.27 ± 0.06 and 1.74 ± 0.11 PBS/Chl *a* relative autofluorescence ratios for the 615 nm grown and 687 nm grown cells, respectively. The more homogenous pattern suggests that PBS autofluorescence originated not only from the thylakoid

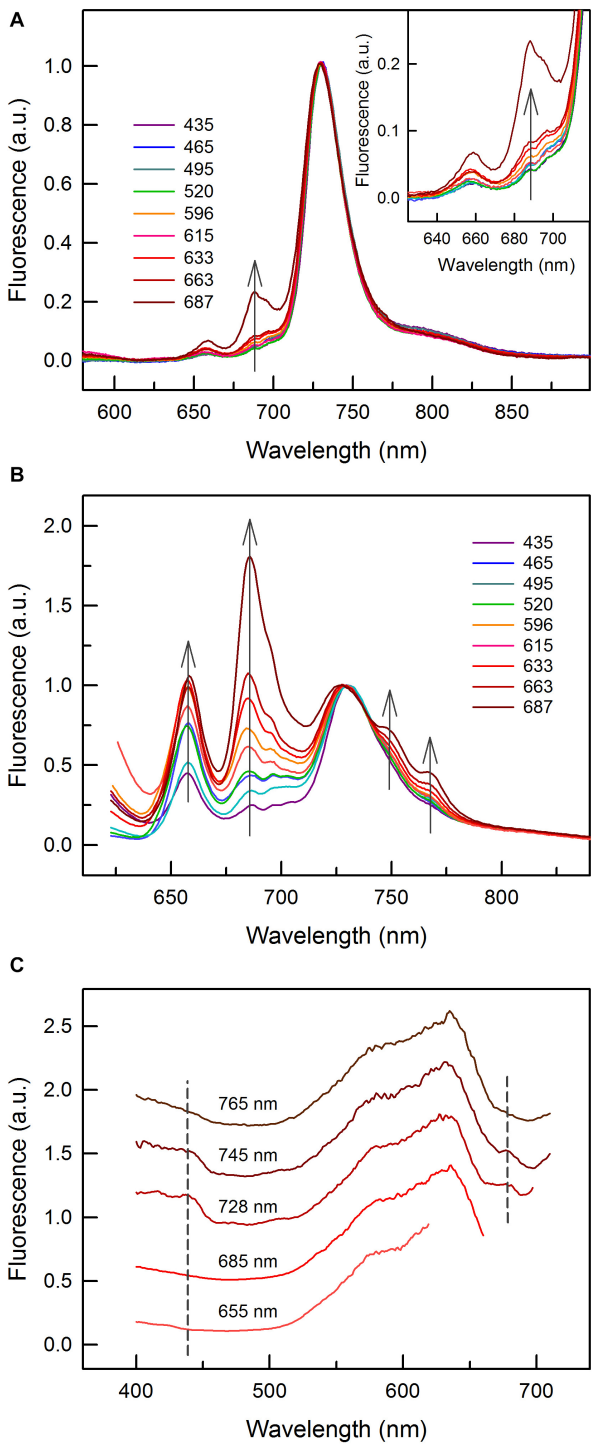

FIGURE 4 | Low temperature (77 K) fluorescence emission and excitation spectra of *C. gracile* sp. ACT 1026. **(A,B)** Fluorescence emission spectra of cells grown under monochromatic lights with 455 nm (Chl *a*) and 590 nm (PBS) excitation, respectively. Three individual spectra of three technical replicates (9 spectra in total for each light condition) were averaged and baseline corrected; error intervals are not shown for clarity. Spectra were normalized to the 685 nm emission. The inset on panel A zooms in the 625 nm – 719 nm spectral region. The gray arrows show the intensification of *(Continued)*

FIGURE 4 | Continued
certain spectral peaks or shoulders with increasing growth wavelengths. **(C)** Fluorescence excitation spectra of the 687 nm grown cells, with various excitation wavelengths as indicated above each spectrum. Three individual spectra were averaged and reference corrected. Spectra were normalized to the maximal signal intensity and shifted vertically for clarity. Dashed lines represent the wavelengths of Chl *a* absorption maxima. The narrower spectra with 655, 685, and 728 nm excitation lights are due to the gap between excitation and emission wavelengths.

membranes, but also from the cytoplasmic space, which is also supported by image analysis. Here, the spatial distribution of Chl *a* autofluorescence remained unchanged as compared to the 615 nm grown cells (77.6 ± 14.9% fluorescence intensities in the central region vs. the membrane region), while the PBS autofluorescence dispersed across the whole cell profile (94.0 ± 4.0% fluorescence intensities in the central region vs. the membrane region, **Figure 5D**).

Photosynthetic Performance

Besides ETR parameters (**Figures 1D–F**), PAM fluorometry allowed for monitoring other photosynthetic parameters. These parameters were either derived from fast OJIP transitions (**Figure 6**) or from traditional (slow) fluorescence induction curves (**Figure 7** and **Supplementary Figure 6**). The shape of the OJIP curves, and especially the fluorescence intensities at the I-step (30 ms), strongly depend on the quality of the growth light (**Figure 6A**). The cells grown under 465 and 495 nm light showed the highest Chl *a* fluorescence at this step, while cells grown under 687 nm displayed the lowest (**Figure 6A**). The kinetics (slope) of the corresponding J–I transition showed the same trend (**Figure 6B**), indicating (i) a more reduced PQ pool in the cultures grown under blue/green light and (ii) an oxidized PQ pool in the 687 nm grown cells. Quantitative analysis of the OJIP kinetics revealed low efficiency of transfer of both PSII (δR_0) and PQH_2 trapped electrons (ψR_0) to PSI acceptors in the blue/blue-green light grown cells and the opposite in the cells grown under 687 nm light (**Figures 6C,D**). No significant changes in the efficiency of electron transfer from Q_A^- to PQ (ψE_0) were found (**Figure 6E**; for definition of OJIP parameters, see Stirbet et al., 2018). These results suggest that the reduced PQ pool in *C. gracile* cells grown under blue/green light was due to a diminished PQH_2 to PSI electron transfer, while there was no change in the corresponding efficiency of the Q_A^- to Q_B^- electron transfer. In other words, the efficiency of reoxidation of a reduced PQ pool by downstream carriers was lower in these cells.

The dependencies of the initial (F_o), steady-state (F_t) and maximal (F_m and F_m') fluorescence yields on the wavelength of growth light showed similar patterns, with maximal and minimal values in the blue/green and red regions, respectively (**Figures 7A,B**). The observed high fluorescence yields in blue/green light grown cultures concur well with the high PBS levels in these cells (c.f. **Figures 2C**, **3A**), while the relatively low F_o and F_m values were in apparent contradiction with the interpretation of fluorescence data (i.e., partial PBS decoupling) in section "Excitation of Photosynthetic

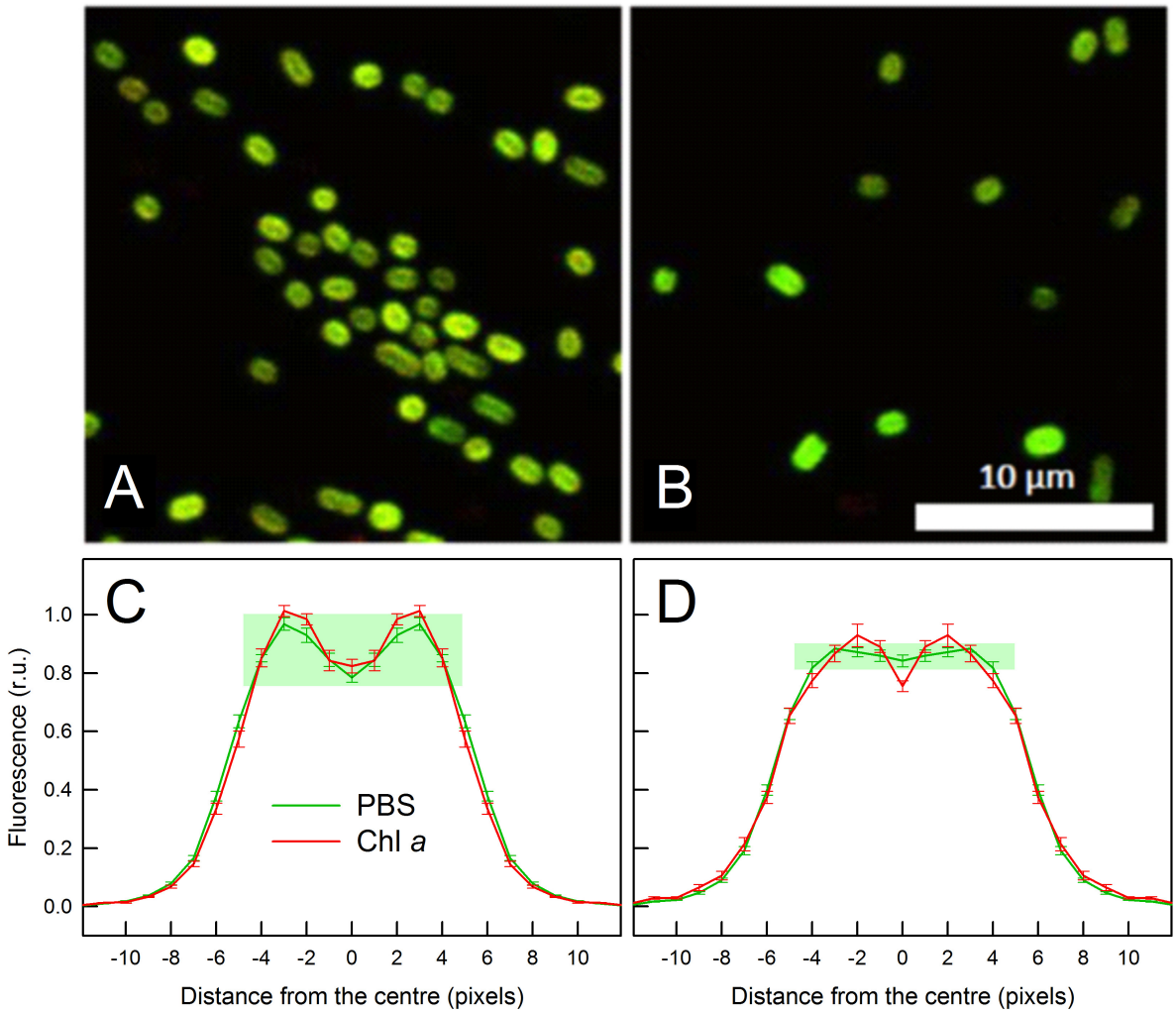

FIGURE 5 | Confocal micrographs **(A,B)** and respective autofluorescence intensity profiles **(C,D)** of *C. gracile* sp. ACT 1026 cells grown under 615 nm **(A,C)** and 687 nm **(B,D)** light. Multicolor images in panels **(A,B)** were composed of PBS (green) and Chl *a* (red) autofluorescence; scale bar is indicated in white. For autofluorescence profiles, fluorescence intensities of 18 **(A,C)** + 10 **(B,D)** = 28 cells were normalized to the integrated intensities along the cross-sectional profile and averaged. Data in panels **(C,D)** are expressed as mean ± standard error; *n* = 36 **(C)** and 20 **(D)**, note the central symmetry of the cells. Distances are expressed in pixel units (1 pixel = 90 nm); pixel Nr. 0 indicates the middle of the cells. The difference between PBS autofluorescence profiles is highlighted by green rectangles in panels **(C,D)**.

Pigment-Protein Complexes" above (see e.g., Acuña et al., 2016; Remelli and Santabarbara, 2018; Santabarbara et al., 2019). However, this could be solved if F_o were normalized to the amount of absorbed light quanta and also to pigment content (**Supplementary Figure 5**). Normalization of F_o to the amount of absorbed light quanta (by 625 nm excitation) revealed high values for the 495 nm and, again, for the 687 nm grown cells, in line with the relatively high PBS content in these cultures (**Figure 3A** and **Supplementary Figure 5A**). Further, the F_o/PBP ratios were remarkably high in all cultures grown under orange-red lights, while the 687 nm grown cells showed an about two-fold higher F_o/Chl ratio as compared to the other cultures (**Supplementary Figures 5B,C**).

Due to the similar patterns of F_o and F_m, not surprisingly, the calculated F_v/F_m values also follow a similar trend, with a maximum at 465 nm (**Figure 7C**). On the contrary, the corresponding PSII effective quantum yields, $Y_{(II)}$, were the lowest in the blue spectral region and the highest in the red region (**Figure 7C**). This, again, indicates an easily reducible PQ pool in the red light grown cells.

To separate changes in the fluorescence yields caused by functional changes in the photosynthetic machinery from the influence of potential alterations in the PBS abundance, we calculated normalized differences of the corresponding fluorescence parameters, i.e., $(F_t - F_o)/F_o$, $(F_m' - F_m)/F_m$, and $1\text{-}(F_v/F_m - Y_{(II)})/(F_v/F_m)$ (**Figures 7D–F**). The analysis revealed high F_t levels (as compared to F_o) in the cultures grown under violet to green and also under near-far red light (**Figure 7D**), which suggests a considerable closure of the PSII reaction centers in these cultures upon AL

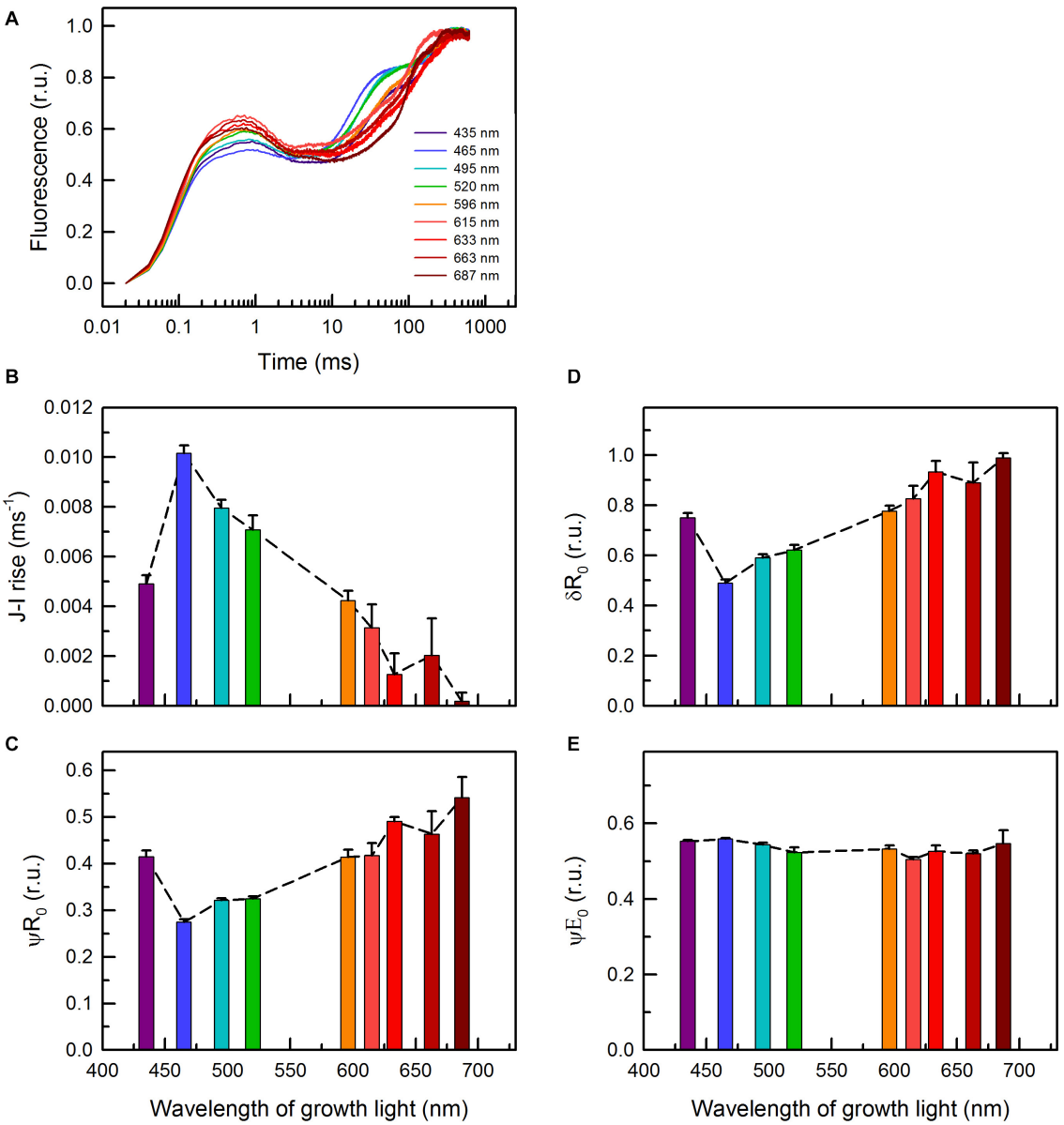

FIGURE 6 | (A) OJIP curves of *C. gracile* sp. ACT 1026 cells grown under monochromatic lights (as detailed in **Figure 1A**) and derived parameters as a function of the wavelength of growth light **(B–E)**. **(B)** Rate of the fluorescence rise during the J-I phase; **(C)** ψR_0, efficiency with which a PSII trapped electron is transferred to final PSI acceptors; **(D)** δR_0, efficiency with which an electron from PQH_2 is transferred to final PSI acceptors; **(E)** ψE_0, efficiency with which a PSII trapped electron is transferred from Q_A^- to PQ; the parameters were derived according to Stirbet et al. (2018). Curves on panel **(A)** represent the mean of three biological replicates, normalized to the P level (error intervals are omitted for clarity), while on panels **(B–E)** standard errors and trendlines are indicated as error bars and dashed lines, respectively. In each case, 625 nm ML and saturating pulse was used. Yet, the traces of parameters in panels **(B–E)** were independent of the applied measuring light wavelength (for more details, see **Supplementary Figure 4**).

illumination. The trend was the opposite for the F_m vs. F_m' and F_v/F_m vs. $Y_{(II)}$ parameters, where the red light grown cells showed the highest relative increase upon (625 nm) AL illumination (**Figures 7E,F** and **Supplementary Figure 6**), showing, in turn, an effective State 2 to State 1 transition. Interestingly, the cells with a redox imbalance (**Figure 6A**) showed the highest non-photochemical quenching (NPQ) using 480 nm AL, whose wavelength is the most effective in inducing cyanobacterial NPQ (**Supplementary Figure 7**; Rakhimberdieva et al., 2004). This suggests an increased abundance of orange carotenoid protein (OCP) in these cultures (see Plohnke et al., 2015) and possibly also the complementary role of short-term light acclimation processes, namely state transitions and blue-light induced OCP quenching, in cyanobacteria (see also Discussion, Kaňa et al., 2012; Bernát et al., 2018).

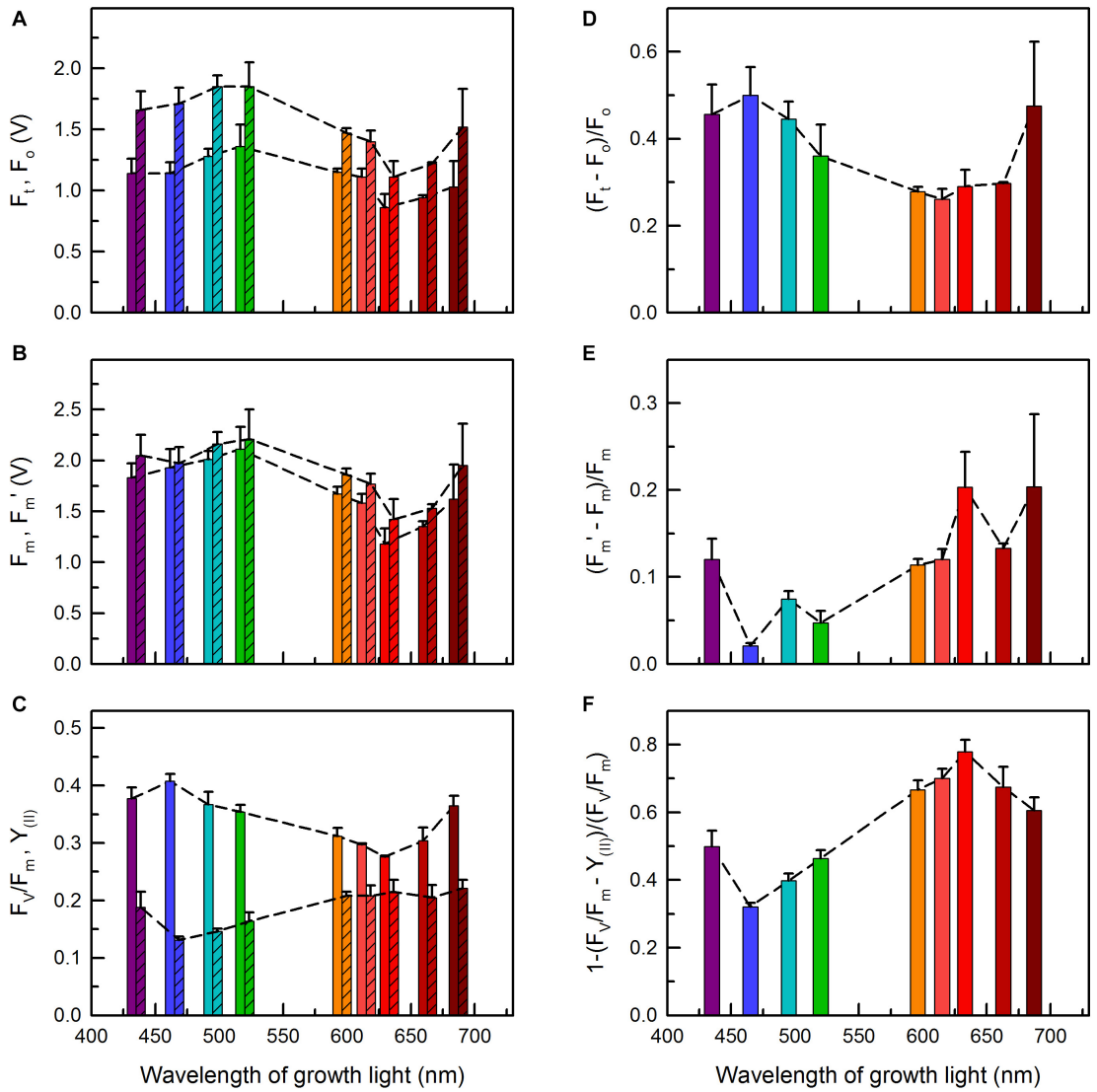

FIGURE 7 | Chl *a* fluorescence parameters of *C. gracile* sp. ACT 1026 cells grown under monochromatic lights (as detailed in **Figure 1A**) as a function of growth light wavelength. **(A)** F_o (open bars) and F_t (striped bars); **(B)** F_m (open bars) and F_m' (striped bars); **(C)** F_v/F_m (open bars) and $Y_{(II)}$ (striped bars); **(D)** $(F_t - F_o)/F_o$; **(E)** $(F_m' - F_m)/F_m$; **(F)** $1-(F_V/F_m - Y_{(II)})/(F_V/F_m)$. In each case, 625 nm ML and AL was used. Values represent the average of three biological replicates; standard errors and trendlines are indicated as error bars and dashed lines, respectively.

DISCUSSION

Plasticity of the Photosynthetic Machinery

Photosynthetic organisms dynamically adjust the number of light quanta reaching the reaction centers and also the light energy distribution between PSII and PSI. In the absence of such adjustment, the electron transport chain would become under- or oversaturated; resulting in sub-optimal photosynthetic performance or damage of the photosynthetic machinery and other cellular components. During long-term light acclimation cells optimize their light-harvesting antenna size and composition, and PSII/PSI ratios according to incident light conditions to poise the redox state of the electron transport chain, and especially of the PQ pool that transports electrons from PSII to downstream carriers (Fujita et al., 1994; Fujita, 1997; Dietzel et al., 2008). Specific form of long-term light acclimation is cyanobacterial CA, in which CA-capable cyanobacteria adjust the pigment composition in their PBS according to light quality (Tandeau de Marsac, 1977; Sanfilippo et al., 2019; see also Introduction). However, according to literature and our data, CA-incapable cyanobacteria (including *C. gracile* according to current classification) are also able to sense and respond to changing light colors (Fujita et al., 1985, 1987, 1994; Fujita and Murakami, 1987; Fujita, 1997; Fiedler et al., 2004; Bernstein et al., 2014; this study).

In this work we comprehensively studied the light color acclimation of *C. gracile*, a common cyanobacterium living in turbid freshwater shallow lakes (like Lake Balaton or other Central-European lakes), using nine different monochromatic growth lights covering the spectral range from 435 to 687 nm. According to our data, *C. gracile* cells performed great plasticity in terms of their pigment composition, antenna size, and photosystem stoichiometry (**Figures 2**–**4**). Oxidation pressure on the intersystem chain via withdrawal of electrons from linear electron transport chain by PSI under orange or red illumination is partially balanced by increasing photosystem II to photosystem I ratios (**Figure 4**). On the other hand, unfavorable light conditions, where neither chlorophyll nor phycobilisomes absorb light sufficiently, are compensated by an enhanced antenna size and/or increased carotenoid levels (**Figures 2**, **3**).

Redox Imbalance in *C. gracile* Grown Under Blue and Near Far-Red Light

In spite of the compensatory strategies described above, *C. gracile*, like other cyanobacteria, uses blue light less efficiently, which involves moderate growth rates, reduced cell volumes and low ETR (**Figure 1**). In the previous work of Luimstra and her co-workers, the less efficient use of blue light in (common) cyanobacteria was explained by a redox imbalance between PSII and PSI, an inherent consequence of PBS-possession of cyanobacteria that are evolutionarily adapted to red-enriched light (Luimstra et al., 2018). Conversely, they explained the fact, why PBS-less marine cyanobacteria, i.e., *Prochlorococcus* species are dominated in deep marine environments that can only be penetrated by blue and green light. We confirmed that hypothesis by PAM-fluorimetry, showing a largely reduced intersystem chain and ineffective photosynthesis in *C. gracile* cells grown under blue light (**Figures 6**, **7**).

Further, we found strong bioenergetic imbalance not only in *C. gracile* cells grown under blue light, but also in cells grown under near far-red (687 nm) light, which is also effectively absorbed by PSI. Surprisingly, orange, red or near far-red growth light triggered a partial excitonic PBS decoupling from photosystems and even from thylakoid membranes, which was the most pronounced in the cells grown under 687 nm light (**Figure 4**). Although energetic decoupling of the PBS antenna from reaction centers occurs even under normal conditions (Chukhutsina et al., 2015), so far, similar phenomenon could have been induced only by strong light (Tamary et al., 2012). It is quite astonishing that under mild physiological conditions it is also possible to induce such permanent decoupling. This strongly suggests that suboptimal photosynthetic performance of near far-red light grown *C. gracile* cells (**Figure 1**) is a consequence of a solid redox-imbalance (PQ pool oxidation, which was opposite to PQ pool reduction in blue/green light grown cells). High levels of the photoprotective carotenoid zeaxanthin in cells grown under 687 nm light (**Figures 2**, **3**) support this assumption. Also, despite the 687 grown cells having oxidized PQ pool upon dark acclimation (**Figure 6**), their intersystem chain turned over-reduced under AL (**Figure 7**, this result does not contradict results of OJIP measurements that were performed after dark acclimation). The permanent excitonic decoupling of PBS from PSII reaction centers (**Figures 4**, **5**) under weak light suggest (i) a physiological role of such light acclimation process (ii) that might be triggered by a different (path)way, rather than via a local heat transient induced process as shown previously (Stoitchkova et al., 2007; Tamary et al., 2012; see also below).

Excitonic Decoupling as a Light Acclimation Process

The two major short-term light acclimation processes in cyanobacteria are state transitions and blue-light induced non-photochemical quenching. They occur in minutes and reflect short-term changes in light intensity. Similarly to long-term light acclimation, these processes also attempt to balance the PQ redox state. Regarding state transitions, it is generally assumed that in state 1 (PQ pool relatively oxidized) and state 2 (PQ pool relatively reduced) the photosynthetic machinery displays optimal quantum yields of photosynthesis in light that has a composition favoring its absorption by PSI or PSII, respectively. Different from higher plants and green algae, cyanobacteria are in state 1 upon illumination and in state 2 in the dark or in very low light due to the respiratory electron flow reducing the PQ pool (that is shared by both photosynthesis and respiration, Mullineaux and Allen, 1986). According to the data available, in cyanobacteria both relative energy transfer from PBS to photosystems and distribution of the absorbed light energy between photosystems are regulated by state transitions (Mullineaux and Emlyn-Jones, 2005), although the detailed molecular mechanism of these processes is still unknown.

Also different from higher plants, NPQ in cyanobacteria is pH-independent and can be exclusively induced by "blue" light. A specific carotenoid molecule was shown to play a central role in this process (Rakhimberdieva et al., 2004). This pigment was identified as a hydroxyechinenone or echinenone chromophore in the water soluble OCP (for current reviews see, Kirilovsky and Kerfeld, 2016; Kerfeld et al., 2017), which is bound to PBS and reversibly converted from the (dark-stable) orange form to the (active) red form upon illumination with strong blue light. The red form is essential for the induction of the photoprotective mechanism (Wilson et al., 2008). Experimental data suggest that the quenching center is formed at the level of the PBS core, most likely at allophycocyanin trimmers emitting light at 660 nm (Tian et al., 2011; Jallet et al., 2012).

Our results show that both state transitions and OCP-quenching can occur in *C. gracile* and their contribution to short-term light acclimation processes is largely dependent on the wavelength of growth light: the efficiency of the state transitions was the highest in the cells grown under red light (**Figure 7**), while OCP-induced NPQ was the maximal in the cultures long-term acclimated either to blue-green or 687 nm light and exhibiting solid redox-imbalance (**Supplementary Figures 7,6A**).

This highlights the increased accumulation of OCP under oxidative stress (Plohnke et al., 2015), possibly in close relation to the essential role of OCP as a singlet oxygen quencher (Sedoud et al., 2014). Moreover, the complementary feature of state transitions and OCP quenching also emphasize the potential interplay between various short-term light acclimation processes (Kaňa et al., 2012; Bernát et al., 2018).

Recently, we have discovered a third type of short-term light acclimation process in cyanobacteria, in which excitonic decoupling of PBSs from PSII reaction centers upon strong illumination plays a central role (Tamary et al., 2012). It was assumed that the process was photon-dose dependent and the mechanism was directly triggered thermally via local heat transients (Stoitchkova et al., 2007; Tamary et al., 2012). In this work we provided evidence that under certain conditions even weak light (i.e., 25 μmol photons m^{-2} s^{-1}) can induce such permanent excitonic decoupling in *C. gracile*. Hence, although the role of local heat transients cannot be neglected, excitonic decoupling from the PBS antenna from PSII can also be induced by a redox signal cascade in this cyanobacterium. PAM-fluorimetry data, showing a largely reduced intersystem chain in AL-illuminated *C. gracile* cells grown under near far-red light (**Figure 7**), supports this hypothesis. High cellular zeaxanthin level (**Figure 3**), which has a general photoprotective role in oxygenic photoautotrophs is also in line with this assumption. In this respect, PBS decoupling induced under weak near far-red light may imply a new type of light acclimation process.

DATA AVAILABILITY STATEMENT

The original contributions presented in the study are included in the article/**Supplementary Material**, further inquiries can be directed to the corresponding author.

AUTHOR CONTRIBUTIONS

GB proposed the research questions, designed the study, performed experiments, contributed to the results analyses, and wrote the manuscript. TZ performed and analyzed cell counting and photosynthesis activity measurements and contributed to growth experiments and analyses. EK and LK performed the HPLC measurements and analyzed the results. GS performed the confocal microscopy and analyzed the results. LV and BS designed the lighting apparatus and contributed to the growth experiments. OP and VT supervised the project. All authors contributed to the article and approved the submitted version.

FUNDING

GB was supported by the Hungarian Academy of Sciences hosted as a distinguished scientist at the Centre for Ecological Research, Balaton Limnological Institute (contract Nr. VK-05/2017). OP was supported by the Czech Science Foundation (GA ČR, grant number 20-17627S). GS was supported by the National Research, Development and Innovation Office (NKFIH; GINOP-2.3.2-15-2016-00001). GB and BS were also supported by NKFIH (grant nos. K128950 and NKFIH-872). TZ was supported by the Ministry of Education, Youth and Sports of the Czech Republic (OP RDE grant number CZ.02.1.01/0.0/0.0/16-026/0008413, project "Strategic Partnership for Environmental Technologies and Energy Production"), and by the Czech Science Foundation (GA ČR, grant number 18–24397S). VT was supported by NKFIH (grants NoK116666, No129505, and No135832).

ACKNOWLEDGMENTS

We thank Jana Hofhanzlová, Tímea Szabó, Balázs Németh and Diana Búzová for their technical assistance. We also thank Doug Campbell as well as the two reviewers for their careful reading of the manuscript and helpful comments and suggestions.

SUPPLEMENTARY MATERIAL

The Supplementary Material for this article can be found online at: https://www.frontiersin.org/articles/10.3389/fpls.2021.612302/full#supplementary-material

REFERENCES

Ackleson, S. G. (2003). Light in shallow waters: a brief research review. *Limnol. Oceanogr.* 48, 323–328. doi: 10.4319/lo.2003.48.1_part_2.0323

Acuña, A. M., Snellenburg, J. J., Gwizdala, M., Kirilovsky, D., van Grondelle, R., and van Stokkum, I. H. M. (2016). Resolving the contribution of the uncoupled phycobilisomes to cyanobacterial pulse-amplitude modulated (PAM) fluorometry signals. *Photosynth. Res.* 127, 91–102. doi: 10.1007/s11120-015-0141-x

Bennett, A., and Bogorad, L. (1973). Complementary chromatic adaptation in a filamentous blue-green alga. *J. Cell Biol.* 58, 419–435. doi: 10.1083/jcb.58.2.419

Bernát, G., Steinbach, G., Kaňa, R., Govindjee, Misra, A. N., and Prášil, O. (2018). On the origin of the slow M–T chlorophyll a fluorescence decline in cyanobacteria: interplay of short-term light-responses. *Photosynth. Res.* 136, 183–198. doi: 10.1007/s11120-017-0458-8

Bernstein, H. C., Konopka, A., Melnicki, M. R., Hill, E. A., Kucek, L. A., Zhang, S., et al. (2014). Effect of mono- and dichromatic light quality on growth rates and photosynthetic performance of *Synechococcus* sp. PCC 7002. *Front. Microbiol.* 5:488. doi: 10.3389/fmicb.2014.00488

Chukhutsina, V., Bersanini, L., Aro, E.-M., and van Amerongen, H. (2015). Cyanobacterial light-harvesting phycobilisomes uncouple from photosystem I during dark-to-light transitions. *Sci. Rep.* 5:14193.

Dietzel, L., Bräutigam, K., and Pfannschmidt, T. (2008). Photosynthetic acclimation: state transitions and adjustment of photosystem stoichiometry - functional relationship between short-term and long-term light quality acclimation in plants. *FEBS J.* 275, 1080–1088. doi: 10.1111/j.1742-4658.2008.06264.x

Engelmann, T. W. (1883). Farbe und Assimilation. Assimilation finder nur in den farbstoffhaltigen Plasmatheilchen statt. II. Näherer Zusammenhang zwischen Lichtabsobtion und Assimilation. III. Weitere folgerungen. *Bot. Z.* 41, 1–19.

Everroad, C., Six, C., Partensky, F., Thomas, J. C., Holtzendorff, J., and Wood, A. M. (2006). Biochemical bases of type IV chromatic adaptation in marine *Synechococcus* spp. *J. Bacteriol.* 188, 3345–3356. doi: 10.1128/jb.188.9.3345-3356.2006

Felföldi, T., Somogyi, B., Márialigeti, K., and Vörös, L. (2011). Notes on the biogeography of non-marine planktonic picocyanobacteria: re-evaluating novelty. *J. Plankton Res.* 33, 1622–1626. doi: 10.1093/plankt/fbr051

Fiedler, B., Broc, D., Schubert, H., Rediger, A., Börner, T., and Wilde, A. (2004). Involvement of cyanobacterial phytochromes in growth under different light qualities and quantities. *Photochem. Photobiol.* 79, 551–555. doi: 10.1562/rn-013r.1

Fujita, Y. (1997). A study on the dynamic features of photosynthetic stoichiometry: accomplishments and problems for future studies. *Photosynth. Res.* 53, 83–93.

Fujita, Y., and Murakami, A. (1987). Regulation of electron transport composition in cyanobacterial photosynthetic system: stoichiometry among photosystem I and II complexes and their light-harvesting antennae and cytochrome b_6f complex. *Plant Cell Physiol.* 28, 1547–1553.

Fujita, Y., Murakami, A., Aizawa, K., and Ohki, K. (1994). "Short-term and long-term adaptation of the photosynthetic apparatus: homeostasic properties of thylakoids," in *The Molecular Biology of Cyanobacteria*, ed. D. A. Bryant (Dordrecht: Kluwer Academic Publishers), 677–692. doi: 10.1007/978-94-011-0227-8_22

Fujita, Y., Murakami, A., and Ohki, K. (1987). Regulation of photosystem composition in the cyanobacterial photosynthetic system: the regulation occurs in response to the redox state of the electron pool located between the two photosystems. *Plant Cell Physiol.* 28, 283–292.

Fujita, Y., Ohki, K., and Murakami, A. (1985). Chromatic regulation of photosystem composition in the photosynthetic system of red and blue-green algae. *Plant Cell Physiol.* 26, 1541–1548.

Gutu, A., and Kehoe, D. (2012). Emerging perspectives on the mechanisms, regulation and distribution of light color acclimation in cyanobacteria. *Mol. Plant* 5, 1–13. doi: 10.1093/mp/ssr054

Ikeuchi, M., and Ishizuka, T. (2008). Cyanobacteriochromes: a new superfamily of tetrapyrrole-binding photoreceptors in cyanobacteria. *Photochem. Photobiol. Sci.* 7, 1159–1167. doi: 10.1039/b802660m

Jallet, D., Gwizdala, M., and Kirilovsky, D. (2012). ApcD, ApcF and ApcE are not required for the Orange Carotenoid Protein related phycobilisome fluorescence quenching in the cyanobacterium *Synechocystis* PCC 6803. *Biochim. Biophys. Acta* 1817, 1418–1427. doi: 10.1016/j.bbabio.2011.11.020

Kaňa, R., Kotabová, E., Komárek, O., Šedivá, B., Papageorgiou, G. C., Govindjee, et al. (2012). The slow S to M fluorescence rise in cyanobacteria is due to a state 2 to state 1 transition. *Biochim. Biophys. Acta* 1817, 1237–1247. doi: 10.1016/j.bbabio.2012.02.024

Kerfeld, C. A., Melnicki, M. R., Sutter, M., and Dominguez-Martin, M. A. (2017). Structure, function and evolution of the cyanobacterial orange carotenoid protein and its homologs. *New. Phytol.* 215, 937–951. doi: 10.1111/nph.14670

Kirilovsky, D., and Kerfeld, C. (2016). Cyanobacterial photoprotection by the orange carotenoid protein. *Nat. Plants* 2:16180.

Komárek, J., Kopecký, J., and Cepák, V. (1999). Generic characters of the simplest cyanoprokaryotes *Cyanobium, Cyanobacterium* and *Synechococcus*. *Cryptogam. Algol.* 20, 209–222. doi: 10.1016/s0181-1568(99)80015-4

Kopečna, J., Komenda, J., Bučinska, L., and Sobotka, R. (2012). Long-term acclimation of the cyanobacterium *Synechocystis* sp. PCC 6803 to high light is accompanied by an enhanced production of chlorophyll that is preferentially channeled to trimeric photosystem I. *Plant Physiol.* 160, 2239–2250. doi: 10.1104/pp.112.207274

Luimstra, V. M., Schuurmans, J. M., Verschoor, A. M., Hellingwerf, K. J., Huisman, J., and Matthijs, H. C. P. (2018). Blue light reduces photosynthetic efficiency of cyanobacteria through an imbalance between photosystems I and II. *Photosynth. Res.* 138, 177–189. doi: 10.1007/s11120-018-0561-5

Maritorena, S., Morel, A., and Gentili, B. (1994). Diffuse reflectance of oceanic shallow waters: influence of water depth and bottom albedo. *Limnol. Oceanogr.* 39, 1689–1703. doi: 10.4319/lo.1994.39.7.1689

Montgomery, B. L. (2017). Seeing new light: recent insights into the occurrence and regulation of chromatic acclimation in cyanobacteria. *Curr. Opin. Plant Biol.* 37, 8–23.

Mullineaux, C. W., and Allen, J. F. (1986). The state 2 transition in the cyanobacterium *Synechococcus* 6301 can be driven by respiratory electron flow into the plastoquinone pool. *FEBS Lett.* 205, 155–160. doi: 10.1016/0014-5793(86)80885-7

Mullineaux, C. W., and Emlyn-Jones, D. (2005). State transition: an example of acclimation to low-light stress. *J. Exp. Bot.* 56, 389–393. doi: 10.1093/jxb/eri064

Palenik, B. (2001). Chromatic adaptation in marine *Synechococcus* strains. *Appl. Environ. Microbiol.* 67, 991–994. doi: 10.1128/aem.67.2.991-994.2001

Plohnke, N., Seidel, T., Kahmann, U., Rögner, M., Schneider, D., and Rexroth, S. (2015). The proteome and lipidome of *Synechocystis* sp. PCC 6803 cells grown under light-activated heterotrophyc growth. *Mol. Cell. Proteomics* 14, 572–584. doi: 10.1074/mcp.m114.042382

Prášil, O., Bína, D., Medová, H., Řeháková, K., Zapomělova, E., Veselá, J., et al. (2009). Emission spectroscopy and kinetic fluorometry studies of phototrophic microbial communities along a salinity gradient in solar saltern evaporation ponds of Eilat, Israel. *Aquat. Microb. Ecol.* 56, 285–296. doi: 10.3354/ame01311

Rakhimberdieva, M. G., Stadnichuk, I. N., Elanskaya, I. V., and Karapetyan, N. V. (2004). Carotenoid-induced quenching of the phycobilisome fluorescence in photosystem II-deficient mutant of *Synechocystis* sp. *FEBS Lett.* 574, 85–88.

Remelli, W., and Santabarbara, S. (2018). Excitation and emission wavelength dependence of fluorescence spectra in whole cells of the cyanobacterium *Synechocystis* sp. PPC6803: influence on the estimation of Photosystem II maximal quantum efficiency. *Biochim. Biophys. Acta* 1859, 1207–1222. doi: 10.1016/j.bbabio.2018.09.366

Rippka, R., and Cohen-Bazire, G. (1983). The cyanobacteriales: a legitimate order based on the type strain *Cyanobacterium staniery*? *Ann. Microbiol.* 134B, 21–36. doi: 10.1016/s0769-2609(83)80094-5

Rockwell, N. C., Duanmu, D., Martin, S. S., Bachy, C., Price, D. C., Bhattacharya, D., et al. (2014). Eukaryotic algal phytochromes span the visible spectrum. *Proc. Natl. Acad. Sci. U.S.A.* 111, 3871–3876. doi: 10.1073/pnas.1401871111

Rockwell, N. C., and Lagarias, J. C. (2010). A brief history of phytochromes. *Chem. Phys. Chem.* 11, 1172–1180. doi: 10.1002/cphc.200900894

Sanfilippo, J. E., Garczarek, L., Partensky, F., and Kehoe, D. M. (2019). Chromatic acclimation in cyanobacteria: a diverse and widespread process for optimizing photosynthesis. *Annu. Rev. Microbiol.* 73, 407–433. doi: 10.1146/annurev-micro-020518-115738

Santabarbara, S., Monteleone, F. V., Remelli, W., Rizzo, F., Menin, B., and Casazza, A. P. (2019). Comparative excitation-emission dependence of the F_V/F_m ratio in model green algae and cyanobacterial strains. *Physiol. Plant.* 166, 351–364. doi: 10.1111/ppl.12931

Schneider, C. A., Rasband, W. S., and Eliceiri, K. W. (2012). NIH Image to ImageJ: 25 years of image analysis. *Nat. Methods* 9, 671–675. doi: 10.1038/nmeth.2089

Schreiber, U., Klughammer, C., and Kolbowski, J. (2012). Assessment of wavelength-dependent parameters of photosynthetic electron transport with a new type of multi-color PAM chlorophyll fluorometer. *Photosynth. Res.* 113, 127–144. doi: 10.1007/s11120-012-9758-1

Sedoud, A., López-Igual, R., Rehman, A. U., Wilson, A., Perreau, F., Boulay, C., et al. (2014). The cyanobacterial photoactive Orange Carotenoid Protein is an excellent singlet oxygen quencher. *Plant Cell* 26, 1781–1791. doi: 10.1105/tpc.114.123802

Stanier, R. Y., Kunisawa, R., Mandel, M., and Cohen-Bazire, G. (1971). Purification and properties of unicellular blue-green algae (order Chroococcales). *Bacteriol. Rev.* 35, 171–205. doi: 10.1128/br.35.2.171-205.1971

Stirbet, A., Lazár, D., Kromdijk, J., and Govindjee. (2018). Chlorophyll a fluorescence induction: Can just a one-second measurement be used to quantify abiotic stress responses? *Photosynthetica* 56, 86–104. doi: 10.1007/s11099-018-0770-3

Stoitchkova, K., Zsiros, O., Jávorfi, T., Páli, T., Andreeva, A., Gombos, Z., et al. (2007). Heat- and light-induced reorganizations in the phycobilisome antenna of Synechocystis sp. PCC 6803. Thermo-optic effect. *Biochim. Biophys. Acta* 1767, 750–756. doi: 10.1016/j.bbabio.2007.03.002

Tamary, E., Kiss, V., Nevo, R., Adam, Z., Bernát, G., Rexroth, S., et al. (2012). Structural and functional alterations of cyanobacterial phycobilisomes induced by high-light stress. *Biochim. Biophys. Acta* 1847, 319–327. doi: 10.1016/j.bbabio.2011.11.008

Tandeau de Marsac, N. (1977). Occurrence and nature of chromatic adaptation in cyanobacteria. *J. Bacteriol.* 130, 82–91.

Tian, L., van Stokkum, I. H. M., Koehorst, R. B. M., Jongerius, A., Kirilovsky, D., and van Amerongen, H. (2011). Site, rate, and mechanism of photoprotective quenching in cyanobacteria. *J. Am. Chem. Soc.* 133, 18304–18311. doi: 10.1021/ja206414m

Wilson, A., Punginelli, C., Gall, A., Bonetti, C., Alexandre, M., Routaboul, J. M., et al. (2008). A photoactive carotenoid protein acting as light sensor. *Proc. Natl. Acad. Sci. U.S.A.* 105, 12075–12080. doi: 10.1073/pnas.0804636105

Wiltbank, L. B., and Kehoe, D. M. (2016). Two cyanobacterial photoreceptors regulate photosynthetic light harvesting by sensing teal, green, yellow, and red light. *mBio* 7:e020130-15.

Wyman, M., and Fay, P. (1986). Underwater light climate and the growth and pigmentation of planktonic blue-green algae (Cyanobacteria) II. The influence of light quality. *Proc. R. Soc. Lond. B* 227, 381–393. doi: 10.1098/rspb.1986.0028

Conflict of Interest: The authors declare that the research was conducted in the absence of any commercial or financial relationships that could be construed as a potential conflict of interest.

frontiers in Plant Science

REVIEW
published: 14 April 2021
doi: 10.3389/fpls.2021.668512

A Holistic Approach to Study Photosynthetic Acclimation Responses of Plants to Fluctuating Light

Armida Gjindali[1†], Helena A. Herrmann[1,2†‡], Jean-Marc Schwartz[2], Giles N. Johnson[1] and Pablo I. Calzadilla[1]*

[1] Department of Earth and Environmental Sciences, Faculty of Science and Engineering, University of Manchester, Manchester, United Kingdom, [2] Division of Evolution & Genomic Sciences, Faculty of Biology, Medicine and Health, University of Manchester, Manchester, United Kingdom

OPEN ACCESS

Edited by:
Michele Grieco,
Martin Luther University of Halle-Wittenberg, Germany

Reviewed by:
Wei Huang,
Chinese Academy of Sciences, China
Amy S. Verhoeven,
University of St. Thomas, United States

***Correspondence:**
Pablo I. Calzadilla
pablo.calzadilla@manchester.ac.uk

[†] These authors have contributed equally to this work

‡Present address:
Helena A. Herrmann,
Faculty of Chemistry, Institute of Analytical Chemistry, University of Vienna, Vienna, Austria

Specialty section:
This article was submitted to Plant Abiotic Stress, a section of the journal Frontiers in Plant Science

Received: 16 February 2021
Accepted: 23 March 2021
Published: 14 April 2021

Citation:
Gjindali A, Herrmann HA, Schwartz J-M, Johnson GN and Calzadilla PI (2021) A Holistic Approach to Study Photosynthetic Acclimation Responses of Plants to Fluctuating Light. Front. Plant Sci. 12:668512. doi: 10.3389/fpls.2021.668512

Plants in natural environments receive light through sunflecks, the duration and distribution of these being highly variable across the day. Consequently, plants need to adjust their photosynthetic processes to avoid photoinhibition and maximize yield. Changes in the composition of the photosynthetic apparatus in response to sustained changes in the environment are referred to as photosynthetic acclimation, a process that involves changes in protein content and composition. Considering this definition, acclimation differs from regulation, which involves processes that alter the activity of individual proteins over short-time periods, without changing the abundance of those proteins. The interconnection and overlapping of the short- and long-term photosynthetic responses, which can occur simultaneously or/and sequentially over time, make the study of long-term acclimation to fluctuating light in plants challenging. In this review we identify short-term responses of plants to fluctuating light that could act as sensors and signals for acclimation responses, with the aim of understanding how plants integrate environmental fluctuations over time and tailor their responses accordingly. Mathematical modeling has the potential to integrate physiological processes over different timescales and to help disentangle short-term regulatory responses from long-term acclimation responses. We review existing mathematical modeling techniques for studying photosynthetic responses to fluctuating light and propose new methods for addressing the topic from a holistic point of view.

Keywords: photosynthesis, fluctuating light, mathematical modeling, acclimation, metabolism

INTRODUCTION

Plants in natural environments are exposed to light and other environmental conditions that fluctuate on timescales ranging over orders of magnitude. The rate of photosynthesis under any given set of conditions will be a function of the light absorbed, the capacity for charge separation in each photosystem, and of the use of that energy to drive carbon assimilation and other metabolic processes. To maximize light capture efficiency at all times, plants need to ensure that the capacities of electron transport and metabolism exceed the maximum rate of light absorption across the

full range of environmental conditions experienced. This, however, is unlikely to be the optimal solution overall, in terms of resource allocation between different processes.

Plants growing under different conditions may be limited by, for example, light and water availability, nitrogen and other nutrients, and other abiotic constraints. Plants exposed to low irradiance will tend to invest less in electron transport proteins and enzymes of carbon assimilation, and more in light capture (antenna proteins), aiming to achieve the best photosynthetic performance given the environmental conditions (Anderson et al., 1988; Stewart et al., 2015). Conversely, a drop in temperature will slow down enzymatic activities and diffusion limited processes but will not affect energy absorption or electron transfer. Thus, plants exposed to prolonged low temperature tend to invest more in enzymes, in order to restore the balance between light capture and carbon assimilation (Stitt and Hurry, 2002).

A response to a sustained change in growth conditions over multiple days which involves a change in gene expression is defined as acclimation. Two different types of acclimation can be distinguished: developmental and dynamic (Walters, 2005; Athanasiou et al., 2010). In both, plants adjust their physiology to suit the prevailing environmental conditions. Developmental acclimation includes morphological changes, occurring when tissues develop under different environmental conditions. Dynamic acclimation occurs in fully developed organs, with fixed morphology, and involves changes in protein content and composition, which in turn affects different metabolic fluxes and metabolite concentration. Such alterations ensure optimum resource use under the new condition, and give plants the necessary plasticity to withstand changes in their environment (such as seasonal temperature and moisture changes, light fluctuation, etc.). Following this definition, we can distinguish photosynthetic acclimation from regulation (Herrmann et al., 2019b), the latter encompassing processes that alter the *activity* of particular steps in photosynthesis over a time scale of seconds or/and minutes, without changing the abundance of the proteins involved. It is important to note that regulatory processes may be involved in pathways controlling acclimation and will in turn be affected by the acclimation response itself.

In natural environments and in crop fields, plants receive light energy in the canopy through sunflecks (Pearcy, 1990). The duration and distribution of these are highly variable, impacting the overall photosynthetic yield (Rascher and Nedbal, 2006; Foo et al., 2020). Due to the high frequency of high-low light cycles, responses that avoid photoinhibition and maximize photosynthetic yield are required. Short-term responses to fluctuating light involves almost immediate changes in the thylakoid membranes [e.g., induction of Non-Photochemical Quenching (NPQ), including high energy-state quenching (qE) and state transitions], alteration in the activation state of enzymes (e.g., Benson-Calvin Cycle) and changes in stomatal conductance (Tikkanen et al., 2006, 2010). Meanwhile, long-term acclimation responses might include, amongst others, an increase in the pool size of the xanthophyll cycle pigments and in the PSBS protein content (Wei et al., 2020), which in turn enhance its photoprotective capacity. The interconnection and overlapping of these processes, which can occur simultaneously or sequentially over time, challenge the study of the sensing and signaling pathways involved in long-term fluctuating light acclimation in plants. Thus, an holistic approach is required, to which mathematical modeling techniques can make important contributions.

Systems modeling applies various mathematical techniques to describe and conceptualize the structural and dynamic components of a system, such as a set of biochemical pathways. Mathematical modeling can be applied at different levels and over different time-scales, describing processes inside an organelle, across the whole cell or even multiple tissues (Dada and Mendes, 2011; Gomes de Oliveira Dal'Molin et al., 2015; Shaw and Cheung, 2018). This approach has been extensively applied in biology, including studies of photosynthetic acclimation and regulation of sugar metabolism in plants (Nägele and Weckwerth, 2014; Zakhartsev et al., 2016; Herrmann et al., 2019a, 2020). Mathematical modeling is restricted by the available biological knowledge, and by the assumptions under which that knowledge is synthesized in the model. However, if the model assumptions represent an accurate description of the biological system under study, *in silico* studies can provide insights into the underlying processes that yield experimentally useful information. Often, modeling techniques are employed to generate new hypotheses about a complex system in an efficient, targeted, and cost-effective manner (Kitano, 2002). Thus, mathematical modeling has the potential to disentangle the many observed biochemical changes in a plant's responses to fluctuating environmental conditions to help identify sensors, signals, or acclimation responses.

For the purpose of this review we will consider immediate changes that occur upon changes in light as the inputs of a plant system (i.e., the sensors), and the long-term responses that result from sustained changes in light regimes as the corresponding outputs (i.e., the long-term acclimation responses). Considering the different timescales in which light can effectively fluctuate in natural environments, we will discuss potential signal transduction pathways that could act as links between the inputs and outputs of the system, triggering acclimation. Overall, we aim to gain a deeper understanding on the following questions: How do plants integrate environmental fluctuations over time and how do they tailor their responses accordingly?

SYSTEM INPUTS: SHORT-TERM RESPONSES TO FLUCTUATING LIGHT

Fluctuations in irradiance are immediately reflected in the chloroplast and in the physiology of leaves, triggering different short-term responses aimed at maximizing photosynthesis, while protecting the photosynthetic apparatus from photo-oxidative damage (Standfuss et al., 2005; Yamori, 2016). These short-term responses can also be important in triggering long-term acclimation, which is determined not only by the intensity of the incident light, but also by the frequency of oscillations (Qiao et al., 2020). In this section, we will address the different

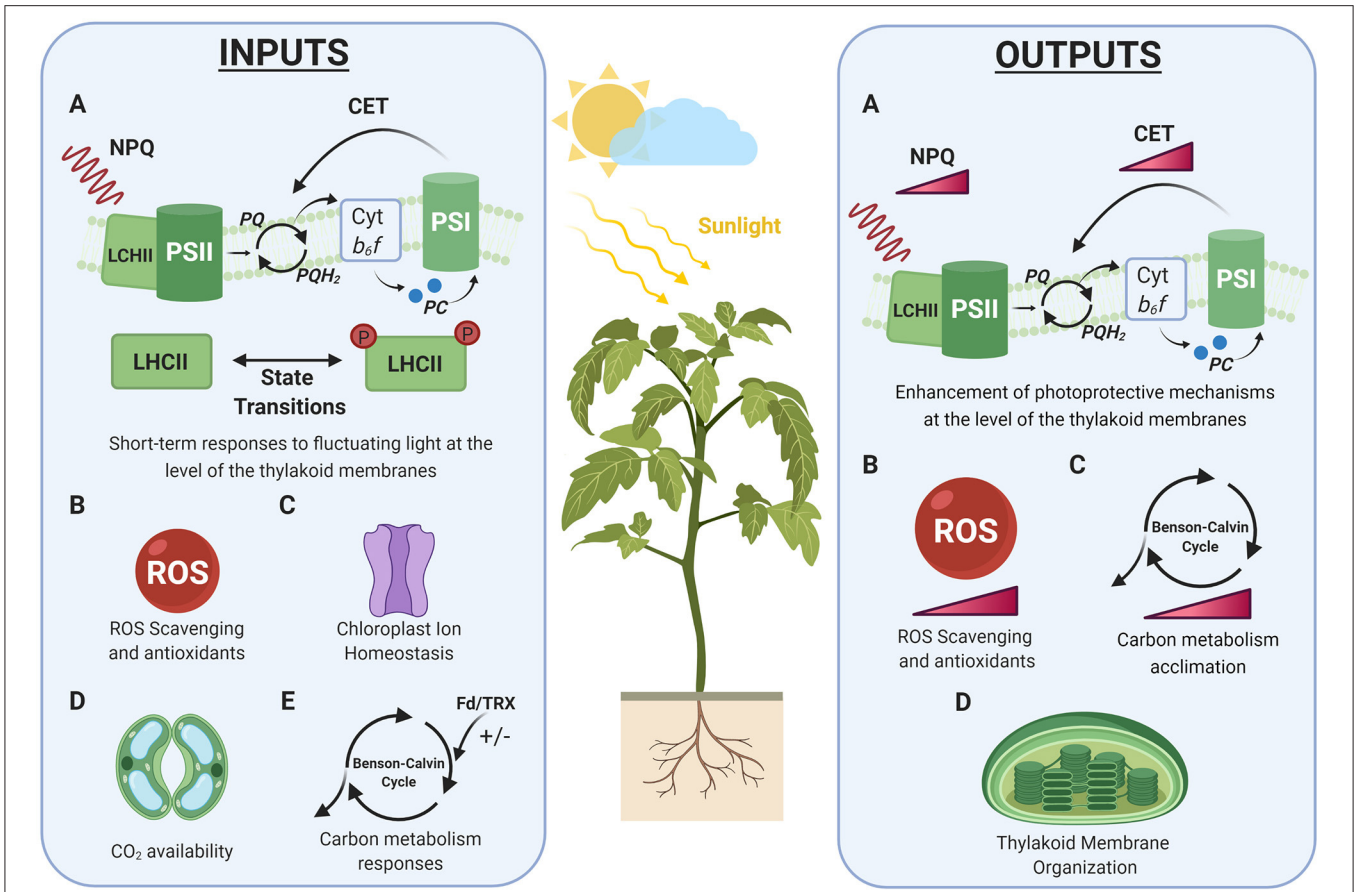

FIGURE 1 | Short and long-term responses to fluctuating light. Schematic representation of the physiological processes defined as inputs and outputs of photosynthetic acclimation to fluctuating light in plants (see sections System Inputs: Short-Term Responses to Fluctuating Light and System Outputs: Long-Term Acclimation to Fluctuating Light). Colored gradient triangles depict accumulation of ROS or intensification of a process. LHCII, Light Harvesting Complex II; PSII, Photosystem II; PSI, Photosystem I; NPQ, Non-Photochemical Quenching; CET, Cyclic Electron Transport; Cyt b_6f, Cytochrome b_6f; PQ, Plastoquinone; PQH2, Plastoquinol. Created with BioRender.com.

regulatory processes that act as potential inputs for the long-term acclimation responses to fluctuating light in plants (**Figure 1**).

Photosynthetic Production of Reactive Oxygen Species (ROS) as a Short-Term Input to the System

Over-reduction of the electron transport chain, which occurs when light absorption exceeds the immediate capacity for CO_2 fixation, can result in electrons "spilling over" to oxygen, leading to the production of Reactive Oxygen Species (ROS). Most directly, this includes singlet excited oxygen ($^1O_2$), superoxide (O_2^-), hydrogen peroxide (H_2O_2), and hydroxyl radicals (HO). ROS generation can be triggered in the chloroplast by many environmental factors, including high light, salinity, drought, pathogens, etc. Therefore, plants have evolved a plethora of ROS scavenging mechanisms to minimize the harmful effects of increased ROS levels (Pospíšil, 2012; Foyer, 2018). Although ROS are also generated in other cell compartments, such as mitochondria and peroxisomes, the main sites of ROS production in the chloroplast are photosystem I (PSI) and photosystem II (PSII; Tripathy and Oelmüller, 2012; Pospíšil, 2016).

Oxygen can be reduced to O_2^- by electrons derived from both photosystems (Zulfugarov et al., 2014; Pospíšil, 2016; Takagi et al., 2016). O_2^- can be converted to H_2O_2 and O_2, a process that is catalyzed by the enzyme superoxide dismutase (SOD) in the chloroplast stroma (Pospíšil, 2012). H_2O_2 can subsequently be converted to water, in the so called water-water cycle, via a series of redox reactions (Awad et al., 2015). Although the scavenging of H_2O_2 can act as an alternative electron sink, the electron flux through this pathway is quickly saturated (Driever and Baker, 2011). Thus, excess H_2O_2 from the chloroplast can pass to the nucleus, where it modulates gene expression and triggers plant acclimation responses (**Figure 1**) (Exposito-Rodriguez et al., 2017).

$^1O_2$ is mainly produced via energy transfer from triplet excited chlorophylls (^{3}Chl*) to oxygen in PSII (Krieger-Liszkay et al., 2008; Pospíšil, 2016). Unlike H_2O_2, $^1O_2$ is believed not to diffuse to the nucleus, due to its short lifetime (~200 ns; Skovsen et al.,

2005). However, $^1O_2$ produced in PSII has been shown to directly react with carotenoids and thylakoid lipids, causing oxidative damage. Oxidative products of carotenoids have been shown to have a signaling role in stress responses (Hideg et al., 1998; Triantaphylidès and Havaux, 2009; Ramel et al., 2012).

Short-Term Photoprotective Responses

Arguably, the most important photo-protective processes in plants are collectively measured by the parameter Non-photochemical quenching (NPQ). This term includes different components that exhibit distinct activation and deactivation kinetics (Standfuss et al., 2005; Johnson and Ruban, 2009; Niyogi, 2009; Ruban et al., 2012; Derks et al., 2015). The major, and fastest, component of NPQ is high energy state quenching (qE). qE is activated by the formation of a pH gradient (ΔpH) between the thylakoid lumen and the chloroplast stroma, and involves protonation of PSII subunit S (PsbS) and the de-epoxidation of zeaxanthin from violaxanthin through the xanthophyll cycle (Pascal et al., 2005; Takizawa et al., 2007; Ruban et al., 2012).

An increase in light intensity results in more protons being transferred from the chloroplast stroma to the thylakoid lumen via photosynthetic electron flow and, as a result, the pH in the thylakoid lumen drops. Protonation of PsbS leads to conformational changes in LHCII, which in turn increase the amount of energy that is quenched as heat, preventing ROS overproduction and protecting PSII from photodamage (Henmi et al., 2004; Vass, 2012; Zavafer et al., 2015). Under fluctuating light conditions, changes in ΔpH are a transient signal for qE, forming and decaying within seconds. However, the interconversion of violaxanthin and zeaxanthin in response to changes in irradiance occurs over a longer timescale (minutes).

Cyclic electron transport (CET) is another regulatory process involved in photoprotection in plants (Finazzi and Johnson, 2016; Yamori et al., 2016; Yamamoto and Shikanai, 2019), which plays an important role in generating the ΔpH required to trigger qE (Suorsa et al., 2016; Nakano et al., 2019). In CET, electrons are transferred from ferredoxin back to the plastoquinone (PQ) pool, and subsequently to PSI through Cyt b_6f and plastocyanin (PC). Thus, CET imports protons from the stroma to the lumen for ATP generation, but without net production of NADPH (Breyton et al., 2006; Joliot and Johnson, 2011). CET helps to balance the ATP:NADPH ratio under circumstances where the rate of consumption of reducing equivalents is reduced. In *Arabidopsis*, *two* main pathways for cyclic electron flow have been identified (Munekage et al., 2008; Shikanai, 2014). In the antimycin A-sensitive pathway, electrons are transferred from ferredoxin to PQ via a pathway involving the PGR5/PGRL1 complex (Munekage et al., 2002; DalCorso et al., 2008). In contrast, in the antimycin A-insensitive pathway, the electron transfer to the PQ pool is facilitated by NADH:plastoquinone oxidoreductase (NDH; Joliot and Johnson, 2011; Shikanai, 2014). For an extensive review of CET, see Nawrocki et al. (2019).

Of the two pathways of CET, the antimycin A-sensitive pathway has been particularly linked to PSI photoprotection under fluctuating conditions (Suorsa et al., 2012; Yamamoto and Shikanai, 2019). Studies in the *pgr5* mutant of Arabidopsis show that PGR5 participates in photosynthetic control of Cyt b_6f (Nandha et al., 2007), protecting PSI from photodamage under low/high light cycles (Suorsa et al., 2012, 2013; Yamamoto and Shikanai, 2019). In addition, PGR5 plays a role in the acceptor-side regulation of PSI. Accordingly, it was recently observed that over-expression of PGR5 in the C4 plant *Flaveria bidentis*, enhances the electron sink downstream of PSI, increasing photoprotection (Tazoe et al., 2020). The water-water cycle has also been suggested as a PSI photoprotective mechanism under fluctuating light conditions, although its activity is strongly species dependent (Huang et al., 2019b; Yang et al., 2020). In this cycle, stromal antioxidants enzymes catalyze ROS conversion into water (Asada, 1999), a process which was recently suggested to be more relevant for PSI photoprotection than CET in angiosperms (Sun et al., 2020).

In addition to qE, another important NPQ component in plants is qT, a form of quenching associated with state transitions (for a review see Minagawa, 2011). This process regulates the distribution of excitation energy between both photosystems, under conditions where the incident light favors the excitation of one over the other. To mitigate such changes, plants can adjust the energy excitation between PSII and PSI within minutes, by altering the distribution of light harvesting proteins between them. The imbalance in the excitation level of the photosystems is sensed through changes in the redox state of the PQ pool (Lemeille and Rochaix, 2010). In particular, reduction of the PQ pool and binding of PQH_2 at the Qo site of the Cyt b_6f, activates a specific kinase (STN7) that phosphorylates LHCII trimers (Wollman and Lemaire, 1988; Vener et al., 1995; Zito et al., 1999; Depège et al., 2003; Bellafiore et al., 2005). Phosphorylation induces LHCII detachment from PSII and partial (or total) attachment to PSI, triggering transition to State II (Kyle et al., 1983; Larsson et al., 1983). Meanwhile, when the PQ pool is oxidized, dephosphorylation of LHCII triggers the opposite phenomenon and transition to State I (Pribil et al., 2010; Shapiguzov et al., 2010). The signals produced from the redox state of the PQ pool are naturally transient, however, evidence shows a direct and rapid regulation of chloroplast gene expression in response to changes in PQ redox state (Pfannschmidt et al., 1999).

Although the classical view of state transitions has been associated with spectral changes in the quality of the incident light, thylakoid phosphorylation can also be triggered dynamically by changes in light intensity (Tikkanen et al., 2010; Grieco et al., 2012; Mekala et al., 2015). While under low white light intensity LHCII phosphorylation levels are maximal, under high light conditions LHCII phosphorylation is down-regulated and PSII core phosphorylation increases (Tikkanen et al., 2010). These opposite states do not change the relative excitation of PSII and PSI, but their regulatory function is related with the maintenance of an equal excitation pressure between both photosystems (Tikkanen et al., 2010). The main kinases and phosphatases involved in this phosphorylation pathway are STN7/STN8 and TAP38/PPH1, respectively; being their regulation particularly relevant under low light conditions (Tikkanen et al., 2010; Mekala et al., 2015). When light intensity increases, other regulatory mechanisms (such as NPQ) become more important for photoprotection (Tikkanen et al., 2010;

Grieco et al., 2012). Under fluctuating light conditions, a role for STN7-dependent phosphorylation was also found in PSI photoprotection, through the maintenance of the redox stability of the electron transport chain (Grieco et al., 2012).

Both STN7 and STN8 are also capable of phosphorylating a range of proteins in the chloroplast (Schönberg et al., 2017), extending their involvement in the short-term response to fluctuating light onto further processes of acclimation. The regulatory pathways related with thylakoid protein phosphorylation have a key role in the photosynthetic responses to a changing environment, and their participation in the signals transduction pathway for acclimation needs further elucidation (reviewed by Grieco et al., 2016).

Changes in Chloroplast Ion Homeostasis

Ion homeostasis in the chloroplast is relevant to light sensing, not only due to its effect on enzymatic activity, but also due to its contribution to the regulation of the proton and electric potentials across the thylakoid membrane (Finazzi et al., 2015). Proton motive force (PMF), the driver of ATP synthesis, consists of two components: $\Delta\Psi$, the electrical potential gradient that is built due to ions moving in and out of the thylakoid lumen, and ΔpH. When proton concentration significantly increases in the thylakoid lumen, qE is activated, leading to the loss of energy as heat (Henmi et al., 2004; Vass, 2012; Zavafer et al., 2015). To maintain ATP production without promoting acidification of the lumen, which leads to NPQ activation, fluxes of counter ions (Cl^- influx, Mg^{2+} and K^+ efflux) regulate the $\Delta\Psi$ component of the PMF (Carraretto et al., 2013; Armbruster et al., 2014; Herdean et al., 2016).

Finetuning ΔpH and $\Delta\Psi$ to better suit different environmental conditions can facilitate fast modulation of photosynthetic activity under fluctuating light conditions. For instance, a transporter that has been linked to fast photosynthetic regulation in *Arabidopsis* is AtVCCN1, which transports Cl^- ions into the chloroplast lumen (Herdean et al., 2016). Influx of Cl^- ions into the lumen triggers an increase in the $\Delta pH/\Delta\Psi$ ratio, by decreasing H^+ efflux from the thylakoid membranes, inducing a faster NPQ response under sudden increases in light intensities. By contrast, potassium influx to the lumen via the K^+ antiport (KEA3), has been identified as an important factor in the transition from high to low light (Armbruster et al., 2014, 2016; Galvis et al., 2020). KEA3 transfers K^+ into the lumen and H^+ out to the chloroplast stroma, decreasing ΔpH but maintaining the $\Delta\Psi$ necessary for ATP production. KEA3 activity accelerates NPQ relaxation during the transition to low light, leading to a fast recovery of CO_2 assimilation (Armbruster et al., 2014).

Another K^+ transporter, the two-pore K^+ channel (TPK3), has been suggested to play a pivotal role in thylakoid ultrastructure organization and plant growth in *Arabidopsis* (Carraretto et al., 2013). TPK3 exports K^+ and Ca^+ ions, and is thought to modulate fast regulation of PMF to optimize photosynthetic activity under different light environments (Carraretto et al., 2013). However, recent results obtained by Höhner et al. (2019) showed that TPK3 is localized in the tonoplast and is not involved in photosynthetic regulation. These authors suggest the involvement of an as yet unknown additional K^+ channel in photosynthetic acclimation to fluctuating light.

Thioredoxins as Signals for Light

The light-induced enzymatic activation of the Benson-Calvin cycle was first discovered by Buchanan and colleagues in the 1960s, showing that CO_2 fixation was activated by light (reviewed by Buchanan et al., 2002; Michelet et al., 2013). This light activation pathway, called the ferredoxin/thioredoxin (Fd/TRX) system, regulates carbon metabolic pathways through post-translational redox modifications (reviewed by Ruelland and Miginiac-Maslow, 1999; Lemaire et al., 2007; Michelet et al., 2013; Nikkanen et al., 2017). Thioredoxins (TRX) in the chloroplast are reduced mainly by ferredoxin (Fd, the PSI electron acceptor), via an enzyme called Ferredoxin-Thioredoxin reductase (FTR). Once reduced, TRX can reduce disulfide bonds in different stromal target proteins, placing the Fd/TRX at the crossroads between the "light" and "dark" reactions of photosynthesis (Ruelland and Miginiac-Maslow, 1999; Lemaire et al., 2007).

Activation of the Fd/TRX system will directly depend on the redox state of the chloroplast, meaning that changes in the photosynthetic electron flow will activate/deactivate different target enzymes under changing light regimes. This on/off switch acts as a significant regulatory process, leading to the adjustment of the carbon metabolism under different conditions. However, most studies on the regulatory role of Fd/TRX have been conducted under continuous light conditions, and research on their involvement in fluctuating light responses is limited (Collin et al., 2004; Nikkanen and Rintamäki, 2014; Geigenberger et al., 2017).

A study performed on the Arabidopsis knockout mutants t*rxm1/m2* showed the role of thioredoxins in the short-term responses to fluctuating light (Thormählen et al., 2017). Mutant plants showed alterations in the light activation of the enzyme malate dehydrogenase (MDH) and the malate/oxaloacetate (Mal/OAA) shuttle, a higher NPQ and a lower PSII quantum efficiency. This phenotype was only evident under fluctuating light conditions, with these alterations being more pronounced with increasing numbers of high-low light cycles. By contrast, no phenotypic differences were seen between the mutants and the WT plants under constant light.

Impact of Fluctuating Light on CO_2 Availability and Photorespiration

Stomatal responses play a critical role in the availability of CO_2 for carbon fixation, and it has been shown that stomatal dynamics limit photosynthesis under fluctuating light (Qu et al., 2016; Papanatsiou et al., 2019; De Souza et al., 2020; Kimura et al., 2020). Since stomatal responses are slower than photochemical and biochemical regulatory changes, a sudden change in light intensity could cause chloroplast CO_2 concentration to decrease (Huang et al., 2015; Vialet-Chabrand et al., 2017). A decrease in CO_2 concentration (and thus carbon fixation) implies that fewer electrons are being directed to the Benson-Calvin cycle, favoring the over-reduction of the electron transport chain and triggering ROS generation. At the same time, a decrease in CO_2 availability also increases O_2 binding to Rubisco, its oxygenase activity

and photorespiration (Huang et al., 2015). Interestingly, it was recently shown that stomatal opening and closure dynamics can acclimate to different growth light regimes, anticipating future variations in light, and adjusting CO_2 availability to the prevailing light condition (Matthews et al., 2018).

Photorespiration is a metabolic pathway that recycles 2-phosphoglycolate (2PG), a toxic product of the oxygenase activity of Rubisco, into 3-phospholycerate (3PGA; reviewed by Foyer et al., 2009; Bauwe et al., 2010; Eisenhut et al., 2019). This recycling requires several enzymatic steps that are distributed across three different organelles: the chloroplast, the peroxisome, and the mitochondrion. Although the photorespiratory pathway can represent a substantial loss of CO_2 fixation, its involvement in photoprotection, nitrogen assimilation, and abiotic stress responses make it a crucial process for plants (reviewed by Foyer et al., 2009; Bauwe et al., 2010; Timm and Bauwe, 2013; Voss et al., 2013; Eisenhut et al., 2019). Nevertheless, its participation under fluctuating light conditions has not been extensively studied (Huang et al., 2015; Schneider et al., 2019). Huang et al. (2015) showed that, under fluctuating light conditions, a strong activation of the photorespiratory pathway allows the consumption of reducing equivalents, decreasing the reduction pressure of the electron transport chain and avoiding ROS generation. In addition, RuBP regeneration is also accelerated, favoring carbon fixation under these circumstances.

SYSTEM OUTPUTS: LONG-TERM ACCLIMATION TO FLUCTUATING LIGHT

Acclimation to environmental fluctuations involves changes in gene expression and protein abundance, which result in the modification of the structure and composition of tissues. In particular, dynamic acclimation occurs in developed tissues, constrained by the existing structures, and involves processes or responses that take several days to be achieved. These responses might depend on the plant species and on the intensity and duration of the environmental fluctuation (Yin and Johnson, 2000). The processes involved in dynamic acclimation are not necessarily irreversible, and they will persist as long as the prevailing environmental condition is maintained. In the following sections, we will focus on the changes involved in the dynamic acclimation of photosynthesis under fluctuating light conditions (**Figure 1**).

Acclimation of Carbon Metabolism

When plants are grown at higher irradiances, they typically develop leaves with a high capacity for photosynthesis (see Walters, 2005). Fully developed leaves transferred from low to high light can also increase their photosynthetic capacity, typically over a period of a week (Athanasiou et al., 2010; Dyson et al., 2015). This acclimation response involves extensive changes across the whole of the leaf proteome, with marked increases in the concentration of Rubisco and other enzymes involved in the Benson-Calvin cycle, as well as down-stream enzymes involved in carbon assimilation (Miller et al., 2017).

Schneider et al. (2019) observed an upregulation of some Benson-Calvin cycle enzyme genes, such as fructose-1,6-bisphosphate aldolase 1 (FBA1) and sedoheptulose-1,7-bisphosphatase (SBSPASE), in Arabidopsis plants subjected to fluctuating light for 3 days. These enzymes were previously shown to participate in the regulation of the metabolic flux of carbon in plants (Lefebvre et al., 2005; Uematsu et al., 2012; Simkin et al., 2015, 2017). In addition, SBSPASE and FBA1 were also found to be regulated by the Fd/TRX system (Breazeale et al., 1978; Sahrawy et al., 1997; Dunford et al., 1998), suggesting a fine-tuning regulation of this long-term acclimation by a short-term mechanism. However, despite the increased activity and/or concentration of their Benson-Calvin enzymes, when compared to constant light conditions, plants under fluctuating light do not necessarily show an enhancement of their CO_2 fixation capacity (Watling et al., 1997; Vialet-Chabrand et al., 2017; Schneider et al., 2019). Studies show that proteomic and transcriptomic changes in response to fluctuating light do not always align, suggesting a role of post-transcriptional regulations in the modulation of long-term acclimation responses (Athanasiou et al., 2010; Dyson et al., 2015; Miller et al., 2017; Schneider et al., 2019; Niedermaier et al., 2020).

Furthermore, as part of the acclimation response of carbon metabolism to fluctuating light, an increase in the expression of photorespiratory genes, and their corresponding protein content, was also observed in Arabidopsis (Schneider et al., 2019; Niedermaier et al., 2020). This metabolic response was shown to be particularly significant under high light fluctuation periods (Huang et al., 2015). Under low light fluctuating regimes, an increase in the photorespiratory pathway was deemed insignificant (Kono et al., 2014), possibly due to a lower accumulation of reducing equivalents.

Thylakoid Membrane Changes During Long-Term Acclimation

In addition to metabolic alterations, changes in the thylakoid membrane protein composition play an important role in light acclimation (reviewed by Walters, 2005; Anderson et al., 2012; Kaiser et al., 2018; Johnson and Wientjes, 2020). For instance, plants grown under high light have been observed to have a lower PSII/PSI ratio, but higher concentrations of Cyt b_6f and ATPase (reviewed by Evans, 1988; Eskins et al., 1991; Walters and Horton, 1994; Bailey et al., 2001; Walters, 2005). Furthermore, high light may also reduce the amount of LHCII and increase the chlorophyll *a*/*b* ratio, which is related with changes in light harvesting complexes concentration and photosystems ratio (Leong and Anderson, 1984; Yang et al., 1998; Bailey et al., 2001). By contrast, LHCII concentration increases when light exposure is limiting for plant growth, although under these conditions, a compensating decrease in PSII levels is also observed (Evans, 1988; Bailey et al., 2001). Some, but not necessarily all, of these responses are seen when plants are exposed to step changes in irradiance. In Arabidopsis, transfer from low to moderately high light resulted in an increase in Cyt b_6f and ATPase, without measurable changes in chlorophyll content or the total amount of LHC proteins (Athanasiou et al., 2010; Miller et al., 2017).

In addition to acclimation to overall light intensity, when plants are exposed to different light *qualities*, the protein composition of the thylakoid membranes may also change (reviewed by Anderson et al., 1988). Long-term acclimation responses include changes in LHCII concentration, and Chl *a*/*b* and PSII/PSI ratio (Chow et al., 1990; Kim et al., 1993; Walters and Horton, 1995; Murchie and Horton, 1998). Such changes, occurring within days; help balance the electron transport rate under situations where either photosystem is preferentially excited by light. Importantly, these alterations differ from state transitions, which occur in seconds to minutes and do not include changes in thylakoid membrane composition, only re-distribution of LHCII and photosystem macro-organization.

Overall, when light intensity or quality change, plant acclimation responses tend to balance light absorption and assimilation (Rott et al., 2011; Yamori et al., 2011). Nevertheless, understanding the effect of fluctuating light in natural environments is far more complex. Sunflecks will have a direct impact on light intensity, but natural shade cast by vegetation will also affect the incident light quality. Thus, natural light fluctuations in the ecosystems result in complex inputs, which might induce contradictory output responses. For instance, the PSII/PSI ratio will change in opposite directions with a decrease in light intensity or with exposure to a high far-red/red ratio, conditions that can be imposed by vegetative shading (Murchie and Horton, 1998; Bailey et al., 2001). Consequently, predicting a thylakoid membrane specific response to fluctuating light in natural environments is not an easy task. Furthermore, many of these responses are species-dependent (Murchie and Horton, 1998; Yin and Johnson, 2000).

Enhancement of the Photoprotective Mechanisms as a Long-Term Acclimation Response

Similar to what happens following sudden increases in light intensity, frequent exposure to oscillating periods of high light induces over-reduction of the electron transport chain, triggering an increase in ROS production and photoinhibition (Shimakawa and Miyake, 2018; Huang et al., 2019a). Thus, long-term acclimation to fluctuating light can also involve an enhancement of photoprotective mechanisms. For instance, Schneider et al. (2019) observed an up-regulation of H_2O_2 scavenging enzymes, such as glutathione peroxidase (GPX7) and catalase (CAT2), in Arabidopsis leaves exposed to 3 days of fluctuating light. In agreement, these plants also increased their ascorbate pool size, indicating an improvement in ROS scavenging and antioxidant response (Schneider et al., 2019).

Fluctuating light can increase PSBS content and the concentration of pigments of the xanthophyll cycle, leading to a strengthening of the photoprotective capacity of NPQ (Barker et al., 1997; Niinemets et al., 1998; Alter et al., 2012; Caliandro et al., 2013). This acclimation response was demonstrated to be, at least partially, regulated at the transcriptional level (Schneider et al., 2019). The relevance of NPQ as a long-term acclimation response to fluctuating light was recently shown using tobacco transgenic lines overexpressing PSBS and zeaxanthin epoxidase (ZEP) and violaxanthin de-epoxidase (VDE), the key enzymes in the xanthophyll cycle (Kromdijk et al., 2016). These plants showed a higher CO_2 assimilation compared to the WT, leading to a higher dry mass accumulation under field conditions.

In addition to NPQ, genes related to CET were also upregulated in response to fluctuating light (Schneider et al., 2019). Proteomic results obtained under the same conditions, and by the same authors, suggest a specific role of the NDH-like complex in this long-term acclimation mechanism (Niedermaier et al., 2020). Nevertheless, mutants lacking PGR5 were shown to suffer strong PSI photoinhibition under fluctuating light (Suorsa et al., 2012; Kono and Terashima, 2016), meaning that the involvement of the antimycin A-sensitive CET pathway in this acclimation process cannot be ruled out. It is worth mentioning that a higher CET flux will contribute to a higher ΔpH, facilitating NPQ generation under photoinhibitory conditions (Munekage et al., 2002). Thus, the involvement of CET in this long-term acclimation response will not only avoid PSI photoinhibition, but also increase thermal dissipation. Consequently, short-term responses to sudden increases in light intensity are also being improved by this long-term response.

SIGNALS TRANSDUCTION PATHWAYS FOR LONG-TERM ACCLIMATION TO FLUCTUATING LIGHT

Short-term input responses, such as redox changes in the photosynthetic apparatus, occur on very rapid timescales (μsec-min), close to those of the natural fluctuations of the light environment. These inputs may trigger cellular changes, such as protein phosphorylation or thiol reductions, which respond more slowly to the changing conditions (minutes). Nevertheless, all these inputs are transient, and so, their putative role in signaling for long-term plant acclimation, which occurs over days, is not obvious. The concentrations of metabolites can also change on rapid timescales, in direct response to changing light conditions; but in some cases their accumulation provides the potential to generate signals which average out the short-term fluctuations in the environment. In the following section, we will address some of the most discussed pathways participating in photosynthetic acclimation to fluctuating light in plants (**Figure 2**).

ROS and the Redox State of the Chloroplast

Retrograde signals originating from photosynthesis have been studied extensively, aiming to describe chloroplast-nucleus communication and regulation of gene expression (Pfannschmidt et al., 1999; Fey et al., 2005b; Wilson et al., 2006; Foyer et al., 2012; Karpiński et al., 2013; Gollan et al., 2015; Matsubara et al., 2016; Leister, 2019). Within these signaling pathways, the participation of ROS originating from photosynthetic electron flow, has been widely discussed (Pfannschmidt et al., 2009; Ramel et al., 2012; Szechyńska-Hebda and Karpiński, 2013; Kim, 2020). For instance, H_2O_2 can diffuse from the chloroplast, creating a signal cascade

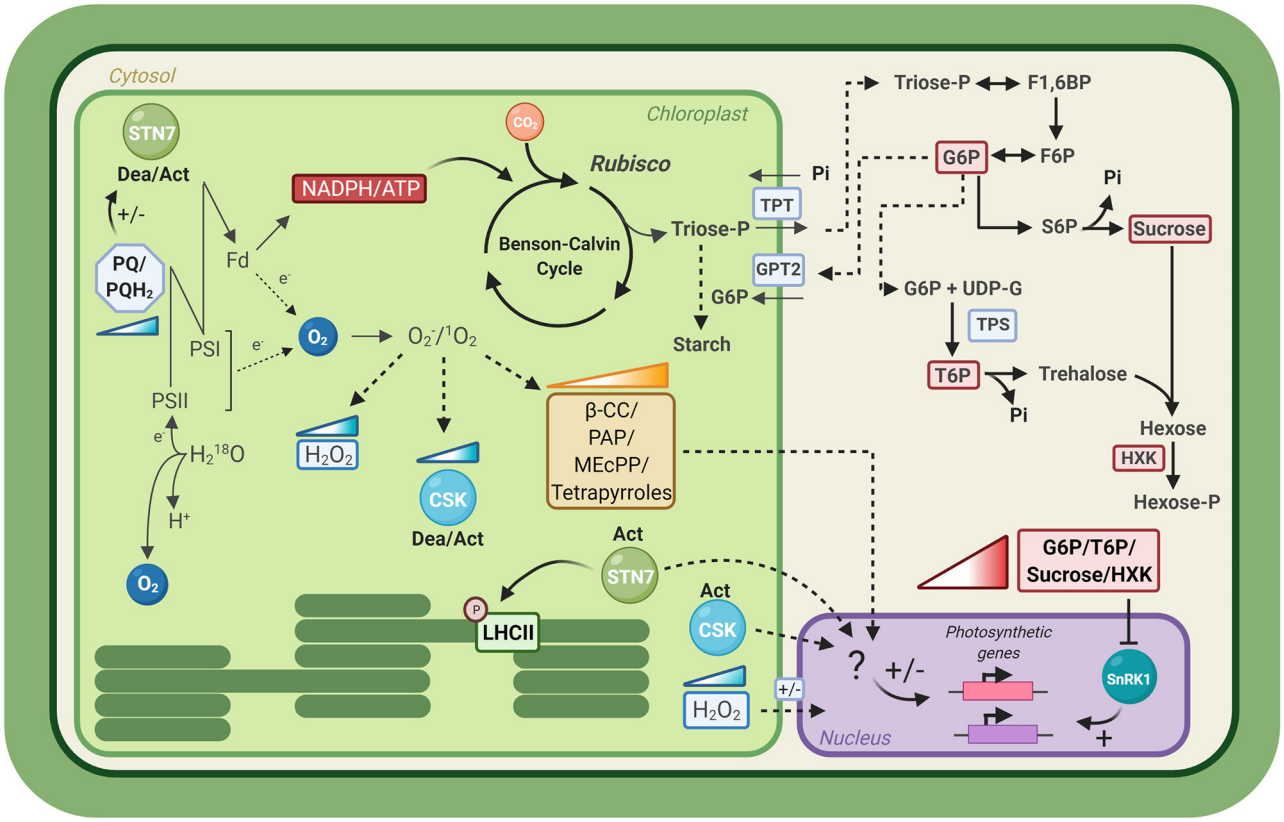

FIGURE 2 | Signals transduction pathways of long-term acclimation to fluctuating light. Schematic representation of the different putative signaling pathways involved in photosynthetic acclimation to fluctuating light, as described in section Signals Transduction Pathways for Long-Term Acclimation to Fluctuating Light. Colored gradient triangles depict accumulation of a metabolite or enzyme. LHCII, Light Harvesting Complex II; PSII, Photosystem II; PSI, Photosystem I; Fd, Ferredoxin; PQ, Plastoquinone; PQH2, Plastoquinol; STN7, STN7 kinase; CSK, Chloroplast Sensor Kinase; SnRK1, SNF1-related kinase 1 β-CC, β-cyclocitral; PAP, 3′-phosphoadenosine 5′-phosphate; MEcPP, methylerythritol cyclodiphosphate; TPT, Triose-phosphate transporter; GTP2, glucose 6-phosphate/phosphate translocator; G6P, glucose-6-phosphate; T6P, trehalose-6-phosphate; F6P, fructose-6-phosphate; S6P, sucrose-6-phosphate; F1,6BP, fructose-1,6-biphosphate; TPS, Trehalose phosphate synthase; HXK, Hexokinase; Dea/Act, Deactivation/Activation. Created with BioRender.com.

ultimately affecting nuclear gene expression (Maruta et al., 2012). Meanwhile, oxidation of β-carotene by $^1O_2$ has been shown to lead to the formation of the volatile compound β-cyclocitral (β-CC), which triggers changes in nuclear gene expression under stress conditions (Ramel et al., 2012; Havaux, 2014; Tian, 2015). Nevertheless, the specific factors participating in this ROS-related signal transduction pathways are still far from being completely elucidated (reviewed by Leister, 2019; Kim, 2020).

In addition, we can think the chloroplast as an environmental sensor for plants, with the redox state of the electron transport chain being a key gear for sensing fluctuations in the environment. Amongst the components of the electron transport chain, the involvement of the PQ pool in retrograde signaling has been suggested, facilitating a rapid physiological response to changing light conditions (El Bissati and Kirilovsky, 2001; Fey et al., 2005a; Bräutigam et al., 2009). Different proteins have been shown to be regulated by the redox state of PQ, and in a ROS-independent manner (Adamska and Kloppstech, 1991; Kimura et al., 2003; Yabuta et al., 2004), and a link between the redox state of the PQ pool and photosystem gene expression has even been observed (Pfannschmidt et al., 1999; El Bissati and Kirilovsky, 2001).

Although it is clear that ROS retrograde signaling and chloroplast redox changes participate in light acclimation, it is still not yet understood how these signals are integrated under fluctuating light. The short lifetime of these chloroplast redox changes imply that other factors might be integrating the redox variations over time. Puthiyaveetil et al. (2008) suggested that a key protein participating in retrograde signaling is the Chloroplast Sensor Kinase (CSK) (**Figure 2**; Puthiyaveetil et al., 2008). This protein is widely seen in photosynthetic organisms and has been shown to bind an iron-sulfur cluster, which can sense changes in the chloroplast redox state (Ibrahim et al., 2020). The activation/deactivation of the kinase regulates the expression of different photosynthetic genes (Puthiyaveetil et al., 2008; Ibrahim et al., 2020), supporting its participation in the adjustment of the stoichiometry of photosynthetic complexes under different light conditions. Interestingly, CSK gene expression was found to be upregulated under fluctuating light in Arabidopsis (Schneider et al., 2019).

STN7 Kinase as a Mediator Between the Chloroplast-Nucleus Communications

The STN7 kinase phosphorylates LHCII and some PSII subunits upon changes in light conditions, triggering state transitions and regulating PSII turnover (Bellafiore et al., 2005; Tikkanen et al., 2006, 2010; Wagner et al., 2008; Pietrzykowska et al., 2014). Although STN7 involvement in short-term regulatory responses to fluctuating light has been well-described, it was also shown that *stn7* mutants are unable to undergo forms of long-term acclimation under changing light regimes (Bonardi et al., 2005; Pesaresi et al., 2009). When *stn7* mutants were grown under fluctuating light they exhibited reduced growth and a lower seed yield and were incapable of adjusting their thylakoid composition to the conditions experienced. In agreement, STN7 gene expression was increased after 3 days of fluctuating light in Arabidopsis (Schneider et al., 2019), again highlighting its potential involvement in long-term acclimation. Thus, STN7 seems to play a critical role in both short- and long-term responses to fluctuating light regimes in plants, either directly or indirectly (Bonardi et al., 2005; Wagner et al., 2008; Bräutigam et al., 2009; Leister, 2019).

Although it is still unknown which proteins participate downstream of STN7 in the long-term acclimation response, one of the putative proteins is TSP9. TSP9 is a plant specific nuclear-encoded protein, found in the thylakoid membranes, which is phosphorylated by STN7 upon illumination (Carlberg et al., 2003; Zer and Ohad, 2003). The phosphorylated form dissociates from the thylakoid membrane and has been proposed to act as a signaling molecule regulating gene expression under changing light conditions (Carlberg et al., 2003; Zer and Ohad, 2003; Fristedt et al., 2009). Nevertheless, downregulation of TSP9 in Arabidopsis plants did not affect the long-term response to light changes (Pesaresi et al., 2009), but its mutation was shown to affect state transitions and NPQ (Fristedt et al., 2009). These results suggest the involvement of TSP9 in the short-term responses to fluctuating light, but not in long-term acclimation. The downstream factors involved in the STN7 long-term acclimation signaling pathway, are still elusive (Leister, 2019).

Metabolites Accumulation as Putative Integrative Factors of the Long-Term Acclimation Response to Fluctuating Light

ROS-Related Metabolites

A putative role for signal integration was suggested for the volatile compound β-cyclocitral (β-CC; Ramel et al., 2012; Havaux, 2014; Tian, 2015); the accumulation of 3′-phosphoadenosine 5′-phosphate (PAP) and its regulation by the SAL1 phosphatase (Estavillo et al., 2011; Chan et al., 2016); and the isopropanoid precursor methylerythritol cyclodiphosphate (MEcPP; Xiao et al., 2012). The accumulation of chloroplast tetrapyrrole biosynthesis intermediates was also suggested to be involved in retrograde signaling (reviewed by Nott et al., 2006; Tabrizi et al., 2016), although this model has been questioned (Mochizuki et al., 2008; Moulin et al., 2008).

The accumulation of these metabolites is directly connected to an increase in ROS production and/or redox changes in the chloroplast (**Figure 2**), and its involvement in the acclimation response to different stress conditions has been described (Estavillo et al., 2011; Ramel et al., 2012; Xiao et al., 2012; Chan et al., 2016). Thus, it is feasible to think that a putative increase in their accumulation over a certain threshold might also trigger an acclimation response to fluctuating light, allowing the integration of different signals over time. This hypothesis is an interesting starting point to close the gap between the short and long-term responses to this environmental condition.

Carbon-Related Metabolites

Sucrose and the Availability of Inorganic Phosphate

The significance of carbon metabolites as signals for acclimation relies on the fact that photosynthate partitioning varies with changes in irradiance and photoperiod (Mengin et al., 2017). Furthermore, different studies support a role for the accumulation of some of these carbon sinks in the plant's response to several environmental conditions. For instance, sucrose shows a significant role in cold acclimation, triggering changes in gene expression and anthocyanin biosynthetic pathways (Solfanelli et al., 2006; Rekarte-Cowie et al., 2008). In addition, evidence supports a sucrose signaling role in many developmental processes in the plant's life cycle (reviewed by Horacio and Martinez-Noel, 2013).

Sucrose concentrations in plant tissues correlate with light intensity, and their synthesizing enzymes fluctuate over the photoperiod (Cheikh and Brenner, 1992; Horacio and Martinez-Noel, 2013). In addition, sucrose downregulates CO_2 fixation through alteration of gene expression (Pamplin and Chapman, 1975; Sheen, 1990; Rook et al., 1998; Wiese et al., 2004), and through a negative feedback regulation due to inorganic phosphate (Pi) availability (Hurry et al., 2000; Ensminger et al., 2006). Sucrose synthesis and degradation participate in Pi cycling between the chloroplast and the cytosol (Hurry et al., 2000). Alterations in sucrose synthesis in the cytosol may decrease Pi availability in the chloroplast, inhibiting ATP synthesis and, as a consequence, RuBP regeneration and carbon fixation (Hurry et al., 2000; Ensminger et al., 2006).

Due to its constitutive presence in the cytosol of plant cells (**Figure 2**), a role for sucrose as a signaling molecule in photosynthetic acclimation may imply that its accumulation needs to exceed a certain threshold (Horacio and Martinez-Noel, 2013). Alter et al. (2012) analyzed the concentration of soluble sugars (glucose, fructose, and sucrose) in Arabidopsis plants under constant and fluctuating light conditions, without observing any differences in total soluble sugar concentration between treatments. Nevertheless, the individual concentration of each sugar was not independently assessed, and changes in sugar ratios under fluctuating light cannot be ruled out.

Glucose-6-Phosphate, Trehalose-6-Phosphate and Hexokinases, Key Molecules in the Starch and Sucrose Synthesis Regulation

Photosynthesis, through the Benson-Calvin cycle, produces glycerate-3-phosphate, which is reduced to triose-phosphate

(triose-P) in successive reactions that consume NADPH and ATP. Triose-P can be used to regenerate ribulose-1,5-*bis*phosphate (RuBP) in the Benson-Calvin cycle, or, when in excess, can be transformed to end products such as sucrose or/and starch (**Figure 2**; reviewed by Ensminger et al., 2006). Sucrose is synthesized in the cytosol, for which triose-P is exported from the chloroplast through the triose-phosphate translocator (TPT; **Figure 2**). When the rate of triose-P export is lower than its rate of synthesis, starch is synthesized in the chloroplast (Zeeman et al., 2004). Carbon flux to starch is also an important strategy to avoid carbon sink limitations under photoinhibitory conditions (Ensminger et al., 2006).

Fixed carbon may also be imported back from the cytosol in the form of glucose-6-phosphate (G6P), through the glucose 6-phosphate/phosphate translocator GPT2 (**Figure 2**; Niewiadomski et al., 2005; Dyson et al., 2015). GTP2 expression is known to be associated with alterations in carbon metabolism and high light responses, leading to photosynthetic acclimation (Athanasiou et al., 2010; Kunz et al., 2010; Dyson et al., 2015). GTP2 might directly affect the relative concentrations of G6P between cell compartments, affecting the metabolic signals triggering photosynthetic responses to different environmental stimulus. For instance, G6P positively regulates sucrose synthesis, by activating SPS and inhibiting sucrose synthase (SUS- an enzyme participating in sucrose catabolism). This inhibition in sucrose degradation is through inhibition of SNF1-related kinase 1 (SnRK1), which participates in the regulation of carbon metabolism, ABA signaling, stress responses and development (Jossier et al., 2009; Zhang et al., 2009; Cho et al., 2012). Thus, regulating the G6P concentration in the cytosol might have a direct impact on metabolism, growth and acclimation under different environmental conditions.

In a similar way to G6P, trehalose-6-phosphate (T6P) has been described as having an important role in the regulation of carbon assimilation and sugar status in plants (reviewed by Ponnu et al., 2011). T6P is an intermediate in trehalose biosynthesis, synthesized from UDP-Glucose and G6P in the cytosol, by the enzyme trehalose phosphate synthase (TPS; **Figure 2**; Häusler et al., 2014). T6P is a signal of sucrose availability, alters the rate of starch biosynthesis in the chloroplast and participates in the cross-talk of metabolic regulations through inhibition of SnRK1 (Lunn et al., 2006; Zhang et al., 2009; Yadav et al., 2014). In particular, T6P was also shown to down-regulate genes related to the photosynthetic process, which are normally up-regulated by SnRK1 (Zhang et al., 2009).

Other proposed sugar sensing molecules are the hexokinases (HXKs), which catalyze the phosphorylation of glucose and fructose and have been defined as evolutionarily conserved glucose sensors (**Figure 2**; reviewed by Granot et al., 2014). HXKs are able to down-regulate the expression of photosynthetic genes, reduce chlorophyll levels and photosynthetic rates (Jang et al., 1997; Dai et al., 1999; Xiao et al., 2000). As a consequence, HXKs are capable of modulating photosynthesis in a glucose dependent-manner, integrating short-term changes in the environment with their corresponding photosynthetic responses (Moore et al., 2003). In agreement, within guard cells, HXK also regulates stomatal closure, supporting a negative coordinated regulation of photosynthesis by hexose availability (Kelly et al., 2013; Granot et al., 2014).

METABOLIC MODELING IN UNRAVELING THE PHOTOSYNTHETIC ACCLIMATION TO FLUCTUATING LIGHT IN PLANTS

Our review of the literature shows that experimental studies that link rapid responses to sustained long-term changes are rare, as they are laborious and often technically infeasible. Mathematical modeling, however, has the potential to overcome some of these limitations, helping to identify mechanisms by which plants integrate short-term responses to the environment over time. A holistic understanding of fluctuating light acclimation is a challenge, involving many timescales. The following section covers a range of mathematical modeling techniques that have previously been applied to study photosynthesis (**Table 1**), and further proposes new modeling techniques that could be employed to deepen our understanding of photosynthetic acclimation to fluctuating light in plants.

Empirical vs. Mechanistic Modeling Techniques to Study Photosynthesis

Mathematical modeling within biology is ruled by two paradigms: empirical modeling and mechanistic modeling. Empirical modeling, also known as statistical modeling, fits a model to the data without considering the underlying biological processes (**Table 1**). Through the observation of a repeated pattern, it is assumed that future events of the same type will result in the same pattern. A straightforward example of an empirical model is the non-rectangular hyperbola of net carbon gas exchange fitted to light response curves (Johnson and Murchie, 2011). While the fit of this model has stood the validation test of time, possible underlying biological mechanisms have only recently been discussed (Retkute et al., 2015; Herrmann et al., 2020). Stegemann et al. (1999) constructed an empirical model relating fluctuating diurnal changes in light intensity to net photosynthesis. By fitting their model parameters to data obtained from two different tree species, they successfully estimated carbon uptake without explaining the mechanisms behind their photosynthetic responses to light.

Empirical models are a powerful tool when the underlying processes are not known and form the premise of machine learning algorithms (Kotsiantis et al., 2007; Angelov and Gu, 2019). The reliability of empirical models improves vastly with the amount of input data available (Kotsiantis et al., 2007), a limitation that is becoming less hindering in the current 'omics era. Nonetheless, extrapolation of empirical models is difficult and, typically, good predictions cannot be made outside of the range of previously measured values. For example, an empirical model of photosynthesis with parameters fitted to a specific light and temperature regime is unlikely to be transferable to another light and temperature regime, and, instead, the model parameters must be estimated anew (Herrmann et al., 2020).

By contrast, mechanistic models, albeit harder to construct, have several advantages over empirical models

TABLE 1 | A brief overview of the primary types of models applied to study photosynthetic responses to fluctuating light.

Type of model	Description	Advantages	Limitations	Examples
Empirical	Statistical methods are used to identify consistently reoccurring patterns in data	No prior knowledge of the underlying biological processes is required	Dependent on high amounts of input data	Stegemann et al., 1999; Louarn et al., 2015
Mechanistic	Systems are broken down into smaller components whose interactions with one another are clearly defined	Can be generalized and used to predict outcomes outside of the range of the input data	Knowledge of the workings of the systems components is required	Farquhar et al., 1980; Kirschbaum et al., 1997; Pearcy et al., 1997
Dynamic	Models mainly consisting of ordinary of partial differential equations that capture changes over time	Can incorporate changes in concentrations over time as well as kinetic and regulatory information	Large models often lead to a combinatorial explosion in parameter estimation	Farquhar et al., 1980; Porcar-Castell et al., 2006; Retkute et al., 2015
Steady-state	Capture the steady-state behavior when internal metabolite concentrations can be assumed to stay constant	Computationally inexpensive; can be used to capture metabolic acclimation	Time-steps typically occur over hours or days; regulatory mechanisms are largely ignored	Cheung et al., 2014; Shaw and Cheung, 2018
Stochastic	Account for a certain unpredictability in the model outcome by considering a probability of occurrence	Can account for randomness, heterogeneity and intrinsic noise	Computationally expensive to run; no single solution	Guerriero et al., 2014; Retkute et al., 2018

The advantages and limitations of each are discussed and examples of where each type of model has been applied are provided.

(**Table 1**). Mechanistic models break down a system into smaller components, and the processes by which these components interact with one another are then captured by mathematical equations. Mechanistic models require an in-depth understanding of the system components and their interactions in space and time. However, once a mechanistic model is constructed and its parameters are successfully estimated, few input data are required for outcome prediction. Furthermore, if the same mechanisms apply under different conditions, or outside the range of the initial input values, the model can be applied beyond the range of the initial training data (Geritz and Kisdi, 2012; Ratti, 2018).

Kinetic models of metabolic pathways are examples of mechanistic models: a pathway is broken down into its metabolites and the way in which these metabolites interact with one another can, for example, be described by mass action law or Michaelis-Menten kinetics (Schallau and Junker, 2010). Many successful kinetic models of photosynthesis have been built, and their ability to capture fluctuating light conditions is discussed in the next section. Kinetic models, as with all others mechanistic models, are limited by our knowledge of the system under study.

Dynamic Modeling to Study Time-Dependent Photosynthetic Responses Under Fluctuating Light

Dynamic models generally encompass time-dependent-models that capture changes over time (**Table 1**). These models employ a set of ordinary differential equations, or partial differential equations, considering one or more independent variables. Dynamic models can be empirical or mechanistic; however, in biochemistry, dynamic models appear most commonly in the form of kinetic models. Kinetic models of biochemical pathways are mechanistic, dynamic models, as they consider changes in metabolite concentrations over time. Due to a combinatorial explosion of the parameter estimation, dynamic models are generally limited to a handful of equations.

Multiple dynamic models of photosynthesis and the Benson-Calvin cycle reactions exist (Farquhar et al., 1980, 2001; Harley and Tenhunen, 1991; Poolman et al., 2000); however, most of them have not been applied to study fluctuating light acclimation. Kirschbaum et al. (1997) and Pearcy et al. (1997) are among the few to have extended the original Farquhar et al. (1980) model to study fluctuating light regimes over a time frame of seconds to hours. Mott and Woodrow (2000), however, addressed the question of nitrogen resource allocation under fluctuating light regimes by using a much simpler model of rubisco and rubisco activase. In addition, Porcar-Castell et al. (2006) incorporated both regulatory and feedback mechanisms in their dynamic model of PSII, and were able to validate experimentally obtained photochemical and non-photochemical quantum yields under fluctuating light. However, none of these models consider a long-term acclimation of plants to changing light regimes, as they have been parametrized for a much shorter timescale.

Retkute et al. (2015) employed a semi-empirical dynamic model to describe carbon uptake over time as a function of light availability and a constant maximum photosynthetic capacity (Pmax). Pmax is calculated to give the maximum possible carbon uptake over the time-weighted average of a light pattern, representing the acclimation state of the plant. How plants shift from one acclimation state to another, and alter their Pmax accordingly, was discussed by Herrmann et al. (2020) using a time- and temperature-dependent model. However, the sensors and signals that trigger a new photosynthetic acclimated state remain elusive.

As discussed in section Signals Transduction Pathways for Long-Term Acclimation to Fluctuating Light, and highlighted in our previous studies (Dyson et al., 2015; Herrmann et al., 2020), carbon fluxes between the cytosol and the chloroplast seem to be important factors in the photosynthetic acclimation responses of plants. In particular, the resulting changes in sugar vs. starch production have been shown to be crucial for acclimation to different light regimes (Dyson et al., 2015). Modeling the changes in carbon metabolism under fluctuating

light could be useful to identify key signals leading to acclimation responses in plants. For instance, using a simple kinetic model and a sensitivity analysis of the model parameters, Nägele and Weckwerth (2014) analyzed the control of sugar homeostasis in plants, and suggested that allosteric effectors alone can account for a considerable readjustment of metabolic homeostasis.

Metabolic control analysis (MCA) quantifies the extent to which fluxes, or concentrations, depend on the model parameters. Thus, when applied to kinetic models, MCA provides a valuable tool for identifying parameters, and thus enzymes, that exert the greatest metabolic control over the fluxes (or species concentrations) in a defined model (ap Rees and Hill, 1994; Poolman et al., 2000). The fact that detailed regulatory information can be included in these dynamic kinetic models represents one of their greater advantages; although at the same time limits the size and complexity over which they can be feasibly solved. Often, a trade-off between the level of mechanistic detail and the feasibility to solve the model is required (Harley and Tenhunen, 1991).

Steady-State Modeling as a Mechanistic Approach to Study Photosynthetic Acclimation to Fluctuating Light

Photosynthetic acclimation to a sustained change in light regime typically occurs over multiple days. As Athanasiou et al. (2010) observed, a new photosynthetic state is reached only 1 week after a change in exposure from low to high light. Acclimation responses to changes in light regimes are typically not represented by kinetic models, which tend to be parametrized over a timescale of seconds to hours. Instead, genome-scale steady-state models which tend to operate over multiple days and weeks can be used to study photosynthetic acclimation (**Table 1**; Herrmann et al., 2019a).

Genome-scale, steady-state, metabolic models, employ what are known as constraint-based modeling (CBM) techniques (Lewis et al., 2012), and operate under the assumption that internal metabolite concentrations are constant over time. This approximation is generally valid over longer time-frames, because the changes in metabolic flux leading to new equilibrium states are usually faster when compared to acclimation responses. Whilst these types of models are able to capture the final acclimated steady-state of plant metabolism, they fail to incorporate the mechanisms that initiate and lead to that new steady-state.

More recent variations of CBM techniques aim to overcome these limitations by employing dynamic CBM techniques (Mahadevan et al., 2002; Grafahrend-Belau et al., 2013). Shaw and Cheung (2018), for example, built a dynamic multi-tissue model by using the output of one steady-state model as the input of another steady-state model. By defining a steady-state model at each time point, they were able to effectively analyse resource allocation in plants over days and weeks. The model by Shaw and Cheung (2018) is based on the diel model first published by Cheung et al. (2014), which combined both a day-time (light-dependent) steady-state model and a night-time (light-independent) steady-state model. Dynamic models constructed of steady-state models are thus able to incorporate time-dependent changes, but typically consider changes over a timescale of multiple days.

Different 'omics datasets can be used to incorporate enzyme regulatory mechanisms into genome-scale stoichiometric models, making it, for instance, possible to study redox changes at a resolution of second to hours with longer process steady-state models (Jamshidi and Palsson, 2010). This kind of analysis, however, has yet to be applied to plants exposed to fluctuating light.

The Challenges and Opportunities of Using a Holistic Approach to Address Photosynthetic Acclimation to Fluctuating Light

Incorporating data measured over different timescales, and both discrete (e.g., state switching) and continuous scales (e.g., sink metabolite accumulation), poses an immense challenge for the study of photosynthetic acclimation under fluctuating light conditions. In order to incorporate models describing different processes over different periods of times, dimensionality reduction techniques will be necessary. These techniques are designed to reduce model complexity by discarding components that have little effect on the overall outcome of interest (Hummer and Szabo, 2015; Snowden et al., 2017). Successful dimensionality reduction should lead to the identification of essential model components required for predictive power; each fine-tuned according to the timescale over which it must operate, and the magnitude for which can shows significant effects on the system itself.

Purvis et al. (2009) use dimensionality reduction to combine multiple small-scale kinetic models in the human platelet P2Y1 signaling system, and convert it into a single holistic model. Employing known dimensionality reduction techniques (Hummer and Szabo, 2015; Ali Eshtewy and Scholz, 2020) on fast existing kinetic models of photosynthesis, may pave the way for their incorporation into slower process models (such as the genetic changes involved in light acclimation). Unfortunately, neither dimensionality reduction nor model validation techniques are frequently employed in plant sciences. Model validation, both at the experimental and theoretical level (Hasdemir et al., 2014), will need to be done before a model is deemed suitable to be integrated holistically.

Hybrid models, which incorporate both discrete and continuous information, are starting to gain attention in other disciplines (Henzinger, 2000; Bortolussi and Policriti, 2008). A simple analogy for such a hybrid automaton is a thermostat, whereby the law of thermodynamics are described by ordinary differential equations (continuous) but the state of the heater is either on or off (discrete). Thus, we can imagine multiple metabolite concentrations changing on a continuous scale in response to environmental fluctuations, which could emerge in an on/off output response (such as the ones described in sections Signals Transduction Pathways for Long-Term Acclimation to Fluctuating Light and System Outputs: Long-Term Acclimation to Fluctuating Light of the present review,

respectively). However, such a system has yet to be identified in plant acclimation to fluctuating light.

The alternative to the mechanistic approaches described above, would be to take an empirical modeling approach. With an ever-increasing and overwhelming amount of multi-omic data available, there are numerous supervised learning algorithms that could be applied to identify "biomarkers" of a given acclimation stage (Mjolsness and DeCoste, 2001; Saeys et al., 2007). While the identification of molecular predictors is promising, these approaches typically do not reveal any information about the mechanisms by which the identified molecules trigger the final acclimated state of the plant. This empirical approach, however, does hold the potential for validating existing hypotheses or generating new hypotheses for experimental validation. For example, if both STN7 and TSP9 were identified as predictors for light acclimation, this would support the idea that TSP9 acts downstream of STN7 in promoting a long-term acclimation response.

Finally, stochastic models can account for random variations in inputs and result in a probability distribution of potential outcomes (**Table 1**; Guerriero et al., 2014; Retkute et al., 2018). The application of stochastic models to photosynthesis remains limited as of today but holds a great potential for identifying potential thresholds for acclimation. For instance, one could imagine a metabolite concentration that fluctuates in response to environmental changes triggering an acclimation process only once a given threshold concentration is passed. This could be the case of the proposed ROS and carbon-related metabolites discussed above (see section Signals Transduction Pathways for Long-Term Acclimation to Fluctuating Light).

To facilitate the integration of different modeling techniques, rigorously standardized tools are required. For instance, the open platform www.e-photosynthesis.org hosts a collection of dynamic plant models, translated to the Systems Biology Mark-up Language (SBML), and provides a good starting point for any modeler interested in photosynthetic acclimation. Currently, the project consists largely of model parametrized over short timescale, but hopefully it will be extended to longer-time physiological processes in the future, such that an effective integration of the two will be possible.

CONCLUDING REMARKS

As this review has shown, there is a gap between studies that consider short-term responses to changes in light conditions, and those that consider long-term acclimation processes. This gap is evident from both an experimental and a theoretical viewpoint, and is likely the result of the difficulties associated with studying interconnected processes that occur over different timescales. The photosynthetic apparatus is highly complex; thus, understanding the regulatory networks of fluctuating light responses over time will require a deeper understanding of the system itself. This situation is even more complex if we consider that many experimental studies focus on well-defined, non-random changes in irradiance that do not necessarily reflect realistic field conditions (Annunziata et al., 2017).

It is also worth mentioning that, in the present review, we mainly describe how changes in light regimes affects processes at a single-cell level. Under field conditions, as captured in canopy level models, fluctuating light often result in heterogeneous light absorbance across leaves and cells. How these differences at the cellular level are integrated within and across tissues remains an important topic for further consideration in the future, given that this heterogeneity may result in emergent properties that cannot be captured by single-cell models. Emergent properties are those which arise from an interaction of model components, and which cannot be described by either of the components on their own (Bhalla and Iyengar, 1999; Peak et al., 2004; Aderem, 2005). Emergent properties are the reason why it is often difficult to explain the mechanistic basis of empirical models, and are why both approaches are needed to enhance our understanding of photosynthetic acclimation to fluctuating light conditions.

It is well-established that realistic models of complex biological signals will require regulation, feedback signals and non-linear dynamic components (Csete and Doyle, 2002). Identifying potential emergent properties of such systems will require the integration and careful dimensionality reduction of multiple processes (Rascher and Nedbal, 2006). Models will need to be specific enough to capture the individual processes that together lead to emergent system properties but, at the same time, need to be general enough to differentiate noise from signal (Gillespie, 2000; Mélykúti et al., 2010). As a conclusion, a combination of existing and emerging modeling techniques will be required to capture the emergent properties and signaling pathways related to photosynthetic acclimation to fluctuating light in plants.

AUTHOR CONTRIBUTIONS

PC, AG, and GJ contributed mainly to the sections System Inputs: Short-Term Responses to Fluctuating Light, System Outputs: Long-Term Acclimation to Fluctuating Light, and Signals Transduction Pathways for Long-Term Acclimation to Fluctuating Light of the present review. HH and J-MS contributed mainly to section Metabolic Modeling in Unraveling the Photosynthetic Acclimation to Fluctuating Light in Plants. All authors co-wrote and approved the manuscript.

FUNDING

This work was support by BBSRC studentships to AG and HH (BB/M011208/1) and BBSRC research grants to GJ and J-MS (BB/J04103/1 and BB/S009078/1).

ACKNOWLEDGMENTS

The authors would like to thank Dr. Beata Czajkowska, Mr. Josef Oliver, and Ms. Norazreen Binti Abd Rahman (University of Manchester) for useful discussions.

REFERENCES

Adamska, I., and Kloppstech, K. (1991). Evidence for an association of the early light-inducible protein (ELIP) of pea with photosystem II. *Plant Mol. Biol.* 16, 209–223. doi: 10.1007/BF00020553

Aderem, A. (2005). Systems biology: its practice and challenges. *Cell* 121, 511–513. doi: 10.1016/j.cell.2005.04.020

Ali Eshtewy, N., and Scholz, L. (2020). Model reduction for kinetic models of biological systems. *Symmetry* 12:863. doi: 10.3390/sym12050863

Alter, P., Dreissen, A., Luo, F.-L., and Matsubara, S. (2012). Acclimatory responses of Arabidopsis to fluctuating light environment: comparison of different sunfleck regimes and accessions. *Photosynth. Res.* 113, 221–237. doi: 10.1007/s11120-012-9757-2

Anderson, J. M., Chow, W. S., and Goodchild, D. J. (1988). Thylakoid membrane organisation in sun/shade acclimation. *Funct. Plant Biol.* 15, 11–26. doi: 10.1071/PP9880011

Anderson, J. M., Horton, P., Kim, E. H., and Chow, W. S. (2012). Towards elucidation of dynamic structural changes of plant thylakoid architecture. *Philos. Trans. R. Soc. B Biol. Sci.* 367, 3515–3524. doi: 10.1098/rstb.2012.0373

Angelov, P. P., and Gu, X. (2019). *Empirical Approach to Machine Learning*. Cham: Springer. doi: 10.1007/978-3-030-02384-3

Annunziata, M. G., Apelt, F., Carillo, P., Krause, U., Feil, R., Mengin, V., et al. (2017). Getting back to nature: a reality check for experiments in controlled environments. *J. Exp. Bot.* 68, 4463–4477. doi: 10.1093/jxb/erx220

ap Rees, T., and Hill, S. A. (1994). Metabolic control analysis of plant metabolism. *Plant Cell Environ.* 17, 587–599. doi: 10.1111/j.1365-3040.1994.tb00151.x

Armbruster, U., Carrillo, L. R., Venema, K., Pavlovic, L., Schmidtmann, E., Kornfeld, A., et al. (2014). Ion antiport accelerates photosynthetic acclimation in fluctuating light environments. *Nat. Commun.* 5, 1–8. doi: 10.1038/ncomms6439

Armbruster, U., Leonelli, L., Correa Galvis, V., Strand, D., Quinn, E. H., Jonikas, M. C., et al. (2016). Regulation and levels of the thylakoid K+/H+ antiporter KEA3 shape the dynamic response of photosynthesis in fluctuating light. *Plant Cell Physiol.* 57, 1557–1567. doi: 10.1093/pcp/pcw085

Asada, K. (1999). The water-water cycle in chloroplasts: scavenging of active oxygens and dissipation of excess photons. *Annu. Rev. Plant Biol.* 50, 601–639. doi: 10.1146/annurev.arplant.50.1.601

Athanasiou, K., Dyson, B. C., Webster, R. E., and Johnson, G. N. (2010). Dynamic acclimation of photosynthesis increases plant fitness in changing environments. *Plant Physiol.* 152, 366–373. doi: 10.1104/pp.109.149351

Awad, J., Stotz, H. U., Fekete, A., Krischke, M., Engert, C., Havaux, M., et al. (2015). 2-cysteine peroxiredoxins and thylakoid ascorbate peroxidase create a water-water cycle that is essential to protect the photosynthetic apparatus under high light stress conditions. *Plant Physiol.* 167, 1592–1603. doi: 10.1104/pp.114.255356

Bailey, S., Walters, R. G., Jansson, S., and Horton, P. (2001). Acclimation of *Arabidopsis thaliana* to the light environment: the existence of separate low light and high light responses. *Planta* 213, 794–801. doi: 10.1007/s004250100556

Barker, D. H., Logan, B. A., Adams, W. W. III., and Demmig-Adams, B. (1997). The response of xanthophyll cycle-dependent energy dissipation in *Alocasia brisbanensis* to sunflecks in a subtropical rainforest. *Funct. Plant Biol.* 24, 27–33. doi: 10.1071/PP96059

Bauwe, H., Hagemann, M., and Fernie, A. R. (2010). Photorespiration: players, partners and origin. *Trends Plant Sci.* 15, 330–336. doi: 10.1016/j.tplants.2010.03.006

Bellafiore, S., Barneche, F., Peltier, G., and Rochaix, J.-D. (2005). State transitions and light adaptation require chloroplast thylakoid protein kinase STN7. *Nature* 433, 892. doi: 10.1038/nature03286

Bhalla, U. S., and Iyengar, R. (1999). Emergent properties of networks of biological signaling pathways. *Science* 283, 381–387. doi: 10.1126/science.283.5400.381

Bonardi, V., Pesaresi, P., Becker, T., Schleiff, E., Wagner, R., Pfannschmidt, T., et al. (2005). Photosystem II core phosphorylation and photosynthetic acclimation require two different protein kinases. *Nature* 437, 1179–1182. doi: 10.1038/nature04016

Bortolussi, L., and Policriti, A. (2008). "Hybrid systems and biology," in *International School on Formal Methods for the Design of Computer, Communication and Software Systems* (Heildelberg: Springer), 424–448. doi: 10.1007/978-3-540-68894-5_12

Bräutigam, K., Dietzel, L., Kleine, T., Ströher, E., Wormuth, D., Dietz, K.-J., et al. (2009). Dynamic plastid redox signals integrate gene expression and metabolism to induce distinct metabolic states in photosynthetic acclimation in Arabidopsis. *Plant Cell* 21, 2715–2732. doi: 10.1105/tpc.108.062018

Breazeale, V. D., Buchanan, B. B., and Wolosiuk, R. A. (1978). Chloroplast sedoheptulose 1, 7-bisphosphatase: evidence for regulation by the ferredoxin/thioredoxin system. *Z. Naturforsch. C* 33, 521–528. doi: 10.1515/znc-1978-7-812

Breyton, C., Nandha, B., Johnson, G. N., Joliot, P., and Finazzi, G. (2006). Redox modulation of cyclic electron flow around photosystem I in C3 plants. *Biochemistry* 45, 13465–13475. doi: 10.1021/bi061439s

Buchanan, B. B., Schürmann, P., Wolosiuk, R. A., and Jacquot, J.-P. (2002). The ferredoxin/thioredoxin system: from discovery to molecular structures and beyond. *Photosynth. Res.* 73, 215–222. doi: 10.1023/A:1020407432008

Caliandro, R., Nagel, K. A., Kastenholz, B., Bassi, R., Li, Z., Niyogi, K. K., et al. (2013). Effects of altered α-and β-branch carotenoid biosynthesis on photoprotection and whole-plant acclimation of Arabidopsis to photo-oxidative stress. *Plant Cell Environ.* 36, 438–453. doi: 10.1111/j.1365-3040.2012.02586.x

Carlberg, I., Hansson, M., Kieselbach, T., Schröder, W. P., Andersson, B., and Vener, A. V. (2003). A novel plant protein undergoing light-induced phosphorylation and release from the photosynthetic thylakoid membranes. *Proc. Natl. Acad. Sci. U.S.A.* 100, 757–762. doi: 10.1073/pnas.0235452100

Carraretto, L., Formentin, E., Teardo, E., Checchetto, V., Tomizioli, M., Morosinotto, T., et al. (2013). A thylakoid-located two-pore K+ channel controls photosynthetic light utilization in plants. *Science* 342, 114–118. doi: 10.1126/science.1242113

Chan, K. X., Mabbitt, P. D., Phua, S. Y., Mueller, J. W., Nisar, N., Gigolashvili, T., et al. (2016). Sensing and signaling of oxidative stress in chloroplasts by inactivation of the SAL1 phosphoadenosine phosphatase. *Proc. Natl. Acad. Sci. U.S.A.* 113, E4567–E4576. doi: 10.1073/pnas.1604936113

Cheikh, N., and Brenner, M. L. (1992). Regulation of key enzymes of sucrose biosynthesis in soybean leaves: effect of dark and light conditions and role of gibberellins and abscisic acid. *Plant Physiol.* 100, 1230–1237. doi: 10.1104/pp.100.3.1230

Cheung, C. Y. M., Poolman, M. G., Fell, D. A., Ratcliffe, R. G., and Sweetlove, L. J. (2014). A diel flux balance model captures interactions between light and dark metabolism during day-night cycles in C3 and crassulacean acid metabolism leaves. *Plant Physiol.* 165, 917–929. doi: 10.1104/pp.113.234468

Cho, Y.-H., Hong, J.-W., Kim, E.-C., and Yoo, S.-D. (2012). Regulatory functions of SnRK1 in stress-responsive gene expression and in plant growth and development. *Plant Physiol.* 158, 1955–1964. doi: 10.1104/pp.111.189829

Chow, W. S., Melis, A., and Anderson, J. M. (1990). Adjustments of photosystem stoichiometry in chloroplasts improve the quantum efficiency of photosynthesis. *Proc. Natl. Acad. Sci. U.S.A.* 87, 7502–7506. doi: 10.1073/pnas.87.19.7502

Collin, V., Lamkemeyer, P., Miginiac-Maslow, M., Hirasawa, M., Knaff, D. B., Dietz, K.-J., et al. (2004). Characterization of plastidial thioredoxins from Arabidopsis belonging to the new y-type. *Plant Physiol.* 136, 4088–4095. doi: 10.1104/pp.104.052233

Csete, M. E., and Doyle, J. C. (2002). Reverse engineering of biological complexity. *Science* 295, 1664–1669. doi: 10.1126/science.1069981

Dada, J. O., and Mendes, P. (2011). Multi-scale modelling and simulation in systems biology. *Integr. Biol.* 3, 86–96. doi: 10.1039/c0ib00075b

Dai, N., Schaffer, A., Petreikov, M., Shahak, Y., Giller, Y., Ratner, K., et al. (1999). Overexpression of Arabidopsis hexokinase in tomato plants inhibits growth, reduces photosynthesis, and induces rapid senescence. *Plant Cell* 11, 1253–1266. doi: 10.1105/tpc.11.7.1253

DalCorso, G., Pesaresi, P., Masiero, S., Aseeva, E., Schünemann, D., Finazzi, G., et al. (2008). A complex containing PGRL1 and PGR5 is involved in the switch between linear and cyclic electron flow in Arabidopsis. *Cell* 132, 273–285. doi: 10.1016/j.cell.2007.12.028

De Souza, A. P., Wang, Y., Orr, D. J., Carmo-Silva, E., and Long, S. P. (2020). Photosynthesis across African cassava germplasm is limited by Rubisco and mesophyll conductance at steady state, but by stomatal conductance in fluctuating light. *New Phytol.* 225, 2498–2512. doi: 10.1111/nph.16142

Depège, N., Bellafiore, S., and Rochaix, J.-D. (2003). Role of chloroplast protein kinase Stt7 in LHCII phosphorylation and state transition in Chlamydomonas. *Science* 299, 1572–1575. doi: 10.1126/science.1081397

Derks, A., Schaven, K., and Bruce, D. (2015). Diverse mechanisms for photoprotection in photosynthesis. Dynamic regulation of photosystem II excitation in response to rapid environmental change. *Biochim. Biophys. Acta* 1847, 468–485. doi: 10.1016/j.bbabio.2015.02.008

Driever, S. M., and Baker, N. R. (2011). The water–water cycle in leaves is not a major alternative electron sink for dissipation of excess excitation energy when CO_2 assimilation is restricted. *Plant Cell Environ.* 34, 837–846. doi: 10.1111/j.1365-3040.2011.02288.x

Dunford, R. P., Durrant, M. C., Catley, M. A., and Dyer, T. A. (1998). Location of the redox-active cysteines in chloroplast sedoheptulose-1, 7-bisphosphatase indicates that its allosteric regulation is similar but not identical to that of fructose-1, 6-bisphosphatase. *Photosynth. Res.* 58, 221–230. doi: 10.1023/A:1006178826976

Dyson, B. C., Allwood, J. W., Feil, R., Xu, Y., Miller, M., Bowsher, C. G., et al. (2015). Acclimation of metabolism to light in *Arabidopsis thaliana*: the glucose 6-phosphate/phosphate translocator GPT2 directs metabolic acclimation. *Plant Cell Environ.* 38, 1404–1417. doi: 10.1111/pce.12495

Eisenhut, M., Roell, M. S., and Weber, A. P. M. (2019). Mechanistic understanding of photorespiration paves the way to a new green revolution. *New Phytol.* 223, 1762–1769. doi: 10.1111/nph.15872

El Bissati, K., and Kirilovsky, D. (2001). Regulation of psbA and psaE expression by light quality in Synechocystis species PCC 6803. A redox control mechanism. *Plant Physiol.* 125, 1988–2000. doi: 10.1104/pp.125.4.1988

Ensminger, I., Busch, F., and Huner, N. P. A. (2006). Photostasis and cold acclimation: sensing low temperature through photosynthesis. *Physiol. Plant.* 126, 28–44. doi: 10.1111/j.1399-3054.2006.00627.x

Eskins, K., Jiang, C. Z., and Shibles, R. (1991). Light-quality and irradiance effects on pigments, light-harvesting proteins and Rubisco activity in a chlorophyll-and light- harvesting-deficient soybean mutant. *Physiol. Plant.* 83, 47–53. doi: 10.1111/j.1399-3054.1991.tb01280.x

Estavillo, G. M., Crisp, P. A., Pornsiriwong, W., Wirtz, M., Collinge, D., Carrie, C., et al. (2011). Evidence for a SAL1-PAP chloroplast retrograde pathway that functions in drought and high light signaling in Arabidopsis. *Plant Cell* 23, 3992–4012. doi: 10.1105/tpc.111.091033

Evans, J. (1988). Acclimation by the thylakoid membranes to growth irradiance and the partitioning of nitrogen between soluble and thylakoid proteins. *Funct. Plant Biol.* 15:93. doi: 10.1071/PP9880093

Exposito-Rodriguez, M., Laissue, P. P., Yvon-Durocher, G., Smirnoff, N., and Mullineaux, P. M. (2017). Photosynthesis-dependent H_2O_2 transfer from chloroplasts to nuclei provides a high-light signalling mechanism. *Nat. Commun.* 8, 1–11. doi: 10.1038/s41467-017-00074-w

Farquhar, G. D., Von Caemmerer, S., and Berry, J. A. (2001). Models of photosynthesis. *Plant Physiol.* 125, 42–45. doi: 10.1104/pp.125.1.42

Farquhar, G. D., von Caemmerer, S., von, and Berry, J. A. (1980). A biochemical model of photosynthetic CO_2 assimilation in leaves of C_3 species. *Planta* 149, 78–90. doi: 10.1007/BF00386231

Fey, V., Wagner, R., Bräutigam, K., and Pfannschmidt, T. (2005a). Photosynthetic redox control of nuclear gene expression. *J. Exp. Bot.* 56, 1491–1498. doi: 10.1093/jxb/eri180

Fey, V., Wagner, R., Braütigam, K., Wirtz, M., Hell, R., Dietzmann, A., et al. (2005b). Retrograde plastid redox signals in the expression of nuclear genes for chloroplast proteins of *Arabidopsis thaliana*. *J. Biol. Chem.* 280, 5318–5328. doi: 10.1074/jbc.M406358200

Finazzi, G., and Johnson, G. N. (2016). Cyclic electron flow: facts and hypotheses. *Photosynth. Res.* 129, 227–230. doi: 10.1007/s11120-016-0306-2

Finazzi, G., Petroutsos, D., Tomizioli, M., Flori, S., Sautron, E., Villanova, V., et al. (2015). Ions channels/transporters and chloroplast regulation. *Cell Calcium* 58, 86–97. doi: 10.1016/j.ceca.2014.10.002

Foo, C. C., Burgess, A. J., Retkute, R., Tree-Intong, P., Ruban, A. V., and Murchie, E. H. (2020). Photoprotective energy dissipation is greater in the lower, not the upper, regions of a rice canopy: a 3D analysis. *J. Exp. Bot.* 71, 7382–7392. doi: 10.1093/jxb/eraa411

Foyer, C. H. (2018). Reactive oxygen species, oxidative signaling and the regulation of photosynthesis. *Environ. Exp. Bot.* 154, 134–142. doi: 10.1016/j.envexpbot.2018.05.003

Foyer, C. H., Bloom, A. J., Queval, G., and Noctor, G. (2009). Photorespiratory metabolism: genes, mutants, energetics, and redox signaling. *Annu. Rev. Plant Biol.* 60, 455–484. doi: 10.1146/annurev.arplant.043008.091948

Foyer, C. H., Neukermans, J., Queval, G., Noctor, G., and Harbinson, J. (2012). Photosynthetic control of electron transport and the regulation of gene expression. *J. Exp. Bot.* 63, 1637–1661. doi: 10.1093/jxb/ers013

Fristedt, R., Carlberg, I., Zygadlo, A., Piippo, M., Nurmi, M., Aro, E.-M., et al. (2009). Intrinsically unstructured phosphoprotein TSP9 regulates light harvesting in *Arabidopsis thaliana*. *Biochemistry* 48, 499–509. doi: 10.1021/bi8016334

Galvis, V. C., Strand, D. D., Messer, M., Thiele, W., Bethmann, S., Hübner, D., et al. (2020). H+ transport by K+ EXCHANGE ANTIPORTER3 promotes photosynthesis and growth in chloroplast ATP synthase mutants. *Plant Physiol.* 182, 2126–2142. doi: 10.1104/pp.19.01561

Geigenberger, P., Thormählen, I., Daloso, D. M., and Fernie, A. R. (2017). The unprecedented versatility of the plant thioredoxin system. *Trends Plant Sci.* 22, 249–262. doi: 10.1016/j.tplants.2016.12.008

Geritz, S. A., and Kisdi, É. (2012). Mathematical ecology: why mechanistic models? *J. Math. Biol.* 65, 1411. doi: 10.1007/s00285-011-0496-3

Gillespie, D. T. (2000). The chemical Langevin equation. *J. Chem. Phys.* 113, 297–306. doi: 10.1063/1.481811

Gollan, P. J., Tikkanen, M., and Aro, E.-M. (2015). Photosynthetic light reactions: integral to chloroplast retrograde signalling. *Curr. Opin. Plant Biol.* 27, 180–191. doi: 10.1016/j.pbi.2015.07.006

Gomes de Oliveira Dal'Molin, C., Quek, L.-E., Saa, P. A., and Nielsen, L. K. (2015). A multi-tissue genome-scale metabolic modeling framework for the analysis of whole plant systems. *Front. Plant Sci.* 6:4. doi: 10.3389/fpls.2015.00004

Grafahrend-Belau, E., Junker, A., Eschenröder, A., Müller, J., Schreiber, F., and Junker, B. H. (2013). Multiscale metabolic modeling: dynamic flux balance analysis on a whole-plant scale. *Plant Physiol.* 163, 637–647. doi: 10.1104/pp.113.224006

Granot, D., Kelly, G., Stein, O., and David-Schwartz, R. (2014). Substantial roles of hexokinase and fructokinase in the effects of sugars on plant physiology and development. *J. Exp. Bot.* 65, 809–819. doi: 10.1093/jxb/ert400

Grieco, M., Jain, A., Ebersberger, I., and Teige, M. (2016). An evolutionary view on thylakoid protein phosphorylation uncovers novel phosphorylation hotspots with potential functional implications. *J. Exp. Bot.* 67, 3883–3896. doi: 10.1093/jxb/erw164

Grieco, M., Tikkanen, M., Paakkarinen, V., Kangasjärvi, S., and Aro, E.-M. (2012). Steady-state phosphorylation of light-harvesting complex II proteins preserves photosystem I under fluctuating white light. *Plant Physiol.* 160, 1896–1910. doi: 10.1104/pp.112.206466

Guerriero, M. L., Akman, O. E., and van Ooijen, G. (2014). Stochastic models of cellular circadian rhythms in plants help to understand the impact of noise on robustness and clock structure. *Front. Plant Sci.* 5:564. doi: 10.3389/fpls.2014.00564

Harley, P. C., and Tenhunen, J. D. (1991). Modeling the photosynthetic response of C3 leaves to environmental factors. *Model. Crop Photosynth. Biochem.* 19, 17–39. doi: 10.2135/cssaspecpub19.c2

Hasdemir, D., Hoefsloot, H. C. J., Westerhuis, J. A., and Smilde, A. K. (2014). How informative is your kinetic model?: using resampling methods for model invalidation. *BMC Syst. Biol.* 8:61. doi: 10.1186/1752-0509-8-61

Häusler, R. E., Heinrichs, L., Schmitz, J., and Flügge, U.-I. (2014). How sugars might coordinate chloroplast and nuclear gene expression during acclimation to high light intensities. *Mol. Plant* 7, 1121–1137. doi: 10.1093/mp/ssu064

Havaux, M. (2014). Carotenoid oxidation products as stress signals in plants. *Plant J.* 79, 597–606. doi: 10.1111/tpj.12386

Henmi, T., Miyao, M., and Yamamoto, Y. (2004). Release and reactive-oxygen-mediated damage of the oxygen-evolving complex subunits of PSII during photoinhibition. *Plant Cell Physiol.* 45, 243–250. doi: 10.1093/pcp/pch027

Henzinger, T. A. (2000). "The theory of hybrid automata," in *Verification of Digital and Hybrid Systems*, eds M. Kemal Inan and R. P. Kurshan (Cham: Springer), 265–292. doi: 10.1007/978-3-642-59615-5_13

Herdean, A., Teardo, E., Nilsson, A. K., Pfeil, B. E., and Johansson, O. N., Ünnep, R., et al. (2016). A voltage-dependent chloride channel fine-tunes photosynthesis in plants. *Nat. Commun.* 7, 1–11. doi: 10.1038/ncomms11654

Herrmann, H. A., Dyson, B. C., Vass, L., Johnson, G. N., and Schwartz, J.-M. (2019a). Flux sampling is a powerful tool to study metabolism

under changing environmental conditions. *NPJ Syst. Biol. Appl.* 5, 1–8. doi: 10.1038/s41540-019-0109-0

Herrmann, H. A., Schwartz, J.-M., and Johnson, G. N. (2019b). Metabolic acclimation—a key to enhancing photosynthesis in changing environments? *J. Exp. Bot.* 70, 3043–3056. doi: 10.1093/jxb/erz157

Herrmann, H. A., Schwartz, J.-M., and Johnson, G. N. (2020). From empirical to theoretical models of light response curves-linking photosynthetic and metabolic acclimation. *Photosynth. Res.* 145, 5–14. doi: 10.1007/s11120-019-00681-2

Hideg, É., Kálai, T., Hideg, K., and Vass, I. (1998). Photoinhibition of photosynthesis *in vivo* results in singlet oxygen production detection via nitroxide-induced fluorescence quenching in broad bean leaves. *Biochemistry* 37, 11405–11411. doi: 10.1021/bi972890+

Höhner, R., Galvis, V. C., Strand, D. D., Völkner, C., Krämer, M., Messer, M., et al. (2019). Photosynthesis in Arabidopsis is unaffected by the function of the vacuolar K+ channel TPK3. *Plant Physiol.* 180, 1322–1335. doi: 10.1104/pp.19.00255

Horacio, P., and Martinez-Noel, G. (2013). Sucrose signaling in plants: a world yet to be explored. *Plant Signal. Behav.* 8:e23316. doi: 10.4161/psb.23316

Huang, W., Hu, H., and Zhang, S. B. (2015). Photorespiration plays an important role in the regulation of photosynthetic electron flow under fluctuating light in tobacco plants grown under full sunlight. *Front. Plant Sci.* 6:621. doi: 10.3389/fpls.2015.00621

Huang, W., Yang, Y.-J., and Zhang, S.-B. (2019a). Photoinhibition of photosystem I under fluctuating light is linked to the insufficient ΔpH upon a sudden transition from low to high light. *Environ. Exp. Bot.* 160, 112–119. doi: 10.1016/j.envexpbot.2019.01.012

Huang, W., Yang, Y.-J., and Zhang, S.-B. (2019b). The role of water-water cycle in regulating the redox state of photosystem I under fluctuating light. *Biochim. Biophys. Acta* 1860, 383–390. doi: 10.1016/j.bbabio.2019.03.007

Hummer, G., and Szabo, A. (2015). Optimal dimensionality reduction of multistate kinetic and Markov-state models. *J. Phys. Chem. B* 119, 9029–9037. doi: 10.1021/jp508375q

Hurry, V., Strand, Å., Furbank, R., and Stitt, M. (2000). The role of inorganic phosphate in the development of freezing tolerance and the acclimatization of photosynthesis to low temperature is revealed by the pho mutants of *Arabidopsis thaliana*. *Plant J.* 24, 383–396. doi: 10.1046/j.1365-313x.2000.00888.x

Ibrahim, I. M., Wu, H., Ezhov, R., Kayanja, G. E., Zakharov, S. D., Du, Y., et al. (2020). An evolutionarily conserved iron-sulfur cluster underlies redox sensory function of the Chloroplast Sensor Kinase. *Commun. Biol.* 3, 1–11. doi: 10.1038/s42003-019-0728-4

Jamshidi, N., and Palsson, B. Ø. (2010). Mass action stoichiometric simulation models: incorporating kinetics and regulation into stoichiometric models. *Biophys. J.* 98, 175–185. doi: 10.1016/j.bpj.2009.09.064

Jang, J.-C., León, P., Zhou, L., and Sheen, J. (1997). Hexokinase as a sugar sensor in higher plants. *Plant Cell* 9, 5–19. doi: 10.1105/tpc.9.1.5

Johnson, G., and Murchie, E. (2011). "Gas exchange measurements for the determination of photosynthetic efficiency in Arabidopsis leaves," in *Chloroplast Research in Arabidopsis*, ed R. Paul Jarvis (Totowa, NJ: Humana Press), 311–326. doi: 10.1007/978-1-61779-237-3_17

Johnson, M. P., and Ruban, A. V. (2009). Photoprotective energy dissipation in higher plants involves alteration of the excited state energy of the emitting chlorophyll(s) in the light harvesting antenna II (LHCII). *J. Biol. Chem.* 284, 23592–23601. doi: 10.1074/jbc.M109.013557

Johnson, M. P., and Wientjes, E. (2020). BBA - Bioenergetics The relevance of dynamic thylakoid organisation to photosynthetic. *Biochim. Biophys. Acta* 1861:148039. doi: 10.1016/j.bbabio.2019.06.011

Joliot, P., and Johnson, G. N. (2011). Regulation of cyclic and linear electron flow in higher plants. *Proc. Natl. Acad. Sci. U.S.A.* 108, 13317–13322. doi: 10.1073/pnas.1110189108

Jossier, M., Bouly, J., Meimoun, P., Arjmand, A., Lessard, P., Hawley, S., et al. (2009). SnRK1 (SNF1-related kinase 1) has a central role in sugar and ABA signalling in *Arabidopsis thaliana*. *Plant J.* 59, 316–328. doi: 10.1111/j.1365-313X.2009.03871.x

Kaiser, E., Matsubara, S., Harbinson, J., Heuvelink, E., and Marcelis, L. F. M. (2018). Acclimation of photosynthesis to lightflecks in tomato leaves: interaction with progressive shading in a growing canopy. *Physiol. Plant.* 162, 506–517. doi: 10.1111/ppl.12668

Karpiński, S., Szechyńska-Hebda, M., Wituszyńska, W., and Burdiak, P. (2013). Light acclimation, retrograde signalling, cell death and immune defences in plants. *Plant Cell Environ.* 36, 736–744. doi: 10.1111/pce.12018

Kelly, G., Moshelion, M., David-Schwartz, R., Halperin, O., Wallach, R., Attia, Z., et al. (2013). Hexokinase mediates stomatal closure. *Plant J.* 75, 977–988. doi: 10.1111/tpj.12258

Kim, C. (2020). ROS-driven oxidative modification: its impact on chloroplasts-nucleus communication. *Front. Plant Sci.* 10:1729. doi: 10.3389/fpls.2019.01729

Kim, J. H., Glick, R. E., and Melis, A. (1993). Dynamics of photosystem stoichiometry adjustment by light quality in chloroplasts. *Plant Physiol.* 102, 181–190. doi: 10.1104/pp.102.1.181

Kimura, H., Hashimoto-Sugimoto, M., Iba, K., Terashima, I., and Yamori, W. (2020). Improved stomatal opening enhances photosynthetic rate and biomass production in fluctuating light. *J. Exp. Bot.* 71, 2339–2350. doi: 10.1093/jxb/eraa090

Kimura, M., Yamamoto, Y. Y., Seki, M., Sakurai, T., Sato, M., Abe, T., et al. (2003). Identification of arabidopsis genes regulated by high light–stress using cDNA microarray. *Photochem. Photobiol.* 77, 226–233. doi: 10.1562/0031-8655(2003)0770226IOAGRB2.0.CO2

Kirschbaum, M. U. F., Küppers, M., Schneider, H., Giersch, C., and Noe, S. (1997). Modelling photosynthesis in fluctuating light with inclusion of stomatal conductance, biochemical activation and pools of key photosynthetic intermediates. *Planta* 204, 16–26. doi: 10.1007/s004250050225

Kitano, H. (2002). Systems biology: a brief overview. *Science* 295, 1662–1664. doi: 10.1126/science.1069492

Kono, M., Noguchi, K., and Terashima, I. (2014). Roles of the cyclic electron flow around PSI (CEF-PSI) and O 2-dependent alternative pathways in regulation of the photosynthetic electron flow in short-term fluctuating light in *Arabidopsis thaliana*. *Plant Cell Physiol.* 55, 990–1004. doi: 10.1093/pcp/pcu033

Kono, M., and Terashima, I. (2016). Elucidation of photoprotective mechanisms of PSI against fluctuating light photoinhibition. *Plant Cell Physiol.* 57, 1405–1414. doi: 10.1093/pcp/pcw103

Kotsiantis, S. B., Zaharakis, I., and Pintelas, P. (2007). Supervised machine learning: A review of classification techniques. *Emerg. Artif. Intell. Appl. Comput. Eng.* 160, 3–24. doi: 10.1007/s10462-007-9052-3

Krieger-Liszkay, A., Fufezan, C., and Trebst, A. (2008). Singlet oxygen production in photosystem II and related protection mechanism. *Photosynth. Res.* 98, 551–564. doi: 10.1007/s11120-008-9349-3

Kromdijk, J., Głowacka, K., Leonelli, L., Gabilly, S. T., Iwai, M., Niyogi, K. K., et al. (2016). Improving photosynthesis and crop productivity by accelerating recovery from photoprotection. *Science* 354, 857–861. doi: 10.1126/science.aai8878

Kunz, H. H., Häusler, R. E., Fettke, J., Herbst, K., Niewiadomski, P., Gierth, M., et al. (2010). The role of plastidial glucose-6-phosphate/phosphate translocators in vegetative tissues of *Arabidopsis thaliana* mutants impaired in starch biosynthesis. *Plant Biol.* 12, 115–128. doi: 10.1111/j.1438-8677.2010.00349.x

Kyle, D. J., Staehelin, L. A., and Arntzen, C. J. (1983). Lateral mobility of the light-harvesting complex in chloroplast membranes controls excitation energy distribution in higher plants. *Arch. Biochem. Biophys.* 222, 527–541. doi: 10.1016/0003-9861(83)90551-9

Larsson, U. K., Jergil, B., and Andersson, B. (1983). Changes in the lateral distribution of the light-harvesting chlorophyll-a/b—protein complex induced by its phosphorylation. *Eur. J. Biochem.* 136, 25–29. doi: 10.1111/j.1432-1033.1983.tb07700.x

Lefebvre, S., Lawson, T., Fryer, M., Zakhleniuk, O. V., Lloyd, J. C., and Raines, C. A. (2005). Increased sedoheptulose-1, 7-bisphosphatase activity in transgenic tobacco plants stimulates photosynthesis and growth from an early stage in development. *Plant Physiol.* 138, 451–460. doi: 10.1104/pp.104.055046

Leister, D. (2019). Piecing the puzzle together: the central role of reactive oxygen species and redox hubs in chloroplast retrograde signaling. *Antioxid. Redox Signal.* 30, 1206–1219. doi: 10.1089/ars.2017.7392

Lemaire, S. D., Michelet, L., Zaffagnini, M., Massot, V., and Issakidis-Bourguet, E. (2007). Thioredoxins in chloroplasts. *Curr. Genet.* 51, 343–365. doi: 10.1007/s00294-007-0128-z

Lemeille, S., and Rochaix, J.-D. (2010). State transitions at the crossroad of thylakoid signalling pathways. *Photosynth. Res.* 106, 33–46. doi: 10.1007/s11120-010-9538-8

Leong, T.-Y., and Anderson, J. M. (1984). Adaptation of the thylakoid membranes of pea chloroplasts to light intensities. I. Study on the distribution of chlorophyll-protein complexes. *Photosynth. Res.* 5, 105–115. doi: 10.1007/BF00028524

Lewis, N. E., Nagarajan, H., and Palsson, B. O. (2012). Constraining the metabolic genotype–phenotype relationship using a phylogeny of *in silico* methods. *Nat. Rev. Microbiol.* 10, 291–305. doi: 10.1038/nrmicro2737

Louarn, G., Frak, E., Zaka, S., Prieto, J., and Lebon, E. (2015). An empirical model that uses light attenuation and plant nitrogen status to predict within-canopy nitrogen distribution and upscale photosynthesis from leaf to whole canopy. *AoB Plants* 7:plv116. doi: 10.1093/aobpla/plv116

Lunn, J. E., Feil, R., Hendriks, J. H. M., Gibon, Y., Morcuende, R., Osuna, D., et al. (2006). Sugar-induced increases in trehalose 6-phosphate are correlated with redox activation of ADPglucose pyrophosphorylase and higher rates of starch synthesis in *Arabidopsis thaliana*. *Biochem. J.* 397, 139–148. doi: 10.1042/BJ20060083

Mahadevan, R., Edwards, J. S., and Doyle, F. J III. (2002). Dynamic flux balance analysis of diauxic growth in *Escherichia coli*. *Biophys. J.* 83, 1331–1340. doi: 10.1016/S0006-3495(02)73903-9

Maruta, T., Noshi, M., Tanouchi, A., Tamoi, M., Yabuta, Y., Yoshimura, K., et al. (2012). H_2O_2-triggered retrograde signaling from chloroplasts to nucleus plays specific role in response to stress. *J. Biol. Chem.* 287, 11717–11729. doi: 10.1074/jbc.M111.292847

Matsubara, S., Schneider, T., and Maurino, V. G. (2016). Dissecting long-term adjustments of photoprotective and photo-oxidative stress acclimation occurring in dynamic light environments. *Front. Plant Sci.* 7:1690. doi: 10.3389/fpls.2016.01690

Matthews, J. S. A., Vialet-Chabrand, S., and Lawson, T. (2018). Acclimation to fluctuating light impacts the rapidity of response and diurnal rhythm of stomatal conductance. *Plant Physiol.* 176, 1939–1951. doi: 10.1104/pp.17.01809

Mekala, N. R., Suorsa, M., Rantala, M., Aro, E.-M., and Tikkanen, M. (2015). Plants actively avoid state transitions upon changes in light intensity: role of light-harvesting complex II protein dephosphorylation in high light. *Plant Physiol.* 168, 721–734. doi: 10.1104/pp.15.00488

Mélykúti, B., Burrage, K., and Zygalakis, K. C. (2010). Fast stochastic simulation of biochemical reaction systems by alternative formulations of the chemical Langevin equation. *J. Chem. Phys.* 132:164109. doi: 10.1063/1.3380661

Mengin, V., Pyl, E., Alexandre Moraes, T., Sulpice, R., Krohn, N., Encke, B., et al. (2017). Photosynthate partitioning to starch in *Arabidopsis thaliana* is insensitive to light intensity but sensitive to photoperiod due to a restriction on growth in the light in short photoperiods. *Plant Cell Environ.* 40, 2608–2627. doi: 10.1111/pce.13000

Michelet, L., Zaffagnini, M., Morisse, S., Sparla, F., Pérez-Pérez, M. E., Francia, F., et al. (2013). Redox regulation of the Calvin-Benson cycle: something old, something new. *Front. Plant Sci.* 4:470. doi: 10.3389/fpls.2013.00470

Miller, M. A. E., O'Cualain, R., Selley, J., Knight, D., Karim, M. F., Hubbard, S. J., et al. (2017). Dynamic acclimation to high light in *Arabidopsis thaliana* involves widespread reengineering of the leaf proteome. *Front. Plant Sci.* 8:1239. doi: 10.3389/fpls.2017.01239

Minagawa, J. (2011). State transitions—the molecular remodeling of photosynthetic supercomplexes that controls energy flow in the chloroplast. *Biochim. Biophys. Acta* 1807, 897–905. doi: 10.1016/j.bbabio.2010.11.005

Mjolsness, E., and DeCoste, D. (2001). Machine learning for science: state of the art and future prospects. *Science* 293, 2051–2055. doi: 10.1126/science.293.5537.2051

Mochizuki, N., Tanaka, R., Tanaka, A., Masuda, T., and Nagatani, A. (2008). The steady-state level of Mg-protoporphyrin IX is not a determinant of plastid-to-nucleus signaling in Arabidopsis. *Proc. Natl. Acad. Sci. U.S.A.* 105, 15184–15189. doi: 10.1073/pnas.0803245105

Moore, B., Zhou, L., Rolland, F., Hall, Q., Cheng, W.-H., Liu, Y.-X., et al. (2003). Role of the Arabidopsis glucose sensor HXK1 in nutrient, light, and hormonal signaling. *Science* 300, 332–336. doi: 10.1126/science.1080585

Mott, K. A., and Woodrow, I. E. (2000). Modelling the role of Rubisco activase in limiting non-steady-state photosynthesis. *J. Exp. Bot.* 51, 399–406. doi: 10.1093/jexbot/51.suppl_1.399

Moulin, M., McCormac, A. C., Terry, M. J., and Smith, A. G. (2008). Tetrapyrrole profiling in Arabidopsis seedlings reveals that retrograde plastid nuclear signaling is not due to Mg-protoporphyrin IX accumulation. *Proc. Natl. Acad. Sci. U.S.A.* 105, 15178–15183. doi: 10.1073/pnas.0803054105

Munekage, Y., Hojo, M., Meurer, J., Endo, T., Tasaka, M., and Shikanai, T. (2002). PGR5 is involved in cyclic electron flow around photosystem I and is essential for photoprotection in Arabidopsis. *Cell* 110, 361–371. doi: 10.1016/S0092-8674(02)00867-X

Munekage, Y. N., Genty, B., and Peltier, G. (2008). Effect of PGR5 impairment on photosynthesis and growth in *Arabidopsis thaliana*. *Plant Cell Physiol.* 49, 1688–1698. doi: 10.1093/pcp/pcn140

Murchie, E. H., and Horton, P. (1998). Contrasting patterns of photosynthetic acclimation to the light environment are dependent on the differential expression of the responses to altered irradiance and spectral quality. *Plant Cell Environ.* 21, 139–148. doi: 10.1046/j.1365-3040.1998.00262.x

Nägele, T., and Weckwerth, W. (2014). Mathematical modeling reveals that metabolic feedback regulation of SnRK1 and hexokinase is sufficient to control sugar homeostasis from energy depletion to full recovery. *Front. Plant Sci.* 5:365. doi: 10.3389/fpls.2014.00365

Nakano, H., Yamamoto, H., and Shikanai, T. (2019). Contribution of NDH-dependent cyclic electron transport around photosystem I to the generation of proton motive force in the weak mutant allele of pgr5. *Biochim. Biophys. Acta* 1860, 369–374. doi: 10.1016/j.bbabio.2019.03.003

Nandha, B., Finazzi, G., Joliot, P., Hald, S., and Johnson, G. N. (2007). The role of PGR5 in the redox poising of photosynthetic electron transport. *Biochim. Biophys. Acta* 1767, 1252–1259. doi: 10.1016/j.bbabio.2007.07.007

Nawrocki, W. J., Bailleul, B., Picot, D., Cardol, P., Rappaport, F., Wollman, F.-A., et al. (2019). The mechanism of cyclic electron flow. *Biochim. Biophys. Acta* 1860, 433–438. doi: 10.1016/j.bbabio.2018.12.005

Niedermaier, S., Schneider, T., Bahl, M.-O., Matsubara, S., and Huesgen, P. F. (2020). Photoprotective acclimation of the *Arabidopsis thaliana* leaf proteome to fluctuating light. *Front. Genet.* 11:154. doi: 10.3389/fgene.2020.00154

Niewiadomski, P., Knappe, S., Geimer, S., Fischer, K., Schulz, B., Unte, U. S., et al. (2005). The Arabidopsis plastidic glucose 6-phosphate/phosphate translocator GPT1 is essential for pollen maturation and embryo sac development. *Plant Cell* 17, 760–775. doi: 10.1105/tpc.104.029124

Niinemets, Ü., Kull, O., and Tenhunen, J. D. (1998). An analysis of light effects on foliar morphology, physiology, and light interception in temperate deciduous woody species of contrasting shade tolerance. *Tree Physiol.* 18, 681–696. doi: 10.1093/treephys/18.10.681

Nikkanen, L., and Rintamäki, E. (2014). Thioredoxin-dependent regulatory networks in chloroplasts under fluctuating light conditions. *Philos. Trans. R. Soc. Lond. B Biol. Sci.* 369:20130224. doi: 10.1098/rstb.2013.0224

Nikkanen, L., Toivola, J., Diaz, M. G., and Rintamäki, E. (2017). Chloroplast thioredoxin systems: prospects for improving photosynthesis. *Philos. Trans. R. Soc. B Biol. Sci.* 372:20160474. doi: 10.1098/rstb.2016.0474

Niyogi, K. K. (2009). Photoprotection and High Light Responses. *Chlamydomonas Sourceb. 3-Vol set* 2, 847–870. doi: 10.1016/B978-0-12-370873-1.00031-9

Nott, A., Jung, H.-S., Koussevitzky, S., and Chory, J. (2006). Plastid-to-nucleus retrograde signaling. *Annu. Rev. Plant Biol.* 57, 739–759. doi: 10.1146/annurev.arplant.57.032905.105310

Pamplin, E. J., and Chapman, J. M. (1975). Sucrose suppression of chlorophyll synthesis in tissue culture: changes in the activity of the enzymes of the chlorophyll biosynthetic pathway. *J. Exp. Bot.* 26, 212–220. doi: 10.1093/jxb/26.2.212

Papanatsiou, M., Petersen, J., Henderson, L., Wang, Y., Christie, J. M., and Blatt, M. R. (2019). Optogenetic manipulation of stomatal kinetics improves carbon assimilation,water use, and growth. *Science* 363, 1456–1459. doi: 10.1126/science.aaw0046

Pascal, A., a, Liu, Z., Broess, K., van Oort, B., van Amerongen, H., Wang, C., et al. (2005). Molecular basis of photoprotection and control of photosynthetic light-harvesting. *Nature* 436, 134–137. doi: 10.1038/nature03795

Peak, D., West, J. D., Messinger, S. M., and Mott, K. A. (2004). Evidence for complex, collective dynamics and emergent, distributed computation in plants. *Proc. Natl. Acad. Sci. U.S.A.* 101, 918–922. doi: 10.1073/pnas.0307811100

Pearcy, R. W. (1990). Sunflecks and photosynthesis in plant canopies. *Annu. Rev. Plant Biol.* 41, 421–453. doi: 10.1146/annurev.pp.41.060190.002225

Pearcy, R. W., Gross, L. J., and He, D. (1997). An improved dynamic model of photosynthesis for estimation of carbon gain in sunfleck light regimes. *Plant Cell Environ.* 20, 411–424. doi: 10.1046/j.1365-3040.1997.d01-88.x

Pesaresi, P., Hertle, A., Pribil, M., Kleine, T., Wagner, R., Strissel, H., et al. (2009). Arabidopsis STN7 kinase provides a link between short- and long-term photosynthetic acclimation. *Plant Cell* 21, 2402–2423. doi: 10.1105/tpc.108.064964

Pfannschmidt, T., Bräutigam, K., Wagner, R., Dietzel, L., Schröter, Y., Steiner, S., et al. (2009). Potential regulation of gene expression in photosynthetic cells by redox and energy state: approaches towards better understanding. *Ann. Bot.* 103, 599–607. doi: 10.1093/aob/mcn081

Pfannschmidt, T., Nilsson, A., and Allen, J. F. (1999). Photosynthetic control of chloroplast gene expression. *Nature* 397, 625–628. doi: 10.1038/17624

Pietrzykowska, M., Suorsa, M., Semchonok, D. A., Tikkanen, M., Boekema, E. J., Aro, E.-M., et al. (2014). The light-harvesting chlorophyll a/b binding proteins Lhcb1 and Lhcb2 play complementary roles during state transitions in Arabidopsis. *Plant Cell* 26, 3646–3660. doi: 10.1105/tpc.114.127373

Ponnu, J., Wahl, V., and Schmid, M. (2011). Trehalose-6-phosphate: connecting plant metabolism and development. *Front. Plant Sci.* 2:70. doi: 10.3389/fpls.2011.00070

Poolman, M. G., Fell, D. A., and Thomas, S. (2000). Modelling photosynthesis and its control. *J. Exp. Bot.* 51, 319–328. doi: 10.1093/jexbot/51.suppl_1.319

Porcar-Castell, A., Bäck, J., Juurola, E., and Hari, P. (2006). Dynamics of the energy flow through photosystem II under changing light conditions: a model approach. *Funct. Plant Biol.* 33, 229–239. doi: 10.1071/FP05133

Pospíšil, P. (2012). Molecular mechanisms of production and scavenging of reactive oxygen species by photosystem II. *Biochim. Biophys. Acta* 1817, 218–231. doi: 10.1016/j.bbabio.2011.05.017

Pospíšil, P. (2016). Production of reactive oxygen species by photosystem II as a response to light and temperature stress. *Front. Plant Sci.* 7:1950. doi: 10.3389/fpls.2016.01950

Pribil, M., Pesaresi, P., Hertle, A., Barbato, R., and Leister, D. (2010). Role of plastid protein phosphatase TAP38 in LHCII dephosphorylation and thylakoid electron flow. *PLoS Biol.* 8:e1000288. doi: 10.1371/journal.pbio.1000288

Purvis, J. E., Radhakrishnan, R., and Diamond, S. L. (2009). Steady-state kinetic modeling constrains cellular resting states and dynamic behavior. *PLoS Comput Biol* 5:e1000298. doi: 10.1371/journal.pcbi.1000298

Puthiyaveetil, S., Kavanagh, T. A., Cain, P., Sullivan, J. A., Newell, C. A., Gray, J. C., et al. (2008). The ancestral symbiont sensor kinase CSK links photosynthesis with gene expression in chloroplasts. *Proc. Natl. Acad. Sci. U.S.A.* 105, 10061–10066. doi: 10.1073/pnas.0803928105

Qiao, M.-Y., Zhang, Y.-J., Liu, L.-A., Shi, L., Ma, Q.-H., Chow, W. S., et al. (2020). Do rapid photosynthetic responses protect maize leaves against photoinhibition under fluctuating light? *Photosynth. Res.* doi: 10.1007/s11120-020-00780-5. [Epub ahead of print].

Qu, M., Hamdani, S., Li, W., Wang, S., Tang, J., Chen, Z., et al. (2016). Rapid stomatal response to fluctuating light: an under-explored mechanism to improve drought tolerance in rice. *Funct. Plant Biol.* 43, 727–738. doi: 10.1071/FP15348

Ramel, F., Birtic, S., Ginies, C., Soubigou-Taconnat, L., Triantaphylidès, C., and Havaux, M. (2012). Carotenoid oxidation products are stress signals that mediate gene responses to singlet oxygen in plants. *Proc. Natl. Acad. Sci. U.S.A.* 109, 5535–5540. doi: 10.1073/pnas.1115982109

Rascher, U., and Nedbal, L. (2006). Dynamics of photosynthesis in fluctuating light. *Curr. Opin. Plant Biol.* 9, 671–678. doi: 10.1016/j.pbi.2006.09.012

Ratti, E. (2018). 'Models of' and 'Models for': on the relation between mechanistic models and experimental strategies in molecular biology. *Br. J. Philos. Sci.* 71, 773–797. doi: 10.1093/bjps/axy018

Rekarte-Cowie, I., Ebshish, O. S., Mohamed, K. S., and Pearce, R. S. (2008). Sucrose helps regulate cold acclimation of *Arabidopsis thaliana*. *J. Exp. Bot.* 59, 4205–4217. doi: 10.1093/jxb/ern262

Retkute, R., Smith-Unna, S. E., Smith, R. W., Burgess, A. J., Jensen, O. E., Johnson, G. N., et al. (2015). Exploiting heterogeneous environments: does photosynthetic acclimation optimize carbon gain in fluctuating light? *J. Exp. Bot.* 66, 2437–2447. doi: 10.1093/jxb/erv055

Retkute, R., Townsend, A. J., Murchie, E. H., Jensen, O. E., and Preston, S. P. (2018). Three-dimensional plant architecture and sunlit–shaded patterns: a stochastic model of light dynamics in canopies. *Ann. Bot.* 122, 291–302. doi: 10.1093/aob/mcy067

Rook, F., Gerrits, N., Kortstee, A., Van Kampen, M., Borrias, M., Weisbeek, P., et al. (1998). Sucrose-specific signalling represses translation of the Arabidopsis ATB2 bZIP transcription factor gene. *Plant J.* 15, 253–263. doi: 10.1046/j.1365-313X.1998.00205.x

Rott, M., Martins, N. F., Thiele, W., Lein, W., Bock, R., Kramer, D. M., et al. (2011). ATP synthase repression in tobacco restricts photosynthetic electron transport, CO_2 assimilation, and plant growth by overacidification of the thylakoid lumen. *Plant Cell* 23, 304–321. doi: 10.1105/tpc.110.079111

Ruban, A. V., Johnson, M. P., and Duffy, C. D. P. (2012). The photoprotective molecular switch in the photosystem II antenna. *Biochim. Biophys. Acta* 1817, 167–181. doi: 10.1016/j.bbabio.2011.04.007

Ruelland, E., and Miginiac-Maslow, M. (1999). Regulation of chloroplast enzyme activities by thioredoxins: activation or relief from inhibition? *Trends Plant Sci.* 4, 136–141. doi: 10.1016/S1360-1385(99)01391-6

Saeys, Y., Inza, I., and Larranaga, P. (2007). A review of feature selection techniques in bioinformatics. *Bioinformatics* 23, 2507–2517. doi: 10.1093/bioinformatics/btm344

Sahrawy, M., Chueca, A., Hermoso, R., Lázaro, J. J., and Gorgé, J. L. (1997). Directed mutagenesis shows that the preceding region of the chloroplast fructose-1, 6-bisphosphatase regulatory sequence is the thioredoxin docking site. *J. Mol. Biol.* 269, 623–630. doi: 10.1006/jmbi.1997.1054

Schallau, K., and Junker, B. H. (2010). Simulating plant metabolic pathways with enzyme-kinetic models. *Plant Physiol.* 152, 1763–1771. doi: 10.1104/pp.109.149237

Schneider, T., Bolger, A., Zeier, J., Preiskowski, S., Benes, V., Trenkamp, S., et al. (2019). Fluctuating light interacts with time of day and leaf development stage to reprogram gene expression. *Plant Physiol.* 179, 1632–1657. doi: 10.1104/pp.18.01443

Schönberg, A., Rödiger, A., Mehwald, W., Galonska, J., Christ, G., Helm, S., et al. (2017). Identification of STN7/STN8 kinase targets reveals connections between electron transport, metabolism and gene expression. *Plant J.* 90, 1176–1186. doi: 10.1111/tpj.13536

Shapiguzov, A., Ingelsson, B., Samol, I., Andres, C., Kessler, F., Rochaix, J.-D., et al. (2010). The PPH1 phosphatase is specifically involved in LHCII dephosphorylation and state transitions in Arabidopsis. *Proc. Natl. Acad. Sci. U.S.A.* 107, 4782–4787. doi: 10.1073/pnas.0913810107

Shaw, R., and Cheung, C. Y. (2018). A dynamic multi-tissue flux balance model captures carbon and nitrogen metabolism and optimal resource partitioning during Arabidopsis growth. *Front. Plant Sci.* 9:884. doi: 10.3389/fpls.2018.00884

Sheen, J. (1990). Metabolic repression of transcription in higher plants. *Plant Cell* 2, 1027–1038. doi: 10.1105/tpc.2.10.1027

Shikanai, T. (2014). Central role of cyclic electron transport around photosystem I in the regulation of photosynthesis. *Curr. Opin. Biotechnol.* 26, 25–30. doi: 10.1016/j.copbio.2013.08.012

Shimakawa, G., and Miyake, C. (2018). Changing frequency of fluctuating light reveals the molecular mechanism for P700 oxidation in plant leaves. *Plant Direct* 2:e00073. doi: 10.1002/pld3.73

Simkin, A. J., Lopez-Calcagno, P. E., Davey, P. A., Headland, L. R., Lawson, T., Timm, S., et al. (2017). Simultaneous stimulation of sedoheptulose 1, 7-bisphosphatase, fructose 1, 6-bisphophate aldolase and the photorespiratory glycine decarboxylase-H protein increases CO_2 assimilation, vegetative biomass and seed yield in Arabidopsis. *Plant Biotechnol. J.* 15, 805–816. doi: 10.1111/pbi.12676

Simkin, A. J., McAusland, L., Headland, L. R., Lawson, T., and Raines, C. A. (2015). Multigene manipulation of photosynthetic carbon assimilation increases CO_2 fixation and biomass yield in tobacco. *J. Exp. Bot.* 66, 4075–4090. doi: 10.1093/jxb/erv204

Skovsen, E., Snyder, J. W., Lambert, J. D. C., and Ogilby, P. R. (2005). Lifetime and diffusion of singlet oxygen in a cell. *J. Phys. Chem. B* 109, 8570–8573. doi: 10.1021/jp051163i

Snowden, T. J., van der Graaf, P. H., and Tindall, M. J. (2017). Methods of model reduction for large-scale biological systems: a survey of current methods and trends. *Bull. Math. Biol.* 79, 1449–1486. doi: 10.1007/s11538-017-0277-2

Solfanelli, C., Poggi, A., Loreti, E., Alpi, A., and Perata, P. (2006). Sucrose-specific induction of the anthocyanin biosynthetic pathway in Arabidopsis. *Plant Physiol.* 140, 637–646. doi: 10.1104/pp.105.072579

Standfuss, J., Terwisscha van Scheltinga, A. C., Lamborghini, M., and Kühlbrandt, W. (2005). Mechanisms of photoprotection and nonphotochemical quenching in pea light-harvesting complex at 2.5 A resolution. *EMBO J.* 24, 919–928. doi: 10.1038/sj.emboj.7600585

Stegemann, J., Timm, H.-C., and Küppers, M. (1999). Simulation of photosynthetic plasticity in response to highly fluctuating light: an empirical model integrating dynamic photosynthetic induction and capacity. *Trees* 14, 145–160. doi: 10.1007/s004680050219

Stewart, J. J., Adams, W. W., Cohu, C. M., Polutchko, S. K., Lombardi, E. M., and Demmig-Adams, B. (2015). Differences in light-harvesting, acclimation to growth-light environment, and leaf structural development between Swedish and Italian ecotypes of *Arabidopsis thaliana*. *Planta* 242, 1277–1290. doi: 10.1007/s00425-015-2368-3

Stitt, M., and Hurry, V. (2002). A plant for all seasons: alterations in photosynthetic carbon metabolism during cold acclimation in Arabidopsis. *Curr. Opin. Plant Biol.* 5, 199–206. doi: 10.1016/S1369-5266(02)00258-3

Sun, H., Yang, Y.-J., and Huang, W. (2020). The water-water cycle is more effective in regulating redox state of photosystem I under fluctuating light than cyclic electron transport. *Biochim. Biophys.* 1861, 148235. doi: 10.1016/j.bbabio.2020.148235

Suorsa, M., Grieco, M., Järvi, S., Gollan, P. J., Kangasjärvi, S., Tikkanen, M., et al. (2013). PGR5 ensures photosynthetic control to safeguard photosystem I under fluctuating light conditions. *Plant Signal. Behav.* 8:e22741. doi: 10.4161/psb.22741

Suorsa, M., Järvi, S., Grieco, M., Nurmi, M., Pietrzykowska, M., Rantala, M., et al. (2012). PROTON GRADIENT REGULATION5 is essential for proper acclimation of Arabidopsis photosystem I to naturally and artificially fluctuating light conditions. *Plant Cell* 24, 2934–2948. doi: 10.1105/tpc.112.097162

Suorsa, M., Rossi, F., Tadini, L., Labs, M., Colombo, M., Jahns, P., et al. (2016). PGR5-PGRL1-dependent cyclic electron transport modulates linear electron transport rate in *Arabidopsis thaliana*. *Mol. Plant* 9, 271–288. doi: 10.1016/j.molp.2015.12.001

Szechyńska-Hebda, M., and Karpiński, S. (2013). Light intensity-dependent retrograde signalling in higher plants. *J. Plant Physiol.* 170, 1501–1516. doi: 10.1016/j.jplph.2013.06.005

Tabrizi, S. T., Sawicki, A., Zhou, S., Luo, M., and Willows, R. D. (2016). GUN4-protoporphyrin IX is a singlet oxygen generator with consequences for plastid retrograde signaling. *J. Biol. Chem.* 291, 8978–8984. doi: 10.1074/jbc.C116.719989

Takagi, D., Takumi, S., Hashiguchi, M., Sejima, T., and Miyake, C. (2016). Superoxide and singlet oxygen produced within the thylakoid membranes both cause photosystem I photoinhibition. *Plant Physiol.* 171, 1626–1634. doi: 10.1104/pp.16.00246

Takizawa, K., Cruz, J. A., Kanazawa, A., and Kramer, D. M. (2007). The thylakoid proton motive force *in vivo*. Quantitative, non-invasive probes, energetics, and regulatory consequences of light-induced pmf. *Biochim. Biophys. Acta* 1767, 1233–1244. doi: 10.1016/j.bbabio.2007.07.006

Tazoe, Y., Ishikawa, N., Shikanai, T., Ishiyama, K., Takagi, D., Makino, A., et al. (2020). Overproduction of PGR5 enhances the electron sink downstream of photosystem I in a C4 plant, Flaveria bidentis. *Plant J.* 103, 814–823. doi: 10.1111/tpj.14774

Thormählen, I., Zupok, A., Rescher, J., Leger, J., Weissenberger, S., Groysman, J., et al. (2017). Thioredoxins play a crucial role in dynamic acclimation of photosynthesis in fluctuating light. *Mol. Plant* 10, 168–182. doi: 10.1016/j.molp.2016.11.012

Tian, L. (2015). Recent advances in understanding carotenoid-derived signaling molecules in regulating plant growth and development. *Front. Plant Sci.* 6:790. doi: 10.3389/fpls.2015.00790

Tikkanen, M., Grieco, M., Kangasjärvi, S., and Aro, E.-M. (2010). Thylakoid protein phosphorylation in higher plant chloroplasts optimizes electron transfer under fluctuating light. *Plant Physiol.* 152, 723–735. doi: 10.1104/pp.109.150250

Tikkanen, M., Mirva, P., Marjaana, S., Sari, S., Paula, M., Julia, V., et al. (2006). State transitions revisited - A buffering system for dynamic low light acclimation of Arabidopsis. *Plant Mol. Biol.* 62, 779–793. doi: 10.1007/s11103-006-9088-9

Timm, S., and Bauwe, H. (2013). The variety of photorespiratory phenotypes–employing the current status for future research directions on photorespiration. *Plant Biol.* 15, 737–747. doi: 10.1111/j.1438-8677.2012.00691.x

Triantaphylidès, C., and Havaux, M. (2009). Singlet oxygen in plants: production, detoxification and signaling. *Trends Plant Sci.* 14, 219–228. doi: 10.1016/j.tplants.2009.01.008

Tripathy, B. C., and Oelmüller, R. (2012). Reactive oxygen species generation and signaling in plants. *Plant Signal. Behav.* 7, 1621–1633. doi: 10.4161/psb.22455

Uematsu, K., Suzuki, N., Iwamae, T., Inui, M., and Yukawa, H. (2012). Increased fructose 1, 6-bisphosphate aldolase in plastids enhances growth and photosynthesis of tobacco plants. *J. Exp. Bot.* 63, 3001–3009. doi: 10.1093/jxb/ers004

Vass, I. (2012). Molecular mechanisms of photodamage in the Photosystem II complex. *Biochim. Biophys. Acta* 1817, 209–217. doi: 10.1016/j.bbabio.2011.04.014

Vener, A. V., van Kan, P. J. M., Gal, A., Andersson, B., and Ohad, I. (1995). Activation/Deactivation Cycle of Redox-controlled Thylakoid Protein Phosphorylation ROLE OF PLASTOQUINOL BOUND TO THE REDUCED CYTOCHROME bf COMPLEX. *J. Biol. Chem.* 270, 25225–25232. doi: 10.1074/jbc.270.42.25225

Vialet-Chabrand, S., Matthews, J. S. A., Simkin, A. J., Raines, C. A., and Lawson, T. (2017). Importance of fluctuations in light on plant photosynthetic acclimation. *Plant Physiol.* 173, 2163–2179. doi: 10.1104/pp.16.01767

Voss, I., Sunil, B., Scheibe, R., and Raghavendra, A. S. (2013). Emerging concept for the role of photorespiration as an important part of abiotic stress response. *Plant Biol.* 15, 713–722. doi: 10.1111/j.1438-8677.2012.00710.x

Wagner, R., Dietzel, L., Bräutigam, K., Fischer, W., and Pfannschmidt, T. (2008). The long-term response to fluctuating light quality is an important and distinct light acclimation mechanism that supports survival of *Arabidopsis thaliana* under low light conditions. *Planta* 228, 573–587. doi: 10.1007/s00425-008-0760-y

Walters, R. G. (2005). Towards an understanding of photosynthetic acclimation. *J. Exp. Bot*. 56, 435–447. doi: 10.1093/jxb/eri060

Walters, R. G., and Horton, P. (1994). Acclimation of *Arabidopsis thaliana* to the light environment: changes in composition of the photosynthetic apparatus. *Planta* 195, 248–256. doi: 10.1007/BF00199685

Walters, R. G., and Horton, P. (1995). Acclimation of *Arabidopsis thaliana* to the light environment: regulation of chloroplast composition. *Planta* 197, 475–481. doi: 10.1007/BF00196669

Watling, J. R., Robinson, S. A., Woodrow, I. E., and Osmond, C. B. (1997). Responses of rainforest understorey plants to excess light during sunflecks. *Funct. Plant Biol.* 24, 17–25. doi: 10.1071/PP96074

Wei, Z., Duan, F., Sun, X., Song, X., and Zhou, W. (2020). Leaf photosynthetic and anatomical insights into mechanisms of acclimation in rice in response to long-term fluctuating light. *Plant Cell Environ.* 44, 747–761. doi: 10.1111/pce.13954

Wiese, A., Elzinga, N., Wobbes, B., and Smeekens, S. (2004). A conserved upstream open reading frame mediates sucrose-induced repression of translation. *Plant Cell* 16, 1717–1729. doi: 10.1105/tpc.019349

Wilson, K. E., Ivanov, A. G., Öquist, G., Grodzinski, B., Sarhan, F., and Huner, N. P. A. (2006). Energy balance, organellar redox status, and acclimation to environmental stress. *Can. J. Bot.* 84, 1355–1370. doi: 10.1139/B06-098

Wollman, F.-A., and Lemaire, C. (1988). Studies on kinase-controlled state transitions in photosystem II and b6f mutants from Chlamydomonas reinhardtii which lack quinone-binding proteins. *Biochim. Biophys. Acta* 933, 85–94. doi: 10.1016/0005-2728(88)90058-8

Xiao, W., Sheen, J., and Jang, J.-C. (2000). The role of hexokinase in plant sugar signal transduction and growth and development. *Plant Mol. Biol.* 44, 451–461. doi: 10.1023/A:1026501430422

Xiao, Y., Savchenko, T., Baidoo, E. E. K., Chehab, W. E., Hayden, D. M., Tolstikov, V., et al. (2012). Retrograde signaling by the plastidial metabolite MEcPP regulates expression of nuclear stress-response genes. *Cell* 149, 1525–1535. doi: 10.1016/j.cell.2012.04.038

Yabuta, Y., Maruta, T., Yoshimura, K., Ishikawa, T., and Shigeoka, S. (2004). Two distinct redox signaling pathways for cytosolic APX

induction under photooxidative stress. *Plant Cell Physiol.* 45, 1586–1594. doi: 10.1093/pcp/pch181

Yadav, U. P., Ivakov, A., Feil, R., Duan, G. Y., Walther, D., Giavalisco, P., et al. (2014). The sucrose–trehalose 6-phosphate (Tre6P) nexus: specificity and mechanisms of sucrose signalling by Tre6P. *J. Exp. Bot.* 65, 1051–1068. doi: 10.1093/jxb/ert457

Yamamoto, H., and Shikanai, T. (2019). PGR5-dependent cyclic electron flow protects photosystem I under fluctuating light at donor and acceptor sides. *Plant Physiol.* 179, 588–600. doi: 10.1104/pp.18.01343

Yamori, W. (2016). Photosynthetic response to fluctuating environments and photoprotective strategies under abiotic stress. *J. Plant Res.* 129, 379–395. doi: 10.1007/s10265-016-0816-1

Yamori, W., Makino, A., and Shikanai, T. (2016). A physiological role of cyclic electron transport around photosystem I in sustaining photosynthesis under fluctuating light in rice. *Sci. Rep.* 6:20147. doi: 10.1038/srep20147

Yamori, W., Takahashi, S., Makino, A., Price, G. D., Badger, M. R., and von Caemmerer, S. (2011). The roles of ATP synthase and the cytochrome b6/f complexes in limiting chloroplast electron transport and determining photosynthetic capacity. *Plant Physiol.* 155, 956–962. doi: 10.1104/pp.110.168435

Yang, D. H., Webster, J., Adam, Z., Lindahl, M., and Andersson, B. (1998). Induction of acclimative proteolysis of the light-harvesting chlorophyll a/b protein of photosystem II in response to elevated light intensities. *Plant Physiol.* 118, 827–834. doi: 10.1104/pp.118.3.827

Yang, Y.-J., Tan, S.-L., Huang, J.-L., Zhang, S.-B., and Huang, W. (2020). The water-water cycle facilitates photosynthetic regulation under fluctuating light in the epiphytic orchid *Dendrobium officinale*. *Environ. Exp. Bot.* 180:104238. doi: 10.1016/j.envexpbot.2020.104238

Yin, Z.-H., and Johnson, G. N. (2000). Photosynthetic acclimation of higher plants to growth in fluctuating light environments. *Photosynth. Res.* 63, 97–107. doi: 10.1023/A:1006303611365

Zakhartsev, M., Medvedeva, I., Orlov, Y., Akberdin, I., Krebs, O., and Schulze, W. X. (2016). Metabolic model of central carbon and energy metabolisms of growing *Arabidopsis thaliana* in relation to sucrose translocation. *BMC Plant Biol.* 16:262. doi: 10.1186/s12870-016-0868-3

Zavafer, A., Cheah, M. H., Hillier, W., Chow, W. S., and Takahashi, S. (2015). Photodamage to the oxygen evolving complex of photosystem II by visible light. *Sci. Rep.* 5:16363. doi: 10.1038/srep16363

Zeeman, S. C., Smith, S. M., and Smith, A. M. (2004). The breakdown of starch in leaves. *New Phytol.* 163, 247–261. doi: 10.1111/j.1469-8137.2004.01101.x

Zer, H., and Ohad, I. (2003). Light, redox state, thylakoid-protein phosphorylation and signaling gene expression. *Trends Biochem. Sci.* 28, 467–470. doi: 10.1016/S0968-0004(03)00173-7

Zhang, Y., Primavesi, L. F., Jhurreea, D., Andralojc, P. J., Mitchell, R. A. C., Powers, S. J., et al. (2009). Inhibition of SNF1-related protein kinase1 activity and regulation of metabolic pathways by trehalose-6-phosphate. *Plant Physiol.* 149, 1860–1871. doi: 10.1104/pp.108.133934

Zito, F., Finazzi, G., Delosme, R., Nitschke, W., Picot, D., and Wollman, F. (1999). The Qo site of cytochrome b6f complexes controls the activation of the LHCII kinase. *EMBO J.* 18, 2961–2969. doi: 10.1093/emboj/18.11.2961

Zulfugarov, I. S., Tovuu, A., Eu, Y.-J., Dogsom, B., Poudyal, R. S., Nath, K., et al. (2014). Production of superoxide from Photosystem II in a rice (*Oryza sativa* L.) mutant lacking PsbS. *BMC Plant Biol.* 14:242. doi: 10.1186/s12870-014-0242-2

Conflict of Interest: The authors declare that the research was conducted in the absence of any commercial or financial relationships that could be construed as a potential conflict of interest.

frontiers in Plant Science

ORIGINAL RESEARCH
published: 15 April 2021
doi: 10.3389/fpls.2021.659439

Leaf Phenological Stages of Winter Oilseed Rape (*Brassica napus* L.) Have Conserved Photosynthetic Efficiencies but Contrasted Intrinsic Water Use Efficiencies at High Light Intensities

Younès Dellero[1]*, *Mathieu Jossier*[2], *Alain Bouchereau*[1], *Michael Hodges*[2] and *Laurent Leport*[1]

[1] Institute for Genetics, Environment and Plant Protection (IGEPP), National Research Institute for Agriculture, Food and Environment (INRAE), Institut Agro, Université Rennes, Le Rheu, France, [2] Université Paris-Saclay, NAtional Committee of Scientific Research (CNRS), National Research Institute for Agriculture, Food and Environment (INRAE), Université Evry, Institute of Plant Sciences Paris-Saclay (IPS2), Orsay, France

OPEN ACCESS

Edited by:
Jeremy Harbinson, Wageningen University and Research, Netherlands

Reviewed by:
Harsh Raman, New South Wales Department of Primary Industries, Australia
Mitsutoshi Kitao, Forestry and Forest Products Research Institute, Japan

***Correspondence:**
Younès Dellero
younes.dellero@inrae.fr

Specialty section:
This article was submitted to Plant Abiotic Stress, a section of the journal Frontiers in Plant Science

Received: 10 February 2021
Accepted: 22 March 2021
Published: 15 April 2021

Citation:
Dellero Y, Jossier M, Bouchereau A, Hodges M and Leport L (2021) Leaf Phenological Stages of Winter Oilseed Rape (Brassica napus L.) Have Conserved Photosynthetic Efficiencies but Contrasted Intrinsic Water Use Efficiencies at High Light Intensities. Front. Plant Sci. 12:659439. doi: 10.3389/fpls.2021.659439

Leaf senescence in source leaves leads to the active degradation of chloroplast components [photosystems, chlorophylls, ribulose-1,5-bisphosphate carboxylase/oxygenase (Rubisco)] and plays a key role in the efficient remobilization of nutrients toward sink tissues. However, the progression of leaf senescence can differentially modify the photosynthetic properties of source leaves depending on plant species. In this study, the photosynthetic and respiratory properties of four leaf ranks of oilseed rape describing leaf phenological stages having different sink-source activities were analyzed. To achieve this, photosynthetic pigments, total soluble proteins, Rubisco amounts, and the light response of chlorophyll fluorescence parameters coupled to leaf gas exchanges and leaf water content were measured. Photosynthetic CO_2 assimilation and electron transfer rates, Rubisco and chlorophyll levels per leaf area were gradually decreased between young, mature and senescent leaves but they remained highly correlated at saturating light intensities. However, senescent leaves of oilseed rape had a lower intrinsic water use efficiency compared to young and mature leaves at saturating light intensities that was mainly due to higher stomatal conductance and transpiration rate with respect to stomatal density and net CO_2 assimilation. The results are in favor of a concerted degradation of chloroplast components but a contrasted regulation of water status between leaves of different phenological stages of winter oilseed rape.

Keywords: ***Brassica napus*, senescence (leaf), source sink relationship, water use efficiency, chlorophyll fluorescence, photosynthesis–respiration imbalance, oilseed rape**

INTRODUCTION

Resource allocation within plant organs, driven by source-sink relationships, is a critical factor determining plant growth capacities and overall productivity for crop species (Smith et al., 2018). Source-sink relationships represent an interesting target for yield improvement and they have undergone a revival of interest recently (Sonnewald and Fernie, 2018). From a functional point

of view, a plant can be divided into source organs, corresponding to photosynthetically active tissues exporting photoassimilates (leaves), and sink organs, i.e., parts of the plant where imported photoassimilates are stored or used (seeds and roots for example) (Fernie et al., 2020). Source organs essentially export carbon and nitrogen resources to sink organs through the phloem in the form of sucrose and nitrogen-rich compounds (glutamine, asparagine, ureides, and peptides) (Julius et al., 2017; Tegeder and Masclaux-Daubresse, 2018). However, depending on the phenological stage and the growth conditions, leaves can have both a source and a sink status (import and export of organic carbon and nitrogen) (Chang et al., 2017). This duality concept is mainly inherent to leaf development and aging, in which senescence represents a major nutrient recycling process ultimately leading to cell death and regulated at multiple levels, notably by leaf age, plant life cycle, and environmental conditions (Woo et al., 2019).

Leaf senescence is characterized by the progressive degradation of chloroplasts through the autophagy machinery (chlorophagy), while mitochondria remain active until the final stages of leaf senescence to support ATP production required for carbon and nitrogen export (Keech et al., 2007; Avila-Ospina et al., 2014). Indeed, during the progression of leaf senescence, the active degradation of major components of chloroplasts (chlorophylls, proteins, and lipids) produces metabolic precursors (amino acids, sugars, and fatty acids) that can be either translocated or used as alternative respiratory substrates for mitochondrial metabolism (Chrobok et al., 2016; Barros et al., 2020). Therefore, leaf senescence can strongly influence plant net CO_2 assimilation, since photosynthesis is progressively inhibited while mitochondrial respiration and associated decarboxylations are strongly stimulated. In parallel, the initiation of leaf senescence induces the degradation of major complexes of the chloroplast electron transfer chain (CETC), notably the reaction centers of photosystems (PS) II and I and their associated antenna (Schottler and Toth, 2014). Such degradations severely reduce linear electron flow through the CETC thus compromising an efficient use of light for the production of ATP and reducing power. Consequently, the activation of photoprotective mechanisms can occur leading to non-photochemical quenching (NPQ), cyclic electron flow and chlororespiration that limit the production of reactive oxygen species (Krieger-Liszkay et al., 2019). However, these mechanisms are dependent of CETC complex ratios that appear to be degraded differentially depending on plant species (Krupinska et al., 2012; Nath et al., 2013; Schottler et al., 2017). Therefore, leaf senescence can also influence the relationship between chloroplastic electron transfer rate and photosynthetic CO_2 assimilation.

Winter oilseed rape (*Brassica napus* L.) is an oleaginous crop of major importance due to the production of seeds being naturally rich in triglycerides and proteins. Unfortunately, while oilseed rape has a high nitrogen uptake efficiency at the vegetative stage, the crop requires large mineral nitrogen (N) inputs (150–250 kg N/ha) compared with other crops, due to a low N remobilization efficiency at both vegetative and reproductive stages (Malagoli et al., 2005; Bouchet et al., 2016). Therefore, the engineering of source-sink relationships of oilseed rape represents a promising target for maintaining crop seed yield and quality with reduced N inputs by targeting either N remobilization efficiency or sink establishment (Stahl et al., 2019; Dellero, 2020). To date, research on source-sink relationships in oilseed rape have been essentially focused on the analysis of proteolysis mechanisms and water status in either well-watered or stress conditions (Albert et al., 2012; Musse et al., 2013; Gironde et al., 2015; Poret et al., 2016). Notably, young leaves of oilseed rape accumulate protease inhibitors to protect them for protein degradation while old leaves of oilseed rape show enhanced protease activities (aspartic, cysteine, and chloroplastic) (Avice and Etienne, 2014). However, at the metabolic level, other mechanisms could also play an important role in nutrient remobilization from source-to-sink tissues such as the fine regulation of leaf primary metabolism (Dellero et al., 2020a,b). Notably, the regulation of photosynthetic and mitochondrial activities during the progression of leaf senescence in oilseed rape represents an interesting area that has yet to be explored.

In this study, the impact of leaf phenological stages and their inherent sink-source activities for nitrogen metabolism on the photosynthetic and respiratory properties of oilseed rape have been evaluated by characterizing four leaf ranks representing leaf phenological stages with contrasted sink/source balances (L15, L11, L7, and L3). Levels of photosynthetic pigments, proteins and Rubisco and chlorophyll fluorescence parameters coupled to leaf gas exchanges during light-response experiments have been measured. Correlation analysis between net CO_2 assimilation, photosynthetic pigment contents, Rubisco levels, stomatal conductance and transpiration rate by using different leaf phenological stages showed interesting results.

MATERIALS AND METHODS

Plant Material and Growth Conditions

All experiments were performed on *B. napus* genotype Aviso ["Bracysol" biological resource center (IGEPP)]. Seeds were first incubated for 3 days on soaked blotting paper to allow seed germination and then transferred in 4 L pots filled with a non-fertilized commercial substrate (Falienor, reference 922016F3). Plant growth was achieved in a 6 m^3 growth chamber with the following climatic conditions: 14 h of light at 22°C and 10 h of dark at 18°C, an ambient air with around 410 μmol $CO_2 \cdot mol^{-1}$ air and a relative humidity of 65–80%, a photosynthetic photon flux density (PPFD) ranging between 100 and 120 μmol photons.$m^{-2}.s^{-1}$ following the position of the leaf within the canopy. Plants were irrigated twice a week with a commercial fertilized solution (Liquoplant Bleu, 2.5% N, 5% P, 2.5% K). All experiments were performed on plants grown for 60 days after sowing, possessing 13 leaf ranks (BBCH-19), annotated from the bottom to the top (L3–L15). The two oldest leaves (L1 and L2) had already fallen off after yellowing, confirming that the remobilization processes between sink and source leaves were operating. A first experiment was performed on three different plants to evaluate and select appropriate leaf ranks for further studies (measurement of fresh weight, leaf area and chlorophyll content in SPAD units using limbs and petioles).

A second experiment was performed on three different plants to measure specific limb fresh and dry weights and water, photosynthetic pigment, soluble protein, and Rubisco contents. A third experiment was performed on three different plants to measure leaf gas-exchange and PSII fluorescence parameters. The chlorophyll content in SPAD units was also measured for each leaf of each experiment to ensure that the leaves selected for the analyses were at similar stages across all experiments. Some of the data obtained in this study were very similar to other works performed on leaves of the same genotype grown in similar conditions and using analogous split experimental setups (Dellero et al., 2020a,b).

Leaf Area and Photosynthetic Pigment Contents

Leaves (L15–L3) were harvested by cutting at the base of their mid-vein and used for the measurements of fresh weight and leaf area in the first experiment. Leaf area was measured with the LI-3100C Area Meter (LiCOR, Lincoln, NE, USA). Chlorophyll levels were first approximated in SPAD units using a non-destructive chlorophyll SPAD-502 meter (Minolta) on leaf limbs (10 measurements per leaf). For photosynthetic pigment determinations, five leaf disks (0.8 cm^2) were punched with a cork-borer in both lamina sides of the leaves and immediately frozen in liquid nitrogen and stored at −80°C. Frozen samples were ground to a fine powder and photosynthetic pigments were extracted in the dark with 400 µL of pure ice-cold acetone. After a 5 min centrifugation step at 12 000 g and 4°C, the supernatant was collected and stored at 4°C in the dark. These steps were repeated three to four times on the pellet with 80% ice-cold acetone until all pigments were extracted (as judged by a fully white pellet). Supernatants were mixed together and 50 µL were diluted in 80% acetone for photosynthetic pigment quantification by spectrophotometry. Chlorophyll a (chl a), chlorophyll b (chl b), carotenoid (carot), and xanthophyll (xant) contents were quantified in $\mu g.mL^{-1}$ from the measurements of A_{663}, A_{646}, and A_{470} nm at 25°C as previously described (Lichtenthaler, 1987): chl a = 12.25 A_{663}-2.79A_{646}; chl b = 21.50 A_{646}-5.10A_{663}; carot+xant = 5.05A_{470}-0.0091chla−0.429chlb.

Water, Soluble Protein, and Rubisco Contents

Ten leaf disks (0.8 cm^2) were punched with a cork-borer from both lamina sides of the leaves, frozen in liquid nitrogen and freeze-dried for 72 h. Water content (WC) was calculated from the measurement of the fresh weight (FW, measured directly after harvesting) and the dry weight (DW, measured after freeze-drying) as follow: WC = (FW-DW)/FW. Specific limb fresh and dry weights were calculated from these samples. Freeze-dried samples were ground to a fine powder and soluble proteins were extracted in a buffer containing 20 mM citrate, 160 mM Na_2HPO_4 (pH 6.8), a pinch of polyvinylpolypyrrolidone (PVPP) and a tablet of a protease inhibitor mixture (Complete Mini, EDTA-free, Roche) for 50 mL. After a 15 min incubation with orbital shaking at 1500 rpm, samples were centrifuged for 30 min at 12 000 g and 4°C then soluble proteins in the supernatant were quantified using the Bradford reagent and bovine serum albumin as a protein standard. For relative quantification of Rubisco content, 20 µg of soluble proteins were separated by SDS-PAGE (10% acrylamide) and stained with Coomassie Brilliant Blue (Laemmli, 1970). Rubisco large subunit (LSU) content was evaluated with ImageJ using the "Gel analyser" on 8-bit images, as previously described (Dellero et al., 2015).

Gas Exchange and Chlorophyll Fluorescence Measurements

For these experiments, an entire working day (8–10 h) was required per plant to achieve all measurements on the four leaf ranks considered in this study. Prior to measurements, each plant was transferred to the laboratory bench 1 h after the beginning of the photoperiod. To accommodate any potential side-effects due to different moisture conditions throughout the day, the order of the leaves used for the light response measurements of A_n and g_{sw} were modified as follows: L15, L11, L7, L3 for day 1; L3, L7, L15, L11 for day 2 and L11, L3, L15, L7 for day 3. For measurements, each leaf was placed in a gas-exchange chamber (LCF 6400-40, LiCOR, Lincoln, NE, USA) connected to a portable photosynthesis system (LI 6400XT, LiCOR, Lincoln, Nebraska, USA). The following conditions were maintained in the chamber: a leaf temperature of 20–21°C, a 60–70% relative humidity (VPD leaf approximately equal to 0.8), a CO_2 concentration of 400 $\mu mol\ CO_2.mol^{-1}$ air and an air flow rate of 300 $\mu mol.s^{-1}$. Chlorophyll fluorescence parameters were measured using default parameters of the leaf fluorescence chamber and calculated as follows (Maxwell and Johnson, 2000): $F_v = F_m\text{-}F_o$, $F_v' = F_m'\text{–}F_0'$, Non Photochemical Quenching (NPQ) = $[(F_m\text{-}F_m')/F_m']$, PSII electron transport rate (J_{PSII}) = $\varphi_{PSII}\times0.5\times PPFD\times\alpha leaf$, with φ_{PSII} corresponding to the quantum yield of PSII $[=(F_m'\text{-}F_t)/F_m']$, PPFD corresponding to the photosynthetic photon flux density in $\mu mol\ photons.m^{-2}.s^{-1}$ and αleaf to the light absorption coefficient of a leaf [α leaf = 0.85 (Peterson and Havir, 2001)]. Prior to the measurement of F_0 and F_m levels, plants were dark-adapted for 30 min. For light-response curves, plants were adapted 10 min to each PPFD level and infrared gas analysers were "matched" together before each measurement. PPFD levels were successively 0, 25, 50, 100, 200, 300, 400, 500, 750, 1000, 1250, 1500, 1500, 1750, and 2000 $\mu mol\ photons.m^{-2}.s^{-1}$. Net CO_2 assimilation rate (A_n, expressed in $\mu mol\ CO_2.m^{-2}.s^{-1}$), stomatal conductance to water vapor (g_{sw}, expressed in mol $H_2O.m^{-2}.s^{-1}$), transpiration (Tr, expressed in mmol $H_2O.m^{-2}.s^{-1}$), and intercellular CO_2 concentration (C_i, expressed in $\mu mol\ CO_2.mol^{-1}$ air) were calculated from CO_2 and H_2O gas exchanges using standard equations described in the LI 6400XT_v6.2 user manual (Part I: The basics/1. System description/Equation summary). The intrinsic water use efficiency (iWUE) was calculated as A_n/g_{sw} using PPFD values > 0.

Stomatal Density

Leaves (L15–L3) were harvested by cutting at the base of their mid-vein and three sections of their limbs were randomly selected. The abaxial epidermis of each section was peeled with a fine clamp at the level of secondary veins. Each epidermis was mounted on a glass slide with water and stomatal density of 0.05 mm^2 sections was measured using a light microscope (Axioskop

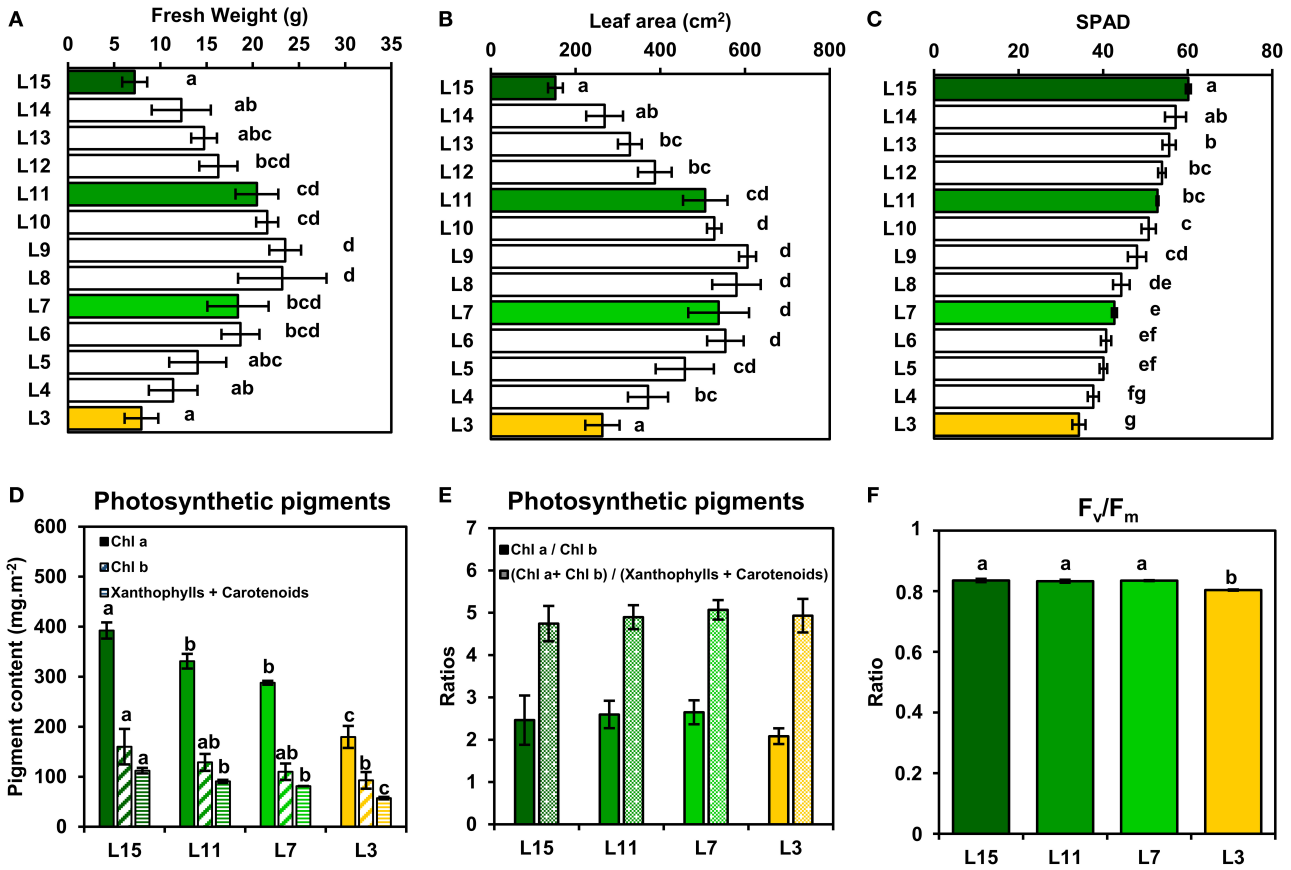

FIGURE 1 | Leaf phenological stages of oilseed rape show a relatively conserved PSII integrity. **(A)** Fresh weight, **(B)** leaf area, and **(C)** chlorophyll content (SPAD units) of oilseed rape leaf ranks. **(D)** Photosynthetic pigment contents and **(E)** ratios and **(F)** PSII maximum quantum yield (F_v/F_m) of four leaf ranks as examples of specific leaf phenological stages (L15: young leaf; L11: pre-mature leaf; L7: post-mature leaf; L3: senescent leaf). Values are means ± SD of three independent biological replicates. Different letters indicate groups of mean values that are significantly different between the different leaf ranks (ANOVA-Tukey HSD, p-value < 0.05).

2 *plus*, Zeiss) at x40 magnification. The mean value obtained from the three sections of a leaf was used as a biological replicate.

Statistical Analysis

Means of different leaf ranks were first compared together with a one-way ANOVA followed by a *post-hoc* Tukey's HSD test for multiple pairwise comparisons. Linear correlations between A_{2000}, $g_{sw\ 2000}$, Tr_{2000}, $C_{i\ 2000}$, photosynthetic pigments, protein levels per leaf area and stomatal density were tested with an F-statistic. For each test, a p-value < 0.05 was applied. All statistical analyses were carried out using R base v3.5.1 (R Core Team, 2018).

RESULTS

In order to evaluate the photosynthetic efficiencies of *B. napus* leaves according to their phenological stage, plants were grown for 2 months at the vegetative stage in growth chambers to reach a 15-leaf stage. At this stage, the two oldest leaves had already fallen off after yellowing, thus confirming the operation of remobilization processes between young, mature and old leaves. Analysis of fresh weight, leaf area and chlorophyll content in SPAD units (**Figures 1A–C**) allowed to distinguish four leaf ranks representing clearly physiologically differentiated phenological stages. Leaf 15 (L15) corresponded to a young growing leaf, with the highest chlorophyll content and a low leaf area and fresh weight. Leaf 11 (L11) and leaf 7 (L7) corresponded, respectively to fully-expanded mature leaves, with the highest leaf areas and fresh weights but with different levels of chlorophylls. Leaf 3 (L3), with the lowest chlorophyll content, corresponded to an old and senescent leaf which can actively remobilise nutrients to younger leaves (L15 notably), as previously described (Dellero et al., 2020a). Since L11, L7, and L3 leaves showed a gradual decrease of their chlorophyll content in SPAD units compared to L15 that may affect the functioning of their CETC, it was decided to measure the content of various photosynthetic pigments and the maximal quantum yield of PSII (F_v/F_m) (**Figures 1D–F**). All photosynthetic pigment contents (chlorophyll a, chlorophyll b, carotenoids and xanthophylls) were progressively decreased from L15 to L3. Chl a/chl b and (chl a + chl b)/(xanthophylls and carotenoids) ratios were not significantly different between the leaf ranks, with values of around 2.5 and 5, respectively, although the L3 chl a/chl b ratio was slightly lower when compared to the other leaf ranks. Consistently, the maximal quantum yield of

PSII (F_v/F_m) remained stable between L15, L11, and L7 (values of around 0.835) whereas L3 showed a significantly lower value of around 0.804. Therefore, although chlorophyll content was altered between young, mature and senescent leaves of oilseed rape, the integrity of PSII and the CETC seemed to remain highly conserved.

Next, it was decided to evaluate further the functioning of the CETC and the photosynthetic CO_2 assimilation capacity of young, mature and senescent leaves of oilseed rape by performing gas exchange and chlorophyll fluorescence measurements in response to light intensity. We also evaluated dark respiration (R_{dark}) as an indicator of mitochondrial respiration. Interestingly, R_{dark} was significantly decreased in L7 and L3 leaf ranks compared to L15 (**Figure 2A**). Net CO_2 assimilation rate (A_n) increased with increasing PPFD for all leaf ranks but it reached a nearly pseudo steady-state level at different PPFD values depending on leaf rank (**Figure 2B**). Indeed, A_n remained relatively stable from 1000 to 2000 PPFD for L11, L7, and L3 and from 1500 to 2000 PPFD for L15. Maximal net CO_2 assimilation rates at saturating light intensities were significantly different between the different leaf ranks (26.96 μmol $CO_2.m^{-2}.s^{-1}$ for L15, 17.83 for L11, 13.60 for L7 and 6.83 for L3 at 2000 PPFD). Analysis of PSII electron transfer rate (J_{PSII}) revealed similar patterns, although it started to reach a pseudo steady-state at an earlier PPFD (**Figure 2C**). Indeed, J_{PSII} was saturated at around 200 PPFD for L3, 500 PPFD for L7, 750 PPFD for L11, and 1000 PPFD for L15. As was seen with A_n, maximal J_{PSII} was also significantly different along the different leaf ranks (139.95 μmol $e^-.m^{-2}.s^{-1}$ for L15, 87.24 for L11, 70.90 for L7, and 36.79 for L3 at 2000 PPFD). Since young, mature and old leaves of oilseed rape had relatively conserved ratios of photosynthetic pigments but showed different PPFD thresholds for A_n and J_{PSII} saturation, it was decided to measure non-photochemical quenching (NPQ) (**Figure 2D**). This parameter is an indicator of an activation of photoprotective mechanism allowing the dissipation of excess excitation energy as heat when light energy absorption exceeds light energy utilization (J_{PSII} saturation) and involves the enzymatic conversion of violaxanthin to zeaxanthin (xanthophyll cycle) (Muller et al., 2001). As perhaps expected, there was a significant increase in NPQ at low PPFD levels for senescent L3 ranked leaves that mirrored J_{PSII} saturation compared to young leaves that were not saturated for J_{PSII} (statistically significant at 200 and 500 PPFD). However, between 1000 and 2000 PPFD, NPQ remained similar for all leaf ranks, except for L3 where NPQ became significantly higher at 2000 PPFD compared to L15 and L11 leaves. Overall, these results show a diminution of both photosynthetic CO_2 assimilation and PSII electron transfer rates from L15 to L3 leaf ranks. Since photosynthetic activity is highly dependent on Rubisco amounts, soluble protein, and Rubisco contents in the young, mature and old leaves of oilseed rape were determined. It was found that soluble protein contents per leaf area gradually decreased from L15 to L3 leaf rank (**Figure 3A**). Using coomassie blue-stained Rubisco large subunit amounts on SDS-PAGE as a proxy (**Figures 3B,C**), it could be seen that relative Rubisco amounts per leaf protein content remained rather stable between the leaf ranks, except for L3, which showed a significant decrease of 25% compared to L15 and L11. Overall, soluble protein contents per leaf area seemed to represent a good proxy for Rubisco amounts per leaf area between the different leaf ranks.

Next, a correlation analysis was performed between A_n at 2000 PPFD (A_{2000}) and either J_{PSII} at 2000 PPFD (J_{2000}), photosynthetic pigments or soluble protein content per leaf area using data obtained from the examined leaf ranks (**Figures 3D–F**). Interestingly, A_{2000} was highly correlated to J_{2000} ($R^2 = 0.99$), and also to photosynthetic pigments ($R^2 = 0.94$) and to soluble protein content ($R^2 = 0.94$). Since CO_2 availability to chloroplasts may also participate to the limitation of A_n between young, mature and senescent leaves of oilseed rape, the light-response of stomatal conductance to water vapor (g_{sw}) and transpiration (Tr) was also examined (**Figures 4A,B**). Stomatal conductance to water vapor (g_{sw}) was constantly increased with increased PPFD but leaf ranks showed significantly different values. L15 showed the highest stomatal conductance, followed by L11 and then L7 and L3. Surprisingly, L7 and L3 leaves exhibited similar stomatal conductance values. The light-response of transpiration (Tr) followed a similar pattern to g_{sw} for the different leaf ranks. Both Tr and g_{sw} did not reach a pseudo steady-state at high light intensities (1500–2000 PPFD) contrary to A_n and J_{PSII} and this was observed for all leaf ranks. Consequently, the intrinsic water use efficiency (iWUE, calculated as A_n/g_{sw}) was the highest at low light intensities (around 200 PPFD) and decreased gradually with increasing PPFD levels for all leaf ranks (**Figure 4C**). However, iWUE was significantly decreased in L3 leaves by up to 50% compared to L15, L11 or L7 leaves at high PPFD values (around 20 vs. 40 μmol CO_2/mol H_2O at 1500 and 2000 PPFD). The analysis of stomatal density on the abaxial epidermis revealed that L15 showed the highest stomatal density followed by L11, then L7 and finally L3 (**Figure 4D**). A correlation analysis between stomatal density, g_{sw}, A_n at 2000 PPFD showed that there was a certain degree of correlation between stomatal conductance (g_{sw2000}) and either stomatal density or photosynthesis (A_{2000}) but only for L15, L11, and L7 leaves (R^2 of 0.90 and 0.72, respectively) (**Figures 5A,B**). Interestingly, senescent leaves (L3) had a higher stomatal conductance compared to their stomatal density thereby suggesting a higher stomatal aperture. However, this was not translated into a higher photosynthetic rate compared to the other leaf ranks (**Figure 5B**). Since changes in stomatal aperture can affect the diffusion of CO_2 within intercellular spaces and subsequently photosynthesis, we also analyzed the intercellular CO_2 concentration at 2000 PPFD ($C_{i\ 2000}$) (**Figure 5C**). $C_{i\ 2000}$ values were gradually increased from L15 to L3 leaves but $C_{i\ 2000}$ was negatively correlated with A_{2000} for all leaf ranks ($R^2 = 0.88$). Considering leaf transpiration rate, we found a high correlation with stomatal conductance between all leaf ranks ($R^2 = 0.97$) and a higher value in the senescent L3 leaves compared to their photosynthetic activity (**Figures 5D,E**). Finally, we analyzed the specific limb dry and fresh weights of young, mature and senescent leaves of oilseed rape. We found that limb water content increased significantly from L15 to L3, and this was associated with a decrease of dry weight per leaf area, while fresh weight per leaf area remained unchanged (**Figures 5F–H**).

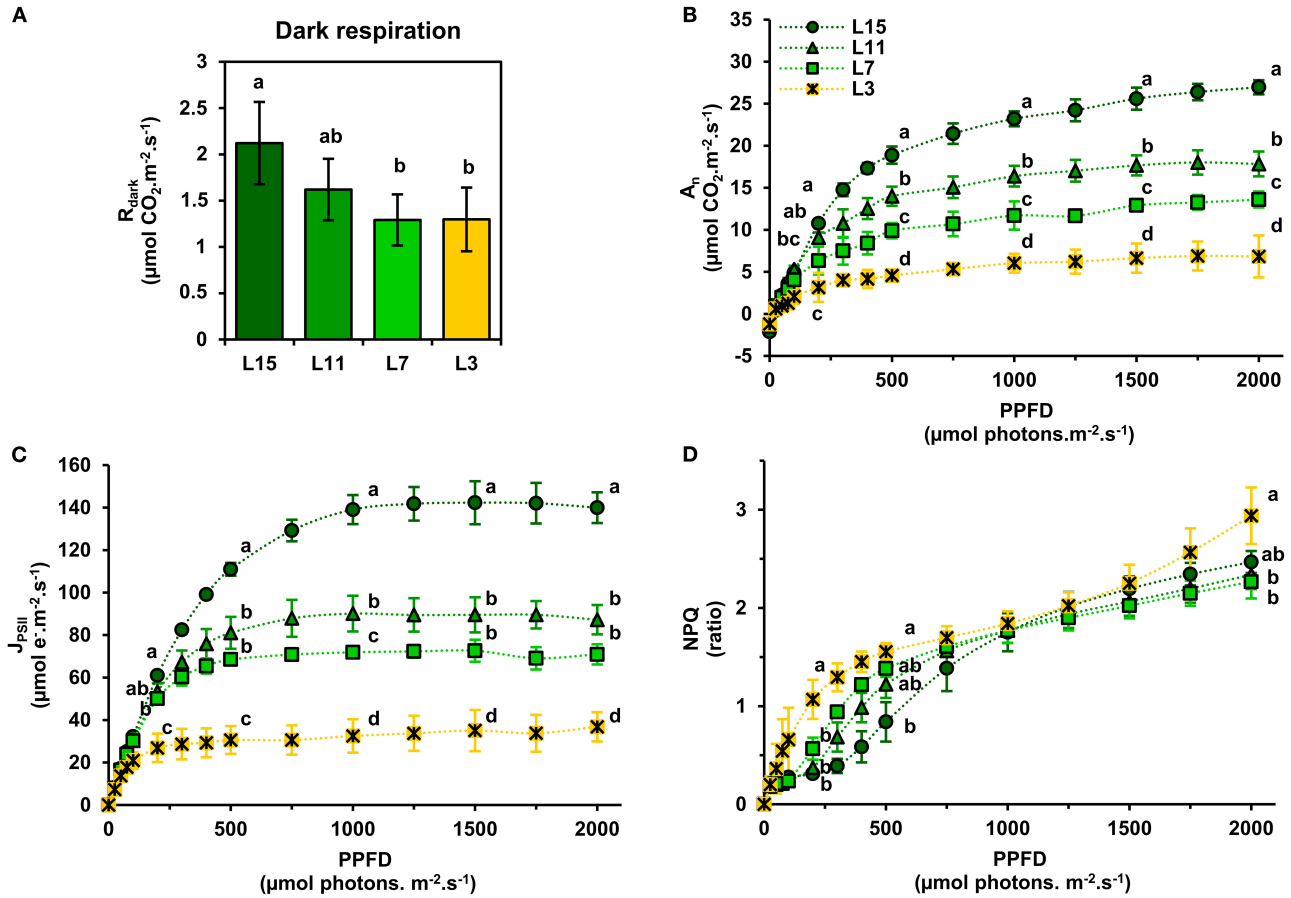

FIGURE 2 | Light-response of net CO_2 assimilation and chlorophyll fluorescence parameters of oilseed rape leaves at different phenological stages. **(A)** Dark respiration (R_{dark}), **(B)** net CO_2 assimilation rate (A_n), **(C)** PSII electron transfer rate (J_{PSII}), and **(D)** non-photochemical quenching (NPQ). Values are means ± SD of three independent biological replicates. Different letters indicate groups of mean values that are significantly different between the different leaf ranks (ANOVA-Tukey HSD, p-value < 0.05) at a given photosynthetic photon flux density (PPFD). L15: young leaf; L11: pre-mature leaf; L7: post-mature leaf; L3: senescent leaf.

DISCUSSION

Source-to-sink remobilization of nutrients is a major process determining plant growth and productivity. Leaf senescence, which leads to the active degradation of chloroplast components (chlorophylls, photosystems, Rubisco) in source leaves while maintaining mitochondrial energy production, plays a key role for the efficient reallocation of carbon and nitrogen to sink tissues. However, the timing of leaf senescence and the kinetics of chloroplast component degradation will modify the photosynthetic properties of source leaves and their net CO_2 assimilation rates (balance between photosynthesis, photorespiration, and mitochondrial respiration). In oilseed rape, source-to-sink nutrient remobilization processes can operate between different leaf phenological stages, when plants are grown at the vegetative stage notably (Clement et al., 2018; Dellero et al., 2020a). Therefore, we took advantage of this to study the impact of leaf phenological stages and their inherent sink-source activities on the photosynthetic and respiratory properties of oilseed rape.

In this study, we found that PSII functioning remained relatively stable between young, mature and senescent leaves, while a gradual decrease of soluble proteins (including Rubisco) and chlorophyll levels was observed. These phenological stages also showed conserved ratios for photosynthetic pigments and PSII fluorescence properties (similar F_v/F_m values and an activation of NPQ at light intensities saturating J_{PSII}) (**Figures 1**, **3**). Since the light intensity used for plant growth in our study (100–120 µmol photons.m^{-2}.s^{-1}) is low when compared to natural daylight (up to 2000 µmol photons.m^{-2}.s^{-1}), it is possible that our growth conditions may have prevented an increase of photoinhibition in senescent leaves that could occur under natural daylight conditions. However, in Arabidopsis plants grown under light intensities similar to those used in our work (100–120 µmol photons.m^{-2}.s^{-1}), the analysis of leaf phenological stages revealed that chlorophyll levels decreased faster than protein levels during natural senescence and this was associated with a decrease of chl a/chl b ratio and PSII maximal quantum yield efficiency (Nath et al., 2013; Tamary et al., 2019). Interestingly, the PSII reaction centers (D1 protein)

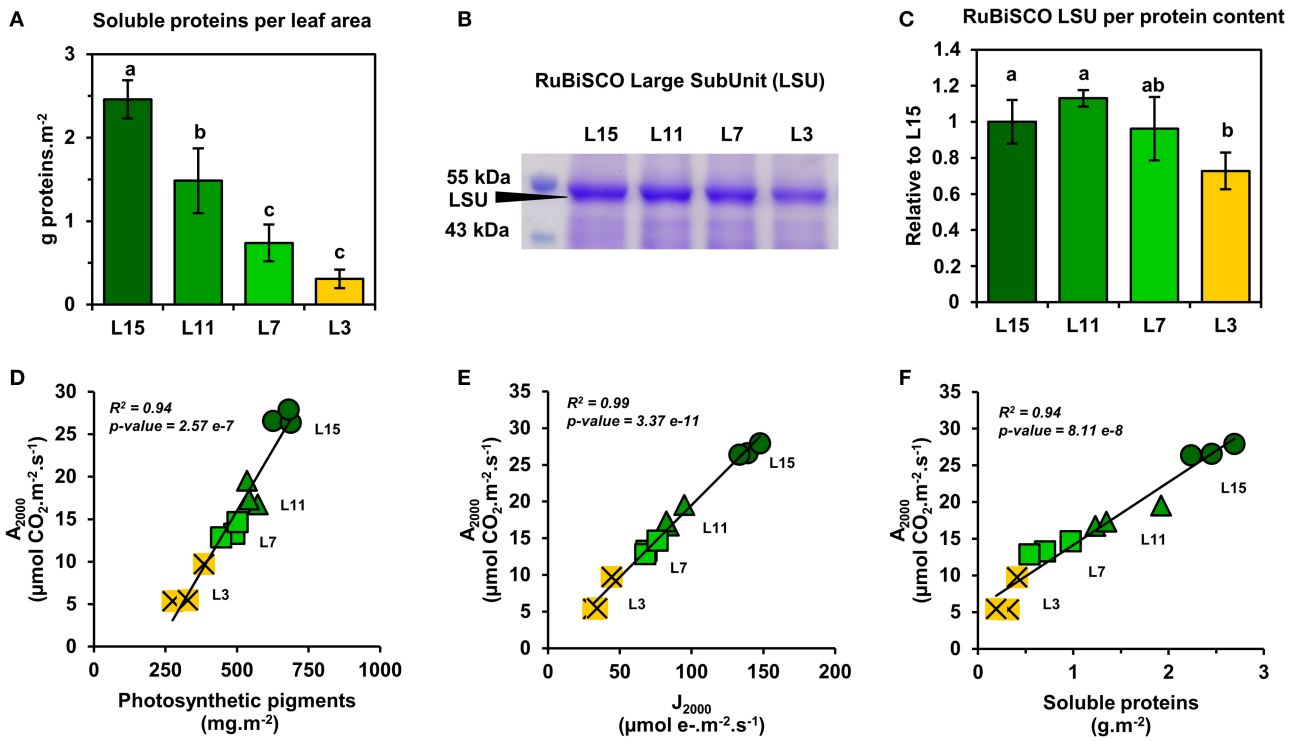

FIGURE 3 | Correlation analysis between the amounts of Rubisco, photosynthetic pigments, J_{PSII}, and net CO_2 assimilation of oilseed rape leaves at different phenological stages and high light intensities. **(A)** Soluble protein contents, **(B)** coomassie blue-stained SDS-PAGE gel showing Rubisco large subunit (LSU), and **(C)** the relative quantification of Rubisco LSU. Correlation analysis at 2000 PPFD between A_n and **(D)** photosynthetic pigments, **(E)** J_{PSII}, and **(F)** soluble protein contents. Values are means ± SD of three independent biological replicates. Different letters indicate groups of mean values that are significantly different between the different leaf ranks (ANOVA-Tukey HSD, p-value < 0.05). L15: young leaf; L11: pre-mature leaf; L7: post-mature leaf; L3: senescent leaf.

were rapidly degraded while antennas from PSII and PSI and PSI reaction centers remained conserved (Nath et al., 2013). Since PSII and PSI reaction centers only harbor chl a while PSII and PSI antennas harbor both chl a and chl b (Caffarri et al., 2014), our results suggest that contrary to Arabidopsis, the sequential dismantling of chloroplast antennas and reaction centers in oilseed rape may proceed through a concerted manner. This hypothesis was also supported by the activation of NPQ mechanisms at light intensities saturating J_{PSII} in young, mature and senescent leaves (**Figures 2C,D**). Indeed, NPQ is triggered by the ΔpH across the thylakoid membrane and it mainly occurs within LHCII and PSII core and requires a functional PsbS protein and the xanthophyll-zeaxanthin cycle (Nicol et al., 2019). Therefore, the activation of NPQ in all of the studied phenological stages suggests a conservation of LHCII and PSII core proteins during chloroplast degradation.

Our results showed that young, mature and senescent leaves of oilseed rape share a similar maximal photosynthetic activity with respect to their photosynthetic capacities (chlorophyll, Rubisco, CETC) at high light intensities (**Figure 3**). Considering the leaf phenological stages studied and their different metabolic states (balance between growth and nutrient remobilization), a conserved correlation between net CO_2 assimilation, chlorophyll levels and Rubisco content was not necessarily expected. Indeed, net CO_2 assimilation rates have been modeled previously as a trade-off between photosynthesis (Rubisco carboxylation steps), photorespiration (CO_2 released by the glycine decarboxylase complex and controlled by Rubisco oxygenation steps) and mitochondrial respiration (CO_2 released by the tricarboxylic acid cycle) (Farquhar et al., 1980). Previous studies reported the central role of mitochondrial metabolism during senescence processes in Arabidopsis (Keech et al., 2007; Chrobok et al., 2016). Particularly, the catabolism of many amino acids is activated to supply the tricarboxylic acid cycle for mitochondrial energy production until late stages of senescence (Hildebrandt et al., 2015; Dellero, 2020). In addition, day mitochondrial ATP production in source leaves can be up to four times higher at high light intensities (1500 PPFD) compared to low light intensities (200 PPFD) (Shameer et al., 2019). Therefore, an increase of mitochondrial respiration at high light unbalancing net CO_2 assimilation with respect to chlorophyll and/or protein content could have been expected in mature and senescent leaves. However, whether amino acid catabolism represents a major flux for mitochondrial respiration in mature and senescent leaves of oilseed rape is still a matter for debate (Dellero et al., 2020a,b). Moreover, boosting mitochondrial respiration may in return have a positive effect on photosynthesis. Indeed, CO_2 released by pyruvate dehydrogenase, isocitrate dehydrogenase

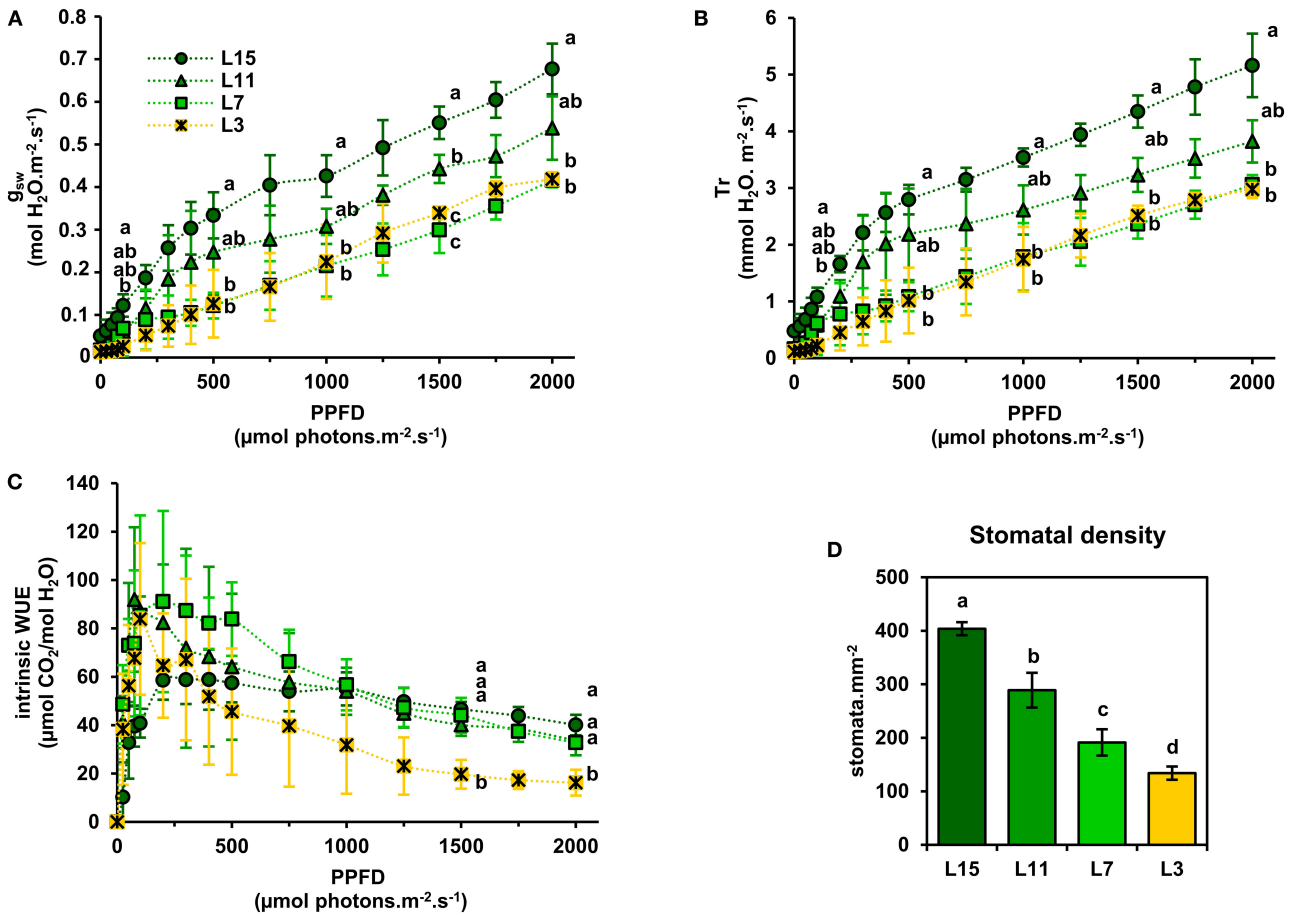

FIGURE 4 | Light-response of stomatal conductance, transpiration, and intrinsic water use efficiency of oilseed rape leaves at different phenological stages. **(A)** Stomatal conductance to water vapor (g_{sw}), **(B)** transpiration rate, **(C)** intrinsic water use efficiency (iWUE), and **(D)** stomatal density (abaxial epidermis). iWUE was calculated as A_n/g_{sw}. Values are means ± SD of three independent biological replicates. Different letters indicate groups of mean values that are significantly different between the different leaf ranks for a given PPFD (ANOVA-Tukey HSD, p-value < 0.05) at 200, 500, 1000, 1500, and 2000 PPFD. L15: young leaf; L11: pre-mature leaf; L7: post-mature leaf; L3: senescent leaf.

and the GABA shunt can significantly diffuse toward chloroplasts and subsequently increase chloroplastic CO_2 concentration (Tcherkez et al., 2017). In addition, we have shown that dark respiration (essentially reflecting mitochondrial respiration) was significantly reduced in mature and senescent leaves of oilseed rape (**Figure 2A**). Although dark respiration still represents 1.3 µmol $CO_2.m^{-2}.s^{-1}$ in L3 leaves (almost 20% of their net CO_2 assimilation), the inhibition of glycolysis and mitochondrial metabolism in the light would lower its overall impact on net CO_2 assimilation rate (Tcherkez et al., 2009). Nevertheless, the ratio for light/dark inhibition of mitochondrial respiration during senescence remains to be investigated in plants.

We found that senescent leaves of oilseed rape had a lower iWUE compared to the other leaf phenological stages, which was mainly due to a higher transpiration rate (Tr) and stomatal aperture (stomatal density/g_{sw}) with respect to the net CO_2 assimilation levels (**Figures 4**, **5**). Previous studies on winter oilseed rape using low-field proton nuclear magnetic resonance demonstrated that leaf senescence re-orchestrated limb structures and intracellular water flux (Musse et al., 2013; Sorin et al., 2015). Interestingly, the size and the vacuolar volume of cells of the palisade parenchyma increased significantly in mature and senescent leaves while cells of the spongy parenchyma remained weakly affected. These morphological changes were also associated with a gradual increase of the leaf water content and a gradual decrease of leaf dry weight between young, mature and senescent leaves. In our study, we found similar results for leaf water content (**Figures 5F–H**) but the differences of iWUE between L3 and L15/L11/L7 were not specifically correlated with the gradual increase of leaf water content, thereby suggesting that the lower iWUE at saturating PPFD in L3 leaves was not specifically associated to the regulation of leaf water status. Whether this water influx within mature and senescent leaves of oilseed rape has an important role for the adjustment of leaf osmotic potential or the export of nutrients from source-to-sink tissues remains an open question (Musse et al., 2013; Sorin et al., 2015). Another hypothesis for the increase of stomatal conductance with respect to photosynthesis in senescent leaves involves the regulation of chloroplastic CO_2 concentration (C_c) by mesophyll conductance.

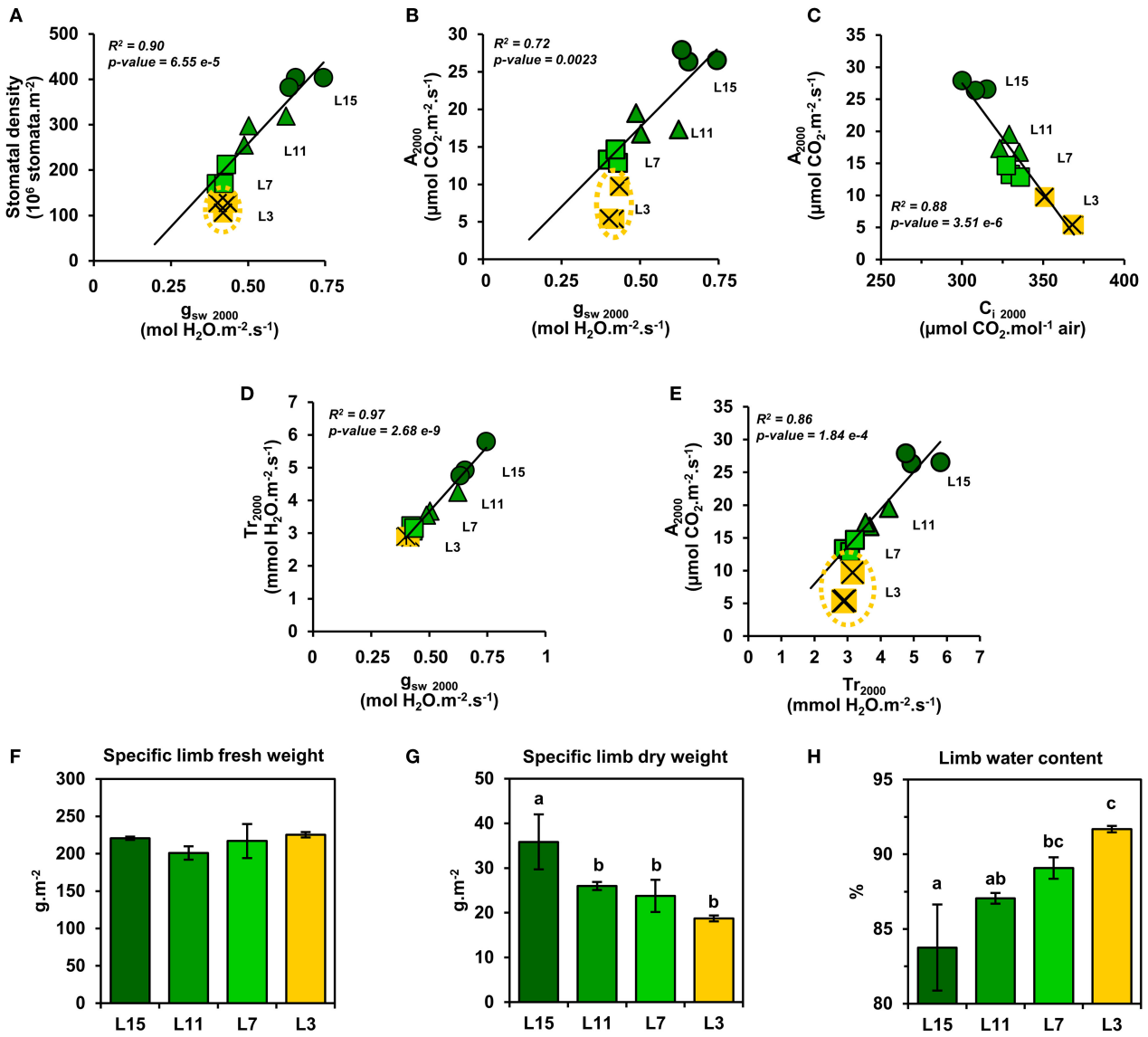

FIGURE 5 | Relationships between stomata and water and CO_2 exchanges of oilseed rape leaves at different phenological stages and high light intensities. Correlation analysis at 2000 PPFD between: stomatal conductance to water vapor (g_{sw}) and **(A)** stomatal density and **(B)** photosynthesis (A_n); **(C)** photosynthesis (A_n) and intracellular CO_2 concentration (C_i); transpiration and **(D)** stomatal conductance to water vapor (g_{sw}) and **(E)** photosynthesis (A_n). **(F)** Specific limb fresh weight, **(G)** Specific limb dry weight, and **(H)** limb water content. Values are means ± SD of three independent biological replicates. Different letters indicate groups of mean values that are significantly different between the different leaf ranks (ANOVA-Tukey HSD, p-value < 0.05). L15: young leaf; L11: pre-mature leaf; L7: post-mature leaf; L3: senescent leaf.

Our results have shown that net CO_2 assimilation was negatively correlated with intracellular CO_2 concentration (C_i) between young, mature and senescent leaves of oilseed rape (**Figure 5C**), thereby suggesting that CO_2 accumulates within intercellular spaces of the leaf when it is not assimilated by Rubisco. However, the Rubisco activity is mainly driven by chloroplastic CO_2 concentration which depends essentially on stomatal aperture and the capacity of intercellular CO_2 to diffuse through cell walls, plasma membranes and chloroplast envelopes (mesophyll conductance) (Gago et al., 2020). In Arabidopsis and oilseed rape, leaf senescence is accompanied by a reduction of cell wall thickness, which should facilitate CO_2 diffusion to chloroplasts (Forouzesh et al., 2013; Musse et al., 2013). On the other hand, leaf senescence also increases palisade parenchyma cell size while reducing the volume of chloroplasts (Musse et al., 2013; Chrobok et al., 2016; Tamary et al., 2019). Thus, a longer path within a liquid phase for CO_2 should affect its diffusion to the chloroplast. Recent studies reported that mesophyll conductance was strongly limited by the cytoplasm in mature leaves of oilseed rape compared to young leaves and significantly contributed to the limitation of net CO_2 assimilation (Lu et al., 2019; Hu et al., 2020). Therefore, the increase of stomatal aperture in

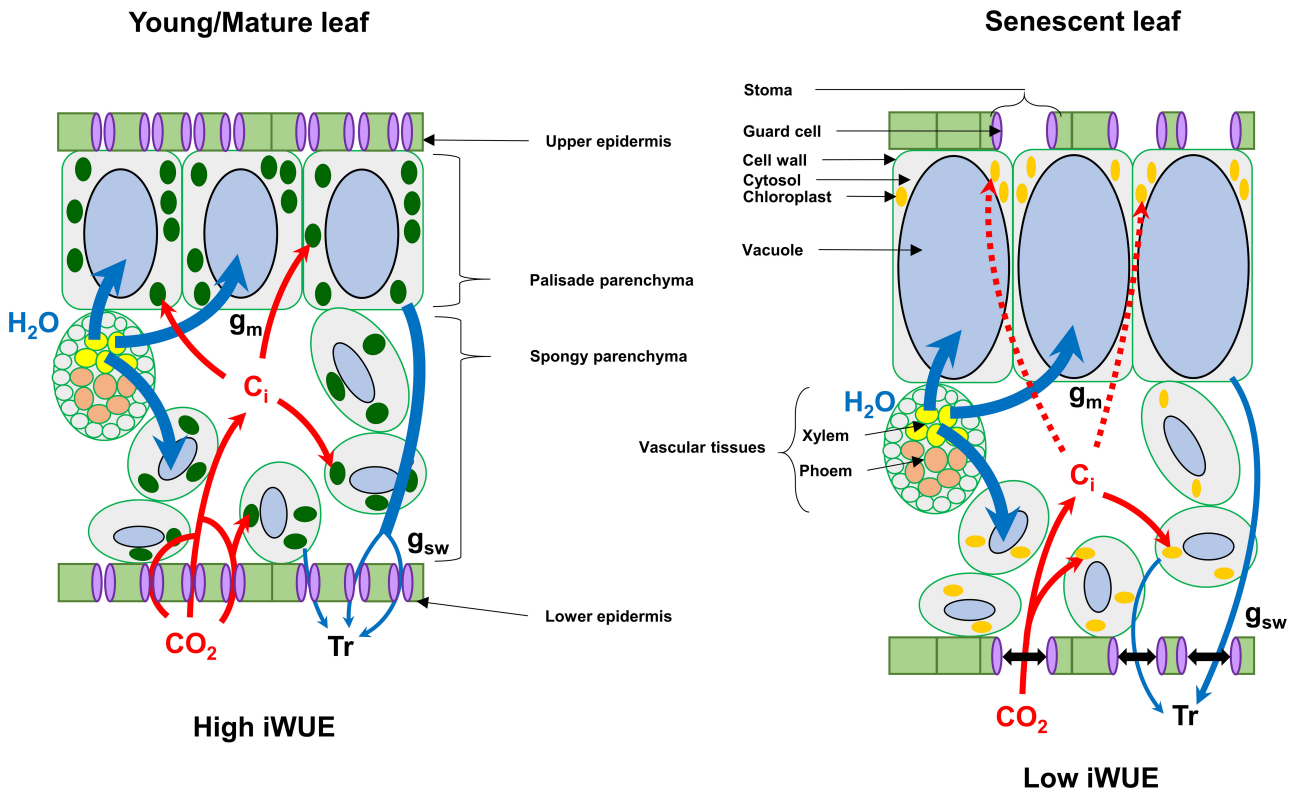

FIGURE 6 | Proposed model for the regulation of intrinsic water use efficiency (iWUE) by senescence in winter oilseed rape leaves at high light intensities. Leaf senescence in winter oilseed rape leads to an increase of the vacuolar volume of cells of the palisade parenchyma, which can limit photosynthesis by decreasing mesophyll conductance of CO_2 (Musse et al., 2013; Sorin et al., 2015; Lu et al., 2019; Hu et al., 2020). In this model, senescent leaves of oilseed rape increase their stomatal aperture compared to young/mature leaves to increase the diffusion of CO_2 toward chloroplasts for photosynthesis. C_i, intercellular CO_2 concentration; Tr, Transpiration; g_m, mesophyll conductance; g_{sw}, stomatal conductance to water vapor.

senescent leaves of oilseed rape could be seen as an adaptive strategy to support photosynthesis with respect to senescence-driven changes of leaf anatomy and Rubisco amounts by boosting CO_2 diffusion toward chloroplasts (**Figure 6**).

In conclusion, leaf phenological stages of winter oilseed rape (*Brassica napus L.*) have different levels for photosynthetic pigments, Rubisco, maximal PSII electron transfer rate and maximal net CO_2 assimilation rates under ambient air but the relative ratios between these components remained strongly conserved per unit of leaf area (photosynthetic efficiency), including an efficient NPQ mechanism. Since these photosynthetic efficiencies remained conserved between the different leaf ranks with respect to their photosynthetic capacities, the results are in favor of a concerted degradation of chloroplast components in winter oilseed rape. Besides this, senescent leaves of oilseed rape have a lower intrinsic WUE at high PPFD compared to young and mature leaves, which seems to be an adaptive strategy to regulate photosynthesis with respect to changes of leaf anatomy (**Figure 6**). An intriguing result that deserves more attention is the gradual decrease of dark respiration between young, mature and senescent leaves. Future work should be focused on the regulation of mitochondrial respiration by the light/dark cycle in young, mature and senescent leaves of oilseed rape at both physiological and metabolic levels to evaluate its contribution to nutrient remobilization processes.

DATA AVAILABILITY STATEMENT

The original contributions presented in the study are included in the article/**Supplementary Material**, further inquiries can be directed to the corresponding author.

AUTHOR CONTRIBUTIONS

YD: conceptualization, data curation, formal analysis, funding acquisition, project administration, supervision, visualization, and writing—original draft. YD and LL: investigation. YD, MJ, and LL: methodology. AB, YD, MH, MJ, and LL: validation, writing—review and editing. All authors have read and agreed to the published version of the manuscript.

FUNDING

This work was supported by the IB2019_FLUCOLSA project of the biology and crop breeding division (INRAE BAP division) and the RAPSODYN project (ANR-11-BTBR-0004) funded by

the program Investments for the Future of the French national agency for research.

ACKNOWLEDGMENTS

We thank Françoise Leprince and Sophie Rolland for help with the measurement of leaf fresh weights, areas, and SPAD levels. We also thank Olivier Coriton and Virginie Huteau for help with the measurement of stomatal density on the abaxial leaf epidermis.

SUPPLEMENTARY MATERIAL

The Supplementary Material for this article can be found online at: https://www.frontiersin.org/articles/10.3389/fpls.2021.659439/full#supplementary-material

REFERENCES

Albert, B., Le Caherec, F., Niogret, M. F., Faes, P., Avice, J. C., Leport, L., et al. (2012). Nitrogen availability impacts oilseed rape (*Brassica napus* L.) plant water status and proline production efficiency under water-limited conditions. *Planta* 236, 659–676. doi: 10.1007/s00425-012-1636-8

Avice, J. C., and Etienne, P. (2014). Leaf senescence and nitrogen remobilization efficiency in oilseed rape (*Brassica napus* L.). *J. Exp. Bot.* 65, 3813–3824. doi: 10.1093/jxb/eru177

Avila-Ospina, L., Moison, M., Yoshimoto, K., and Masclaux-Daubresse, C. (2014). Autophagy, plant senescence, and nutrient recycling. *J. Exp. Bot.* 65, 3799–3811. doi: 10.1093/jxb/eru039

Barros, J. A. S., Siqueira, J. A. B., Cavalcanti, J. H. F., Araujo, W. L., and Avin-Wittenberg, T. (2020). Multifaceted roles of plant autophagy in lipid and energy metabolism. *Trends Plant Sci.* 25, 1141–1153. doi: 10.1016/j.tplants.2020.05.004

Bouchet, A.-S., Laperche, A., Bissuel-Belaygue, C., Snowdon, R., Nesi, N., and Stahl, A. (2016). Nitrogen use efficiency in rapeseed. a review. *Agron. Sustain. Dev.* 36:38. doi: 10.1007/s13593-016-0371-0

Caffarri, S., Tibiletti, T., Jennings, R. C., and Santabarbara, S. (2014). A comparison between plant photosystem I and photosystem II architecture and functioning. *Curr. Protein Pept. Sci.* 15:36. doi: 10.2174/1389203715666140327102218

Chang, T. G., Zhu, X. G., and Raines, C. (2017). Source-sink interaction: a century old concept under the light of modern molecular systems biology. *J. Exp. Bot.* 68, 4417–4431. doi: 10.1093/jxb/erx002

Chrobok, D., Law, S. R., Brouwer, B., Linden, P., Ziolkowska, A., Liebsch, D., et al. (2016). Dissecting the metabolic role of mitochondria during developmental leaf senescence. *Plant Physiol.* 172, 2132–2153. doi: 10.1104/pp.16.01463

Clement, G., Moison, M., Soulay, F., Reisdorf-Cren, M., and Masclaux-Daubresse, C. (2018). Metabolomics of laminae and midvein during leaf senescence and source-sink metabolite management in *Brassica napus* L. leaves. *J. Exp. Bot.* 69, 891–903. doi: 10.1093/jxb/erx253

Dellero, Y. (2020). Manipulating amino acid metabolism to improve crop nitrogen use efficiency for a sustainable agriculture. *Front. Plant Sci.* 11:1857. doi: 10.3389/fpls.2020.602548

Dellero, Y., Clouet, V., Marnet, N., Pellizzaro, A., Dechaumet, S., Niogret, M. F., et al. (2020a). Leaf status and environmental signals jointly regulate proline metabolism in winter oilseed rape. *J. Exp. Bot.* 71, 2098–2111. doi: 10.1093/jxb/erz538

Dellero, Y., Heuillet, M., Marnet, N., Bellvert, F., Millard, P., and Bouchereau, A. (2020b). Sink/source balance of leaves influences amino acid pools and their associated metabolic fluxes in winter oilseed rape (*Brassica napus* L.). *Metabolites* 10:16. doi: 10.3390/metabo10040150

Dellero, Y., Lamothe-Sibold, M., Jossier, M., and Hodges, M. (2015). Arabidopsis thaliana ggt1 photorespiratory mutants maintain leaf carbon/nitrogen balance by reducing RuBisCO content and plant growth. *Plant J.* 83, 1005–1018. doi: 10.1111/tpj.12945

Farquhar, G. D., Von Caemmerer, S., and Berry, J. A. (1980). A biochemical model of photosynthetic CO_2 assimilation in leaves of C 3 species. *Planta* 149:13. doi: 10.1007/BF00386231

Fernie, A. R., Bachem, C. W. B., Helariutta, Y., Neuhaus, H. E., Prat, S., Ruan, Y. L., et al. (2020). Synchronization of developmental, molecular, and metabolic aspects of source-sink interactions. *Nat. Plants* 6, 55–66. doi: 10.1038/s41477-020-0590-x

Forouzesh, E., Goel, A., Mackenzie, S. A., and Turner, J. A. (2013). *In vivo* extraction of Arabidopsis cell turgor pressure using nanoindentation in conjunction with finite element modeling. *Plant J.* 73, 509–520. doi: 10.1111/tpj.12042

Gago, J., Daloso, D. M., Carriqu,í, M., Nadal, M., Morales, M., Araújo, W. L., et al. (2020). Mesophyll conductance: the leaf corridors for photosynthesis. *Biochem. Soc. Trans.* 48, 429–439. doi: 10.1042/BST20190312

Gironde, A., Etienne, P., Trouverie, J., Bouchereau, A., Le Caherec, F., Leport, L., et al. (2015). The contrasting N management of two oilseed rape genotypes reveals the mechanisms of proteolysis associated with leaf N remobilization and the respective contributions of leaves and stems to N storage and remobilization during seed filling. *BMC Plant Biol.* 15:59. doi: 10.1186/s12870-015-0437-1

Hildebrandt, T. M., Nunes Nesi, A., Araujo, W. L., and Braun, H. P. (2015). Amino acid catabolism in plants. *Mol. Plant* 8, 1563–1579. doi: 10.1016/j.molp.2015.09.005

Hu, W., Lu, Z., Meng, F., Li, X., Cong, R., Ren, T., et al. (2020). The reduction in leaf area precedes that in photosynthesis under potassium deficiency: the importance of leaf anatomy. *New Phytol.* 227, 1749–1763. doi: 10.1111/nph.16644

Julius, B. T., Leach, K. A., Tran, T. M., Mertz, R. A., and Braun, D. M. (2017). Sugar transporters in plants: new insights and discoveries. *Plant Cell Physiol.* 58, 1442–1460. doi: 10.1093/pcp/pcx090

Keech, O., Pesquet, E., Ahad, A., Askne, A., Nordvall, D., Vodnala, S. M., et al. (2007). The different fates of mitochondria and chloroplasts during dark-induced senescence in Arabidopsis leaves. *Plant Cell Environ.* 30, 1523–1534. doi: 10.1111/j.1365-3040.2007.01724.x

Krieger-Liszkay, A., Krupinska, K., and Shimakawa, G. (2019). The impact of photosynthesis on initiation of leaf senescence. *Physiol. Plant* 166, 148–164. doi: 10.1111/ppl.12921

Krupinska, K., Mulisch, M., Hollmann, J., Tokarz, K., Zschiesche, W., Kage, H., et al. (2012). An alternative strategy of dismantling of the chloroplasts during leaf senescence observed in a high-yield variety of barley. *Physiol. Plant* 144, 189–200. doi: 10.1111/j.1399-3054.2011.01545.x

Laemmli, U. K. (1970). Cleavage of structural proteins during the assembly of the head of bacteriophage T4. *Nature* 227:6. doi: 10.1038/227680a0

Lichtenthaler, H. K. (1987). ChlorolShylls and carotenoids: pigments of photosynthetic biomembranes. *Methods Enzymol.* 148:33. doi: 10.1016/0076-6879(87)48036-1

Lu, Z., Xie, K., Pan, Y., Ren, T., Lu, J., Wang, M., et al. (2019). Potassium mediates coordination of leaf photosynthesis and hydraulic conductance by modifications of leaf anatomy. *Plant Cell Environ.* 42, 2231–2244. doi: 10.1111/pce.13553

Malagoli, P., Laine, P., Rossato, L., and Ourry, A. (2005). Dynamics of nitrogen uptake and mobilization in field-grown winter oilseed rape (Brassica napus) from stem extension to harvest. II. An 15N-labelling-based simulation model of N partitioning between vegetative and reproductive tissues. *Ann. Bot.* 95, 1187–1198. doi: 10.1093/aob/mci131

Maxwell, K., and Johnson, G. N. (2000). Chlorophyll fluorescence—a practical guide. *J. Exp. Bot.* 51:10. doi: 10.1093/jexbot/51.345.659

Muller, P., Li, X.-P., and Niyogi, K. K. (2001). Non-photochemical quenching. A response to excess light energy. *Plant Physiol.* 125:9. doi: 10.1104/pp.125.4.1558

Musse, M., De Franceschi, L., Cambert, M., Sorin, C., Le Caherec, F., Burel, A., et al. (2013). Structural changes in senescing oilseed rape leaves at tissue and subcellular levels monitored by nuclear magnetic resonance relaxometry through water status. *Plant Physiol.* 163, 392–406. doi: 10.1104/pp.113.223123

Nath, K., Phee, B. K., Jeong, S., Lee, S. Y., Tateno, Y., Allakhverdiev, S. I., et al. (2013). Age-dependent changes in the functions and compositions of

photosynthetic complexes in the thylakoid membranes of Arabidopsis thaliana. *Photosynth. Res.* 117, 547–556. doi: 10.1007/s11120-013-9906-2

Nicol, L., Nawrocki, W. J., and Croce, R. (2019). Disentangling the sites of non-photochemical quenching in vascular plants. *Nat. Plants* 5, 1177–1183. doi: 10.1038/s41477-019-0526-5

Peterson, R. B., and Havir, E. A. (2001). Photosynthetic properties of an Arabidopsis thaliana mutant possessing a defective PsbS gene. *Planta* 214, 142–152. doi: 10.1007/s004250100601

Poret, M., Chandrasekar, B., Van Der Hoorn, R. A. L., and Avice, J. C. (2016). Characterization of senescence-associated protease activities involved in the efficient protein remobilization during leaf senescence of winter oilseed rape. *Plant Sci.* 246, 139–153. doi: 10.1016/j.plantsci.2016.02.011

R Core Team (2018). *R: A Language and Environment for Statistical Computing*. Vienna: R Foundation for Statistical Computing.

Schottler, M. A., Thiele, W., Belkius, K., Bergner, S. V., Flugel, C., Wittenberg, G., et al. (2017). The plastid-encoded PsaI subunit stabilizes photosystem I during leaf senescence in tobacco. *J. Exp. Bot.* 68, 1137–1155. doi: 10.1093/jxb/erx009

Schottler, M. A., and Toth, S. Z. (2014). Photosynthetic complex stoichiometry dynamics in higher plants: environmental acclimation and photosynthetic flux control. *Front. Plant Sci.* 5:188. doi: 10.3389/fpls.2014.00188

Shameer, S., Ratcliffe, R. G., and Sweetlove, L. J. (2019). Leaf energy balance requires mitochondrial respiration and export of chloroplast NADPH in the light. *Plant Physiol.* 180, 1947–1961. doi: 10.1104/pp.19.00624

Smith, M. R., Rao, I. M., and Merchant, A. (2018). Source-sink relationships in crop plants and their influence on yield development and nutritional quality. *Front. Plant Sci.* 9:1889. doi: 10.3389/fpls.2018.01889

Sonnewald, U., and Fernie, A. R. (2018). Next-generation strategies for understanding and influencing source-sink relations in crop plants. *Curr. Opin. Plant Biol.* 43, 63–70. doi: 10.1016/j.pbi.2018.01.004

Sorin, C., Musse, M., Mariette, F., Bouchereau, A., and Leport, L. (2015). Assessment of nutrient remobilization through structural changes of palisade and spongy parenchyma in oilseed rape leaves during senescence. *Planta* 241, 333–346. doi: 10.1007/s00425-014-2182-3

Stahl, A., Vollrath, P., Samans, B., Frisch, M., Wittkop, B., and Snowdon, R. J. (2019). Effect of breeding on nitrogen use efficiency-associated traits in oilseed rape. *J. Exp. Bot.* 70, 1969–1986. doi: 10.1093/jxb/erz044

Tamary, E., Nevo, R., Naveh, L., Levin-Zaidman, S., Kiss, V., Savidor, A., et al. (2019). Chlorophyll catabolism precedes changes in chloroplast structure and proteome during leaf senescence. *Plant Direct* 3:e00127. doi: 10.1002/pld3.127

Tcherkez, G., Gauthier, P., Buckley, T. N., Busch, F. A., Barbour, M. M., Bruhn, D., et al. (2017). Leaf day respiration: low CO2 flux but high significance for metabolism and carbon balance. *New Phytol.* 216, 986–1001. doi: 10.1111/nph.14816

Tcherkez, G., Mahe, A., Gauthier, P., Mauve, C., Gout, E., Bligny, R., et al. (2009). In folio respiratory fluxomics revealed by 13C isotopic labeling and H/D isotope effects highlight the noncyclic nature of the tricarboxylic acid "cycle" in illuminated leaves. *Plant Physiol.* 151, 620–630. doi: 10.1104/pp.109.142976

Tegeder, M., and Masclaux-Daubresse, C. (2018). Source and sink mechanisms of nitrogen transport and use. *New Phytol.* 217, 35–53. doi: 10.1111/nph.14876

Woo, H. R., Kim, H. J., Lim, P. O., and Nam, H. G. (2019). Leaf senescence: systems and dynamics aspects. *Annu. Rev. Plant Biol.* 70, 347–376. doi: 10.1146/annurev-arplant-050718-095859

Conflict of Interest: The authors declare that the research was conducted in the absence of any commercial or financial relationships that could be construed as a potential conflict of interest.

frontiers in Plant Science

ORIGINAL RESEARCH
published: 04 August 2021
doi: 10.3389/fpls.2021.612702

Evaluation of Light-Dependent Photosynthetic Reactions in *Reynoutria japonica* Houtt. Leaves Grown at Different Light Conditions

Selma Mlinarić[1], Lidija Begović[1], Neven Tripić[1], Antonija Piškor[1] and Vera Cesar[1,2]*

[1] Department of Biology, Josip Juraj Strossmayer University of Osijek, Osijek, Croatia, [2] Faculty of Dental Medicine and Health, Josip Juraj Strossmayer University of Osijek, Osijek, Croatia

The Japanese knotweed (*Reynoutria japonica* Houtt.) is considered as one of the most aggressive and highly successful invasive plants with a negative impact on invaded habitats. Its uncontrolled expansion became a significant threat to the native species throughout Europe. Due to its extensive rhizome system, rapid growth, and allelopathic activity, it usually forms monocultures that negatively affect the nearby vegetation. The efficient regulation of partitioning and utilization of energy in photosynthesis enables invasive plants to adapt rapidly a variety of environmental conditions. Therefore, we aimed to determine the influence of light conditions on photosynthetic reactions in the Japanese knotweed. Plants were grown under two different light regimes, namely, constant low light (CLL, 40 μmol/m^2/s) and fluctuating light (FL, 0–1,250 μmol/m^2/s). To evaluate the photosynthetic performance, the direct and modulated chlorophyll *a* fluorescence was measured. Plants grown at a CLL served as control. The photosynthetic measurements revealed better photosystem II (PSII) stability and functional oxygen-evolving center of plants grown in FL. They also exhibited more efficient conversion of excitation energy to electron transport and an efficient electron transport beyond the primary electron acceptor Q_A, all the way to PSI. The enhanced photochemical activity of PSI suggested the formation of a successful adaptive mechanism by regulating the distribution of excitation energy between PSII and PSI to minimize photooxidative damage. A faster oxidation at the PSI side most probably resulted in the generation of the cyclic electron flow around PSI. Besides, the short-term exposure of FL-grown knotweeds to high light intensity increased the yield induced by downregulatory processes, suggesting that the generation of the cyclic electron flow protected PSI from photoinhibition.

Keywords: Japanese knotweed, invasive species, modulated 820 nm reflectance, JIP-test, total driving forces, non-photochemical quenching

OPEN ACCESS

Edited by:
Jeremy Harbinson, Wageningen University and Research, Netherlands

Reviewed by:
Luca Vitale, Institute for Agricultural and Forestry Systems in the Mediterranean, National Research Council of Italy (CNR), Italy
Filippos Bantis, Aristotle University of Thessaloniki, Greece

****Correspondence:***
Selma Mlinarić
smlinaric@biologija.unios.hr;
selma.mlinaric@biologija.unios.hr

Specialty section:
This article was submitted to Plant Abiotic Stress, a section of the journal Frontiers in Plant Science

Received: *30 September 2020*
Accepted: *29 June 2021*
Published: *04 August 2021*

Citation:
Mlinarić S, Begović L, Tripić N, Piškor A and Cesar V (2021) Evaluation of Light-Dependent Photosynthetic Reactions in Reynoutria japonica Houtt. Leaves Grown at Different Light Conditions. Front. Plant Sci. 12:612702. doi: 10.3389/fpls.2021.612702

INTRODUCTION

In the natural environment, plants are exposed to fluctuations of quantity and quality of the incident light. They can adjust the physiological and biochemical processes to sudden changes in light conditions. However, in the experimental conditions, plants are often grown at the continuous light regime. At low-light conditions, they have to adjust the functioning to use the

available light efficiently for the optimal photosynthesis, while at high-light conditions, they have to protect themselves from photoinhibition damage. Often, such adjustments include structural changes at different levels, including, thylakoid, photosystem (PS), pigment, and/or protein (Keren et al., 1997; Lichtenthaler et al., 2007; Kouřil et al., 2013). Contrary to the short-term adaptation to low–light conditions, the long-term strategies involved different structural changes, such as increased leaf mass and thickness, increased amount of thylakoids, or/and higher chlorophyll content (Lichtenthaler and Burkart, 1999; Lichtenthaler et al., 2007). Low light was shown to induce alterations in the photosynthetic apparatus in beech and barley, which resulted in the limitation of the electron transport due to the lower amount of electron carriers and due to a lower connectivity of PSII units in shaded leaves (Desotgiu et al., 2012; Živčak et al., 2014). However, the response to the fluctuating-light (FL) conditions depends on the environmental and experimental conditions, as well as on the species, developmental stage, and physiological factors of the plants (Yin and Johnson, 2000; Kaiser et al., 2018), and usually includes the reprogramming of gene expression connected to the photosynthetic processes (Armbruster et al., 2017; Schneider et al., 2019) and stomatal acclimation (Matthews et al., 2018; Yamori et al., 2020). When plants grow in natural, FL, they have to develop the long-term acclimation responses that differ from those found in plants growing at constant high-light or constant low-light (CLL) conditions (Schneider et al., 2019). Although, recently, the technology and availability of illumination systems are more acceptable and they could simulate natural light conditions, sudden changes in light intensity, clouds, or even wind in nature could occur in less than a second. Therefore, to understand how plants behave in such environments, it is desirable to study the photosynthetic processes under natural environmental conditions.

The Japanese knotweed (*Reynoutria japonica* Houtt.) is one of the most widespread invasive species in Croatia (Boršić et al., 2008; CABI, 2019; FCD, 2020). It is a fast-growing and perennial shrub, very invasive due to its rapid spread in various ecosystems, and very difficult to remove. It is characterized by the ability of the exceptional reproduction and the rapid physiological adaptation to the conditions in the new environment (Spiering, 2011). The Japanese knotweed can also be potentially beneficial to the human society. Its high resistance and efficient accumulation of heavy metals from the environment make it an ideal candidate for soil phytoremediation. It has proven to be an acceptable source of food for humans, domestic animals, and bees, and its metabolism creates compounds that are of potential importance for the herbicide medicine and industry (Beerling et al., 1994; Barney et al., 2006).

One of the most important mechanisms that allows invasive plants to achieve success in a variety of environmental conditions is attributed to the higher photosynthetic rate compared with the native plants (Li and Xiao, 2012; Bajwa et al., 2016). An important aspect of the monitoring and detection of plant responses and their survival under natural conditions is the estimation of their physiological status. Recently, the chlorophyll *a* fluorescence has been extensively used as a non-invasive, very sensitive, and fast method for the estimation of the photosynthetic performance that can provide a reliable source of information on plant conditions (Goltsev et al., 2016; Bussotti and Pollastrini, 2017; Mlinarić et al., 2017; Pollastrini et al., 2017; Kalaji et al., 2018b; Begović et al., 2020).

Since the Japanese knotweed is a heliophilic species, it is adapted to grow under the conditions of increased light intensity. Due to its fast-spreading nature and by creating monocultures, it has become a serious threat to the biodiversity. It is easily cultivated, can grow in various types of soils, and can adapt to a large scale of environmental factors (Beerling et al., 1994; Barney et al., 2006). As an invasive species, it is capable of developing certain adaptations to less favorable conditions. However, one of the major environmental factors that can control its performance is the availability of light. It affects the above- and below-ground biomass of knotweed directly by reducing its performance and, consequently, its invasiveness (Dommanget et al., 2013; Dommanget et al., 2019). Specifically, the below-ground system of the knotweeds presents the majority of its biomass. Plants grown in high-light conditions, in comparison with those grown in low-light conditions, allow the allocation of more resources to the below-ground system, indicating a strong effect of light, hence, enabling colonization and competitiveness of the Japanese knotweed (Price et al., 2002). The most recent study revealed that the Japanese knotweed adopts differential strategies of growth and space occupancy when grown in full sunlight and in shaded habitats (Martin et al., 2020). Therefore, we hypothesized that plants grown at different light regimes, e.g., CLL and fluctuating natural light, would develop certain adaptations to such conditions in photosynthetic reactions. An efficient photosynthesis was recognized to be one of the most important mechanisms that allow invasive plants to achieve success in various environmental conditions (Bajwa et al., 2016). Thus, the main objective of this study was to determine the influence of different illumination regimes on the efficiency of the photosynthetic apparatus and to gain detailed insight into its functioning in the invasive Japanese knotweed by using mainly non-destructive methods, simultaneous measurements of prompt fluorescence, modulated 820 nm reflection (MR), and saturating pulse method, as well as by the determination of the content of the photosynthetic pigment. To our knowledge, the obtained results in this investigation will reveal the most detailed insight into the light-driven reactions in the invasive Japanese knotweed and the adaptations of the photosynthetic apparatus to CLL and FL conditions. Therefore, our investigation results could contribute to a better understanding of mechanisms that play a role in the success of this invasive species.

MATERIALS AND METHODS

Experimental Setup

Rhizomes of the Japanese knotweed (*R. japonica* Houtt.) were planted in a mixture of commercial soil and sand (3:1) in six plastic containers (50 cm × 19 cm × 16.5 cm). The soil used was natural peat (pH = 5.5–7) with the addition of the fertilizer (**Supplementary Table 2**). Three of them were

placed in the room near the window facing south, exposed directly to sunlight. The light intensity (Quantitherm QRT1 light meter, Hansatech, United Kingdom) varied from 30 to 1,250 μmol/m^2/s. The photoperiod changed from 11 to 16 h of FL, while the temperature was 23°C ± 1°C. A detailed information on the distribution of the light throughout the day, the changes in photoperiod, light intensity, and zenith angle that occurred for 110 days is shown in **Supplementary Table 1**. The other three containers were placed in the growth chamber with the day/night photoperiod of 16/8 h (day/night), CLL intensity (i.e., 40 μmol/m^2/s), and a constant temperature of 23°C ± 1°C. The combination of warm white light (i.e., 3,000 K), cool white light (i.e., 4,000 K), and cool daylight (i.e., 6,500 K) from fluorescent tubes (Osram, Munich, Germany) provided a range of visible-light spectra within the visible range between 300 and 700 nm, with maximum peaks at blue, green, and red parts of the spectra (**Supplementary Figure 1**). The plants grown in CLL were used as the control group. They were watered regularly. They started to emerge at 2 weeks after the planting. In each container, at least five plants were growing from one rhizome. The measurements were carried out 110 days after planting on the fully grown leaves (third leaf from the top of the plant).

Simultaneous Measurements of the Prompt Fluorescence and Modulated 820 nm Reflection

The prompt chlorophyll *a* fluorescence (PF) and MR were simultaneously recorded *in vivo* on five plants in each container (n = 15) using Multichannel Plant Efficiency Analyser, M-PEA (Hansatech Instruments, Norfolk, United Kingdom). All measurements were performed on attached, fully dark-adapted leaves (for 30 min). During the measurements, the leaves were exposed to a pulse of high intensity red light-emitting diode (LED) at 625 nm and intensity of up to 5,000 μmol photons/m^2/s to ensure an effective light saturation of exposed leaf surface (i.e., 4-mm diameter). Recorded PF data were analyzed using the JIP-test that represents the translation of the original data to biophysical parameters that quantify the energy fluxes through PSII (Strasser et al., 2000; Strasser et al., 2004). The OJIP transients are presented as mean values of 15 measurements for each group of plants. To evaluate the condition of the photosynthetic apparatus in CLL- and FL-grown Japanese knotweed plants, the selected structural and functional parameters calculated from the JIP-test were chosen. The description of the calculated OJIP test parameters is given in **Table 1**. To compare the recorded OJIP transients for specific events in the OP, OK, OJ, JP, and IP phases, the difference in the relative variable fluorescence (ΔVt) was calculated and presented as a difference ΔV_{OP}, ΔV_{OK}, ΔV_{OJ}, ΔV_{JP}, and ΔV_{IP} normalized to the control (CLL-grown plants) (Yusuf et al., 2010; Dąbrowski et al., 2019). The total driving force (DF_{total}) of the total photosynthetic electron transport, shown as log PI_{total}, was summed up by the corresponding partial DFs: log $\gamma_{RC}/(1-\gamma_{RC})$, log $\varphi_{P0}/(1-\varphi_{P0})$, log $\psi_{E0}/(1-\psi_{E0})$, and log $\delta_{R0}/(1-\delta_{R0})$ (van Heerden et al., 2007). The MR measurements for high-quality P700 reflectance were performed by using modulated 820-nm LED. From the MR signal of the reflected beam, the MR/MR_0 ratio was calculated. The first reliable MR measurement (MR_0) value was taken at 0.7 ms (Strasser et al., 2010; Oukarroum et al., 2013; Salvatori et al., 2014; Salvatori et al., 2015). The parameters and formulas used are listed in **Table 1**.

Double-Pulse Method

For the calculation of Q_B-reducing and non-Q_B-reducing centers, the double-hit measurement protocol was used. The protocol was set up at M-PEA, and it was measured simultaneously with PF and MF. After the first pulse that was used to measure PF followed a second pulse after the dark period of 500 ms. The relative fraction of Q_B-reducing and non-Q_B-reducing centers was calculated as described in the studies of Mathur et al. (2011) and Tomar et al. (2015).

Saturation Pulse Method

The effect of light intensity on the PSII activity was determined by measuring chlorophyll *a* fluorescence *in vivo* on two randomly selected leaves per container using amplitude-modulated fluorometer MiniPAM (Walz, Effeltrich, Germany). The minimal (F_0) and maximal (F_m) fluorescence yields were measured in the dark-adapted leaves (30 min). Same parameters (F') and (F_m') were measured at the photosynthetically active photon flux density (PPFD) at 100, 250, 500, 1,000, and 2,000 μmol photons/m^2/s. The following parameters were calculated: maximum quantum yield of PSII, effective quantum yield of PSII [Y(PSII)], the relative rate of the electron transport (relETR; Genty et al., 1989), non-photochemical quenching (NPQ; Bilger and Björkman, 1990), quantum yield induced by downregulatory processes in PSII [Y(NPQ)], and quantum yield of non-regulated energy dissipated in PSII [Y(NO)] (Kramer et al., 2004).

Determination of the Photosynthetic Pigments

After the measurements of PF and MR, the same leaves were used for the determination of the concentration of photosynthetic pigments. The leaves were powdered using liquid nitrogen, and the photosynthetic pigments were extracted using cold acetone. The concentrations of chlorophylls (Chl *a* and Chl *b*) and carotenoids (Car) were determined spectrophotometrically (Specord 40, Analytik Jena, Germany) at 470, 661.6, and 644.8 nm. The total chlorophyll (Chl $a + b$) concentration, as well as the chlorophyll *a* and *b* ratio (Chl a/b) and the Chl $a + b$ to Car ratio (Chl $a + b$/Car), was calculated (Lichtenthaler, 1987).

Data Analysis

The Student's *t*-test was used to analyze the statistical differences between the leaves exposed to CLL and FL conditions. The asterisk (*) indicates a significant difference between the compared parameters. For simultaneous DF and MR, as well as for double-pulse measurements, five leaves per container were used (n = 15). For the photosynthetic pigment concentration, same leaves were collected into composite sample and six (n = 6) replicates were measured per treatment. For modulated

TABLE 1 | Description of used JIP-test parameters.

Prompt fluorescence (PF)	
Technical parameters	
F_0	Fluorescence intensity at 20 μs
F_m	Maximal fluorescence intensity
F_t	Fluorescence intensity at time *t* after the onset of actinic illumination
F_v	Maximal variable fluorescence
t_{Fm}	Time to reach maximal fluorescence intensity F_m
Area	Total complementary area between the fluorescence induction curve and $F = F_m$
S_m	Normalized total area above OJIP curve, reflecting multiple-turnover events
S_m/t_{Fm}	Index quantifying the average excitation energy of open RCs from $t = 0$ to t_{Fm}
N	Turnover number
M_0	Initial slope of the curve at the origin of the relative variable fluorescence rise
Vt	Relative variable fluorescence at time *t*
Density and overall grouping probability of RCs	
RC/CS_0	Measure for Q_A^- reducing RCs per excited leaf cross-section (CS)
Q_B reducing centers	The fraction of Q_B reducing reaction centers
Non-Q_B reducing centers	The fraction of non-Q_B reducing reaction centers
OEC centers	The fraction of Oxygen Evolving Complexes (OEC)
P_{2G}	Overall grouping probability for the use of the absorbed energy in photochemical reactions
Quantum efficiencies and flux ratios	
$\varphi_{P0} = TR_0/ABS$	Maximum quantum yield of primary photochemistry, the probability that an absorbed photon will be trapped by the PSII RC and will reduce one Q_A
$\psi_{E0} = ET_0/TR_0$	Electron transport efficiency, the probability that an absorbed photon will enter the electron transport chain
$\varphi_{E0} = ET_0/ABS$	Probability that a photon trapped by the PSII RC enters the electron transport chain
$\delta_{R0} = RE_0\text{-}ET_0$	Probability that an electron is transported from reduced PQ to the electron acceptor side of PSI
$\varphi_{R0} = RE_0/ABS$	Quantum yield of electron transport from Q_A^- to the PSI end electron acceptors
ABS/RC	Effective antenna size of an active reaction center (RC). Expresses the total number of photons absorbed by Chl molecules of all RC divided by the total number of active RCs
ET_0/RC	Electron transport in an active RC
TR_0/RC	Maximal trapping rate of PSII. Describes the maximal rate by which excitation is trapped by the RC
DI_0/RC	Effective dissipation in an active RC
RE_0/RC	Electron flux reducing end electron acceptors at the PSI acceptor side per RC
Performance indices and driving forces	
$PI_{ABS} = \gamma_{RC}/(1\text{-}\gamma_{RC}) \times \varphi_{P0}/(1\text{-}\varphi_{P0}) \times \psi_{E0}/(1\text{-}\psi_{E0})$	Performance index (potential) for energy conservation from photons absorbed by PSII to the reduction of intersystem electron acceptors.
$PI_{total} = \gamma_{RC}/(1\text{-}\gamma_{RC}) \times \varphi_{P0}/(1\text{-}\varphi_{P0}) \times \psi_{E0}/(1\text{-}\psi_{E0}) \times \delta_{R0}/(1\text{-}\delta_{R0})$	Performance index (potential) for energy conservation from photons absorbed by PSII to the reduction of PSI end acceptors
$DF_{total} = \log PI_{total}$	Total driving forces for photosynthesis of the observed system, created by summing up the partial driving forces for each of the several bifurcations
Modulated reflection (MR)	
V_{ox}	Rate of P700 and PC oxidation, calculated as the maximum slope decrease of MR_t/MR_0
V_{red}	Rate of P700 and PC re-reduction, calculated as the maximum slope increase of MRt/MR_0
MR_{min}	A transitory steady state, with equal oxidation and re-reduction rates of P700 and PC, calculated as the minimum of MRt/MR_0

fluorescence measurements, two leaves per container were measured ($n = 6$). The difference between the parameters measured in CLL and FL plants, as well as between the parameters at different PPFD, was analyzed by one-way analysis of variance (ANOVA), followed by the Fisher's least significant difference (LSD) *post hoc* test. The results were expressed as means ± standard deviation (SD), and the differences were considered significant at $p < 0.05$. For all statistical analyses, Statistica 13.4.0.14 software (TIBCO Software Inc., Palo Alto, CA, USA) was used.

RESULTS

Analysis of Prompt Chlorophyll *a* Fluorescence Transients and Parameters of the JIP-Test

Prompt chlorophyll *a* fluorescence and MR were measured in knotweed plants grown at CLL and FL conditions. The curve normalized between O and P steps (**Figure 1A**) showed higher values in FL-grown plants compared with CLL–grown

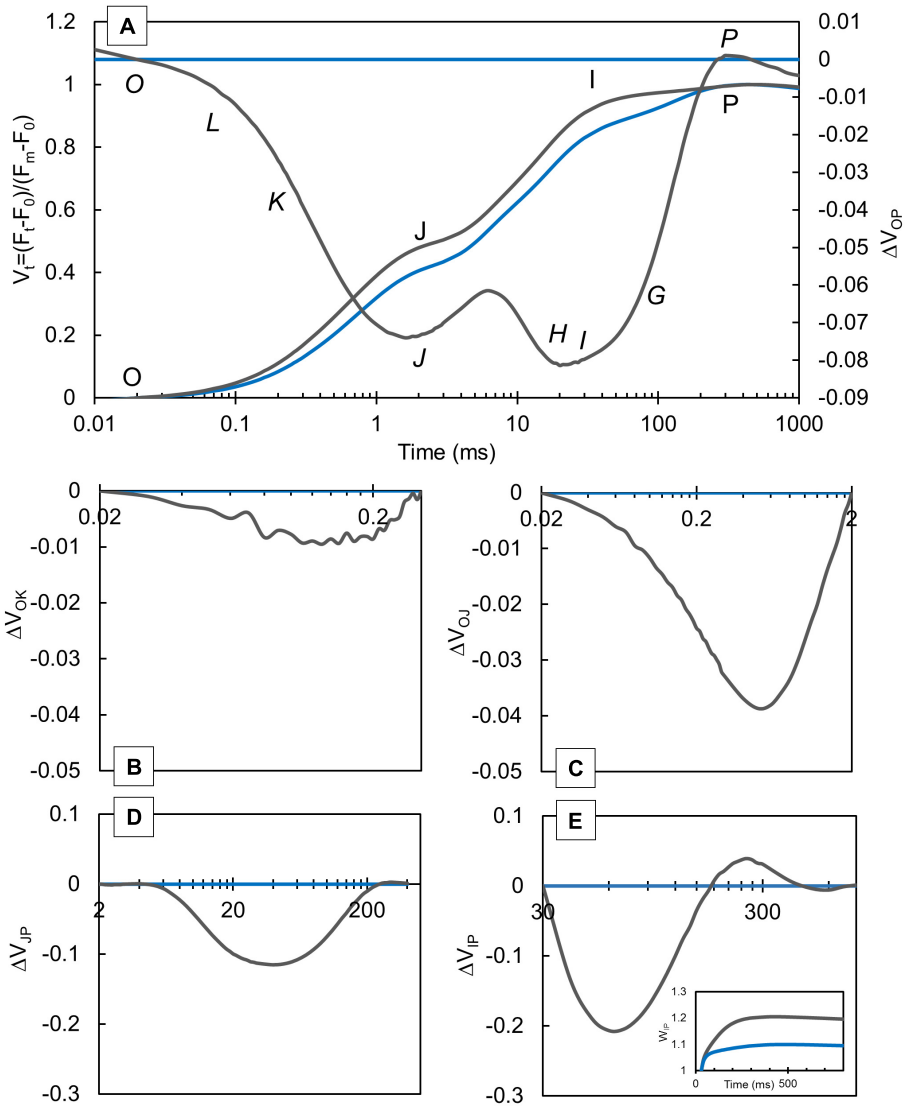

FIGURE 1 | Variations in the shape of the transient curves of the chlorophyll *a* fluorescence measured in the Japanese knotweed (*Reynoutria japonica* Houtt.) leaves exposed to constant low light (blue lines) and fluctuating light (gray lines). Each curve represents the average kinetics of 15 measurements (n = 15) per treatment. Average fluorescence data were normalized between OP **(A)**, OK **(B)**, OJ **(C)** JP **(D)**, and IP **(E)** steps and plotted as difference kinetics ΔVt in a different time range. Average values measured in constant low light were used as referent values. The relative variable fluorescence transient, V_t **(A)**, shows typical O-J-I-P steps, while in difference kinetics, ΔV_{OP}, specific bands *O-L-K-J-I-H-G-P* can be distinguished.

plants. The ΔVt (**Figures 1A–E**) was calculated as the difference between FL-grown and CLL–grown plants, which was used as a reference for data normalization. Our results revealed negative ΔL (**Figure 1B**), ΔK (**Figure 1C**), and ΔH (**Figure 1D**) bands, while the ΔG band (**Figure 1E**) showed a negative amplitude followed by a slight positive inflection in FL-grown knotweeds. The $V_{IP} \geq 1$, plotted in the 30–300 ms range (**Figure 1E**, insert), showed a higher amplitude in FL-grown plants.

The fluorescence intensity at 20 s (F_0) (**Table 2**) showed significantly lower values in FL-grown plants compared with CLL-grown plants, while the F_m showed no difference between the two plant groups. The total complementary area between the curves of fluorescence induction and F_m (Area) revealed almost two times higher values in FL-grown plants compared with CLL-grown plants. The time to reach the maximal fluorescence intensity (t_{Fm}) as well as the M_0, the initial slope of relative variable fluorescence, was low in FL-grown plants when compared with CLL-grown plants. The parameters including S_m, that provides an amount of the energy that is needed to close all reaction centers, S_m/t_{Fm}, that describes the average fraction of open reaction centers during the time needed to complete their closure, N, the turnover number, and the fraction of oxygen-evolving complex (OEC) revealed significantly higher values in FL-grown plants than in CLL–grown plants. The density of active reaction centers (RC) per cross-section, RC/CS_0, the

TABLE 2 | Selected parameters of the chlorophyll *a* fluorescence, characterizing PSII functioning gained from measurements of the Japanese knotweed (*Reynoutria japonica* Houtt.) leaves exposed to constant low and fluctuating light.

	Constant low light	Fluctuating light	*t*-value	*p*
F_0	6540.467 ± 1305.285	5347.333 ± 581.853	−3.233	0.003*
F_m	26239.000 ± 2584.880	25021.933 ± 2636.281	−1.277	0.212
F_v/F_0	3.095 ± 0.474	3.687 ± 0.225	4.371	< 0.001*
F_0/F_m	0.247 ± 0.029	0.214 ± 0.011	−4.208	< 0.001*
Area	279006.792 ± 32506.227	464173.496 ± 40850.223	13.737	< 0.001*
t_{Fm}	500.000 ± 65.465	432.667 ± 73.724	−2.644	0.013*
S_m	14.238 ± 1.948	23.771 ± 2.515	11.606	< 0.001*
S_m/t_{Fm}	0.029 ± 0.004	0.056 ± 0.011	9.365	< 0.001*
N	4.448 ± 0.416	6.574 ± 0.605	8.014	< 0.001*
M_0	0.611 ± 0.109	0.470 ± 0.041	−4.708	< 0.001*
RC/CS_0	3845.759 ± 450.251	3626.533 ± 268.331	1.620	0.116
OEC fraction	0.653 ± 0.040	0.683 ± 0.030	2.308	0.029*
Q_B reducing RCs	0.600 ± 0.035	0.606 ± 0.023	0.492	0.627
non-Q_B reducing RCs	0.400 ± 0.035	0.394 ± 0.023	−0.492	0.627
P_{2G}	0.284 ± 0.121	0.304 ± 0.091	0.501	0.143
V_L	0.079 ± 0.019	0.059 ± 0.005	−3.876	< 0.001*
V_K	0.167 ± 0.031	0.129 ± 0.011	−4.585	< 0.001*
V_J	0.478 ± 0.038	0.408 ± 0.042	−4.776	< 0.001*
V_I	0.909 ± 0.017	0.827 ± 0.033	−8.592	< 0.001*

Data are presented as mean ± SD.
*An asterisk (*) represents a significant difference at $p \leq 0.05$ (using the Student's t-test). For parameter abbreviations, see **Table 1**.*

fraction of Q_B and non-Q_B reducing centers and an overall grouping probability, P_{2G}, showed no significant difference between two differentially grown plant groups. However, the variable fluorescence measured at all chosen time points, V_L, V_K, V_I, and V_J, showed significantly lower values in FL-grown plants compared with CLL–grown plants.

The spider plot (**Figure 2**) represents the normalized curves of the calculated biophysical parameters derived from the JIP-test which characterize the functioning of PSII. Results are represented as the difference between FL-grown plants and CLL-grown plants that were used as control. The performance index (PI_{ABS}) showed significantly higher values of FL-grown plants compared with CLL-grown plants. The quantum yields and probabilities (φ_{P0}, ψ_{E0}, φ_{E0}, δ_{R0}, and φ_{R0}) were significantly higher in FL-grown plants when compared with CLL-grown plants. The specific energy fluxes per reducing PSII RCs, absorption (ABS/RC), and dissipation (DI_0/RC) were significantly lower in FL-grown plants; trapping (TR_0/RC) and electron flux reducing end electron acceptors at the PSI acceptor side (RE_0/RC) showed significantly higher values, while the electron transport further than Q_A^- (ET_0/RC) showed no significant difference compared with CLL-grown plants.

Total Driving Forces

The performance index for the energy conservation from the exciton to the reduction of PSI end acceptors (PI_{total}) showed three times higher values in FL-grown plants than in CLL-grown plants (**Figure 3A**). DF_{total} (**Figure 3B**) for photosynthesis in the observed system are presented as corresponding partial DFs: log $\gamma_{RC}/(1-\gamma_{RC})$, log $\varphi_{P0}/(1-\varphi_{P0})$, log $\psi_{E0}/(1-\psi_{E0})$, and log $\delta_{R0}/(1-\delta_{R0})$. All calculated partial DFs showed a significant difference between FL-grown and CLL-grown plants. The PI_{total}

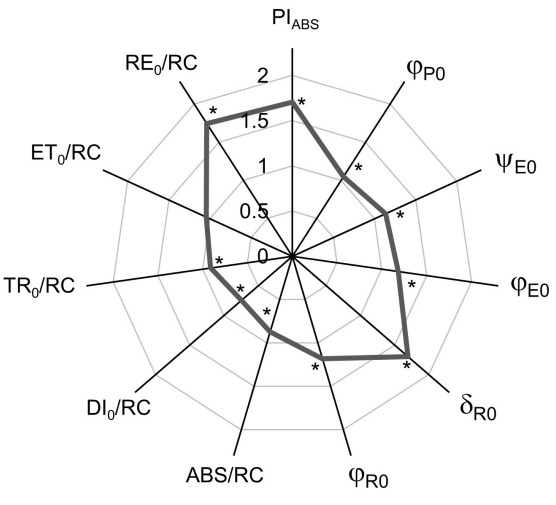

FIGURE 2 | Spider plots display the normalized values of selected parameters of chlorophyll *a* fluorescence characterizing PSII functioning: performance index (PI_{ABS}), quantum yields (φ_{P0}, ψ_{E0}, φ_{E0}, δ_{R0}, and φ_{R0}), and specific energy fluxes per Q_A^- reducing PSII RC (ABS/RC, DI_0/RC, TR_0/RC, ET_0/RC, and RE_0/RC) of Japanese knotweed (*Reynoutria japonica* Houtt.) leaves exposed to fluctuating light (gray line). The values for plants grown in fluctuating light were shown as the difference compared with low-light-grown plants (control = 1). The curve represents the mean values of 15 replicates. The asterisk (*) represents a significant difference at $p \leq 0.05$ (using the Student's *t*-test) compared with control.

(**Figure 3A**) in FL–grown plants increased due to an increase in log $\gamma_{RC}/(1-\gamma_{RC})$ and log $\psi_{E0}/(1-\psi_{E0})$, as well as less negative values of log $\delta_{R0}/(1-\delta_{R0})$.

Analysis of Modulated 820 nm Reflection Transients

Modulated 820 nm reflection signals (**Figure 4A**) were presented as MR/MR_0 ratio. The differences in kinetics at 820 nm reveal the redox states of P700 and PC. The typical MR transient comprises of fast decreasing phase from MR_0 to MR_{min} (at ∼0.7–7 ms, respectively) and a slow increasing phase from MR_{min} to MR_{max} (at ∼300 ms). Our results showed a similar slope for the fast part of the transient, while the slow part of the transient revealed an obvious difference between CLL-grown and FL-grown plants. CLL-grown plants showed a substantial slowdown in the slow phase of transient compared with FL-grown plants. Two additional parameters that can be derived from MR_{820} signals, V_{ox} and V_{red} (**Figure 4B**), represent the oxidation rate of PC and P700 and the re-reduction rate of PC^+ and $P700^+$, respectively. FL-grown plants showed a significantly higher V_{ox} value, while the V_{red} was significantly lower compared with CLL-grown plants.

Rate of Electron Transport and Quantum Efficiencies of the Photosystem II

To determine the effect of light intensity on the PSII activity, relETR, Y(PSII), Y(NO), and Y(NPQ) were measured at different light intensities (**Figure 5**). FL-grown plants showed significantly

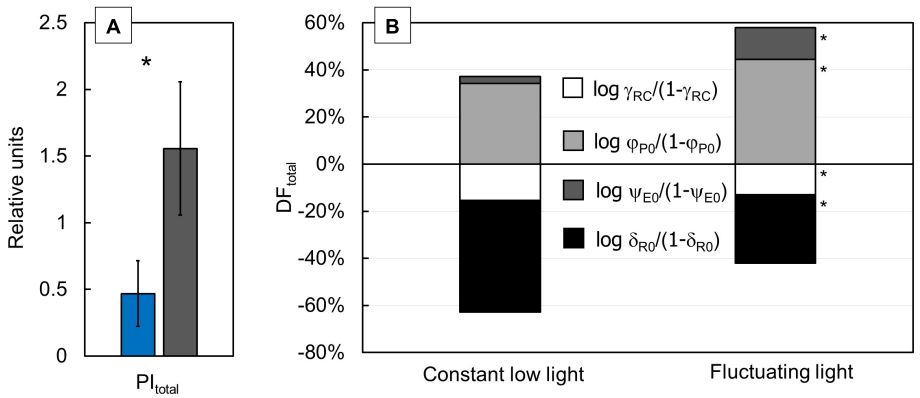

FIGURE 3 | Difference of the performance index for energy conservation from exciton to the reduction of the PSI end acceptors [PI_{total} **(A)**] was measured in the Japanese knotweed (*Reynoutria japonica* Houtt.) leaves exposed to constant low light (blue bar) and fluctuating light (gray bar). Variation in the total driving forces [DF_{total} **(B)**] for each group of plants was calculated by summing up their partial driving forces: log $\gamma_{RC}/(1-\gamma_{RC})$ (white), log $\varphi_{P0}/(1-\varphi_{P0})$ (light gray), log $\psi_{E0}/(1-\psi_{E0})$ (dark gray), and log $\delta_{R0}/(1-\delta_{R0})$ (black). Represented values are the mean of 15 replicates per treatment. The asterisk (*) represents a significant difference at $p \leq 0.05$ (using the Student's *t*-test); error bars represent ± SD.

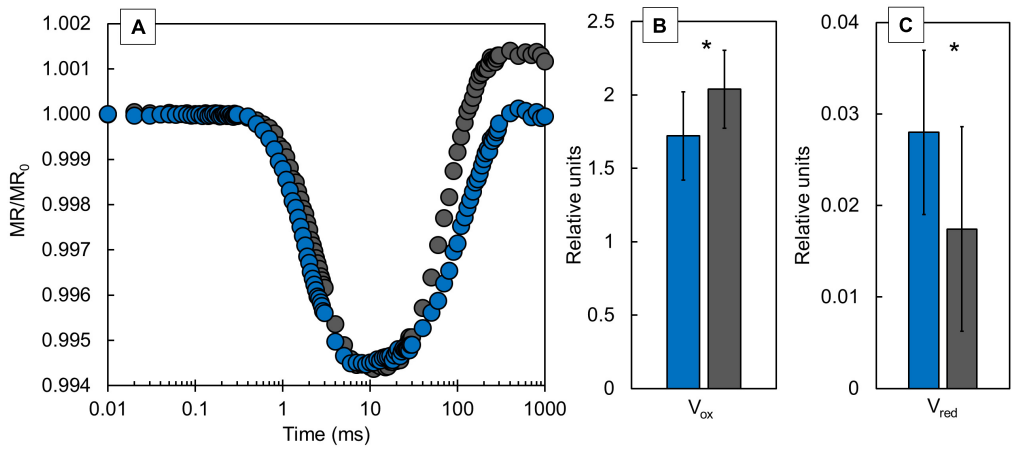

FIGURE 4 | The kinetics of modulated 820 nm reflection (MR) normalized to MR_0 **(A)**, values of the oxidation rate of PC and P700 [V_{ox} **(B)**], and re-reduction rate of PC^+ and $P700^+$ [V_{red} **(C)**] were measured in the Japanese knotweed (*Reynoutria japonica* Houtt.) leaves exposed to constant low light (blue) and fluctuating light (gray). The represented values are the mean of 15 replicates per treatment. The asterisk (*) represents a significant difference at $p \leq 0.05$ (using the Student's *t*-test); error bars represent ± SD.

higher relETR values (**Figure 5A**) at moderate (500 PPFD) and high light intensities (1,000 and 2,000 PPFD), while at lower light intensities (100 and 250 PPFD), there was no significant difference between CLL-grown and FL-grown plants. The effective photochemical quantum yield of PSII [Y(PSII)], the quantum yield of non-regulated energy dissipation [Y(NO)], and the quantum yield for dissipation by downregulation [Y(NPQ)] describe the energy distribution through PSII (**Figure 5B**). Both CLL-grown and FL-grown plants revealed a similar response of measured parameters. Nevertheless, there was a significant difference for Y(PSII) and Y(NPQ) parameters at all applied light intensities between both the plant groups. Except for the significantly lower Y(NO) measured at 2,000 PPFD compared with the lower light intensities in CLL-grown plants, Y(NO) showed that there was no significant change regardless of the applied light intensity between CLL-grown and FL-grown plants.

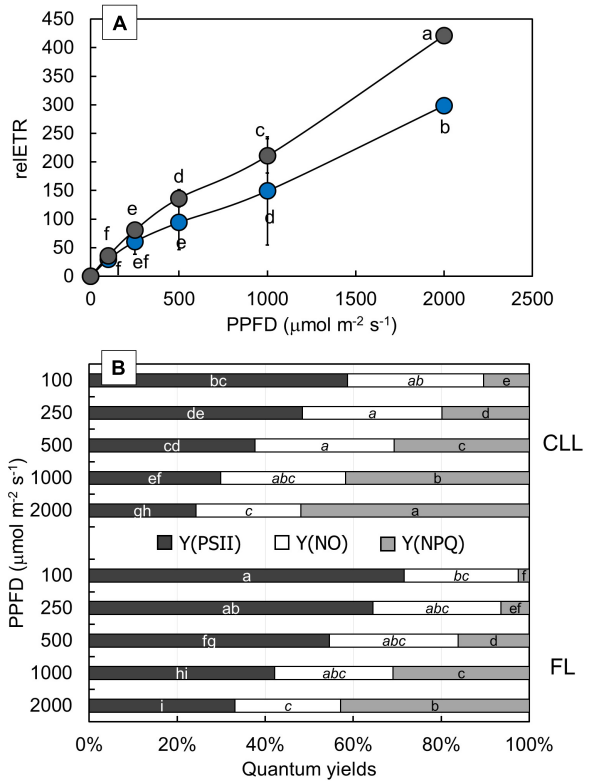

FIGURE 5 | Changes of relative electron transport rate [relETR **(A)**] were measured at 100, 250, 500, 1,000, and 2,000 μmol/m^2/s in the Japanese knotweed (*Reynoutria japonica* Houtt.) leaves exposed to constant low light (blue dots) and fluctuating light (gray dots). Complementary changes of quantum yields **(B)**: quantum efficiency of PSII photochemistry (Y(PSII), dark gray), quantum yield of non-regulated energy dissipated in PSII (Y(NO), white), and quantum yield for dissipation through downregulation in PSII (Y(NPQ), light gray) were represented for each applied light intensity for both investigated plant groups. Data are shown as means of six replicates (n = 6). Different letters represent significant difference at $p \leq 0.05$ (using the ANOVA LSD test) between two investigated plant groups at each light intensity within each quantum yield [white letters for Y(PSII), letters in italic for Y(NO), and black letters for Y(NPQ)].

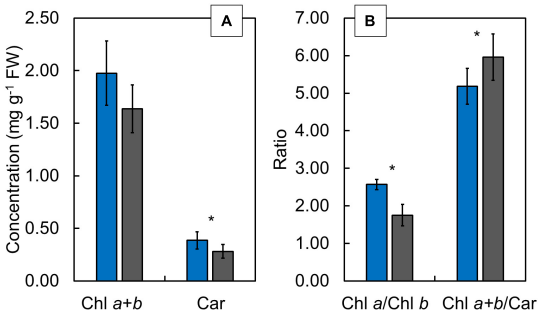

FIGURE 6 | The Chl $a + b$ (mg/g FW) and carotenoids (Car; mg/g FW) **(A)**, as well as Chl a/b and Chl $a + b$/Car ratios **(B)**, determined in the Japanese knotweed (*Reynoutria japonica* Houtt.) leaves exposed to constant low light (blue bars) and fluctuating light (gray bars). The values are represented as means ± SD. The asterisk (*) represents a significant difference at $p \leq 0.05$ (using the Student's t-test).

Content of Photosynthetic Pigments

Although the Chl $a + b$ showed no significant difference between CLL-grown and FL-grown plants (**Figure 6A**), the Car (**Figure 6A**) and the Chl a/b ratio (**Figure 6B**) showed significantly lower values, while the Chl $a + b$/Car ratio (**Figure 6B**) revealed significantly higher values in FL-grown plants compared with CLL-grown plants.

DISCUSSION

The Japanese knotweed plants grown in CLL and FL conditions exhibited a differential response of photosynthetic light-dependent reactions. Our results suggested that the knotweed plants grown in FL acclimated under such conditions by showing better overall photosynthetic reactions compared with plants grown in CLL, thus showing high acclimation potential. FL-grown knotweeds showed a protected integrity of thylakoid membranes, showing better grouping and connectivity between the reaction centers of PSII. This allows them for an efficient allocation of absorbed energy that can be efficiently utilized in primary photochemistry. A larger acceptor pool enables them to achieve an efficient electron transport due to higher amount of free-electron acceptors, as well as more efficient reduction rate at the PSI acceptor side. The fully functional OEC enables replacement of sufficient amount of electrons toward PSII to drive the functional photosynthetic reactions. As a result, FL-grown knotweeds revealed a functional electron transport all the way to PSI, as well as enhanced the photochemical activity of PSI at the acceptor side. In addition, the results after short-term light treatments suggested that FL-grown plants generate a cyclic electron flow to protect PSI by preventing overreduction of the PSI acceptor side.

When exposed to different growth conditions, the photosynthetic apparatus comprises various strategies for adaptation and/or protection at different levels of light conversion throughout the electron transport chain. The OJIP transient curves give us the perception of the status of the plant; therefore, its shape was shown to be a good indicator of the

pool size of the electron carriers in the photosynthetic electron transport chain. Stressful conditions, therefore, cause the change in the intensity of the characteristic points of the OJIP curve. Subsequently, the intensity in the J, I, and P steps, and also in the intermediate L and K bands, changes (Strasser et al., 2000; Kalaji et al., 2018b). It was proposed that low light induces higher J step and, hence, higher V_J and also higher ψ_{E0} due to the limited re-oxidation of Q_A (Strasser et al., 2007). Therefore, a smaller pool of plastoquinone (PQ) disables CLL-grown knotweeds to achieve an efficient electron transport since they had a lower amount of free-electron acceptors (Gao et al., 2014). Stress can induce higher I step due to the accumulation of a higher amount of reduced Q_A and PQ, which subsequently blocks the electron transport between Q_A and Q_B and further to PSI (Strasser et al., 2010; Kalaji et al., 2014). It was reported for the Norway spruce vegetative buds (Katanić et al., 2012), developing common fig leaves (Mlinarić et al., 2017), and radish plants exposed to sulfur deficiency (Samborska et al., 2019) that V_I increase is connected with reoxidation and turnover rate. Based on that, our results imply that Q_A of CLL-grown plants could be reduced, but not reoxidized as efficient as FL-grown plants.

The good grouping and connectivity between the reaction centers of PSII enable an efficient allocation of the absorbed energy to the primary acceptor Q_A (Yusuf et al., 2010). The occurrence of the K-band and the parameter F_v/F_0 reflects the activity of the OEC on the donor site of PSII (Kalaji et al., 2011). Therefore, the tolerance to various stress, such as salinity (Dąbrowski et al., 2019) or drought (Oukarroum et al., 2007), is often connected with the appearance of a negative L-band. Likewise, a negative K-band is often associated with the plants that exhibit tolerance to stress such as heavy metals (Żurek et al., 2014; Begović et al., 2016), salinity (Pavlović et al., 2019), chilling (Krüger et al., 2014), and drought (Oukarroum et al., 2009; Begović et al., 2020), suggesting that functional OEC can replace a sufficient amount of electrons toward PSII to drive functional photosynthetic reactions. However, recent investigation on low-light-grown and high-light-grown *Phalenopsis* plants revealed a lower P_{2G} in high-light-grown plants (Ceusters et al., 2019), suggesting the higher connectivity under the light limitation. Our results, however, suggested that FL-grown plants had closely connected thylakoids that are considered stable and not likely to undergo structural changes. The negative shape of the L-band is the reliable indicator of better grouping and connectivity between the reaction centers of PSII that enables an efficient allocation of the absorbed energy to the primary acceptor Q_A (Yusuf et al., 2010). Such closely connected thylakoids are considered stable and not likely to undergo structural changes. Therefore, the negative L-band and higher, although not significantly, P_{2G}, the overall grouping probability within the PSII antennae in FL-grown plants suggested better grouping and connectivity between the reaction centers of PSII in FL-grown plants, which is related with the preservation of integrity of thylakoid membranes in FL-grown plants. In addition, FL-grown plants carry out efficient photosynthetic reactions due to fully functional OEC that was able to replace necessary amount of electrons in the direction of PSII.

The most recent investigations also involved the calculations of H- and G-bands. The H-band is connected to the redox state of the Q_A, and the negative amplitude is the result of the inhibited reoxidation of Q_A^- (Kalaji et al., 2018a; Dąbrowski et al., 2019). Negative amplitudes of G-band were associated with the adaptation mechanism in nutrient-deficient rapeseed plants that compensate the functionality by increasing the number of $NADP^+$ molecules per active RC (Kalaji et al., 2018a). A similar response of FL-grown plants in our investigation suggests certain adaptation to the FL. Additionally, the maximal amplitude of $W_{OI} \geq 1$ reveals the IP phase, where larger amplitudes suggest larger acceptors pool (Yusuf et al., 2010; Guo et al., 2020). Therefore, a higher W_{OI} amplitude in FL-grown plants indicated a bigger pool of the end electron acceptors at the PSI acceptor side compared with CLL-grown plants. Our results for FL-grown plants were consistent with those implicating more efficient reduction rate at the PSI acceptor side in FL-grown knotweeds compared with CLL-grown knotweeds.

Recently, it was suggested that a good connection of PSII would ensure an efficient utilization of absorbed light into the electron transport and the excitation energy from closed RCs will be transferred to open ones, but without connectivity, the excitation energy will be mainly dissipated. Hence, an increased connectivity is often associated with more efficient processing of light energy (Ceusters et al., 2019). In our investigation, considering connectivity, FL-grown plants showed a similar behavior pattern as HL-grown *Phalenopsis*, indicating that light limitation of CLL-grown plants diminished energy fluctuations through PSII. Such specific fluxes consider only active RCs that can reduce Q_A (Force et al., 2003; Yusuf et al., 2010). A significantly lower Chl *a/b* ratio in FL-grown plants suggests a higher acclimation potential due to the formation of smaller, but more efficient, photosynthetic units (Oguchi et al., 2003; Brestič et al., 2014). Furthermore, F_m and Chl $a + b$ did not differ between FL-grown and CCL-grown plants. It was suggested that there was a strong correlation between F_m and Chl content and that changes in the chlorophyll content do not affect the antenna size but reflect its ability to acclimate to the light environment (Dinç et al., 2012). FL-grown knotweed plants generated an efficient mechanism to regulate the amount of excitation energy needed to reach the RC as acclimation to fluctuations in the light intensity. Moreover, the absorbed light energy in FL-grown knotweeds was efficiently utilized in the primary photochemistry and revealed functional electron transport all the way to PSI.

The PI_{total} was known to be the most sensitive parameter that describes the functional activity of PSII, PSI, and intersystem electron transport chain (Yusuf et al., 2010; Krüger et al., 2014; Dąbrowski et al., 2016), and therefore, it allows the extensive analyses of the photosynthetic performance. It was suggested that a higher value of log $\varphi_{P0}/(1\text{-}\varphi_{P0})$ is associated with an efficient primary photochemistry due to the light reactions (Pereira et al., 2000; Kalaji et al., 2011). An increase of this log $\psi_{E0}/(1\text{-}\psi_{E0})$ suggests the improved ability of the photosynthetic system for the conversion of the excitation energy to electron transport beyond Q_A^- in plants grown in the FL (van Heerden et al., 2007; Krüger et al., 2014). Based on that, our results imply that FL-grown plants revealed highly regulated photosynthetic processes

between the light-dependent reactions and the reactions leading to CO_2 assimilation compared with CCL-grown ones.

The modulated reflection at 820 nm represents the oxidation state of PC and P700 and re-reduction state of PC^+ and $P700^+$ and depends on the available pool of electron acceptors on the acceptor side of PSI (Strasser et al., 2010; Guo et al., 2020). The faster oxidation of PC and P700 reflects the enhanced photochemical activity of PSI at the acceptor side (Gao et al., 2014; Salvatori et al., 2015). It was suggested that a higher PSI activity could be an adaptive mechanism for minimizing the photooxidative damage by regulating the distribution of excitation energy between PSII and PSI (Zhang et al., 2016). It was reported recently that FL primarily damages PSI in the wild-type *Arabidopsis* plants. In that case, the generation of the cyclic electron flow around PSI could play an important role in the photoprotection of the PSI donor side (Yamamoto and Shikanai, 2019). Therefore, based on the above-mentioned studies, our results suggested that in FL-grown plants, there were too few electrons transferred to PSI, which were not able to completely reduce $P700^+$ and PC^+ compared with CLL-grown knotweeds.

The photosynthetic efficiency is known to decrease under high irradiation, and at the same time, heat dissipation and the relative electron transport increase (Bajkán et al., 2012; Sperdouli and Moustakas, 2012; Brestič et al., 2014; Huang et al., 2018). Several components can be involved in the increase of non-photochemical quenching, and most usually, its increase is associated with the dissipation of the active energy *via* the carotenoids (Demmig-Adams and Adams, 1996; Brestič et al., 2014). CLL-grown plants dissipated greater amount of energy by downregulation, implying an effective mechanism to cope with the photoinhibitory conditions. Such an increase could be the case in our investigation since the higher Car, as well as higher Chl $a + b$ to Car ratio, was observed in CLL-grown plants. Recently, it was suggested that such a mechanism could be directly associated with the P700 redox status (Brestič et al., 2014; Zhang et al., 2016). The short-term exposure of FL-grown knotweeds could cause accumulation of electrons in PSI, resulting in oxidative damage. To prevent overreduction of the PSI acceptor side, cyclic electron flow limits the production of reactive oxygen species, thus protecting the acceptor side of PSI (Salvatori et al., 2015). In such case, FL-grown plants can generate a cyclic electron flow to protect PSI (Yamamoto and Shikanai, 2019).

The parallel measurements of the photosynthetic parameters used several non-destructive methods, and the determination of photosynthetic pigments showed that CLL led to a lower functionality of the light-driven photosynthetic reaction in the Japanese knotweed compared with plants grown in FL. The growth in FL, however, induced fully efficient PSII and PSI, reaction centers, and intersystem electron transport. To our knowledge, obtained results in this investigation revealed the most detailed insight into the light-driven reactions in the invasive Japanese knotweed and the adaptations of the photosynthetic apparatus to the FL conditions. Recent study on the growth dynamics of this invasive species based on the light availability showed that the Japanese knotweed grew faster and explored larger area when cultivated in full sunlight (Martin et al., 2020). They found that plants grown in full sunlight had higher vigor compared with those grown in shaded area. This corresponds to our findings that CLL-grown plants had a poor photosynthetic performance compared with FL-grown plants, which could be one of the key roles of its invasive success.

CONCLUSION

It can be concluded that Japanese knotweed plants grown in FL built distinct adaptations to the changing light conditions compared with the plants grown in CLL. Our results revealed that FL exhibited more efficient photosynthetic reactions compared with the plants grown in CLL due to the better grouping and connectivity between the PSII units compared with CLL-grown plants. The fully functional OEC in FL-grown plants was able to replace a sufficient amount of electrons toward PSII to drive functional photochemical reactions. The formation of smaller photosynthetic units in FL-grown plants caused a lower absorption and trapping but a more efficient conversion of excitation energy to the electron transport beyond the primary electron acceptor Q_A. An efficient reduction and reoxidation of Q_A in FL-grown plants ensured rather undisturbed electron transport all the way to PSI, while the larger PQ pool enabled them to achieve an efficient electron transport due to a higher amount of free-electron acceptors. Due to the larger acceptor pool at the PSI acceptor side, FL-grown plants were more capable of reduction of their end acceptor than CLL-grown ones. The enhanced photochemical activity of PSI in FL-grown plants suggested the formation of a successful adaptive mechanism for minimizing the photooxidative damage by regulating the distribution of the excitation energy between PSII and PSI. In contrast, CLL-grown plants accumulated a higher amount of reduced Q_A and PQ that could be reduced but not reoxidized as efficient as in FL-grown plants. That subsequently blocked the electron transport between Q_A and Q_B and further to PSI. However, FL-grown knotweeds exhibited faster oxidation at the PSI side, which could be the result of generating the cyclic electron flow around PSI. Despite the better effective quantum yield of PSII and the linear electron transport observed in FL-grown plants, an exposure to the short-term high light intensity increased Y(NPQ), the yield induced by the downregulatory processes, suggesting that the generation of the cyclic electron flow around PSI was due to the functional adaptation of the FL-grown plants to protect PSI from photoinhibition.

AUTHOR CONTRIBUTIONS

SM proposed a conceptual framework, supervised the research, analyzed the data, and wrote the manuscript. LB performed measurements and statistical analysis, reviewed, and edited the manuscript. NT and AP performed the measurements. VC reviewed the manuscript. All authors contributed to the manuscript revision, read, and approved the submitted version.

ACKNOWLEDGMENTS

The authors wish to thank Ksenija Doboš for valuable technical assistance and Dubravka Špoljarić Maronić for helpful corrections and improvements in the manuscript.

SUPPLEMENTARY MATERIAL

The Supplementary Material for this article can be found online at: https://www.frontiersin.org/articles/10.3389/fpls.2021.612702/full#supplementary-material

REFERENCES

Armbruster, U., Galvis, V. C., Kunz, H.-H., and Strand, D. D. (2017). The regulation of the chloroplast proton motive force plays a key role for photosynthesis in fluctuating light. *Curr. Opin. Plant Biol* 37, 56–62. doi: 10.1016/j.pbi.2017.03.012

Bajkán, S., Várkonyi, Z., and Lehoczki, E. (2012). Comparative study on energy partitioning in photosystem II of two Arabidopsis thaliana mutants with reduced non-photochemical quenching capacity. *Acta Physiol. Plant* 34, 1027–1034. doi: 10.1007/s11738-011-0899-1

Bajwa, A. A., Chauhan, B. S., Farooq, M., Shabbir, A., and Adkins, S. W. (2016). What do we really know about alien plant invasion? A review of the invasion mechanism of one of the world's worst weeds. *Planta* 244, 39–57. doi: 10.1007/s00425-016-2510-x

Barney, J. N., Tharayil, N., DiTommaso, A., and Bhowmik, P. C. (2006). The biology of invasive alien plants in Canada. 5. Polygonum cuspidatum Sieb. & Zucc.[= Fallopia japonica (Houtt.) Ronse Decr.]. *Can. J. Plant Sci.* 86, 887–906. doi: 10.4141/P05-170

Beerling, D. J., Bailey, J. P., and Conolly, A. P. (1994). *Fallopia japonica* (Houtt.) ronse decraene. *J. Ecol.* 82, 959–979. doi: 10.2307/2261459

Begović, L., Galić, V., Abičić, I., Lončarić, Z., Lalić, A., and Mlinarić, S. (2020). Implications of intra-seasonal climate variations on chlorophyll a fluorescence and biomass in winter barley breeding program. *Photosynthetica* 58, 995–1008. doi: 10.32615/ps.2020.053

Begović, L., Mlinarić, S., Antunović Dunić, J., Katanić, Z., Lončarić, Z., Lepeduš, H., et al. (2016). Response of *Lemna minor* L. to short-term cobalt exposure: the effect on photosynthetic electron transport chain and induction of oxidative damage. *Aquat. Toxicol.* 175, 117–126. doi: 10.1016/j.aquatox.2016.03.009

Bilger, W., and Björkman, O. (1990). Role of the xanthophyll cycle in photoprotection elucidated by measurements of light-induced absorbance changes, fluorescence and photosynthesis in leaves of Hedera canariensis. *Photosynth. Res.* 25, 173–185. doi: 10.1007/BF00033159

Boršić, I., Milović, M., Dujmović, I., Bogdanović, S., Cigić, P., Rešetnik, I., et al. (2008). Preliminary check-list of invasive alien plant species (IAS) in Croatia. *Nat. Croat.* 17, 55–71.

Brestič, M., Živčak, M., Olsovska, K., Shao, H.-B., Kalaji, H. M., and Allakhverdiev, S. I. (2014). Reduced glutamine synthetase activity plays a role in control of photosynthetic responses to high light in barley leaves. *Plant Physiol. Biochem.* 81, 74–83. doi: 10.1016/j.plaphy.2014.01.002

Bussotti, F., and Pollastrini, M. (2017). Observing climate change impacts on European forests: what works and what does not in ongoing long-term monitoring networks. *Front. Plant Sci.* 8:629. doi: 10.3389/fpls.2017.00629

CABI (2019). *Fallopia Japonica (Japanese Knotweed)* [Online]. Available online at: https://www.cabi.org/isc/datasheet/23875 (accessed September 23, 2020).

Ceusters, N., Valcke, R., Frans, M., Claes, J. E., Van den Ende, W., and Ceusters, J. (2019). Performance index and PSII connectivity under drought and contrasting light regimes in the CAM orchid phalaenopsis. *Front. Plant Sci.* 10:1012. doi: 10.3389/fpls.2019.01012

Dąbrowski, P., Baczewska, A. H., Pawluśkiewicz, B., Paunov, M., Alexantrov, V., Goltsev, V., et al. (2016). Prompt chlorophyll a fluorescence as a rapid tool for diagnostic changes in PSII structure inhibited by salt stress in *Perennial ryegrass*. *J. Photochem. Photobiol. B Biol.* 157, 22–31. doi: 10.1016/j.jphotobiol.2016.02.001

Dąbrowski, P., Baczewska-Dąbrowska, A. H., Kalaji, H. M., Goltsev, V., Paunov, M., Rapacz, M., et al. (2019). Exploration of chlorophyll a fluorescence and plant gas exchange parameters as indicators of drought tolerance in perennial ryegrass. *Sensors* 19:2736. doi: 10.3390/s19122736

Demmig-Adams, B., and Adams, W. W. (1996). The role of xanthophyll cycle carotenoids in the protection of photosynthesis. *Trends Plant Sci.* 1, 21–26. doi: 10.1016/S1360-1385(96)80019-7

Desotgiu, R., Cascio, C., Pollastrini, M., Gerosa, G., Marzuoli, R., and Bussotti, F. (2012). Short and long term photosynthetic adjustments in sun and shade leaves of *Fagus sylvatica* L., investigated by fluorescence transient (FT) analysis. *Plant Biosyst.* 146, 206–216. doi: 10.1080/11263504.2012.705350

Dinç, E., Ceppi, M. G., Tóth, S. Z., Bottka, S., and Schansker, G. (2012). The chl a fluorescence intensity is remarkably insensitive to changes in the chlorophyll content of the leaf as long as the chl a/b ratio remains unaffected. *Biochim. Biophys. Acta Biomembr.* 1817, 770–779. doi: 10.1016/j.bbabio.2012.02.003

Dommanget, F., Evette, A., Breton, V., Daumergue, N., Forestier, O., Poupart, P., et al. (2019). Fast-growing willows significantly reduce invasive knotweed spread. *J. Environ. Manage.* 231, 1–9. doi: 10.1016/j.jenvman.2018.10.004

Dommanget, F., Spiegelberger, T., Cavaillé, P., and Evette, A. (2013). Light availability prevails over soil fertility and structure in the performance of Asian knotweeds on riverbanks: new management perspectives. *Environ. Manage.* 52, 1453–1462. doi: 10.1007/s00267-013-0160-3

FCD (2020). *Flora Croatica Database*. Available online at: https://hirc.botanic.hr/fcd/DetaljiFrame.aspx?IdVrste=8449&taxon=Reynoutria+japonica+Houtt (accessed September 23, 2020).

Force, L., Critchley, C., and van Rensen, J. J. (2003). New fluorescence parameters for monitoring photosynthesis in plants. *Photosynth. Res.* 78, 17–33. doi: 10.1023/A:1026012116709

Gao, J., Li, P., Ma, F., and Goltsev, V. (2014). Photosynthetic performance during leaf expansion in *Malus micromalus* probed by chlorophyll a fluorescence and modulated 820 nm reflection. *J. Photochem. Photobiol. B Biol.* 137, 144–150. doi: 10.1016/j.jphotobiol.2013.12.005

Genty, B., Briantais, J.-M., and Baker, N. R. (1989). The relationship between the quantum yield of photosynthetic electron transport and quenching of chlorophyll fluorescence. *Biochim. Biophys. Acta Gen. Subj.* 990, 87–92. doi: 10.1016/S0304-4165(89)80016-9

Goltsev, V., Kalaji, H., Paunov, M., Bąba, W., Horaczek, T., Mojski, J., et al. (2016). Variable chlorophyll fluorescence and its use for assessing physiological condition of plant photosynthetic apparatus. *Russ. J. Plant Physiol.* 63, 869–893. doi: 10.1134/S1021443716050058

Guo, Y., Lu, Y., Goltsev, V., Strasser, R. J., Kalaji, H. M., Wang, H., et al. (2020). Comparative effect of tenuazonic acid, diuron, bentazone, dibromothymoquinone and methyl viologen on the kinetics of Chl a fluorescence rise OJIP and the MR820 signal. *Plant Physiol. Biochem.* 156, 39–48. doi: 10.1016/j.plaphy.2020.08.044

Huang, W., Yang, Y.-J., Zhang, S.-B., and Liu, T. (2018). Cyclic electron flow around photosystem I promotes ATP synthesis possibly helping the rapid repair of photodamaged photosystem II at low light. *Front. Plant Sci.* 9:239. doi: 10.3389/fpls.2018.00239

Kaiser, E., Morales, A., and Harbinson, J. (2018). Fluctuating light takes crop photosynthesis on a rollercoaster ride. *Plant Physiol.* 176, 977–989. doi: 10.1104/pp.17.01250

Kalaji, H. M., Bąba, W., Gediga, K., Goltsev, V., Samborska, I. A., Cetner, M. D., et al. (2018a). Chlorophyll fluorescence as a tool for nutrient status identification in rapeseed plants. *Photosynth. Res.* 136, 329–343. doi: 10.1007/s11120-017-0467-7

Kalaji, H. M., Bosa, K., Kościelniak, J., and Żuk-Gołaszewska, K. (2011). Effects of salt stress on photosystem II efficiency and CO2 assimilation of two Syrian barley landraces. *Environ. Exp. Bot.* 73, 64–72. doi: 10.1016/j.envexpbot.2010.10.009

Kalaji, H. M., Oukarroum, A., Alexandrov, V., Kouzmanova, M., Brestic, M., Zivcak, M., et al. (2014). Identification of nutrient deficiency in maize and tomato plants by in vivo chlorophyll a fluorescence measurements. *Plant Physiol. Biochem.* 81, 16–25. doi: 10.1016/j.plaphy.2014.03.029

Kalaji, H. M., Rastogi, A., Živčák, M., Brestic, M., Daszkowska-Golec, A., Sitko, K., et al. (2018b). Prompt chlorophyll fluorescence as a tool for crop phenotyping:

an example of barley landraces exposed to various abiotic stress factors. *Photosynthetica* 56, 953–961. doi: 10.1007/s11099-018-0766-z

Katanić, Z., Atić, L., Ferhatović, D., Cesar, V., and Lepeduš, H. (2012). PSII photoscemistry in vegetative buds and needles of Norway spruce (*Picea abies* L. Karst.) probed by OJIP chlorophyll a fluorescence measurement. *Acta Biol. Hung.* 63, 218–230. doi: 10.1556/abiol.63.2012.2.5

Keren, N., Berg, A., Van Kan, P. J., Levanon, H., and Ohad, I. (1997). Mechanism of photosystem II photoinactivation and D1 protein degradation at low light: the role of back electron flow. *Proc. Natl. Acad. Sci. U.S.A.* 94, 1579–1584. doi: 10.1073/pnas.94.4.1579

Kouřil, R., Wientjes, E., Bultema, J. B., Croce, R., and Boekema, E. J. (2013). High-light vs. low-light: effect of light acclimation on photosystem II composition and organization in *Arabidopsis thaliana*. *Biochim. .Biophys Acta Biomembr.* 1827, 411–419. doi: 10.1016/j.bbabio.2012.12.003

Kramer, D. M., Johnson, G., Kiirats, O., and Edwards, G. E. (2004). New fluorescence parameters for the determination of QA redox state and excitation energy fluxes. *Photosynth. Res.* 79:209. doi: 10.1023/B:PRES.0000015391.99477.0d

Krüger, G. H. J., De Villiers, M. F., Strauss, A. J., de Beer, M., van Heerden, P. D. R., Maldonado, R., et al. (2014). Inhibition of photosystem II activities in soybean (*Glycine max*) genotypes differing in chilling sensitivity. *S. Afr. J. Bot.* 95, 85–96. doi: 10.1016/j.sajb.2014.07.010

Li, Q., and Xiao, H. (2012). The interactions of soil properties and biochemical factors with plant allelopathy. *Ecol. Environ. Sci.* 21, 2031–2036.

Lichtenthaler, H. K. (1987). Chlorophylls and carotenoids: pigments of photosynthetic biomembranes. *Methods Enzymol.* 148, 350–382.

Lichtenthaler, H. K., Ač, A., Marek, M. V., Kalina, J., and Urban, O. (2007). Differences in pigment composition, photosynthetic rates and chlorophyll fluorescence images of sun and shade leaves of four tree species. *Plant Physiol. Biochem.* 45, 577–588. doi: 10.1016/j.plaphy.2007.04.006

Lichtenthaler, H. K., and Burkart, S. (1999). Photosynthesis and high light stress. *Bulgarian J. Plant Physiol.* 25, 3–16.

Martin, F.-M., Dommanget, F., Lavallée, F., and Evette, A. (2020). Clonal growth strategies of Reynoutria japonica in response to light, shade, and mowing, and perspectives for management. *NeoBiota* 56, 89–110.

Mathur, S., Allakhverdiev, S. I., and Jajoo, A. (2011). Analysis of high temperature stress on the dynamics of antenna size and reducing side heterogeneity of Photosystem II in wheat leaves (*Triticum aestivum*). *Biochim. Biophys. Acta Biomembr.* 1807, 22–29. doi: 10.1016/j.bbabio.2010.09.001

Matthews, J. S., Vialet-Chabrand, S., and Lawson, T. (2018). Acclimation to fluctuating light impacts the rapidity of response and diurnal rhythm of stomatal conductance. *Plant Physiol.* 176, 1939–1951. doi: 10.1104/pp.17.01809

Mlinarić, S., Antunović Dunić, J., Skendrović Babojelić, M., Cesar, V., and Lepeduš, H. (2017). Differential accumulation of photosynthetic proteins regulates diurnal photochemical adjustments of PSII in common fig (*Ficus carica* L.) leaves. *J. Plant Physiol.* 209, 1–10. doi: 10.1016/j.jplph.2016.12.002

Oguchi, R., Hikosaka, K., and Hirose, T. (2003). Does the photosynthetic light-acclimation need change in leaf anatomy? *Plant Cell Environ.* 26, 505–512. doi: 10.1046/j.1365-3040.2003.00981.x

Oukarroum, A., El Madidi, S., Schansker, G., and Strasser, R. J. (2007). Probing the responses of barley cultivars (*Hordeum vulgare* L.) by chlorophyll a fluorescence OLKJIP under drought stress and re-watering. *Environ. Exp. Bot.* 60, 438–446. doi: 10.1016/j.envexpbot.2007.01.002

Oukarroum, A., Goltsev, V., and Strasser, R. J. (2013). Temperature effects on pea plants probed by simultaneous measurements of the kinetics of prompt fluorescence, delayed fluorescence and modulated 820 nm reflection. *PLoS One* 8:e59433. doi: 10.1371/journal.pone.0059433

Oukarroum, A., Schansker, G., and Strasser, R. J. (2009). Drought stress effects on photosystem I content and photosystem II thermotolerance analyzed using Chl a fluorescence kinetics in barley varieties differing in their drought tolerance. *Physiol. Plant.* 137, 188–199. doi: 10.1111/j.1399-3054.2009.01273.x

Pavlović, I., Mlinarić, S., Tarkowská, D., Oklestkova, J., Novak, O., Lepeduš, H., et al. (2019). Early Brassica crops responses to salinity stress: a comparative analysis between Chinese cabbage, white cabbage and kale. *Front. Plant Sci.* 10:450. doi: 10.3389/fpls.2019.00450

Pereira, W. E., de Siqueira, D. L., Martínez, C. A., and Puiatti, M. (2000). Gas exchange and chlorophyll fluorescence in four citrus rootstocks under aluminium stress. *J. Plant Physiol.* 157, 513–520. doi: 10.1016/S0176-1617(00)80106-6

Pollastrini, M., Nogales, A. G., Benavides, R., Bonal, D., Finer, L., Fotelli, M., et al. (2017). Tree diversity affects chlorophyll a fluorescence and other leaf traits of tree species in a boreal forest. *Tree Physiol.* 37, 199–208. doi: 10.1093/treephys/tpw132

Price, E. A., Gamble, R., Williams, G. G., and Marshall, C. (2002). "Seasonal patterns of partitioning and remobilization of 14 C in the invasive rhizomatous perennial Japanese knotweed (*Fallopia japonica* (Houtt.) Ronse Decraene)," in *Ecology and Evolutionary Biology of Clonal Plants*, eds J. F. Stuefer, B. Erschbamer, H. Huber, and J. I. Suzuki (Dordrecht: Springer), 125–140.

Salvatori, E., Fusaro, L., Gottardini, E., Pollastrini, M., Goltsev, V., Strasser, R. J., et al. (2014). Plant stress analysis: application of prompt, delayed chlorophyll fluorescence and 820 nm modulated reflectance. Insights from independent experiments. *Plant Physiol. Biochem.* 85, 105–113. doi: 10.1016/j.plaphy.2014.11.002

Salvatori, E., Fusaro, L., Strasser, R. J., Bussotti, F., and Manes, F. (2015). Effects of acute O3 stress on PSII and PSI photochemistry of sensitive and resistant snap bean genotypes (*Phaseolus vulgaris* L.), probed by prompt chlorophyll "a" fluorescence and 820 nm modulated reflectance. *Plant Physiol. Biochem.* 97, 368–377. doi: 10.1016/j.plaphy.2015.10.027

Samborska, I. A., Kalaji, H. M., Sieczko, L., Borucki, W., Mazur, R., Kouzmanova, M., et al. (2019). Can just one-second measurement of chlorophyll a fluorescence be used to predict sulphur deficiency in radish (*Raphanus sativus* L. sativus) plants?. *Curr. Plant Biol.* 19:100096. doi: 10.1016/j.cpb.2018.12.002

Schneider, T., Bolger, A., Zeier, J., Preiskowski, S., Benes, V., Trenkamp, S., et al. (2019). Fluctuating light interacts with time of day and leaf development stage to reprogram gene expression. *Plant Physiol.* 179, 1632–1657. doi: 10.1104/pp.18.01443

Sperdouli, I., and Moustakas, M. (2012). Differential response of photosystem II photochemistry in young and mature leaves of *Arabidopsis thaliana* to the onset of drought stress. *Acta Physiol. Plant.* 34, 1267–1276. doi: 10.1007/s11738-011-0920-8

Spiering, D. J. (2011). Effectiveness of two alternative herbicides compared to a conventional chemical herbicide for control of Japanese knotweed (*Polygonum cuspidatum*). *Bull. Buffalo Soc. Nat. Sci.* 40, 49–58.

Strasser, R. J., Srivastava, A., and Tsimilli-Michael, M. (2000). "The fluorescence transient as a tool to characterize and screen photosynthetic samples," in *Probing Photosynthesis: Mechanism, Regulation & Adaptation*, 1st Edn, eds M. Yunus, U. Pathre, and P. Mohanty (New York, NY: CRC), 445–483.

Strasser, R. J., Tsimilli-Michael, M., Dangre, D., and Rai, M. (2007). "Biophysical phenomics reveals functional building blocks of plants systems biology: a case study for the evaluation of the impact of mycorrhization with Piriformospora indica," in *Advanced Techniques in Soil Microbiology*, eds A. Varma and R. Oelmüller (Berlin: Springer Verlag), 319–341.

Strasser, R. J., Tsimilli-Michael, M., Qiang, S., and Goltsev, V. (2010). Simultaneous in vivo recording of prompt and delayed fluorescence and 820-nm reflection changes during drying and after rehydration of the resurrection plant Haberlea rhodopensis. *Biochim. Biophys. Acta Bioenerg.* 1797, 1313–1326. doi: 10.1016/j.bbabio.2010.03.008

Strasser, R. J., Tsimilli-Michael, M., and Srivastava, A. (2004). "Analysis of the chlorophyll a fluorescence transient," in *Chlorophyll a Fluorescence: A Signature of Photosynthesis*, eds G. C. Papageorgiou and Govinjee (Dordrecht: Springer), 321–362.

Tomar, R., Sharma, A., and Jajoo, A. (2015). Assessment of phytotoxicity of anthracene in soybean (Glycine max) with a quick method of chlorophyll fluorescence. *Plant Biol.* 17, 870–876. doi: 10.1111/plb.12302

van Heerden, P. D. R., Swanepoel, J. W., and Kruger, G. H. J. (2007). Modulation of photosynthesis by drought in two desert scrub species exhibiting C3-mode CO2 assimilation. *Environ. Exp. Bot.* 61, 124–136. doi: 10.1016/j.envexpbot.2007.05.005

Yamamoto, H., and Shikanai, T. (2019). PGR5-dependent cyclic electron flow protects photosystem I under fluctuating light at donor and acceptor sides. *Plant Physiol.* 179, 588–600. doi: 10.1104/pp.18.01343

Yamori, W., Kusumi, K., Iba, K., and Terashima, I. (2020). Increased stomatal conductance induces rapid changes to photosynthetic rate in response to

naturally fluctuating light conditions in rice. *Plant Cell Environ.* 43, 1230–1240. doi: 10.1111/pce.13725

Yin, Z.-H., and Johnson, G. N. (2000). Photosynthetic acclimation of higher plants to growth in fluctuating light environments. *Photosynth. Res.* 63, 97–107. doi: 10.1023/A:1006303611365

Yusuf, M. A., Kumar, D., Rajwanshi, R., Strasser, R. J., Tsimilli-Michael, M., Govindjee, et al. (2010). Overexpression of γ-tocopherol methyl transferase gene in transgenic *Brassica juncea* plants alleviates abiotic stress: physiological and chlorophyll a fluorescence measurements. *Biochim. Biophys. Acta* 1797, 1428–1438. doi: 10.1016/j.bbabio.2010.02.002

Zhang, D., Zhang, Q. S., Yang, X. Q., Sheng, Z. T., and Nan, G. N. (2016). The alternation between PSII and PSI in ivy (*Hedera nepalensis*) demonstrated by in vivo chlorophyll a fluorescence and modulated 820 nm reflection. *Plant Physiol. Biochem.* 108, 499–506. doi: 10.1016/j.plaphy.2016.08.018

Živčak, M., Brestič, M., and Kalaji, H. M. (2014). Photosynthetic responses of sun- and shade-grown barley leaves to high light: is the lower PSII connectivity in shade leaves associated with protection against excess of light? *Photosynth. Res.* 119, 339–354. doi: 10.1007/s11120-014-9969-8

Żurek, G., Rybka, K., Pogrzeba, M., Krzyżak, J., and Prokopiuk, K. (2014). Chlorophyll a fluorescence in evaluation of the effect of heavy metal soil contamination on *Perennial grasses*. *PLoS One* 9:e91475. doi: 10.1371/journal.pone.0091475

Conflict of Interest: The authors declare that the research was conducted in the absence of any commercial or financial relationships that could be construed as a potential conflict of interest.

Publisher's Note: All claims expressed in this article are solely those of the authors and do not necessarily represent those of their affiliated organizations, or those of the publisher, the editors and the reviewers. Any product that may be evaluated in this article, or claim that may be made by its manufacturer, is not guaranteed or endorsed by the publisher.

frontiers in Plant Science

ORIGINAL RESEARCH
published: 03 January 2022
doi: 10.3389/fpls.2021.615253

Effectiveness of Light-Quality and Dark-White Growth Light Shifts in Short-Term Light Acclimation of Photosynthesis in *Arabidopsis*

*Elisabeth Hommel[1], Monique Liebers[2], Sascha Offermann[3] and Thomas Pfannschmidt[3]**

[1] Pflanzenphysiologie, Institut für Biologie, Universität Leipzig, Leipzig, Germany, [2] Molekulare Pflanzenphysiologie, Institut für Pflanzenwissenschaften und Mikrobiologie, Universität Hamburg, Hamburg, Germany, [3] Pflanzenphysiologie, Institut für Botanik, Naturwissenschaftliche Fakultät, Leibniz-Universität Hannover, Hanover, Germany

OPEN ACCESS

Edited by:
Fiamma Longoni,
Université de Neuchâtel, Switzerland

Reviewed by:
Wojciech Jacek Nawrocki,
VU Amsterdam, Netherlands
Alexey Shapiguzov,
University of Helsinki, Finland

***Correspondence:**
Thomas Pfannschmidt
Thomas.Pfannschmidt@botanik.uni-hannover.de

Specialty section:
This article was submitted to Plant Abiotic Stress, a section of the journal Frontiers in Plant Science

Received: *08 October 2020*
Accepted: *07 December 2021*
Published: *03 January 2022*

Citation:
Hommel E, Liebers M, Offermann S and Pfannschmidt T (2022) Effectiveness of Light-Quality and Dark-White Growth Light Shifts in Short-Term Light Acclimation of Photosynthesis in Arabidopsis. Front. Plant Sci. 12:615253. doi: 10.3389/fpls.2021.615253

Photosynthesis needs to run efficiently under permanently changing illumination. To achieve this, highly dynamic acclimation processes optimize photosynthetic performance under a variety of rapidly changing light conditions. Such acclimation responses are acting by a complex interplay of reversible molecular changes in the photosynthetic antenna or photosystem assemblies which dissipate excess energy and balance uneven excitation between the two photosystems. This includes a number of non-photochemical quenching processes including state transitions and photosystem II remodeling. In the laboratory such processes are typically studied by selective illumination set-ups. Two set-ups known to be effective in a highly similar manner are (i) light quality shifts (inducing a preferential excitation of one photosystem over the other) or (ii) dark-light shifts (inducing a general off-on switch of the light harvesting machinery). Both set-ups result in similar effects on the plastoquinone redox state, but their equivalence in induction of photosynthetic acclimation responses remained still open. Here, we present a comparative study in which dark-light and light-quality shifts were applied to samples of the same growth batches of plants. Both illumination set-ups caused comparable effects on the phosphorylation of LHCII complexes and, hence, on the performance of state transitions, but generated different effects on the degree of state transitions and the formation of PSII super-complexes. The two light set-ups, thus, are not fully equivalent in their physiological effectiveness potentially leading to different conclusions in mechanistic models of photosynthetic acclimation. Studies on the regulation of photosynthetic light acclimation, therefore, requires to regard the respective illumination test set-up as a critical parameter that needs to be considered in the discussion of mechanistic and regulatory aspects in this subject.

Keywords: photosynthesis, state transitions, photosystem II super-complexes, light-quality control, dark-light shifts

INTRODUCTION

In oxygenic photosynthesis of plant and algae chloroplasts photosystem II (PSII) and photosystem I (PSI) work electrochemically in series. Efficient electron transport from the donor at PSII, water, to the final acceptor at PSI, $NADP^+$, therefore, requires a balanced action of both photosystems. The reaction centers possess slightly different absorption maxima of 680 nm for PSII and 700 nm for PSI. Enrichment of either wavelength in the incident light, thus, can cause imbalances in photosystems excitation which in turn reduces the efficiency in photosynthetic energy conversion (Allen and Pfannschmidt, 2000). Many abiotic and biotic influences can lead to variations in the illumination of plants. A number of highly sophisticated regulation mechanisms evolved that acclimate the process of photosynthetic light harvesting to variations in both light intensity and light-quality that can occur at time scales ranging from seconds to minutes as well as from daily to seasonal variations (Kanervo et al., 2005; Walters, 2005; Eberhard et al., 2008).

In dense populations of terrestrial plants one can observe an exponential decrease in light intensity and a concomitant enrichment of far-red light wavelengths both caused by selective absorption of photosynthetically active radiation (PAR) from the top leaves of the canopy (Terashima and Hikosaka, 1995; Dietzel et al., 2008; Johnson and Wientjes, 2020). Far-red light enriched environments typically lead to relative over-excitation of PSI and a subsequent oxidation of the intermittent electron carriers such as plastoquinone (PQ). Sudden light flashes or long-term exposure to direct sun-light caused by leaf movement through wind or growth can induce the opposite situation in which preferential excitation of PSII creates a more reduced state of the PQ pool. The PQ oxidation at the cytochrome b_6f complex, an electron transport complex functionally placed between PSII and PSI, is the slowest and, therefore, rate-limiting step of the photosynthetic electron transport. It, thus, represents an ideal sensor for environmental fluctuations (Pfannschmidt, 2003). Indeed, the reduction/oxidation (redox) state of the PQ pool was found to be a key regulator of important photosynthetic acclimation processes including short-term and long-term acclimation responses, such as state transitions and photosystem stoichiometry adjustment (Dietzel et al., 2008; Johnson and Wientjes, 2020 (Goldschmidt-Clermont and Bassi, 2015).

State transitions represent a short-term regulation mechanism for excitation energy redistribution in which the relative antenna cross section of PSII and PSI is modulated through selective phosphorylation of the light harvesting complex of PSII (LHCII) (Allen and Forsberg, 2001). Upon preferential excitation of PSII the PQ pool becomes more reduced. This activates by still unclear mechanistic means the thylakoid-bound kinase STN7 (Bellafiore et al., 2005) that phosphorylates the PSII-bound LHCII. This phosphorylation induces a lateral migration of parts of the LHCII to PSI, thereby reducing the PSII antenna cross section (and its photon absorption capability) and enlarging that of PSI with the goal to redirect more light energy to the rate limiting PSI (state 2) (Rochaix, 2013; Pan et al., 2018). In the opposite case oxidation of the PQ pool was observed to be accompanied by an inactivation of STN7 and a constitutively active thylakoid bound phosphatase PPH1/TAP38 (Pribil et al., 2010; Shapiguzov et al., 2010) de-phosphorylates the LHCII bound to PSI inducing a lateral re-migration to PSII (state 1). PSII core proteins are phosphorylated by another kinase called STN8 that is not under direct control of the PQ pool (Bonardi et al., 2005; Vainonen et al., 2005). It, however, displays a partial substrate overlap with STN7 and is involved in many aspects of photosynthetic regulation that are related to STN7-controlled functions. Understanding photosynthetic regulation by phosphorylation, therefore, requires considering both kinase activities (Rochaix, 2013). Recent studies uncovered that phosphorylated Lhcb1 and Lhcb2 proteins perform different roles during state transitions with Lhcb2 being the dominant protein in this process (Pietrzykowska et al., 2014; Crepin and Caffarri, 2015; Longoni et al., 2015).

Our understanding of the mechanistic steps triggering state transitions is highly complicated by the fact that the linear electron transfer function is not reflected in the structure of the photosynthetic apparatus. The thylakoid membrane system in which the photosystems reside possesses a highly organized three-dimensional structure and can be distinguished into grana membranes with tightly appressed membrane stacks and the interconnecting stroma lamellae. The precise structure of the thylakoid membrane system is still under investigation (Pribil et al., 2014; Kowalewska et al., 2016), however, it is commonly accepted that PSII and its LHCII are located within the grana stacks while PSI (and also the ATPase) are located in grana margins and stroma lamellae since their stromal protein extrusions sterically prevent a presence within the appressed grana membrane stacks (Dekker and Boekema, 2005). Movement of LHCII complexes between PSII and PSI would not only require lateral migration in a membrane but also a movement between grana and stroma lamellae sections. Such directed migration is mechanistically difficult to explain regarding the complex structure of the thylakoid membrane and its crowding with embedded protein complexes that cause steric hindrances (Kirchhoff et al., 2011). The topic of LHCII migration during state transitions is still not fully understood and alternative models for these movements (and thus for state transitions) are proposed in which not only the LHCII but also the photosystems move in order to generate PSII/LHCII/PSI hyper-complexes (Tikkanen et al., 2011).

The structure of the thylakoid membrane system is not fixed but highly dynamic. Phosphorylation of LHCII complexes and/or PSII core proteins within the grana stacks induces a (partial) de-stacking of the membrane structure probably by introducing negative charges on both sides of the membrane stack that repel each other (Allen, 1992). It is important to note that the LHCII kinase STN7 likely cannot enter the grana due to an extruding stromal domain (Rochaix, 2013). Phosphorylation of LHCII, thus, can occur only at the grana margins where the kinase is located. LHCII phosphorylation and subsequent grana membrane de-stacking, therefore, can happen only step-wise from outside to inside and its kinetic depends on the number of available LHCII complexes that reach the STN7 kinase domain. Similar structural constraints may occur

also in PSII core phosphorylation events that are suggested to play a role in antenna dissociation and core monomerization (Puthiyaveetil and Kirchhoff, 2013).

Functional PSII complexes within grana stacks typically form dimers that associate with various amounts of LHCII trimers generating so-called PSII super-complexes. The largest association stably isolated after detergent treatment consists of two PSII core (C) complexes with each having one strongly (S) and one moderately (M) bound LHCII trimer generating the $C_2S_2M_2$ complex (Caffarri et al., 2009). *In vivo* larger associations might be possible. Partial dissociation of this $C_2S_2M_2$ complex generates smaller super-complexes while aggregations of it create so-called mega-complexes that can even form para-crystalline structures in the grana membranes (Dekker and Boekema, 2005). Upon a state 1-to-state 2 transition a decrease in $C_2S_2M_2$ complexes and a concomitant increase of $C_2S_2M_1$ complexes has been observed that suggest an involvement of the M complexes in state transitions (Kouril et al., 2005). In addition, extra LHCII trimers with only very loose contact to the PSII core are located between the super-complexes and in the grana margins providing further candidate trimers that potentially migrate during state transitions (Kouril et al., 2013).

Phosphorylation of PSII core and LHCII trimers is a major determinant of the highly complex arrangement of the photosynthetic apparatus and the thylakoid membrane structure, but the precise sequence of events is far from being clear. We recently could demonstrate that light-quality shifts that either reduce or oxidize the photosynthetic electron transport chain do have pronounced effects not only on STN7 activity and state transitions but also on the formation and the release of PSII super-complexes (Dietzel et al., 2011). These changes in PSII super-complex accumulation occur in the same time range as state transitions and appear to be a limiting factor for them as the amount of PSII super-complexes correlates inversely with the speed of state transitions. According to current data the PSII super-complex release (and presumably the release of PSII super-complexes attached to each other) starts most likely with the phosphorylation of CP43, a core protein of PSII. Stn7/Stn8 double mutants that lack any PSII/LHCII phosphorylation cannot release PSII super-complexes (and likely also structures of higher order such as mega-complexes) and do not display any state transitions. Conversely, in mutants that cannot form PSII super-complexes state transitions run faster. This effect is likely caused by a faster LHCII trimer phosphorylation that is required for state transitions because of higher mobility of the trimers in the membrane (Damkjaer et al., 2009; Dietzel et al., 2011; Garcia-Cerdan et al., 2011). The trimer identity and role of LHCII phosphorylation during PSII remodeling is, however, still under debate as also alternative models have been presented proposing that the so-called extra LHCII trimers are phosphorylated and migrate to PSI during a state 1-to-state 2 transition (Wientjes et al., 2013). Concomitant with that the LHCII trimers in PSII super-complexes were found to be phosphorylated but did not induce a release of the complexes. It was concluded that phosphorylation is not sufficient for a release of PSII super-complexes and that these are stable during a state 1-to-state 2 transition (Wientjes et al., 2013). Recent studies revealed that also the activity of the chloroplast acetyltransferase NSI is required for state transitions and thylakoid membrane remodeling (Koskela et al., 2018, 2020). While the precise mechanistic involvement of protein acetylation requires further investigation these studies reveal that photosynthetic light acclimation is not only dependent on phosphorylation of LHCII proteins but may involve additional post-translational modifications of thylakoid membrane proteins.

Research on processes involved in state transitions typically is done in the laboratory on plants grown under defined light conditions that induce either reduction or oxidation of the PQ pool, respectively. These conditions may be induced by technically slightly different test set-ups, but not much attention has been given yet to such details. We were wondering whether illumination set-ups with small different technical settings but with comparable effects on the PQ pool redox state do induce equivalent physiological effects on photosynthetic acclimation. To this end, we compared light-quality shifts and dark-white light shifts in their effectiveness on state transitions, photosynthetic antenna phosphorylation and PSII super-complex formation.

MATERIALS AND METHODS

Plant Material

Arabidopsis thaliana var. Columbia-O (Col-0) plants were grown on soil for 14 days under long day (LD) conditions (16 h light/8 h dark) at 50 μmol m^{-2} s^{-1} white light (Lumilux "Cool White" L 18W/840, Osram) at 23°C and 60% humidity before subsequent light treatments. Plants subjected to long-term light-quality treatment (6 days under continuous PSI- or PSII-light) were grown for 5 days in LD conditions followed by 3 days of continuous WL (to adapt the plants to the continuous illumination) matching a final age of 14 days. Plant material was grown in several parallel pots allowing to split plant sets for individual light treatments after a common initial growth phase. All growth experiments and their subsequent physiological and molecular characterizations were done with at least three independent biological replicates.

Illumination Set-Ups and Thylakoid Membrane Isolation

After 14 days of pre-cultivation under LD conditions (if not indicated otherwise) plants were subjected to various illumination set-ups for the indicated time periods. White light (WL) treatments were performed under the identical light sources as used for pre-cultivation. The technological set-up for PSI- and PSII-light treatments was identical to that described in Wagner et al. (2008) and Dietzel et al. (2011). For better understanding and interpretation of the physiological effects the emission spectra of the WL, PSI- and PSII-light sources within the growth chambers were recorded with a spectrometer (LI-180, LI-COR Biosciences). These spectra are given in the **Supplementary Figure S1**. After the respective light treatments (compare **Table 1**) plant material was harvested directly under the light source and put immediately into ice-cold homogenization buffer followed by isolation of thylakoid

TABLE 1 | Summary of illumination programs and the corresponding physiological questions investigated by these approaches.

Abbreviation	Illumination program	Physiological state in question
Control		
Dark	14 d of growth in 16 h WL/8 h dark; harvest under safe green light before beginning of next light period	State of PS at the end of a dark period in a standard dark-light growth schedule (state 1 as in Wientjes et al., 2013).
Light-quality shifts		
Dark - PSII 50	14 d of growth in 16 h WL/8 h dark + 50 min PSII-light	Induction of state 2 by 50 min of PSII-light instead of WL.
Dark - PSII 50 - PSI 30	14 d of growth in 16 h WL/8 h Dark + 50 min PSII-light + 30 min PSI-light	Induction of state 1 by additional 30 min of PSI-light.
Dark-white light (WL) shifts		
Dark - WL 50	14 d of growth in 16 h WL/8 h dark + 50 min WL	State of PS after 50 min of WL following the last dark period (state 2 as in Wientjes et al., 2013).
Dark - WL 50 - Dark 15	14 d of growth in 16 h WL/8 h dark + 50 min WL + 15 min dark	Effect of additional 15 min of dark after 50 min illumination (re-opening of PSII centers).
Dark - WL 2 h	14 d of growth in 16 h WL/8 h dark + 2 h WL	Approval of state 2 after extended illumination with WL.
Dark - WL 2 h - Dark 15 min	14 d of growth in 16 h WL/8 h dark + 2 h WL + 15 min dark	Effect of additional 15 min of dark after extended WL acclimation (re-opening of PSII centers).

All plants analyzed were 14 days old. For plants subjected to long-term light-quality treatments the pre-growth phase was correspondingly shortened. Abbreviations used: d, days; h, hours; min, minutes; PS, photosynthesis apparatus. Abbreviations for light sources are as given in main text.

membranes as described (Järvi et al., 2011). Chlorophyll concentration of resulting samples was determined according to Porra et al. (1989). Thylakoid samples isolated for BN-PAGE analysis were immediately processed after isolation. Aliquots from these samples were frozen for western-immune-blot analyses after SDS-PAGE and kept at −80°C until further use.

Room Temperature Chlorophyll Fluorescence Measurements

Time course and degree of Chl fluorescence transients of 14-to-21-day-old WT plants and *stn7* mutants grown under DL conditions subjected to indicated shifts in illumination were detected using a pulse amplitude modulation (PAM)-based fluorometer (Junior-PAM, Walz). The measurements aimed to analyze the general dynamics in the Chl fluorescence changes induced by the indicated light shifts with a special emphasis on the process of state transitions. As reference a standard state transition experiment using the internal monochromatic light sources (blue LED, 450 nm, far-red LED, 730 nm) of the Junior-PAM device was performed. To this end plants in their growth pots were placed under the Junior-PAM detector in a way that Chl fluorescence detection was yielding sufficient intensity, but without using a clamp for the leaf that could influence gas exchange. The distance between the fiber optics probe and the leaf surface was adjusted to 5 mm. After 1 h of dark acclimation F_0 and F_m were determined for calculation of F_v/F_m ($F_v = F_m - F_0$) using the Junior-PAM internal measuring light and saturation pulses. Then, actinic light (blue LED, 45 μmol photons m^{-2} s^{-1}) was switched on for 30 min for induction of state 2. At steady state fluorescence in state 2 (F_{s2}) a saturation pulse was given for detection of F_{m2}'. Then, far-red light (Junior-PAM, level 12) was added for further 30 min to induce state 1. When reaching a steady state fluorescence in state 1 (F_{s1}) another saturation pulse was given for detection of F_{m1}'. Reversibility of the light-induced acclimation responses was checked in each replicate by switching off the far-red LED allowing for returning to state 2. Determination of Chl fluorescence transients and state transitions induced by growth light sources were done essentially in the same manner as described for the LED-driven reference experiment, but using shifts between the growth lights instead of the internal LEDs. In light quality shift experiments state 2 was induced in 1 h dark-acclimated plants by 50 min illumination with PSII-light, while state 1 was induced by subsequent illumination with PSI-light for 30 min. Reversibility of state transitions in these conditions was checked by a switch back to PSII-light for each replicate. Dark-light shift experiments were performed analogously starting with 1 h dark-acclimation, followed by a 50 min illumination period with white light to induce state 2, followed by a 30 min shift to darkness to induce state 1. Again, reversibility of state transitions was checked by another 30 min of illumination with white light. Calculations of state transition parameters for all light set-ups are given in legend of **Table 2**.

Detection of Thylakoid Membrane Proteins and Their Phosphorylation States

Total accumulation and phosphorylation state of proteins or complexes were determined by western-immune-analyses using protein-specific antisera directed against D1, D2, CP43, Lhcb1 (Agrisera No. AS05084, AS06146, AS111787, AS01004) or an anti-phospho-threonine antibody (Cell Signaling Technology®) and the enhanced chemiluminescence (ECL) assay. Indicated amounts of samples were separated by either denaturing SDS-PAGE or BN-PAGE and transferred to nitrocellulose membrane (®PROTAN Whatman) by semi-dry-western blotting using standard protocols (Sambrook and Russel, 2001). ECL visualization of primary antisera was done using suitable secondary anti-sera fused to horseradish peroxidase and a Chemi-Doc-^{TM}MP Imaging System (BioRad Laboratories).

Recording of large differences in signal intensities occurring on one and the same membrane (especially those between phosphorylated core and light harvesting proteins) was done by a series of increasing exposition times in the camera system allowing for respecting the linearity between protein loading and signal intensity. Optimal loading of SDS-PAGE gels with respect to equality of protein amounts between different samples and the linearity between loaded protein amount and resulting ECL signal was systematically determined by serial dilution of WL extracts and determination of the corresponding phosphothreonine signals. Best signal ratios were obtained in the range of 20–30 μg total chlorophyll in the protein extracts and all subsequent experiments were adjusted to this range. In addition, equal loading of each SDS-PAGE gel was tested after the immune-detection using amido-black or Ponceau S staining of the respective membranes.

BN-PAGE and 2D BN-PAGE

Both BN-PAGE and 2D BN-PAGE were performed essentially as described earlier (Dietzel et al., 2011). Thylakoid sample volumes corresponding to 20 or 30 μg chlorophyll were used for solubilization of thylakoid membranes by adding β-dodecyl-maltoside (β-DM) to a final concentration of 1% (w/v). Samples were separated on 0.75 mm × 12 cm × 18 cm native 5–12% acrylamide gradient gels. The BN gel run was performed for 15 h (over-night) at 70 V in a cold chamber at 4°C. The voltage was then adjusted to 250 V until the run was finished. The cathode blue buffer was replaced by colorless buffer after 2/3 of the gel run. The BN gels were photographically documented, disassembled and cut into slices isolating the different sample lanes. These slices were incubated in denaturing Laemmli buffer [138 mM Tris/HCL pH 6.8, 6M urea, 22.2% (w/v) glycerol, 4.3% (w/v) SDS, 5% (v/v) 2-mercaptoethanol] for 1 h in a Petri dish under gentle shaking, loaded on a denaturing 6–12% acrylamide SDS gradient gel and separated over night at 12 mA. Finally, the gels were silver-stained following standard protocols (Sambrook and Russel, 2001) and photographically documented.

RESULTS

Induction and Dynamics of Photosynthetic Acclimation in Response to Light Quality and Dark-White Light Shifts

Recent studies reported 77K fluorescence emission spectra indicating that both, light-quality and dark-white light shifts, induce a significant lateral movement of the mobile LHCII antenna between PSII and PSI resulting in considerable changes of the respective antenna cross sections. The state transition deficient *Arabidopsis* mutant *stn7* was devoid of such changes indicating that the differences in the observed 77K spectra of WT and mutant were caused by short-term antenna movements, i.e., state transitions (Dietzel et al., 2011; Koskela et al., 2018). The 77K measurements, however, provide only static start and end point comparisons missing the dynamics of the respective acclimation responses. In order to follow the course of photosynthetic acclimation induced by light-quality or dark-white light shifts we recorded room temperature (RT) Chl fluorescence transients of plants subjected to corresponding growth light shifts. The *Arabidopsis* state transition mutant *stn7* was used as reference throughout all experiments in order to distinguish between the impact of energy dependent quenching (qE) and state transitions (qT). The impact of photoinhibition-dependent quenching (qI) was regarded as negligible since only weak actinic light was used for excitation in these experiments.

As technical reference for the two illumination set-ups studied we recorded Chl fluorescence changes of WL-grown wild-type control plants (WT) subjected to standard LEDs providing monochromatic blue and far-red light as typically used in PAM-derived Chl fluorescence measurements (for detection of state transitions) (**Figure 1A**). Illumination with blue light as actinic light source was used to induce a stable steady state fluorescence resulting in state 2 in WT plants (dark gray traces, **Figure 1A**). Additionally applied far-red light resulted in a sudden fluorescence drop caused by enhanced excitation of PSI that accelerates the withdrawal of electrons from the inter-photosystem transport chain leading to the oxidation of the PQ pool. Subsequently a sigmoidal increase in fluorescence was observed (corresponding to a state 2–state 1 transition) that reached the steady state (state 1) after ∼10 min, a time frame comparable to earlier reports (Dietzel et al., 2011; Koskela et al., 2018). After switching off the far-red light source the Chl fluorescence values exhibited a sharp increase followed by rapid quenching reaching a steady state after ∼10 min corresponding to a state 1–state 2 transition. This sharp fluorescence peak is caused by the sudden over-excitation of PSII due to the decelerated removal of electrons from the PQ pool. Notably, the steady state fluorescence in state 2 and state 1 stabilized at the same values indicating the balancing effect of state transition in electron transport. Performing the same light quality shifts with the *stn7* mutant resulted in a completely different response pattern (red traces, **Figure 1A**). Far-red illumination of the mutant caused a much stronger drop in fluorescence than in WT which is most likely caused by the large immobile PSII antenna since the mutant is unable to perform a transition to state 2. Unlike the WT the mutant was unable to return to the steady state fluorescence level, although we observed a weak increase within the first 15 min that may indicate that the mutant was still able to perform some minor antenna re-arrangements of unknown origin. Switching off the far-red light source resulted in a jump of the fluorescence signal back to the original values followed by a slow further increase again suggesting some minor re-arrangements in the antenna or the photosynthetic electron transport chain. It must be noted that the fluorescence values of WT and mutant were normalized to the values in state 2. Since Chl fluorescence measurements provide only relative values, it is not possible to compare Chl fluorescence values in absolute terms. Likely the state 2 fluorescence in the *stn7* mutant is higher than in WT but since an internal control is not available this could not be quantified.

Subjecting WT plants to shifts between PSII- and PSI-growth lights resulted in Chl fluorescence changes highly comparable to the LED based system (**Figure 1B**). The fluorescence drop after

shift from PSII- to PSI-light was somewhat more pronounced than with the addition of far-red LED light, therefore the subsequent fluorescence rise took a bit longer in total time, but fully recovered. A shift back to PSII-light induced a slightly stronger fluorescence peak that, however, was fully quenched in a similar time range as in the LED-based system. Also the *stn7* mutant displayed Chl fluorescence changes in response to the light shifts which were highly similar to those in the LED-based system. In sum, the obtained data indicate that shifts between the PSI- and PSII-growths are able to effectively induce state transitions.

Next, we performed corresponding experiments using dark-white light shifts for manipulation of photosynthetic electron transport (**Figure 1C**). Dark-acclimated wild-type plants were illuminated for 30 min with white light in a comparable intensity as with the PSII-light source until the plants reached a stable steady state fluorescence. Shifting plants to dark conditions induced a drop in Chl fluorescence that was followed by a slow sigmoidal increase in fluorescence that reached the steady state (state 1) after ∼30 min. A shift back to white light induced a sharp fluorescence rise that was quickly quenched by the light activation of photochemical and non-photochemical quenching (NPQ) processes. The same experiments done with the *stn7* mutant resulted in a significant drop in fluorescence after shift to darkness. The mutant was unable to return to the starting level in Chl fluorescence, thus the slow sigmoidal return observed in WT can be regarded as a transition to state 1. A shift back to white light induced a fluorescence rise that was considerably smaller than in WT followed by rapid quenching comparable to the WT control.

The dark-to-white light shift is used in standard experimental photosynthesis set-ups to determine the effectiveness of photochemical (PQ) and non-photochemical quenching (NPQ) processes. Since these processes occur in parallel their relative contribution to the overall Chl fluorescence quenching is difficult to quantify, but for determination of state transition dependent quenching (qT) an established protocol exists. This quantification of qT requires saturation light pulses that close the PSII reaction centers and indicate their relative antenna size in either state 1 or state 2 (Haldrup et al., 2001). However, this type of protocol functions properly only under conditions in which the excitation energy of the actinic light source remains stable during measurement without inducing differences in energy-dependent quenching (qE). Since dark-to-WL shifts include intrinsic differences in actinic light intensity a different way of quantification for the contribution of state transitions under these conditions was required. To this end, we determined state transitions in two different ways according to published protocols (Haldrup et al., 2001) as (i) relative change in maximal fluorescence in state 1 and state 2 (qT) and as (ii) relative Chl fluorescence change (F_r) that describes the relative difference of fluorescence in state 2 and state 1 upon changes between either PSI- or PSII-light (Haldrup et al., 2001). In order to eliminate the contribution of energy dependent quenching in these calculations we determined all values in parallel for WT and the state transition mutant *stn7* (both grown and measured under identical conditions). Then we subtracted the values of the mutant from WT assuming that the remaining values provide an approximation for the contribution of state transitions to the fluorescence changes in the growth light systems (given as $qT_{approx.}$ and ΔF_r in **Table 2**). According to these results we found that in both growth light set-ups, illumination shifts induce state transitions comparable to the LED-based detection system. All plant batches were in a comparable viability state as indicated by highly similar F_v/F_m values (see **Table 2**) excluding the possibility of interference by stress responses. The Chl fluorescence traces provided also a rough estimate for the speed of state transitions in the different illumination systems. According to these data the state transitions in the LED-based test system and the PSI-PSII-growth light sources were comparable in speed, while

TABLE 2 | Chlorophyll fluorescence parameters in the different light set-ups.

Set-up	F_v/F_m	qT_1	qT_1 approx	qT_2	qT_2 approx	F_r	ΔF_r
Internal LED lights	**WT:** 0.76 ± 0.01 ***stn7:*** 0.79 ± 0.01	**WT:** 0.028 ± 0.008 ***stn7:*** −0.025 ± 0.002	**0.053** ± 0.007	**WT:** 0.049 ± 0.022 ***stn7:*** −0.032 ± 0.003	**0.082** ± 0.019	**WT:** 0.67 ± 0.05 ***stn7:*** −0.2 ± 0.02	**0.87** ± 0.087
PSII-/PSI-light system	**WT:** 0.81 ± 0.00 ***stn7:*** 0.77 ± 0.03	**WT:** 0.04 ± 0.02 ***stn7:*** 0.01 ± 0.01	**0.05** ± 0.071	**WT:** 0.07 ± 0.013 ***stn7:*** 0.027 ± 0.021	**0.047** ± 0.034	**WT:** 0.47 ± 0.2 ***stn7:*** 0.04 ± 0.08	**0.43** ± 0.11
Dark/white- light system	**WT:** 0.82 ± 0.00 ***stn7:*** 0.77 ± 0.01	**WT:** 0.101 ± 0.014 ***stn7:*** 0.044 ± 0.024	**0.057** ± 0.025	**WT:** 0.166 ± 0.036 ***stn7:*** 0.064 ± 0.017	**0.102** ± 0.036	**WT:** 0.9 ± 0.02 ***stn7:*** 0.6 ± 0.03	**0.3** ± 0.066

Calculation of Chl fluorescence parameters was done with data obtained in experiments shown in ***Figure 1****. Results are means of three independent biological replicates. Standard deviations are given. Calculation of* F_v/F_m*:* $F_m - F_0/F_m$*. Calculation of qT (state transition dependent quenching) with the saturation pulse method was done separately for the transitions from state 2 to state 1 (*qT_1*) and from state 1 to state 2 (*qT_2*) as:* $qT_1 = (F_{m1} - F_{m2})/F_{m1}$ *and* $qT_2 = (F_{m1} - F_{m2}')/F_{m1}$*; with* F_{m1}*,* F_{m2} *and* F_{m2}' *as maximum fluorescence yields obtained in stable state 1 and 2, respectively (compare* ***Supplementary Figure S1****). Approximation of state transitions in the light quality and dark-light shift systems is calculated as:* $qT_{n\ approx} = qT_{n\ WT} - qT_{n\ stn7}$*. Calculation of* F_r *according to Haldrup et al. (2001):* $F_r = [(F_i' - F_i) - (F_{ii}' - F_{ii})]/(F_i' - F_i)$ *with* F_i *and* F_{ii} *as fluorescence yield in state 1 or 2, and with* F_i' *and* F_{ii}' *as fluorescence yield in state 1 or 2 directly after illumination shift. Approximation of state transitions on base of* F_r *in WT and stn7 is given as:* $\Delta F_r = F_{r\ WT} - F_{r\ stn7}$*.*

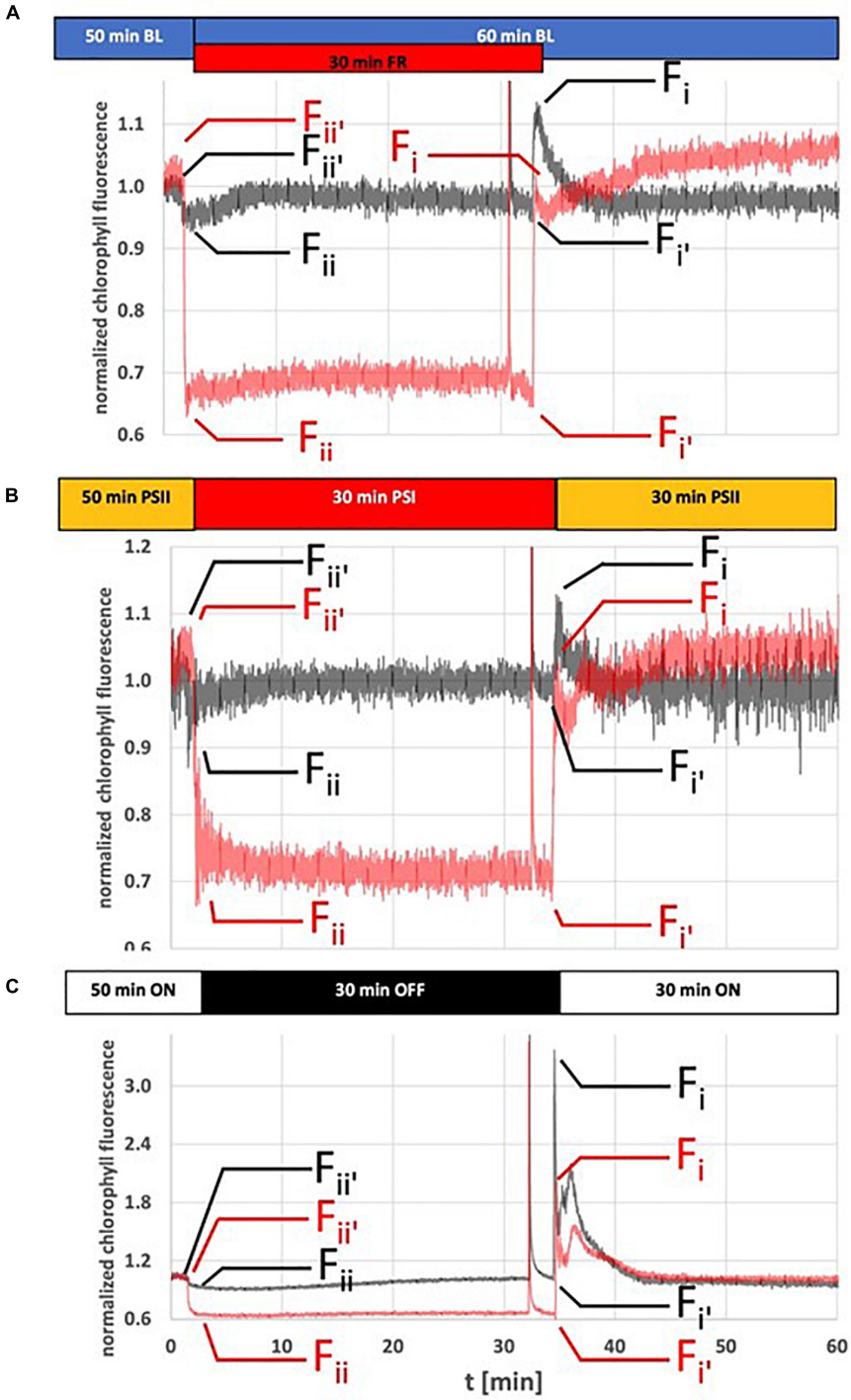

FIGURE 1 | Dynamics of Chl fluorescence changes in response to light quality or dark-light shifts. *Arabidopsis* WT plants (gray traces) and *stn7* mutants (red traces) were grown for 14 days under LD conditions and then used for Chl fluorescence measurements using a pulse amplitude modulated fluorometer. **(A)** Reference measurement using internal LED based light sources of the measurement device for induction of state transitions. **(B)** Chl fluorescence changes caused by shifts between the PSI- and PSII-light sources at equal PAR. **(C)** Chl fluorescence changes caused by dark-white light shifts. Duration of and shifts in illumination are indicated by horizontal bars on top of the fluorescence traces. All experiments started with a 60 min dark-adaptation followed by the light regime indicated in the figure. A saturation light pulse was given 2 min before a change in light condition. Only the pulse in state 1 is visible at this magnification of the figure. F_{ii}', F_{ii}, F_i', and F_i values were taken at indicated time point (small arrows) in order to calculate F_r according to the protocol by Haldrup et al. (2001). Chl fluorescence is given as normalized values. The figure depicts representative results. Each experiment was repeated at least three times with three different biological samples. For understanding of Chl fluorescence nomenclature compare legend of **Table 2**. Full data sets for all graphs including a full representation of saturation light pulses are available in **Supplementary Figure S2**.

that in the white light-to-dark shift was considerably slower (especially for the state 2-to-state 1 transition). A precise determination of the speed of the state 1-to-state 2 transition remained difficult because of the interfering photochemical quenching and NPQ processes, however, in all cases it is likely faster than the state 2-to-state 1 transition since the steady state levels were reached faster.

Phosphorylation Changes Induced by Light-Quality or Dark-Light Shifts

In order to obtain independent experimental proof for the effectiveness of the two growth light systems in inducing state transitions we determined the phosphorylation state of thylakoid membrane proteins in the different illumination set-ups by standard procedures (**Figure 2**). To this end *Arabidopsis thaliana* plants were grown for 2 weeks and subjected to various illumination protocols using light-quality (PSI- or PSII-light) or dark-white light (WL) shifts (explained in **Table 1**). 50 min illumination with PSII-light after the last dark phase induced a strong phosphorylation of LHCII while additional 30 min of PSI-light resulted in a very low phosphorylation state (**Figure 2**, P-LHCII, lanes 1–2). The phosphorylation state of control plants harvested at the end of the last dark period was found to be low, but apparently stronger than after the PSI-light treatment (**Figure 2**, lane 3). When we replaced the PSII-light by WL we observed a strong LHCII phosphorylation that appeared to be slightly stronger than that after PSII-light illumination. Returning such samples for 15 min to the dark partly reversed the phosphorylation state of LHCII (**Figure 2**, P-LHCII, lanes 4, 5). For PSII core proteins D1, D2 and CP43 we observed similar patterns in phosphorylation changes with the exception that the phosphorylation state was found strongest in the dark control (**Figure 2**, top panel, lane 3). 50 min of PSII-light slightly weakened this phosphorylation state, but additional 30 min of PSI-light led to almost complete de-phosphorylation. Illumination of plants with 50 min of WL resulted in a comparable effect as with PSII-light and additional 15 min in the dark resulted in a very minor further decrease (**Figure 2**, top panel, lanes 4, 5).

The observations on LHCII phosphorylation are consistent with earlier reports (Bellafiore et al., 2005; Bonardi et al., 2005; Pesaresi et al., 2009; Tikkanen et al., 2010) and indicate that light-quality shifts as well as dark-light shifts are able to induce LHCII phosphorylation changes that are required for state transitions, i.e., strong LHCII phosphorylation after illumination with PSII-light or WL; and LHCII de-phosphorylation after illumination with PSI-light or transfer to the dark. Control experiments indicated that neither the total protein composition of the thylakoid membrane fractions (**Supplementary Figure S3A**) nor the accumulation of selected PSII proteins (**Supplementary Figure S3B**) displayed major changes in response to the applied light shifts. Most importantly, Lhcb1 (one of the major LHCII proteins) remained fully stable under all tested conditions (**Supplementary Figure S3B**, bottom panel) indicating that the observed variations in phosphorylation state of the antenna (**Figure 2**) are not caused by differences in protein accumulation.

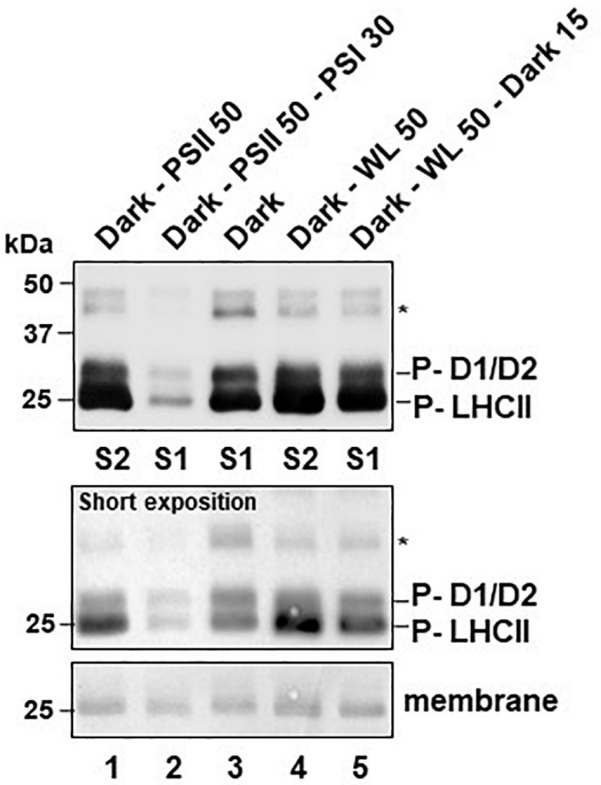

FIGURE 2 | Effects of light-quality or dark-white light shifts on phosphorylation state of thylakoid membrane proteins. Isolated thylakoid protein samples corresponding to 20 μg total chlorophyll were separated by SDS-PAGE. For detection of phosphorylation state proteins were transferred to a nitrocellulose membrane *via* western blot and immuno-decorated using an anti-phospho-threonine antiserum (Cell Signaling Technologies). Labeling was done according to published work (Fristedt et al., 2009; Samol et al., 2012). This phospho-immuno-detection was done once to confirm the state transition results from the Chl fluorescence data and produced results that are in full accordance to earlier studies. A comprehensive statistical treatment of data including triplicate independent biological repetitions, therefore, was regarded as negligible. Relative changes in signal intensities can be sufficiently estimated by comparison to the loading controls given by the respective amido-black stained membranes at the migration front of LHCII trimers (membrane). Additional loading controls are given in **Supplementary Figure S3**. Sizes of marker proteins are given in the left margins in kDa. Signals from phosphorylated CP43 (labeled by asterisk) and another unidentified protein were very weak requiring long exposition times to be visualized. Signals from phosphorylated D1, D2 and LHCII (P-D1/D2, P-LHCII) were reaching saturation under such conditions and a second short exposition time of the same membrane is given (short exposition) as control. All plants were grown for 2 weeks under LD conditions and treated as indicated before sampling. Dark-PSII 50: 50 min PSII-light after dark. Dark-PSII 50–PSI 30: 50 min PSII-light after dark followed by 30 min of PSI-light. Dark: Control at the end of the last dark period. Dark-WL 50: 50 min WL after dark. Dark-WL 50 - Dark 15: 50 min WL after dark followed by 15 min dark. The respective state induced by the illumination program is indicated at the bottom (S1: state 1; S2: state 2).

This indicates that both light set-ups are suitable to control the activity of the redox-responsive STN7 kinase (and hence are suitable for the control of the PQ redox state). However, the two light set-ups may generate subtle differences in PSII core

protein phosphorylation that could be an interesting target for more specific investigations in future.

Phosphorylation State of Native Photosystem Complexes and Photosystem II Remodeling in Response to Light-Quality and Dark-Light Shifts

Assessments of the phosphorylation state of PS proteins after denaturing SDS-PAGE determines the phosphorylation state of the total fraction of a given protein, but cannot distinguish between different association states of native PS complexes in the membrane. Since state transitions and PSII core protein phosphorylation are known to be also connected to PSII remodeling events we determined the phosphorylation state of the diverse PS complexes after mild solubilization and blue native (BN)-PAGE as reported earlier (Dietzel et al., 2011). Strongest changes in phosphorylation states could be observed for free LHCII trimers and (to a minor degree) for so-called LHCII assemblies (**Figure 3A**). As in the denaturing approach, illumination with WL and PSII-light (the latter as long-term or short-term application) resulted in a high phosphorylation state while dark or PSI-light illumination induced low phosphorylation states. Further significant differences in phosphorylation states were found in PSII monomers and super-complexes (**Figure 3A**). The phosphorylation signal of PSII-super-complexes in response to PSII-light was found to be much more pronounced than after PSI-light exposure confirming earlier studies (Dietzel et al., 2011). WL treatment, however, was less effective and could not induce the same strong phosphorylation response as PSII-light (especially after the short-term light shift, **Figure 3A**, lane 4). The signal intensity in the WL samples was more comparable to that from the dark and PSI-light treated samples. The results indicate that PSII-light and WL illumination induce also at the native level a significant phosphorylation of LHCII complexes confirming the effectiveness of both light set-ups in induction of state transitions. Interpretation of the phosphorylation intensities of PSII super-complexes, however, is more difficult since core protein and LHCII phosphorylation contribute to the resulting signal. Furthermore, the signal intensity might be affected by the actual amount of the respective PSII super-complexes.

In order to study such potentially different effects of light-quality and dark-light shifts on PSII super-complexes, thylakoid membrane complexes from *Arabidopsis thaliana* plants grown under corresponding light conditions were analyzed for their assembly states. To this end plant material was harvested under the respective condition, thylakoids were isolated, membranes were solubilized and blue native (BN) PAGE (**Figure 3B**) was performed as described earlier (Dietzel et al., 2011). For testing the impact of light-quality on PSII super-complex formation, plants at the end of the night period were illuminated 50 min with PSII-light, one sample was harvested and the remaining plants were further illuminated with PSI-light for 30 min (**Figure 3B**). While in PSII-light plants only small amounts of PSII super-complexes were detectable, PSI-light exposure induced a strong formation of super-complexes within just 30 min. This is in full accordance with earlier data (Dietzel et al., 2011). Control plants harvested in the dark exhibited only minor amounts of PSII super-complexes that appear to be even less abundant than after PSII-light treatment. In contrast, 50 min of WL exposure caused significant PSII super-complex formation, however, less than after PSI-light treatment (especially with respect to the two largest complexes that correspond to $C_2S_2M_1$ and $C_2S_2M_2$ complexes) (**Figure 3B**). Since in the dark much less PSII super-complexes were found than under WL we concluded that these must exhibit a stronger phosphorylation state than the ones detected in the WL sample (compare to **Figure 3A**, lanes 1, 2). Quantification of the relative changes in phosphorylation signals and Coomassie staining of PSII super-complexes using ImageJ software confirmed that PSII super-complexes from dark samples exhibited stronger phosphorylation than those isolated from samples exposed to 50 min of WL (see **Supplementary Table S1**). This indicates that the phosphorylation states of PSII super-complexes isolated from the dark and 50 min WL samples are opposing the respective states of the LHCII trimers within the same samples. These data are in line with the observation that dark samples display higher core protein phosphorylation states (compare to **Figure 2**). Dark-light shifts, thus, induced state transitions comparable to light-quality shifts, but they caused the opposite effect on PSII super-complex formation. In addition, the PSII super-complex formation induced by WL was found to be not reversible when plants were shifted for 15 min back to dark conditions (**Figure 3C**). Such a dark treatment is commonly used in room temperature Chl fluorescence experiments to re-open all PSII reaction centers and to transfer all antenna complexes back to PSII. Our observations described here strongly suggest that even though all PSII reaction centers might have re-opened a full PSII remodeling is not achieved within 15 min. A longer dark adaptation phase in such kind of experiments, thus, appears to be recommendable. Prolongation of WL illumination to 2 h did not further increase the accumulation of PSII super-complexes indicating that the 50 min WL exposition was already saturating the response (**Figure 3D**). In sum, we conclude that dark-light shifts induce (at least in part) different mechanisms in PSII super-complex formation than light-quality shifts. Alternatively, the release mechanisms might be not the same. As a side observation we found that regardless of which light treatment was used, a high abundance of PSII super-complexes was always accompanied by a strong accumulation of an additional green band in the BN-PAGE (**Figures 3B–D**) that most likely corresponds to LHCII assemblies (Chen et al., 2018) suggesting that the same mechanism that causes the PSII super-complex formation is also involved in the agglomeration of LHCII trimers (or *vice versa*).

Subunit Composition of Photosystem Complexes After Different Light Treatments

Next we analyzed the subunit composition of the different protein complexes identified in the BN-PAGE. Lanes with corresponding material separated by BN-PAGE were cut and subjected to a second denaturing dimension as done earlier (Dietzel et al., 2011). Protein subunits contained in the various

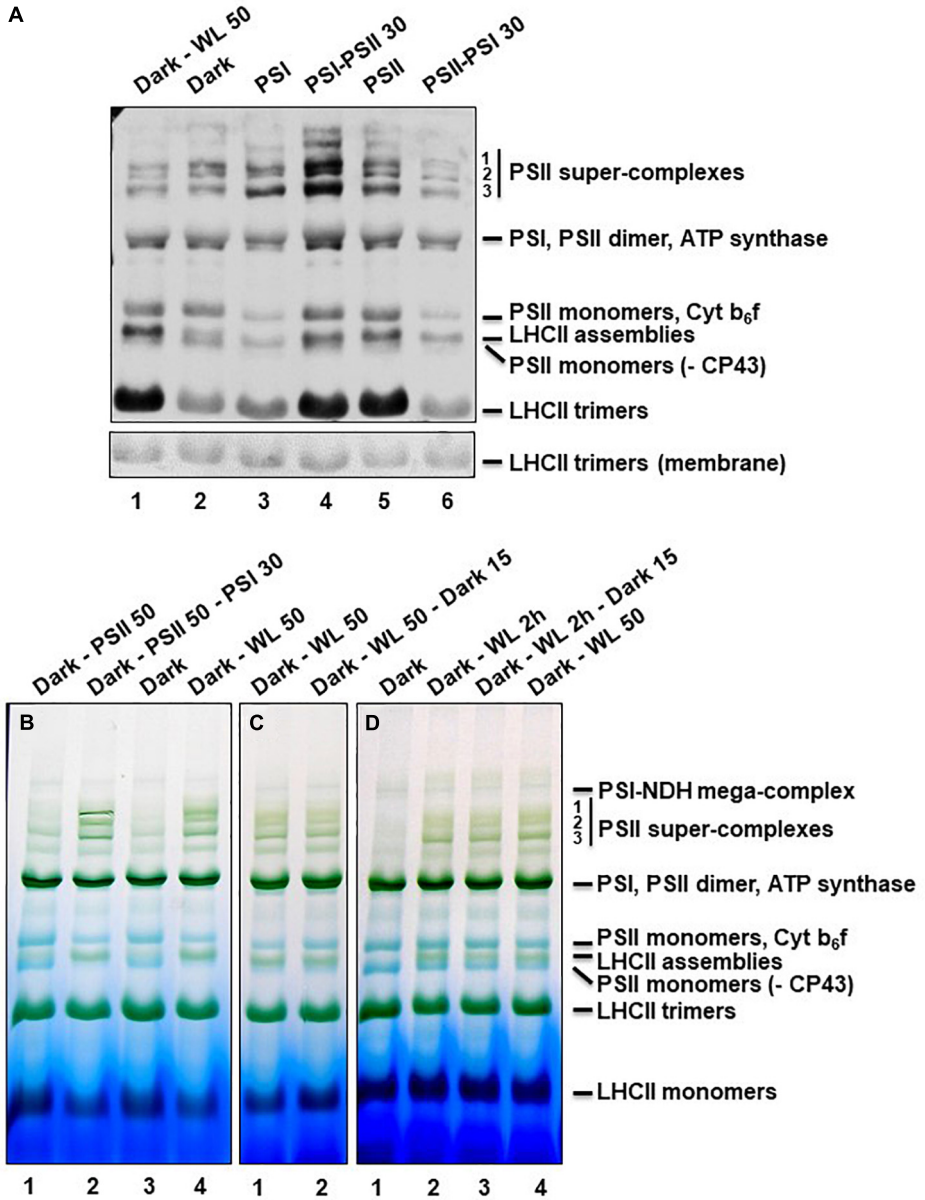

FIGURE 3 | Phosphorylation and assembly states of thylakoid membrane protein complexes after BN-PAGE. **(A)** Thylakoid protein samples corresponding to 20 μg total chlorophyll were separated by BN-PAGE. Material for the first two wells was isolated from plants grown under LD conditions for 2 weeks. Dark-WL 50: 50 min illumination with WL after dark period. Dark: Sample harvested at the end of the night period. All other plants were grown for 5 days under LD conditions, afterward shifted for 3 days to continuous white light and subsequently grown for 6 days under the light-quality regimes indicated on top (matching in total 2 weeks of growth). These samples served as control allowing for comparison with results published earlier (Dietzel et al., 2011). PSI: 6 days PSI-light; PSI-PSII 30: 6 days PSI-light followed by 30 min PSII-light; PSII: 6 days PSII-light; PSII-PSI 30: 6 days PSII-light followed by 30 min PSI-light. The protein complexes separated by the BN-PAGE were denatured in gel by incubation in Laemmli buffer and transferred to a nitrocellulose membrane *via* western blot. Phosphorylation state of thylakoid membrane proteins was detected by incubation with anti-phospho-threonine antibodies. The amido-black stained membrane at the height of LHCII trimers is shown as loading control. Bands were labeled as described (Järvi et al., 2011). The experiment was repeated three times with results showing only marginal variations, thus one representative result is given. Note that the phosphorylation states of the free LHCII trimers correspond well to those shown in **Figure 2**. **(B–D)** Thylakoid protein samples corresponding to 30 μg total chlorophyll were separated by BN-PAGE. Material separated on the same gel always was isolated from the same growth batch of plants that were all grown under LD conditions for 2 weeks prior to the different short-term illumination treatments indicated on top of each well. Dark samples were harvested at the end of the night period and served as control. All material was harvested directly under the respective light source. **(B)** Dark - PSII 50: 50 min PSII-light after dark; Dark - PSII 50 - PSI 30: 50 min PSII- light after dark followed by 30 min PSI-light; Dark: control at end of dark period; Dark - WL 50: 50 min WL after dark (same in panels **(B)** and **(C)**). **(C)** Dark - WL 50 - dark 15: 50 min WL after dark followed by a 15 min shift into dark. **(D)** Dark - WL 2 h: 2 h WL after dark; Dark - WL 2 h - dark 15: 2 h WL after dark followed by a 15 min shift into dark. Panels **(B–D)** are from individual gels each and display representative results. Each experiment was done at least three times. Bands were labeled (right margin) as described (Dietzel et al., 2011; Järvi et al., 2011). As common control Dark - WL 50 was included in all gels.

native complexes were subsequently visualized by silver-staining (**Figures 4A,B**), and identified according to their reported migration behavior in these gel systems as well as by own confirmation by mass spectrometry (Aro et al., 2005). PSII-light acclimation for 50 min caused a very low accumulation of PSII super-complexes (especially of the two largest ones corresponding to $C_2S_2M_1$ and $C_2S_2M_2$ complexes) when compared to the subsequent PSI-light acclimation (see broadly boxed area in **Figure 4A**). Instead high accumulation of PSII monomers with or without CP43 became visible (small boxed area in **Figure 4A**). In addition the PSII monomers containing CP43 displayed a very high proportion of phosphorylated CP43 (indicated by an asterisk). PSI-light acclimation caused the opposite reaction with low amounts of monomeric PSII complexes and apparently undetectable traces of phosphorylated CP43. Interestingly, PSII monomers without CP43 were less abundant in these samples suggesting that they may be involved in the formation of the LHCII assemblies.

The same 2D BN-PAGE analysis was performed with material from *Arabidopsis thaliana* plants harvested shortly before the end of the night phase and after 50 min of WL treatment. Material isolated from the dark phase was almost devoid of PSII super-complexes, but displayed a very high proportion of monomeric PSII complexes and a strong accumulation of phosphorylated CP43 (**Figure 4B**, left side of gel), the latter being consistent with the results presented in **Figure 2**. 50 min WL treatment induced formation of some PSII super-complexes (mainly the lower two bands). Accumulation of monomeric PSII and of phosphorylated CP43 was less when compared to the dark sample but more when compared to PSI-light acclimated samples (**Figure 4A**). This indicates that the structure of PSII super-complexes under dark conditions resembles very much that under PSII-light conditions while WL treatment for 50 min induces a condition being somewhat intermediate between PSI- and PSII-light. We conclude that although PSII-light and WL treatments both induce a significant phosphorylation of LHCII they induce different responses in PSII super-complex formation.

DISCUSSION

Variations in illumination caused by abiotic and biotic factors are one prime source of deleterious effects on photosynthetic efficiency that are counteracted by a multitude of compensation responses such as non-photochemical quenching, state transitions and PSII remodeling events (Morales and Kaiser, 2020). These responses are very complex and typically include structural rearrangements in the photosynthetic apparatus, most of them in the antenna complexes of PSII and PSI (Johnson and Wientjes, 2020). Many details in these antenna rearrangements are not understood yet and, therefore, are investigated in a variety of set-ups. Growth conditions in climate-controlled growth chambers cannot reflect the multitude of variations in the natural environment of a plant, but allow for the analysis of isolated parameters and their effects under standardized conditions. These set-ups, however, are often highly specific and may generate subtle physiological differences that are not apparent on first sight. A careful and detailed analysis, therefore, is highly recommendable for each set-up. Measurement of room temperature Chl fluorescence parameters typically done in a pulse-amplitude modulation (PAM) mode is very informative (Maxwell and Johnson, 2000; Kalaji et al., 2017). However, for these measurements usually the plants are taken out of their growth condition and placed into a measurement room or chamber where they are subjected to highly specific analytic lights. State transition measurements in vascular plants (note that protocols for algae might be different) are often performed with LEDs within the blue range (∼450–470 nm) as actinic light source (compare **Figure 1A**). This actinic light excites PSII and PSI, drives photosynthetic electron flow and reduces the PQ pool resulting in state 2. Induction of state 1 then is induced by illumination with far-red LEDs (∼730–735 nm) either in replacement or in addition resulting in the oxidation of the PQ pool (compare **Figure 1A**). Such measurements report on the ability of the plant to perform state transitions, but they do not report whether or not the growth light system is inducing the respective responses. To obtain this information it is required to perform state transition measurements with the growth light sources as analytic lights. This requires to do the measurements directly within the growth unit (compare **Figures 1B,C**).

Most laboratory growth light systems for plants of at least the last five decades were based on illumination with fluorescent tube lamps, sometimes combined with incandescent bulbs. These light systems are efficient and long-lasting concerning plant growth, but with respect to their light spectrum somewhat limited when compared to natural conditions. When studying photosynthetic light acclimation responses it is, therefore, recommendable to take these specific conditions into consideration. Here we have compared the direct effects of dark-light and PSI-PSII-light shifts of two fluorescent tube-based growth light systems on thylakoid membrane protein phosphorylation, the performance of state transitions and PSII super-complex remodeling in *Arabidopsis* WT plants in order to test how far these two illumination set-ups are comparable.

In principle, one could expect that both conditions, darkness and PSI-light, cause an oxidation of the photosynthetic electron transport chain since in the first case no charge separation can occur while in the second case PSI is working more efficiently than PSII. In contrast, WL and PSII-light should induce a reduction of it including corresponding changes in the PQ pool redox state as both promote charge separation in PSII and subsequent electron transport toward the PQ pool. Consequently, we would expect inactivation or activation of the thylakoid membrane kinase STN7, respectively, and correspondingly we would expect less and more phosphorylation of LHCII. This, indeed, we could observe in the RT Chl fluorescence traces (**Figure 1**) and the thylakoid membrane phosphorylation state (**Figures 2**, **3A**). It must, however, be noted that the changes in the RT Chl fluorescence traces represent the combined action of several quenching processes and the proportion that state transitions contribute could be determined only by the inclusion of the *stn7* mutant as negative control. This approach provided a reasonable approximation of the extent to which state transitions contribute to the changes in the Chl fluorescence signal observed

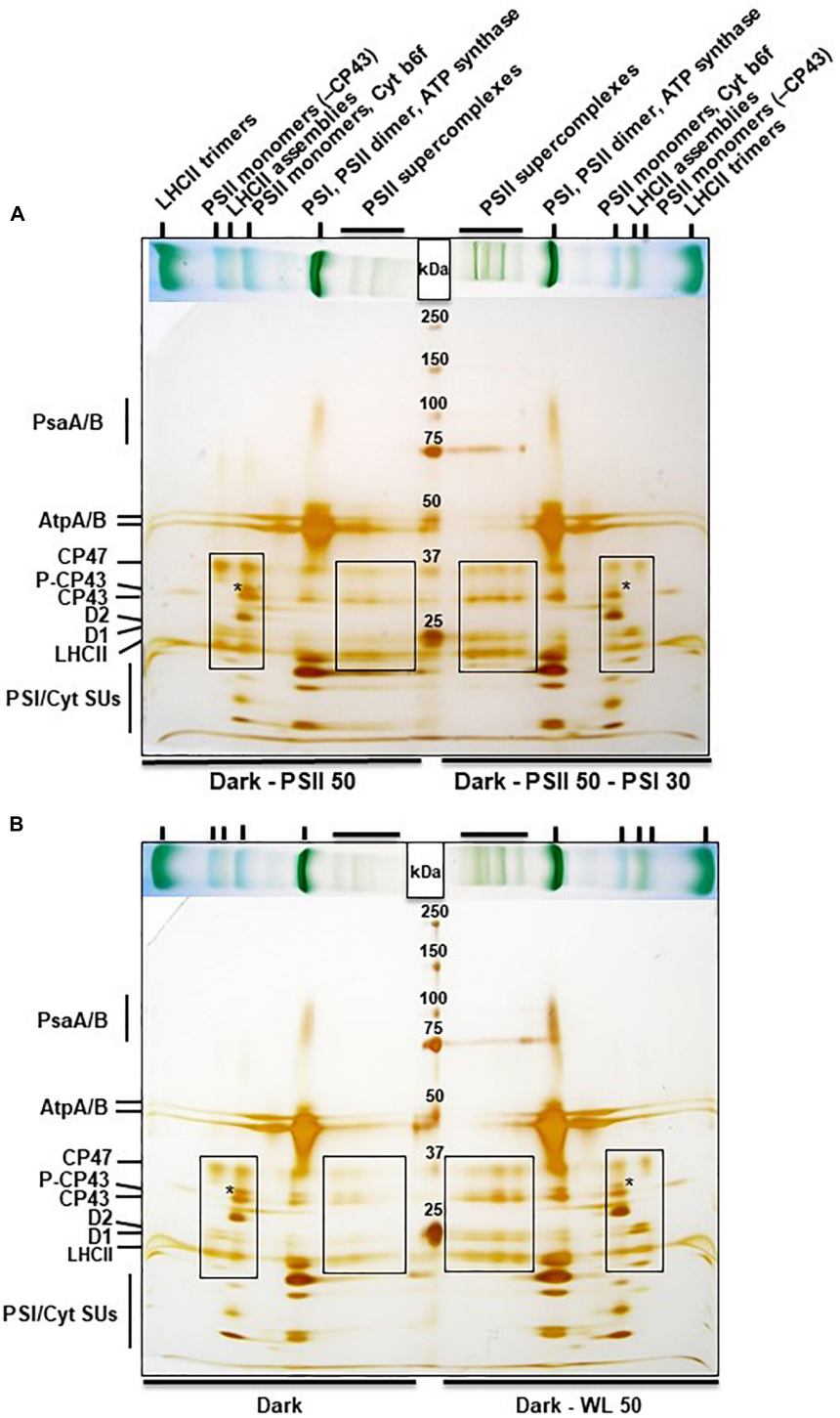

FIGURE 4 | 2D BN-PAGE of thylakoid membrane proteins from *A. thaliana* subjected to light quality or dark light shifts. Stripes from BN-PAGE (placed horizontally on top of gels, compare **Figure 3**) were cut out, denatured in Laemmli buffer and run on a SDS-PAGE as second dimension with a head-to-head orientation. Marker proteins (sizes are given in kDa) were loaded in between. The gels were stained with silver. **(A)** Dark - PSII 50: 50 min PSII-light after dark period; Dark - PSII 50 - PSI 30: 50 min PSII-light after dark period followed by a shift for 30 min to PSI-light. **(B)** Dark: Material harvested at the end of the night phase; Dark - WL 50: 50 min WL illumination after dark phase. Labeling of bands in the BN-PAGE given on top of panel **(A)** is also valid for panel **(B)**, corresponding bands are marked by vertical small lines. Individual protein bands in the second dimension are given in the left margins. Asterisks mark the position of phosphorylated CP43 (right or left from the asterisk, respectively). Broad boxed areas indicate subunits of PSII super-complexes, small boxed areas indicate subunits of PSII monomers. Experiments have been performed three times with results showing only minor variations. Continuous protein bands at 75 kDa in the right half of the gels are leakages from the protein marker.

upon shifts between growth lights. Based on the assumption that the *stn7* mutant performs photochemical quenching comparable to WT we estimate that state transitions contribute between 30 and 50% to the total Chl fluorescence change after the growth light shifts [PSI- to- PSII-light (**Figure 1B**) and dark- to white light (**Figure 1C**)]. The proportion of mobile LHCII in vascular plants is estimated to be around just 15–20% (in contrast to 80% in the unicellular alga *Chlamydomonas*) (Rochaix, 2007). Therefore, state transitions are regarded to play only a minor role as quenching process in vascular plants. However, state transitions represent an acclimation response acting preferentially in the low light range (below 100 μE light intensity in vascular plants) since in higher light intensities the LHCII kinase is inactivated (Rintamaki et al., 2000). Our data suggest that in this low light range state transitions may play a more prominent role than anticipated so far in plants, most likely because state transition measurements are typically not done with the growth light source as analytic lights.

In sum, we regard the two light set-ups as equally effective to induce short term photosynthetic acclimation responses in the antenna, i.e., changes in LHCII phosphorylation and corresponding state transitions. With respect to PSII super-complex formation, however, the two illumination set-ups induce different reactions (**Figure 5**). The question arises whether this difference in PSII super-complex formation is relevant for state transitions. Analysis of PSII super-complex remodeling induced by light-quality shifts indicated that CP43 phosphorylation in PSII super-complexes (and probably also in mega-complexes) most likely initiates the release of these super-complexes (Dietzel et al., 2011). Indeed, we observed high accumulation of phosphorylated CP43 both in the dark and after PSII-light treatment (**Figures 4A,B**, asterisks) where only weak super-complex formation is found. In contrast, strong PSII super-complex formation after PSI-light treatment correlated with low accumulation of phosphorylated CP43. More moderate PSII super-complex formation as observed after 50 min WL treatment also correlated with a moderate accumulation of phosphorylated CP43 (**Figures 4A,B**, asterisks). The phosphorylation states of the native complexes indicate that WL mainly induces the phosphorylation of free LHCII trimers (**Figure 3A**) that are readily available since in the dark only a minor fraction of PSII super-complexes exists and most LHCII trimers appear to be present as free unbound trimers (**Figure 3B**). This is in agreement with a recent study reporting that it is a loosely bound (L) LHCII trimer rather than an S or M LHCII trimer from the PSII super-complexes that is involved in the formation of the state-transition induced PSI-LHCII complex (Galka et al., 2012). The STN8 kinase was identified as an enzyme targeting PSII core proteins (Bonardi et al., 2005; Vainonen et al., 2005), however, CP43 phosphorylation dynamics differ from that of other core proteins suggesting the action of another yet unidentified kinase activity (Fristedt et al., 2010). In addition, the degree of PSII phosphorylation was found to differ between genetic accessions of *Arabidopsis* (Yin et al., 2012). Phosphorylation and dephosphorylation of thylakoid photosynthesis proteins depends on a complex interplay of the STN7 and STN8 kinases and their counteracting TAP38/PPH1 and PBCP phosphatases (Wunder et al., 2013). Although already studied in great detail at biochemical and physiological level our understanding of the regulation of these enzymes has still gaps and the involvement of additional enzyme activities such as a kinase activity being responsible for CP43 phosphorylation in the dark might be possible under specific conditions not tested yet. This argues for more systematic studies analyzing phosphorylation/dephosphorylation of thylakoid membrane proteins under a large variety of illumination conditions and in different genetic backgrounds in order to achieve a comprehensive understanding of these processes.

In sum, we conclude that WL illumination does induce a state transition by phosphorylating free LHCII trimers, but at the same time it induces a moderate formation of PSII super-complexes (and a concomitant de-phosphorylation of them) which is in contrast to PSII-light illumination (**Figures 2–4**), which induces strong phosphorylation of PSII super-complexes (and its subsequent partial release) generating more free LHCII trimers (**Figure 5**). Some highly phosphorylated PSII super-complexes appear to remain stable suggesting that not alone the phosphorylation state but also other determinants such as crowding of the membrane may have an impact on the release (**Figure 3**; Dietzel et al., 2011; Kirchhoff, 2014). PSII-light, thus, can induce migration of bound and free LHCII trimers while WL likely induces only that of free LHCII trimers which may explain differing observations (Dietzel et al., 2011; Wientjes et al., 2013). Interestingly, since both light sources are able to induce state transitions this suggests that LHCII complexes that migrate during state transitions may potentially originate from different pools of LHCII making it difficult to definitely identify which trimer is actually migrating during state transitions (Minagawa, 2011).

Another difference between the two light systems relates to the metabolic state of the plants in state 1. The original observations describing state 1–state 2 transitions trace back to two studies on photosynthesis in algae; both done in the light (Bonaventura and Myers, 1969; Murata, 1969). The original definition of state 1 and state 2, thus, refers to an illuminated state of the organism. A dark condition at the end of the night may exhibit the same low phosphorylation state/pattern of the LHCII as under PSI-light, but it is not identical with respect to the metabolism of the organism; e.g., the redox state of the thioredoxin pool controlling enzyme activities in the Calvin-Benson cycle (Dietz and Pfannschmidt, 2011). This is partly reminiscent to the induction of state transitions in *Chlamydomonas reinhardtii* where state 1 and state 2 represent two different metabolic states (Wollman, 2001). In *Arabidopsis* (as in all green plants) a shift from dark to light conditions represents a shift from heterotrophic to autotrophic life style (Smith and Stitt, 2007) while a PSI-light/PSII-light shift represents a shift under autotrophic conditions between two different light harvesting states. In the first case energy resources collected in the previous light phase are consumed and the light harvesting machinery is shut off while in the second case energy from photosynthesis is used and the light harvesting machinery works with two different efficiencies leading to two distinct light-adapted metabolic states (Bräutigam et al., 2009).

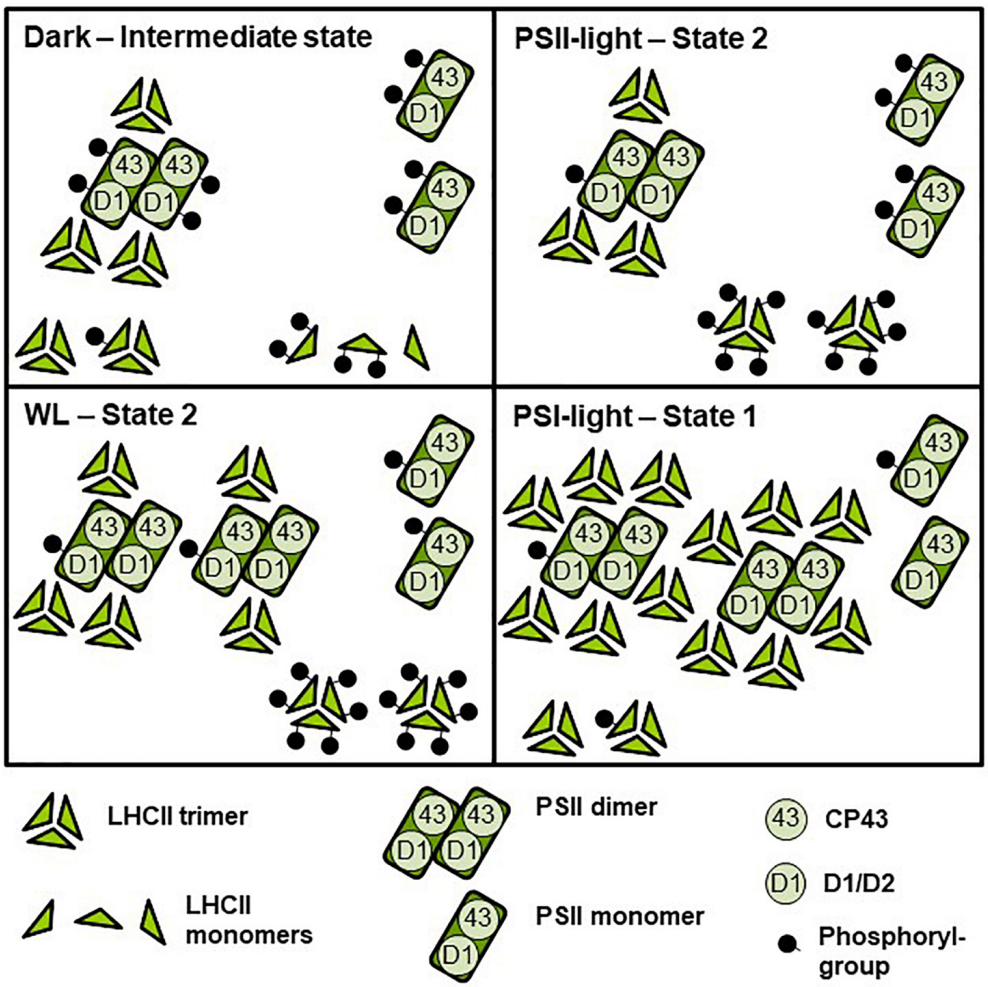

FIGURE 5 | Model depicting effects of light-quality or dark-white light shifts on assembly and phosphorylation states of thylakoid membrane proteins. The simplified scheme integrates the central biochemical data from **Figures 2**–**4** and **Supplementary Table S1**. Symbol representations are defined at the bottom of the scheme. The number of protein complexes and of phosphoryl-groups per protein complex indicates relative accumulation and degree of phosphorylation between the four different conditions. Dark: Low accumulation of PSII super-complexes, moderate phosphorylation state of PSII-bound LHCII and free LCHII trimers, PSII monomers with strongly phosphorylated CP43. PSII-light – State 2: Low accumulation of PSII super-complexes, PSII monomers with strongly phosphorylated CP43, high phosphorylation state of LHCII trimers. WL: High accumulation of PSII super-complexes (mostly C_2S_1 and C_2S_2), PSII monomers with low to moderately phosphorylated CP43, very high phosphorylation of LHCII trimers. PSI-light – State 1: Very high accumulation of PSII super-complexes (including $C_2S_2M_2$ to C_2S_1), low phosphorylation state of PSII-bound and free LHCII trimers and of PSII dimers. PSII monomers with largely dephosphorylated CP43. For functional implications of the different assembly and phosphorylation states, see "Discussion" section.

For the degree of LHCII phosphorylation (and thus for redox-controlled STN7 kinase activity) this appears to be of no major difference; however, we observed a significant difference in PSII core phosphorylation between dark and PSI-light conditions (**Figure 2**). This specific difference might be a cause for the different PSII super-complex formation in these two conditions and, thus, could potentially influence the number of LHCII trimers available for the state transition process. It, therefore, is possible that metabolic activities in the dark support to some extent selective thylakoid membrane protein phosphorylation (and possibly the activity of a corresponding kinase activity). In fact, such dark phosphorylation states have been observed. CP43 was reported to be more phosphorylated in the dark than in the light (Fristedt et al., 2010) being in agreement with these observations, however, the responsible kinase activity remains to be elucidated. Our observations are also compatible with a recent study investigating the association of LHCII to PSI in dark-acclimated plants (Chukhutsina et al., 2020). This study revealed that in several plant species LHCII appears to be part of the LHCI-PSI complex in the dark. It was concluded that the plants are in a state between state 1 and state 2 because Lhcb2 is partly phosphorylated. This is consistent with our finding that LHCII at the end of the night still exhibits partial phosphorylation (**Figure 2**), suggesting that a complete state 1 is reached only under conditions when electrons are actively withdrawn from the PQ pool, e.g., by far-red or PSI-light illumination

(**Figures 1**, **2**). Whether a dark-induced state 1 is different from the corresponding light-induced state 1 (e.g., in terms of LHCII trimers involved) or simply remains incomplete needs to be further investigated. However, comparison of total LHCII phosphorylation (**Figure 2**) with LHCII trimer phosphorylation (**Figure 3A**) suggests a potentially higher phosphorylation state of free LHCII monomers under these conditions arguing for two different types of state 1 (**Figure 5**).

In sum, our study reveals that growth light set-ups with highly similar physiological effects and only minor technically different properties may still induce differences in photosynthetic acclimation responses which can be of importance for our understanding of the studied processes. The question of comparability of results between different illumination set-ups may become even more urgent with the advent of LED based illumination systems that are increasingly used now for plant growth (Seiler et al., 2017; Matsuda et al., 2021). A recent study investigated wavelength-specific effects on the redox state of the PQ pool using monochromatic LED illumination of different colors (Mattila et al., 2020). The authors observed varying efficiencies within the 400–700 nm range. These variations may explain the differences between various artificial light sources with divergent light emission spectra. The WL and PSII-light used in this study are highly similar in the range of 580–700 nm and reduce both the PQ pool with high efficiency as visible by the high LHCII phosphorylation (e.g., **Figures 2**, **3**). The orange filter of the PSII-light, however, cuts off green and especially blue light wavelengths (**Supplementary Figure S1**) that may be responsible for the differences in the PS super-complex phosphorylation through the action of additional enzyme activities (see above). This will be investigated in more detail in future. In consequence, a very detailed description of the used growth light system and its spectral qualities will become mandatory for future studies on photosynthetic acclimation responses.

DATA AVAILABILITY STATEMENT

The original contributions presented in the study are included in the article/**Supplementary Material**, further inquiries can be directed to the corresponding author.

AUTHOR CONTRIBUTIONS

TP designed the research. EH, ML, and SO performed the research. All authors discussed the data and contributed to the writing of the article.

FUNDING

This work was supported by funding from the DFG to TP (Pf323-5).

ACKNOWLEDGMENTS

We thank Birgit Lippmann and Julia Gunia for their help in plant growth, chlorophyll fluorescence measurements, and western immunoblot analyses. We are especially grateful to Dr. Tatjana Kleine who provided us seed badges of the *Arabidopsis stn7* mutant.

SUPPLEMENTARY MATERIAL

The Supplementary Material for this article can be found online at: https://www.frontiersin.org/articles/10.3389/fpls.2021.615253/full#supplementary-material

REFERENCES

Allen, J. F. (1992). Protein phosphorylation in regulation of photosynthesis. *Biochim. Biophys. Acta* 1098, 275–335.

Allen, J. F., and Forsberg, J. (2001). Molecular recognition in thylakoid structure and function. *Trends Plant Sci.* 6, 317–326. doi: 10.1016/s1360-1385(01)02010-6

Allen, J. F., and Pfannschmidt, T. (2000). Balancing the two photosystems: photosynthetic electron transfer governs transcription of reaction centre genes in chloroplasts. *Philos. Trans. R. Soc. London B Biol. Sci.* 355, 1351–1357. doi: 10.1098/rstb.2000.0697

Aro, E. M., Suorsa, M., Rokka, A., Allahverdiyeva, Y., Paakkarinen, V., Saleem, A., et al. (2005). Dynamics of photosystem II: a proteomic approach to thylakoid protein complexes. *J. Exp. Bot.* 56, 347–356. doi: 10.1093/jxb/eri041

Bellafiore, S., Barneche, F., Peltier, G., and Rochaix, J. D. (2005). State transitions and light adaptation require chloroplast thylakoid protein kinase STN7. *Nature* 433, 892–895. doi: 10.1038/nature03286

Bonardi, V., Pesaresi, P., Becker, T., Schleiff, E., Wagner, R., Pfannschmidt, T., et al. (2005). Photosystem II core phosphorylation and photosynthetic acclimation require two different protein kinases. *Nature* 437, 1179–1182. doi: 10.1038/nature04016

Bonaventura, C., and Myers, J. (1969). Fluorescence and oxygen evolution from *Chlorella pyrenoidosa*. *Biochim. Biophys. Acta* 189, 366–383. doi: 10.1016/0005-2728(69)90168-6

Bräutigam, K., Dietzel, L., Kleine, T., Ströher, E., Wormuth, D., Dietz, K. J., et al. (2009). Dynamic plastid redox signals integrate gene expression and metabolism to induce distinct metabolic states in photosynthetic acclimation in *Arabidopsis*. *Plant Cell* 21, 2715–2732. doi: 10.1105/tpc.108.062018

Caffarri, S., Kouril, R., Kereiche, S., Boekema, E. J., and Croce, R. (2009). Functional architecture of higher plant photosystem II super-complexes. *EMBO J.* 28, 3052–3063. doi: 10.1038/emboj.2009.232

Chen, Y. E., Su, Y. Q., Mao, H. T., Wu, N., Zhu, F., Yuan, M., et al. (2018). Terrestrial plants evolve highly assembled photosystem complexes in adaptation to light shifts. *Front. Plant Sci.* 9:1811. doi: 10.3389/fpls.2018.01811

Chukhutsina, V. U., Liu, X., Xu, P., and Croce, R. (2020). Light-harvesting complex II is an antenna of photosystem I in dark-adapted plants. *Nat. Plants* 6, 860–868. doi: 10.1038/s41477-020-0693-4

Crepin, A., and Caffarri, S. (2015). The specific localizations of phosphorylated Lhcb1 and Lhcb2 isoforms reveal the role of Lhcb2 in the formation of the PSI-LHCII supercomplex in *Arabidopsis* during state transitions. *Biochim. Biophys. Acta* 1847, 1539–1548. doi: 10.1016/j.bbabio.2015.09.005

Damkjaer, J. T., Kereiche, S., Johnson, M. P., Kovacs, L., Kiss, A. Z., Boekema, E. J., et al. (2009). The photosystem II light-harvesting protein Lhcb3 affects the macrostructure of photosystem II and the rate of state transitions in *Arabidopsis*. *Plant Cell* 21, 3245–3256. doi: 10.1105/tpc.108.064006

Dekker, J. P., and Boekema, E. J. (2005). Supramolecular organization of thylakoid membrane proteins in green plants. *Biochim. Biophys. Acta Bioenerget.* 1706, 12–39. doi: 10.1016/j.bbabio.2004.09.009

Dietz, K. J., and Pfannschmidt, T. (2011). Novel regulators in photosynthetic redox control of plant metabolism and gene expression. *Plant Physiol.* 155, 1477–1485. doi: 10.1104/pp.110.170043

Dietzel, L., Bräutigam, K., and Pfannschmidt, T. (2008). Photosynthetic acclimation: state transitions and adjustment of photosystem stoichiometry - functional relationships between short-term and long-term light quality acclimation in plants. *FEBS J.* 275, 1080–1088. doi: 10.1111/j.1742-4658.2008.06264.x

Dietzel, L., Brautigam, K., Steiner, S., Schuffler, K., Lepetit, B., Grimm, B., et al. (2011). Photosystem II supercomplex remodeling serves as an entry mechanism for state transitions in *Arabidopsis*. *Plant Cell* 23, 2964–2977. doi: 10.1105/tpc.111.087049

Eberhard, S., Finazzi, G., and Wollman, F. A. (2008). The dynamics of photosynthesis. *Annu. Rev. Genet.* 42, 463–515.

Fristedt, R., Granath, P., and Vener, A. V. (2010). A protein phosphorylation threshold for functional stacking of plant photosynthetic membranes. *PLoS One* 5:e10963. doi: 10.1371/journal.pone.0010963

Fristedt, R., Willig, A., Granath, P., Crevecoeur, M., Rochaix, J. D., and Vener, A. V. (2009). Phosphorylation of photosystem II controls functional macroscopic folding of photosynthetic membranes in *Arabidopsis*. *Plant Cell* 21, 3950–3964. doi: 10.1105/tpc.109.069435

Galka, P., Santabarbara, S., Khuong, T. T., Degand, H., Morsomme, P., Jennings, R. C., et al. (2012). Functional analyses of the plant photosystem I-light-harvesting complex II supercomplex reveal that light-harvesting complex II loosely bound to photosystem II is a very efficient antenna for photosystem I in state II. *Plant Cell* 24, 2963–2978. doi: 10.1105/tpc.112.100339

Garcia-Cerdan, J. G., Kovacs, L., Toth, T., Kereiche, S., Aseeva, E., Boekema, E. J., et al. (2011). The PsbW protein stabilizes the supramolecular organization of photosystem II in higher plants. *Plant J.* 65, 368–381. doi: 10.1111/j.1365-313X.2010.04429.x

Goldschmidt-Clermont, M., and Bassi, R. (2015). Sharing light between two photosystems: mechanism of state transitions. *Curr. Opin. Plant Biol.* 25, 71–78. doi: 10.1016/j.pbi.2015.04.009

Haldrup, A., Jensen, P. E., Lunde, C., and Scheller, H. V. (2001). Balance of power: a view of the mechanism of photosynthetic state transitions. *Trends Plant Sci.* 6, 301–305. doi: 10.1016/s1360-1385(01)01953-7

Järvi, S., Suorsa, M., Paakkarinen, V., and Aro, E. M. (2011). Optimized native gel systems for separation of thylakoid protein complexes: novel super- and mega-complexes. *Biochem. J.* 439, 207–214. doi: 10.1042/BJ20102155

Johnson, M. P., and Wientjes, E. (2020). The relevance of dynamic thylakoid organisation to photosynthetic regulation. *Biochim. Biophys. Acta Bioenerg.* 1861:148039. doi: 10.1016/j.bbabio.2019.06.011

Kalaji, H. M., Schansker, G., Brestic, M., Bussotti, F., Calatayud, A., Ferroni, L., et al. (2017). Frequently asked questions about chlorophyll fluorescence, the sequel. *Photosynth. Res.* 132, 13–66. doi: 10.1007/s11120-016-0318-y

Kanervo, E., Suorsa, M., and Aro, E. M. (2005). Functional flexibility and acclimation of the thylakoid membrane. *Photochem. Photobiol. Sci.* 4, 1072–1080. doi: 10.1039/b507866k

Kirchhoff, H. (2014). Structural changes of the thylakoid membrane network induced by high light stress in plant chloroplasts. *Philos. Trans. R. Soc. Lond. B Biol. Sci.* 369:20130225. doi: 10.1098/rstb.2013.0225

Kirchhoff, H., Hall, C., Wood, M., Herbstova, M., Tsabari, O., Nevo, R., et al. (2011). Dynamic control of protein diffusion within the granal thylakoid lumen. *Proc. Natl. Acad. Sci. U.S.A.* 108, 20248–20253. doi: 10.1073/pnas.1104141109

Koskela, M. M., Brunje, A., Ivanauskaite, A., Grabsztunowicz, M., Lassowskat, I., Neumann, U., et al. (2018). Chloroplast acetyltransferase NSI is required for state transitions in *Arabidopsis thaliana*. *Plant Cell* 30, 1695–1709. doi: 10.1105/tpc.18.00155

Koskela, M. M., Brunje, A., Ivanauskaite, A., Lopez, L. S., Schneider, D., DeTar, R. A., et al. (2020). Comparative analysis of thylakoid protein complexes in state transition mutants nsi and stn7: focus on PSI and LHCII. *Photosynth. Res.* 145, 15–30. doi: 10.1007/s11120-020-00711-4

Kouril, R., Wientjes, E., Bultema, J. B., Croce, R., and Boekema, E. J. (2013). High-light vs. low-light: effects of light acclimation on photosystem II composition and organization in *Arabidopsis thaliana*. *Biochim. Biophys. Acta* 1827, 411–419. doi: 10.1016/j.bbabio.2012.12.003

Kouril, R., Zygadlo, A., Arteni, A. A., de Wit, C. D., Dekker, J. P., Jensen, P. E., et al. (2005). Structural characterization of a complex of photosystem I and light-harvesting complex II of *Arabidopsis thaliana*. *Biochemistry* 44, 10935–10940. doi: 10.1021/bi051097a

Kowalewska, L., Mazur, R., Suski, S., Garstka, M., and Mostowska, A. (2016). Three-dimensional visualization of the tubular-lamellar transformation of the internal plastid membrane network during runner bean chloroplast biogenesis. *Plant Cell* 28, 875–891. doi: 10.1105/tpc.15.01053

Longoni, P., Douchi, D., Cariti, F., Fucile, G., and Goldschmidt-Clermont, M. (2015). Phosphorylation of the light-harvesting complex II isoform Lhcb2 is central to state transitions. *Plant Physiol.* 169, 2874–2883. doi: 10.1104/pp.15.01498

Matsuda, R., Ito, H., and Fujiwara, K. (2021). Effects of artificially reproduced fluctuations in sunlight spectral distribution on the net photosynthetic rate of cucumber leaves. *Front. Plant Sci.* 12:675810. doi: 10.3389/fpls.2021.675810

Mattila, H., Khorobrykh, S., Hakala-Yatkin, M., Havurinne, V., Kuusisto, I., Antal, T., et al. (2020). Action spectrum of the redox state of the plastoquinone pool defines its function in plant acclimation. *Plant J.* 104, 1088–1104. doi: 10.1111/tpj.14983

Maxwell, K., and Johnson, G. N. (2000). Chlorophyll fluorescence–a practical guide. *J. Exp. Bot.* 51, 659–668. doi: 10.1093/jxb/51.345.659

Minagawa, J. (2011). State transitions-The molecular remodeling of photosynthetic super-complexes that controls energy flow in the chloroplast. *Biochim. Biophys. Acta* 1807, 897–905. doi: 10.1016/j.bbabio.2010.11.005

Morales, A., and Kaiser, E. (2020). Photosynthetic acclimation to fluctuating irradiance in plants. *Front. Plant Sci.* 11:268. doi: 10.3389/fpls.2020.00268

Murata, N. (1969). Control of excitation transfer in photosynthesis. I. Light-induced change of chlorophyll a fluorescence in *Porphyridium cruentum*. *Biochim. Biophys. Acta* 172, 242–251. doi: 10.1016/0005-2728(69)90067-x

Pan, X., Ma, J., Su, X., Cao, P., Chang, W., Liu, Z., et al. (2018). Structure of the maize photosystem I supercomplex with light-harvesting complexes I and II. *Science* 360, 1109–1113. doi: 10.1126/science.aat1156

Pesaresi, P., Hertle, A., Pribil, M., Kleine, T., Wagner, R., Strissel, H., et al. (2009). *Arabidopsis* STN7 kinase provides a link between short- and long-term photosynthetic acclimation. *Plant Cell* 21, 2402–2423. doi: 10.1105/tpc.108.064964

Pfannschmidt, T. (2003). Chloroplast redox signals: how photosynthesis controls its own genes. *Trends Plant Sci.* 8, 33–41. doi: 10.1016/s1360-1385(02)00005-5

Pietrzykowska, M., Suorsa, M., Semchonok, D. A., Tikkanen, M., Boekema, E. J., Aro, E. M., et al. (2014). The light-harvesting chlorophyll a/b binding proteins Lhcb1 and Lhcb2 play complementary roles during state transitions in *Arabidopsis*. *Plant Cell* 26, 3646–3660. doi: 10.1105/tpc.114.127373

Porra, R. J., Thompson, W. A., and Kriedemann, P. E. (1989). Determination of accurate extinction coefficients and simultaneous-equations for assaying Chlorophyll-a and Chlorophyll-B extracted with 4 different solvents - verification of the concentration of chlorophyll standards by atomic-absorption spectroscopy. *Biochim. Biophys. Acta* 975, 384–394. doi: 10.1016/s0005-2728(89)80347-0

Pribil, M., Labs, M., and Leister, D. (2014). Structure and dynamics of thylakoids inland plants. *J. Exp. Bot.* 65, 1955–1972. doi: 10.1093/jxb/eru090

Pribil, M., Pesaresi, P., Hertle, A., Barbato, R., and Leister, D. (2010). Role of plastid protein phosphatase TAP38 in LHCII dephosphorylation and thylakoid electron flow. *PLoS Biol.* 8:e1000288. doi: 10.1371/journal.pbio.1000288

Puthiyaveetil, S., and Kirchhoff, H. (2013). A phosphorylation map of the photosystem II supercomplex C2S2M2. *Front. Plant Sci.* 4:459. doi: 10.3389/fpls.2013.00459

Rintamaki, E., Martinsuo, P., Pursiheimo, S., and Aro, E. M. (2000). Cooperative regulation of light-harvesting complex II phosphorylation via the plastoquinol and ferredoxin-thioredoxin system in chloroplasts. *Proc. Natl. Acad. Sci. U.S.A.* 97, 11644–11649. doi: 10.1073/pnas.180054297

Rochaix, J. (2013). Redox regulation of thylakoid protein kinases and photosynthetic gene expression. *Antioxid. Redox Signal.* 18, 2184–2201. doi: 10.1089/ars.2012.5110

Rochaix, J. D. (2007). Role of thylakoid protein kinases in photosynthetic acclimation. *FEBS Lett.* 581, 2768–2775. doi: 10.1016/j.febslet.2007.04.038

Sambrook, J., and Russel, D. W. (2001). *Molecular Cloning: A Laboratory Manual*, 3rd Edn. Cold Spring Harbor, NY: Cold Spring Harbor Laboratory Press.

Samol, I., Shapiguzov, A., Ingelsson, B., Fucile, G., Crevecoeur, M., Vener, A. V., et al. (2012). Identification of a photosystem II phosphatase involved in light acclimation in *Arabidopsis*. *Plant Cell* 24, 2596–2609. doi: 10.1105/tpc.112.095703

Seiler, F., Soll, J., and Bolter, B. (2017) Comparative phenotypical and molecular analyses of arabidopsis grown under fluorescent and LED light. *Plants* 6:24. doi: 10.3390/plants6020024

Shapiguzov, A., Ingelsson, B., Samol, I., Andres, C., Kessler, F., Rochaix, J.-D., et al. (2010). The PPH1 phosphatase is specifically involved in LHCII dephosphorylation and state transitions in *Arabidopsis*. *Proc. Natl. Acad. Sci. U.S.A.* 107, 4782–4787. doi: 10.1073/pnas.0913810107

Smith, A. M., and Stitt, M. (2007). Coordination of carbon supply and plant growth. *Plant Cell Environ.* 30, 1126–1149. doi: 10.1111/j.1365-3040.2007.01708.x

Terashima, I., and Hikosaka, K. (1995). Comparative ecophysiology of leaf and canopy photosynthesis. *Plant Cell Environ.* 18, 1111–1128. doi: 10.1111/j.1365-3040.1995.tb00623.x

Tikkanen, M., Grieco, M., and Aro, E. (2011). Novel insights into plant light-harvesting complex II phosphorylation and 'state transitions'. *Trends Plant Sci.* 3, 126–131. doi: 10.1016/j.tplants.2010.11.006

Tikkanen, M., Grieco, M., Kangasjärvi, S., and Aro, E.-M. (2010). Thylakoid protein phosphorylation in higher plant chloroplasts optimizes electron transfer under fluctuating light. *Plant Physiol.* 152, 723–735. doi: 10.1104/pp.109.150250

Vainonen, J. P., Hansson, M., and Vener, A. V. (2005). STN8 protein kinase in *Arabidopsis thaliana* is specific in phosphorylation of photosystem II core proteins. *J. Biol. Chem.* 280, 33679–33686. doi: 10.1074/jbc.M505729200

Wagner, R., Dietzel, L., Bräutigam, K., Fischer, W., and Pfannschmidt, T. (2008). The long-term response to fluctuating light quality is an important and distinct light acclimation mechanism that supports survival of *Arabidopsis thaliana* under low light conditions. *Planta* 228, 573–587. doi: 10.1007/s00425-008-0760-y

Walters, R. G. (2005). Towards an understanding of photosynthetic acclimation. *J. Exp. Bot.* 56, 435–447. doi: 10.1093/jxb/eri060

Wientjes, E., Drop, B., Kouril, R., Boekema, E. J., and Croce, R. (2013). During State 1 to State 2 transition in *Arabidopsis thaliana*, the photosystem II supercomplex gets phosphorylated but does not dissassemble. *J. Biol. Chem.* 288, 32821–32826. doi: 10.1074/jbc.M113.511691

Wollman, F. A. (2001). State transitions reveal the dynamics and flexibility of the photosynthetic apparatus. *EMBO J.* 20, 3623–3630. doi: 10.1093/emboj/20.14.3623

Wunder, T., Xu, W., Liu, Q., Wanner, G., Leister, D., and Pribil, M. (2013). The major thylakoid protein kinases STN7 and STN8 revisited: effects of altered STN8 levels and regulatory specificities of the STN kinases. *Front. Plant Sci.* 4:417. doi: 10.3389/fpls.2013.00417

Yin, L., Fristedt, R., Herdean, A., Solymosi, K., Bertrand, M., Andersson, M. X., et al. (2012). Photosystem II function and dynamics in three widely used *Arabidopsis thaliana* accessions. *PLoS One* 7:e46206. doi: 10.1371/journal.pone.0046206

Conflict of Interest: The authors declare that the research was conducted in the absence of any commercial or financial relationships that could be construed as a potential conflict of interest.

Publisher's Note: All claims expressed in this article are solely those of the authors and do not necessarily represent those of their affiliated organizations, or those of the publisher, the editors and the reviewers. Any product that may be evaluated in this article, or claim that may be made by its manufacturer, is not guaranteed or endorsed by the publisher.

frontiers | Frontiers in Plant Science

TYPE Original Research
PUBLISHED 09 March 2023
DOI 10.3389/fpls.2023.1070218

OPEN ACCESS

EDITED BY
Luisa M. Sandalio,
Department of Biochemistry (CSIC), Spain

REVIEWED BY
Lorenzo Ferroni,
University of Ferrara, Italy
Ladislav Nedbal,
Palacký University, Olomouc, Czechia

*CORRESPONDENCE
Emilie Wientjes
emilie.wientjes@wur.nl
Jeremy Harbinson
Jeremy.Harbinson@wur.nl

SPECIALTY SECTION
This article was submitted to Plant Abiotic Stress, a section of the journal Frontiers in Plant Science

RECEIVED 14 October 2022
ACCEPTED 03 February 2023
PUBLISHED 09 March 2023

CITATION
Schiphorst C, Koeman C, Caracciolo L, Staring K, Theeuwen TPJM, Driever SM, Harbinson J and Wientjes E (2023) The effects of different daily irradiance profiles on Arabidopsis growth, with special attention to the role of PsbS. *Front. Plant Sci.* 14:1070218. doi: 10.3389/fpls.2023.1070218

The effects of different daily irradiance profiles on Arabidopsis growth, with special attention to the role of PsbS

Christo Schiphorst[1], Cas Koeman[1], Ludovico Caracciolo[1], Koen Staring[1], Tom P. J. M. Theeuwen[2], Steven M. Driever[3], Jeremy Harbinson[1*] and Emilie Wientjes[1*]

[1]Laboratory of Biophysics, Wageningen University & Research, Wageningen, Netherlands, [2]Laboratory of Genetics, Wageningen University & Research, Wageningen, Netherlands, [3]Centre for Crop Systems Analysis, Wageningen University & Research, Wageningen, Netherlands

In nature, light is never constant, while in the controlled environments used for vertical farming, *in vitro* propagation, or plant production for scientific research, light intensity is often kept constant during the photoperiod. To investigate the effects on plant growth of varying irradiance during the photoperiod, we grew *Arabidopsis thaliana* under three irradiance profiles: a square-wave profile, a parabolic profile with gradually increasing and subsequently decreasing irradiance, and a regime comprised of rapid fluctuations in irradiance. The daily integral of irradiance was the same for all three treatments. Leaf area, plant growth rate, and biomass at time of harvest were compared. Plants grown under the parabolic profile had the highest growth rate and biomass. This could be explained by a higher average light-use efficiency for carbon dioxide fixation. Furthermore, we compared the growth of wild type plants with that of the PsbS-deficient mutant *npq4*. PsbS triggers the fast non-photochemical quenching process (qE) that protects PSII from photodamage during sudden increases in irradiance. Based mainly on field and greenhouse experiments, the current consensus is that *npq4* mutants grow more slowly in fluctuating light. However, our data show that this is not the case for several forms of fluctuating light conditions under otherwise identical controlled-climate room conditions.

KEYWORDS

fluctuating light, photosynthesis, CO_2 assimilation, leaf area, Arabidopsis

1 Introduction

In nature, the irradiance incident on a leaf changes over the course of a day. These fluctuations occur on multiple timescales, ranging from a second to minutes for sunflecks caused by air movement moving leaves higher in the canopy or by cloud movement, to fluctuations caused by cloud movement lasting between minutes and hours, to the diurnal

change in irradiance as the sun rises and sets as a result of the rotation of the Earth around its axis (Pearcy, 1990; Ruban, 2009; Kaiser et al., 2018; Wang et al., 2020). In low light, when photosynthesis is light-limited, plants must absorb as much light as possible for photosynthesis and use it as efficiently as possible. In contrast, in high light, when photosynthesis is light-saturated, more energy is absorbed than can be used for photosynthesis. If left unchecked, this excess of energy can actually damage the plant. As a result of these changing priorities, plants must constantly maintain a balance between efficient photosynthesis in low light and photoprotection in high light (Pearcy, 1990; Ruban, 2009; Kaiser et al., 2018; Wang et al., 2020; Long et al., 2022). Matters are complicated in cases of fluctuating irradiance because an increase in irradiance (provided that assimilation is not already light-saturated) will produce an increase in assimilation, which results in a decrease in the degree of excess of irradiation. As a result, the degree to which irradiance is in excess changes (and normally decreases) with time.

Plants have developed multiple ways to respond to changes in light intensity (Ruban, 2009; Murchie and Niyogi, 2011; Kaiser et al., 2018). A major adaptation mechanism is the circadian rhythm, based on the oscillating day–night cycle of terrestrial daylight. It is estimated that 25-35% of the *Arabidopsis thaliana* (Arabidopsis) genome is controlled by the circadian rhythm (Covington and Harmer, 2007; Hazen et al., 2009). Unsurprisingly, photosynthesis is also influenced by circadian oscillations *via* various pathways and mechanisms (Dodd et al., 2014). This is reflected in the fact that photosynthesis, as assessed by net CO_2 assimilation rate (A_{net}) and stomatal conductance, continues to display a circadian rhythm in plants exposed to constant light (Hennessey and Field, 1991). As plants have evolved under a natural daytime light regime, in which potential irradiance increases gradually until noon and then decreases until sunset, it can be hypothesized that plants should be adapted to this irradiance profile and thus should grow more quickly under a natural, approximately parabolic (or sinusoidal) irradiance profile than under square-wave (on/off) light conditions. Knowledge of such an adaptation would be important in guiding the control of irradiance in vertical farming, where crops such as lettuce are grown indoors under light-emitting diode lamps (LEDs) (van Delden et al., 2021). An increase in plant biomass produced per unit kWh of electricity used for lighting would provide an economic advantage. A hint that sinusoidal light does provide an advantage comes from the work of Chiang et al. (2020), which shows that the leaf area of several species is larger for plants grown under sinusoidal light than for plants grown under square-wave light conditions with the same daily integral of irradiance.

Rapid fluctuations in light intensity, on the timescale of seconds to minutes, are very common in the understory of forests and in the canopy of densely packed crops growing in the field (Pearcy, 1990; Ruban, 2009; Kaiser et al., 2018; Wang et al., 2020; Long et al., 2022). Such fluctuations are challenging for plants and have been shown to negatively affect plant growth and fitness (Kulheim et al., 2002; Alter et al., 2012; Poorter et al., 2016; Vialet-Chabrand et al., 2017; Kaiser et al., 2018; Qiao et al., 2021). The main mechanism of protection against sudden high light is qE, or energy-dependent non-photochemical quenching (NPQ), the process in PSII that underlies the protective conversion to heat of those excited states of chlorophyll that are in excess of the needs of photochemistry. Excess irradiance above the requirements of photosynthetic metabolism leads to acidification of the thylakoid lumen, which is sensed by the protein PsbS and catalyzes the quenching of excited states, thereby giving rise to the phenomenon of qE (Li et al., 2000; Li et al., 2002). The enzymatic conversion of the carotenoid violaxanthin into zeaxanthin further amplifies qE (Demmig-Adams, 1990; Niyogi et al., 1998). The establishment and relaxation of qE is slow relative to the more rapid fluctuations of irradiance encountered in the field (seconds or tens of seconds for qE versus seconds or less for irradiance fluctuations). Based on *in silico* experiments, the slow relaxation of qE, which can limit the light-use efficiency of PSII electron transport for photosynthesis, has been proposed to be potentially a limiting factor for photosynthesis and crop carbon gain (Zhu et al., 2004). Accelerating the relaxation of qE *via* over-expression of PsbS and the enzymes involved in the reversible conversion of violaxanthin into zeaxanthin has been found to result in increased crop productivity in the field in tobacco plants (Kromdijk et al., 2016) and increased crop yield in soybean (De Souza et al., 2022). On the other hand, the same mutations have been found to impair growth rate in Arabidopsis (Garcia-Molina and Leister, 2020). It is generally believed that lacking PsbS negatively affects plant performance under light fluctuations: a PsbS knock-out, known as *npq4*, produces fewer seeds (Kulheim et al., 2002; Krah and Logan, 2010), has a reduced leaf area (Logan et al., 2008; Krah and Logan, 2010), and exhibits reduced CO_2 assimilation (Hubbart et al., 2012). However, under constant irradiance during the photoperiod, a lack of PsbS does not seem to confer any disadvantages (Kulheim et al., 2002; Khuong et al., 2019) and could even represent an advantage under constant low irradiance (Khuong et al., 2019).

Thus far, most fluctuating light studies on the *npq4* mutant have been performed under uncontrolled field conditions or in greenhouses. As such, it is unclear under which kind of light fluctuations possession of PsbS is required for optimal plant growth and biomass production. If we are to engineer plants with improved photosynthetic efficiency for higher crop yields (Zhu et al., 2010), it is important to understand under which light conditions photoprotective quenching is beneficial for plant growth. A similar question could be asked for Stn7, the kinase of the major light-harvesting complex II that restores the balance of excitation of photosystems I and II under certain conditions of imbalance and thus improves the light-use efficiency of assimilation (Bellafiore et al., 2005; Taylor et al., 2019). It has been shown that absence of this protein also diminishes plant fitness and growth under fluctuating light conditions (Kulheim et al., 2002; Frenkel et al., 2007; Tikkanen et al., 2010; Grieco et al., 2012).

Several studies have investigated the effects of fluctuating light on plant growth, e.g., through use of a square-wave irradiance profile (Tikkanen et al., 2010), fluctuations that mimic a measured natural daytime light profile (Vialet-Chabrand et al., 2017; Chiang et al., 2020), or a natural increasing and decreasing intensity profile with added random fluctuations (Ferroni et al., 2020; von Bismarck et al., 2022). Here we have investigated the effects of different light regimes on the growth rate and biomass production of Arabidopsis

plants. We compared the effects on wild type (WT) plants, *stn7* plants (lacking Stn7), and *npq4* plants. This comparison produced two interesting results. First, when they were grown under fluctuating light that mimics natural light conditions, the relative growth rate and above-ground biomass production of *npq4* and *stn7* plants were not significantly reduced compared to those of WT plants. Second, growing plants of each of these genotypes under a parabolic irradiance profile, resembling the natural diurnal increase and decrease in light intensity, resulted in enhanced biomass production. To investigate this further, we studied the effect of different fluctuating light conditions and temperatures on the growth of *npq4* plants compared to WT plants. Finally, the CO_2 assimilation rate of WT plants was compared for the square-wave and parabolic irradiance regimes.

2 Materials and methods

2.1 Growth conditions

A. thaliana plants, accession *Columbia*, from lines WT, *npq4* (Li et al., 2000), and *stn7* (Bellafiore et al., 2005), were grown in controlled conditions of 24°C during the day and 20°C during the night, under a short-day light regime of 8 hours light and 16 hours darkness, with a light intensity of 125 µmol m^{-2} s^{-1}. Seeds were allowed to germinate for 10 days before being transplanted into individual pots, where they were grown for another week before the experiments were started.

2.2 Growth under square-wave, parabolic, and fluctuating light conditions

Growth irradiance was provided by an LED array (Fluence Vypr 2p, Fluence Europe, Rotterdam, the Netherlands). The light intensity provided by this array is linearly dependent on the supply output current generated by the LED power supply. This output current was controlled using the dimmer function of the supply, which was linearly dependent on the value of a resistor placed between the dimmer control pins. Adjustable resistance between these pins was provided by an optocoupled light-dependent resistor actuated by a microcontroller (ESP32 – Espressif Systems; https://www.espressif.com). This digital controller allowed the irradiance to be altered every 3 seconds, this limit on the rate being set by the control electronics of the LED power supply.

For the square wave, a continuous light intensity of 150 µmol m^{-2} s^{-1} was used throughout the photoperiod. The parabolic profile was interpolated from irradiance data based on measurements made available at solcast.com. The cloudless irradiance values used for this purpose were measured on 2021-11-11 at 21.9028° N, 12.4964° E, a location in the Sahara in Niger. The fluctuating light condition was based on measurements made on September 20th 2020 in Wageningen (the Netherlands, 51° 59'20.0"N, 5°39'43.2"E) 1.5m above ground in a mature maize canopy. Using a Licor quantum sensor, a laboratory-built transimpedance amplifier, and a Picolog ADC-24 datalogger, an irradiance dataset with 100 ms resolution was recorded. The average over 3-second intervals was used for the fluctuating condition, adjusted for the 8-hour photoperiod by taking a 2-hour slice of data from the middle of the day. Irradiance levels between 0 and 60 µmol m^{-2} s^{-1} could not be achieved by our system owing to limitations in the control of the LED power supply. As a result, both the parabolic profile and fluctuating light profile began with a stepwise increase. The three different illumination conditions were normalized to the same total daily integrated photosynthetic photon flux density (PPFD) over an 8-hour photoperiod (Figure 1).

In order to image the growth of plants in the growth cabinet, a Raspberry Pi device connected to 6 different USB webcams was programmed to collect images multiple times per day. The images were first corrected for fish-eye distortion using the Python module OpenCV. Subsequently, the coordinates of every individual plant pot were measured using ImageJ, which allowed the images to be sliced to form sub-images, each containing a single plant, and the area of each plant was measured. Leaf area was determined by converting the RGB image to the CIELAB color space, where the a^* channel was inverted and converted to a mask before the leaf areas were automatically selected using an ImageJ script. Growth in leaf area (A) for each individual plant was then fitted using an expolinear growth model (Goudriaan and Monteith, 1990):

$$A = \frac{C_m}{R_m} ln(1 + e^{R_m * (t - t_b)})$$

where R_m is the maximum relative growth rate in the exponential phase, C_m is the maximum relative growth rate in the linear phase, t is elapsed time, and t_b is the time at which the linear phase starts.

2.3 Measurement of CO_2 assimilation using a custom-built system

CO_2 assimilation measurements were performed as described in Taylor et al. (2019) using an LI-7000 CO_2/H_2O analyzer (LI-COR, NE, USA) operating in differential mode. The gas mix used for the measurements contained 400 µmol CO_2 mol^{-1} (400ppm CO_2), 200 mmol O_2 mol^{-1} (20% oxygen), and 18.8 mmol H_2O mol^{-1}, and the remainder of the gas mix consisted of N_2. The gas stream was divided between the reference cell of the gas analyzer and a custom-made leaf chamber, after which the gas stream was supplied to the analysis cell of the gas analyzer. The leaf chamber allowed an entire Arabidopsis leaf to be enclosed within the chamber *via* the petiole. The upper transparent window of the chamber was sealed against the metal rim of the lower half of the leaf chamber by a hard rubber O-ring coated with silicone grease, forming a gas-tight seal with no diffusive leaks.

An LED array was fitted on top of the leaf chamber; this was controlled by a constant-current LED driver (Mean Well LCM-40, Haarlem, the Netherlands) capable of rapid changes in current output. This driver was controlled by an ESP32 microcontroller *via* an optocoupler with a 2s interval in the case of the simulated parabolic irradiance profile.

10.3389/fpls.2023.1070218

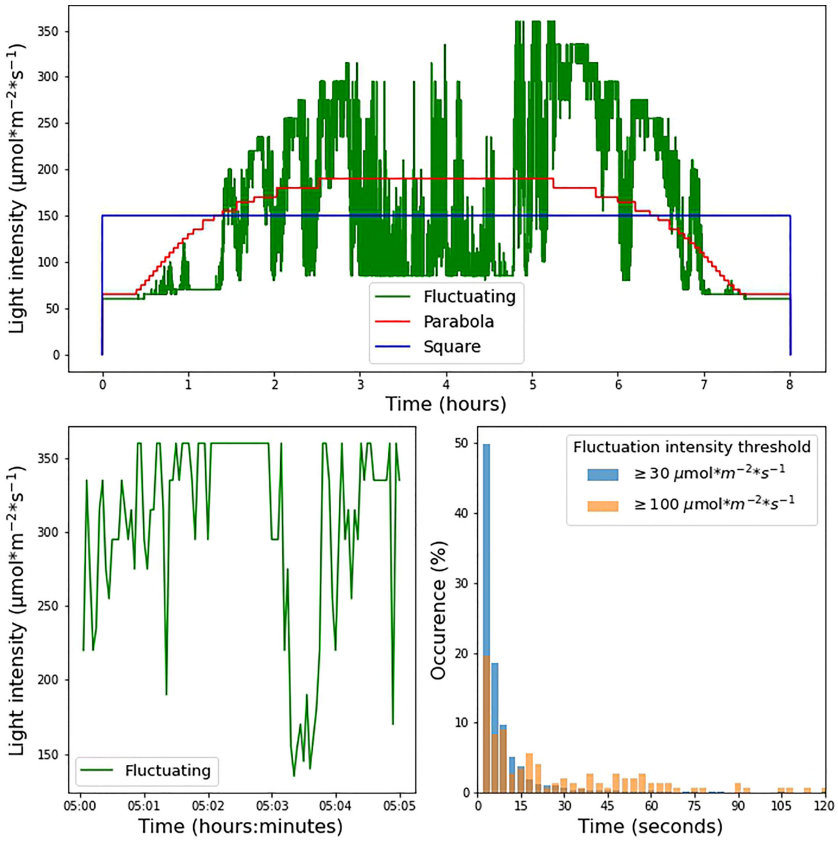

FIGURE 1
(A) Experimental light intensity conditions during the 8-hour photoperiod under which the plants were grown. **(B)** Zoomed-in visualization of 5 min under the fluctuating light condition. **(C)** Incidence of fluctuations in the fluctuating light condition. The histograms show the proportion of instances in which light intensity remained within a range of 30 µmol m^{-2} s^{-1} (blue bars) and 100 µmol m^{-2} s^{-1} (orange bars) for a given amount of time.

Gas exchange measurements were performed on 5-week-old plants grown under square wave irradiance of 125 µmol m^{-2} s^{-1} during the photoperiod. Leaves were adapted for 15 minutes after being placed in the leaf chamber before the measurement was started.

CO_2 assimilation was calculated by correcting for gas dilution by H_2O released by the leaf using the following formula:

$$J_{CO_2} = \frac{J_{gas_{in}}}{A_{leaf}}\left(x_{CO_{2_{in}}} - x_{CO_{2_{out}}}\left(\frac{1 - x_{H_2O_{in}}}{1 - x_{H_2O_{out}}}\right)\right)$$

where $J_{gas_{in}}$ is the total gas influx, A_{leaf} is the total leaf area in the chamber, and x is the molar fraction of the respective gas measured at the influx or the outflux of the leaf chamber. Transpiration was calculated according to the following formula:

$$J_{H_2O} = \frac{J_{gas_{in}}}{A_{leaf}} * \left(\frac{x_{H_2O_{out}} - x_{H_2O_{in}}}{1 - x_{H_2O_{out}}}\right)$$

2.4 Combined measurement of CO_2 assimilation and chlorophyll fluorescence

Combined measurements of CO_2 assimilation and chlorophyll fluorescence were taken for individual leaves using an open infrared gas-exchange system (LI-6400XT; LI-COR, Lincoln, NE) and a 2-cm^2 leaf chamber with an integral blue–red LED light source and fluorometer (LI-6400–40; LI-COR, Lincoln, NE). Plants were dark acclimated and then exposed to three cycles of approximately 5 min of low light (100 µmol m^{-2} s^{-1}) and 1 min of high light (1000 µmol m^{-2} s^{-1}), followed by three cycles of 5 min of low light and 5 min of high light. Light supplied was a combination of red and 10% blue light. The operating efficiency of PSII electron transport (Φ_{PSII}) was determined as (F_m'– F')/F_m' (Genty et al., 1989), where F' is the steady-state fluorescence and F_m' is the maximum fluorescence during the saturating light pulse, as determined by the multiphase flash method (Loriaux et al., 2013). The level of non-photochemical quenching (NPQ) was determined as (F_m – F_m')/F_m', where F_m is the maximum fluorescence in the dark-acclimated state and F_m' is the maximum fluorescence during the light-adapted state, both as determined by a multiphase flash (after (Loriaux et al., 2013); total duration was 0.9 seconds (0.3 seconds per phase), the ramp rate was 40%, and the maximum flash intensity was ~ 6000 µmol m^{-2} s^{-1}). Conditions in the leaf cuvette were maintained at a CO_2 concentration of 400 ppm, a VPD of approximately 1 kPa, and a leaf temperature of 25°C. Recordings of gas exchange and chlorophyll fluorescence were made every minute for the duration of the measurement period.

10.3389/fpls.2023.1070218

2.5 PSII quantum efficiency measurements

The ratio of maximum variable to maximum total Chl *a* fluorescence (F_v/F_m), determined after 30 min dark-adaptation, served as a measure of PSII quantum efficiency. Fluorescence measurements were performed with a PAM-101 fluorometer (Walz, Effeltrich, Germany). F_m was measured as the maximum fluorescence during a saturating pulse of 0.8 seconds with an intensity of ~6000 µmol m^{-2} s^{-1}.

2.6 Fluctuating light; WT vs *npq4*

A lighting system was created in a plant growth cabinet using LED bars for the low-irradiance conditions (100 µmol m^{-2} s^{-1}, LL) combined with an additional 4 high-power 3W LEDs with a 15° focusing lens to provide the high-irradiance (1000 µmol m^{-2} s^{-1}, HL) conditions. Plants were grown under a short-day light regime of 8 hours light and 16 hours darkness at three different temperatures (4°C, 10°C, or 24°C). The temperature was unchanged throughout the day/night cycle. The switch to the high-power LEDs between LL and HL was managed using a relay controlled by a programmable Arduino microcontroller (https://www.arduino.cc). Three different conditions were programmed: 1h HL (1000 µmol m^{-2} s^{-1}) and 30 min LL (100 µmol m^{-2} s^{-1}); 1 min HL and 5 min LL; and 5 min HL and 5 min LL.

Growth was monitored by taking photographs of the plants (including a minimum of 10 plants for each genotype and each condition) every 3 or 4 days and counting the pixels for each plant using Adobe Photoshop CS6, using a 1-euro coin as a size reference in the images. After each experiment, the fresh above-ground weight of the plants was determined.

3 Results

3.1 The effect of square-wave, parabolic, and fluctuating light conditions on plant growth

We investigated the effects of different light regimes on the growth of WT, *npq4*, and *stn7* Arabidopsis plants. After 17 days of growth under continuous light (125 µmol m^{-2} s^{-1}, 8-hour photoperiod), the plants were exposed to three different light conditions, all with an 8-hour photoperiod and the same daily integral of photosynthetic photon flux density (PPFD). The conditions were: 1) square-wave irradiance of 150 µmol m^{-2} s^{-1}; 2) parabolic irradiance ranging from 65 to 190 µmol m^{-2} s^{-1}, resembling the natural increase and decrease in light intensity during the day; and 3) rapidly fluctuating irradiance ranging from 60 to 360 µmol m^{-2} s^{-1}, based on the measurements of light intensity fluctuations in a maize canopy in the field. The three light intensity profiles are shown in Figure 1A while Figure 1B shows a zoomed-in view of the fluctuating light profile (condition 3 above). We analyzed the changes imposed under the fluctuating light regime; Figure 1C shows the distribution of the time taken for the light intensity to change by ≥ 30 µmol m^{-2} s^{-1} or ≥ 100 µmol m^{-2} s^{-1}. This analysis shows that periods of constant irradiance lasting 3 seconds occurred most frequently (this was the shortest time-interval over which the intensity was changed), while periods of constant irradiance lasting up to 1 minute were frequent. Periods of constant light intensity lasting more than 2 minutes were uncommon (1.8% of the total for changes ≥ 30 µmol m^{-2} s^{-1} and 10.5% of the total for changes ≥ 100 µmol m^{-2} s^{-1}).

In order to evaluate plant growth (Supplementary Movie 1), at least 3 images of the plants were collected each day, and the projected leaf area was measured using these images (Supplementary Movie 2). Based on these data, we plotted the increase in leaf area over time (Figure 2). Treating increase in leaf area as a metric for overall growth, we found that fluctuating irradiance significantly ($p < 0.05$) reduced plant growth in WT and *npq4* plants, compared to the two other conditions (Figure 3). For *stn7* plants, growth was fastest under a parabolic irradiance profile; the other two conditions (fluctuating and square) did not differ significantly from each other in terms of growth speed, but in both cases this was slower than under the parabolic profile.

Next, in order to analyze the effect of different irradiance profiles on the rate of plant growth in greater detail, growth in projected leaf area as function of time was parameterized by fitting an expolinear growth model (see Materials and Methods). Plant growth was initially exponential, but became linear as the canopy began to close (i.e., when the leaves began to overlap). We found that while R_m (the maximum relative growth rate) could be estimated reliably from our data, due to the relatively short

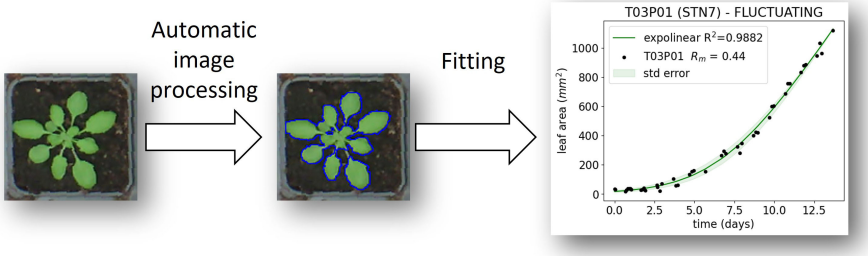

FIGURE 2
Workflow for analysis of increase in leaf area over time.

10.3389/fpls.2023.1070218

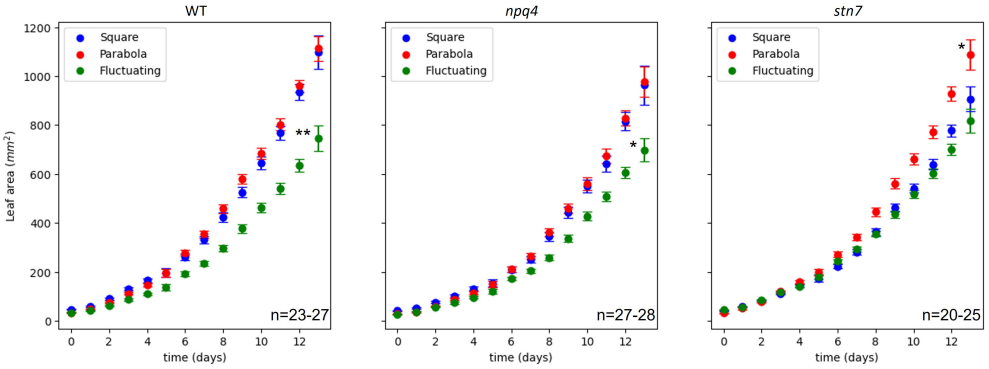

FIGURE 3
Increase in leaf area (mm^2) during growth of WT, *npq4*, and *stn7* Arabidopsis plants under square-wave, parabolic, and fluctuating light conditions. The SE is shown. The number of plants (n) analyzed is displayed on each graph. Differences in final leaf area were tested via one-way ANOVA, followed by a Tukey HSD test. Significantly different values are indicated by asterisks, * for p<0.05 and ** for p<0.01.

duration of this experiment, the uncertainty was large for the estimated values of C_m (the maximum growth rate in the linear phase); therefore, this parameter was not used for further analysis. Figure 4A shows the R_m values for the WT, *npq4*, and *stn7* plants under each of the three light conditions. Both WT and *stn7* plants showed a significantly higher R_m under a parabolic irradiance profile compared to the two other irradiance conditions. In contrast, *npq4* plants exhibited a significantly higher maximum relative growth rate under the parabolic irradiance than under the square-wave condition, but there were no significant differences in relative growth rate between fluctuating irradiance and the other two irradiance profiles. The total above-ground fresh weight of the plants at the end of the experiment showed a similar trend. Fresh weight was significantly higher for WT and *stn7* plants grown under a parabolic irradiance profile; *npq4* plants also had a higher fresh weight under parabolic irradiance compared to the other two profiles, but in this case the difference was not significant. For *npq4* plants, fresh weight was significantly lower when they were grown under fluctuating light conditions compared to square-wave and parabolic irradiance profiles. Finally, WT plants grown under fluctuating irradiance also had a fresh weight lower than those grown under parabolic or square-wave profiles, but in this case the difference was not significant.

Taken together, the data on leaf area and fresh weight from WT, *npq4*, and *stn7* plants showed similar overall trends in terms of the effects of different irradiance profiles on plant growth (Figures 3, 4).

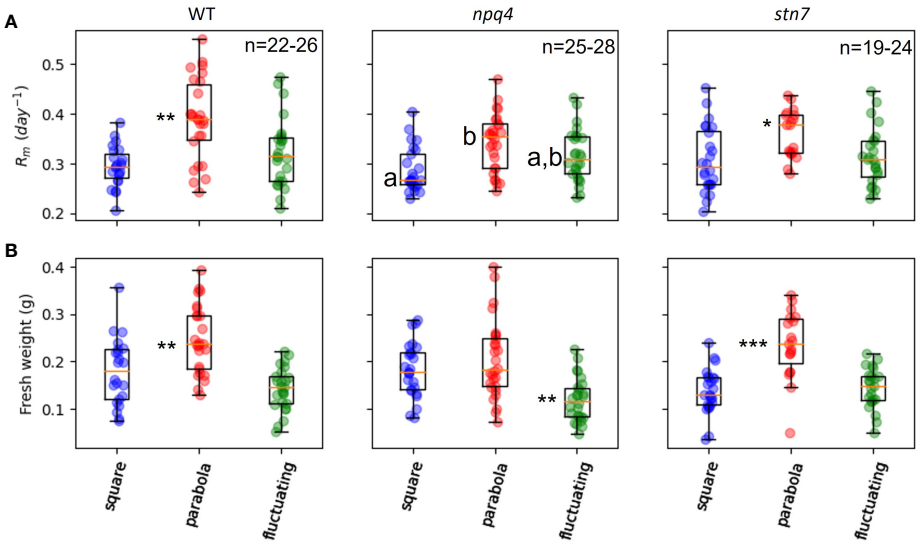

FIGURE 4
Maximal exponential growth rate **(A)** and fresh weight **(B)** of WT, npq4, and stn7 plants under square, parabolic, and fluctuating light conditions. Measurements are displayed in boxplot form. The middle line represents the median value of the data; values inside the box represent 50% of the measured data; and the whiskers together with the box comprise 95% of the measured values. Differences were tested for via one-way ANOVA, followed by a Tukey HSD test. Significantly different values are indicated by asterisks: * for p<0.05, ** for p<0.01, *** for p<0.001. For npq4 plants, the Rm values for the square and parabolic light conditions are significantly different (p<0.001), while there is no significant difference between the square and fluctuating conditions (p=0.122) or between the parabolic and fluctuating conditions (p=0.166).

Growth (as indexed by R_m and fresh weight) was greatest under the parabolic profile condition relative to the square-wave and fluctuating profiles; note that a square-wave profile is conventionally used in controlled-environment systems.

3.2 Under which fluctuating light conditions does the absence of PsbS or Stn7 result in a growth disadvantage?

We compared the maximum relative growth rates (R_m, Figure 5A), fresh weights (Figure 5B), and increases in leaf area (Supplementary Figure 1) of WT plants, *npq4* plants (which lack PsbS), and *stn7* plants (which lack Stn7) grown under fluctuating light conditions. The maximum relative growth rate was very similar for the three plant types. Although the fresh weight and final leaf area of *npq4* plants were lower than those of WT and *stn7* plants, the difference was not statistically significant (p=0.17 for fresh weight and p=0.487 for final leaf area in a comparison of *npq4* with WT). Therefore, no significant disadvantage arising from the absence of Stn7 or PsbS was found under the fluctuating light irradiance condition. Having PsbS or Stn7 also did not confer an advantage under this specific fluctuating light condition (fluctuations are shown in Figure 1). The question remained as to whether there is any fluctuating irradiance regime under which a lack of these proteins results in a growth impairment. This has already been shown for *stn7* plants, which show strongly impaired growth under 5 min of low light (50-60 µmol m^{-2} s^{-1}) alternating with 1 min of high light (500-600 µmol m^{-2} s^{-1}) (Tikkanen et al., 2010; Grieco et al., 2012). The smaller size of the intensity fluctuations (60-360 µmol m^{-2} s^{-1}) applied in our light condition was most likely the reason why we did not observe a difference in growth.

We decided to focus in more detail on the need for PsbS, as this protein is directly related to qE and is generally believed to be required for optimal plant growth and fitness under fluctuating light conditions (Kulheim et al., 2002; Alter et al., 2012; Poorter et al., 2016; Vialet-Chabrand et al., 2017; Kaiser et al., 2018; Qiao et al., 2021). In the literature, *npq4* plants have been compared to WT plants under outdoor conditions, and in a climate-controlled room under one specific fluctuating light condition. Here we tested several irradiance fluctuations. Given that temperature might also play a role in the need for qE through its effect on photosynthesis irradiance curves and rate of response to fluctuating light this factor was also included.

3.2.1 What is the effect of fluctuating light on *npq4* plants?

The growth of WT and *npq4* Arabidopsis plants was assessed by quantifying the increase in projected leaf area during growth and their final fresh weight. First, a constant irradiance condition (125 µmol m^{-2} s^{-1}) was tested (at 24 °C). As expected, no difference between the WT and *npq4* plants in terms of leaf area (Figure 6A) or fresh weight (Supplementary Figure 2) was found (Table 1). Next, we tested fluctuations occurring on a rather slow timescale: 1 hour of high light (HL, 1000 µmol m^{-2} s^{-1})/0.5 hours of low light (LL, 100 µmol m^{-2} s^{-1}), fluctuating during the full 8-hour photoperiod (Figure 6B). Again, no difference was found between WT and *npq4*, even though the plants were being exposed to a 10-fold irradiance fluctuation. We continued by testing a higher-frequency fluctuation similar to those used by Tikkanen et al. (2010) and Grieco et al. (2012); specifically, this consisted of 5 min of LL alternating with 1 min of HL (Figure 6C; Supplementary Figure 2). Even under these light conditions no differences were observed, in agreement with an earlier observation (Tikkanen et al., 2010). This clearly demonstrates that not all intensity fluctuations negatively impact plant growth in the *npq4* mutant. Only when we applied an equal duration of HL and LL by prolonging the exposure to high irradiance (5 min HL /5 min LL) did we find that *npq4* plants showed a significant decrease in growth rate (Figure 6D) and fresh weight (Supplementary Figure 2) relative to the WT.

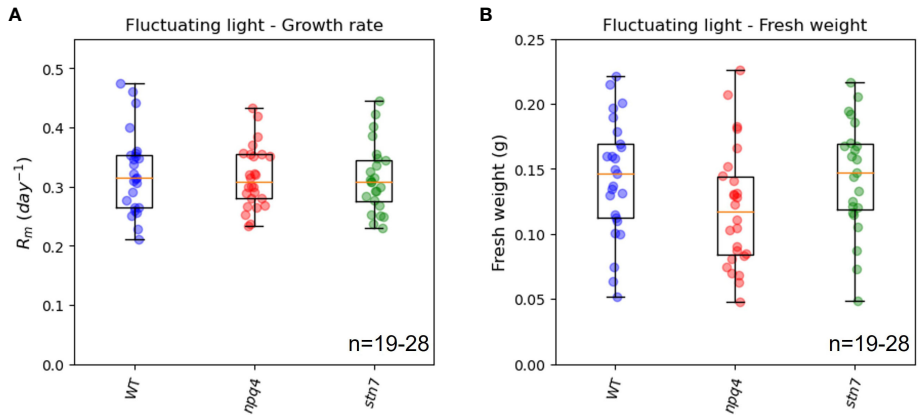

FIGURE 5
Exponential growth rate **(A)** and above-ground fresh weight **(B)** of WT, *npq4*, and *stn7* plants grown under fluctuating light. Measurements are displayed in boxplot form. The middle line represents the median value of the data; values inside the box represent 50% of the measured data; and the whiskers together with the box comprise 95% of the measured values. The number of plants (n) is indicated in the figure. The differences between the genotypes were not significant, p>0.1.

10.3389/fpls.2023.1070218

We then further challenged the plants by lowering the temperature to increase the light stress. At 10°C, WT and *npq4* plants showed the same amount of growth under continuous light (Figure 7A; Table 1), although this growth was diminished compared to the same conditions at 24°C. At 10°C, under a regime of 5 min HL (600 µmol m^{-2} s^{-1})/5 min LL (Figure 7B) and under a regime of 5 min HL (1000 µmol m^{-2} s^{-1})/5 min LL (Figure 7C), *npq4* growth was diminished relative to WT, and this diminution was stronger at the higher HL intensity applied. Comparison of the leaf area of WT plants relative to *npq4* plants (leaf area ratio: WT/*npq4*, Supplementary Figure 3) showed that the disadvantage associated with a lack of PsbS is more severe at 10°C compared to 24°C. Decreasing the temperature further to 4°C resulted in half of the *npq4* plants dying after 4 days of exposure to fluctuating light (5 min HL/5 min LL), while 91% of the WT plants survived (Figure 8, n≥10). After 7 days, nearly all plants had died in the case of both WT and *npq4*. This indicates that PsbS increases the chance of survival under low temperature conditions, although WT plant mortality was still high.

3.2.2 Improved CO_2 fixation under fluctuating light

Among the three fluctuating light conditions under which we compared plant growth of WT and *npq4* at 24°C, only the 5 *min* HL/5 min LL regime had a negative impact on *npq4* relative to WT. This shows that *npq4* plants, despite their lack of qE, can grow as well as the WT under continuous light or moderate fluctuations (Figures 6A–C, 7A), but there is a growth penalty under harsher treatments involving more rapid fluctuations with longer periods of high irradiance (Figure 6D) or fluctuations at lower temperatures (Figures 7B, C). The question remains as to whether there are conditions under which the possession of PsbS is a disadvantage—in other words, whether the amount of PsbS is the result of optimization of a trade-off. For instance, it has been shown that tobacco plants lacking PsbS have more open stomata, which decreases the stomatal limitation on CO_2 assimilation, allowing (all other things being equal) for more assimilation. If water were not a limiting factor and the water vapor pressure deficit only small, then the penalty in terms of plant water

TABLE 1 Effects of light conditions on the growth of *npq4* vs WT plants as assessed by leaf area and above-ground fresh weight.

Temperature (°C)	Light conditions during photoperiod (µmol m^{-2} s^{-1})	Decreased growth in *npq4* vs WI
24	125	No
24	1 hour 1000/0.5 hour 100	No
24	1 min 1000/5 min 100	No
24	5 min 1000/5 min 100	Yes
10	125	No
10	5 min 1000/5 min 100	Yes
10	5 min 600/5 min 100	Yes
4	100	No
4	5 min 1000/5 min 100	Yes

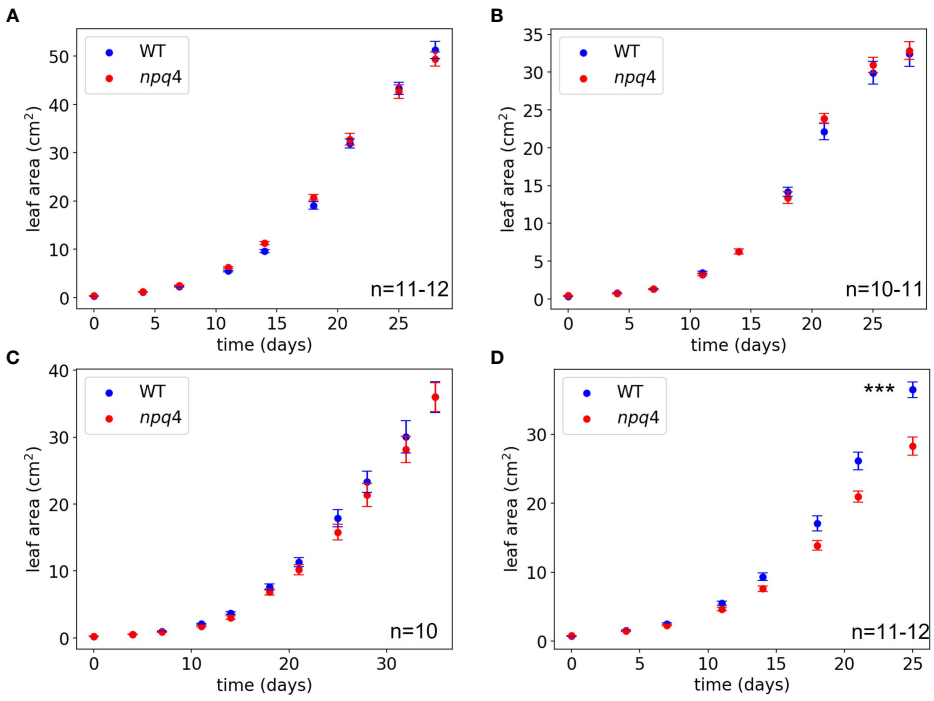

FIGURE 6
Growth of WT vs npq4 Arabidopsis plants at 24°C under **(A)** continuous light conditions of 125 µmol m^{-2} s^{-1}, **(B)** fluctuating light under a regime of 1 hour at 1000 µmol m-2 s-1/0.5 hour 100 µmol m-2 s-1, **(C)** fluctuating light under a regime of 1 min at 1000 µmol m-2 s-1/ 5 min at 100 µmol m-2 s 1. **(D)** fluctuating light under a regime of 5 min at 1000 µmol m-2 s-1/ 5 min at 100 µmol m-2 s 1. The number of plants (n) and SEs are indicated in the figure. Asterisks indicate significant differences in final leaf area, based on a two-tailed independent t-test: *** for p<0.001.

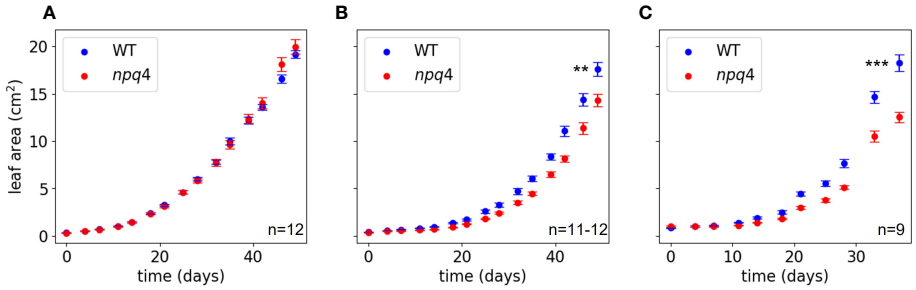

FIGURE 7
Leaf area in WT and npq4 plants grown at 10 °C under continuous light **(A)**, a regime of 5 min HL (600 µmol m^{-2} s^{-1})/5 min LL **(B)**, and a regime of 5 min HL (1000 µmol m-2 s-1)/5 min LL **(C)**. Asterisks indicate a significant difference in final leaf area, based on a two-tailed independent t-test: ** for p<0.01 and *** for p<0.001.

balance of having more open stomata would be small. In the case of tobacco, however, despite the increased stomatal conductance arising from knock-out of PsbS, complementary changes in photosynthetic capacity and in the amount of rubisco and its activation left the overall assimilation rate almost unchanged (Glowacka et al., 2018). Furthermore, when WT plants transition from HL to LL, the dissipation of excess energy in the PSII pigment bed through qE does not switch off instantaneously, and as result qE activity limits photosynthesis, wasting potentially useful energy in the PSII pigment bed as heat (Zhu et al., 2004; De Souza et al., 2022). In absence of PsbS, this problem of diminished photosynthesis arising from the slow relaxation of qE ought not to apply, which could make *npq4* more photosynthetically efficient in the immediate aftermath of a high-to-low light transition. Indeed, faster relaxation of qE (which could be achieved by undertaking lower levels of qE to start with) results in greater growth in tobacco plants (Kromdijk et al., 2016), but not in Arabidopsis (Garcia-Molina and Leister, 2020). An obvious disadvantage of lacking PsbS is the increased risk of photodamage under at least some HL conditions. To address these effects on carbon dioxide fixation and photodamage, we explored how the operating efficiency of PSII electron transport (Φ_{PSII}) and carbon dioxide fixation were affected by different fluctuating light treatments.

First, we compared the CO_2 assimilation rate (Figure 9A) and Φ_{PSII} (Supplementary Figure 4) of WT and *npq4* plants under fluctuating light conditions. Dark-adapted plants, grown under constant light, were exposed to three cycles of approximately 5 min LL/1 min HL, followed by three cycles of 5 min LL/5 min HL. A portable gas exchange system (LI-6400XT) equipped with red and blue actinic light was used for these measurements. Under these conditions, CO_2 assimilation during the 5 min of HL was higher for *npq4* plants than for WT plants. To explore the cause of this enhanced assimilation, we plotted gross CO_2 assimilation rate (i.e., the assimilation rate referenced to the respiration rate during the dark period after the end of the photorespiratory burst and other short-lived transients occurring after the cessation of irradiance) against relative electron transport rate (rETR) through photosystem II. rETR, an index for the rate of linear electron transport, is obtained by multiplying Φ_{PSII} by the light intensity, assuming that leaf absorption is the same for WT and *npq4* plants (Figure 9B). *npq4* plants showed a higher assimilation rate per unit

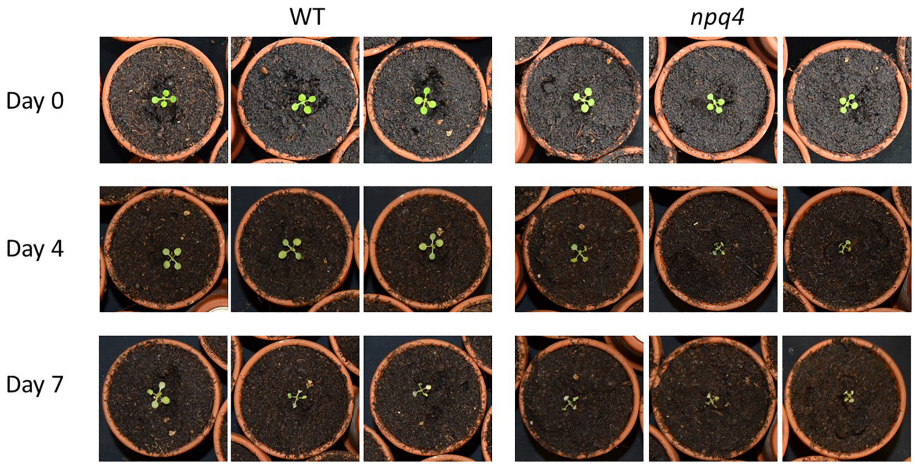

FIGURE 8
Growth of WT and *npq4* plants under fluctuating light conditions (5 min 1000 µmol m-2 s-1/5 min 100 µmol m^{-2} s^{-1}) at 4°C. Number of days after the start of the light treatment is indicated.

10.3389/fpls.2023.1070218

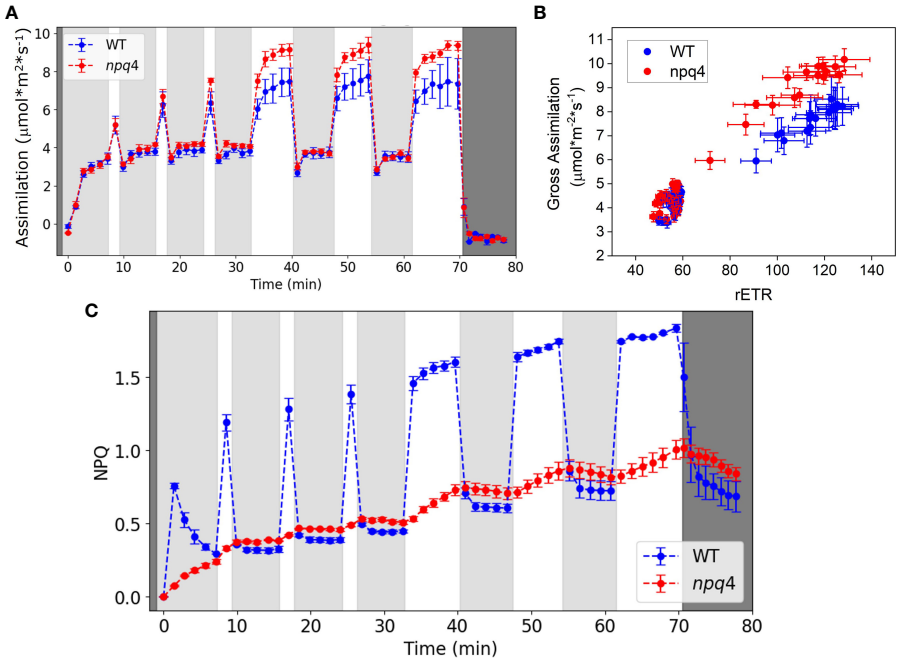

FIGURE 9
(A) Net CO_2 assimilation in WT and *npq4* plants under fluctuating light conditions. Light gray areas indicate periods of low light (100 µmol m^{-2} s^{-1}), white areas indicate high light (1000 µmol m-2 s-1), and dark gray indicates darkness. **(B)** Relationship between gross CO_2 assimilation and the relative electron transport rate (rETR) of photosystem II. **(C)** NPQ in WT and npq4 plants under fluctuating light conditions. SEs are indicated; n=3. Plants were grown in continuous light.

rETR (p<0.0001, two-tailed test). This might be explained by a higher internal CO_2 concentration in *npq4* plants, consistent with their larger stomatal conductance as compared to WT plants (Supplementary Figure 5).

In Figure 9C, the NPQ levels of WT and *npq4* plants are compared under the same fluctuating light cycles used to investigate the assimilation responses. As expected, WT plants showed qE under HL, and this was lower in *npq4* plants. Despite lacking PsbS, however, the *npq4* plants did develop a substantial level of NPQ during the experiment. qE in the *npq4* plants tracked qE in the WT plants during the low light periods but increased only slowly during the high light periods. The slow increase of NPQ in *npq4* plants during the high light periods paralleled the slow increase in NPQ in WT plants under high light. NPQ levels during the LL illumination periods were even slightly higher in *npq4* plants than in WT plants. Although they do have a limited, slow NPQ response, the *npq4* plants lack the large and rapid NPQ response of the WT plants that can be seen immediately following the beginning and end of the HL periods.

Next, to assess CO_2 assimilation directly after a switch from HL to LL in greater detail, we exposed WT and *npq4* plants to a regime consisting of 30 min of LL/30 min HL/30 min LL under atmospheric (21%) oxygen levels (Figure 10A). In this case, data were collected using a custom-built gas analysis system with white actinic LEDs; this enabled the measurement of the assimilation of a single Arabidopsis leaf. Under these conditions, similar assimilation rates were measured for WT and *npq4* leaves. Upon transition from HL to LL, the drop in assimilation was also very similar for both types of plants, so we did not observe any advantage associated with a lack of PsbS in the period immediately following a switch from HL to LL. The drop in net assimilation after a switch to LL is partially attributable to the CO_2 burst that occurs following the high-to-low irradiance step, which itself is due to photorespiratory carbon dioxide release (Vines et al., 1983). To remove this feature from the assimilation response, we reduced the oxygen level to 2% (Figure 10B). However, even without photorespiration and qE (*npq4*), a post-high-irradiance drop in assimilation was still observed to some extent after the transition to LL, although the time course of the transient post-illumination drop in assimilation was slower under non-photorespiratory (2% O_2) conditions compared to photorespiratory conditions. The effect of removing qE (as observed through comparison of *npq4* with WT) on this post-high-light drop is limited (Figure 10B).

An obvious disadvantage that *npq4* plants can be expected to have relative to WT plants is their increased risk of photodamage in HL conditions. We used the maximum quantum efficiency of PSII (F_v/F_m) as a proxy for the degree of photodamage. Plants were grown for 5 days under a fluctuating regime of 5 min HL/5 min LL. After growth at 24°C, F_v/F_m was significantly (although only slightly) lower in *npq4* plants (0.803 ± 0.003; ± indicates the standard error) compared to WT plants (0.822 ± 0.002); see Supplementary Figures 6A, B. However, when the temperature was 10°C, the difference was larger: 0.770 ± 0.006 for WT vs 0.710 ± 0.006 for *npq4* (Supplementary Figure 6C). This indicates that PsbS protects PSII against photodamage under this more extreme fluctuating light treatment.

10.3389/fpls.2023.1070218

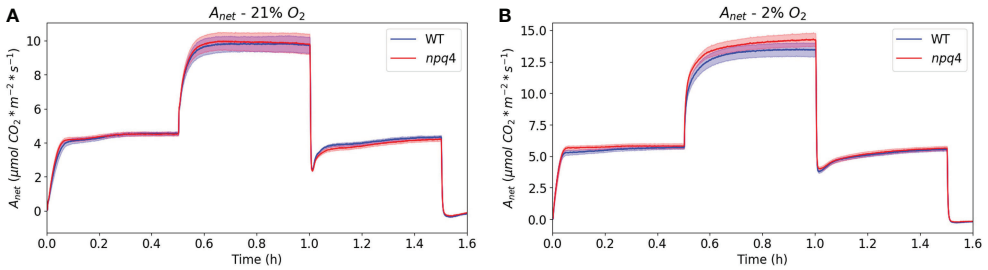

FIGURE 10
Net CO_2 assimilation in WT and *npq4* plants under a regime of 30 min LL – 30 min HL – 30 min LL with 21% oxygen **(A)** and 2% oxygen **(B)**. SEs are indicated; n=9. Plants were grown in continuous light.

3.3 Improved CO_2 fixation under parabolic light

The question remains as to why plants grow faster in parabolic light. Given that plants have evolved under conditions in which light intensity naturally increases and decreases gradually during the day, it can be hypothesized that short- or longer-term control of net carbon assimilation rate and stomal conductance has been in some way optimized for the conditions. To investigate this possibility, plants were grown under square-wave irradiance (PAR: 125 µmol m^{-2} s^{-1}), after which they were tested under square-wave white light (120 µmol m^{-2} s^{-1}) or parabolic white light (minimum PAR of 15 µmol m^{-2} s^{-1}; maximum of 180 µmol m^{-2} s^{-1}) with the same integral PPFD (Figure 11A). Carbon assimilation rates (Figure 11B) and transpiration rates (Supplementary Figure 7) were measured over an entire photoperiod. For square-wave light, carbon assimilation rate rapidly rose and reached its maximum after ~20 minutes, after which it slowly and slightly increased over the remainder of the photoperiod. The parabolic irradiance profile showed a gradual increase and decrease, following the light intensity pattern (Figures 11A, B). The most interesting data were obtained by dividing carbon assimilation rate by light intensity as an index of light-use efficiency (LUE) (Figure 11C). For the plants grown and tested under parabolic light conditions, LUE reached its maximum value in under 2 minutes, while this took 20 minutes for the plants tested under square-wave light conditions (see Supplementary Figure 8 for a zoomed-in visualization of the first hour). Furthermore, the LUE of plants exposed to a parabolic irradiance profile was higher at the beginning and end of the day, when the

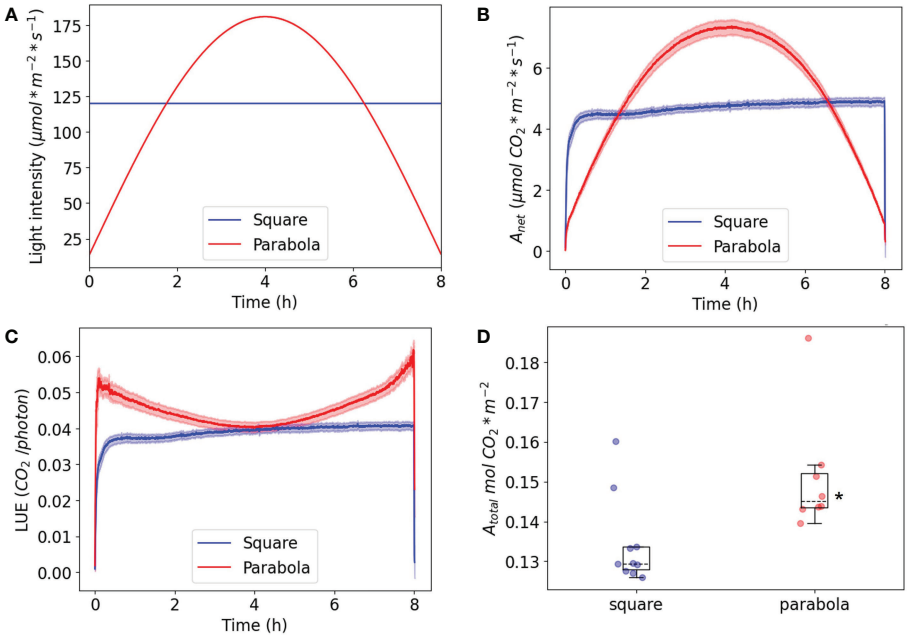

FIGURE 11
Plants were grown and measured under a square-wave irradiance profile and a parabolic irradiance profile with the same daily integral PPFD. **(A)** The irradiance profile during the 8h measurement. **(B)** The net CO_2 assimilation rate. **(C)** The net light-use efficiency (LUE). **(D)** The total CO_2 assimilation per day. The SE is shown; n=8 for the parabola condition, n=10 for the square condition. The asterisk is D indicates a significant difference based on a two-tailed independent t-test ($p < 0.05$).

leaves received a lower intensity of light compared to the plants exposed to the square-wave condition. This is to be expected, as gross CO_2 assimilation LUE is known to be highest under low-light conditions (Bjorkman and Holmgren, 1963). Interestingly, the LUE of plants grown under a parabolic irradiance profile was the same in the middle of the day as that of plants grown under a square-wave irradiance profile, while the light intensity at midday was 180 μmol m^{-2} s^{-1} for the parabolic profile and 120 μmol m^{-2} s^{-1} for the square-wave profile. Taken together, these findings indicate that, over the course of a full day, light presented with a parabolic profile can be used more efficiently; this finding also implies that Arabidopsis plants acclimate their photosynthesis processes differently to each of the two regimes, resulting in the same light-use efficiency at the peak irradiance of both regimes.

To evaluate further this apparent improvement in assimilation in response to a parabolic irradiance profile, total CO_2 assimilation (mol CO_2 m^{-2}) per day was compared for the two growth conditions (Figure 11D). This comparison showed that the parabolic irradiance profile resulted in significantly higher levels of total assimilation per day than the square-wave profile ($n \geq 8$), even though the daily integral of irradiance was the same. This is partly due to the parabolic profile containing lower irradiances than the square-wave profile, since lower irradiances will be associated with higher light-use efficiency in terms of assimilation, all other things being equal. It is also due to the parabolic profile producing higher light-use efficiency than the square-wave profile at higher irradiances, thereby enabling the plants to make better use of the higher irradiances. The higher daily integral of assimilation can explain why the WT plants grown under the parabolic irradiance profile had a significantly higher fresh weight and exponential growth rate (Figure 4) compared to the plants grown under a square-wave profile.

4 Discussion

4.1 Plants under natural light conditions

Over recent decades, photosynthesis research has focused on photosynthesis under constant light conditions. However, in nature and for crops that grow in the field, light is essentially never constant, and under these circumstances photosynthetic responses to fluctuating light become more important (Harbinson and Woodward, 1984; Pearcy, 1990; Ruban, 2009; Kaiser et al., 2018; Wang et al., 2020; Long et al., 2022). When plants transition from shade into full sunlight, absorbed irradiance can increase over the sub-second time range, but the reactions of photosynthesis, especially the dark reactions and stomatal responses, take many minutes to reach new steady-state levels, with the slowest phases of this response being limited by the rates of rubisco activation and stomatal opening (Allen and Pearcy, 2000; Mott and Woodrow, 2000; McAusland et al., 2016; Kaiser et al., 2018; De Souza et al., 2020). This relatively slow increase in the rate of photosynthesis leads to the loss of potential canopy CO_2 assimilation (Taylor and Long, 2017). Furthermore, the excess of light energy that is harvested by the plant may lead to photodamage, particularly in PSII, due to the formation of reactive oxygen species. To minimize photodamage, plants rapidly upregulate qE in order to safely thermally dissipate the excess energy (Horton et al., 1996). When plants shift from sunlight into the shade, however, qE takes on the order of minutes to relax to a new lower level. As a result, useful excitation energy is wasted, and assimilation is transiently limited by the depressed light-use efficiency of PSII photochemistry, which lowers the potential carbon gain (Zhu et al., 2004; De Souza et al., 2022). There is, therefore, an intriguing trade-off between photoprotection when transitioning to a high irradiance and wasting energy when transitioning to a low irradiance. It can be hypothesized that in conditions of overall low light with brief spikes of high light (on a seconds-to-minutes timescale, typical for sun flecks), it is more efficient to endure photodamage in high light rather than switching to a dissipative state that does not instantly switch off in the period after the spike.

When the periods of high light are as long as the periods of low light, on a timescale of minutes, the prolonged exposure to excess light means that inducing qE could be more worthwhile in order to reduce photodamage and thus allow for increased CO_2 assimilation as a result of higher LUE and eventually greater plant growth. This benefit of qE over longer periods of high light would be in spite of the loss of carbon assimilation that occurs immediately after the high–low light transition due to the slow relaxation of qE. The following questions arise: first, under which light conditions does photoprotection represent an advantage for plant growth, and under which conditions it is not beneficial and may it even impair plant growth?; and second, is a light intensity profile involving a gradual increase and decrease during the day better for plant growth than a square-wave irradiance profile, of the kind often used in growth cabinets? To answer these questions, we have grown plants under various light conditions and compared their increase in leaf area and biomass production. These growth conditions made use of rather unnatural square-wave profiles of the kind that are nonetheless widely used in fluctuating light research, as well a fluctuating light profile recorded in a maize canopy and an approximately parabolic profile that is similar to the natural diurnal daylight profile of a cloudless sky. WT plants were compared with *npq4* plants, which lack the PsbS protein that is key to the qE component of NPQ, and *stn7* plants, which are impaired in their regulation and optimization of light-harvesting *via* state transitions.

4.2 When does PsbS represent an advantage?

Comparing the growth of WT vs *npq4* Arabidopsis plants under various fluctuating light conditions at controlled temperatures (24°C, 10°C, and 4°C) allowed us to investigate the circumstances under which having PsbS represented an advantage. The plants were well watered and fertilized to ensure that water and nutrient stress would not compound the effects of light and temperature stress. First, the effect of a natural fluctuating light profile (Figure 1), measured under a maize canopy, was tested. No significant difference was found between WT and *npq4* plants in leaf area or fresh weight (Figure 5). Alternating 1h of HL (1000 μmol m^{-2} s^{-1})

with 0.5h of LL (100 μmol m^{-2} s^{-1}) also resulted in no differences between WT and *npq4* plants. We cannot rule out an effect of acclimation processes, such as a decrease in PSII antenna size and the increase in linear electron transport efficiency that occurs when plants are acclimated to HL for several days (Bailey et al., 2004; Albanese et al., 2016; Schumann et al., 2017; van Rooijen et al., 2017). Such acclimation could make qE less important for photoprotection. Furthermore, the increased opening of stomata in *npq4* plants could represent an advantage for plant growth (Drake et al., 2013; Glowacka et al., 2018) (Figure 9B), while the corresponding natural disadvantage of lower water use efficiency would be less of a problem under our growth conditions, as the plants were well watered (Glowacka et al., 2018). Our measurements did indeed show an increased CO_2 assimilation rate in *npq4* plants during conditions involving 5 min of high red and blue light illumination, but this advantage was not confirmed under 30 min high white light illumination.

Next, we tested the plant growth response to a regimen of 5 min of LL (100 μmol m^{-2} s^{-1}) alternating with 1 min of HL (1000 μmol m^{-2} s^{-1}). Again, no difference in plant growth was observed. It can be hypothesized that a certain amount of extra photodamage might be induced in *npq4* plants during the brief period of HL illumination; however, this could be compensated for by the reduced impact of qE on electron transport following a shift to LL. To test whether *npq4* plants do indeed perform better immediately after a shift from HL to LL, we compared CO_2 assimilation in WT and *npq4* plants. No advantage of a lack of PsbS was observed (Figure 10), so this cannot explain why *npq4* plants did not show impaired growth under the regime of 5 min of LL (100 μmol m^{-2} s^{-1}) alternating with 1 min of HL (1000 μmol m^{-2} s^{-1}). Instead, our NPQ measurements suggest that this can be explained by the higher overall NPQ levels occurring in the *npq4* plants during the periods of LL illumination. It is interesting to see that the level of NPQ during the LL periods is even slightly higher for *npq4* plants than for WT plants and increases on the same trend during each illumination cycle. Additionally, the decay of NPQ in the dark follows a similar trend for *npq4* and WT plants (Figure 9C); furthermore, this residual NPQ in *npq4* plants has been shown to largely decay within 15 min (Takahashi et al., 2009). This is clearly a faster process than the PSII repair cycle, which takes hours to complete (Koivuniemi et al., 1995) and includes a D1 degradation half-time of ~30 min (Aro et al., 1993). As such, the NPQ that has developed in *npq4* plants appears to be largely photoprotective (that is, like qE) and occurs only in part due to permanent PSII damage. This conclusion is in agreement with the work of Johnson and Ruban (2010), who showed that photoprotective energy dissipation does build up in the *npq4* mutant, albeit with a far slower kinetics.

Finally, alternating 5 min of HL with 5 min of LL did result in better growth in WT plants, signifying that having PsbS represents an advantage under this fluctuating light regime. Analysis of dark-acclimated F_v/F_m after one week of this fluctuating light regime showed that dark-adapted quantum efficiency of PSII was lower for *npq4* plants than for WT plants. This effect was stronger at 10°C than at 24°C. This shows that PsbS plays a photoprotective role that becomes more important at lower temperatures under more extreme fluctuating light conditions (Figures 6D, 7B, C). This could be due to a lower rate of PSII repair, or to a larger PSII acceptor-side limitation upon shift from LL to HL, as the induction of photosynthesis will be slower (Tikkanen et al., 2014; Huang et al., 2021). In agreement with this observation, we found that the combination of this fluctuating light regime with a lower temperature of 10°C increased the difference in plant growth between WT and *npq4* plants. Furthermore, at 4°C, *npq4* seedlings died after 4 days of exposure to the fluctuating light regime, while nearly all WT seedlings survived. This points to a clear survival benefit if Arabidopsis plants were to be exposed to cold days with high light levels, as might occur in late autumn, winter, and spring (Arabidopsis is a winter annual over much of its European distribution).

In nature, stresses often occur together. For example, on a summer day, high irradiance can be accompanied by high temperatures and drought stress. Examining individual factors in isolation is essential in order to understand their effects in detail; however, this approach might not capture the actual conditions in nature. With the increasing opportunities for high-throughput phenotyping, the time is ripe to study the combined effect of heat, drought, and light stress under controlled conditions. The disadvantage of this approach is that the number of possibilities to be tested is infinite. It is therefore important that the research community selects specific conditions to be tested. To investigate the role of PsbS in photoprotection, we recommend including a regime consisting of the alternation of 5 min of high light with 5 min of low light, which shows a clear phenotype for *npq4* plants. Given that the major component of PsbS-dependent NPQ is activated over the course of minutes and deactivated on a timescale of tens of seconds (Li et al., 2000), it would also be interesting to investigate whether these more rapid fluctuations have a greater impact on *npq4* vs WT plant growth. Past research on the effects of fluctuating light on growth have been largely limited by the ability to modulate growth room irradiance. In most cases, irradiance could only be modulated at low frequencies and amplitudes (compared to those of natural irradiances, which can reach 2,000 μmol m^{-2} s^{-1}). With the advent of LED lighting in controlled environments and the higher irradiances that can be produced by LEDs, it will become possible to explore a wider range of frequencies and amplitudes of irradiance. Given the complexity of the regulation of photosynthesis, with which qE regulation is interwoven, and the way in which photodamage arises from this regulation, a question that emerges is which frequencies and amplitudes of irradiance result in the greatest negative impact on plant growth, especially in a comparison between *npq4* and WT. For example, in regard to photodamage and fluctuating light, other targets exist apart from PSII; e.g., PSI has also been shown to be vulnerable to photodamage at low temperatures, and this damage is influenced by qE in PSII (Zhang and Scheller, 2004; Tikkanen et al., 2014; Allahverdiyeva et al., 2015). A valuable aspect of examining effects on plant growth as a way to monitor factors like the absence of PsbS is that this approach integrates across different sources of stress and will include any positive consequences of an apparently deleterious mutation on growth.

4.3 Gradual day/night regime improves plant growth by more efficient photosynthesis

Recent advances in LED technology have made this the primary choice of light source for vertical farming and for growth cabinets used for scientific research. The favorable characteristics of LEDs include low energy requirements (or high quantum efficiency), a low heat output, fast response time, and flexibility in light intensity, with attendant wide variation in the spectral composition of the irradiance that can be produced (Proietti et al., 2021; van Delden et al., 2021). When plants are grown under artificial light, it is important that the energy input is efficiently converted into crop yield. In this project, we used the controllability of LED output to simulate a natural diurnal pattern of increasing and decreasing light intensity in order to investigate whether this would lead to higher LUE, which would be of interest for vertical farming. In the case of WT Arabidopsis plants grown under a parabolic irradiance profile, we did indeed observe an increase in maximal exponential growth rate and final fresh weight in comparison to those grown under a square-wave profile (Figure 4). Further investigation of LUE in terms of assimilation (Figure 9) showed that the low-irradiance part of the parabolic profile occurring at the beginning of the day can be used very efficiently and efficiency rises quickly with duration of irradiance. This indicates that assimilation is hardly limited by photosynthetic induction (particularly rubisco activation and stomatal opening). On the other hand, the sudden increase of irradiance in the square-wave regime results in a low LUE for the first ~20 minutes because of the time required to strongly activate assimilation. It remains to be seen whether a slow onset of light intensity in combination with stepwise switching off of the light (at the end of the photoperiod) provides the same increase in biomass and total CO_2 assimilation, or whether the natural gradual rise and decrease in light intensity provides the highest overall LUE.

Data availability statement

The original contributions presented in the study are included in the article/Supplementary Material. Further inquiries can be directed to the corresponding authors.

Author contributions

CS, JH, and EW contributed to conception and design of the study. LC designed and built the system to grow plants under fluctuating light. CS, LC, KS, CS, TT, and SD performed the experiments. CS organized the data, made the figures and performed the statistical analysis. EW and CS wrote the draft of the manuscript, SD and JH substantially improved the manuscript. All authors contributed to the article and approved the submitted version.

Funding

This work was supported by the Dutch Organization for scientific research (NWO) *via* Vidi grant no. VI.Vidi 192.042 (EW) and ALWGS.2016.012 (TT).

Conflict of interest

The authors declare that the research was conducted in the absence of any commercial or financial relationships that could be construed as a potential conflict of interest.

Publisher's note

Supplementary material

The Supplementary Material for this article can be found online at: https://www.frontiersin.org/articles/10.3389/fpls.2023.1070218/full#supplementary-material

References

Albanese, P., Manfredi, M., Meneghesso, A., Marengo, E., Saracco, G., Barber, J., et al. (2016). Dynamic reorganization of photosystem II supercomplexes in response to variations in light intensities. *Biochim. Biophys. Acta* 1857, 1651–1660. doi: 10.1016/j.bbabio.2016.06.011

Allahverdiyeva, Y., Suorsa, M., Tikkanen, M., and Aro, E. M. (2015). Photoprotection of photosystems in fluctuating light intensities. *J. Exp. Bot.* 66, 2427–2436. doi: 10.1093/jxb/eru463

Allen, M. T., and Pearcy, R. W. (2000). Stomatal behavior and photosynthetic performance under dynamic light regimes in a seasonally dry tropical rain forest. *Oecologia* 122, 470–478. doi: 10.1007/s004420050968

Alter, P., Dreissen, A., Luo, F. L., and Matsubara, S. (2012). Acclimatory responses of arabidopsis to fluctuating light environment: comparison of different sunfleck regimes and accessions. *Photosynth Res.* 113, 221–237. doi: 10.1007/s11120-012-9757-2

Aro, E. M., Virgin, I., and Andersson, B. (1993). Photoinhibition of photosystem II. inactivation, protein damage and turnover. *Biochim. Biophys. Acta* 1143, 113–134. doi: 10.1016/0005-2728(93)90134-2

Bailey, S., Horton, P., and Walters, R. G. (2004). Acclimation of arabidopsis thaliana to the light environment: The relationship between photosynthetic function and chloroplast composition. *Planta* 218, 793–802. doi: 10.1007/s00425-003-1158-5

Bellafiore, S., Bameche, F., Peltier, G., and Rochaix, J. D. (2005). State transitions and light adaptation require chloroplast thylakoid protein kinase STN7. *Nature* 433, 892–895. doi: 10.1038/nature03286

Bjorkman, O., and Holmgren, P. (1963). Adaptability of photosynthetic apparatus to light intensity in ecotypes from exposed and shaded habitats. *Physiologia Plantarum* 16, 889–914. doi: 10.1111/j.1399-3054.1963.tb08366.x

Chiang, C., Bankestad, D., and Hoch, G. (2020). Reaching natural growth: The significance of light and temperature fluctuations in plant performance in indoor growth facilities. *Plants* 9, 1–18. doi: 10.3390/plants9101312

Covington, M. F., and Harmer, S. L. (2007). The circadian clock regulates auxin signaling and responses in arabidopsis. *PloS Biol.* 5, e222. doi: 10.1371/journal.pbio.0050222

Demmig-Adams, B. (1990). Carotenoids and photoprotection in plants - a role for the xanthophyll zeaxanthin. *Biochim. Et Biophys. Acta* 1020, 1–24. doi: 10.1016/0005-2728(90)90088-L

De Souza, A. P., Burgess, S. J., Doran, L., Hansen, J., Manukyan, L., Maryn, N., et al. (2022). Soybean photosynthesis and crop yield are improved by accelerating recovery from photoprotection. *Science* 377, 851–854. doi: 10.1126/science.adc9831

De Souza, A. P., Wang, Y., Orr, D. J., Carmo-Silva, E., and Long, S. P. (2020). Photosynthesis across African cassava germplasm is limited by rubisco and mesophyll conductance at steady state, but by stomatal conductance in fluctuating light. *New Phytol.* 225, 2498–2512. doi: 10.1111/nph.16142

Dodd, A. N., Kusakina, J., Hall, A., Gould, P. D., and Hanaoka, M. (2014). The circadian regulation of photosynthesis. *Photosynth Res.* 119, 181–190. doi: 10.1007/s11120-013-9811-8

Drake, P. L., Froend, R. H., and Franks, P. J. (2013). Smaller, faster stomata: Scaling of stomatal size, rate of response, and stomatal conductance. *J. Exp. Bot.* 64, 495–505. doi: 10.1093/jxb/ers347

Ferroni, L., Zivcak, M., Sytar, O., Kovar, M., Watanabe, N., Pancaldi, S., et al. (2020). Chlorophyll-depleted wheat mutants are disturbed in photosynthetic electron flow regulation but can retain an acclimation ability to a fluctuating light regime. *Environ. Exp. Bot.* 178, 1–20. doi: 10.1016/j.envexpbot.2020.104156

Frenkel, M., Bellafiore, S., Rochaix, J. D., and Jansson, S. (2007). Hierarchy amongst photosynthetic acclimation responses for plant fitness. *Physiologia Plantarum* 129, 455–459. doi: 10.1111/j.1399-3054.2006.00831.x

Garcia-Molina, A., and Leister, D. (2020). Accelerated relaxation of photoprotection impairs biomass accumulation in arabidopsis. *Nat. Plants* 6, 9–12. doi: 10.1038/s41477-019-0572-z

Genty, B., Briantais, J. M., and Baker, N. R. (1989). The relationship between the quantum yield of photosynthetic electron-transport and quenching of chlorophyll fluorescence. *Biochim. Et Biophys. Acta* 990, 87–92. doi: 10.1016/S0304-4165(89)80016-9

Glowacka, K., Kromdijk, J., Kucera, K., Xie, J. Y., Cavanagh, A. P., Leonelli, L., et al. (2018). Photosystem II subunit s overexpression increases the efficiency of water use in a field-grown crop. *Nat. Commun.* 9. Article number 868. doi: 10.1038/s41467-018-03231-x

Goudriaan, J., and Monteith, J. L. (1990). A mathematical function for crop growth based on light interception and leaf-area expansion. *Ann. Bot.* 66, 695–701. doi: 10.1093/oxfordjournals.aob.a088084

Grieco, M., Tikkanen, M., Paakkarinen, V., Kangasjarvi, S., and Aro, E. M. (2012). Steady-state phosphorylation of light-harvesting complex II proteins preserves photosystem I under fluctuating white light. *Plant Physiol.* 160, 1896–1910. doi: 10.1104/pp.112.206466

Harbinson, J., and Woodward, F. I. (1984). Field measurements of the gas exchange of woody plant species in simulated sunflecks. *Ann. Bot.* 53, 841–851. doi: 10.1093/oxfordjournals.aob.a086754

Hazen, S. P., Naef, F., Quisel, T., Gendron, J. M., Chen, H., Ecker, J. R., et al. (2009). Exploring the transcriptional landscape of plant circadian rhythms using genome tiling arrays. *Genome Biol.* 10. doi: 10.1186/gb-2009-10-2-r17

Hennessey, T. L., and Field, C. B. (1991). Circadian rhythms in photosynthesis : Oscillations in carbon assimilation and stomatal conductance under constant conditions. *Plant Physiol.* 96, 831–836. doi: 10.1104/pp.96.3.831

Horton, P., Ruban, A. V., and Walters, R. G. (1996). Regulation of light harvesting in green plants. *Annu. Rev. Plant Physiol. Plant Mol. Biol.* 47, 655–684. doi: 10.1146/annurev.arplant.47.1.655

Huang, W., Hu, H., and Zhang, S. B. (2021). Photosynthetic regulation under fluctuating light at chilling temperature in evergreen and deciduous tree species. *J. Photochem. Photobiol. B-Biology* 219, 1–8. doi: 10.1016/j.jphotobiol.2021.112203

Hubbart, S., Ajigboye, O. O., Horton, P., and Murchie, E. H. (2012). The photoprotective protein PsbS exerts control over CO(2) assimilation rate in fluctuating light in rice. *Plant J.* 71, 402–412. doi: 10.1111/j.1365-313X.2012.04995.x

Johnson, M. P., and Ruban, A. V. (2010). Arabidopsis plants lacking PsbS protein possess photoprotective energy dissipation. *Plant J.* 61, 283–289. doi: 10.1111/j.1365-313X.2009.04051.x

Kaiser, E., Morales, A., and Harbinson, J. (2018). Fluctuating light takes crop photosynthesis on a rollercoaster ride. *Plant Physiol.* 176, 977–989. doi: 10.1104/pp.17.01250

Khuong, T. T. H., Robaglia, C., and Caffarri, S. (2019). Photoprotection and growth under different lights of arabidopsis single and double mutants for energy dissipation (npq4) and state transitions (pph1). *Plant Cell Rep.* 38, 741–753. doi: 10.1007/s00299-019-02403-3

Koivuniemi, A., Aro, E. M., and Andersson, B. (1995). Degradation of the D1- and D2-proteins of photosystem II in higher plants is regulated by reversible phosphorylation. *Biochemistry* 34, 16022–16029. doi: 10.1021/bi00049a016

Krah, N. M., and Logan, B. A. (2010). Loss of psbS expression reduces vegetative growth, reproductive output, and light-limited, but not light-saturated, photosynthesis in arabidopsis thaliana (Brassicaceae) grown in temperate light environments. *Am. J. Bot.* 97, 644–649. doi: 10.3732/ajb.0900163

Kromdijk, J., Glowacka, K., Leonelli, L., Gabilly, S. T., Iwai, M., Niyogi, K. K., et al. (2016). Improving photosynthesis and crop productivity by accelerating recovery from photoprotection. *Science* 354, 857–861. doi: 10.1126/science.aai8878

Kulheim, C., Agren, J., and Jansson, S. (2002). Rapid regulation of light harvesting and plant fitness in the field. *Science* 297, 91–93. doi: 10.1126/science.1072359

Li, X. P., Bjorkman, O., Shih, C., Grossman, A. R., Rosenquist, M., Jansson, S., et al. (2000). A pigment-binding protein essential for regulation of photosynthetic light harvesting. *Nature* 403, 391–395. doi: 10.1038/35000131

Li, X. P., Muller-Moule, P., Gilmore, A. M., and Niyogi, K. K. (2002). PsbS-dependent enhancement of feedback de-excitation protects photosystem II from photoinhibition. *Proc. Natl. Acad. Sci. United States America* 99, 15222–15227. doi: 10.1073/pnas.232447699

Logan, B. A., Hammond, M. P., and Stormo, B. M. (2008). The French paradox: Determining the superoxide-scavenging capacity of red wine and other beverages. *Biochem. Mol. Biol. Educ.* 36, 39–42. doi: 10.1002/bmb.20140

Long, S. P., Taylor, S. H., Burgess, S. J., Carmo-Silva, E., Lawson, T., De Souza, A. P., et al. (2022). Into the shadows and back into sunlight: Photosynthesis in fluctuating light. *Annu. Rev. Plant Biol.* 73, 617–648. doi: 10.1146/annurev-arplant-070221-024745

Loriaux, S. D., Avenson, T. J., Welles, J. M., Mcdermitt, D. K., Eckles, R. D., Riensche, B., et al. (2013). Closing in on maximum yield of chlorophyll fluorescence using a single multiphase flash of sub-saturating intensity. *Plant Cell Environ.* 36, 1755–1770. doi: 10.1111/pce.12115

McAusland, L., Vialet-Chabrand, S., Davey, P., Baker, N. R., Brendel, O., and Lawson, T. (2016). Effects of kinetics of light-induced stomatal responses on photosynthesis and water-use efficiency. *New Phytol.* 211, 1209–1220. doi: 10.1111/nph.14000

Mott, K. A., and Woodrow, I. E. (2000). Modelling the role of rubisco activase in limiting non-steady-state photosynthesis. *J. Exp. Bot.* 51, 399–406. doi: 10.1093/jexbot/51.suppl_1.399

Murchie, E. H., and Niyogi, K. K. (2011). Manipulation of photoprotection to improve plant photosynthesis. *Plant Physiol.* 155, 86–92. doi: 10.1104/pp.110.168831

Niyogi, K. K., Grossman, A. R., and Bjorkman, O. (1998). Arabidopsis mutants define a central role for the xanthophyll cycle in the regulation of photosynthetic energy conversion. *Plant Cell* 10, 1121–1134. doi: 10.1105/tpc.10.7.1121

Pearcy, R. W. (1990). Sunflecks and photosynthesis in plant canopies. *Annu. Rev. Plant Physiol. Plant Mol. Biol.* 41, 421–453. doi: 10.1146/annurev.pp.41.060190.002225

Poorter, H., Fiorani, F., Pieruschka, R., Wojciechowski, T., van der Putten, W. H., Kleyer, M., et al. (2016). Pampered inside, pestered outside? differences and similarities between plants growing in controlled conditions and in the field. *New Phytol.* 212, 838–855. doi: 10.1111/nph.14243

Proietti, S., Moscatello, S., Riccio, F., Downey, P., and Battistelli, A. (2021). Continuous lighting promotes plant growth, light conversion efficiency, and nutritional quality of eruca vesicaria (L.) cav. in controlled environment with minor effects due to light quality. *Front. Plant Sci.* 12, 730119. doi: 10.3389/fpls.2021.730119

Qiao, M. Y., Zhang, Y. J., Liu, L. A., Shi, L., Ma, Q. H., Chow, W. S., et al. (2021). Do rapid photosynthetic responses protect maize leaves against photoinhibition under fluctuating light? *Photosynthesis Res.* 149, 57–68. doi: 10.1007/s11120-020-00780-5

Ruban, A. V. (2009). Plants in light. *Commun. Integr. Biol.* 2, 50–55. doi: 10.4161/cib.2.1.7504

Schumann, T., Paul, S., Melzer, M., Dormann, P., and Jahns, P. (2017). Plant growth under natural light conditions provides highly flexible short-term acclimation properties toward high light stress. *Front. Plant Sci.* 8. doi: 10.3389/fpls.2017.00681

Takahashi, S., Milward, S. E., Fan, D. Y., Chow, W. S., and Badger, M. R. (2009). How does cyclic electron flow alleviate photoinhibition in arabidopsis? *Plant Physiol.* 149, 1560–1567. doi: 10.1104/pp.108.134122

Taylor, S. H., and Long, S. P. (2017). Slow induction of photosynthesis on shade to sun transitions in wheat may cost at least 21% of productivity. *Philos. Trans. R Soc. Lond B Biol. Sci.* 372, 1–9. doi: 10.1098/rstb.2016.0543

Taylor, C. R., van Ieperen, W., and Harbinson, J. (2019). Demonstration of a relationship between state transitions and photosynthetic efficiency in a higher plant. *Biochem. J.* 476, 3295–3312. doi: 10.1042/BCJ20190576

Tikkanen, M., Grieco, M., Kangasjarvi, S., and Aro, E. M. (2010). Thylakoid protein phosphorylation in higher plant chloroplasts optimizes electron transfer under fluctuating light. *Plant Physiol.* 152, 723–735. doi: 10.1104/pp.109.150250

Tikkanen, M., Mekala, N. R., and Aro, E. M. (2014). Photosystem II photoinhibition-repair cycle protects photosystem I from irreversible damage. *Biochim. Et Biophys. Acta-Bioenergetics* 1837, 210–215. doi: 10.1016/j.bbabio.2013.10.001

van Delden, S. H., SharathKumar, M., Butturini, M., Graamans, L. J. A., Heuvelink, E., Kacira, M., et al. (2021). Current status and future challenges in implementing and upscaling vertical farming systems. *Nat. Food* 2, 944–956. doi: 10.1038/s43016-021-00402-w

van Rooijen, R., Kruijer, W., Boesten, R., van Eeuwijk, F. A., Harbinson, J., and Aarts, M. G. M. (2017). Natural variation of YELLOW SEEDLING1 affects photosynthetic acclimation of arabidopsis thaliana. *Nat. Commun.* 8, 1421. doi: 10.1038/s41467-017-01576-3

Vialet-Chabrand, S., Matthews, J. S., Simkin, A. J., Raines, C. A., and Lawson, T. (2017). Importance of fluctuations in light on plant photosynthetic acclimation. *Plant Physiol.* 173, 2163–2179. doi: 10.1104/pp.16.01767

Vines, H. M., Tu, Z. P., Armitage, A. M., Chen, S. S., and Black, C. C. (1983). Environmental responses of the post-lower illumination CO_2 burst as related to leaf photo-respiration. *Plant Physiol.* 73, 25–30. doi: 10.1104/pp.73.1.25

von Bismarck, T., Korkmaz, K., Ruß, J., Skurk, K., Kaiser, E., Correa Galvis, V., et al. (2022). Light acclimation interacts with thylakoid ion transport to govern the dynamics of photosynthesis in arabidopsis. *New Phytol* 237 (1), 160–176. doi: 10.1111/nph.18534

Wang, Y., Burgess, S. J., de Becker, E. M., and Long, S. H. P. (2020). Photosynthesis in the fleeting shadows: An overlooked opportunity for increasing crop productivity? *Plant J.* 101, 874–884. doi: 10.1111/tpj.14663

Zhang, S. P., and Scheller, H. V. (2004). Photoinhibition of photosystem I at chilling temperature and subsequent recovery in arabidopsis thaliana. *Plant Cell Physiol.* 45, 1595–1602. doi: 10.1093/pcp/pch180

Zhu, X. G., Long, S. P., and Ort, D. R. (2010). Improving photosynthetic efficiency for greater yield. *Annu. Rev. Plant Biol.* 61, 235–261. doi: 10.1146/annurev-arplant-042809-112206

Zhu, X. G., Ort, D. R., Whitmarsh, J., and Long, S. P. (2004). The slow reversibility of photosystem II thermal energy dissipation on transfer from high to low light may cause large losses in carbon gain by crop canopies: a theoretical analysis. *J. Exp. Bot.* 55, 1167–1175. doi: 10.1093/jxb/erh141

Advantages of publishing in Frontiers

OPEN ACCESS
Articles are free to read for greatest visibility and readership

FAST PUBLICATION
Around 90 days from submission to decision

HIGH QUALITY PEER-REVIEW
Rigorous, collaborative, and constructive peer-review

TRANSPARENT PEER-REVIEW
Editors and reviewers acknowledged by name on published articles

Frontiers
Avenue du Tribunal-Fédéral 34
1005 Lausanne | Switzerland

Visit us: www.frontiersin.org
Contact us: frontiersin.org/about/contact

REPRODUCIBILITY OF RESEARCH
Support open data and methods to enhance research reproducibility

DIGITAL PUBLISHING
Articles designed for optimal readership across devices

FOLLOW US
@frontiersin

IMPACT METRICS
Advanced article metrics track visibility across digital media

EXTENSIVE PROMOTION
Marketing and promotion of impactful research

LOOP RESEARCH NETWORK
Our network increases your article's readership